Copy No. ______________

[redacted]

FACILITY FORM 602

N66-16389 (ACCESSION NUMBER)	(THRU)
414 (PAGES)	1 (CODE)
CR-68285 (NASA CR OR TMX OR AD NUMBER)	30 (CATEGORY)

GPO PRICE $ ______________

CFSTI PRICE(S) $ ______________

Hard copy (HC) 7.00

Microfiche (MF) 2.00

ff 653 July 65

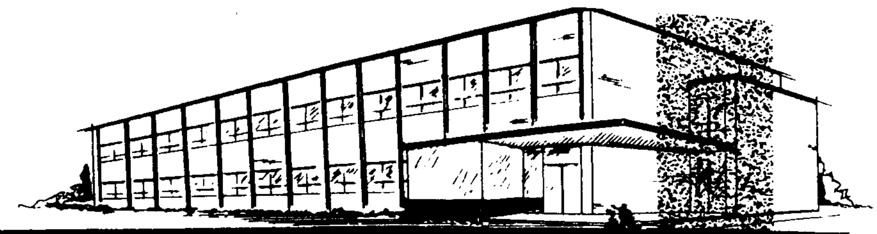

THE Bendix CORPORATION

BENDIX SYSTEMS DIVISION • ANN ARBOR MICHIGAN

LUNAR NAVIGATION STUDY
FINAL REPORT
(June 1964 to May 1965)

BSR 1134

June 1965

Sections 8 through 10 and Appendices

Prepared for:
George C. Marshall Space Flight Center
Huntsville, Alabama
under
Contract No. NAS8-11292

Authors:

L. J. Abbeduto	W. G. Green
M. E. Amdursky	T. F. King
D. K. Breseke	R. B. Odden
J. T. Broadbent	P. I. Pressel
R. A. Gill	T. T. Trexler
H. C. Graboske	C. Waite

BENDIX SYSTEMS DIVISION
OF
THE BENDIX CORPORATION
Ann Arbor, Michigan

SECTION 8

CONCEPT ANALYSIS

A generalized accuracy analysis of navigation concepts in which component capabilities are to be stressed embodies two areas of investigation: (1) a parametric study of total concept performance as a function of component capabilities for a parameterized, standard vehicle traverse and (2) an analysis emphasizing the navigation requirements imposed upon the total concept and evaluation of component requirements as a function of the total concept requirements. The first analysis yields a large quantity of concept performance data as a result of component functioning. The second phase leads to specific requirements which the generalized concepts and the associated components must meet to satisfy the lunar navigation problem.

The analytic approach described above implies the following analytic objectives:

1. Component capabilities

2. Component requirements.

Since the first objective is general and the results are given with interpretation provided by the user of the data, this approach is termed mission independent. Inherent to the problem of making recommendations for component R&D is the necessity for specific missions and mission requirements. Therefore, objective 2 is a result of a mission dependent analysis.

8.1 ANALYSIS APPROACH

The objective of the mission independent analysis was the accumulation of data such that application of the resultant curves will lead to a design point system dependent upon the set of traverse ranges, mission duration, and terminal requirements specified by an analyst applying the curves. Both position fix subconcepts and dead reckoning subconcepts were subject to component accuracy parameter variation to cover the full range of total concept accuracy (or homing range requirements) for a set of standardized trajectories and concept accuracy values. An objective of this analysis is the definition of critical components, or large error sources, for each concept and then minimization of these inputs through selected operating point geometry defined by sensitivity coefficient analysis.

The mission dependent analysis is necessary to make recommendations for component research and development. This analysis applies the set of postulated missions and mission independent analysis data to achieve the goal of defining component accuracy requirements. The postulated missions (described in Section 2) are parameterized for computer simulation as discussed in Section 7.4. The combination of the mission independent analysis with further computer analysis of selected accuracy type systems allows the definition of component accuracy requirements as a function of mission era and component and physical knowledge state of the art. Error reduction techniques, such as periodic position fix operations, are included in the analysis to assess the alleviation of accuracy requirements upon the dead reckoning components.

8.2 ERROR SENSITIVITY COEFFICIENTS

This section discusses the numerical analysis of the following partial derivative error sensitivity coefficients. The coefficients—primarily celestial tracking coefficients—were selected for study because of the importance of self-contained position fixing techniques for lunar navigation concepts.

1. Position Fix

   $C_1, C_2 \ldots C_{12}$ Section 7.2.2

2. Azimuth Alignment; Continuous Azimuthal Reference

   $C_{17}, C_{18} \ldots C_{21}$ Section 7.2.3

3. True Elevation

   $C_{13}, C_{14}, C_{15}, C_{16}$ Section 7.2.5

4. True Azimuth

   $C_{22}, C_{23}, C_{24}, C_{25}$ Section 7.2.5

The purpose of the study was to determine the conditions for minimal error sensitivity coefficients so that the condition for minimal transference of equipment and physical errors to vehicle position and azimuth errors would be established. The results of the analysis define the operating point of celestial and vehicle geometry which minimizes the effect of equipment errors and physical uncertainties. For preliminary results, see Appendix B.

The coefficients basically represent the celestial tracker error model. This position fixing and azimuth alignment technique applies to Concept 1 and Concept 2. However, the results of the analysis of coefficients $C_{17} \ldots C_{21}$ are applicable to the techniques of vehicle animuth measurement utilizing celestial or earth tracking equipments. In this case, the results pertain to calculations on an incremental leg of the dead reckoning traverse.

8.2.1 Position Fix

Since the error sensitivity coefficients are actually partial derivatives, there are a prohibitive number of vehicle-celestial geometries which could be examined. However, becasue the purpose of this analysis is minimization of interdependencies and difinition of critical variables, the need is for a trend of coefficient values rather than specific numerical values. Hence, three vehicle positions on the lunar surface were chosen as operating points, and the celestial geometries were varied about these locations. The total situations are shown in Table 8-1.

Plots of the absolute magnitude of the coefficients are shown in Figures 8-1 to 8-21.* The coefficients for each operating point are plotted versus the elevation angle to the first observable, for parametric values of azimuthal separation of the two stars $\Delta\alpha^*$.

The coefficients evaluated for Point I also are plotted versus the azimuthal separation for parametric values of the elevation angle to the first observable.

Examination of the curves shows the coefficients to:

1. Remain relatively constant for varying ϵ_1^*.

2. Increase in a second order fashion as ϵ_2^* is changed from 10° to 85°.

---

*Figures are presented at the end of the section, beginning on p. 8-58.

TABLE 8-1

CONDITIONS FOR POSITION FIX EVALUATIONS

Variable	Point I	Point II	Point III
x	4°	-60°	0
y	-40°	16°	0
r	0	0	0
p	0	0	0
ϵ_1^*	$0 \rightarrow 80^\circ$		
α_1^*	$30^\circ \rightarrow 110^\circ$		
ϵ_2^*	10°, 85°		
α_2^*	20°		
$\Delta\alpha^*$	$10^\circ \rightarrow 90^\circ$		
	$\Delta\alpha^* = \alpha_1^* - \alpha_2^*$		

3. Vary considerably for varying $\Delta\alpha^*$. (The plots of C_i vs $\Delta\alpha^*$ emphasize this fact in comparison to C_i vs ϵ_1^*).

4. Approach minimal values for $\Delta\alpha^* = 90^\circ$. (The minimal values for $\Delta\alpha^* = 70^\circ \Longrightarrow u_1 = x$).

5. Remain relatively independent of lunar location when final vehicle position error is calculated.

Conclusions:

1. $C_1 \ldots C_{12}$ are generally minimal for $\Delta\alpha^* = 90^\circ$.

2. $C_1 \ldots C_{12}$ are relatively independent of ϵ_1^*, ϵ_2^*, but are minimal for $\epsilon_1^*, \epsilon_2^* \longrightarrow 0$.

3. $C_1 \ldots C_{12}$ as affecting vehicle position error are relatively independent of vehicle lunar position.

4. The ideal operating point is defined as $70^\circ \leq |\alpha_1^* - \alpha_2^*| \leq 110^\circ$.

8.2.2 Azimuth Alignment/Measurement

The operating conditions for the azimuth error study are shown in Table 8-2. Only one observable is required to establish vehicle azimuth once vehicle position is known.

TABLE 8-2

CONDITIONS FOR INITIAL AZIMUTH EVALUATIONS

Variable	Point I	Point II	Point III
x	4°	-60°	0
y	-40°	16°	0
r	0	0	0
p	0	0	0
A	0	0	0
ϵ_1^*	$0 \longrightarrow 80^\circ$		
α_1^*	$30^\circ \longrightarrow 110^\circ$		

Plots of the absolute magnitude of the coefficients C_{17}, C_{19}, and C_{20} are shown in Figures 8-22 to 8-24. Coefficients C_{18} and C_{21} are not plotted since

$$|C_{18}| = 1.0$$

$$|C_{20}| = |C_{21}| \text{ for all conditions.}$$

The coefficients are plotted versus ϵ_1^* for parametric values of α_1^*.

Examination of the curves shows the coefficients to:

1. Remain relatively independent of vehicle lunar position when the total effects upon vehicle azimuth alignment are considered.

   However, in the particular instance of $|C_{20}|$ and $|C_{21}|$, there is minimal dependence with $u_1 \longrightarrow$ polar latitudes with $x \longrightarrow$ equatorial latitudes, and maximal dependence with $x \longrightarrow$ polar latitudes and $u_1 \longrightarrow$ equatorial latitudes.

2. Increase greatly as $\epsilon_1^* \longrightarrow 90^\circ$, and are approximately equal to unity for $\epsilon_1^* \leq 20^\circ$ for all conditions.

3. Show an artificial dependency upon $|A - \alpha_1^*|$. The coefficients C_{17}, C_{19} are minimum for $\alpha_1^* = 0$ not because $|A - \alpha^*| = 0$ but since $y = w_1$. Similarly C_{20} is minimum for the condition $x = u_1$ ($\alpha^* \cong 90^\circ$). But, these conditions serve no useful purpose when aligning the system because the conditions $y = w_1$ and $x = u_1$ are never known without error.

Conclusions:

1. $C_{17} \ldots C_{21}$ are minimal for low elevation angles.

2. C_{17}, C_{18}, and C_{19}, as affecting vehicle azimuth alignment, are relatively independent of vehicle lunar position.

3. The ideal operating point is defined as:

$$\epsilon_1 \leq 20^\circ$$

$$\left\{ \begin{array}{lcl} x & = & \text{equatorial latitudes} \\ u & = & \text{polar latitudes} \end{array} \right\}$$

8.2.3 True Elevation

The coefficients $C_{13} \ldots C_{16}$ represent the sensitivity of vertical errors, elevation and azimuth measurement errors made in a body-fixed space to true elevation error in the analytic space. Hence, the operating points for this analysis are independent of vehicle lunar position and only involve functionally the observable true azimuth $(A + \alpha^*)$, true elevation ϵ^*, and vehicle roll r and pitch p. The operating conditions for the study are shown in Table 8-3.

TABLE 8-3

CONDITIONS FOR TRUE ELEVATION EVALUATION

Variable	Range
x	0
y	0
r	$0 \longrightarrow 30^\circ$
p	$0 \longrightarrow 30^\circ$
A	0
ϵ^*	$0 \longrightarrow 80^\circ$
α^*	$0 \longrightarrow 90^\circ$

Plots of the absolute magnitude of the coefficients are shown in Figures 8-25 to 8-31, with C_i plotted versus vehicle roll angle r for parametric values of vehicle pitch angle p. Sequential plots show parametric variations in ϵ^* and α, respectively.

Examination of the curves shows:

$|C_{13}|$ is

1. < 1.
2. Minimal for p, $r \longrightarrow 0$.

3. Generally increases as $\alpha^* \longrightarrow 90^\circ$.

4. Relatively independent of ϵ^*.

$|C_{14}|$ is

1. ≤ 1.

2. Minimal for $p \longrightarrow 30^\circ$.

3. Generally decreases as $r \longrightarrow 30^\circ$.

4. Generally decreases as $\epsilon^* \longrightarrow 90^\circ$.

5. Relatively independent of α^*.

$|C_{15}|$ is

1. ≤ 1.

2. Generally decreases for $p \longrightarrow 30^\circ$.

3. Relatively constant for r, ϵ^*.

4. Maximum for $\alpha^* = 90^\circ$.

$|C_{16}|$ is

1. ≤ 1.

2. Relatively independent of r, ϵ^*.

3. Maximum for $\alpha^* = 0^\circ$.

Conclusions:

Since these coefficients are less than or equal to unity for all of the above parametric combinations, no significant operating condition constraints are imposed.

8.2.4 True Azimuth

The coefficients $C_{22} \ldots C_{25}$ represent the sensitivity of vertical errors, elevation and azimuth measurement errors in the body fixed space to true azimuth errors in the analytic space. The operating conditions for the numerical analysis are those shown in Table 8-3, and plots of the absolute magnitude of the coefficients are shown in Figures 8-32 through 8-44.

Examination of the plots shows:

$|C_{22}|$ is

1. < 1 for all r, p, α^* and $\epsilon^* \leq 10^\circ$.
2. Maximal for $\epsilon^* \longrightarrow 90^\circ$.
3. Minimal for large p when $\epsilon^* \leq 10^\circ$.
4. Relatively fixed with respect to r for above conditions.

$|C_{23}|$ is

1. < 1 for all r, p, α^* and $\epsilon^* \leq 10^\circ$.
2. Maximal for $\epsilon^* \longrightarrow 90^\circ$.
3. Minimal for $p \longrightarrow 0$, $\epsilon^* \leq 10^\circ$ and all r.
4. Variable with r for above conditions.

$|C_{24}|$ is

1. < 1 for all values r, p, α^*, and $\epsilon^* \leq 10^\circ$.
2. Maximal for $\epsilon^* \longrightarrow 90^\circ$.
3. Minimal as $\alpha^* \longrightarrow 90^\circ$; p, $\epsilon^* \longrightarrow 0$ and all r.

$|C_{25}|$ is

1. < 1 for all values r, p, α^*, and $\epsilon^* \leq 10^\circ$.

2. Maximal for $\epsilon^* \longrightarrow 90^\circ$.

3. Minimal for p, $\epsilon^* \longrightarrow 0$ and all r.

Conclusions:

1. $C_{22} \ldots C_{25}$ are minimal for low ϵ^*.

2. $C_{22} \ldots C_{25}$ are ≤ 1 for $\epsilon^* \leq 10^\circ$.

3. $C_{22} \ldots C_{25}$ are rather insensitive to r, p at low ϵ^*.

4. An ideal operating point is

$$\epsilon^* \leq 10^\circ$$

$$|r| \leq 10^\circ$$

$$|p| \leq 10^\circ.$$

8.2.5 Conclusions

Results of the numerical study for each coefficient type imply that the following operating points are desired for minimal dependence or transference of equipment and physical errors to vehicle position and azimuth errors:

Position Fix

Tracker Stabilized:

1. $70^\circ \leq |\alpha_1^* - \alpha_2^*| \leq 110^\circ$

2. $\epsilon_1^*, \epsilon_2^* \leq 20^\circ$.

3. Any x, y

4. r, p subject only to maximum equipment, vehicle bounds.

Tracker Body Fixed:

1. $70^{\circ} \leq \left|\alpha_1^* - \alpha_2^*\right| \leq 110^{\circ}$

2. $\epsilon_1^* \leq 10^{\circ}$

3. $|r| \leq 10^{\circ}$

4. $|p| \leq 10^{\circ}$

5. Any x, y

Azimuth Alignment/Measurement

The operating conditions for minimum error sensitivity are identical to the above, but with the following additional constraint (if possible):

$$x \equiv \text{equatorial latitudes}$$

$$u_1 \equiv \text{polar latitudes.}$$

This constraint is a result of computing vehicle azimuth in a selenographic system with polar orientation. Equivalently, a latitude longitude grid shift, if precise azimuth measurement is required, to the direction of the reference observable will minimize vehicle azimuth errors due to vehicle position and observable longitude subpoint errors.

8.3 NONGYRO CONCEPT

8.3.1 Mission Independent Analysis

8.3.1.1 Position Fix, Initial Azimuth Error Analysis

The results of a general, mission independent position fix and initial azimuth alignment study are presented for lunar surface navigation systems using the following position fix and azimuth alignment techniques. The results are applicable to both the nongyro and inertial concepts.

Position Fix:

1. Celestial Tracking

2. CSM Angular Tracking

3. CSM Ranging.

Initial Azimuth Alignment:

1. Celestial Tracking

2. CSM Tracking.

Position fix errors and initial azimuth alignment errors are plotted against input errors for parametric variations in observable geometry, CSM orbit geometry, and vehicular positions. See Figures 8-45 to 8-96.

The objectives of the analysis were evaluation of:

1. Critical error sources

2. Geometrical effects on output errors as a function of input errors

3. Maximum and particularly minimum bounds of vehicle position error and azimuth error as a function of error inputs

4. The feasibility of the CSM as a navigational satellite.

The imposition of navigational requirements upon the position fix system is discussed in Section 8. 3. 2. . The emphasis of this section is the magnitude of the position and azimuth errors as a function of error inputs.

The situations as represented in the curves referenced above are easily understood if the standardized mission parametric variations in Table 8-4 are considered. For each system type, critical operating points were selected and then varied. The reason and importance of each parametric variation is discussed below with reference to the case number, i. e. , I-1 versus I-2, etc. Additional parameter values of x, y, r, p were studied, but only insignificant changes to the following results were observed.

TABLE 8-4

SYSTEM AND SUBSYSTEM ANALYSIS PARAMETERS

System	Subsystem	Parameters								Case
		x	y	A, r, p	ϵ_1^*	ϵ_2^*	α_1^*	α_2^*	$\Delta\alpha^*$	
Celestial Tracking	Position Fix	4	-40	0	10	10	45	-45	90	I-1
		4	-40	0	10	10	45	20	25	I-2
	Initial Azimuth	4	-40	0	10	10	45	-45		II-1
		4	-40	0	10	10	45	20		II-2
		4	-40	0	60	10	45	-45		II-3
		60	-40	0	10	10	45	-45		II-4
CSM Tracking	Position Fix	4	-40	0	12.3	19.2			134	III-1
		4	-40	0	31	41			70	III-2
	Initial Azimuth	4	-40	0	12.3	19.2			134	IV-1
		4	-40	0	31	41			70	IV-2
		S_1	S_2	S_3						
CSM Ranging	Position Fix	.25	.5	.75						V-1
		.4	.5	.6						V-2

CSM Orbital Parameters

$w_o = -30^\circ$

$i = 10^\circ$

$V_c = 5753.6$ km/hr

$R_c = 1923$ km

S_i = The proportionate point at which CSM is visible

The objectives of case comparisons are:

I-I: Optimum celestial geometry since $\Delta\alpha^* = 90^\circ$. Curves indicate minimum position errors as a function of error inputs.

I-2: Nominal celestial geometry, since $\Delta\alpha^* = 25^\circ$ or 155°. Curves indicate upper bound of position errors as a function of error inputs.

II-1: Optimal celestial geometry since position error is minimum, latitude of vehicle is equatorial with star subpoint polar, and $\epsilon_1^* = 10^\circ$. The curves indicate minimum azimuth error as a function of error inputs.

II-2: This is a repeat of Case II-1 but with the vehicle position error induced by conditions of Case I-2. The curves indicate slightly greater azimuth errors as a function of error inputs.

II-3: A repeat of Case II-1 with $\epsilon_1^* = 60^\circ$. The curves indicate an upper bound on initial azimuth error as a function of error inputs.

II-4: Optimal celestial geometry but with vehicle in polar latitudes and observable subpoint in equatorial latitudes. The curves indicate minimal bearing errors as a function of error inputs for polar traverse.

III-1: Nominal CSM geometry since $\Delta\alpha^* = 135^\circ$ or 45° and low altitudes. The curves represent upper bounds on vehicle position error as a function of error inputs.

III-2: Geometry approaching optimal with $\Delta\alpha^* = 70^\circ$ or 110°. The curves indicate approximate minimal position error as a function of error inputs.

IV-1: Repeat of Case III-1 with curves indicating minimal initial azimuth alignment error as a function of error inputs. (This case is minimal due to lower ϵ_1^*).

IV-2: Repeat of Case III-2 with curves indicating upper bounds on azimuth error as a function of error inputs.

V-1: Relatively widely spaced points of CSM range measurements. Curves indicate approximate minimal position error as a function of error inputs.

V-2: The points of CSM range measurements more closely spaced. Curves indicate upper bound of position error as a function of error inputs.

Celestial Tracking

For each of the above cases, celestial tracker error curves (Figures 8-45 to 8-78) are plotted as a function of error inputs. The symbols A, B, C, D shown on each set of curves have the definitions shown in Table 8-5 and described below.

TABLE 8-5

NONGYRO/INERTIAL CONCEPT CELESTIAL TRACKING ERROR TABLE

Case	$\sigma_{\epsilon}, \sigma_{\alpha}$ deg	σ_{r}, σ_{p} deg	σ_{t} hr	σ_{R}, σ_{D} deg	σ_{γ} deg	Type System
A	0.0	0.0	0.0	0.0	0.0	Errorless
A'	0.001	0.001	0.00003	0.0001	0.005	SOA
B	0.001	0.001	0.00003	0.0001	0.02	SOA
C	0.01	0.01	0.003	0.005	0.04	Nominal
D	0.04	0.1	0.03	0.03	0.06	Maximum

For each curve, the parametric values of error inputs were selected from Table 8-5. For example, in the plot of Position Fix Error versus Celestial Tracker Error, σ_ϵ, σ_α are equal independent variables. Curve A in this plot represents Position Error as a function of Celestial Tracker Error with other component and physical errors zero. Thus, the values of Case A in the error table were applied, with the exception of the independent variable which is varied from minimum to maximum.

Similarly for curve B in the same plot; while σ_α, σ_ϵ range from minimum to maximum, the remaining error inputs maintain the values given by row B in the error table.

Another illustration is the plot of Position Fix Error versus Timer Error. Curve C in this plot implies the error inputs σ_ϵ, σ_α, σ_r, σ_p, σ_R, σ_D, σ_γ remain fixed at the values given by row C of the error table, while σ_t runs from minimum to maximum. The extension of this logic applies to all other curves.

The vertical dashed line in each curve indicates the SOA, nominal, or maximum value of the equipment error input, or the respective estimates of the physical uncertainties.

Critical dependency of vehicle errors to component errors is demonstrated if there is a significant change in the position error or azimuth error curves for a particular "accuracy type system", i.e. A, B, C, D as the independent variable is varied from minimum to maximum. The lower the slope, the less effect an error input has. Maximum dependency is shown for curves with slopes approximating that of curve A.

Because of the parametric values of the error inputs selected from the error table, the implication follows that:

Case A	$\Longrightarrow$	Errorless System (with the exception of the independent variable)
Case A'	$\Longrightarrow$	SOA System ($\sigma_\gamma = 0.005^\circ$)
Case B	$\Longrightarrow$	SOA System ($\sigma_\gamma = 0.020^\circ$)
Case C	$\Longrightarrow$	Nominal System
Case D	$\Longrightarrow$	Maximum System

Although Case A' and Case B are termed SOA accuracy-type concepts, the nominal case values, Case C, more closely correspond to the error values of an implemented system. Case A' and Case B are not fictitious values, but refer to SOA values which generally reflect laboratory test values and which are usually more optimistic than those of an implemented system.

CSM Tracking

Tracking of the Command and Service Module is an alternate technique for establishing vehicle position. Angular tracking and ranging techniques (assuming the necessary equipments and data are available in the nongyro and inertial position fixing subconcepts) are analyzed in the manner of the celestial tracking error study.

Table 8-6 is the error table for the CSM angular tracking study. The resulting curves are shown in Figures 8-79 to 8-94.

TABLE 8-6

CSM ANGULAR TRACKING ERROR TABLE

Case	σ_ϵ, σ_α deg	σ_r, σ_p deg	σ_γ deg	σ_{hc}, Δ_{RN}, Δ_{RE} km	Type System
A	0. 0	0. 0	0. 0	0. 0	Errorless
B	0. 001	0. 001	0. 02	0. 5	SOA
C	0. 01	0. 01	0. 04	1. 0	Nominal
D	0. 04	0. 1	0. 06	3. 0	Maximum

No error table is constructed for CSM ranging techniques; instead the CSM ranging system position errors are shown in Figures 8-95 and 8-96 plotted against range measurement errors for parametric values of CSM orbital errors.

Results and Conclusions

Celestial Tracking:

1. Position Fix:

   a. Critical Error Source

(1)	Vertical Anomalies	Primary
(2)	Vertical Sensor	Primary
(3)	Celestial Tracker	Secondary
(4)	Ephemeris	Secondary

   The importance of the vertical anomaly as a large error source is emphasized by Figure 8-49. Position Fix Error vs Vertical Anomalies for an optimal geometry situation. For an optimal or SOA system (Case B), and for $\sigma\ \gamma > 0.002^{\circ}$, the position error is a heavily weighted function of the anomalies. The same is true for a nominal accuracy system (Case C). Therefore, absolute navigation to an extremely precise degree is significantly hindered regardless of the quality of the navigational components unless the vertical anomalies are compensated for. The series of curves reflecting the optimal celestial vehicle geometry were replotted (Figures 8-50 through 8-53) with the vertical anomaly term set identically to zero.

   b. Geometrical Effects

   The changing of celestial geometry relative to the vehicle from optimal $\Delta\alpha^{*} = 90^{\circ}$ to nominal $\Delta\alpha^{*} \approx 25^{\circ}$, doubled the minimal values of position error. Hence, for minimal error, or maximum component accuracy requirement, the necessity of optimal geometry should not be under emphasized while performing the position fix function.

   The results of a study not described show that vehicle roll, pitch, and lunar location have negligible effects upon vehicle position error.

c. Minimal Position Error

For optimal geometry, and for the error inputs:

Celestial Tracker

$\sigma_{\alpha}, \alpha_{\epsilon} = 0.001^{\circ}$

Vertical Sensor

$\sigma_{r}, \sigma_{p} = 0.001^{\circ}$

Timer

$\sigma_{t} = 0.00003$ hr

Ephemeris

$\sigma_{R}, \sigma_{D} = 0.0083^{\circ}$

Vertical Anomalies

$\sigma_{\gamma} = 0.005$

PE $\cong$ 0.300 km.

With the vertical anomaly term set to zero, the following accuracies are attainable in an optimal geometry system:

SOA accuracy type system: 0.260 km

Nominal-accuracy type system: 0.490 km

2. Initial Azimuth Alignment:

a. Critical Error Source:

$$\left.\begin{array}{l}\text{1. Ephemeris}\\ \text{2. Celestial Tracker}\\ \text{3. Vertical Sensor}\\ \text{4. Vertical Anomalies}\end{array}\right\}\ \text{Equally}$$

The timer contributions are negligible.

When consideration is given to the effects of geometrical results discussed below, the initial azimuth error is relatively low. The requirements already imposed by the position fix function are such that the component and physical uncertainty parameter values will suffice for the azimuth alignment function.

b. Geometrical Effects

The increase in position error caused by altering the azimuthal separation of the two observables from $\Delta\alpha^* = 90^\circ$, optimal, to $\Delta\alpha^*, = 25^\circ$, nominal, also increased azimuth error generally by 1.25. But the error remains at a relatively low level.

Increasing the elevation angle of the observable from 10° to 60° caused a change in alignment error by a factor greater than 10.

The effect induced by vehicle positions in polar latitudes sighting upon stars with subpoints in equatorial latitudes also increased the azimuth error. The effect varied depending upon the system type, but generally an increase of 1.5 to 5.0 was observed.

c. Minimal Alignment Error

For optimal geometry, equatorial latitudes, and error sources listed for minimum position error:

$$\sigma_{AO} \cong 0.009^\circ$$

For identical conditions but polar vehicle position:

$$\sigma_{AO} \cong 0.017^\circ.$$

CSM Angular Tracking:

Position Fix and Initial Azimuth

The results of the curves, Figures 8-79 through 8-94, are self-explanatory. Until the CSM orbit can be known to accuracy greater than 0. 5 km, this concept appears impractical when compared to celestial tracking methods.

However, if the orbital uncertainty were substantially reduced, the critical error inputs would be vertical anomalies.

It is obvious that the CSM as a navigational satellite is not in an optimal orbit. Thus by changing the orbit inclination, orbit radius and other orbit parameters to adapt to a particular vehicle-navigational satellite geometric configuration, the system errors might be substantially reduced.

CSM Ranging:

Position Fix

The critical error source is not the range measurement error but again the knowledge of the CSM orbit. This concept appears impractical when compared to the Celestial Tracking Method.

Again however, the CSM is not in an optimal orbit to serve as a navigation satellite, and should an optimal combination of range sightings, orbital error, and orbital parameters be combined, the system errors might be substantially reduced.

8.3.1.2 Dead Reckoning

This mission independent analysis determines critical error sources of the dead reckoning subsystem of the nongyro concept. The concept was operated in a relative navigation mode on a standard trajectory in a selenographic region free of navigational singularities; thus, such effects as equatorial navigation near the earth subpoint are avoided and do not enter the evaluation. The resultant curves are dead reckoning system errors for typical non-singular type traverses and provide the base data when navigation requirements are imposed upon the dead reckoning systems.

The approach selected to analyze the extensive parametric combinations was to establish a standard or base path, then vary the parameters of the path which affect vehicle position errors in the most dependent manner. The parameter selected was range of traverse, and three specific ranges were used. The vehicle, path, and geometrical parameters are shown in Table 8-7.

Figures 8-97 through 8-102 are typical standard trajectories in planar and altitude coordinates generated from the data in Table 8-7. The paths are relatively free of extensive obstacle maneuvering and would correspond to a fairly flat, mild lunar traverse. This is indicated by the % EDT of 2 to 3. Although only a single nominal velocity parameter of 8 km/hr was used due to the parametric values of range, the parametric effect of time is achieved if the duration of mission traverse is considered as opposed to range of traverse. Therefore, from the following,

Path 1 $\quad R \cong 11 \text{ km} \Longrightarrow t \cong 1.4 \text{ hr}$

Path 2 $\quad R \cong 50 \text{ km} \Longrightarrow t \cong 6.4 \text{ hr}$

Path 3 $\quad R \cong 101 \text{ km} \Longrightarrow t \cong 12.9 \text{ hr}$

the association of short range, short duration of time and long range, long duration of time implies the full spectra of standard missions from both a distance and time viewpoint.

TABLE 8-7

DEAD RECKONING SUBSYSTEM OPERATING CHARACTERISTIC

	Selenographic Region				Traverse Length, Duration			Terrain Charazterizations				
Path	x_o deg	Y_o deg	$h_o = h_D$ km	A_{OD} deg	≈ Range km	≈ t hr	V km/hr	ΔA_{max} deg	Δr_{max} deg	Δp_{max} deg	$\Delta \beta_{max}$ deg	EDT %
1	4	-40	0	45	11	1.4	8	30	10	10	5	3
2	4	-40	0	45	51	6.4	8	30	10	10	5	2
3	4	-40	0	45	101	12.9	8	30	10	10	5	2

Vehicle Constraints			Celestial Geometry	
V km/hr	K_{vr} km/hr deg^{-1}	K_{vp} km/hr deg^{-1}	u_E deg	w_E deg
8	0.1	0.1	8	8

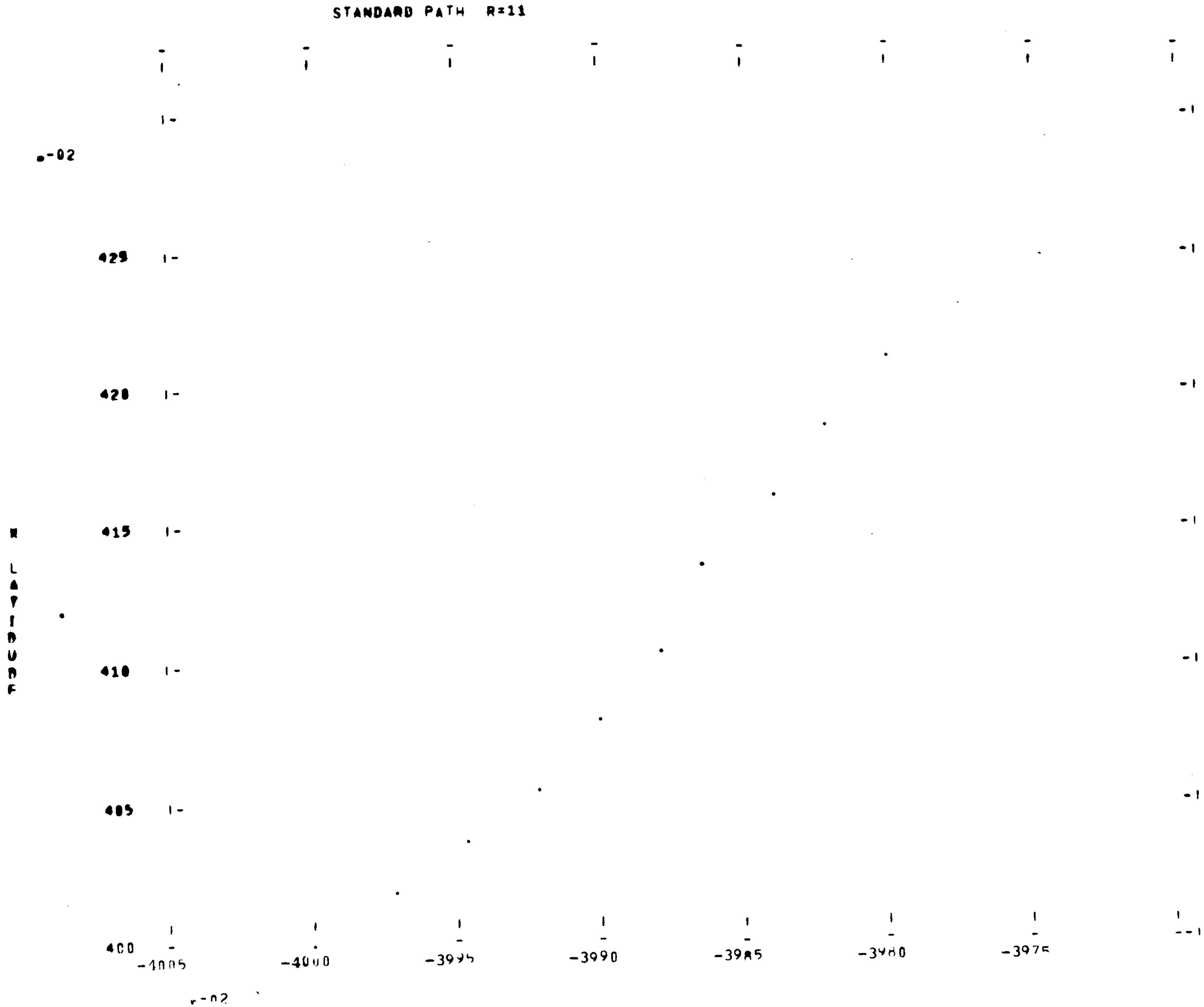

Figure 8-97 Planar Path

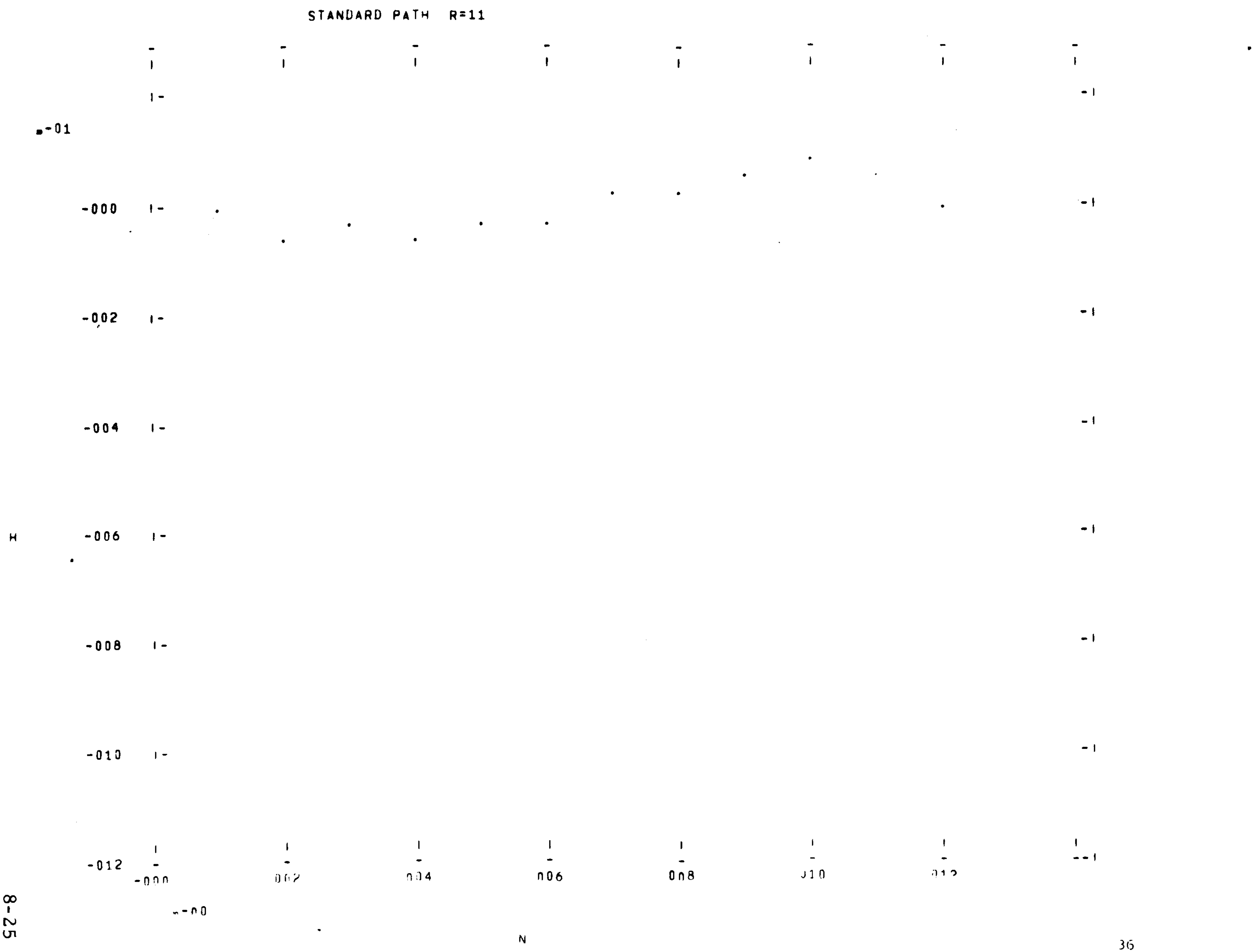

36

Figure 8-98 Altitude Path

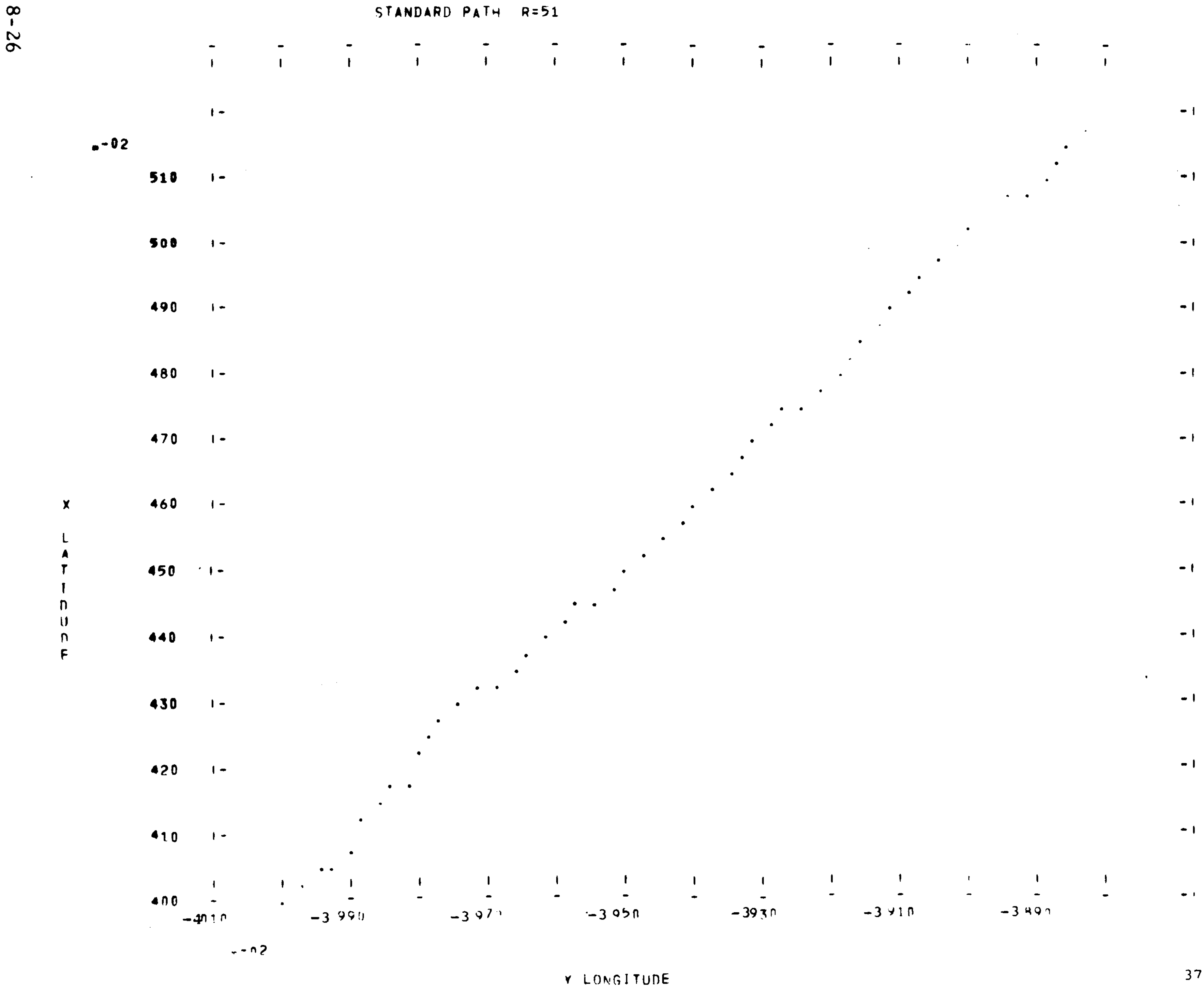

Figure 8-99 Planar Path

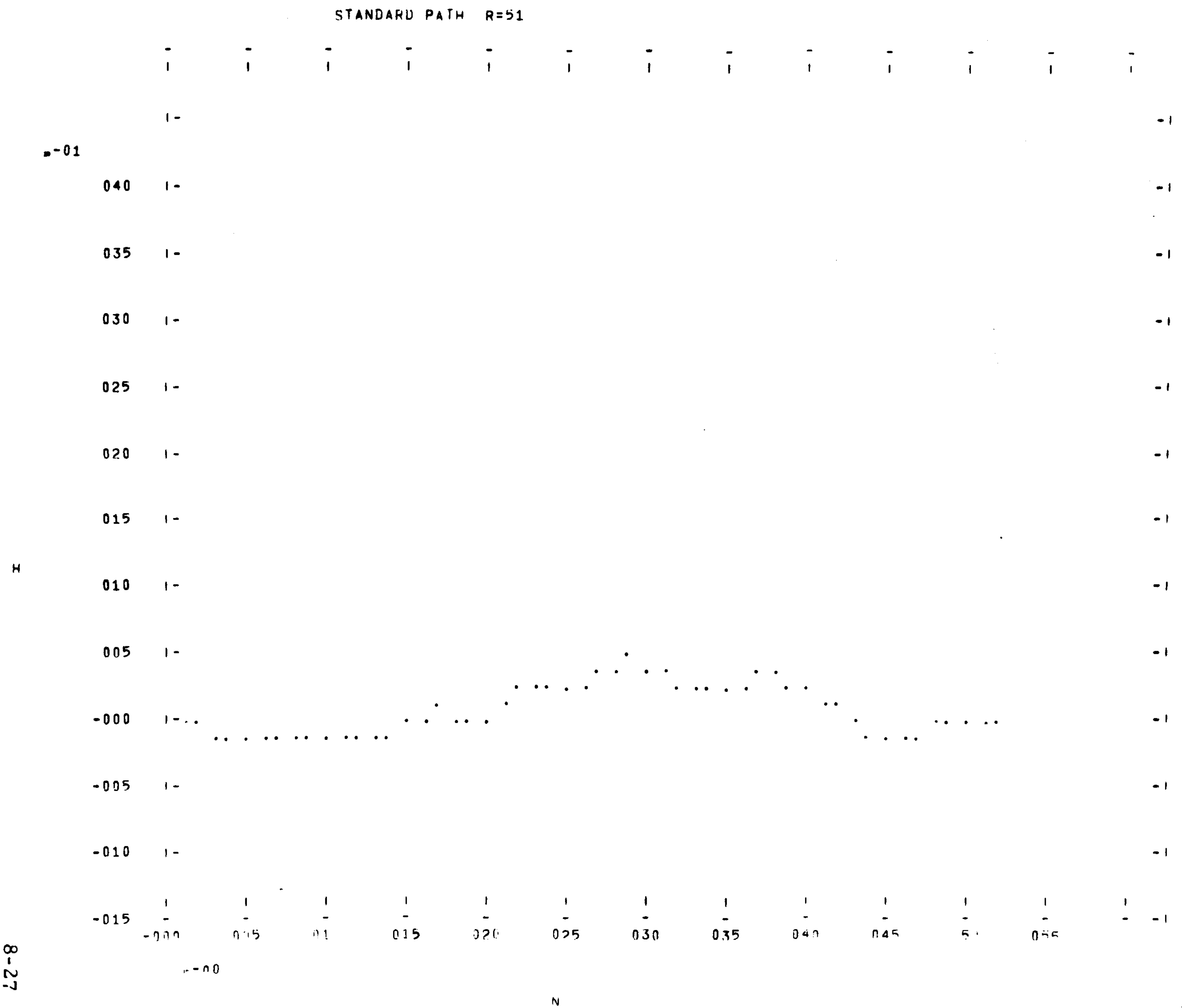

Figure 8-100 Altitude Path

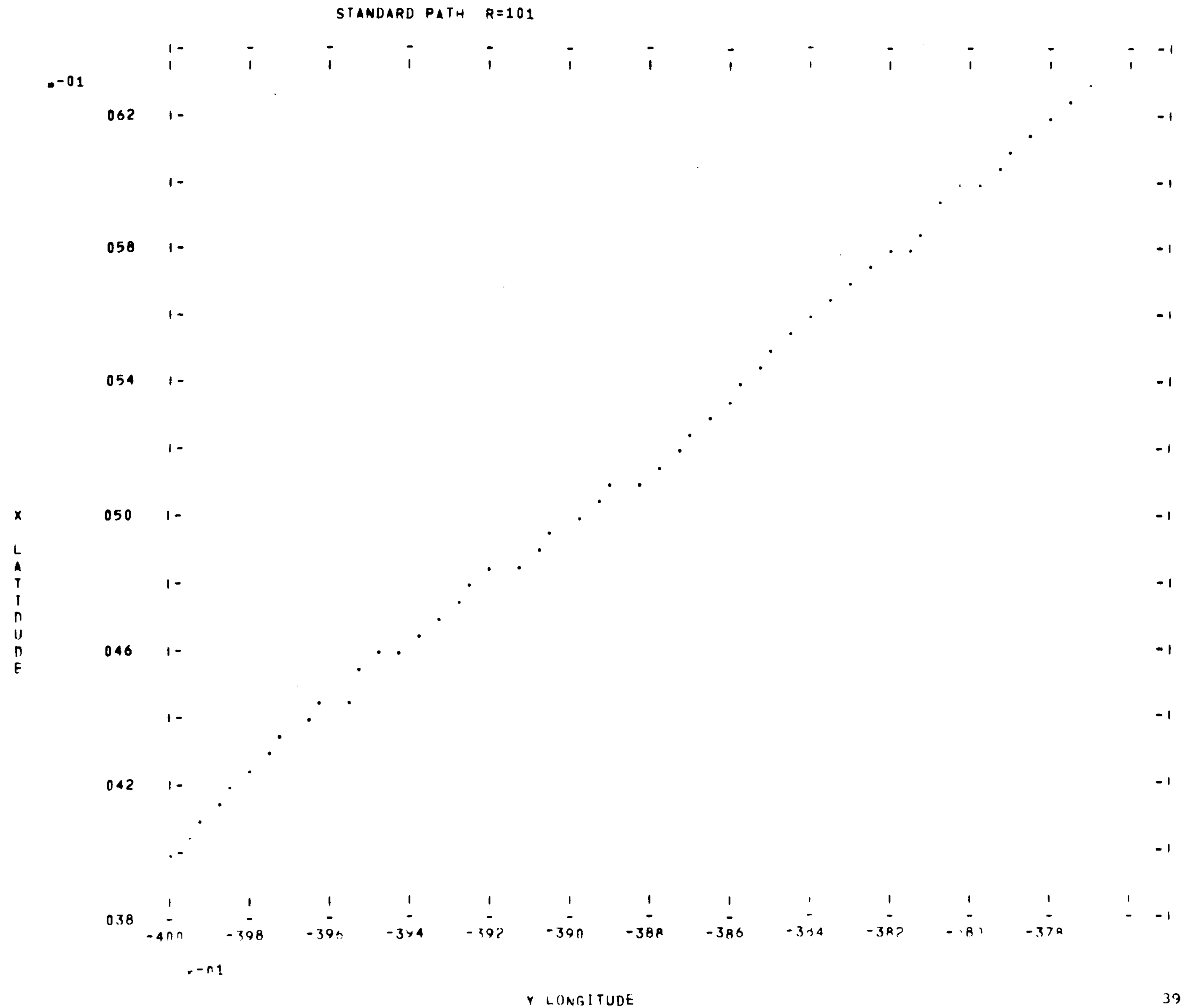

Figure 8-101 Planar Path

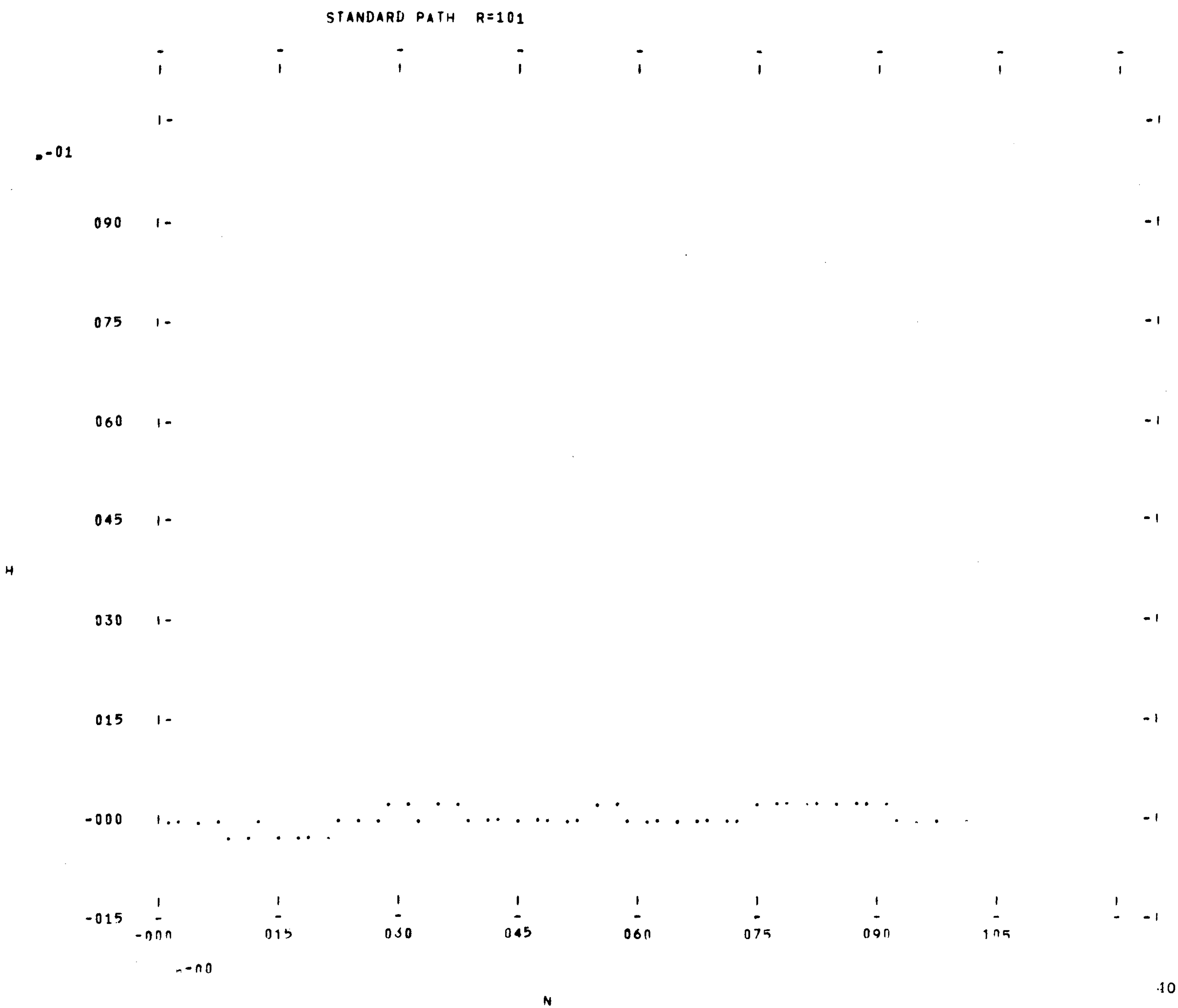

Figure 8-102 Altitude Path

The dead reckoning system of the nongyro concept was evaluated on the standard paths which served as the reference trajectories. The results are typical position error PE curves (Figures 8-103 to 8-119) and altitude error curves $(PE)_Z$ (Figures 8-120 to 8-128) plotted as a function of component error or physical uncertainty value for parametric values of traverse range. The composition of component errors is indicated in Table 8-8, the Nongyro Concept Dead Reckoning Error Table.

The interpretation and use of the error table follows from the treatment of the position fix error table discussed in Section 8. 3. 1. 1. Briefly, each row of the table represents an accuracy type system. This accuracy type system is held fixed and the independent variable or component error under investigation is varied from minimum to maximum, or through the given values: zero, projected state of the art, SOA, nominal, and maximum. Then the total concept error at the terminal or end point of the traverse is plotted as a function of the independent variable. The SOA, nominal, and maximum values of error inputs are denoted by dashed lines on the respective error curves. The curves plotted on linear paper represent concept errors for the "errorless" system.

Five particular classes of accuracy type systems were selected:

Case 0 $\Longrightarrow$ Errorless

Case 1 $\Longrightarrow$ Projected State of the Art (Proj SOA)

Case 2 $\Longrightarrow$ SOA

Case 3 $\Longrightarrow$ Nominal (Nom)

Case 4 $\Longrightarrow$ Maximum (Max)

8. 3. 1. 3 Results and Conclusions

Examination of the dead reckoning error curves (Figures 8-103 to 8-128) points to two critical components of the nongyro concept. The odometer, the distance sensor, and the IR earth tracker, the heading reference, are the components which contribute to the major portion of the concept position error during the dead reckoning process. Table 8-9 summarizes the relaxation or tightening of component requirements for the projected SOA, SOA, and nominal accuracy type systems to meet the specified

TABLE 8-8

NONGYRO CONCEPT DEAD RECKONING ERROR TABLE

Accuracy Type System	σ_c	K_s	K_{sp}	σ_a, σ_e	σ_r, σ_p	K_r, K_p	σ_{RE}, σ_{DE}	σ_t	K_t	σ_γ
0 Errorless	0.0	0.0	0.0	0.0	0.0	0.0	0.0	0.0	0.0	0.0
1 Proj SOA	0.0001	10^{-6}	10^{-5}	0.002	0.0001	10^{-7}	0.0001	≈ 0.0	≈ 0.0	0.0
2 SOA	0.001	10^{-5}	0.0001	0.02	0.0006	10^{-6}	0.001	3×10^{-6}	≈ 0.0	0.0
3 Nom	0.01	0.0001	0.001	0.2	0.01	0.0001	0.01	3×10^{-5}	0.001	0.0
4 Max.	0.03	0.0003	0.004	1.0	0.1	0.001	0.03	0.0001	0.01	0.0

TABLE 8-9

NONGYRO DEAD RECKONING STANDARD REQUIREMENT TABLE
(HORIZONTAL)

Dead Reckoning Requirement		1/20	1/50	1/100	1/200	1/500	1/1000
Range - km		10, 50, 100	10, 50, 100	10, 50, 100	10, 50, 100	10, 50, 100	10, 50, 100
Error	Accuracy Type System						
σ_c, σ_s	Proj. SOA 1	+	.019	.01	.005	.002	.001
	SOA 2	+	.019	.01	.005	.002	.001
	Nom 3	+	.018	.009	.003	0	0
σ_a, σ_e	Proj. SOA 1	+	+	.52	.27	.13	.08
	SOA 2	+	+	.50	.26	.12	0
	Nom 3	+	.96	.02	0	0	0

V = 8 km/hr

+: The dead reckoning requirement is satisfied with the given accuracy type system, and for all component error values from projected SOA to maximum.

0: The dead reckoning requirement is not satisfied for any value of the respective component error since the accuracy type system does not satisfy the requirement.

dead reckoning rate requirements. Since the odometer and IR earth tracker were the prime contributors, only these component requirements are tabulated. The ephemeris errors, timer errors, pendulous vertical errors, and vertical anomalies have comparatively little effect upon the total planar error and are omitted.

The dead reckoning requirement is designated as allowable error per distance traveled for a specific vehicle velocity. The nongyro requirements are evaluated for a vehicle velocity of 8 km/hr. The interpretation of the dead reckoning rate requirement may be total allowable dead reckoning error to satisfy a homing requirement if the mission length is known. If, for example, the traverse range is 100 km, the total dead reckoning rate to satisfy a 1-km homing range is 1/100. Therefore, the postulation of the six standard dead reckoning rates 1/20, 1/50, 1/100, 1/200, 1/500, 1/1000, together with a traverse range and vehicle velocity specification, allows the creation of the mission independent component requirements tabulated in Table 8-9.

1/20: This requirement is satisfied by the complete range of component errors, contained in the error table, Table 8-5. Any combination of the errors satisfy the requirement.

1/50: The odometer error for each of the three accuracy type systems can be relaxed to 0.018 to satisfy this requirement. The earth tracker errors can be relaxed to the maximum value 1.0° for the Proj. SOA and SOA systems, but the upper bound of 0.96° must be met for the nominal system.

1/100: For the Proj. SOA and SOA systems the odometer error can be increased to 0.01. However, for the nominal accuracy type system, the requirement is tightened to 0.009.

The earth tracker requirement can be relaxed to about 0.50° for the Proj. SOA and SOA type systems. However, the nominal accuracy type system requirement is only fulfilled if the error is decreased to 0.02° for the 10 km range trajectory. But for 50 km and 100 km, the accuracy requirement cannot be met.

1/200: The odometer error for the Proj. SOA and SOA systems can be relaxed to 0.005. However, for the nominal accuracy type system the requirement of odometer error is 0.003.

A quarter of a degree earth tracker is required for the Proj. SOA and SOA type systems, but the 1/200 requirement is not attainable for the nominal accuracy type system.

1/500: The odometer accuracy requirement for the Proj. SOA and SOA systems can be relaxed to 0.002. But the errors contributed by the other components of the nominal accuracy type system prevent this requirement to be achieved with any value of odometer error. A tenth of a degree earth tracker is required to achieve 1/500 accuracy for the Proj. SOA and SOA systems. However, the nominal accuracy type system cannot meet the requirement regardless of the earth tracker error.

1/1000: The odometer error that can match the requirement is 0.001 for the Proj. SOA and SOA accuracy type systems. The nominal system cannot meet the requirement.

The earth tracker maximum error allowable is 0.08° for the Proj. SOA system. The SOA and nominal systems cannot satisfy the requirement.

Since the terminology "SOA accuracy type system" refers to and implies component errors for components functioning in an extremely ideal, regulated, laboratory-type environment, and the term "nominal accuracy type system" implies SOA implementation of navigation systems, the conclusion is reached from the standard trajectory analysis that to achieve 1/500 and 1/1000 dead reckoning rates, R&D must be directed towards reduction of odometer and earth tracker errors by an order of magnitude from the current nominal values to SOA and Proj. SOA values in the final implemented design.

The planar error contributions from ephemeris, pendulous vertical, timer, and vertical anomalies are negligible in comparison to the IR earth tracker and odometer errors. In fact, depending upon mission requirements, serious consideration should be given to the technique of determining vehicle bearing without earth ephemeris and timer data. The PE vs Earth Tracker Error plot (Figure 8-107) shows typical results.

The mission independent analysis shows that the primary error sources of vehicle vertical error are the pendulous vertical sensor, vertical anomalies, and odometric contributions. Since vertical error is such a path dependent quantity, no convenient assessment criteria exist to interpret concept errors in terms of equipment requirements. However, remembering that the standard trajectory simulated a traverse over fairly flat terrain (maximum slope: 17/100) the nominal accuracy type system error was 0.050 km at 100 km. Reducing the pendulous vertical error does not decrease the magnitude of altitude error. However, decreasing allowable odometer error to 0.001 decreases the altitude error to 0.020 km. If the pendulous vertical error is increased by an order of magnitude, vehicle altitude error is roughly 0.180 km. Hence, the attempt to maintain vertical sensor error in the 36 arc sec region is advisable with a simultaneous reduction in odometer error.

8.3.2 Mission Dependent Analysis

The objectives of the analysis are to define component accuracy requirements, as a function of mission era, to meet the most stringent postulated concept requirement of that time period. Only through the evaluation of navigation component performance on mission requirements can recommendations of research and development be made. Hence, the resultant data of this analysis emphasize component accuracy requirements which enable a functioning concept to satisfy the mission requirements of terminal range T_R, velocity V, and traverse range R. The systems formed to meet the requirements will be the Projected SOA, SOA and nominal accuracy type systems with variations of component errors from the base value comprising the accuracy type systems.

If the homing range or terminal requirement T_R is fixed for specific mission leg (range, velocity, selenographic location, terrain characterizations), the only method of alleviating or reducing component accuracy requirements is to increase the number of position fixes on the mission leg. Of course, the constraint is required that the position fix error be less than the terminal requirement in order that the homing mode of navigation be effected. Error reduction techniques such as position fixing are available, but the purpose of the dead reckoning subsystem is to conserve astronaut time and effort during the performance of the navigation functions. Therefore, the frequency of position fixing should be kept to an absolute minimum. Due to the nature of this generalized navigation study, it is necessary to first postulate the frequency of position fixing based on total mission range and duration as compared to the standard approach of defining the position fix frequency as a function of dead reckoning accuracy capabilities. Due to the adverse environment of the moon, there are two criteria to establish the basic postulations of position fixing frequency:

1. Every x km

2. Every y hours.

Certainly, basing the assumption of position fixing every x km unduly restricts the time dependent inertial concept. However, position fixing every y hours also restricts the effectively time independent nongyro concept. The additional variable, vehicle velocity, obscures the criteria, but a combination of range and time will ensure coverage of all cases. The guideline establishing position fix frequency is:

1. 1/50 km

or

2. 1/8 hr.

This criteria is used to establish the accuracy type systems which can satisfy the strictest mission requirements of each mission era. (The missions are tabulated in Section 2.) The mission legs imposing the tightest navigation requirements on both the dead reckoning and position fix concepts for a particular era are listed in Table 8-10. The computer terrain characterizations describing and correlated to the terrain type are shown in Table 8-11. The approximate % EDT which results from the application of this data is also tabulated. These descriptors together with the mission coordinates, vehicle velocity, and terminal requirements completely characterize the mission.

The objective of this analysis is to determine which of the accuracy type concepts or design point systems can meet the postulated mission requirements. Due to the severe terminal requirements, two assumptions are necessary to properly encompass or to constrain the analysis.

1. The allowable position fix errors must be minimal so that the terminal requirement can be met with the combination of system errors from both the position fix and dead reckoning subconcepts.

TABLE 8-10

MISSIONS AND DESCRIPTORS

Mission	Leg	Initial Coordinates			Destination Coordinates			≈ Range km	Terrain Type	V km/hr	T_R km
		x_o	y_o	h_o	x_D	y_D	h_D				
I 1972	C	2.0	-46.0	0	2.267	-46	0	8	SM	3	0.400
II 1976	E	6.2	-40.5	0	6.3	-40	0.05	18	RM	5	0.400
III 1978	A	12.5	-50.2	0	13.9	-47.8	0	83	SM	8	2.830
	B	13.9	-47.8	0	16.3	-47.3	0.05	62	RM	8	0.450
IV 1980	C	-14.3	-17.0	0	-15.0	-13.5	0	100	SM	10	0.450
	E	-25.0	- 6.0	0.1	-23.3	- 6.3	0.3	50	RH	5	0.450
V 1980	A	13.7	-60.0	0	15.0	-63.1	0	100	SM	8	2.290
	B	15.0	-78.3	0	15.6	-80.0	0.05	50	RM	5	1.430
	*C	16.2	-93.0	0.05	17.0	-94.6	0.20	50	GH	5	0.450
VI 1984	B	51.5	-16.6	0.1	53.2	-17.0	0.5	50	RH	5	0.450

*Backside of Moon

TABLE 8-11

TERRAIN CHARACTERIZATIONS

Terrain Type	D_j km	Δh_{max} km	$\Delta\beta_{max}$ deg	ΔA_{max} deg	Δr_{max} deg	Approximate % EDT
SM	1	0.173	3.0	45.0	10.0	5.0
RM	1	0.255	6.0	90.0	12.0	25.0
GH	1	0.340	15.0	120.0	15.0	40.0
RH	1	0.577	25.0	160.0	20.0	80.0

2. To eliminate excessive updating and extensive position fixing, the criteria pertaining to the period of the position fix operation discussed above must be applied so that a realistic design point system can be devised.

Application of these two statements requires the constraints:

1. For minimal terminal requirements, 0.400 km, the position fix and dead reckoning error will be approximately equally weighted. Hence

$$(PE)_{PF} \leq 0.300 \text{ km}$$

This value can be met with a SOA celestial tracking system with no vertical anomaly error, optimal geometry, nominal ephemeris error, and star tracker accuracy relaxed to greater than the SOA value:

i.e.,

$$\sigma_{\gamma} = 0$$

$$\sigma_R, \sigma_D = 0.005^{o}$$

$\sigma_t = 0.00003$ hr

$\sigma_\epsilon, \sigma_\alpha = 0.004^\circ$

$\sigma_{rs} = \sigma_r, \sigma_p = 0.001^\circ$

These equipment and physical uncertainty values are used for the position fix error inputs of Concepts 1 and 2. The RF concept also requires a position fix error of 0.300 km. This is achievable with about 1 week of earth-based ranging (Section 8.5.1.1).

2. The design point dead reckoning concept was selected from the accuracy type systems available in the error tables. The selection criteria was based on that accuracy concept which satisfies the terminal requirement and has minimum utilization of position fixing within the alloted position fix frequency rates.

The latitude-longitude and altitude plots of the mission legs of Table 8-10 are shown in Figure 8-129 through 8-148. The altitude plots, ordinate labeled H in km, abscissa labeled N, correspond to the altitude variation, relative to 1738 km, along the vehicle path. The symbol N designates the nth point of the path.

The vehicle position error PE and altitude error PE_Z, for the nongyro concept are plotted as functions of time (hr) in Figures 8-149 through 8-164b. The planar position errors and altitude errors are the output of each accuracy type system evaluated on the corresponding mission leg depicted in the mission path graphs, Figures 8-129 through 8-148. Figure 8-164a, as an example, shows dead reckoning subsystem updating by taking a position fix at the point selected by the J function (Section 7.3.5). Table 8-12 summarizes the nongyro accuracy type systems which satisfy the postulated mission terminal requirements. The error plots are the output errors of these accuracy type systems.

TABLE 8-12

NONGYRO DEAD RECKONING DESIGN POINT SYSTEMS

Mission	Leg	Accuracy Type System+	# PF	J (see Sec. 7.3.5)
I 1972	C	Nom	0	0.39
II 1976	E	Nom	0	0.67
III 1978	A	Nom	0	0.10
	B	Nom; $\sigma_c = 0.005$	1	1.77, 0.64
IV 1980	C	Nom; $\sigma_c = 0.005$	3	4.36, 1.31, 0.55
	E	Nom; $\sigma_c = 0.005$	1	2.46, 0.90
V 1980	A	Nom	1	0.23
	B	Nom	1	0.22
VI 1984	B	Nom; $\sigma_c = 0.005$	1	2.07, 0.81

The vertical anomaly error σ_γ was set to zero so that the full assessment of equipment errors can be realized.

In Table 8-12 it is noted that Mission V, 1980, Leg C is not included. This mission is located on the far side of the moon and dramatically points to the near side selenographic restriction imposed upon the dead reckoning concept which employs an earth tracker as a basic heading reference. The tabulation of the number of position fixes required for homing, # PF, indicates the position fixes taken, other than initial alignment. When, for example, one position fix is indicated, it implies a position fix is performed midway from initial coordinates to destination coordinates. Since homing is assured for $J \leq 1$, the relative proximity of the J value to unity is a measure of the tight tolerance on component errors. If J is near zero, component errors may be increased; if J > unity but near the value unity, component errors can be reduced and homing achieved without a mid traverse position fix. Thus, in the case of Mission IV, 1980, Leg C, where three position fixes are indicated, if σ_c had been reduced to the SOA value, the second J function would be less than unity and homing achieved with one position fix.

+Table 8-8, p. 8-31.

The approximate values of vehicle altitude error, the error with respect to the last position fix, are usually on the order of 0.050 km for the nominal accuracy type system.

For the nine mission legs, the employment of error reduction techniques, such as position fixing, allows the nominal nongyro dead reckoning accuracy type system, with odometer error reduced to 0.005, to satisfy the majority of the terminal requirements. Tightening the odometer error to the SOA value 0.001, would provide a significant safety factor, and would partly eliminate intermediate range position fixing.

Inclusion of vertical anomaly error would affect the dead reckoning results negligibly, but by increasing substantially the position fix error, homing could not be affected for the given terminal ranges and the accuracy of the dead reckoning subconcept would be superfluous. Thus, the importance of position fixing by vertical independent techniques is again emphasized.

8.4 INERTIAL CONCEPT

8.4.1 Mission Independent Analysis

8.4.1.1 Position Fix, Initial Azimuth Alignment

The position fix subsystem of the inertial concept is identical to the nongyro position fix subconcept with the exception that its vertical sensor is a vertical gyro. However, interpreting the error input of the vertical sensor as the null or resolution error of the vertical gyro rather than a pendulous vertical sensor, the curves in Figures 8-45 to 8-96 which resulted from the analysis of Section 8.3.1.1 apply to the inertial concept position fix, azimuth alignment subsystem. Hence, the position fix and azimuth alignment results and analysis of Section 8.3.1.1 hold for the inertial concept.

However, an additional important conclusion can be drawn. Current values of null and resolution error of a vertical gyro are presented in Table 8-13.

TABLE 8-13

VERTICAL GYRO NULL ERRORS

Curve	Case	σ_r, σ_p
A, B	SOA	0.01
C	Nom	0.1
D	Max	1.0

The requirement is imposed upon the inertial system, Concept 2, that an extremely high quality vertical gyro be used as a vertical reference during the position fix operation. Present SOA figures indicate inertial quality gyros would supply a minimal position error of about 0.4 km (Case A', optimal geometry, σ_r, $\sigma_p = 0.01^\circ$ and no drift error). But if the vertical gyro is no more accurate than 0.1°, the minimal position error is about 4.3 km. Hence, the optimal geometry curves (Figures 8-45 to 8-53) indicate a recommendation for a static vertical sensor to replace the vertical gyro during the position fix operation.

8.4.1.2 Dead Reckoning

The analysis of the inertial concept, dead reckoning subsystem was performed as defined in Section 8.3.1.2. The subconcept was operated in a relative navigation mode along the set of reference trajectories (Figure 8-97 to 8-102) defined by Table 8-7 and discussed in Section 8.3.1.2. However, since the position error of the inertial concept is a heavily weighted function of traverse time, a minimum vehicle velocity of 3 km/hr and maximum velocity of 18 km/hr were used to bracket the concept errors. But an intermediate velocity of 8 km/hr was used to perform the "errorless" analysis. Therefore, Table 8-7, the standard trajectory data table, remains unchanged except for the parametric velocities:

V = 3, 8, 18 km/hr

The application and utilization of Table 8-14, the Inertial Concept Dead Reckoning Error Table, follow the usage of the error table discussed in Section 8.3.1.2. The inertial concept dead reckoning standard error curves are shown in Figures 8-165 to 8-215.

8.4.1.3 Results and Conclusions

The inertial concept standard dead reckoning requirements are shown in Tables 8-15 and 8-16. The treatment of determination of component requirements is similar to that discussed in Section 8.3.1.2 for the nongyro dead reckoning concept. Because of the heavily weighted time dependency of the inertial concept errors, the planar error requirements are generated from the standard trajectory analysis for a minimum velocity of 3 km/hr and maximum velocity of 18 km/hr. The ranges of traverse for the former are 10, 20, and 30 km which imply approximately 3, 6, and 10 hour durations; the latter case is considered for ranges of 10, 50, and 100 km, or approximately 0.5, 3, and 6 hours. Hence, the full spectrum of range and duration are considered for each accuracy type system.

The critical components of the inertial dead reckoning subconcept are the accelerometers and directional gyro. The main error sources are the accelerometer null or resolution errors and the directional gyro drift and resolution errors. These component requirements are summarized in the following standard requirement tables. Since the component requirements for the inertial concept are heavily weighted functions of both range and velocity (time) for each specific parametric and accuracy type system,

TABLE 8-14

INERTIAL CONCEPT, DEAD RECKONING ERROR TABLE

	Accuracy Type System	σ_{Ax} σ_{Ay} σ_{A_z}	K_{A3}	σ_{GA}	σ_{gD}	σ_r, σ_p	K_r, K_p	σ_{pD}, σ_{rD}	$\sigma\gamma$
0	Errorless	0.0	0.0	0.0	0.0	0.0	0.0	0.0	0.0
1	Proj. SOA	0.00127	10^{-7}	0.0001	0.001	0.001	10^{-5}	0.001	0.0
2	SOA	0.0127	10^{-6}	0.001	0.005	0.01	0.003	0.01	0.0
3	Nom	0.127	10^{-5}	0.1	0.08	0.1	0.001	0.05	0.0
4	Max	0.127	0.0001	1.0	1.0	1.0	0.005	0.5	0.0

$$\sigma_{Ax}, \sigma_{Ay}, \sigma_{Az} = 0.127 \frac{\text{Km}}{\text{Hr}^2} = 10^{-6} \text{ earth g}$$

TABLE 8-15

INERTIAL DEAD RECKONING PLANAR STANDARD REQUIREMENT

Error		σ_{Ax}, σ_{Ay}, σ_{Az}			σ_{GA}			σ_{gD}		
Accuracy Type System		1	2	3	1	2	3	1	2	3
DR Reqt.	Range	Proj. SOA	SOA	Nom	Proj. SOA	SOA	Nom	Proj. SOA	SOA	Nom
1/20	10, 50	+	+	+	+	+	+	+	+	+
	100	+	+	+	+	+	+	+	+	.50
1/50	10	+	+	+	+	+	+	+	+	+
	50	+	+	+	+	+	.34	.78	.76	.27
	100	.080*	.080*	.064*	+	+	0	.36	.34	0
1/100	10	+	+	+	.56	.50	.44	+	+	+
	50	.67*	.67*	.052*	.56	.50	0	.38	.36	0
	100	.042*	.042*	.025*	.56	.50	0	.19	.16	0
1/200	10	+	+	+	.24	.23	.14	.94	.92	.30
	50	.038*	.038*	.020*	.29	.25	0	.20	.17	0
	100	.025*	.025*	.003**	.28	.27	0	.092	.04*	0
1/500	10	.066*	.066*	0	.12	.11	0	.38	.34	0
	50	.014*	.014*	0	.12	.12	0	.076	.023*	0
	100	.013*	.013*	0	.12	.10	0	.02*	0	0
1/1000	10	.034*	.034*	0	.066*	.045*	0	.20	.15	0
	50	.008**	.008**	0	.03*	0	0	.025*	0	0
	100	.004**	.004**	0	.005*	0	0	.006*	0	0

V = 18 km/hr

For σ_{Ax}, σ_{Ay}, σ_{Az}; 0.127 km/hr^2 = 10^{-6} earth g

* : Requirement exceeds nominal error value

**: Requirement exceeds SOA error value

+ : The dead reckoning requirement is satisfied with the given accuracy type system, and for all component error values from projected SOA to maximum.

0 : The dead reckoning requirement is not satisfied for any value of the respective component error since the accuracy type system does not satisfy the requirement.

TABLE 8-16

INERTIAL DEAD RECKONING STANDARD REQUIREMENT

Error		$\sigma_{Ax}, \sigma_{Ay}, \sigma_{Az}$			σ_{GA}			σ_{gD}		
Accuracy Type System		1	2	3	1	2	3	1	2	3
DR Reqt.	Range km	Proj. SOA	SOA	Nom	Proj. SOA	SOA	Nom	Proj. SOA	SOA	Nom
1/20	10	.042*	.042*	.040*	+	+	0	+	+	+
	20	.024*	.024*	.022*	+	+	0	.65	.54	0
	30	.015*	.015*	.015*	+	+	0	.44	.23	0
1/50	10	.018*	.018*	.016*	+	.7	0	+	+	0
	20	.011**	.011**	.010**	+	0	0	.23	0	0
	30	.006**	.006**	.005**	+	0	0	.17	0	0
1/100	10	.011**	.011**	.008**	.54	0	0	.27	0	0
	20	.007**	.007**	.004**	.54	0	0	.20	0	0
	30	.0045**	.0045**	.002**	.54	0	0	.10	0	0
1/200	10	.007**	.007**	.0035**	.26	0	0	.15	0	0
	20	.004**	0	0	.10	0	0	.08	0	0
	30	.001**	0	0	0	0	0	.03*	0	0
1/500	10	.004**	0	0	0	0	0	.02*	0	0
	20	0	0	0	0	0	0	0	0	0
	30	0	0	0	0	0	0	0	0	0
1/1000	10	.003**	0	0	0	0	0	0	0	0
	20	0	0	0	0	0	0	0	0	0
	30	0	0	0	0	0	0	0	0	0

V = 3 km/hr

For $\sigma_{Ax}, \sigma_{Ay}, \sigma_{Az}$; 0.127 km/hr^2 = 10^{-6} earth g

* : Requirement exceeds nominal error value

**: Requirement exceeds SOA error value

+ : The dead reckoning requirement is satisfied with the given accuracy type system, and for all component error values from projected SOA to maximum.

0 : The dead reckoning requirement is not satisfied for any value of the respective component error since the accuracy type system does not satisfy the requirement.

a different relaxation or tightening of component requirements occurs. Hence the severity of the error requirement is indicated by the asterisk * above the requirement. The asterisk definitions are given below the tables. It is to be emphasized that the SOA values are optimistic, bench-type component values and nominal values more closely correspond to actual implemented values.

With this statement as background, the critical component or main error contributor is definitely observed to be the accelerometers. The maximum dead reckoning route which can be met with a nominal system and nominal accelerometer errors (10^{-6} earth g) is 1/50 at 50 km with an 18 km/hr vehicle velocity. For ranges of 10 km, at 18 km/hr, the maximum achievable rate with a nominal accuracy accelerometer is 1/200. With a SOA accuracy type system, the maximum requirement that can be met is 1/1000 at 100 km with the accelerometer requirement tightened to about 10^{-8} earth g. The nominal accuracy type system is unable to meet either the 1/500 or the 1/1000 requirement regardless of accelerometer error since the remaining component errors, the nominal values, exceed the dead reckoning requirement.

Table 8-15 indicates the maximum allowable accelerometer requirement bounds for the ranges of 10, 50, and 100 km since the vehicle velocity is maximum. To relax the stringent requirements, error reduction techniques such as position fixing will reduce the requirements; however, if dead reckoning rates of greater accuracy than 1/500 are desired, even position fixing every 10 km will require accelerometers on the order of 10^{-7} earth g (0.127 km/hr^2). Although this is quoted as an SOA value by many vendors, implementation of the device in a functioning system casts doubts upon the final component error.

Table 8-16, which lists the inertial concept standard requirement for vehicle velocity of 3 km/hr, indicates a tighter requirement imposed upon accelerometer accuracy. In all instances of ranges, 10, 20, and 30 km, of accuracy-type systems, projected SOA, SOA, and nominal, a 10^{-7} earth g type accelerometer is required to satisfy the dead reckoning requirements. For dead reckoning rates equivalent to or greater than 1/100, an accelerometer of the type 10^{-8} earth g is required, and for the more exacting missions (1/500, 1/1000) system errors for particular accuracy-type systems exceed the dead reckoning requirement irrespective of accelerometer accuracy.

For direction gyro null error or alignment error, the most difficult requirement to meet at 18 km/hr is the 1/500 value. A tenth of a degree gyro will achieve this requirement with remaining concept errors at the SOA values. The nominal requirement cannot be met since the accelerometer error is too large. To achieve the 1/1000 requirement, the projected SOA accuracy type system must hold and σ_{GA} must be tightened to greater than the nominal accuracy value of 0.1°.

The dead reckoning requirement of 1/200, with V = 18 km/hr, is the maximum requirement which can be met at a distance of 100 km with the SOA accuracy type system. The DG drift must be less than the nominal value but greater than the SOA value at σ_{GD} = 0.04 deg/hr. Only for the 10 km range can the nominal accuracy-type system satisfy the 1/200 requirement. In this instance, the gyro drift rate can be relaxed to 0.30 deg/hr. Only with the projected SOA system, and a gyro drift rate less than the nominal value, can an accuracy of 1/1000 be met for a 100 km traverse.

With vehicle velocities on the order of 3 km/hr, the primary error source is the accelerometer null error which completely negates the directional gyro alignment errors and gyro drift rates. This is evidenced by the large number of accuracy-type systems which cannot satisfy the standard dead reckoning requirement.

The conclusion is reached that to achieve concept dead reckoning accuracies on the order of 1/500 and 1/1000 for a full spectrum of vehicle velocities, accelerometers of the class 10^{-7}, 10^{-8}, and 10^{-9} earth g must be operational and functional in an implemented system; 10^{-5} earth g and 10^{-6} earth g accelerometers perform sufficiently well for vehicle ranges (10 km @ 8 km/hr) to satisfy 1/20 and 1/50 requirements, respectively. In this manner, continual position fixing and updating allow greater accuracy for extended range missions. In addition, should 10^{-8} earth g accelerometers be available, to achieve 1/1000 accuracy on extended missions (100 km @ 18 km/hr) DG null accuracies of 0.01° and drift rates of 0.005 deg/hr will be required.

The primary error sources of vehicle altitude error are vertical gyro drift and null errors, and the accelerometer null error. High velocity, short range traverses negate the accelerometer and VG drift terms. However, for extensive operating times, these terms dominate.

8.4.2 Mission Dependent Analysis

The postulated missions, simulated for the mission dependent analysis of the inertial concept, are the missions described in Section 8.3.2 and shown in Figures 8-129 to 8-148. These mission legs form the most restrictive set of accuracy requirements upon the concept for the particular era of interest and exploration. The analysis framework, discussed in Section 8.3.2, is applied to obtain the inertial concept accuracy-type system or design point system, which satisfies the mission leg requirements. The position fix and dead reckoning error allocations are equal for the minimum terminal requirements mission, and the accuracy-type celestial tracking position fix subconcept selected is that described in Section 8.3.2.

The vehicle position error and altitude error plot for the respective systems in Table 8-17 are shown in Figures 8-216 to 8-235. Table 8-17 summarizes the results.

TABLE 8-17

INERTIAL DEAD RECKONING DESIGN POINT SYSTEM

Mission	Leg	Accuracy Type System+	#PF	J (see Sec. 7.3.5)
I 1972	C	Nom; $\sigma_{Ax} \ldots = 10^{-7}$*	0	0.40
II 1976	E	Nom; $\sigma_{Ax} \ldots = 10^{-7}$*	0	0.93
III 1978	A	Nom; $\sigma_{Ax} \ldots = 10^{-7}$*	0	0.29
	B	Nom; $\sigma_{Ax} \ldots = 10^{-7}$*	3	22.62, 1.91, 0.41
IV 1980	C	Proj. SOA	0	0.44
	E	Proj. SOA	1	1.67; 0.44
V 1980	A	SOA	0	0.61
	B	SOA	1	1.48, 0.13
	C	Proj. SOA	0	0.55
VI 1984	B	Proj. SOA	1	1.16, 0.42

+ Table 8-14, p. 8-44.

* Earth g's.

The inertial concept dead reckoning error grows rapidly with extended operating and mission times due to the doubly integrated accelerometer outputs. This enormous growth is reflected in the large initial J value of Mission III, 1978, leg B. The second J value is slightly less than two and indicates that, if an SOA accuracy-type directional gyro had been used as the vehicle heading reference, homing could have been achieved with only one intermediate position fix and realignment. However, the main error can be attributed to the accelerometers, and in order to satisfy future missions with strict terminal accuracy requirements, at least 10^{-7} earth g accelerometers are required. For the 1980-type missions, the nominal accuracy-type system no longer suffices, and the SOA and projected SOA accuracy-type design point systems are required. The error table, Table 8-14, defines these accuracy-type systems in terms of component errors.

The inertial concept is not restricted to near-side operation and can be evaluated for far-side performance. Mission V, 1980, Leg C, (the far-side mission) was satisfied with a Proj. SOA accuracy-type system. However, the J function was 0.55 with no intermediate position fixes. An SOA accuracy-type system with one intermediate position fix would solve the requirement.

Relative magnitudes of vehicle altitude errors, referenced to the last position fix, range from 0.040 km to about 0.400 km.

8.5 RF CONCEPT

8.5.1 Mission Independent Analysis

8.5.1.1 Position Fix

The RF concept utilizes a position fix subconcept consisting of a vehicle-mounted active RF beacon which is tracked by earth-based equipment. Earth-based tracking in conjunction with earth-based computation allows the fixing of vehicle position. Current capabilities of the DSIF tracking network are shown in Table 8-18 (Ref. 154). Tabulated is the time in days to reduce the semi-major axis of the three-sigma ellipse to specified values. Interpretation of these figures in terms of errors in the lunar latitude, longitude, altitude selenographic system should be carefully made due to the uncertainty and errors in the celestial mechanics description of the lunar center. Various estimates of the moon's distance from the earth give an error range of ±1 km to ±1.2 km (Ref. 34). Assuming these values to be probable errors and converting to 3σ values gives an error range of 5 km to 5.34 km.

An interesting comparison of earth-based tracking versus self contained position fixing can be made if a position fix error of 3 km is specified. Roughly two days of tracking time are required to achieve this quoted accuracy, while the nominal celestial tracking accuracy-type system achieves 3 km error with vertical anomalies of 0.09° (5.4 arc min).

TABLE 8-18

DSIF TRACKING CAPABILITY VERSUS TRACKING TIME

3σ Semi major Axis	Ranging (days)		Doppler (days)	
	One Station A	Two Stations A and B	One Station A	Two Stations A and B
15	<1.0	<1.0	1.9	1.2
6	1.4	<1.0	3.6	2.6
3	2.1	1.0	6.2	4.6
1.5	2.6	2.4	10.4	8.2
0.75	3.4	2.9	18.4	15.4
0.30	7.0	5.2	>28.0	>28.0
Station A: Goldstone Station B: Woomera				

8.5.1.2 Dead Reckoning

The dead reckoning subsystem of the RF concept was evaluated on the standard trajectories of Section 8.3.1.2. The parametric velocities of 3, 8, and 18 km/hr are identical to the inertial concept velocities. The error table, Table 8-19, was applied in the manner of the former tables. PE curves and $(PE)_Z$ curves (Figures 8-236 to 8-278) were obtained from the data application.

TABLE 8-19

RF CONCEPT DEAD RECKONING ERROR TABLE

	Accuracy Type System	σ_δ	σ_b	T	σ_a, σ_e	σ_{RE}, σ_{DE}	σ_r, σ_p	K_r, K_p	σ_t	K_t	σ_γ
0	Errorless	0.0	0.0	0.0	0.0	0.0	0.0	0.0	0.0	0.0	0.0
1	Proj. SOA	0.1	10^{-5}	0.01	0.001	0.0001	0.0001	10^{-7}	3×10^{-6}	0.0	0.0
2	SOA	0.5	0.0001	0.0035	0.01	0.001	0.0006	10^{-6}	0.00003	0.0	0.0
3	Nom	1.0	0.001	0.0026	0.1	0.01	0.01	0.0001	0.0003	0.001	0.0
4	Max	5.0	0.01	0.0024	1.0	0.03	0.03	0.001	0.003	0.01	0.0

8.5.1.3 Results and Conclusions

The standard error requirement tables constructed for the RF dead reckoning concept are Tables 8-20 and 8-21. The distance measuring device of the RF dead reckoning concept is a cw or pulsed single beam doppler radar which completely dominates the requirement table. The primary error contributors to concept velocity errors are antenna pointing error and errors in modulated frequency detection. Generally, the errors in the frequency detection limit the total concept accuracy to 1/50 or a 2% system. For example, a nominal accuracy-type system with a data smoothing interval of 0.0036 hr (13 sec) provides an accuracy of 1/50 for a range of 100 km at 18 km/hr. Because of low vehicle velocities, a low signal-to-noise ratio (or extensive smoothing time) persists and the frequency detection error limits the dead reckoning performance to a maximum attainable rate of 1/50. An important error contributor obscured by the doppler radar is the RF earth tracker pointing errors. However, at 18 km/hr to achieve the 1/50 requirement for ranges of 10, 50 and 100 km, the RF earth tracker pointing error requirements can be relaxed to 0.4°.

Accuracies equivalent to or greater than 1/100 cannot be met with any of the accuracy-type systems using projected SOA, SOA, or nominal, regardless of the relaxation or tightening of all component error requirements. The reason, as stated above, is low signal-to-noise ratios; the extensive duration of smoothing data required of the doppler data places the accuracy bounds at 1/50. Also, reduction of vehicle velocities to approximately 3 km/hr decreases the attainable accuracy to 1/20 for the reduced accuracy-type systems. This is evidenced by the preponderance of 0's in the 3 km/hr standard error requirement table, Table 8-17.

The primary vertical error contributors are the doppler radar and the pendulous vertical sensor.

Ephemeris, timer, and the effect of vertical anomalies are minimal and the linear curves of the nongyro concept can be applied.

8.5.2 Mission Dependent Analysis

The missions simulated for the mission dependent analysis are described in Section 8.3.2 and plotted in Figures 8-129 to 8-148. The guidelines for the RF concept analysis are the same as those described in Section 8.3.2 for the nongyro concept.

TABLE 8-20

RF DEAD RECKONING CONCEPT STANDARD REQUIREMENT TABLE

Dead Reckoning Requirement		1/20			1/50			1/100		
Range		10	50	100	10	50	100	10	50	100
Error	Accuracy Type System									
σ_b	Proj. SOA 1	+	+	+	+	+	+	0	0	0
	SOA 2	+	+	+	+	+	+	0	0	0
	Nom 3	+	+	+	0	0	0	0	0	0
T	Proj. SOA 1	+	+	+	.0026	.0026	.0026	0	0	0
	SOA 2	+	+	+	.0029	.0029	.0029	0	0	0
	Nom 3	+	+	+	.0036	.0036	.0036	0	0	0
σ_δ	Proj. SOA 1	4.9	4.9	4.9	1.6	1.6	1.6	0	0	0
	SOA 2	4.6	4.6	5.6	.9	.9	.9	0	0	0
	Nom 3	4.4	4.4	4.4	0	0	0	0	0	0
σ_e, σ_a	Proj. SOA 1	+	+	+	1.0	1.0	1.0	0	0	0
	SOA 2	+	+	+	.44	.44	.44	0	0	0
	Nom 3	+	+	+	0	0	0	0	0	0

V = 18 km/hr

+: The dead reckoning requirement is satisfied with the given accuracy type system, and for all values from projected SOA to maximum for the respective component error

0: The dead reckoning requirements is not satisfied for any value of the respective component error since the accuracy type system does not satisfy the requirement.

TABLE 8-21

RF DEAD RECKONING CONCEPT STANDARD REQUIREMENT TABLE

Dead Reckoning Requirement			1/20			1/50			1/100		
Range			10	50	100	10	50	100	10	50	100
Error	Accuracy Type System										
σ_δ	Proj.SOA	1	4.0	4.1	3.9	0	0	0	0	0	0
	SOA	2	1.8	2.2	1.8	0	0	0	0	0	0
	Nom	3	0	0	0	0	0	0	0	0	0
σ_b	Proj. SOA	1	+	+	+	0	0	0	0	0	0
	SOA	2	+	+	+	0	0	0	0	0	0
	Nom	3	0	0	0	0	0	0	0	0	0
T	Proj.SOA	1	.0026	.0026	.0026	0	0	0	0	0	0
	SOA	2	.0027	.0027	.0027	0	0	0	0	0	0
	Nom	3	.0028	.0028	.0028	0	0	0	0	0	0
σ_e, σ_a	Proj.SOA	1	+	+	+	0	0	0	0	0	
	SOA	2	+	+	+	0	0	0	0	0	
	Nom	3	0	0	0	0	0	0	0	0	

V = 3 km/hr

+: The dead reckoning requirement is satisfied with the given accuracy type system, and for all values from projected SOA to maximum for respective component error

0: The dead reckoning requirement is not satisfied for any value of the respective component error since the accuracy type system does not satisfy the requirement.

Position error PE and attitude error PE_Z plots as a function of time for the RF concept are shown in Figures 8-279 to 8-296. These plots are the result of selected accuracy-type systems (Table 8-22) evaluated on the mission paths.

As stated in Section 8.3.2, the position fix error is limited to less than 0.300 km. At present, this requires a quoted vehicle tracking time of about one week. However to fully assess the RF dead reckoning concept component errors, it is necessary to postulate this tracking accuracy as an initial condition upon the dead reckoning system. Table 8-22 summarizes the analytical results.

TABLE 8-22

RF CONCEPT DEAD RECKONING DESIGN POINT SYSTEMS

Mission		Leg	Accuracy Type System+	#PF	J (see Sec. 7.3.5)
I	1972	C	Nom	-	1.60
II	1976	E	SOA	-	3.74
III	1978	A	Nom	0	0.87
		B	Proj. SOA	3	9.35, 2.633, 1.01, .59
IV	1980	C	Proj. SOA	7	13.19, 3.58, 1.20, .64
		E	Proj. SOA	7	16.95, 4.76, 1.53, .75
V	1980	A	Nom	1	1.95, .52
		B	Nom	1	2.67, .75
VI	1984	B	Proj. SOA	7	15.83, 4.47, 1.48, .73

+Table 8-19, p. 8-52.

The RF earth tracker error values were modified for the mission dependent analysis. Pointing errors for the accuracy-type systems were set at 0.2°, 0.02°, and 0.002°.

The results shown in Table 8-22 emphasize the necessity of an increased homing range capability for the RF concept. Due to the large error contribution of frequency detection in the doppler radar, only three of the nine postulated missions are satisfied under the guidelines of Section 8.3.2. The requirements of Mission I, 1972, Leg E, can be solved if an SOA accuracy-type system is employed; and the second mission requirements can be met if the accuracy-type system is reduced to Proj. SOA. However, because of the extensive, tracking time required to position fix the vehicle, an absolute minimum of position fixing is required. Hence, the Mission IV, 1980, and Mission VI, 1984, traverse requirements cannot be achieved. Little consideration should be given to employment of the RF dead reckoning concept on a mission requiring better than 2% accuracy to eliminate extensive dead reckoning updating.

Because of the RF earth tracker which measures vehicle bearing, the RF concept is restricted to near-side operations.

Vehicle altitude errors are approximately 0.050 km to 0.130 km, with the above accuracy-type concepts.

Figure 8-1 CELESTIAL TRACKER ERROR SENSITIVITY COEFFICIENTS
POSITION FIX

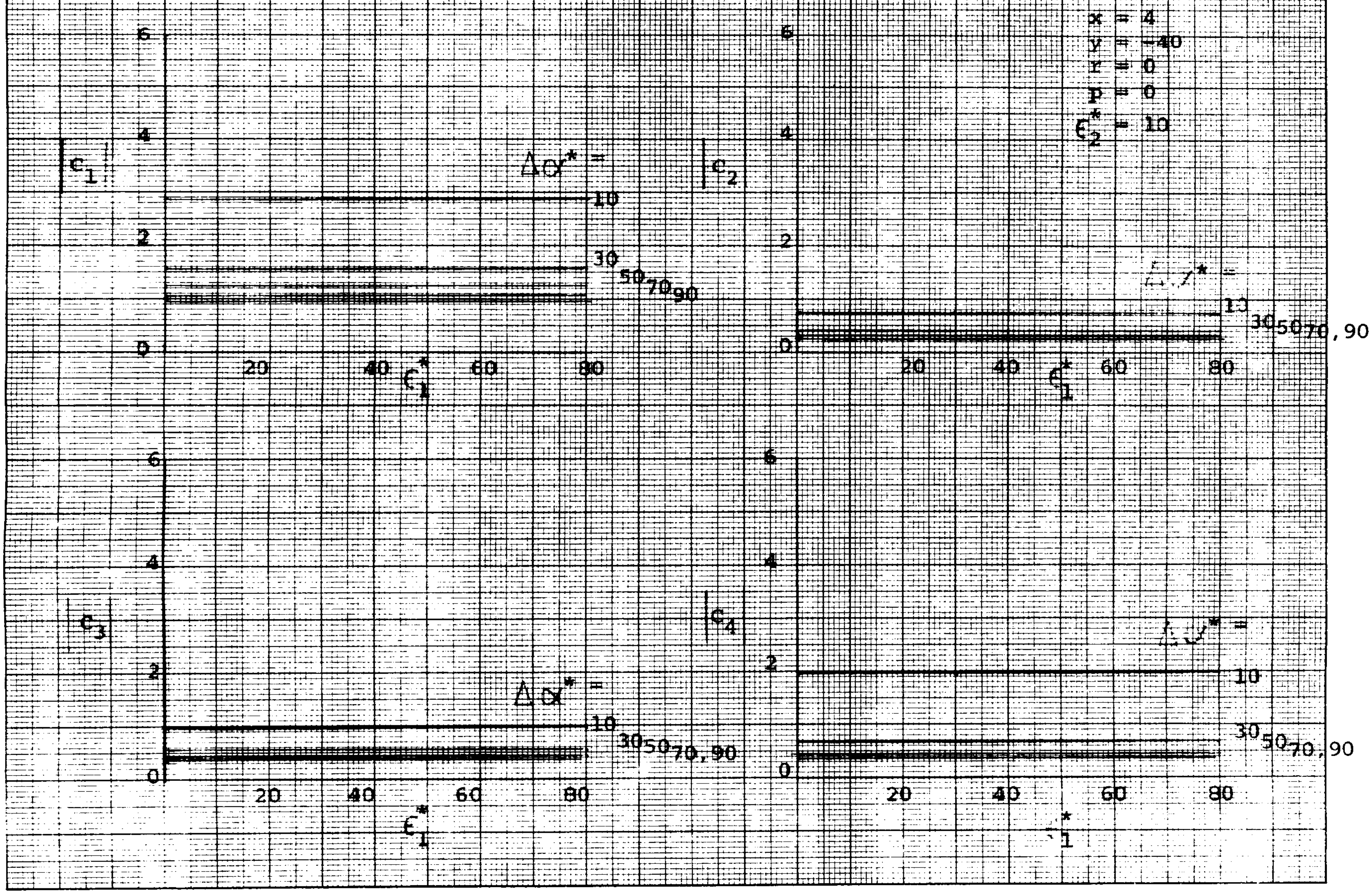

Figure 8.2 CELESTIAL TRACKER ERROR SENSITIVITY COEFFICIENTS
POSITION FIX

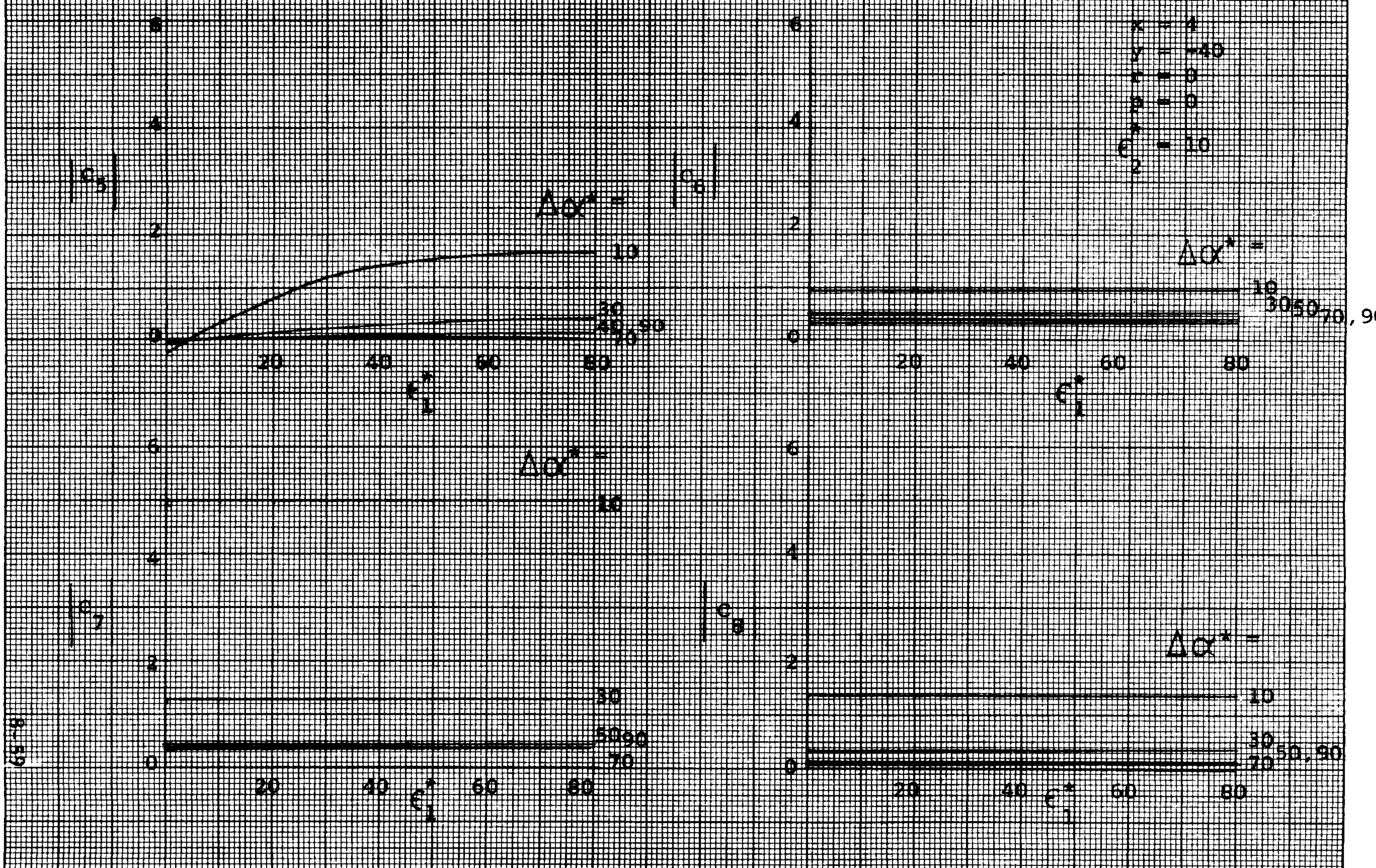

Figure 8-7 CELESTIAL TRACKER ERROR SENSITIVITY COEFFICIENTS
POSITION FIX

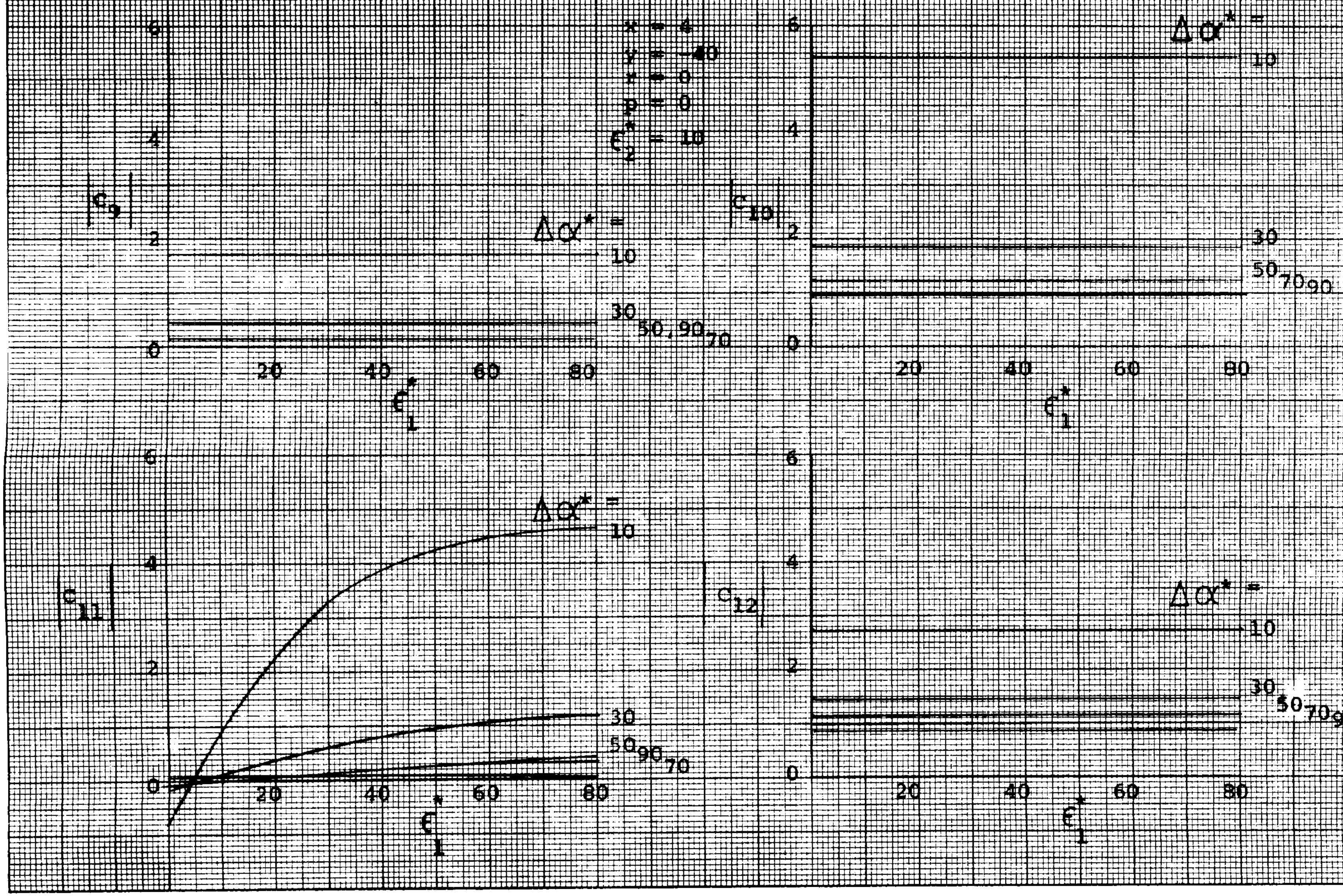

Figure 8-4 CELESTIAL TRACKER ERROR SENSITIVITY COEFFICIENTS POSITION FIX

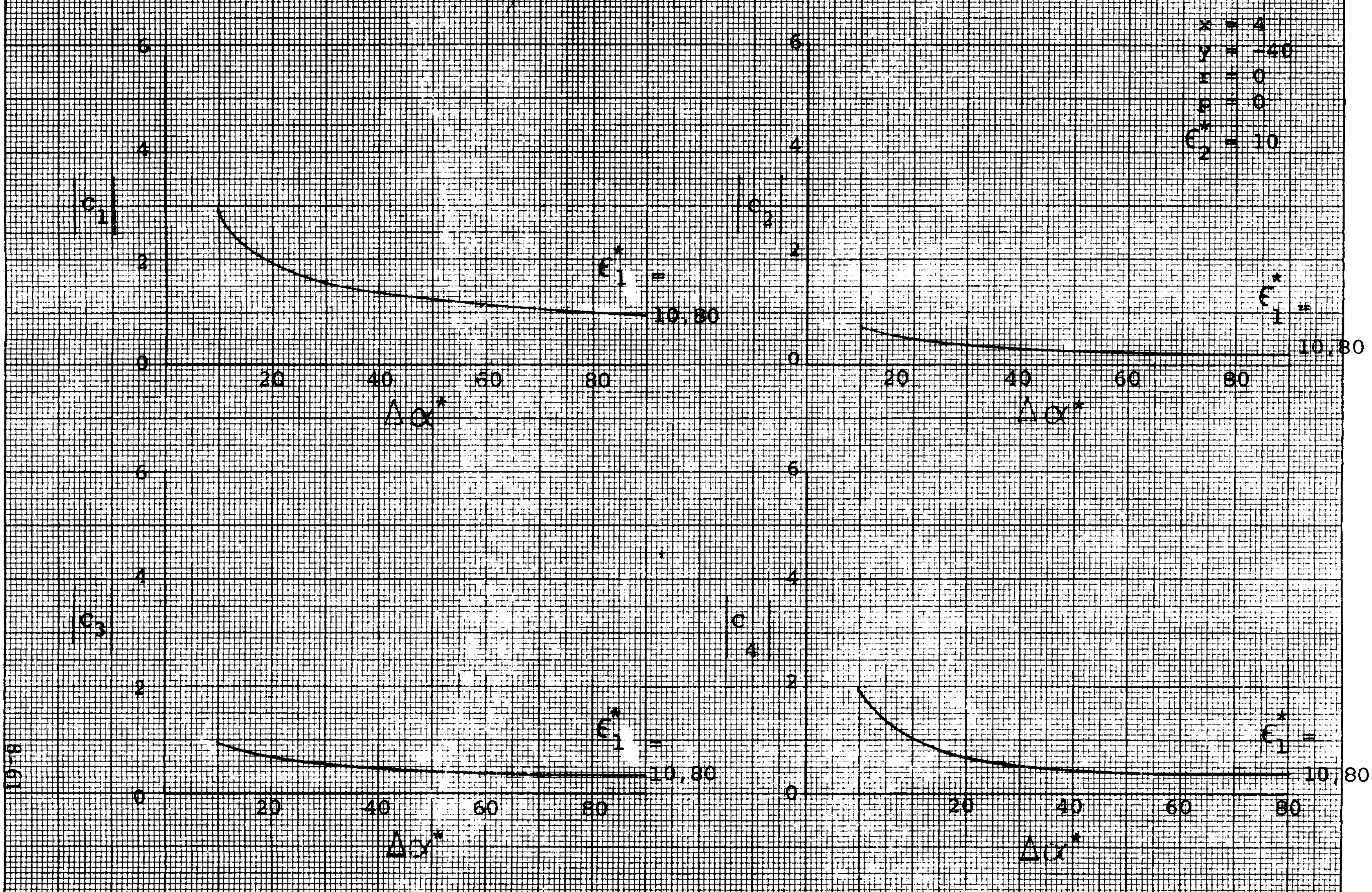

Figure B-5 CELESTIAL TRACKER ERROR SENSITIVITY COEFFICIENTS POSITION FIX

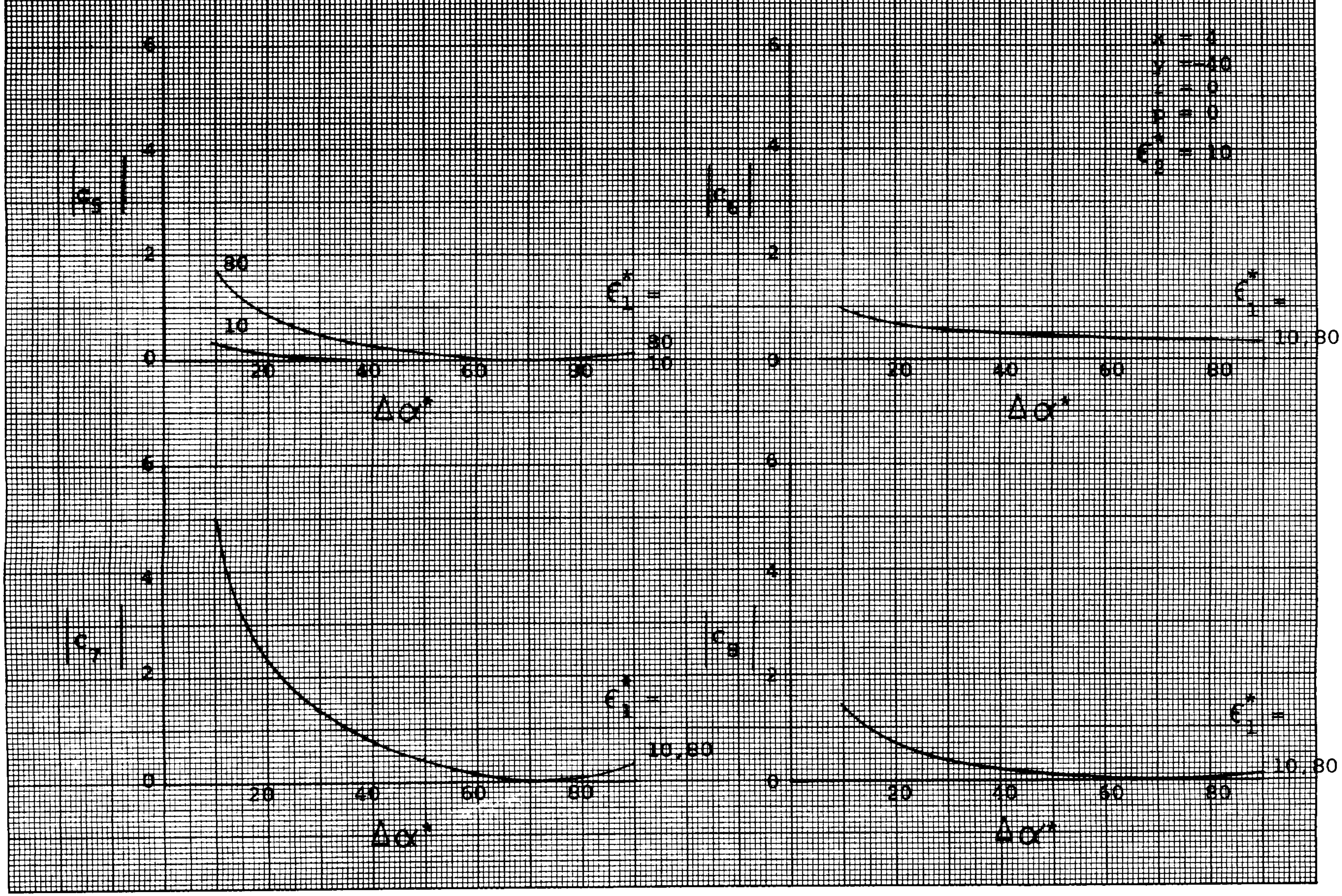

Figure 8-6 CELESTIAL TRACKER ERROR SENSITIVITY COEFFICIENTS POSITION FIX

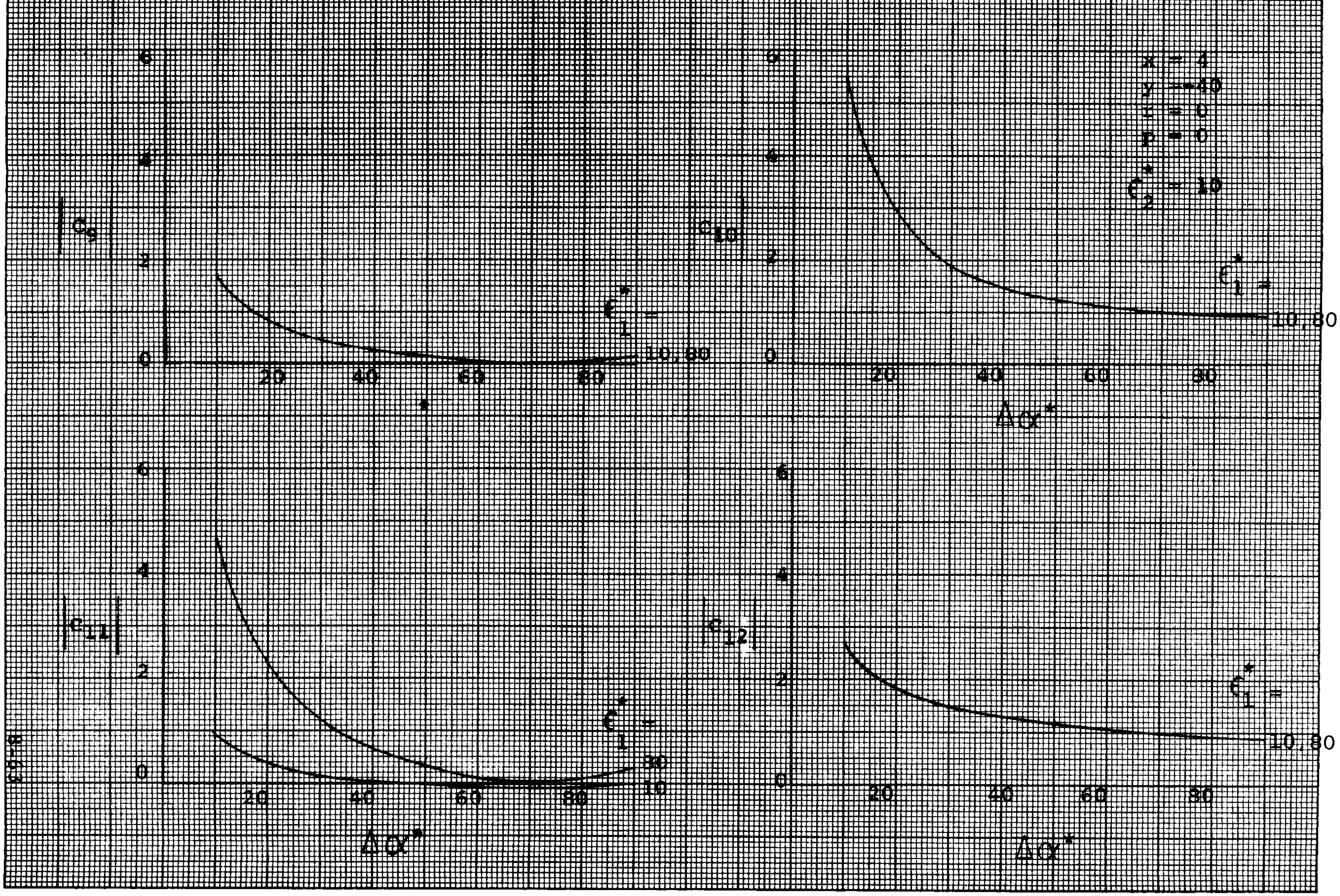

Figure 8-7 CELESTIAL TRACKER ERROR SENSITIVITY COEFFICIENTS
POSITION FIX

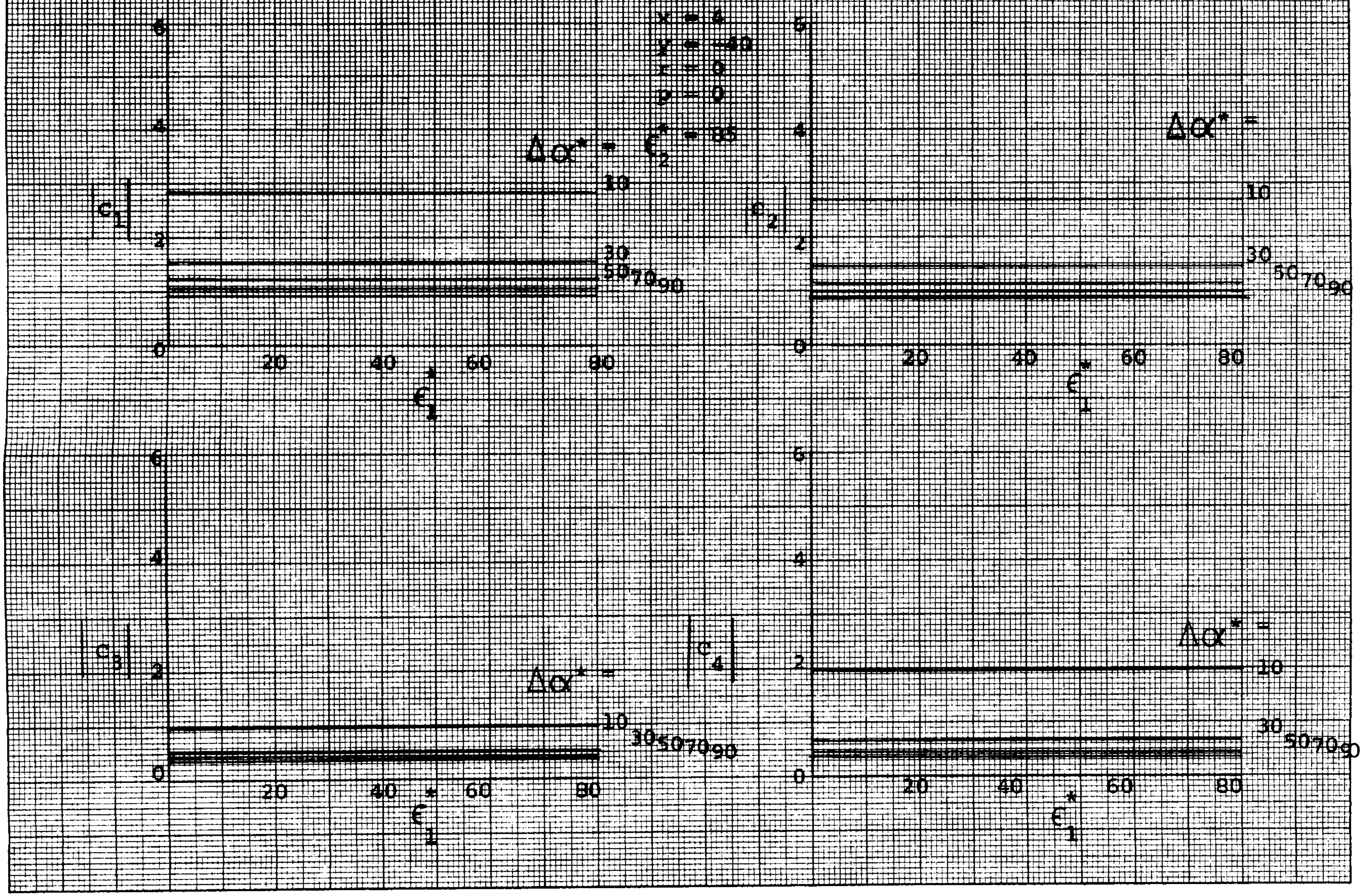

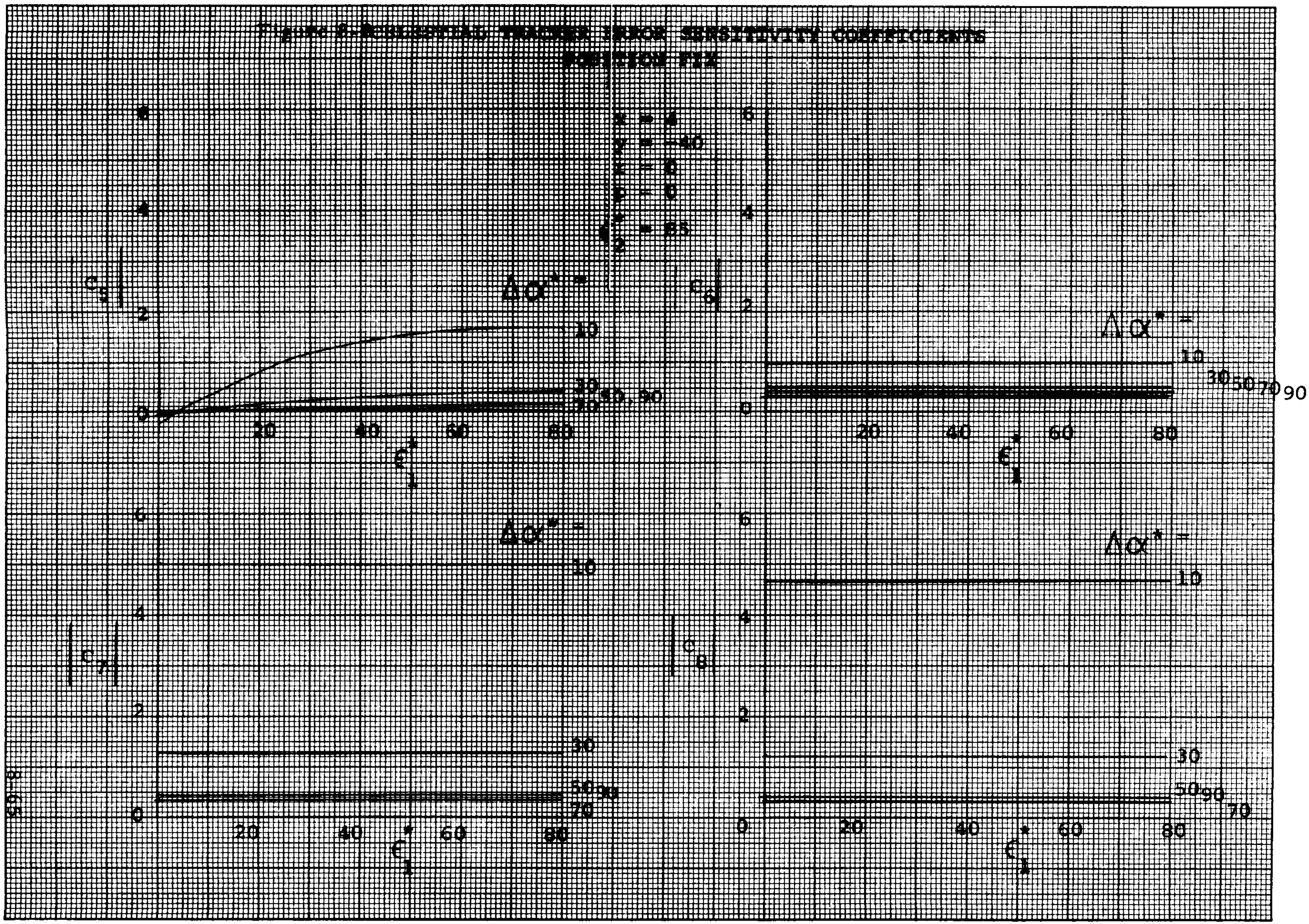

Figure 8-? CELESTIAL TRACKER ERROR SENSITIVITY COEFFICIENTS
POSITION FIX

Figure 8-9 CELESTIAL TRACKER ERROR SENSITIVITY COEFFICIENTS
POSITION FIX

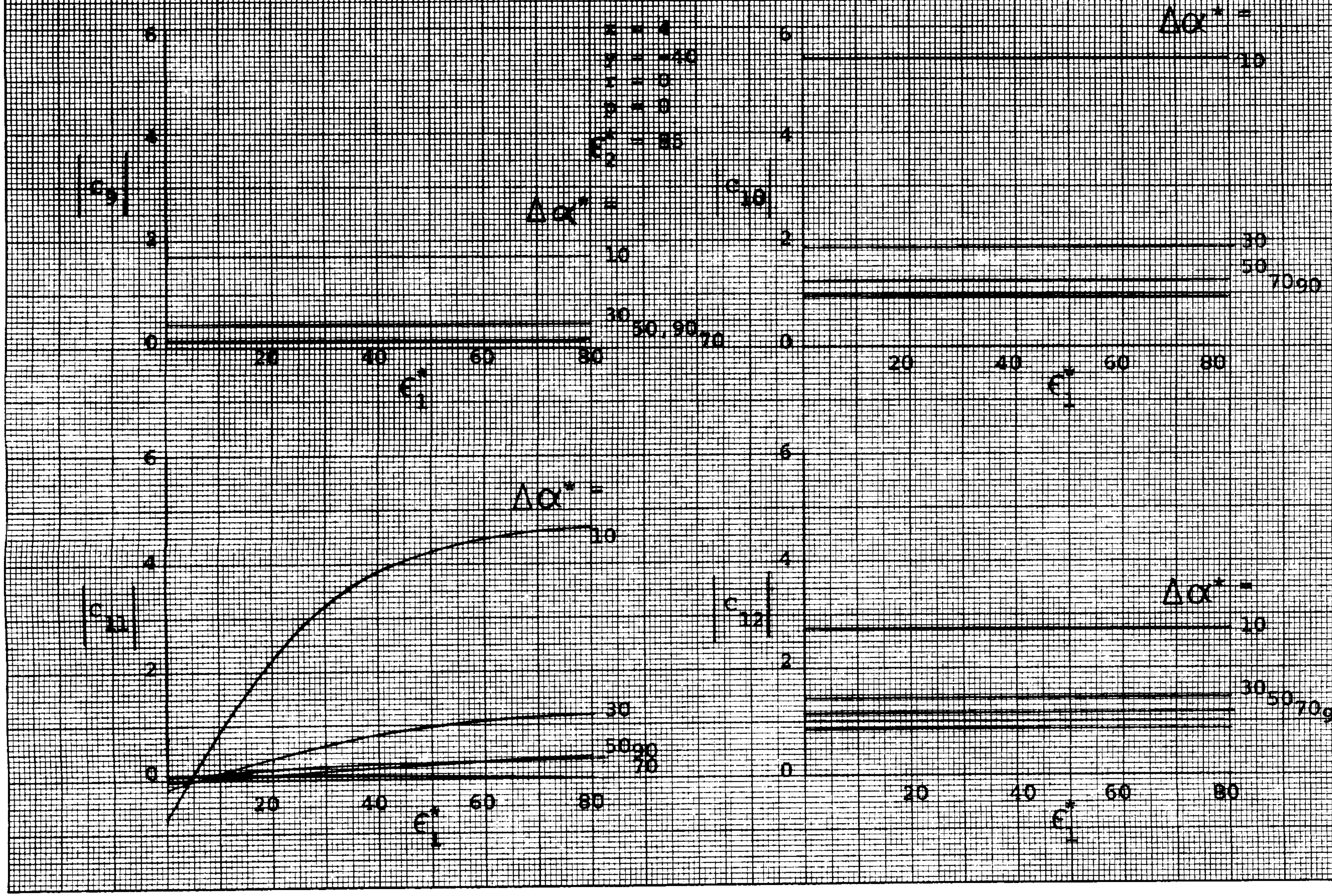

Figure 8-16 CELESTIAL TRACKER ERROR SENSITIVITY COEFFICIENTS
POSITION FIX

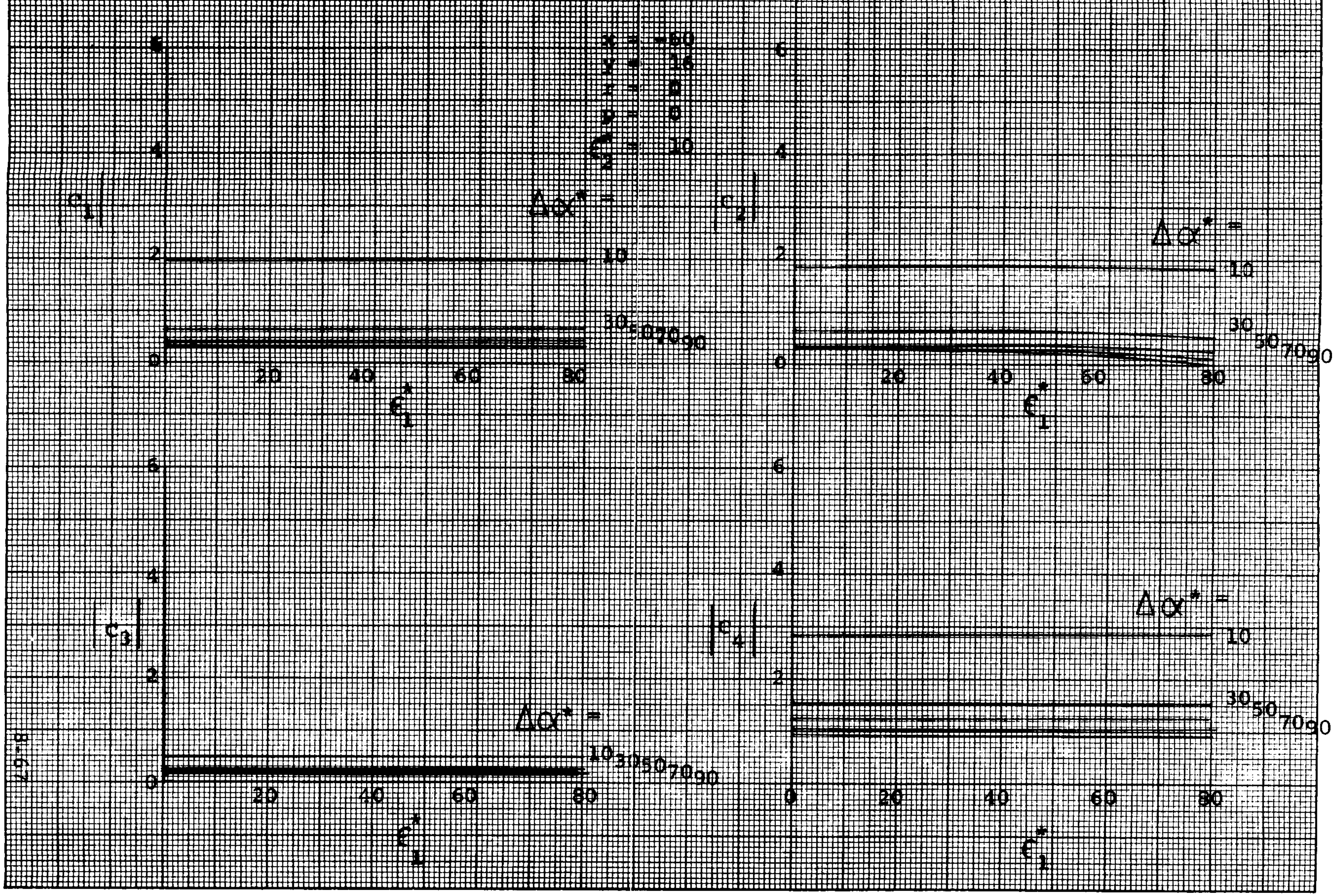

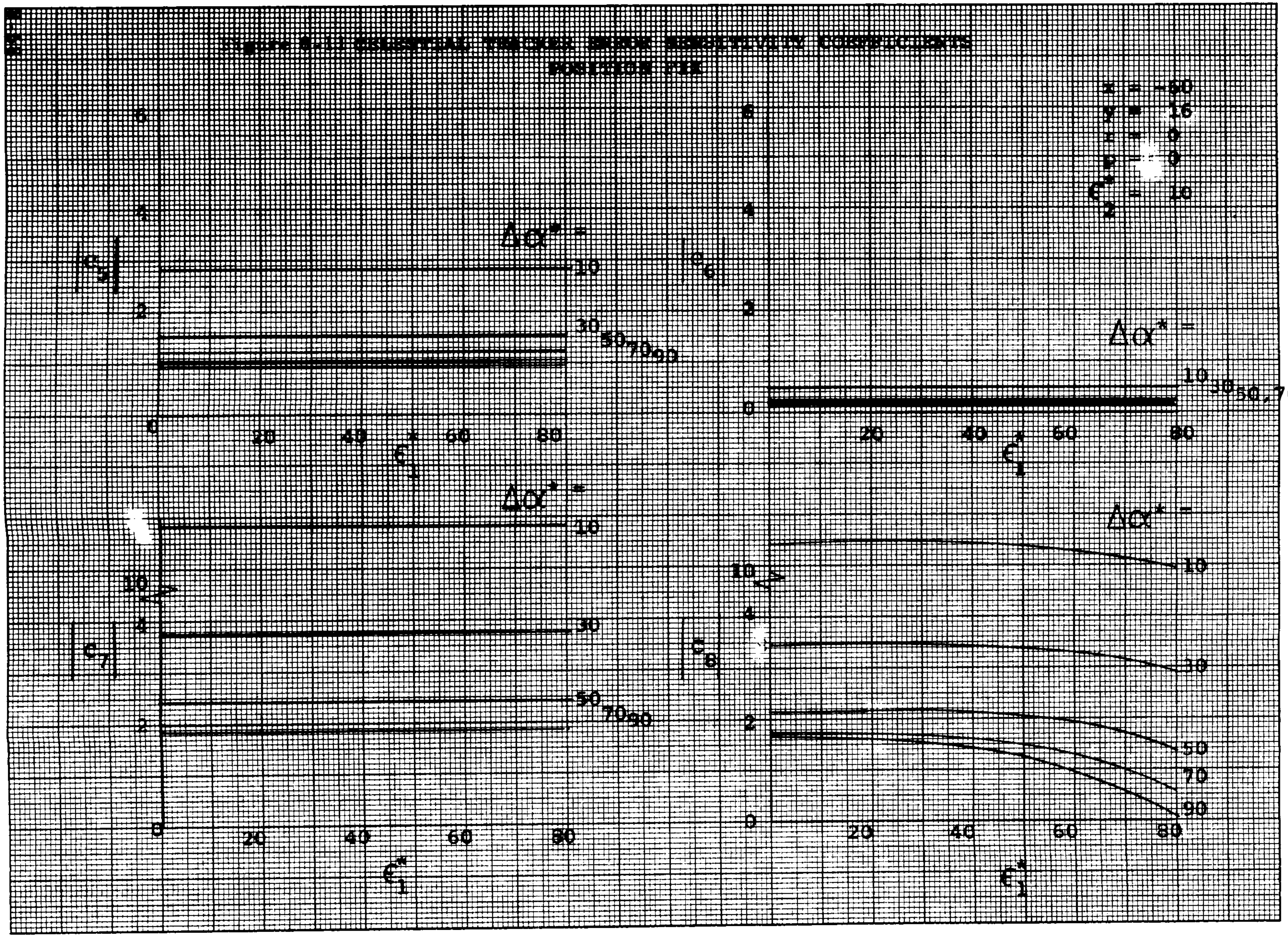
CELESTIAL TRACKER ERROR SENSITIVITY COEFFICIENTS
POSITION FIX
x = -60
y = 16
z = 0
p = 0
ϵ_2^* = 10
$|c_5|$
$|c_6|$
$|c_7|$
$|c_8|$
$\Delta\alpha^*$ =
10
30
50
70
90
ϵ_1^*
0
20
40
60
80
2
4
6

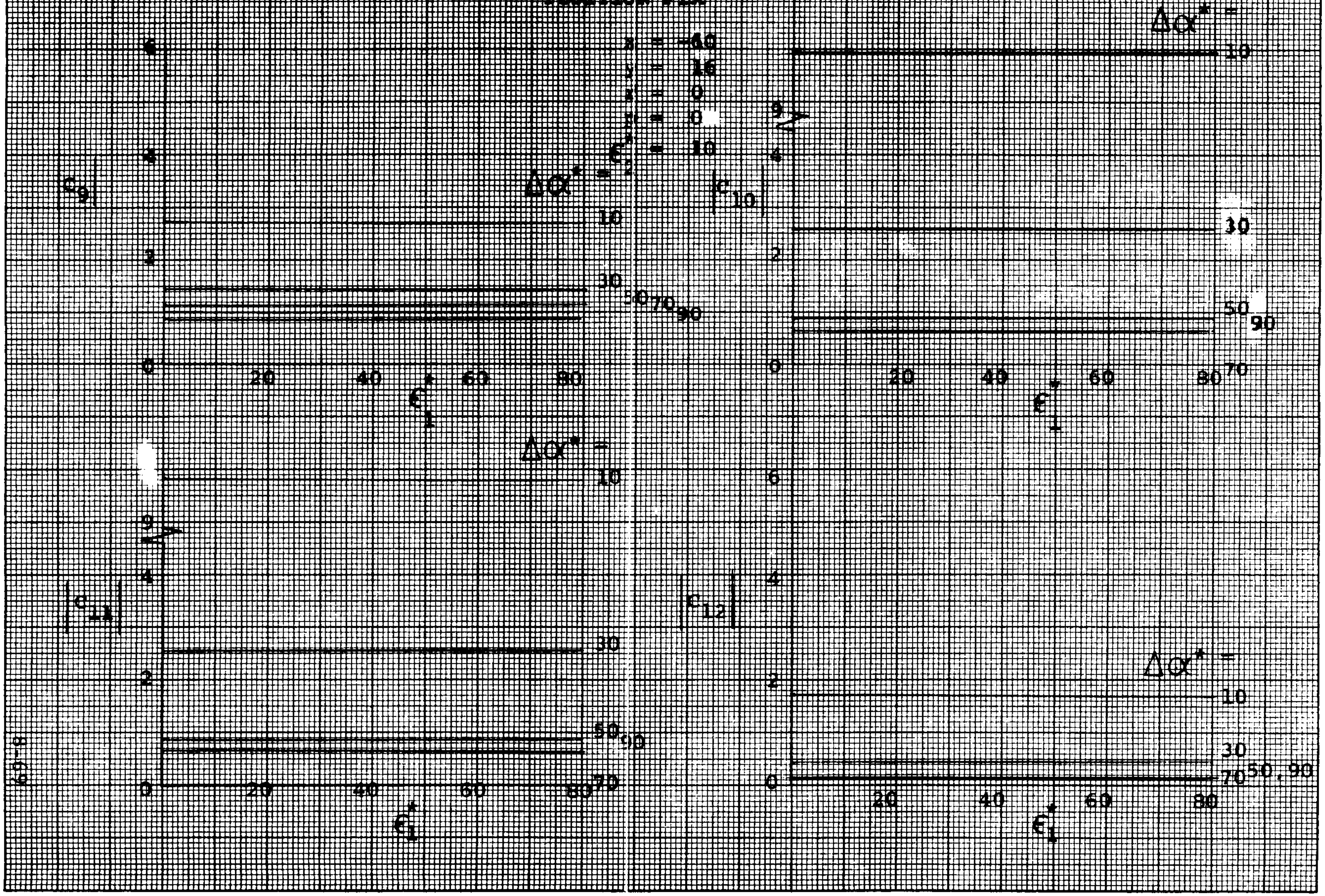

Figure 8-12 CELESTIAL TRACKER ERROR SENSITIVITY COEFFICIENTS POSITION FIX

Figure 8-13 CELESTIAL TRACKER ERROR SENSITIVITY COEFFICIENTS
POSITION FIX

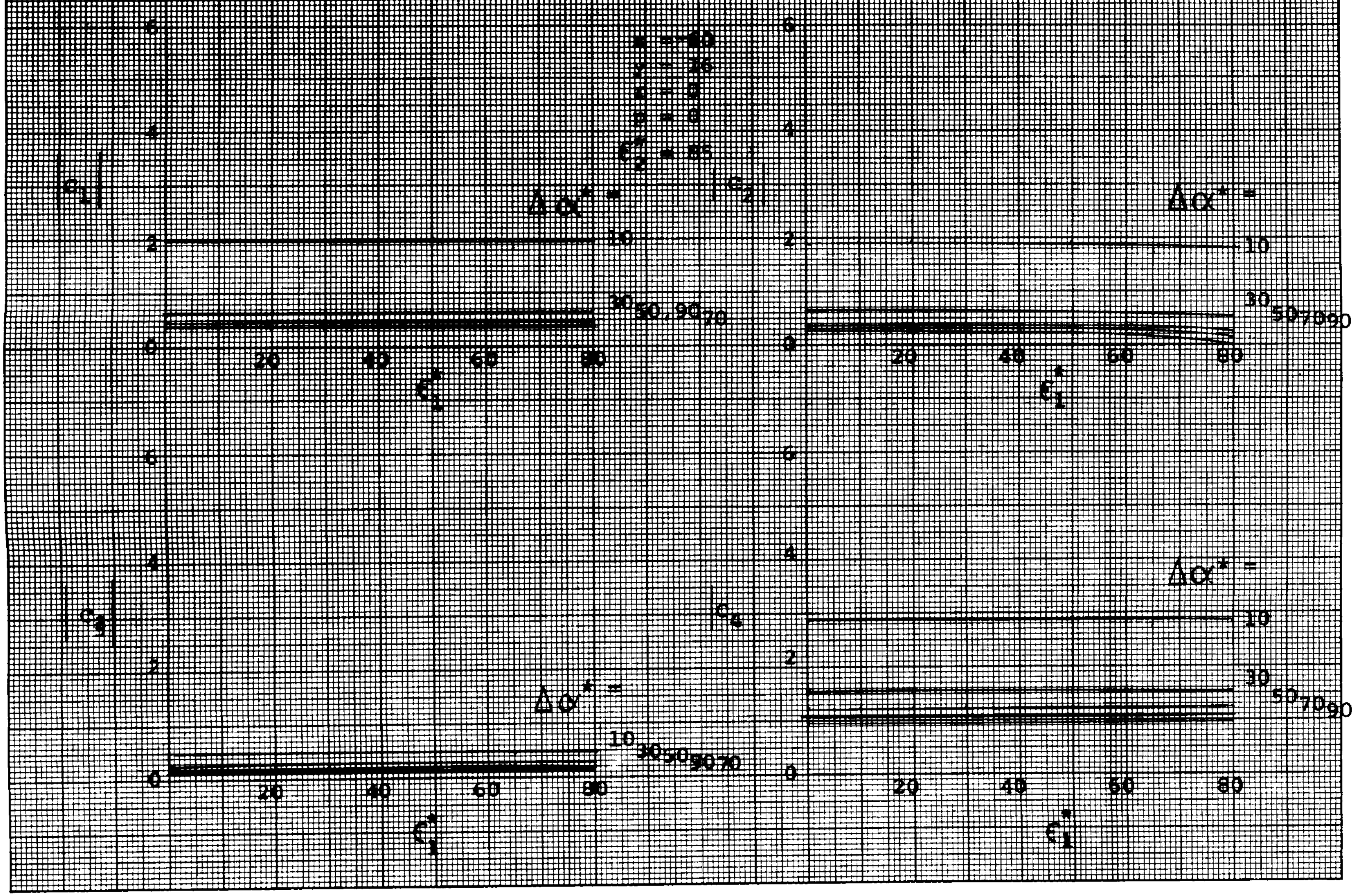

Figure 8-14 CELESTIAL TRACKER ERROR SENSITIVITY COEFFICIENTS POSITION FIX

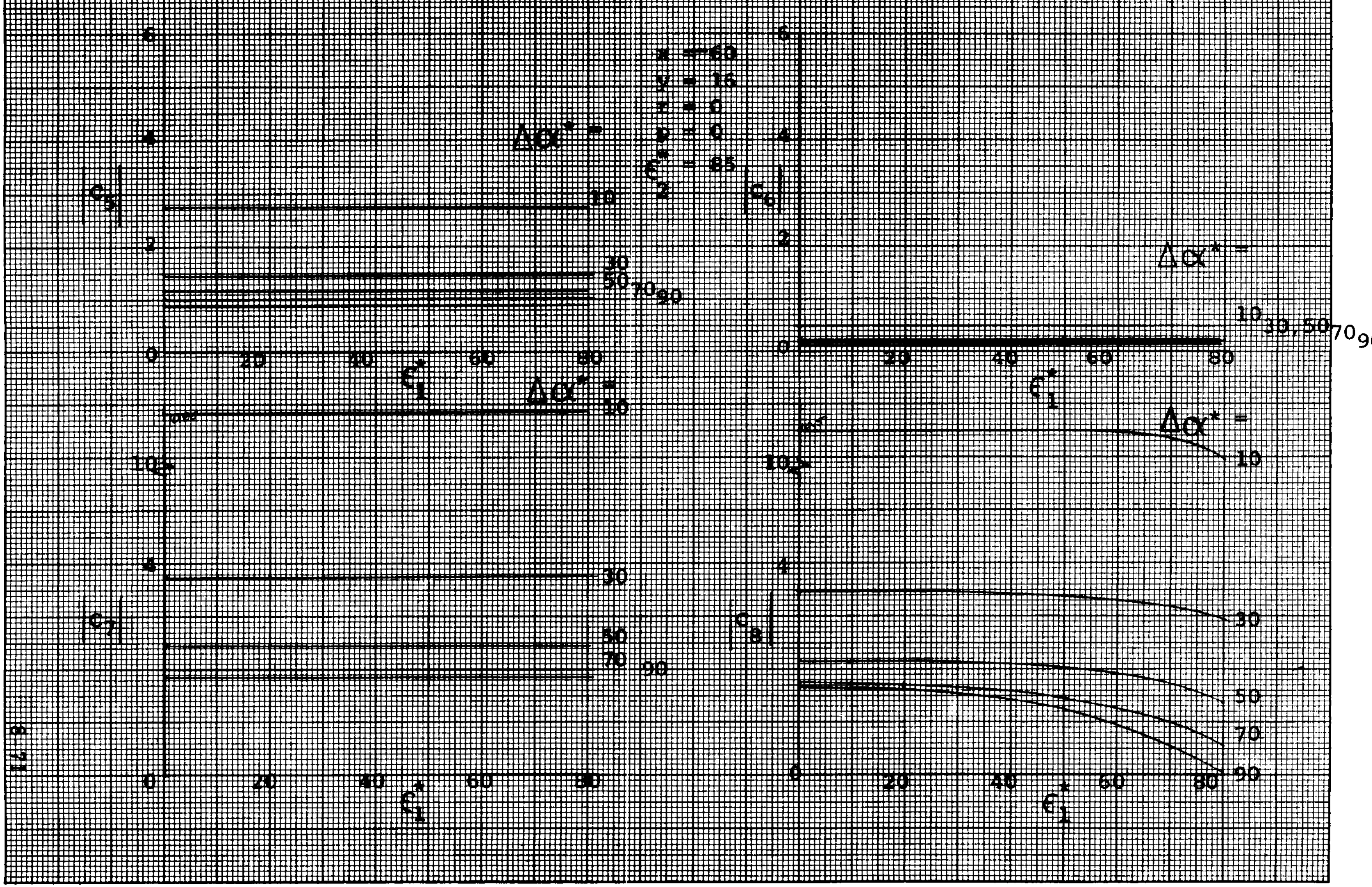

Figure 8-15 CELESTIAL TRACKER ERROR SENSITIVITY COEFFICIENTS
POSITION FIX

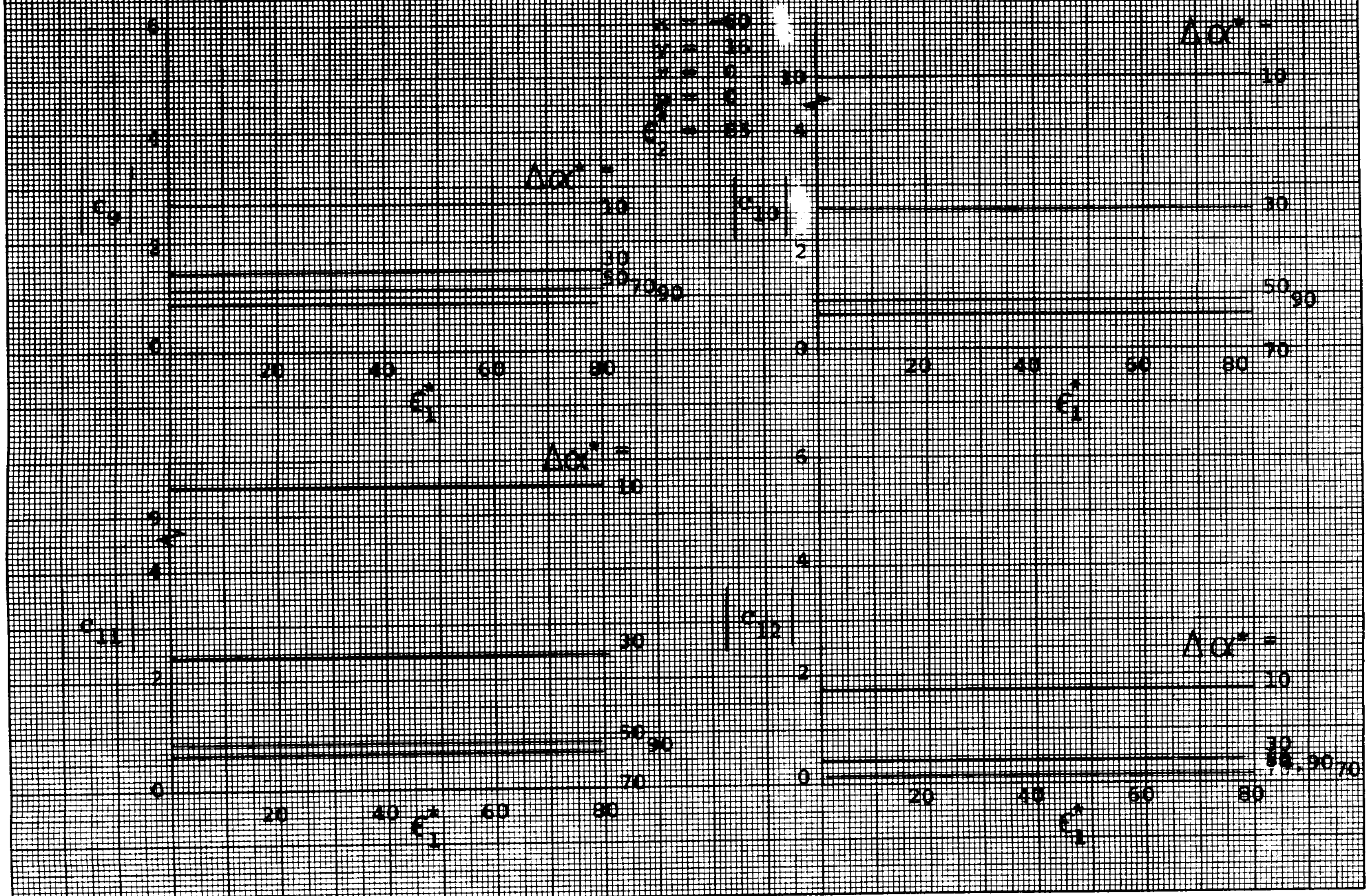

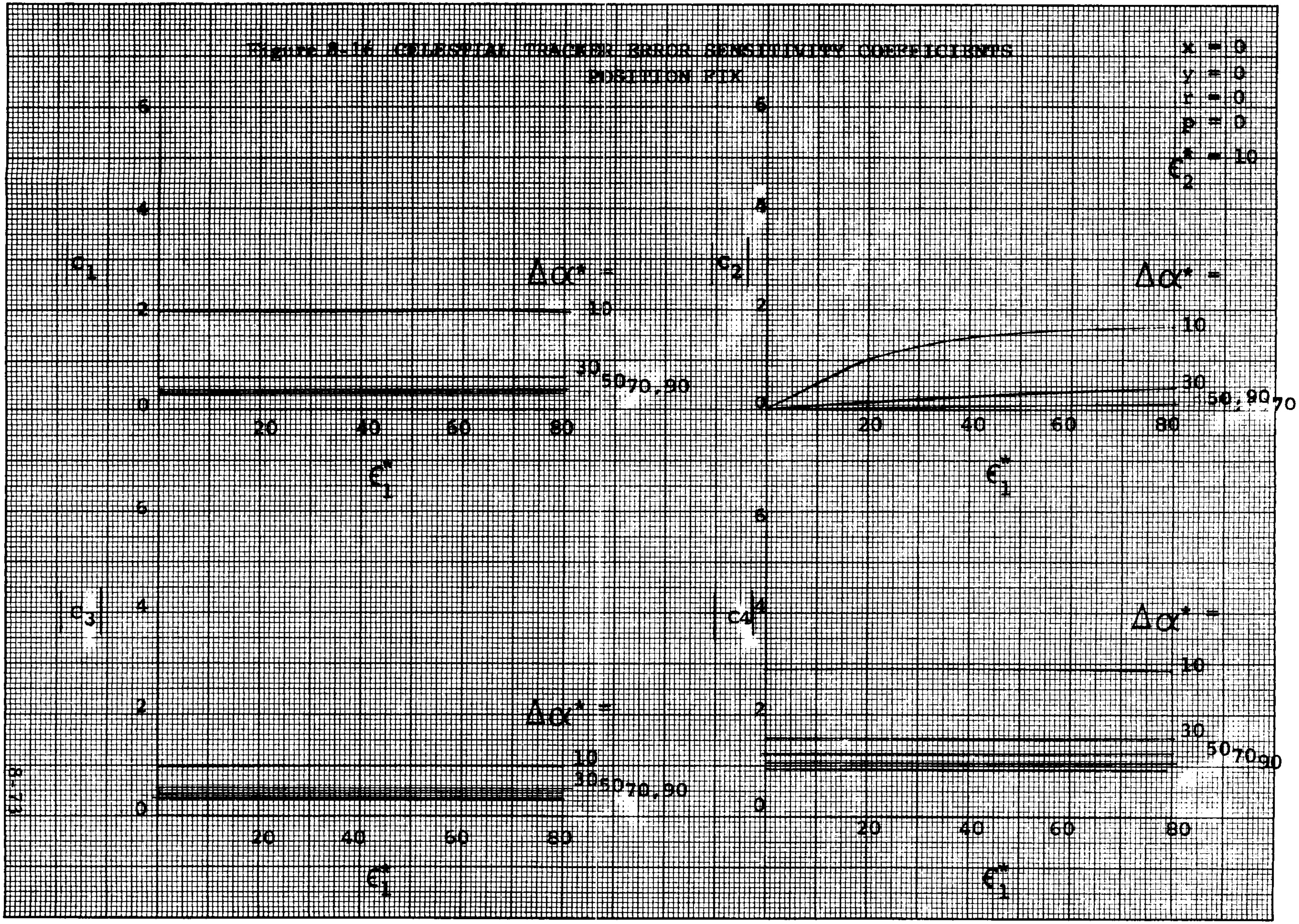

Figure 8-16 CELESTIAL TRACKER ERROR SENSITIVITY COEFFICIENTS
POSITION FIX

Figure 3-17 CELESTIAL TRACKER ERROR SENSITIVITY COEFFICIENTS
POSITION FIX

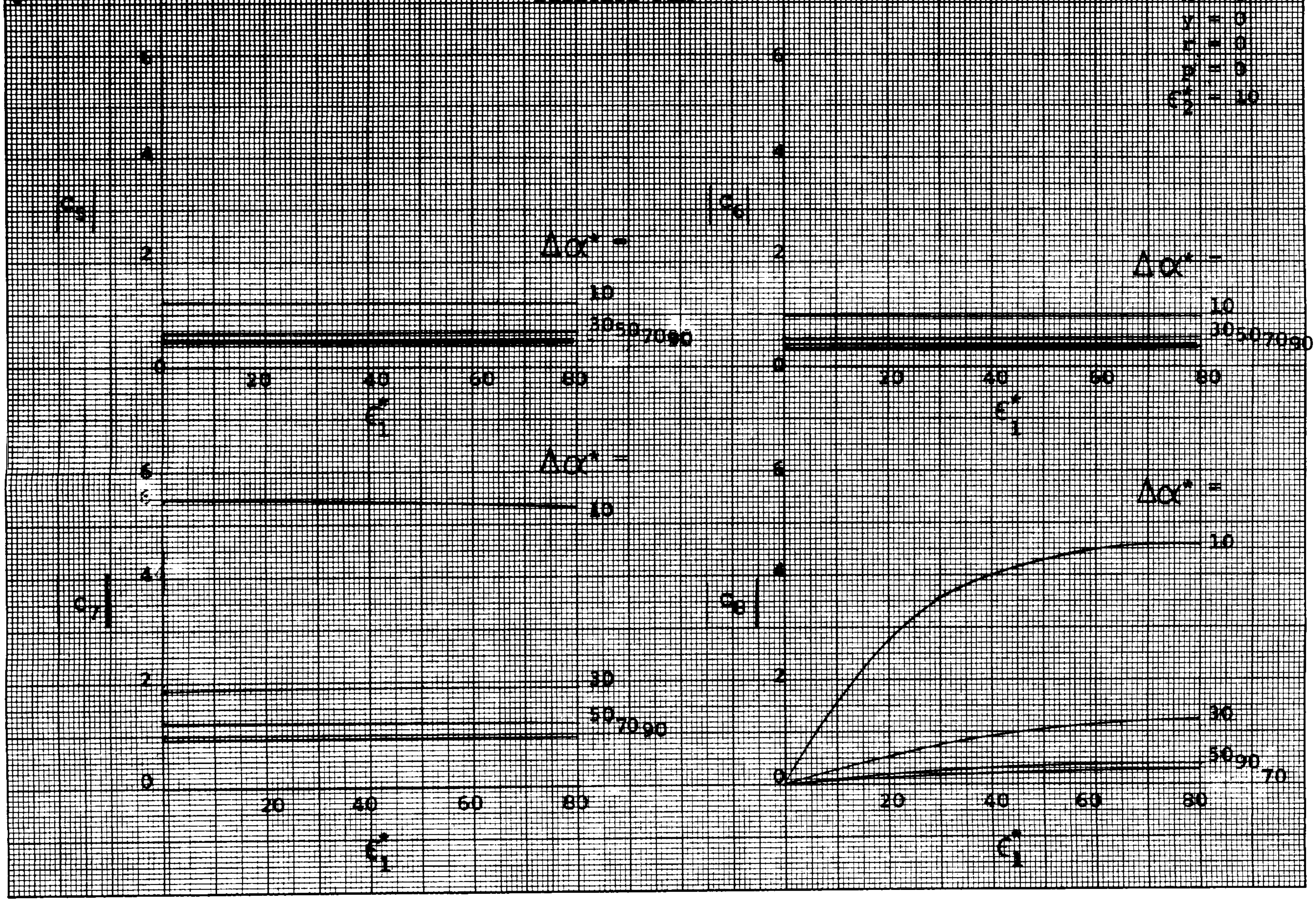

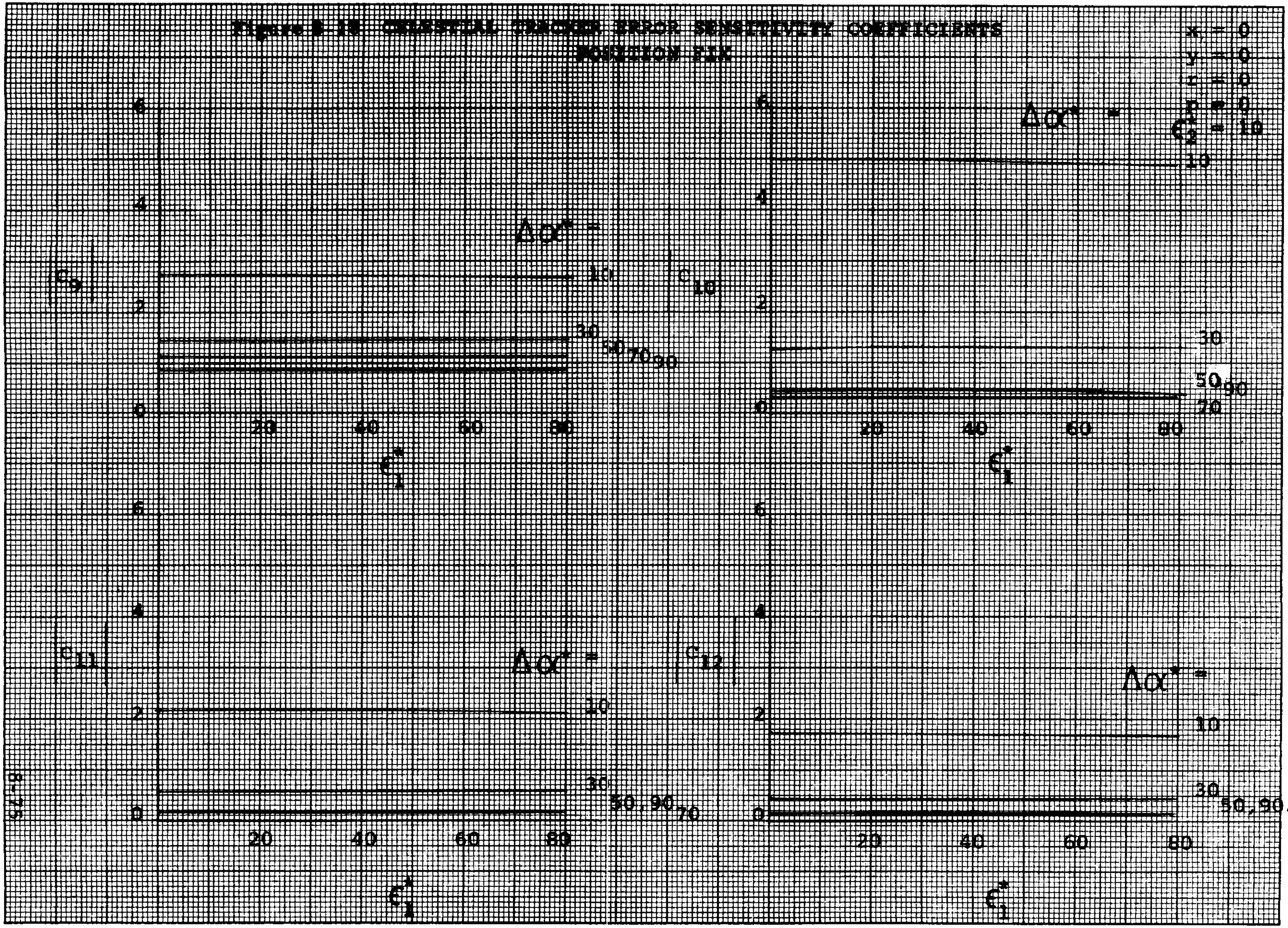

Figure 8-18 CELESTIAL TRACKER ERROR SENSITIVITY COEFFICIENTS POSITION FIX

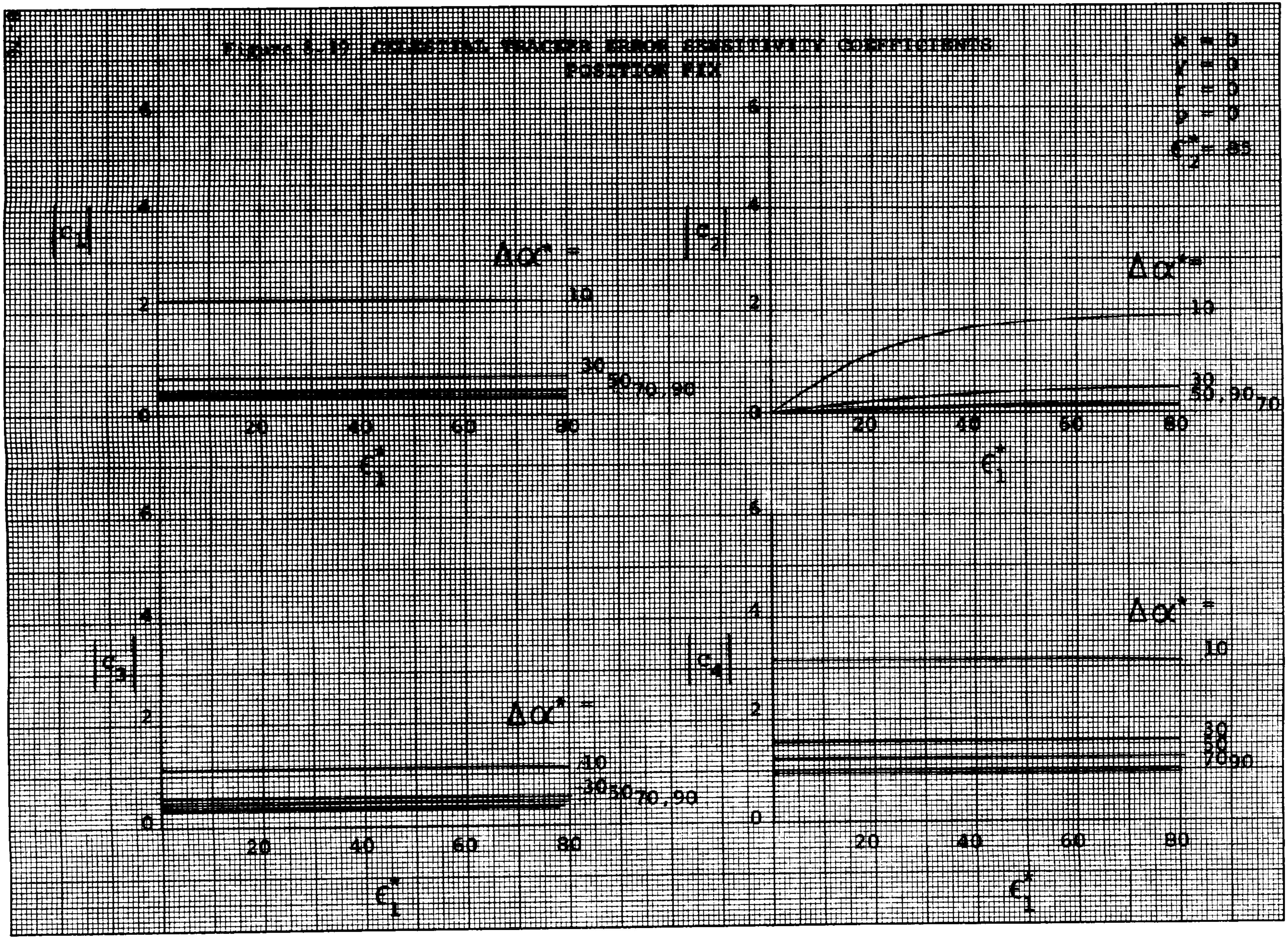

Figure 8-19 CELESTIAL TRACKER ERROR SENSITIVITY COEFFICIENTS
POSITION FIX

Figure 8-20 CELESTIAL TRACKER ERROR SENSITIVITY COEFFICIENTS
POSITION FIX

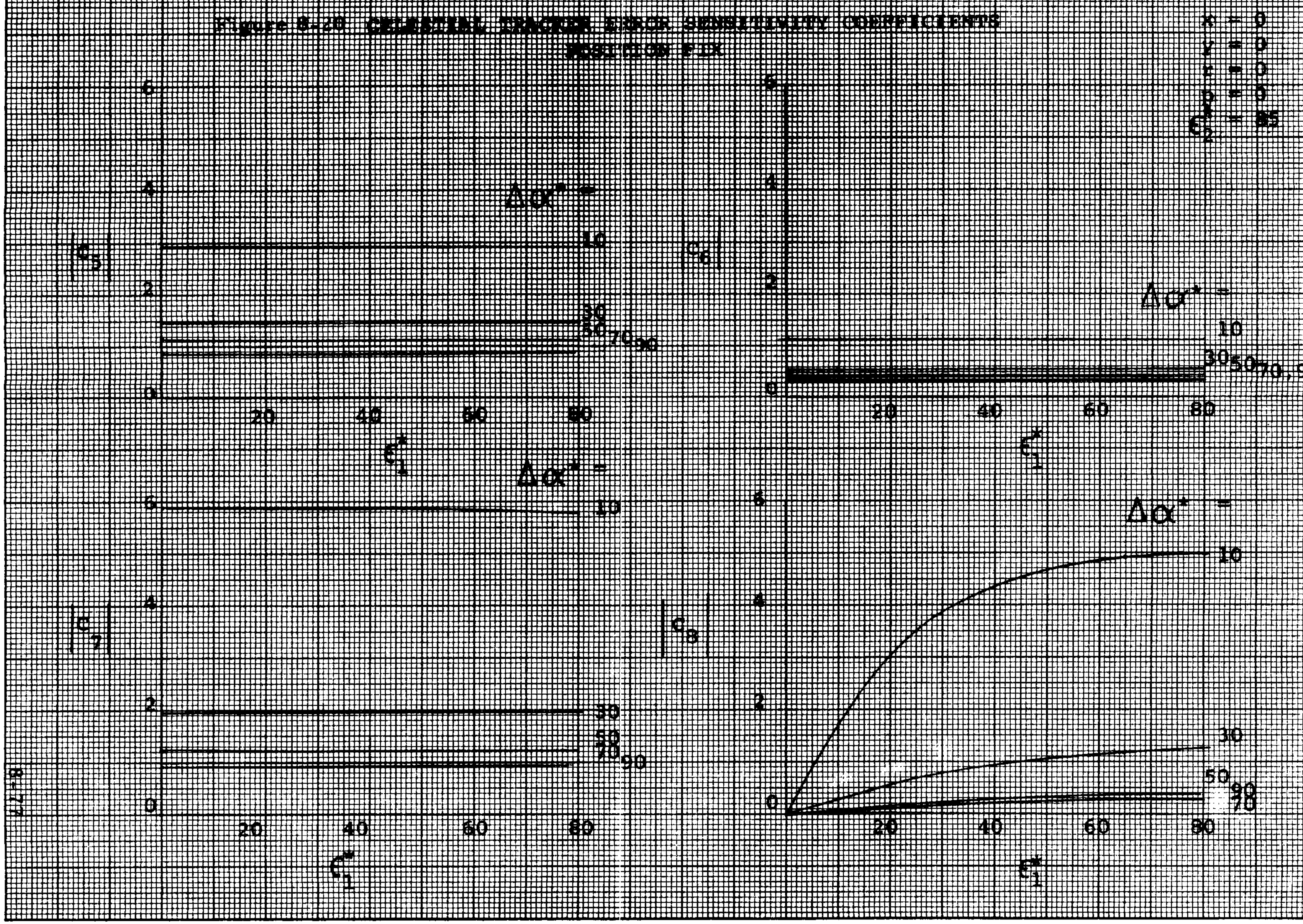

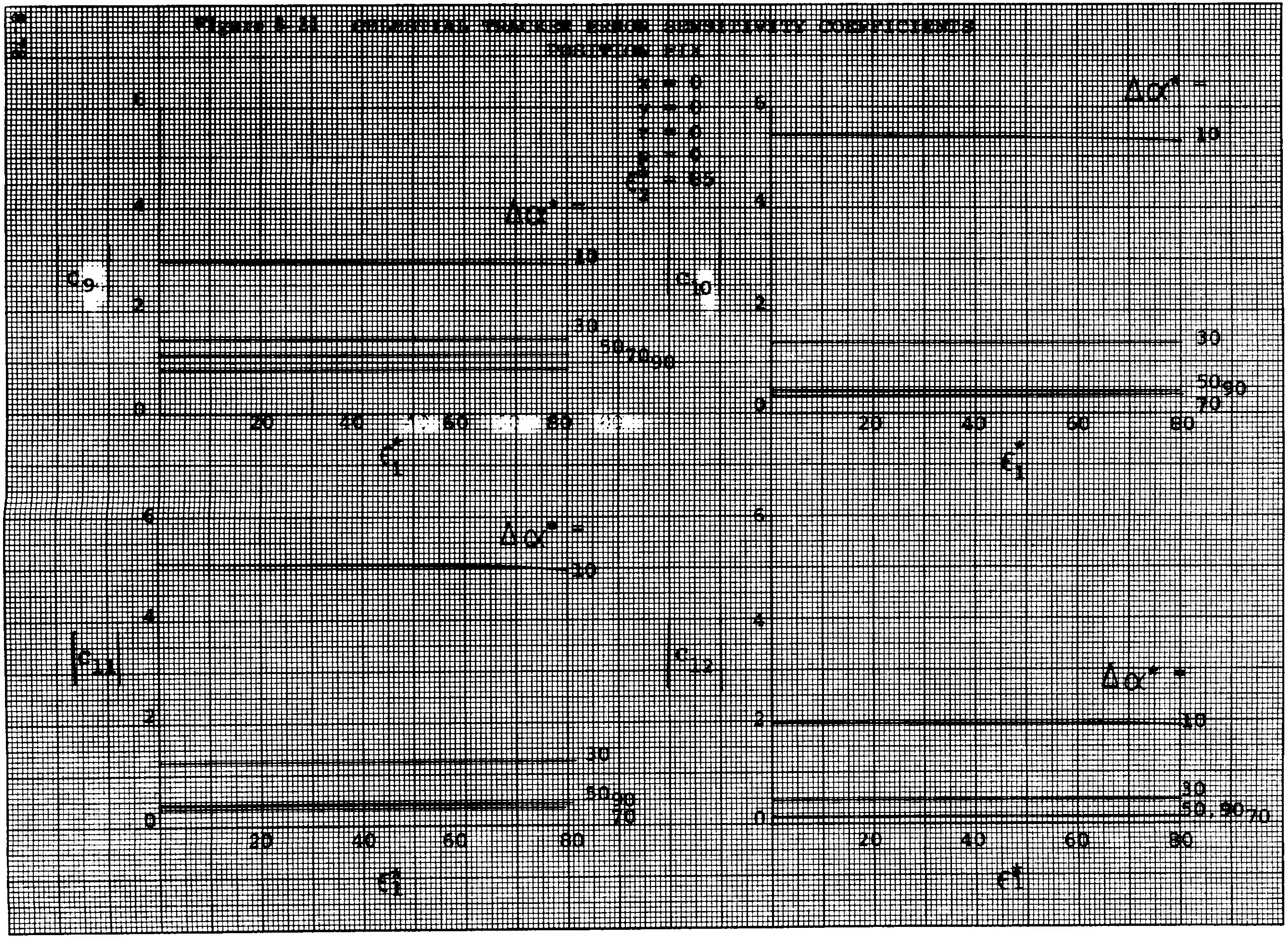

TRACKER ERROR SENSITIVITY COEFFICIENTS
POSITION FIX
x = 0
y = 0
z = 0
ϵ_2^* = 85
$|C_9|$
$|C_{10}|$
$|C_{11}|$
$|C_{12}|$
$\Delta\alpha^*$ =
10
30
50
70
90
0
2
4
6
20
40
60
80
ϵ_1^*

Figure 8.22 CELESTIAL TRACKER ERROR SENSITIVITY COEFFICIENTS
AZIMUTH ALIGNMENT

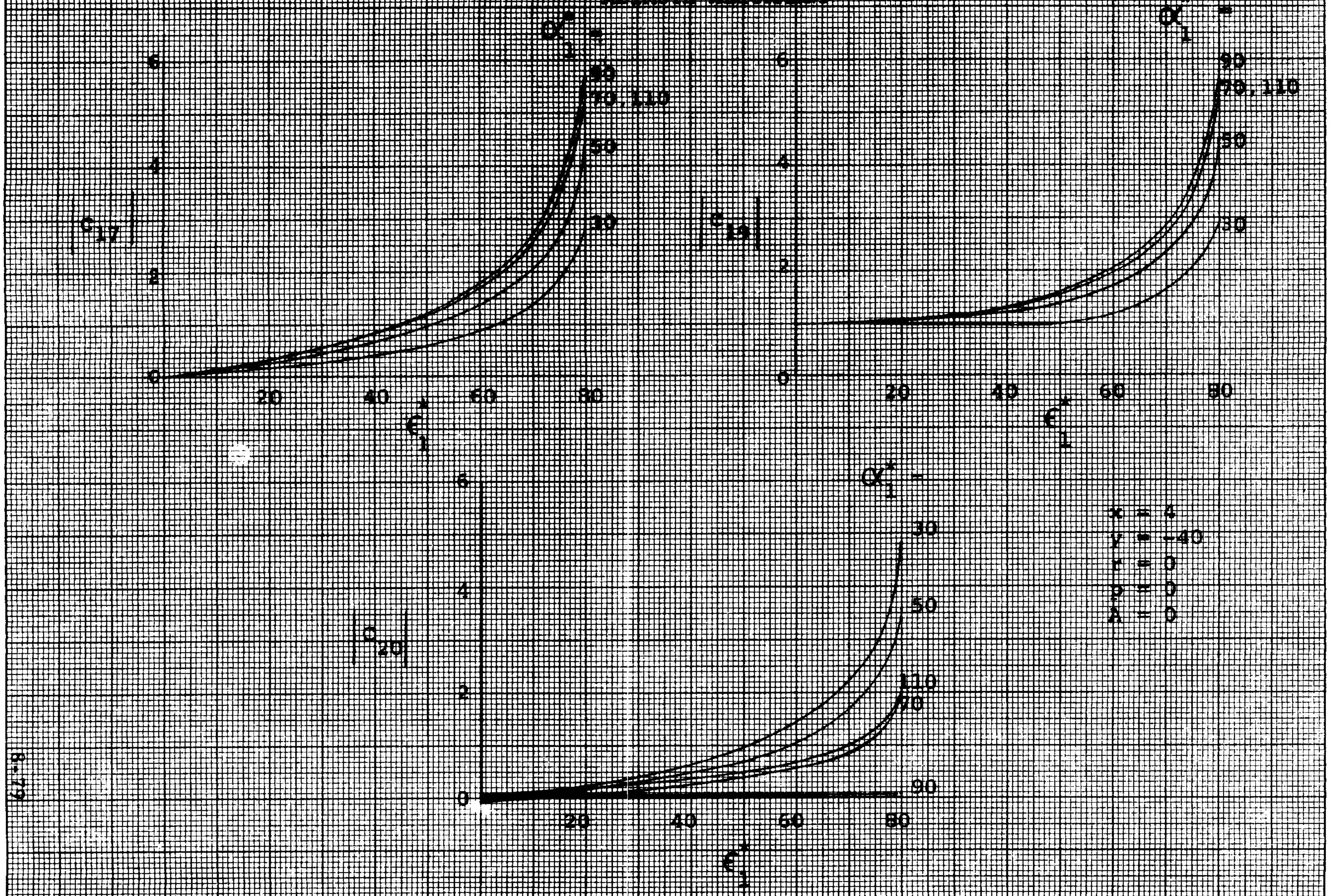

Figure 5.25 CELESTIAL TRACKER ERROR SENSITIVITY COEFFICIENTS
AZIMUTH ALIGNMENT

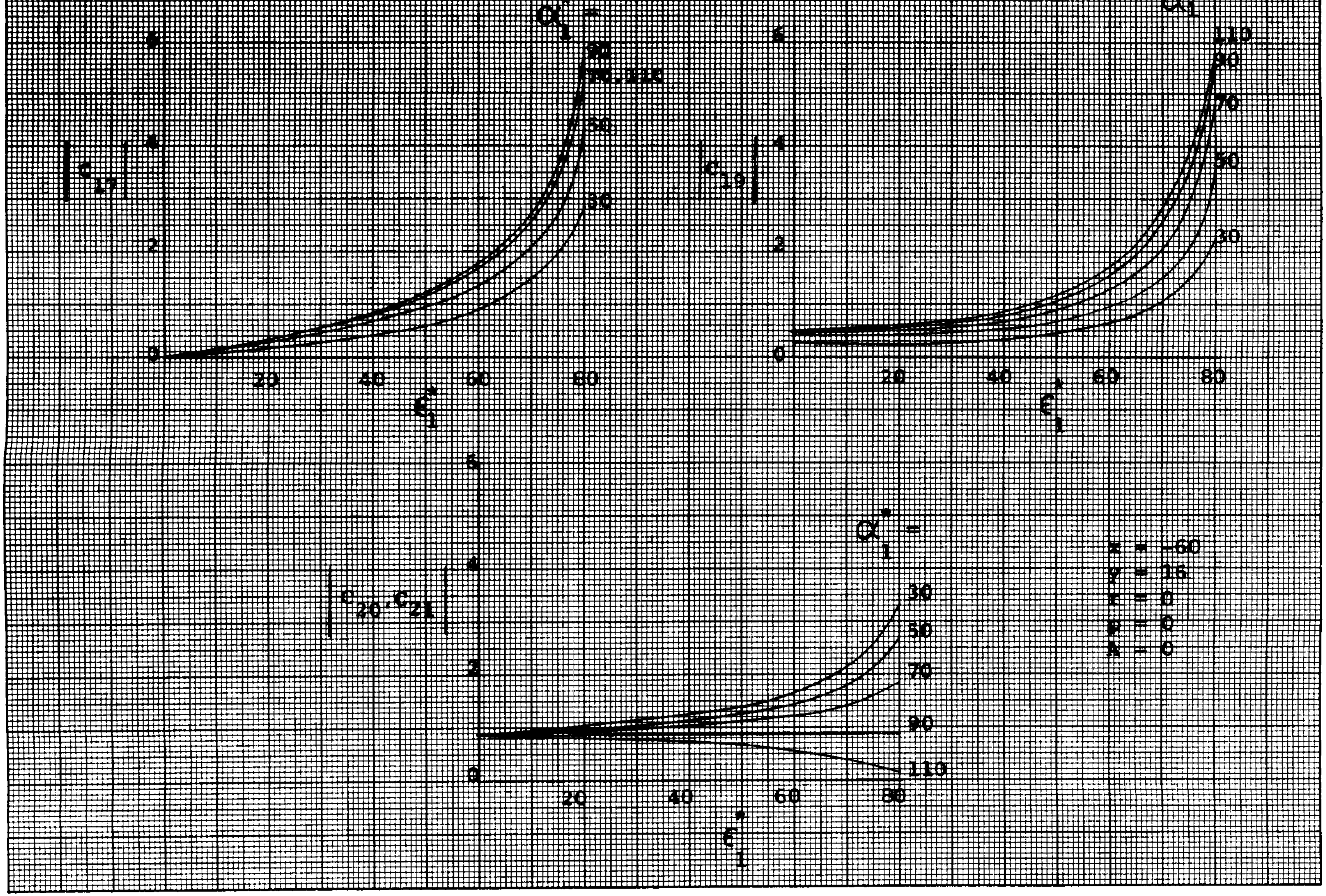

Figure 8-24 CELESTIAL TRACKER ERROR SENSITIVITY COEFFICIENTS
AZIMUTH ALIGNMENT

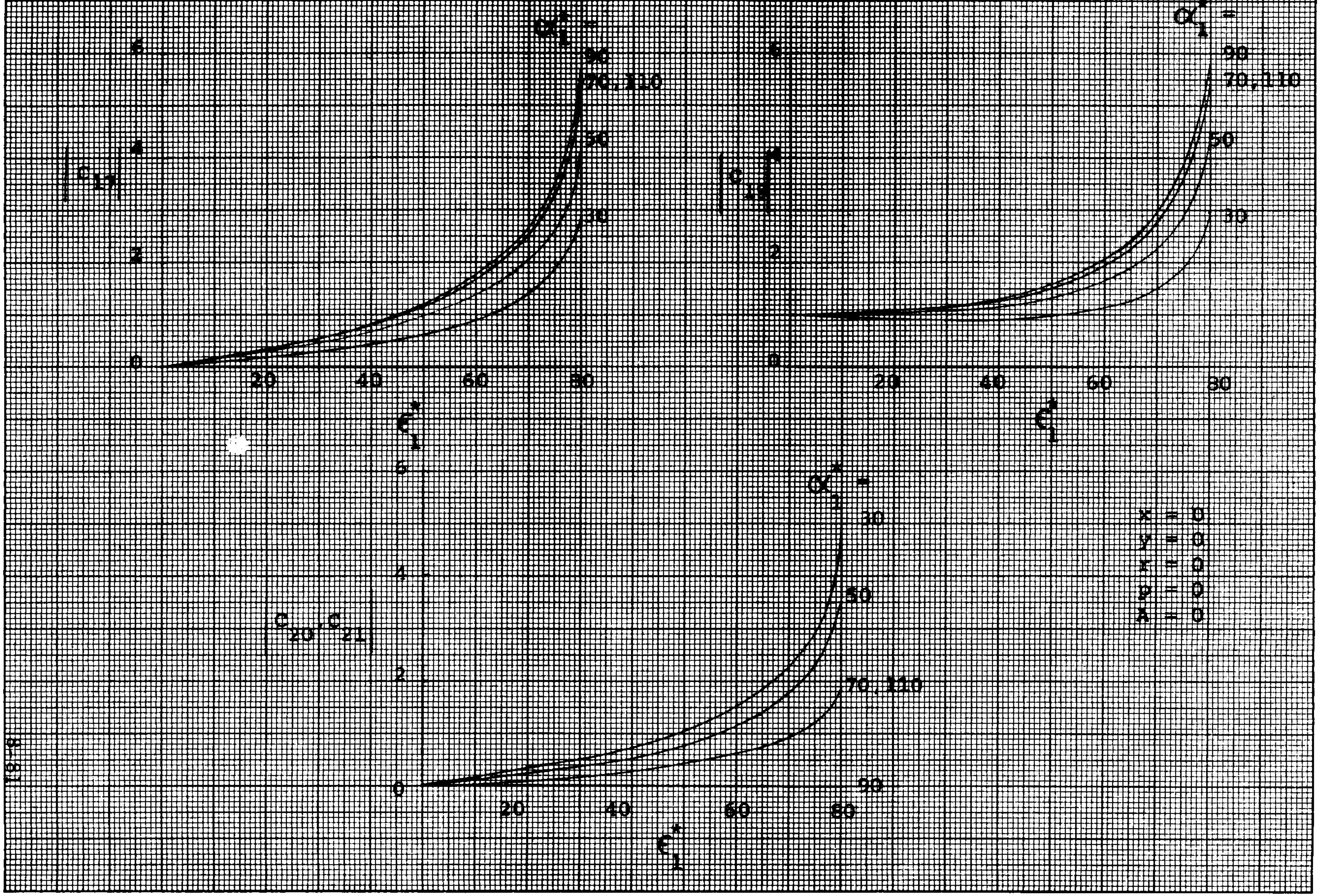

Figure B-18 ERROR SENSITIVITY COEFFICIENTS CELESTIAL TRACKER TRUE ELEVATION

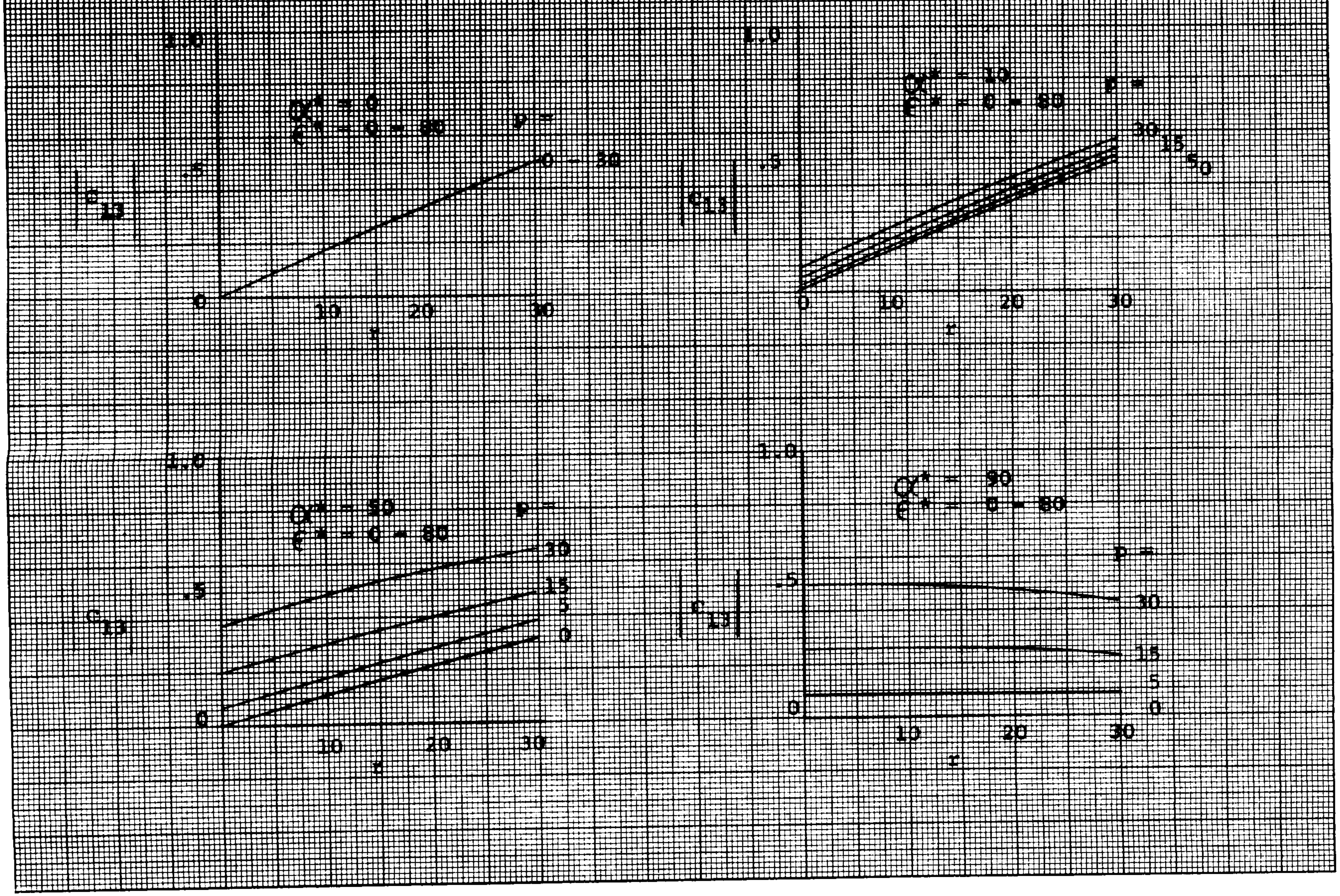

Figure 8-26 ERROR SENSITIVITY COEFFICIENTS CELESTIAL TRACKER TRUE ELEVATION

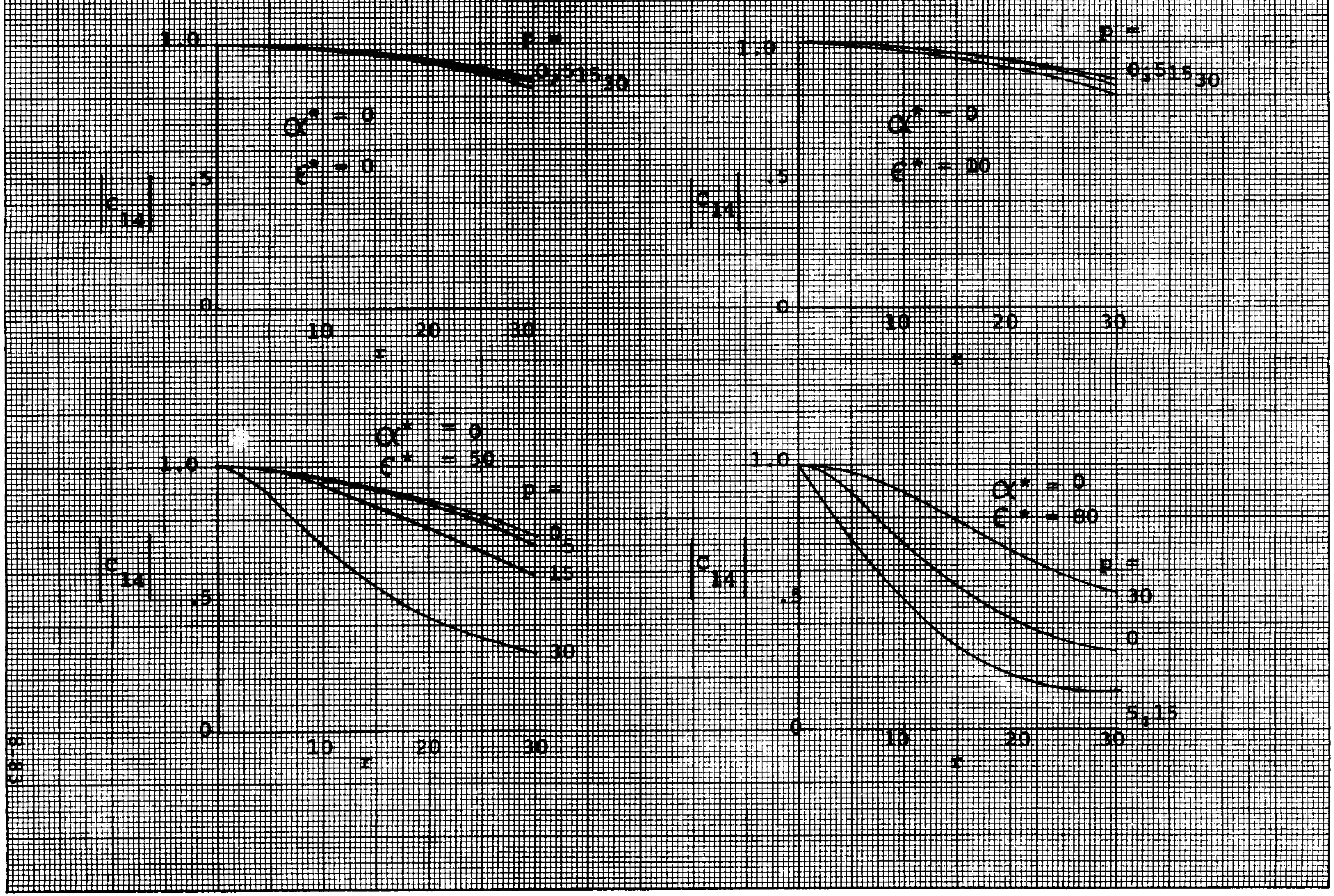

Figure 8-27 ERROR SENSITIVITY COEFFICIENTS CELESTIAL TRACKER TRUE ELEVATION

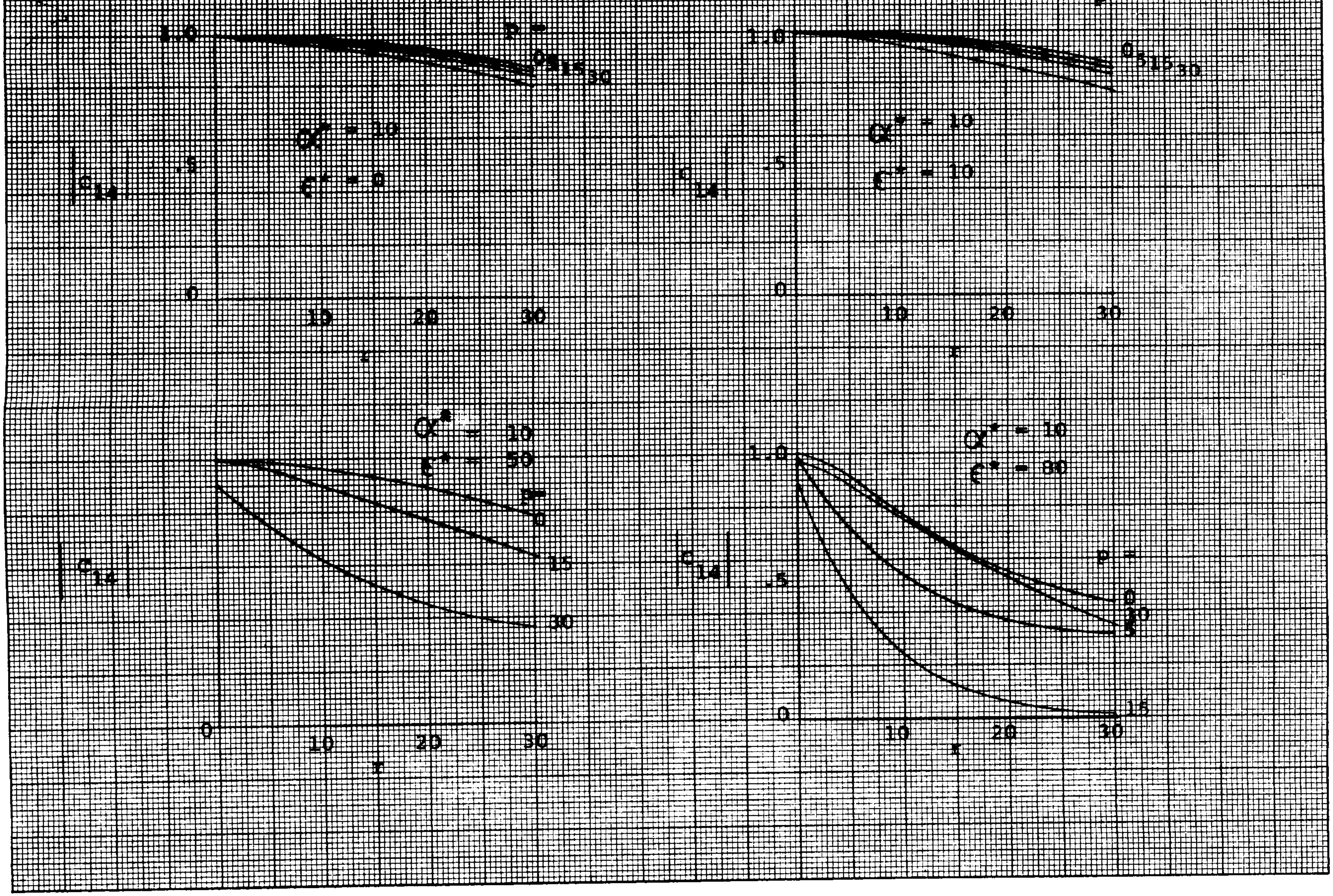

ERROR SENSITIVITY COEFFICIENTS CELESTIAL TRACKER TRUE ELEVATION

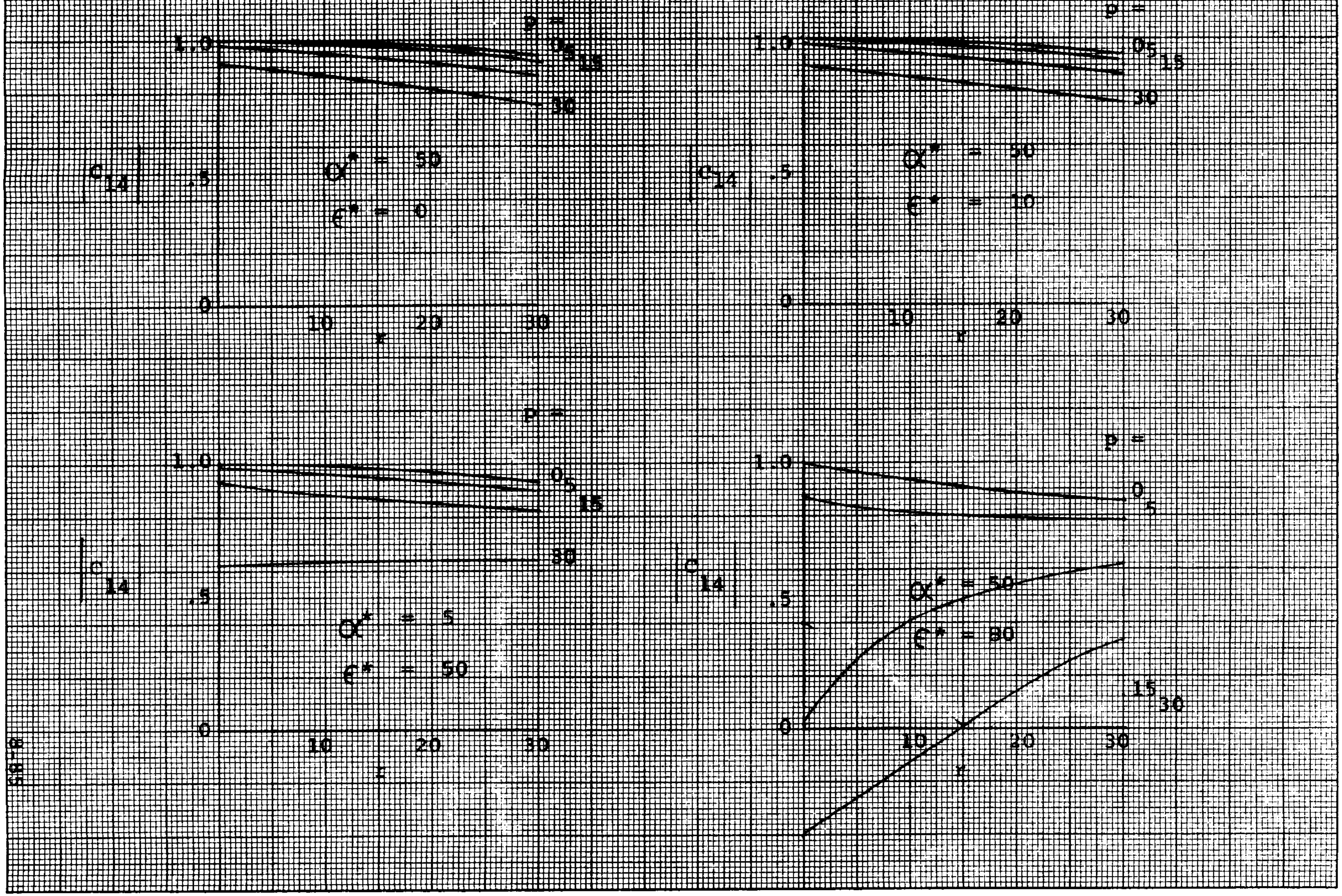

Figure [illegible] ERROR SENSITIVITY COEFFICIENTS CELESTIAL TRACKER TRIM ELEVATION

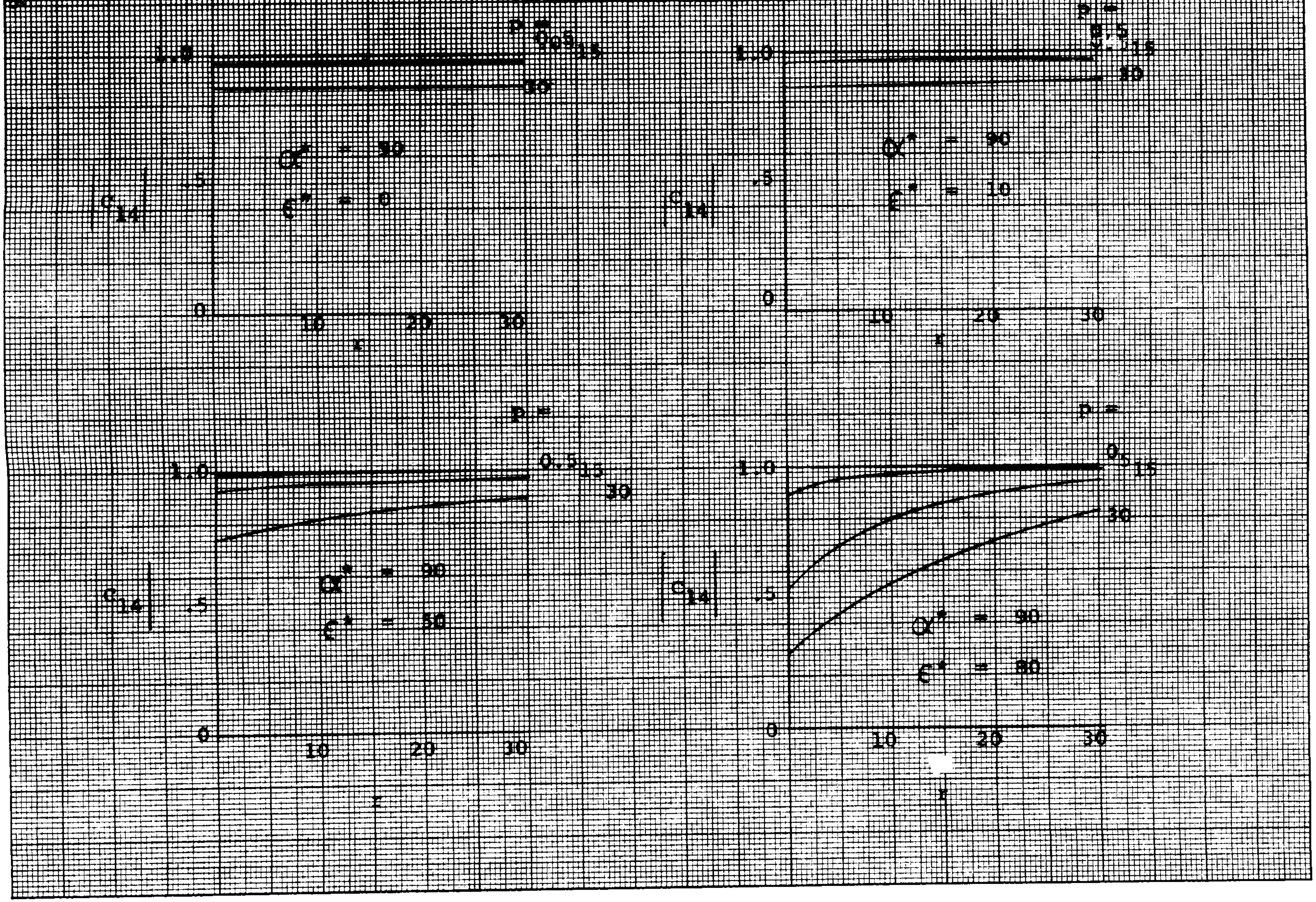

Figure 8-30 ERROR SENSITIVITY COEFFICIENTS CELESTIAL TRACKER TRUE ELEVATION

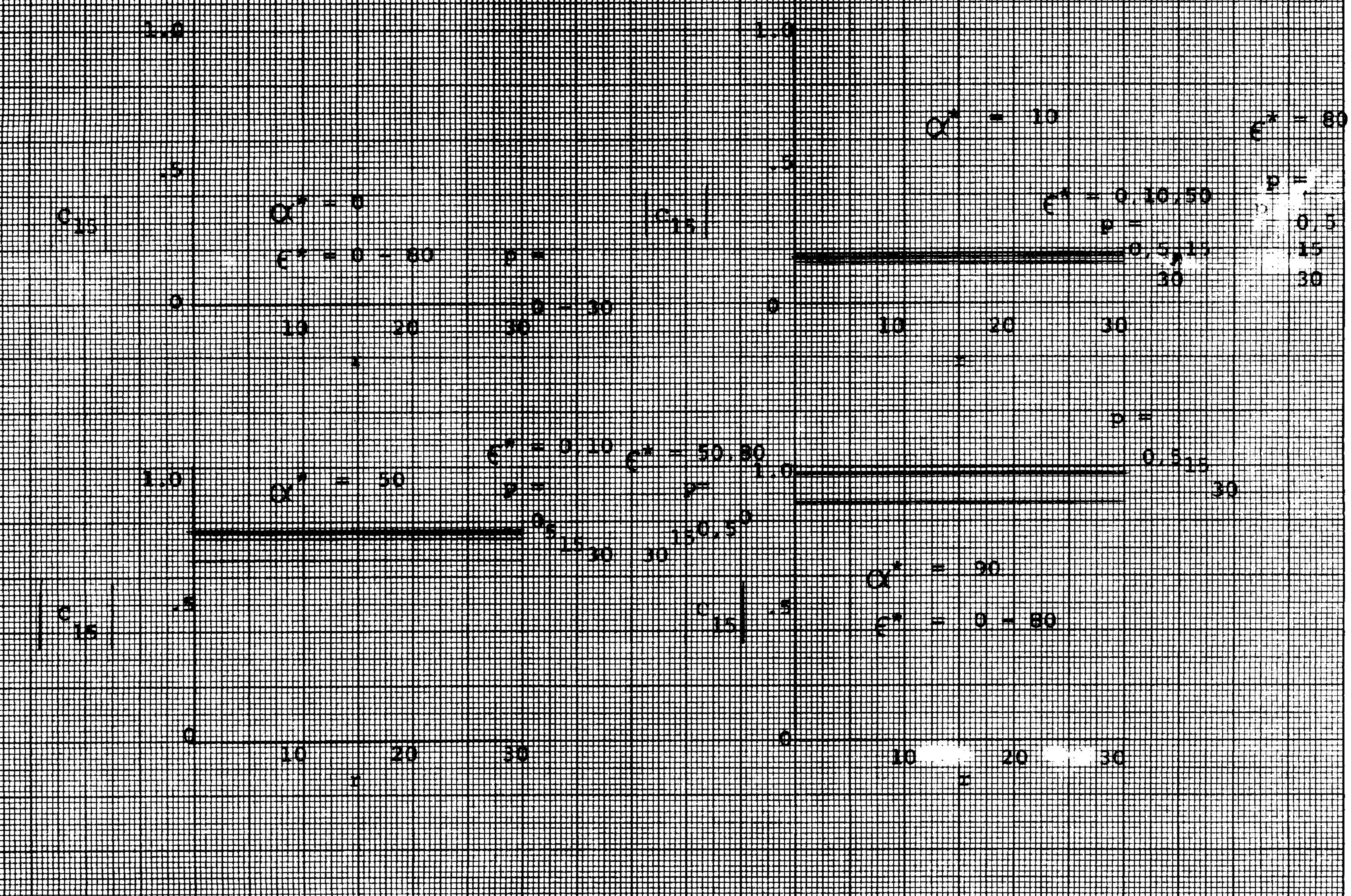

Figure B-31 ERROR SENSITIVITY COEFFICIENTS CELESTIAL TRACKER TRUE ELEVATION

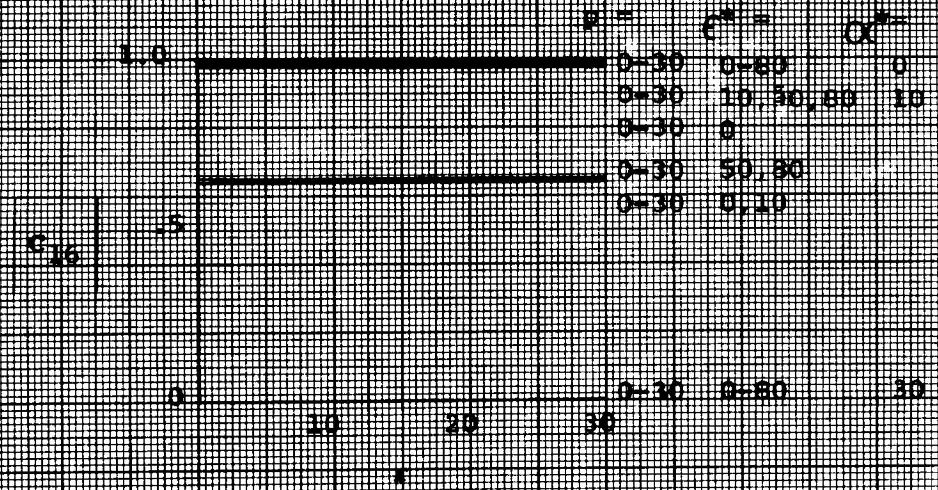

Figure 8-32 ERROR SENSITIVITY COEFFICIENTS CELESTIAL TRACKER TRUE AZIMUTH

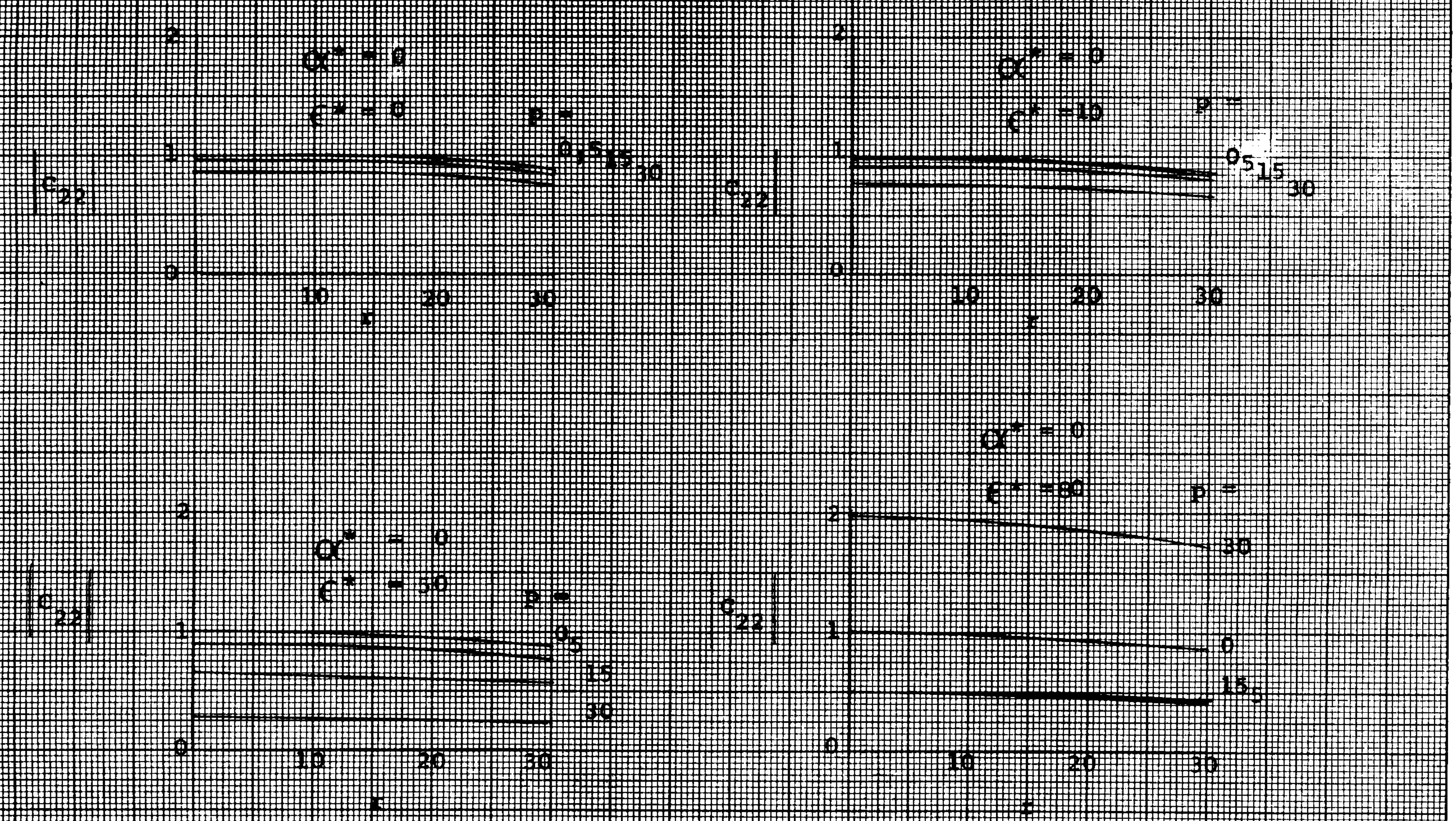

Figure 8-33 ERROR SENSITIVITY COEFFICIENTS CELESTIAL TRACKER TRUE AZIMUTH

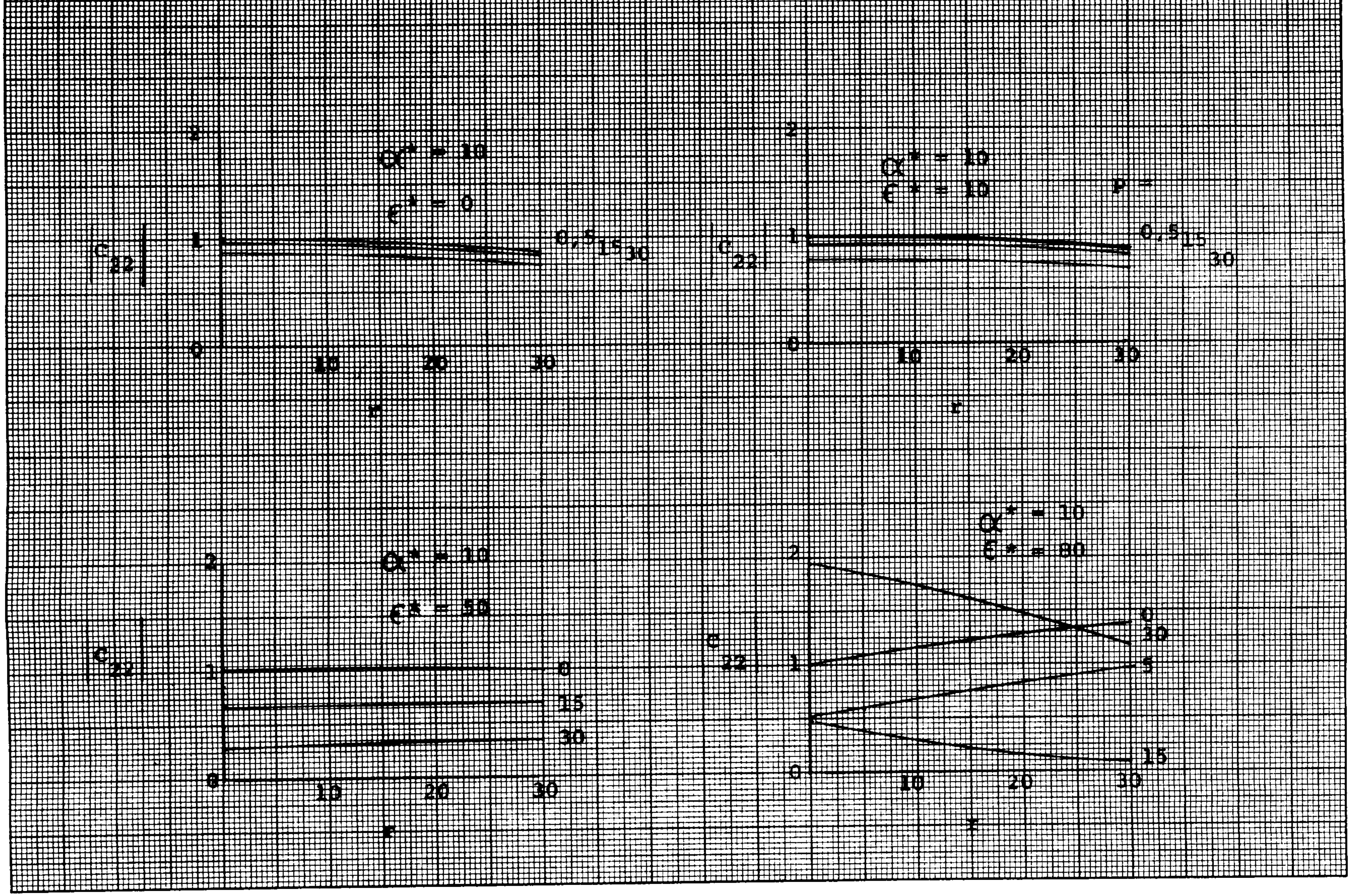

Figure 8-34 ERROR SENSITIVITY COEFFICIENTS CELESTIAL TRACKER TRUE AZIMUTH

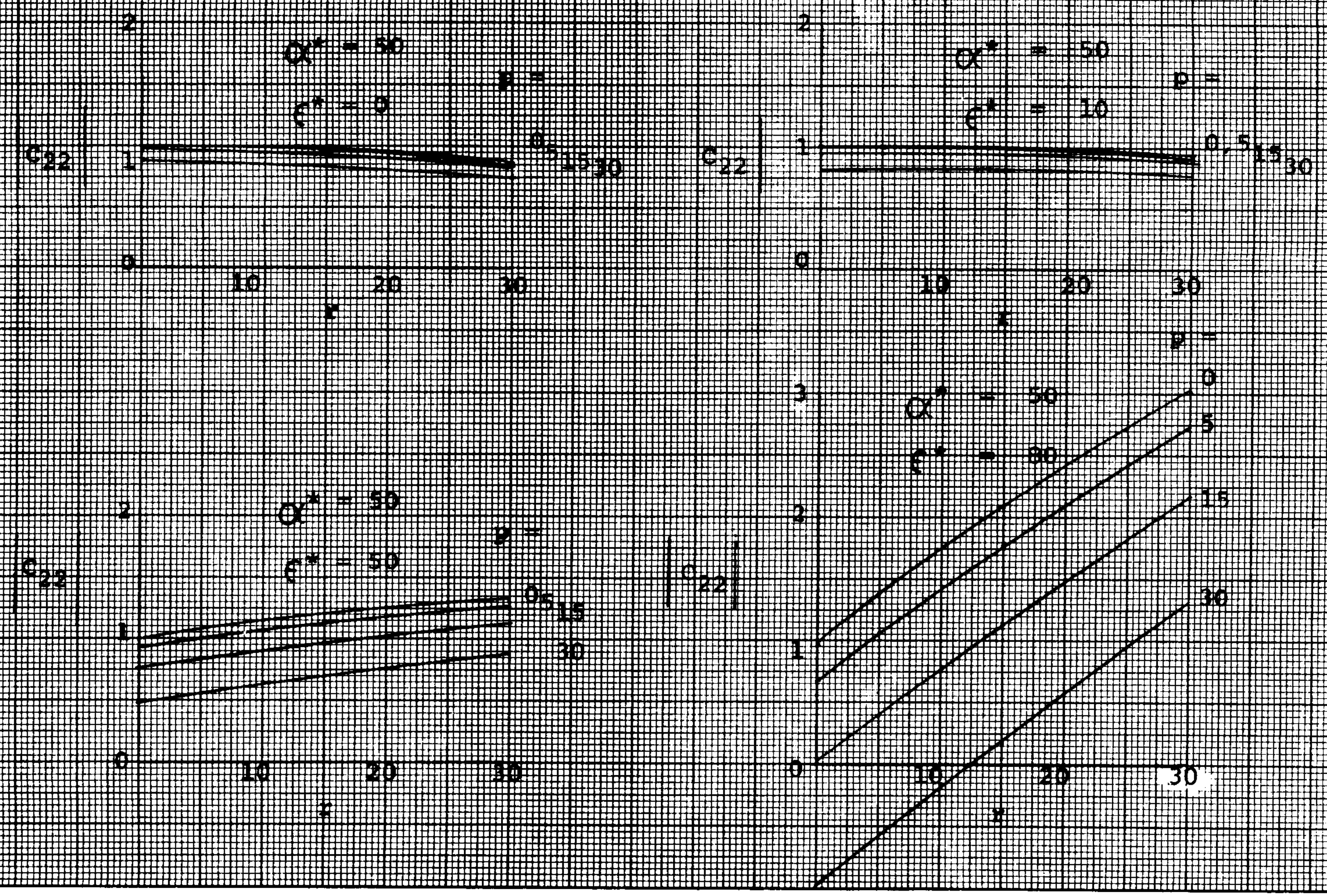

Figure 8-35 ERROR SENSITIVITY COEFFICIENTS CELESTIAL TRACKER TRUE AZIMUTH

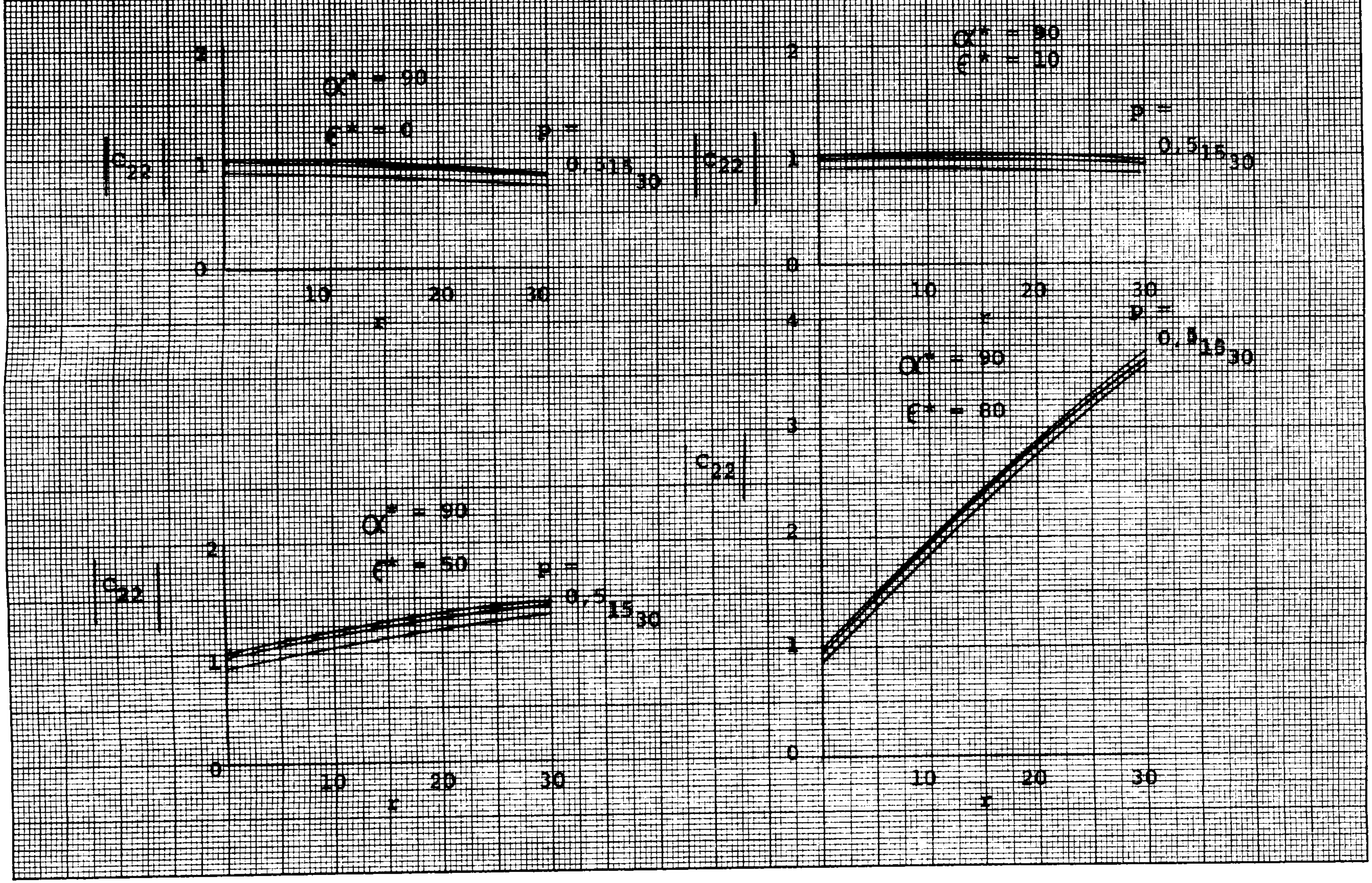

Figure 8-36 ERROR SENSITIVITY COEFFICIENTS CELESTIAL TRACKER TRUE AZIMUTH

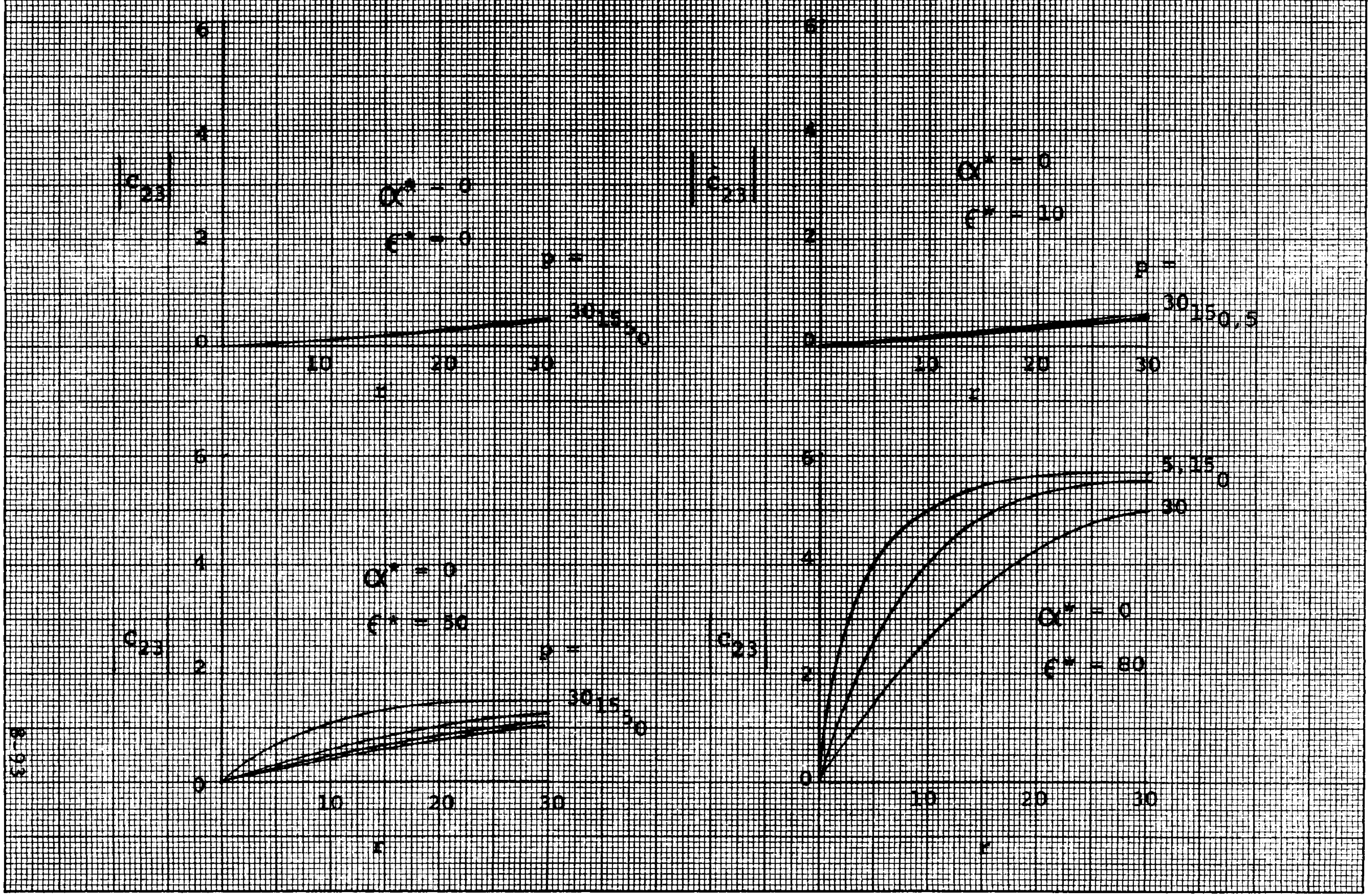

Figure 8.37 ERROR SENSITIVITY COEFFICIENTS CELESTIAL TRACKER TRUE AZIMUTH

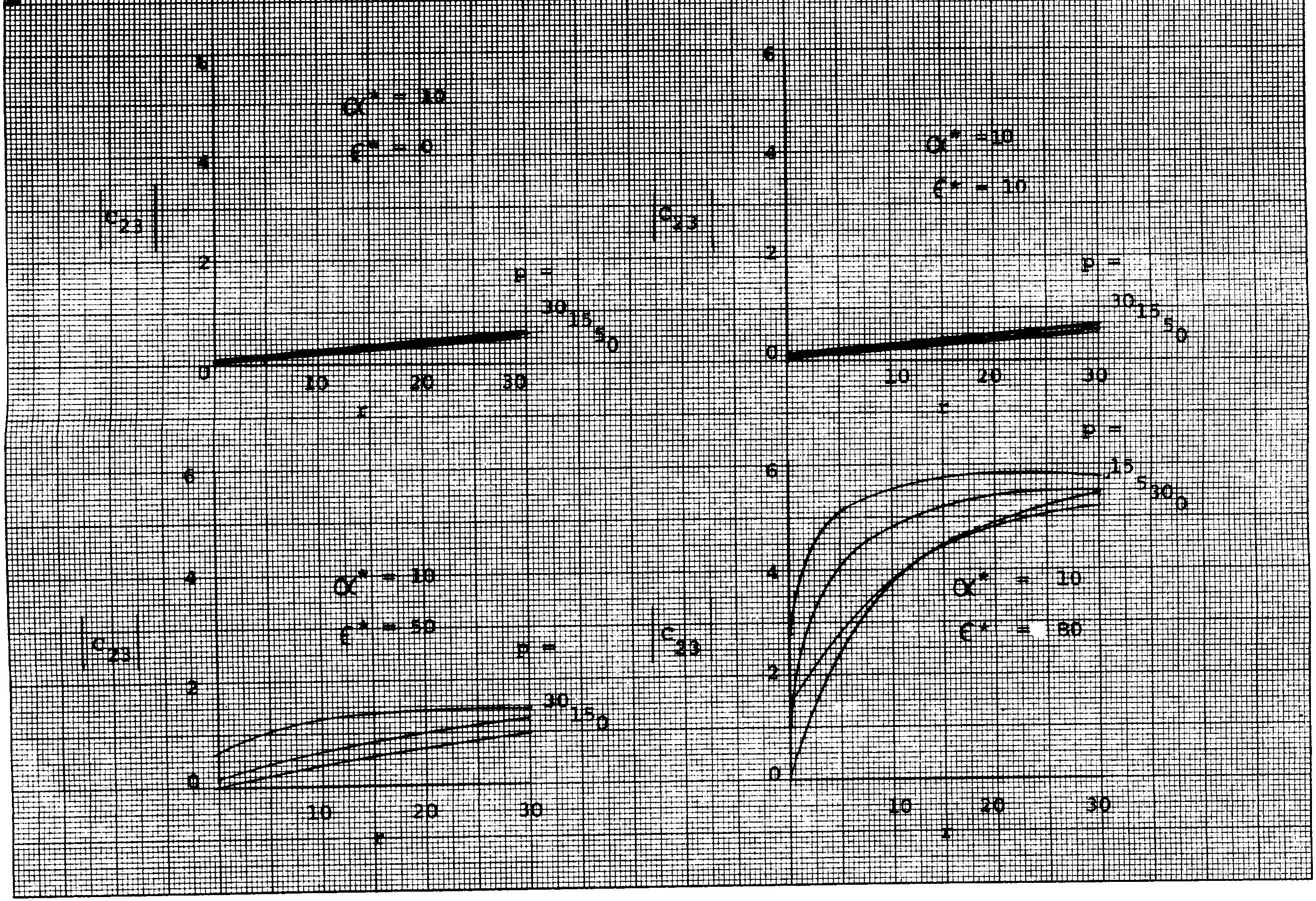

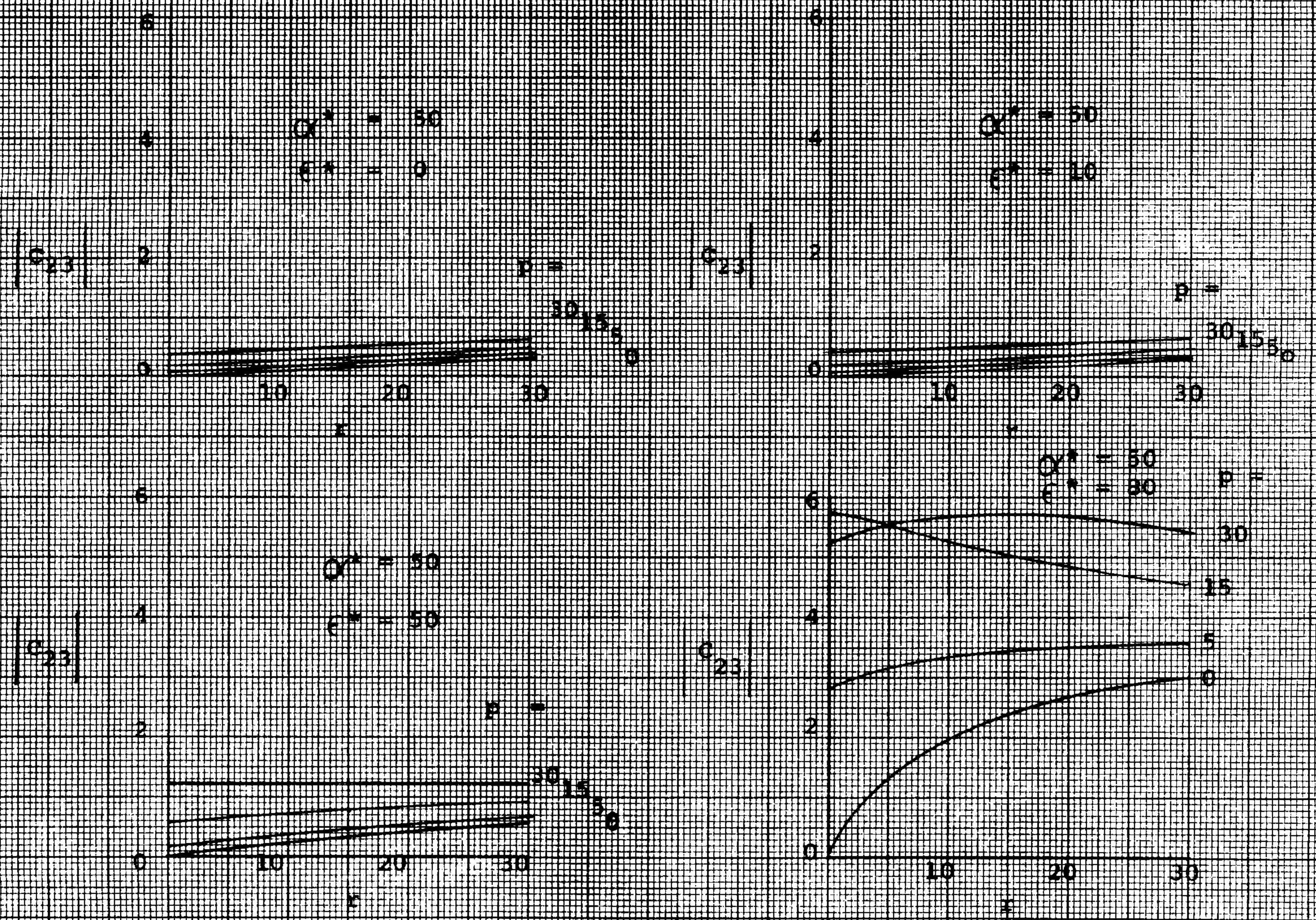

Figure 8-38 ERROR SENSITIVITY COEFFICIENTS CELESTIAL TRACKER TRUE AZIMUTH

Figure 8-39 ERROR SENSITIVITY COEFFICIENTS CELESTIAL TRACKER TRUE AZIMUTH

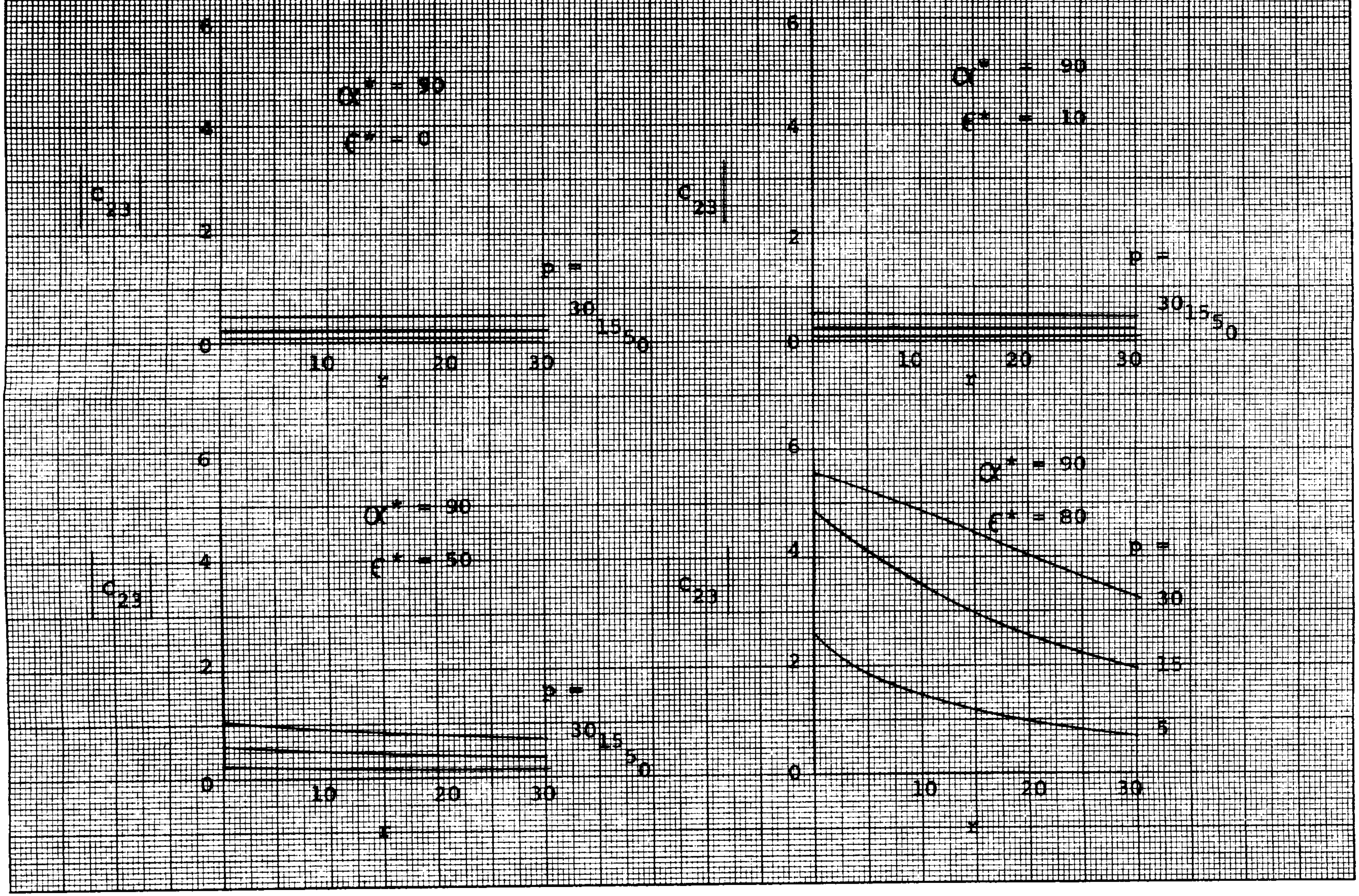

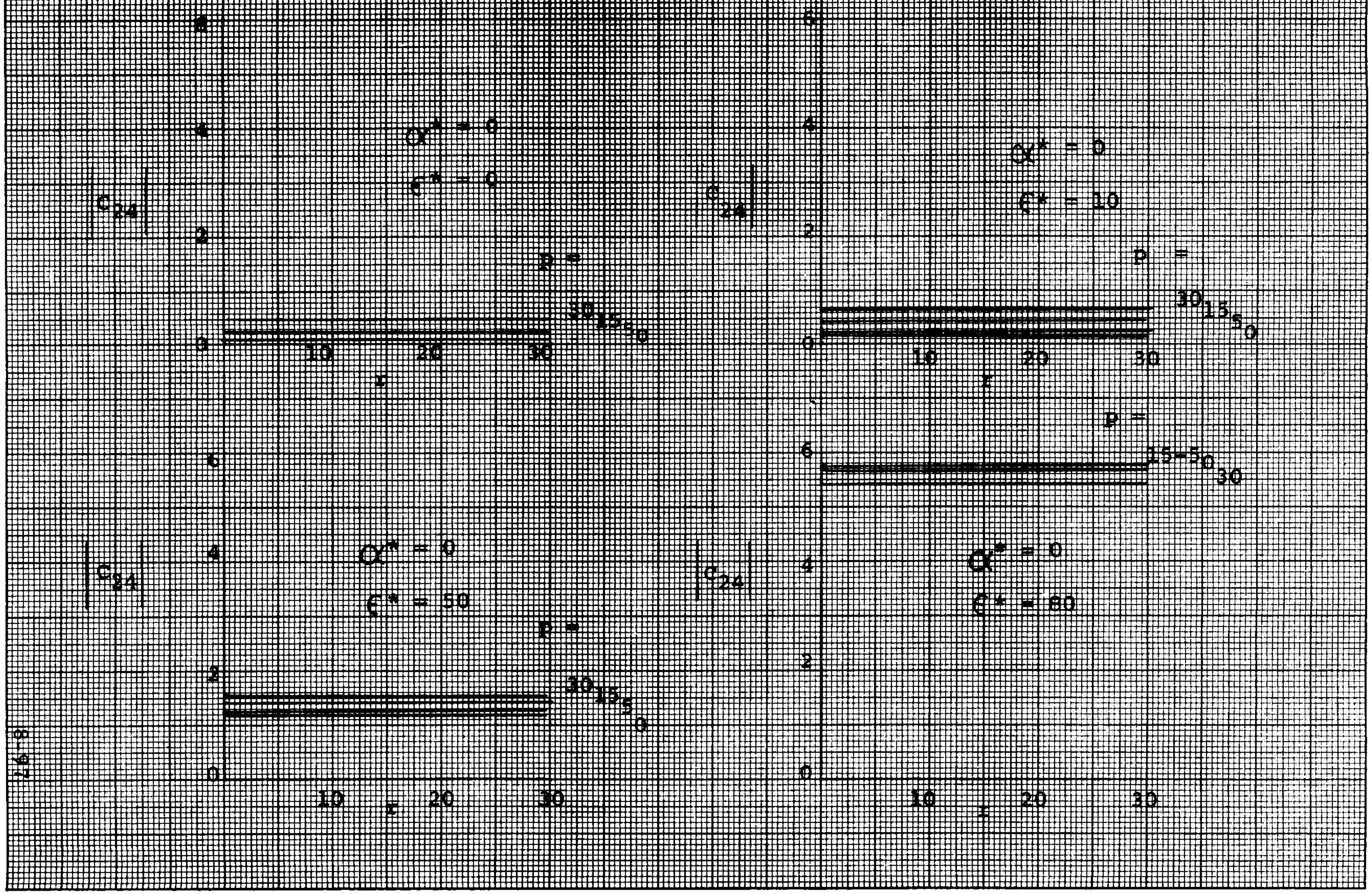

Figure 8-40 ERROR SENSITIVITY COEFFICIENTS CELESTIAL TRACKER TRUE AZIMUTH

Figure 8-41 ERROR SENSITIVITY COEFFICIENTS CELESTIAL TRACKER TRUE AZIMUTH

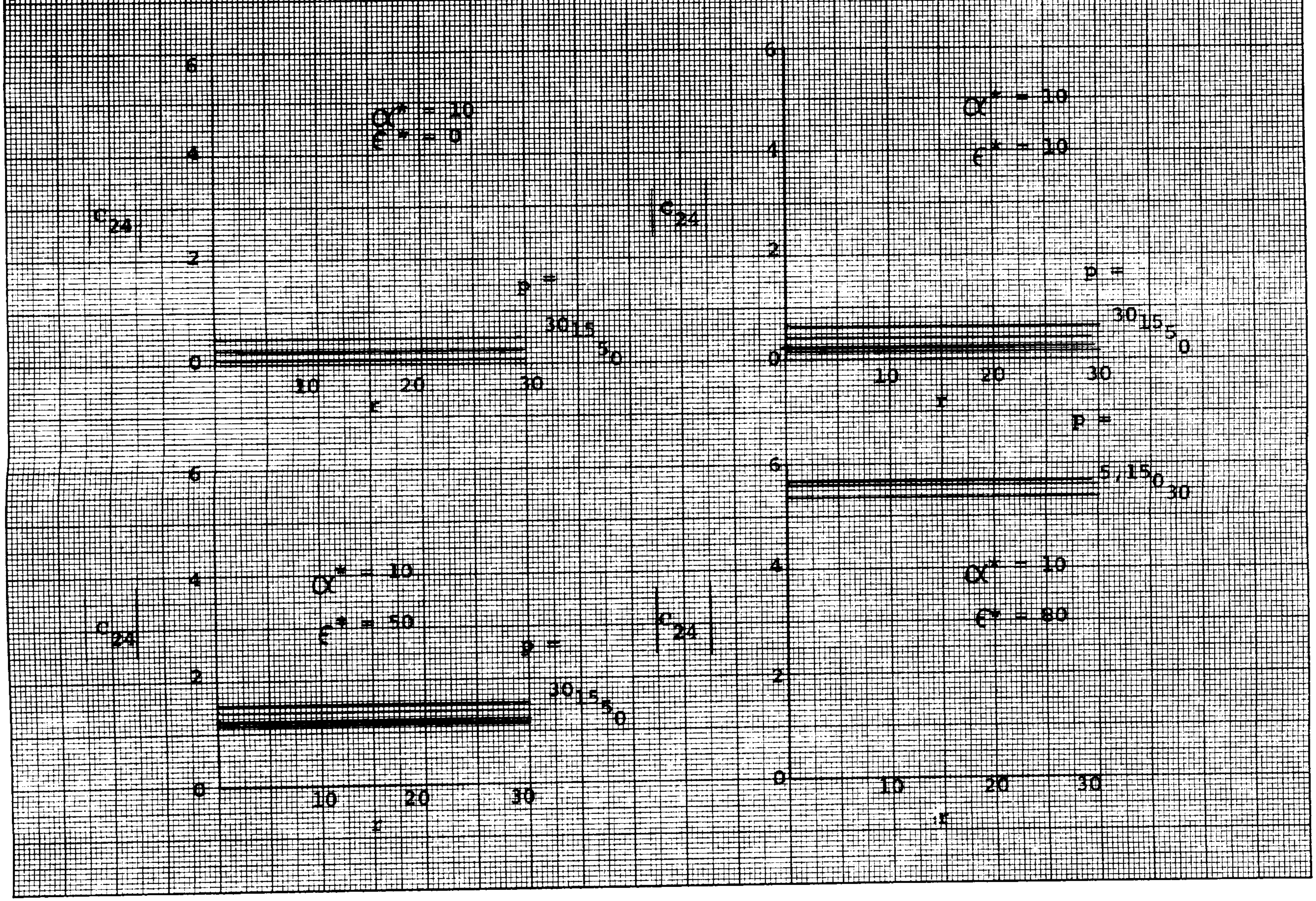

Figure 8-42 ERROR SENSITIVITY COEFFICIENTS CELESTIAL TRACKER TRUE AZIMUTH

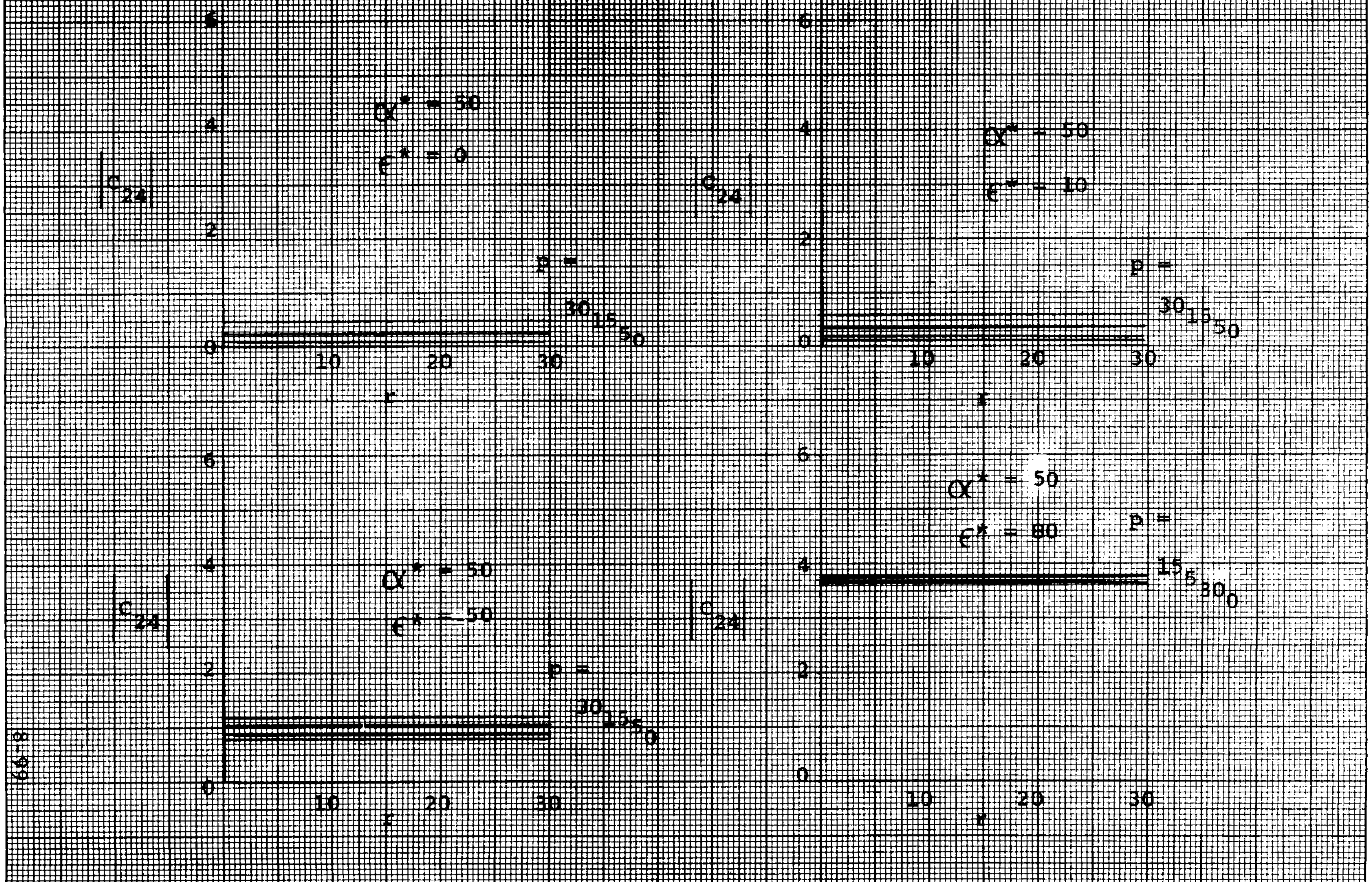

Figure 8-43 ERROR SENSITIVITY COEFFICIENTS CELESTIAL TRACKER TRUE AZIMUTH

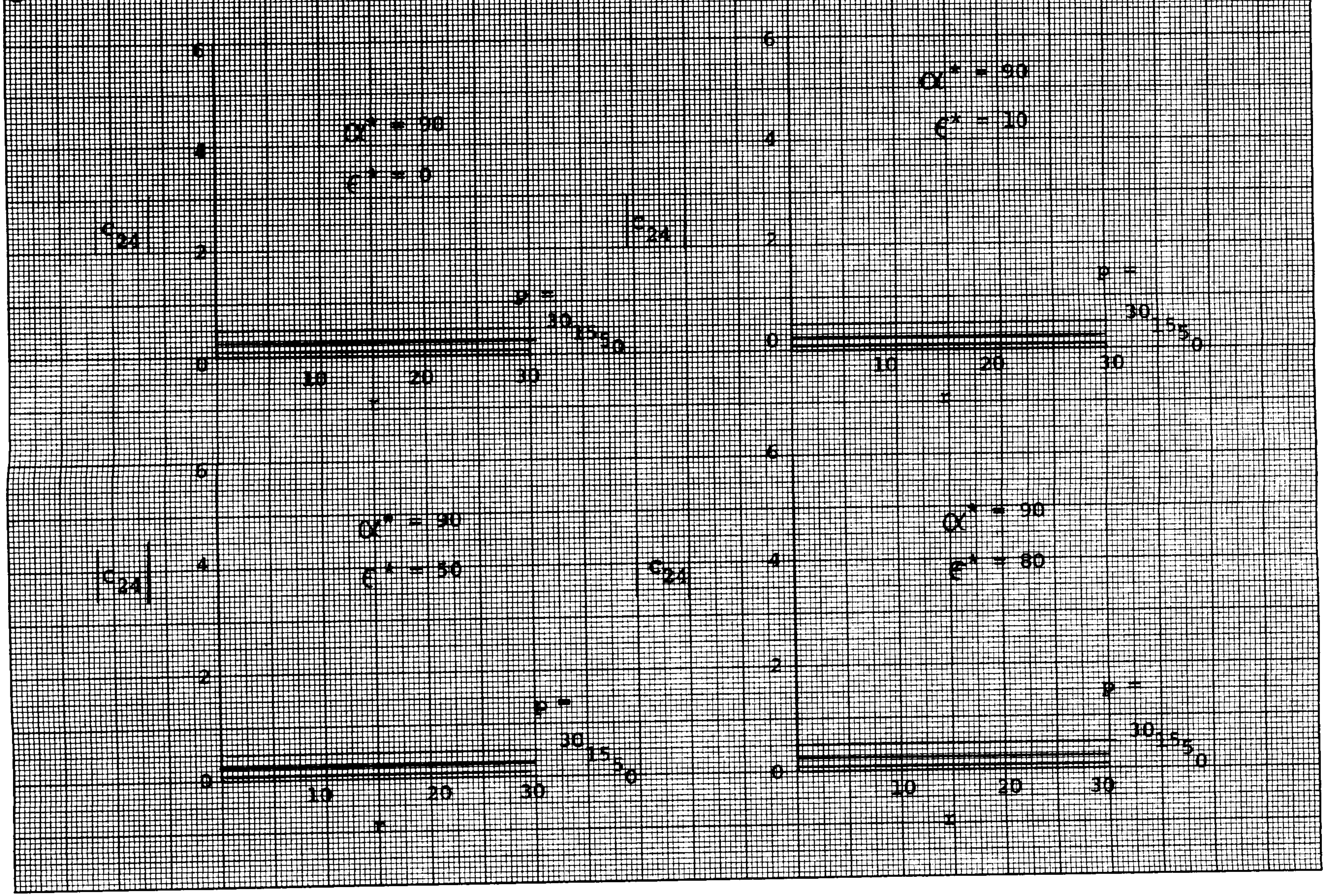

Figure 8-44 ERROR SENSITIVITY COEFFICIENTS CELESTIAL TRACKER TRUE AZIMUTH

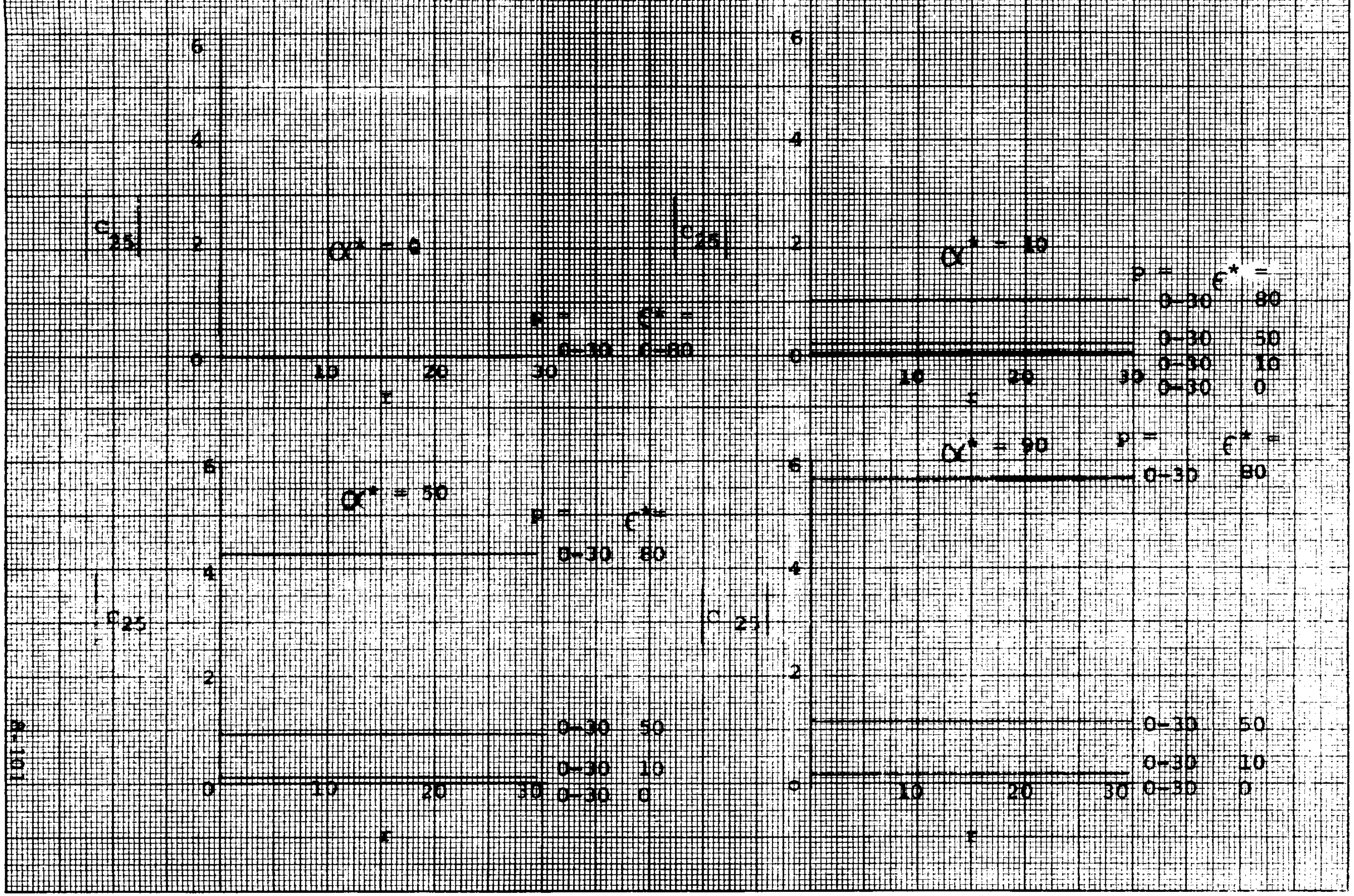

NON GYRO / INERTIAL CONCEPT

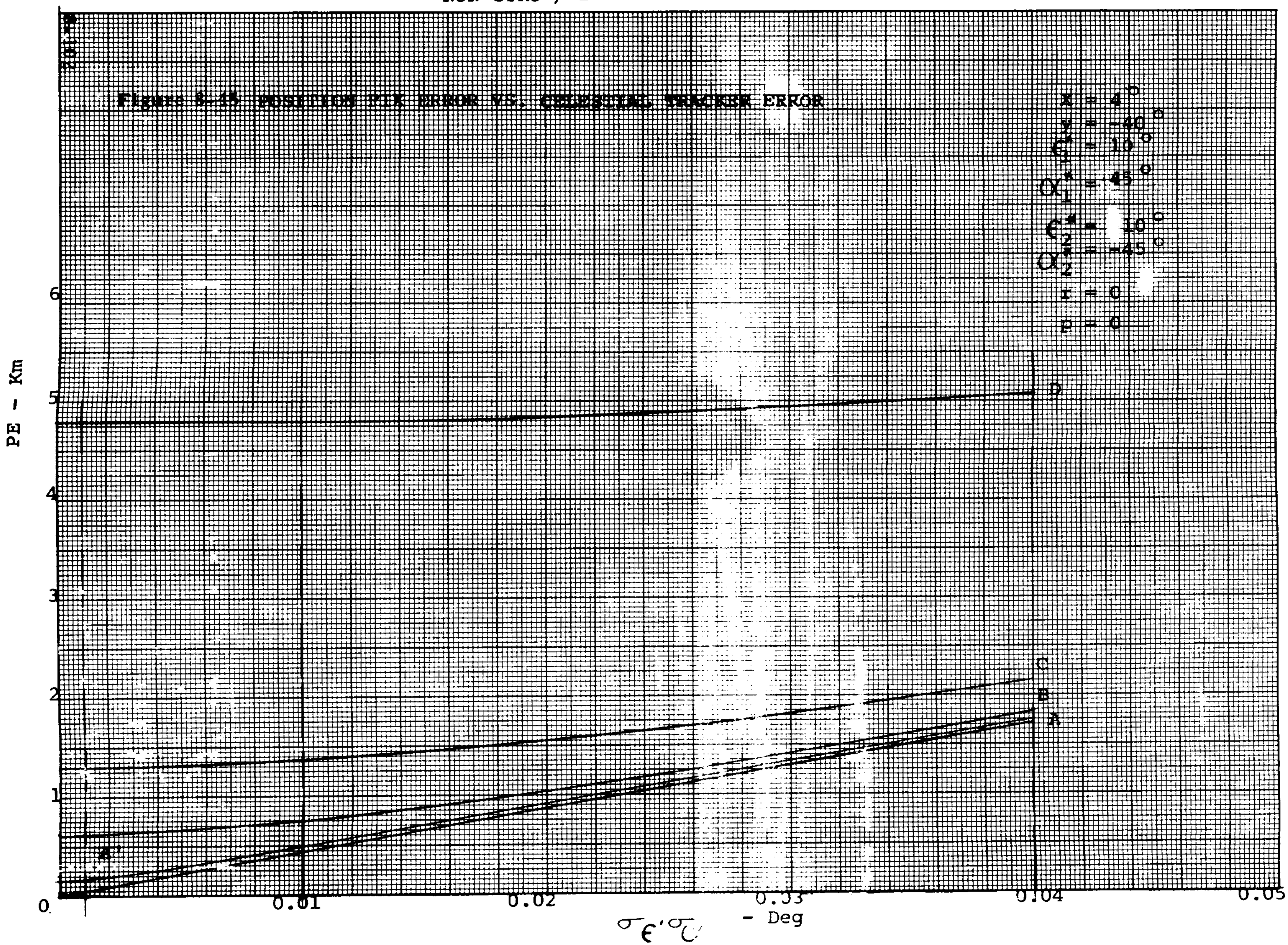

Figure 8-45 POSITION FIX ERROR VS. CELESTIAL TRACKER ERROR

NON GYRO / INERTIAL CONCEPT

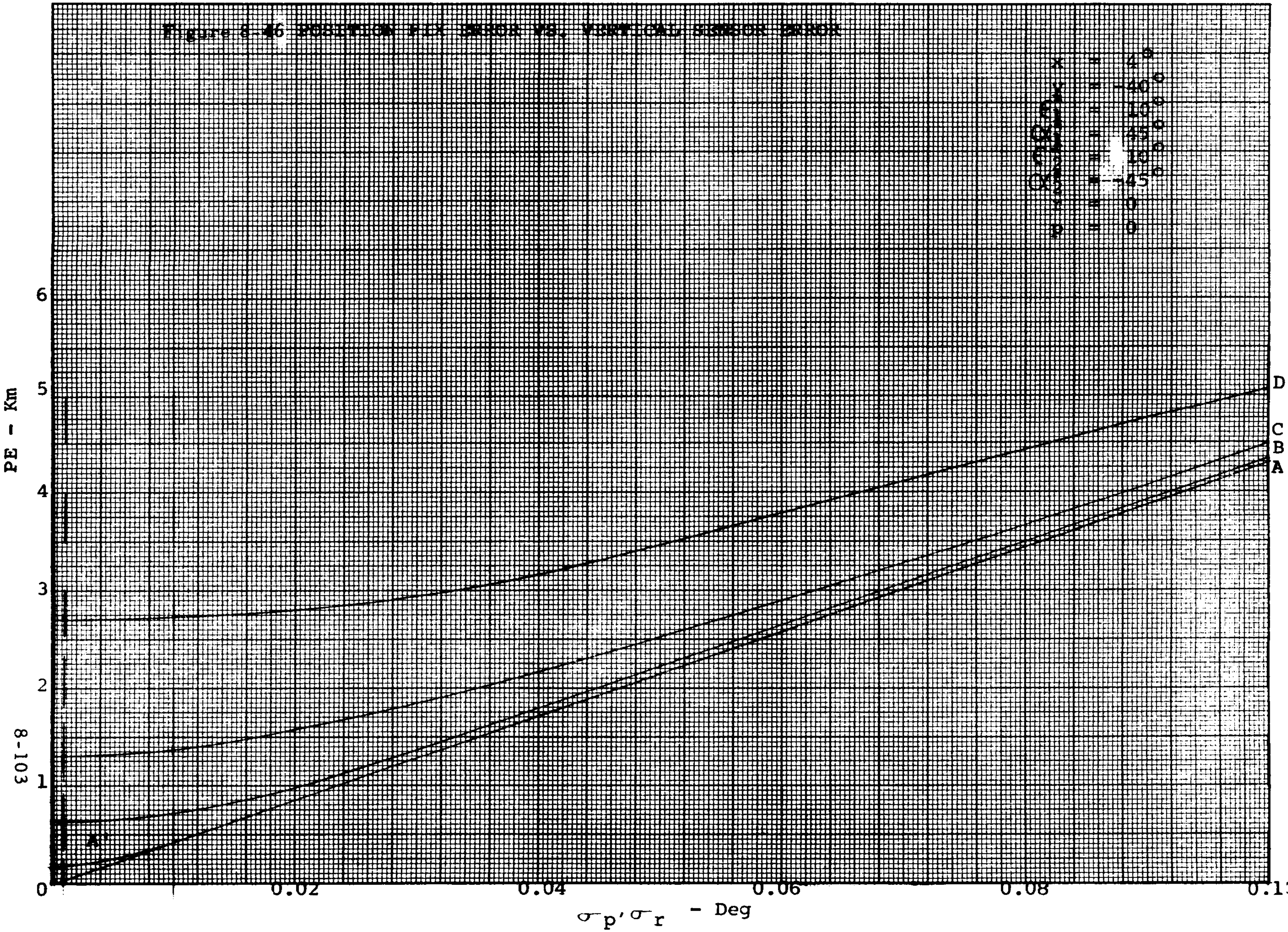

Figure 8-46 POSITION FIX ERROR VS. VERTICAL SENSOR ERROR

NON GYRO / INERTIAL CONCEPT

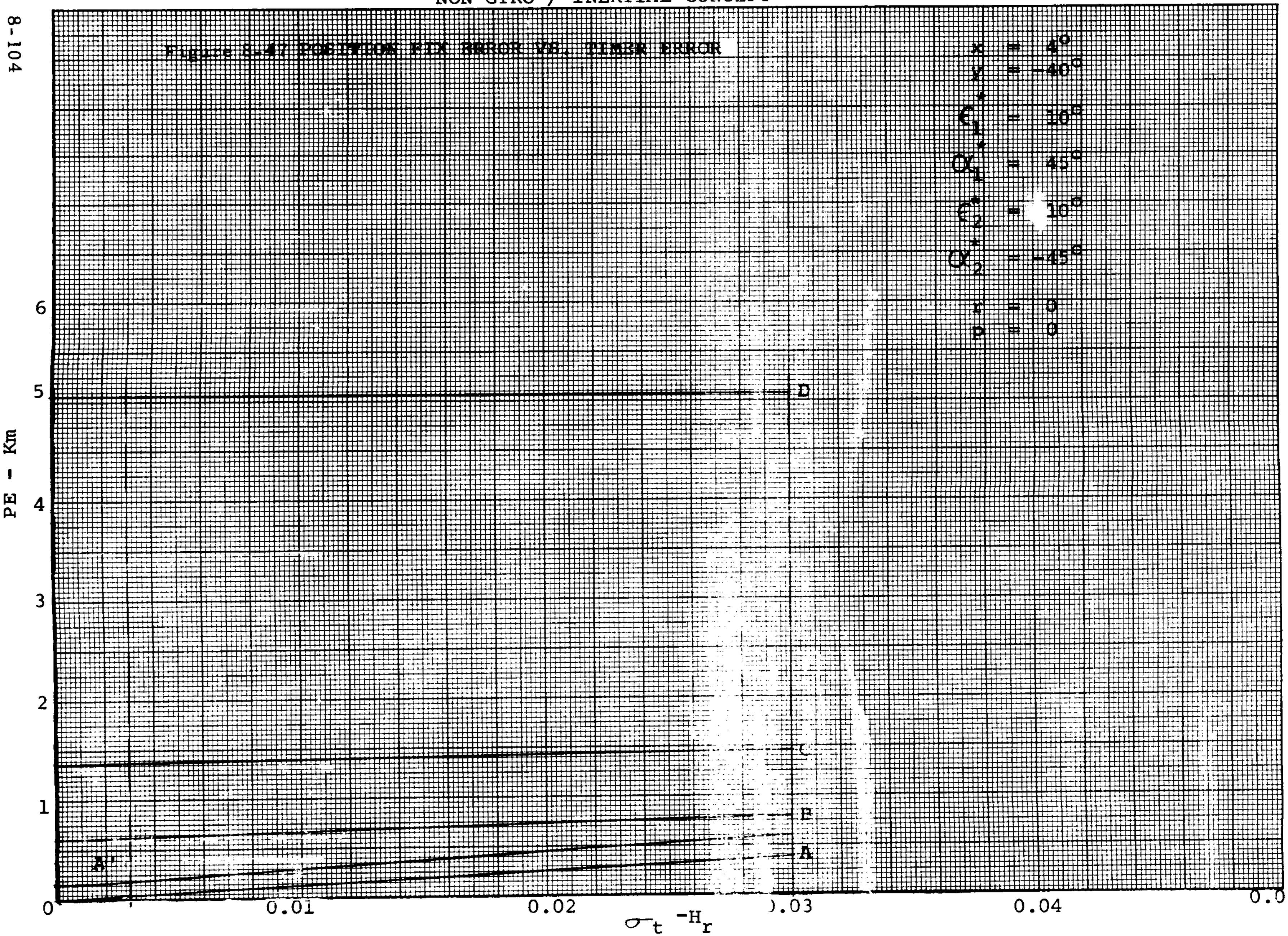

Figure 8-47 POSITION FIX ERROR VS. TIMER ERROR

NON GYRO / INERTIAL CONCEPT

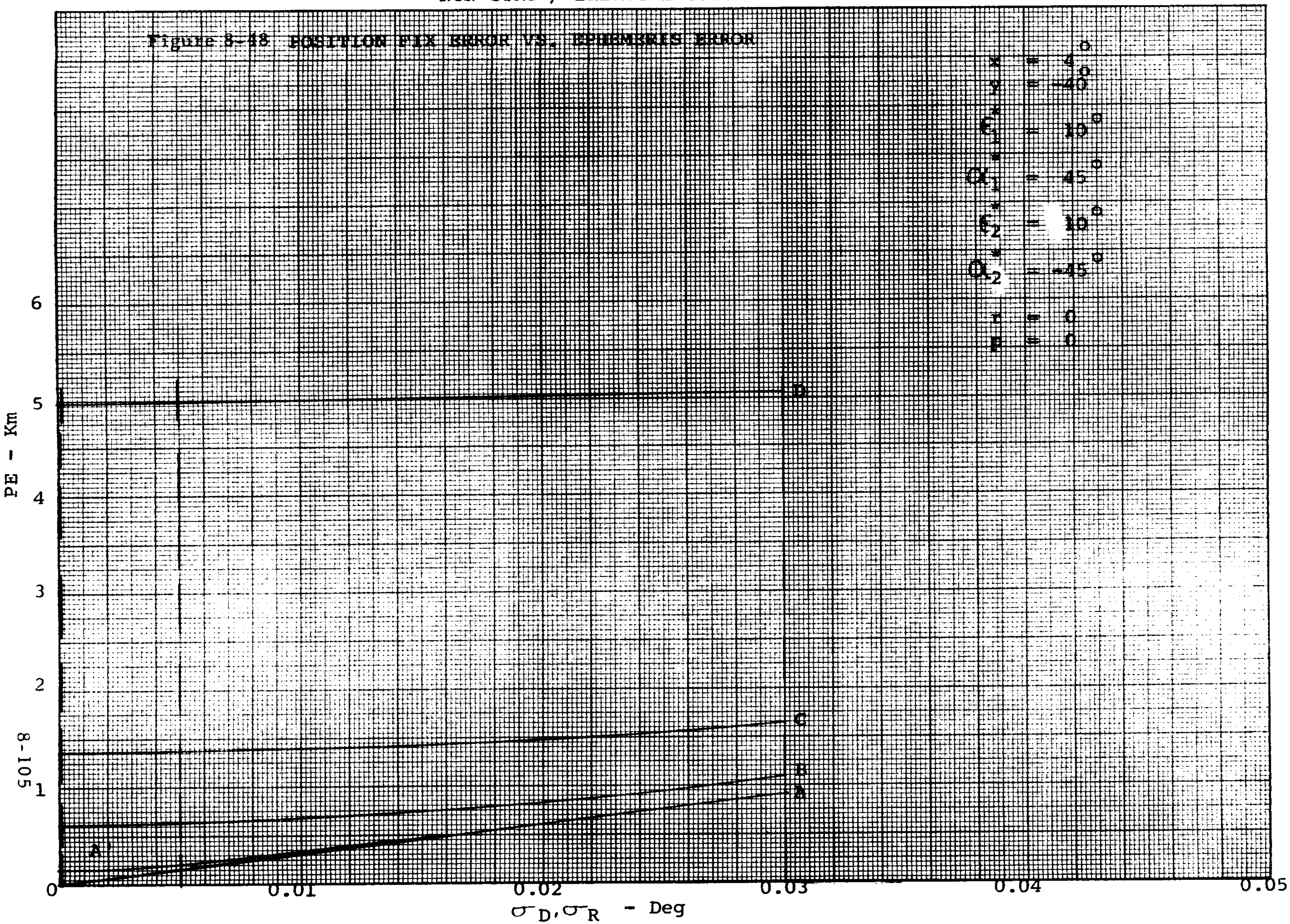

Figure 8-48 POSITION FIX ERROR VS. EPHEMERIS ERROR

NON GYRO / INERTIAL CONCEPT

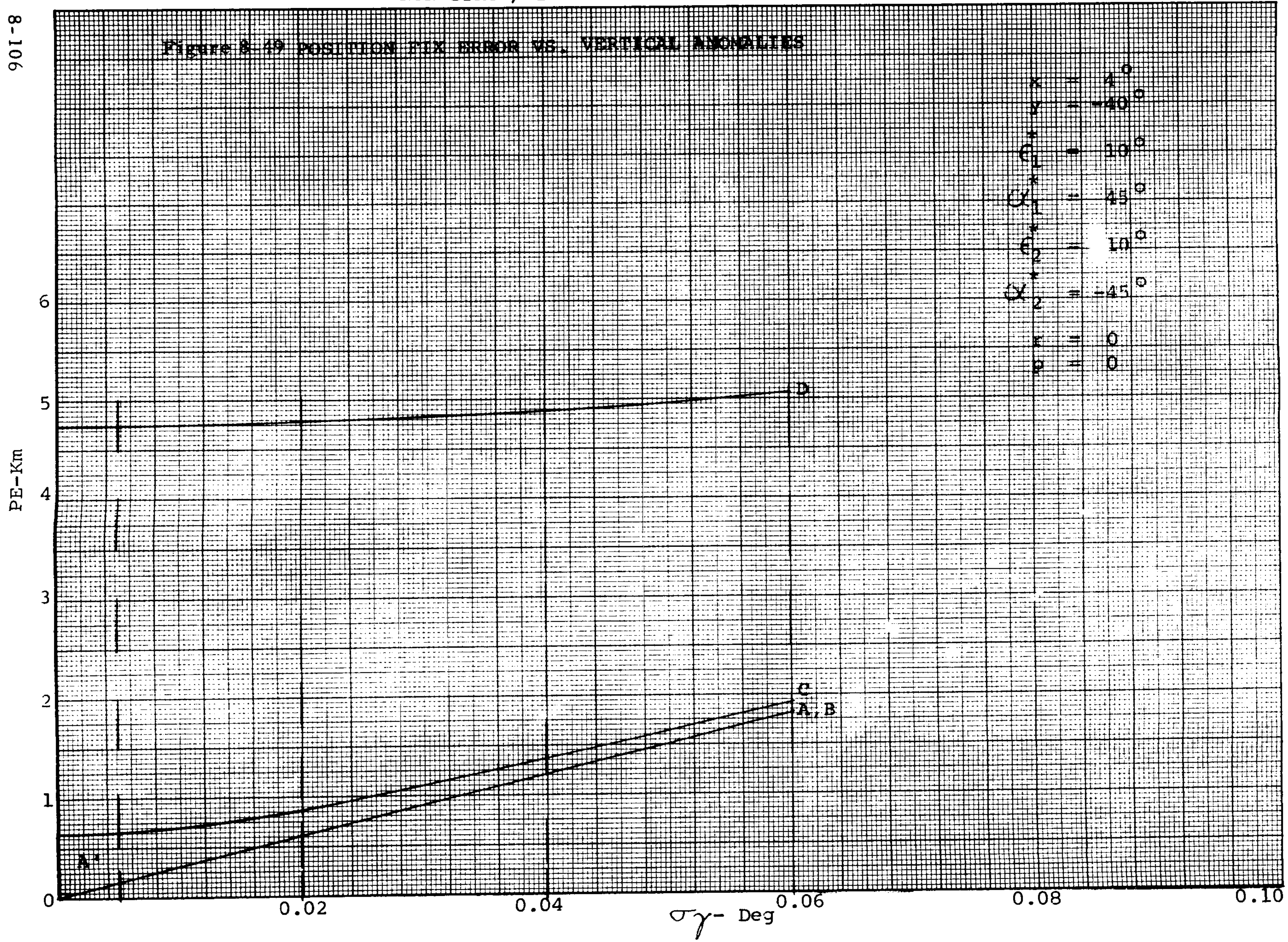

Figure 8.49 POSITION FIX ERROR VS. VERTICAL ANOMALIES

NON GYRO / INERTIAL CONCEPT

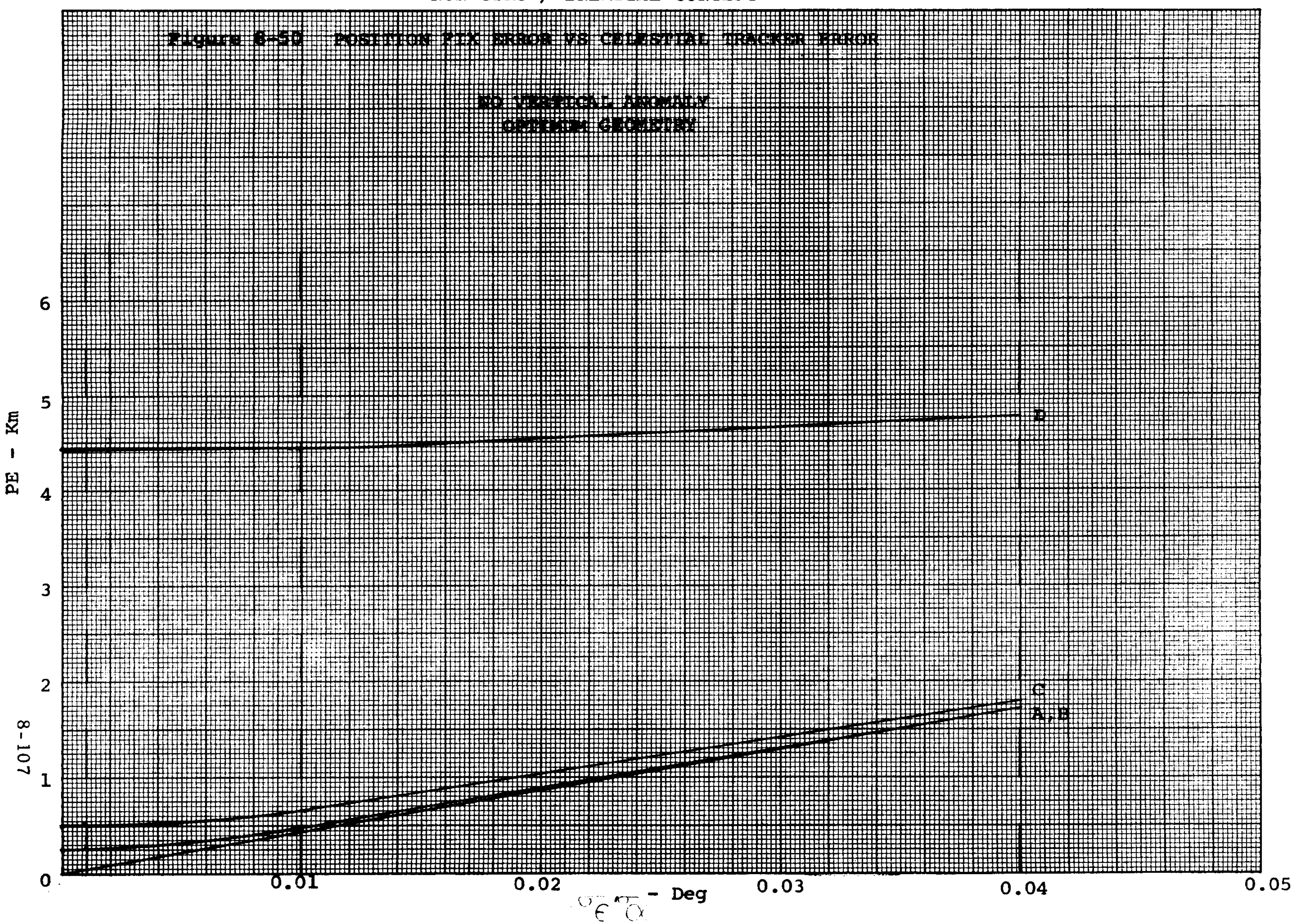

Figure 8-50 POSITION FIX ERROR VS CELESTIAL TRACKER ERROR

NON GYRO / INERTIAL CONCEPT

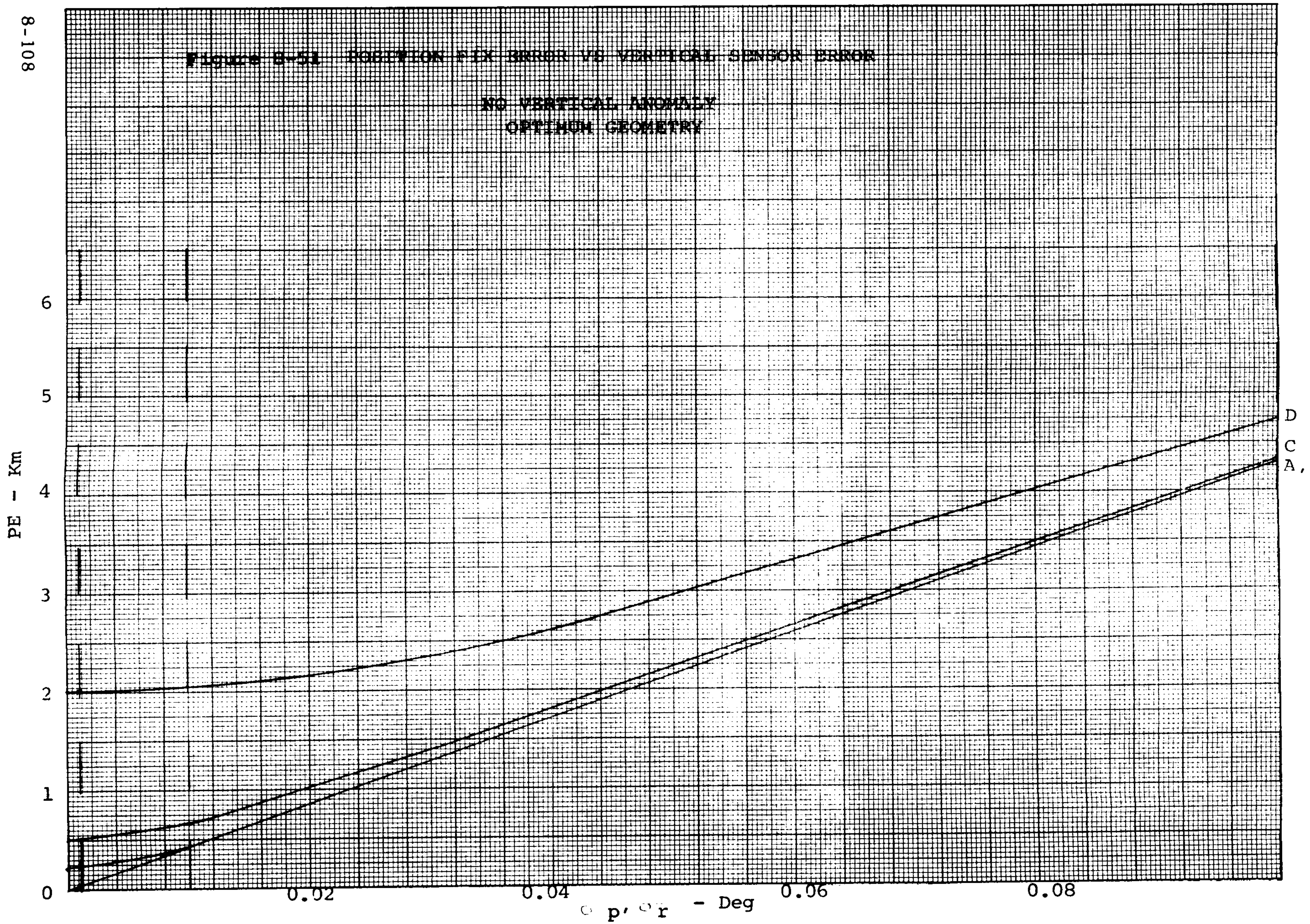

Figure 8-51 POSITION FIX ERROR VS VERTICAL SENSOR ERROR

NON GYRO / INERTIAL CONCEPT

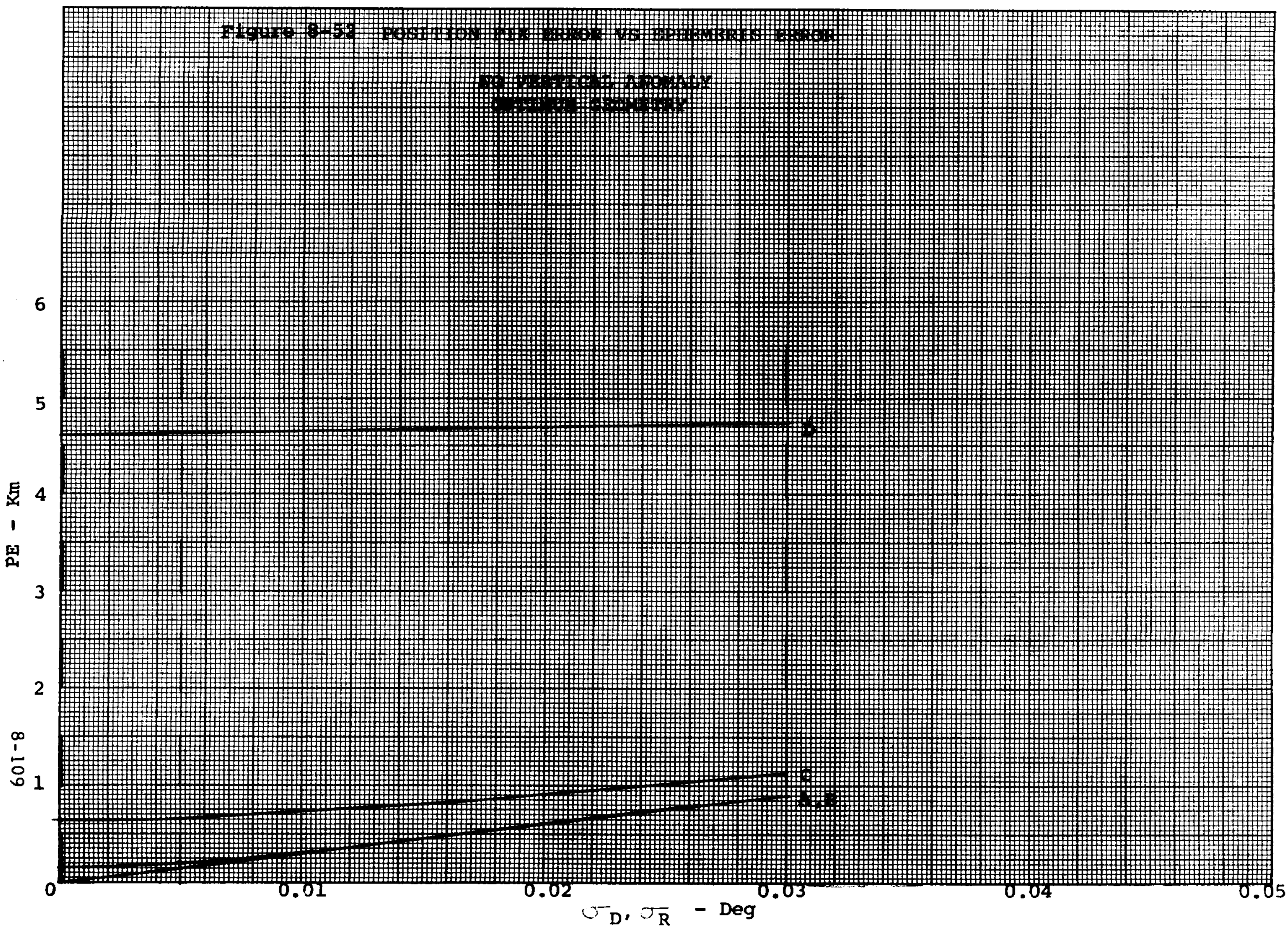

Figure 8-52 POSITION FIX ERROR VS EPHEMERIS ERROR

NO VERTICAL ANOMALY
OPTIMUM GEOMETRY

NON GYRO / INERTIAL CONCEPT

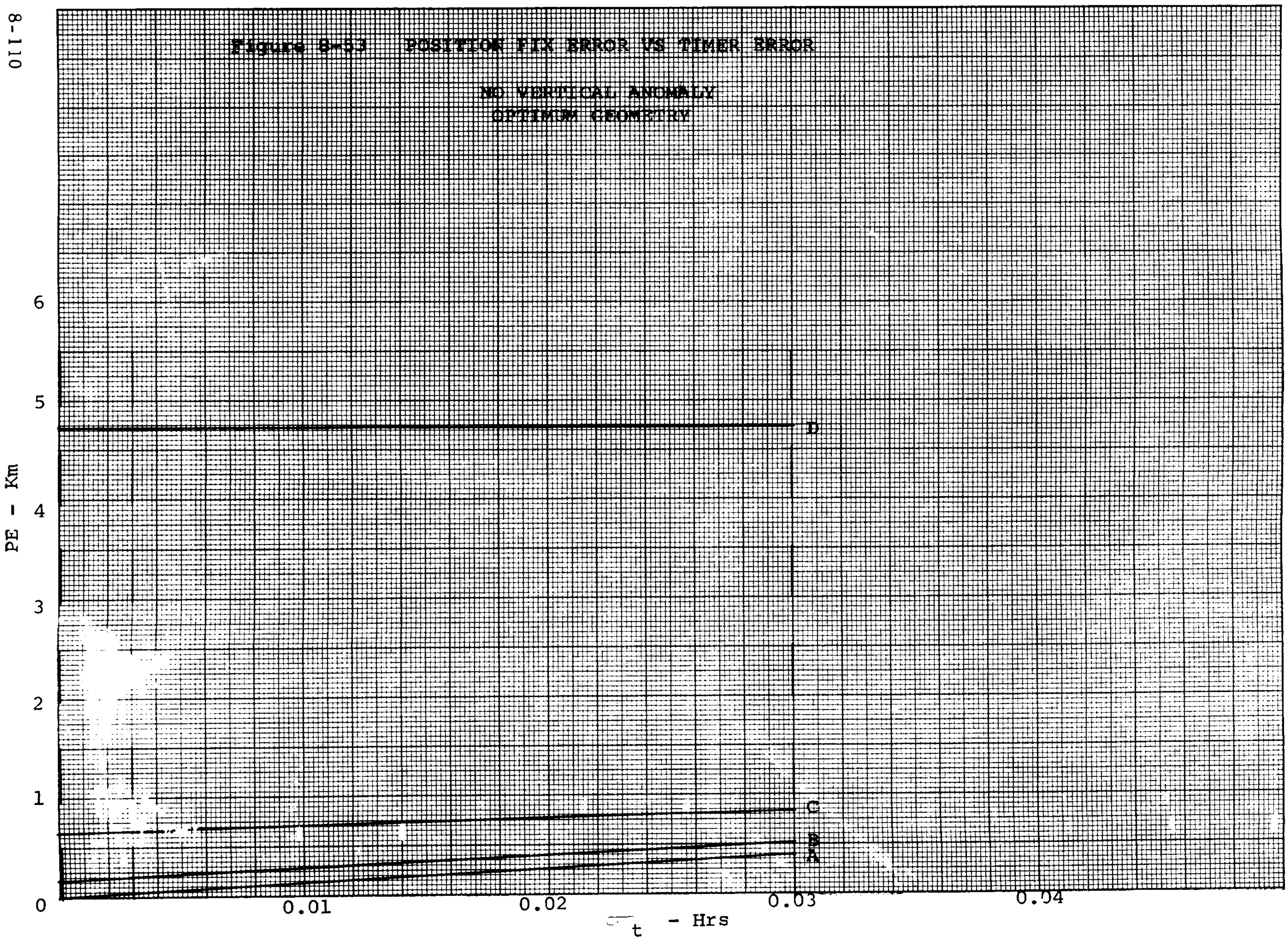

NON GYRO / INERTIAL CONCEPT

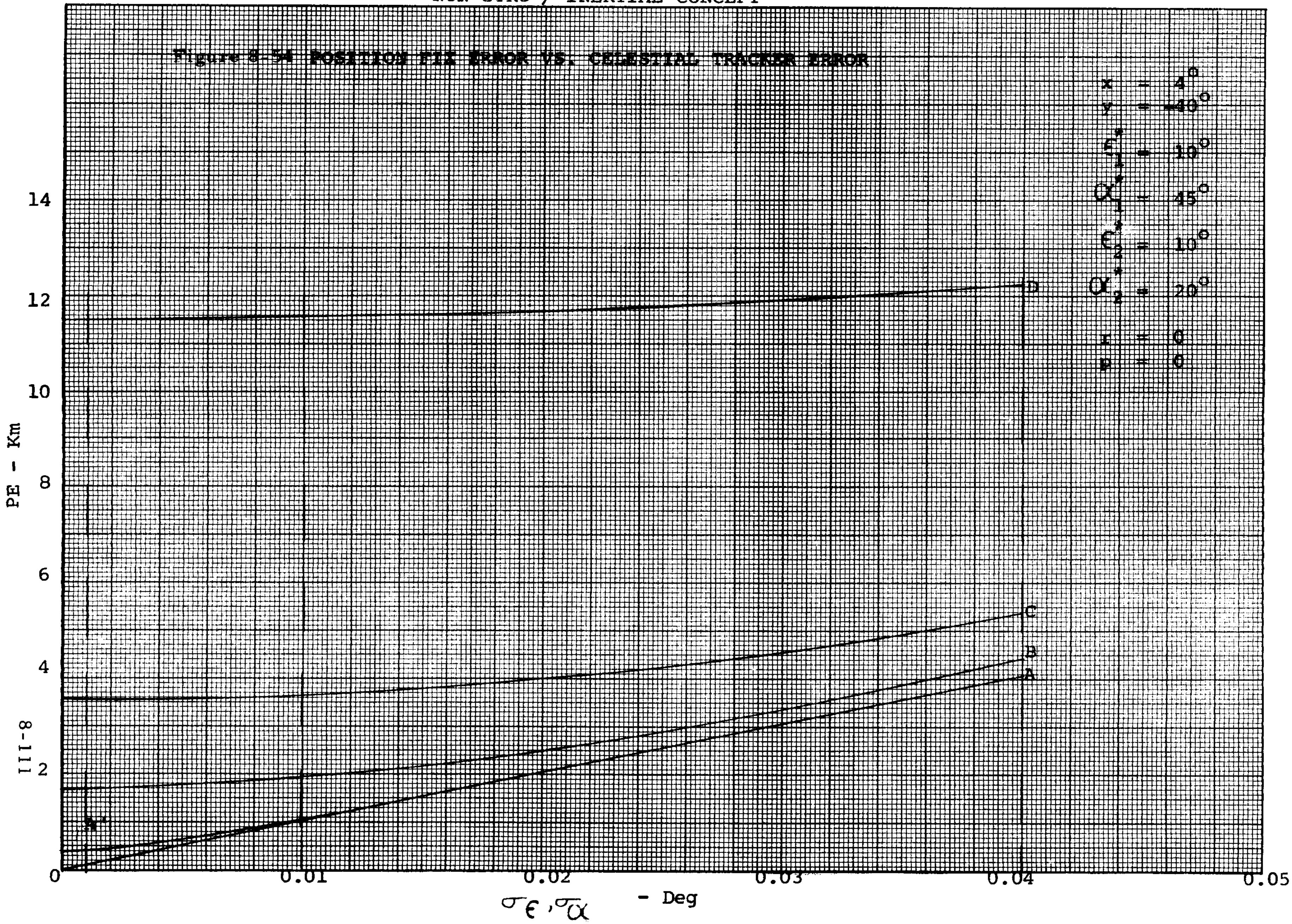

Figure 8-54 POSITION FIX ERROR VS. CELESTIAL TRACKER ERROR

NON GYRO / INERTIAL CONCEPT

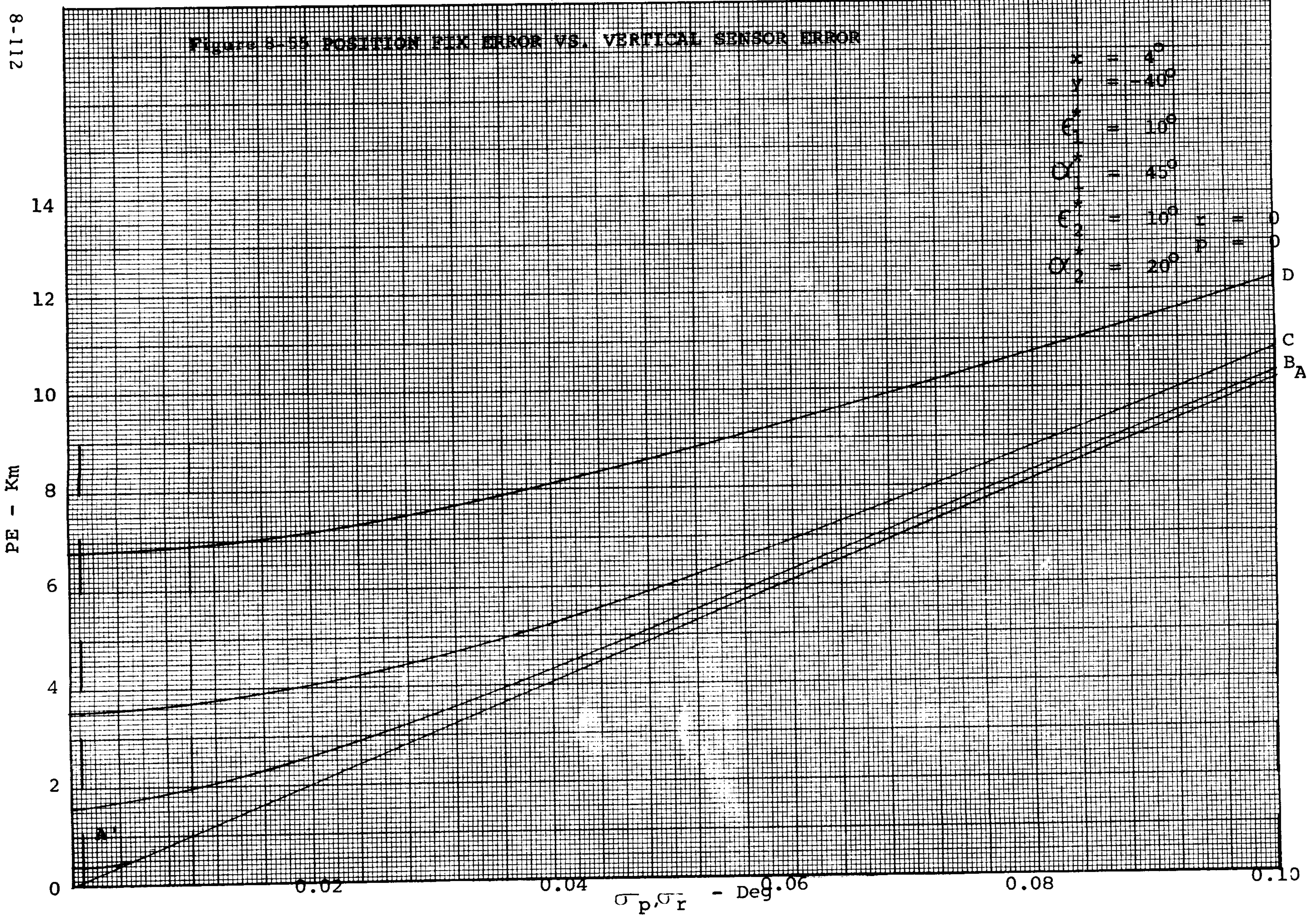

Figure 8-55 POSITION FIX ERROR VS. VERTICAL SENSOR ERROR

NON GYRO / INERTIAL CONCEPT

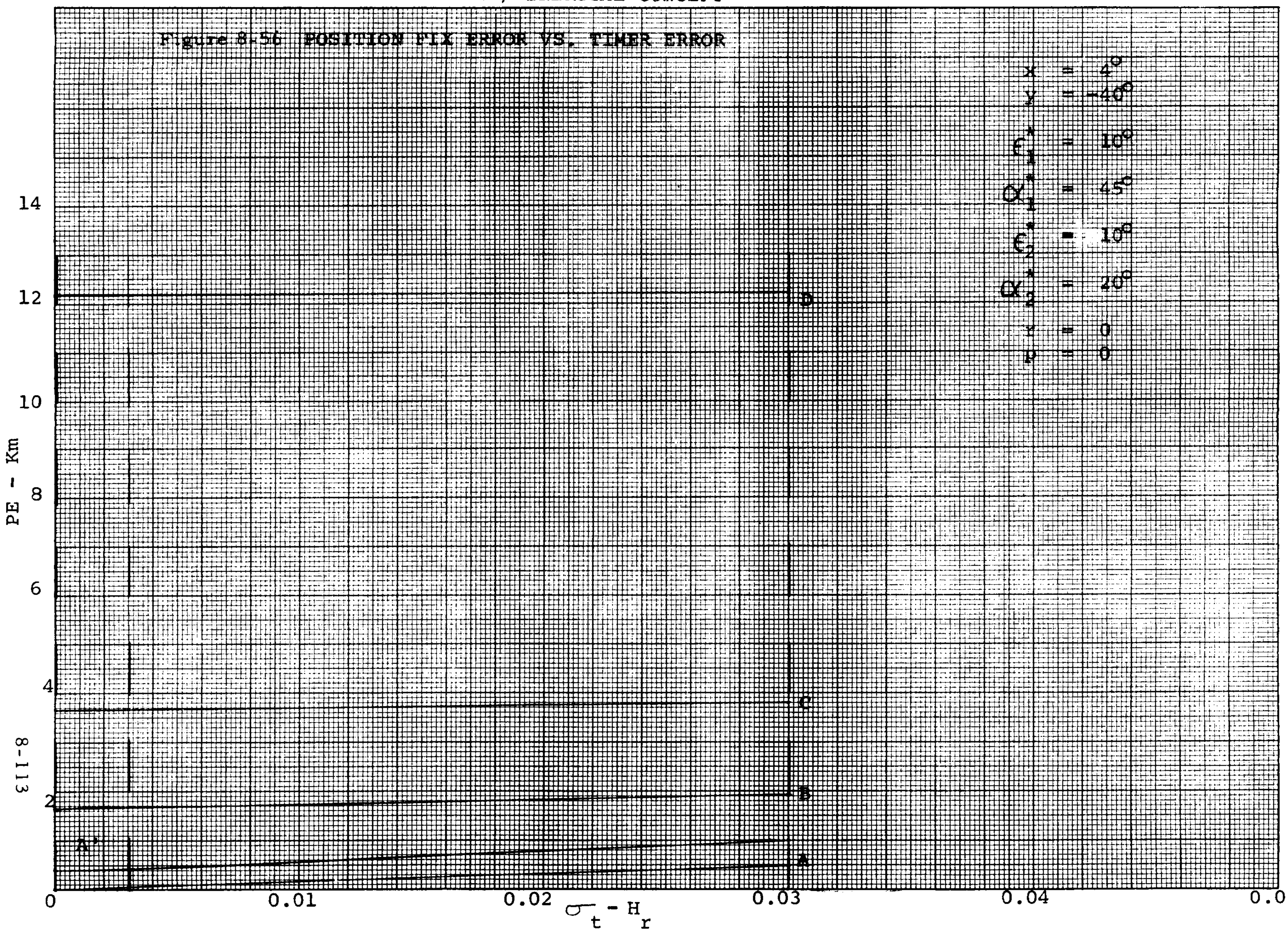

Figure 8-56 POSITION FIX ERROR VS. TIMER ERROR

NON GYRO / INERTIAL CONCEPT

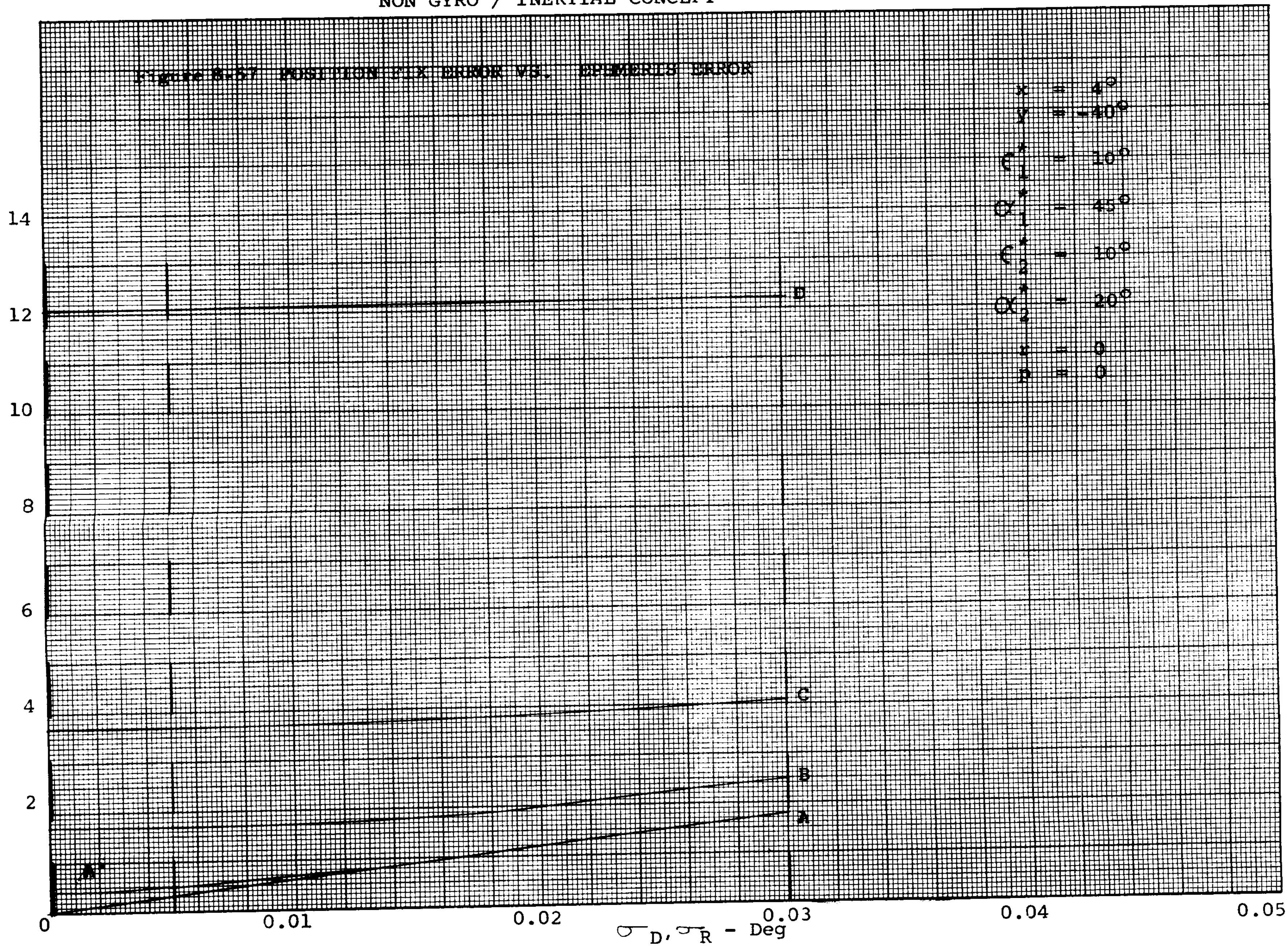

Figure 8-57 POSITION FIX ERROR VS. EPHEMERIS ERROR

NON GYRO / INERTIAL CONCEPT

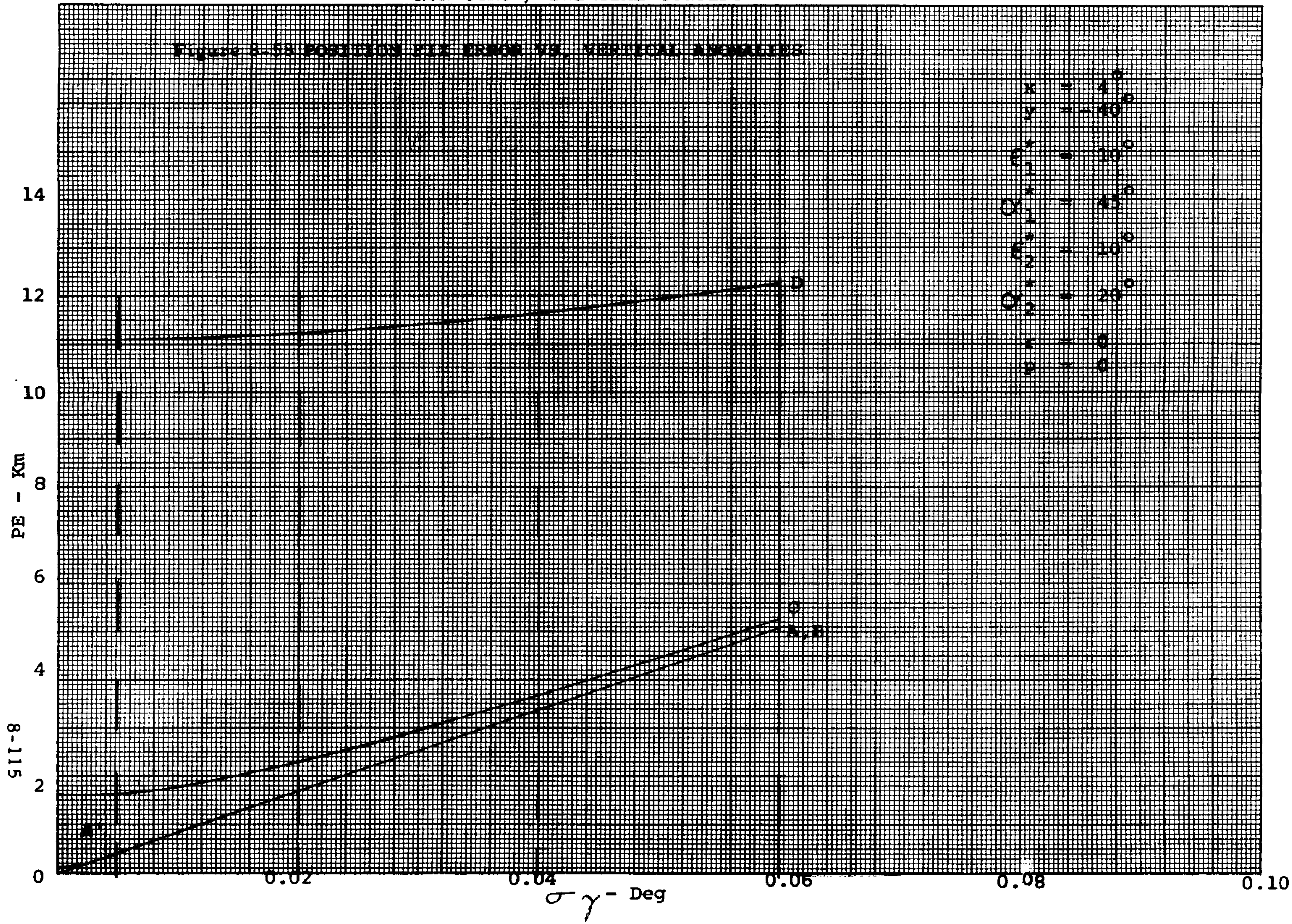

Figure 8-58 POSITION FIX ERROR VS. VERTICAL ANOMALIES

NON GYRO / INERTIAL CONCEPT

Figure 8-59 INITIAL AZIMUTH ERROR VS. CELESTIAL TRACKER ERROR

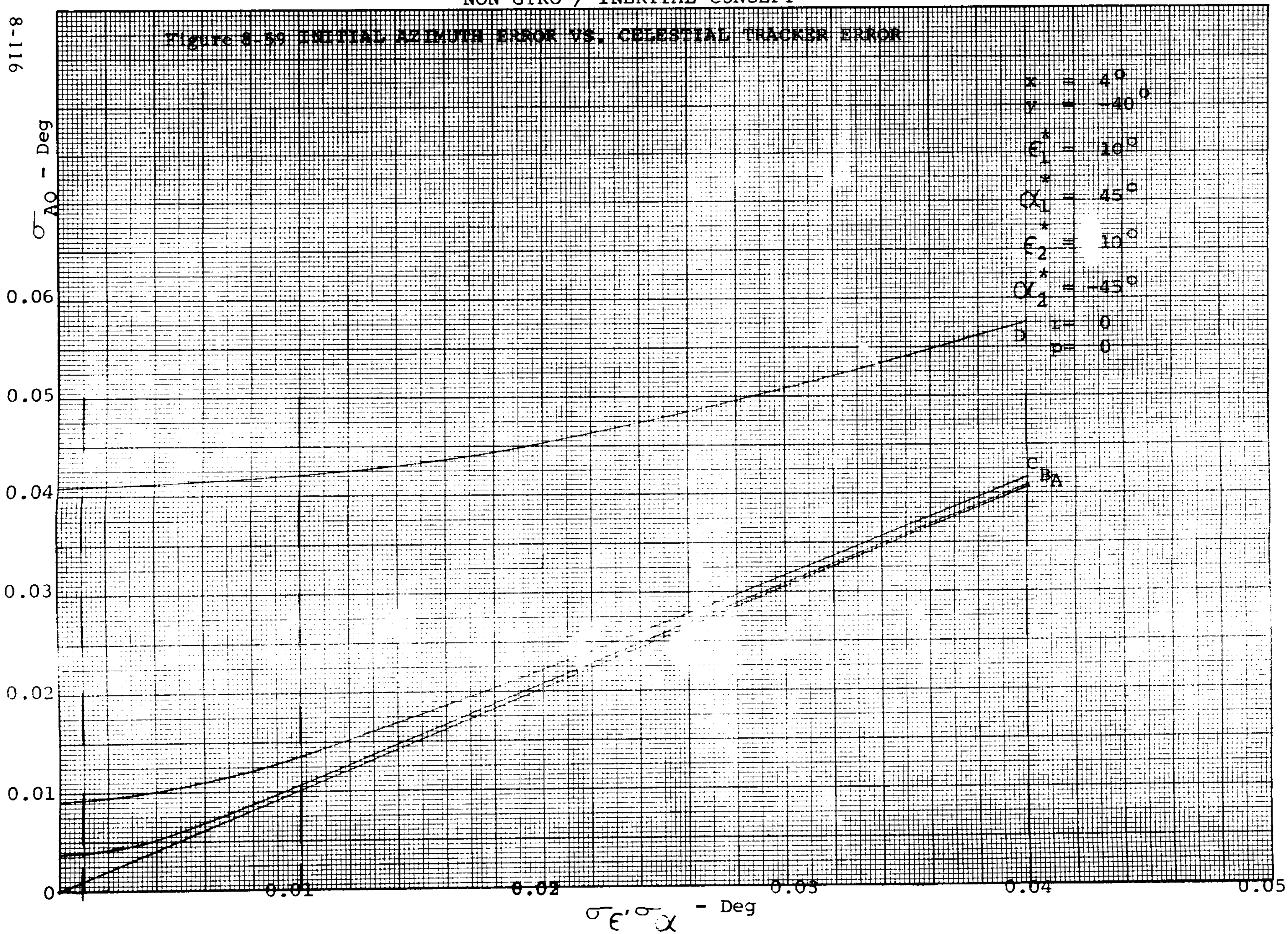

NON GYRO / INERTIAL CONCEPT

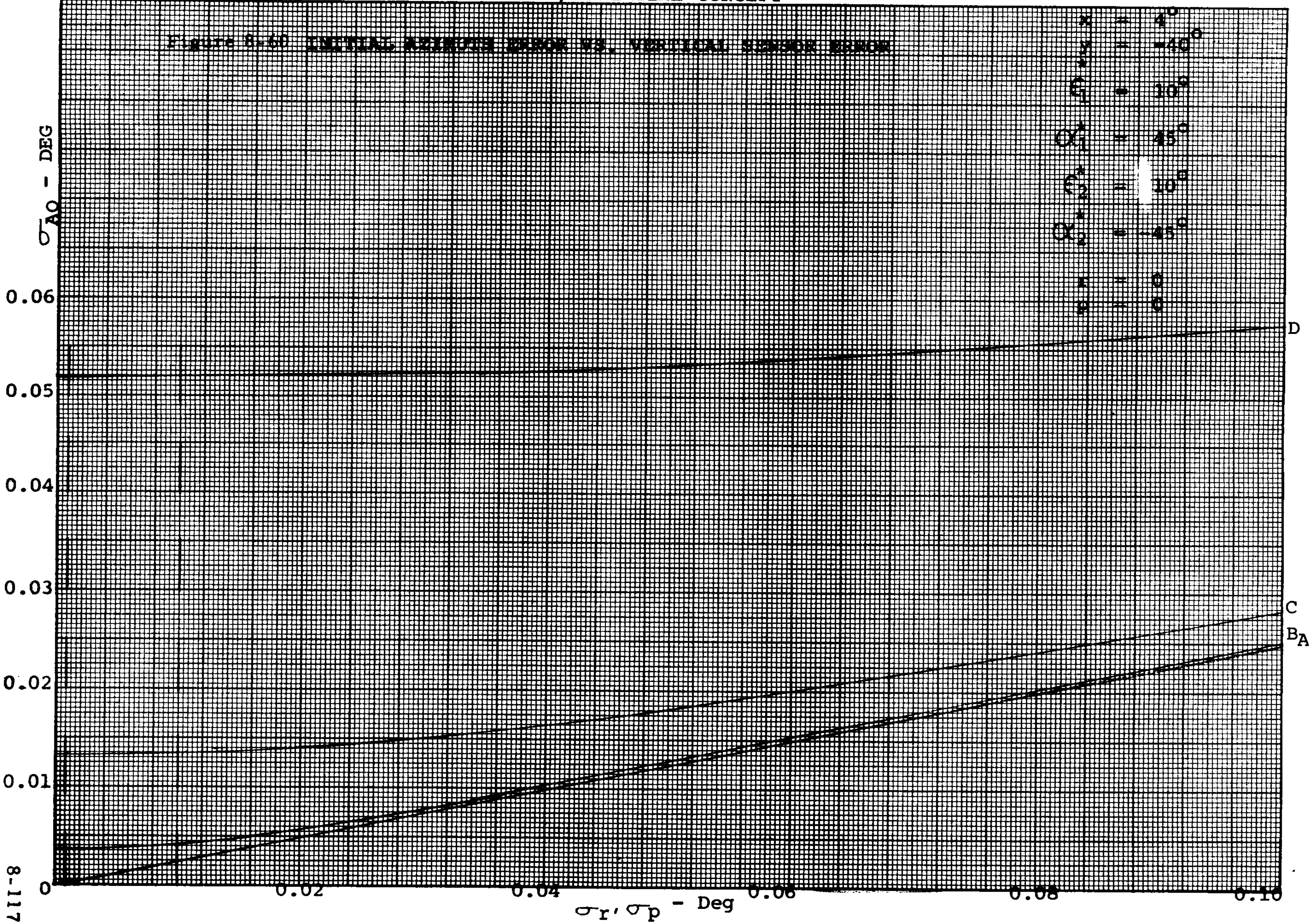

Figure 8-60 INITIAL AZIMUTH ERROR VS. VERTICAL SENSOR ERROR

NON GYRO / INERTIAL CONCEPT

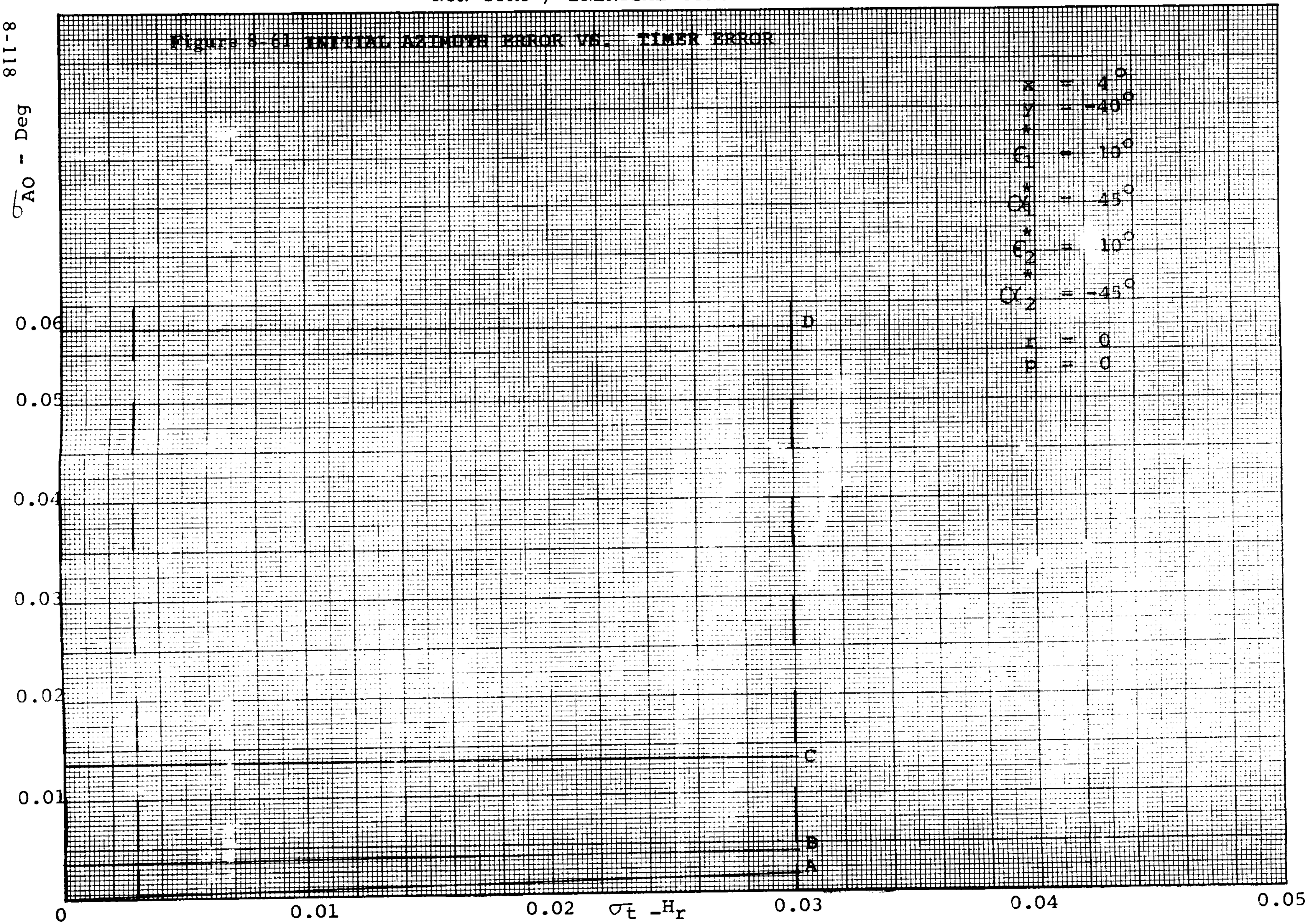

Figure 8-61 INITIAL AZIMUTH ERROR VS. TIMER ERROR

NON GYRO / INERTIAL CONCEPT

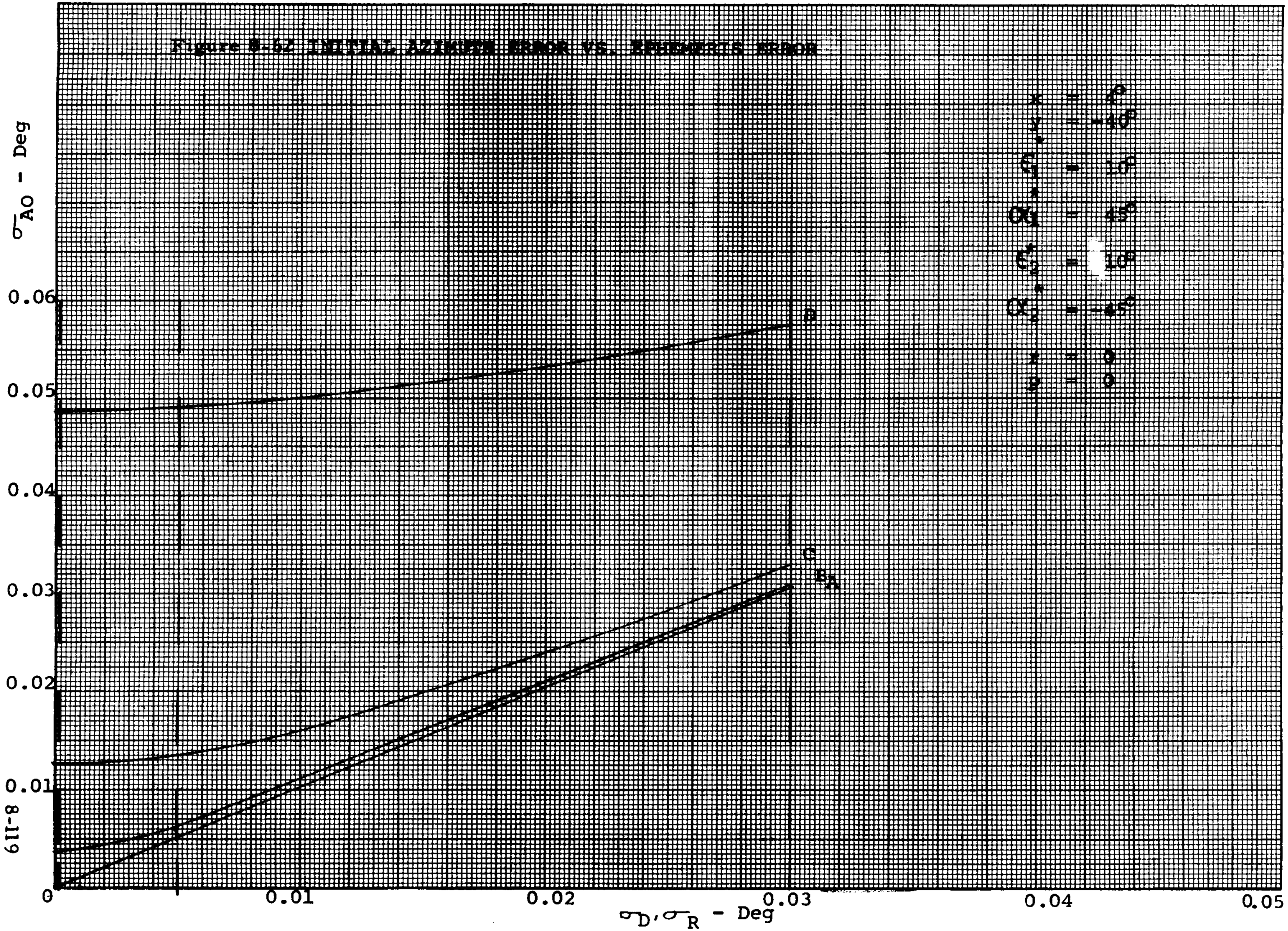

Figure 8-62 INITIAL AZIMUTH ERROR VS. EPHEMERIS ERROR

NON GYRO / INERTIAL CONCEPT

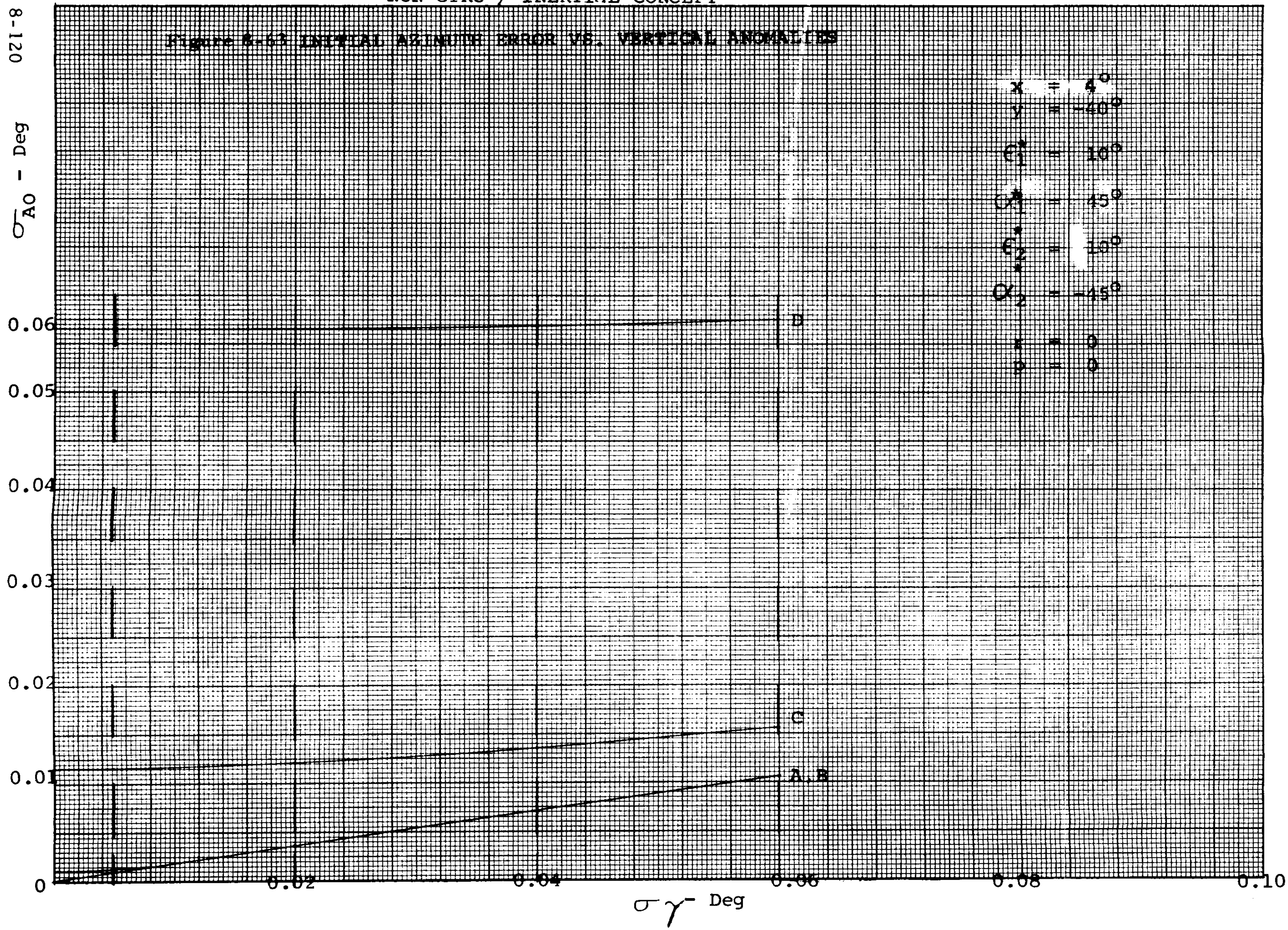

Figure 8-63 INITIAL AZIMUTH ERROR VS. VERTICAL ANOMALIES

NON GYRO / INERTIAL CONCEPT

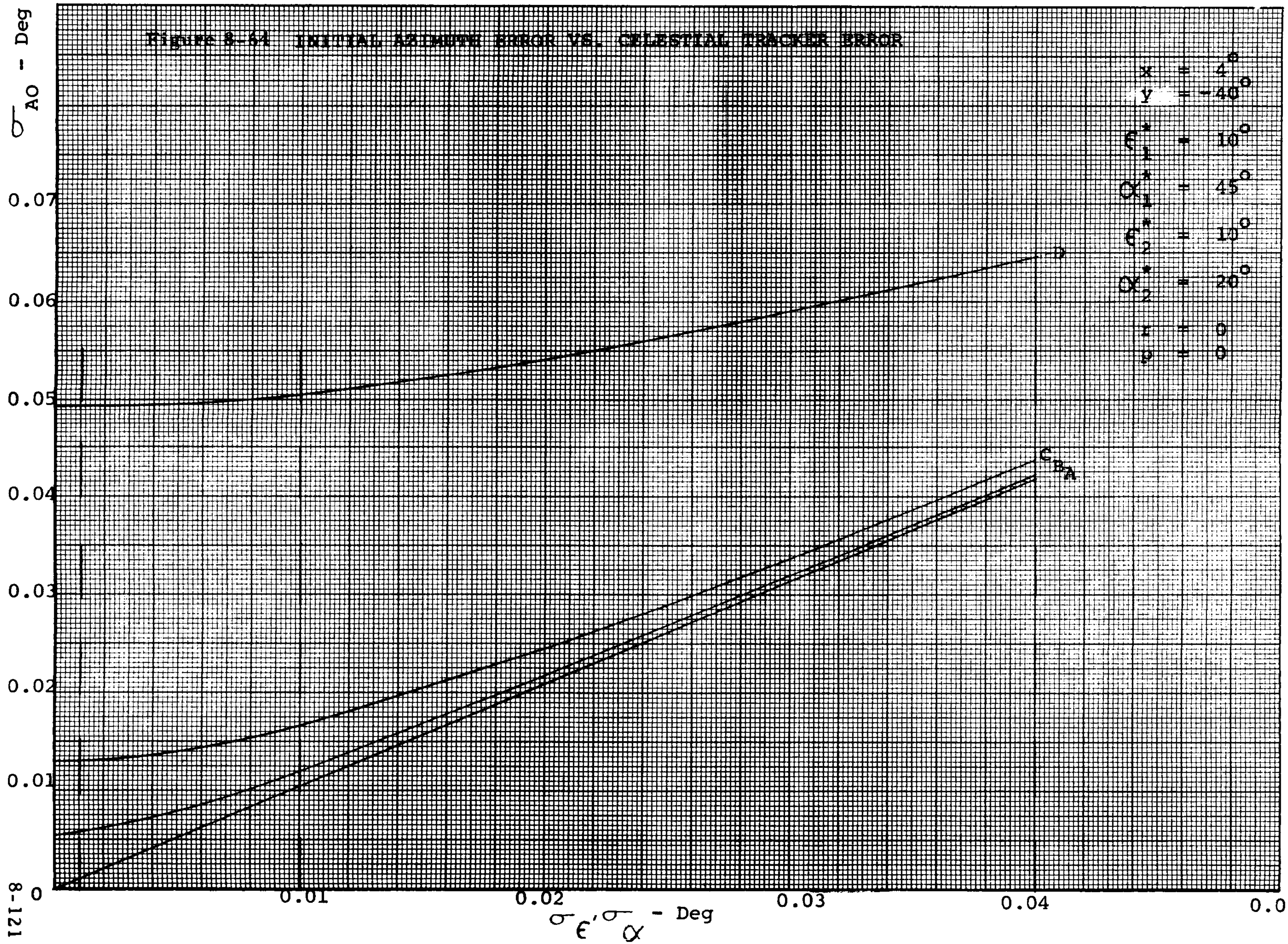

Figure 8-65 NON GYRO / INERTIAL CONCEPT

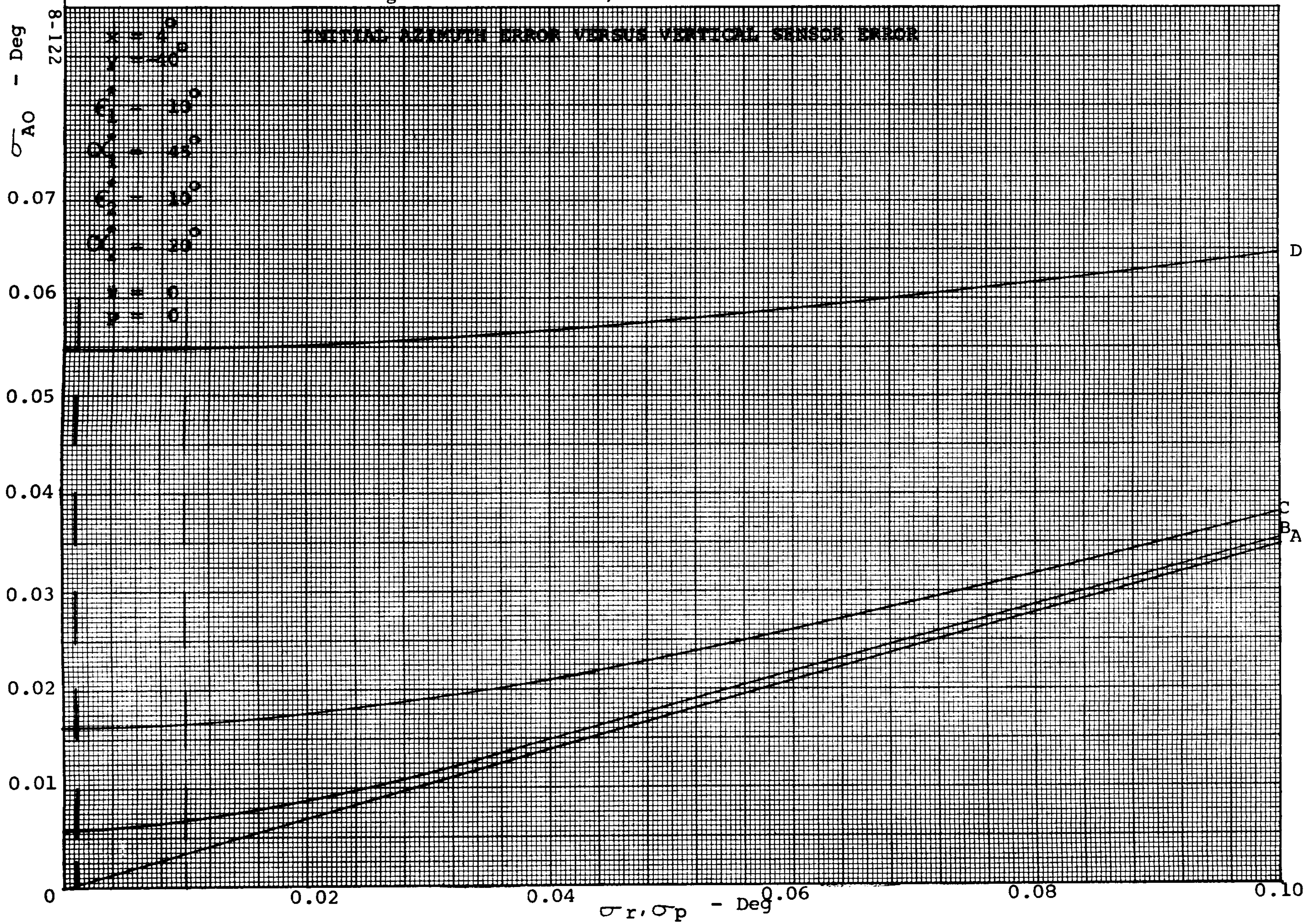

NON GYRO / INERTIAL CONCEPT

Figure 8-66 INITIAL AZIMUTH ERROR VS. TIMER ERROR

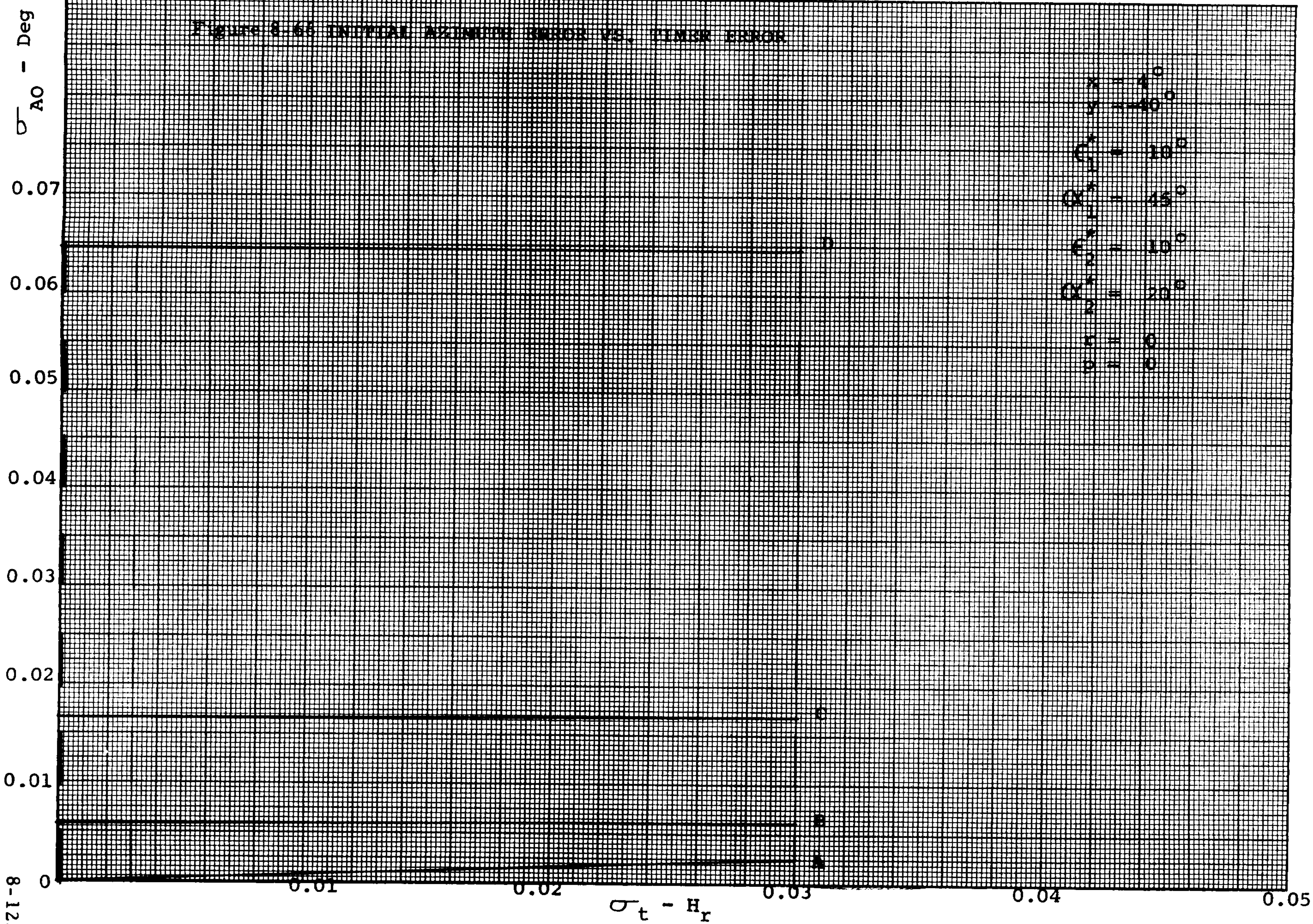

NON GYRO / INERTIAL CONCEPT

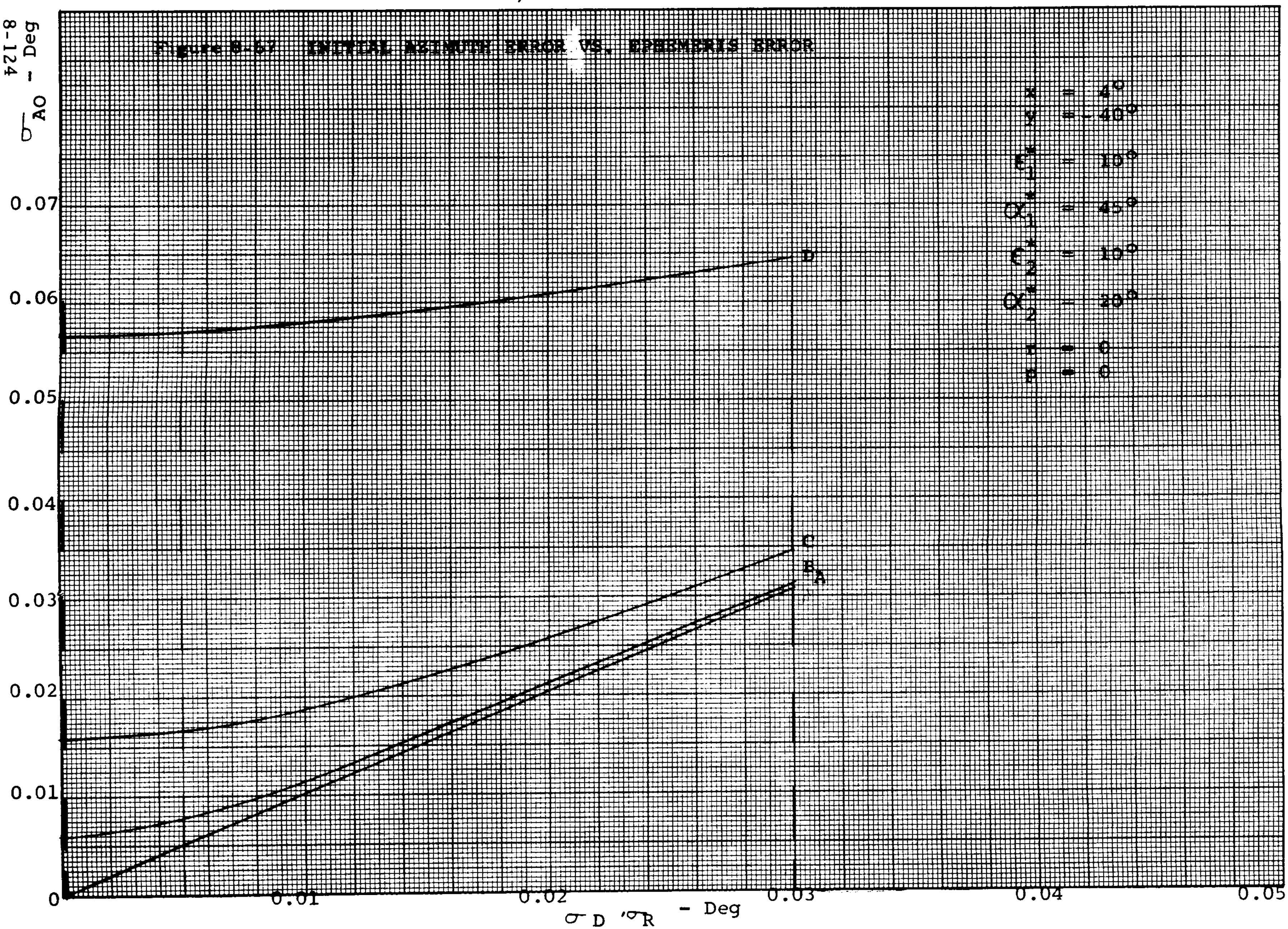

Figure 8-67 INITIAL AZIMUTH ERROR VS. EPHEMERIS ERROR

NON GYRO / INERTIAL CONCEPT

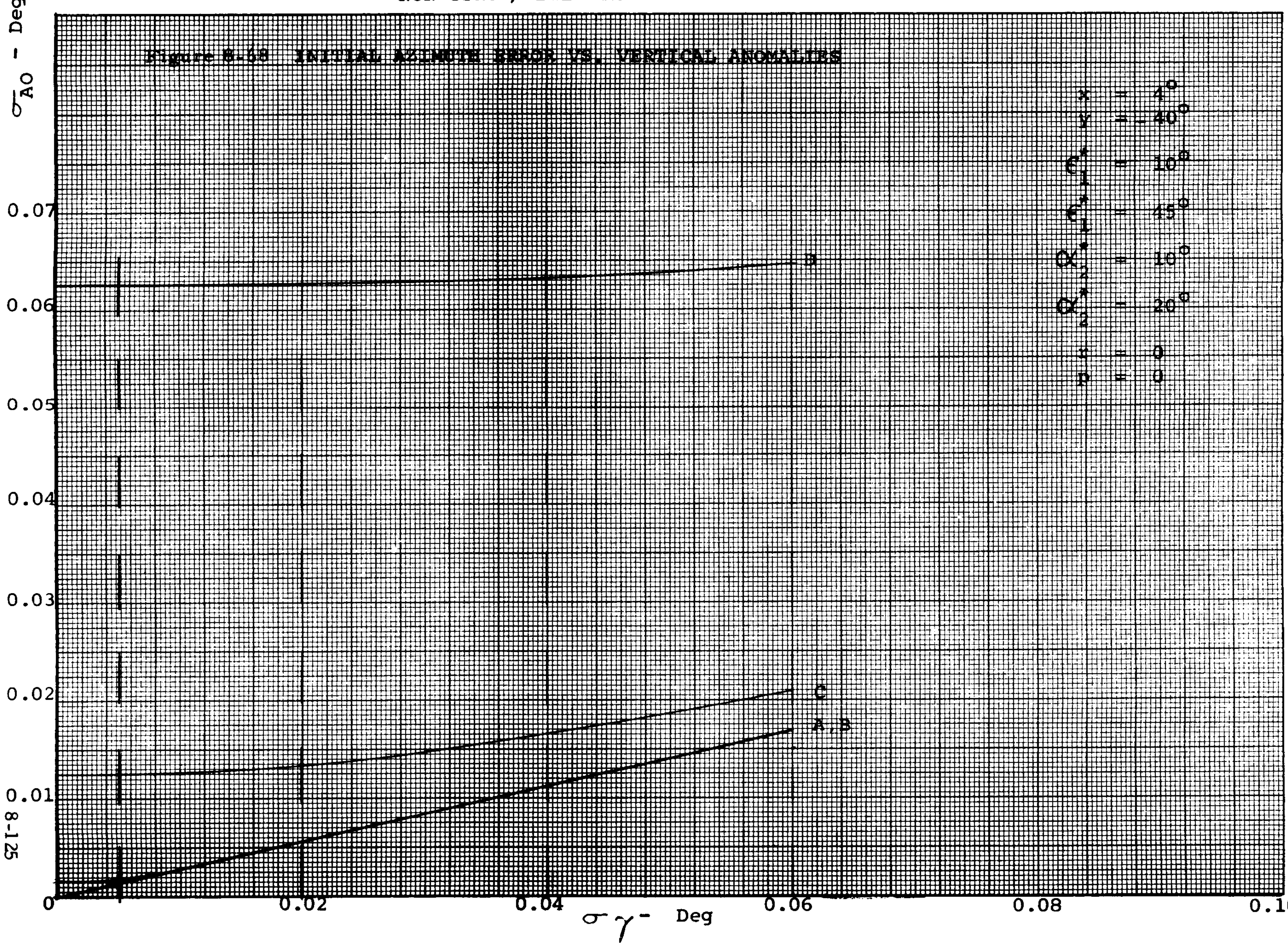

Figure 8-68 INITIAL AZIMUTH ERROR VS. VERTICAL ANOMALIES

NON GYRO / INERTIAL CONCEPT

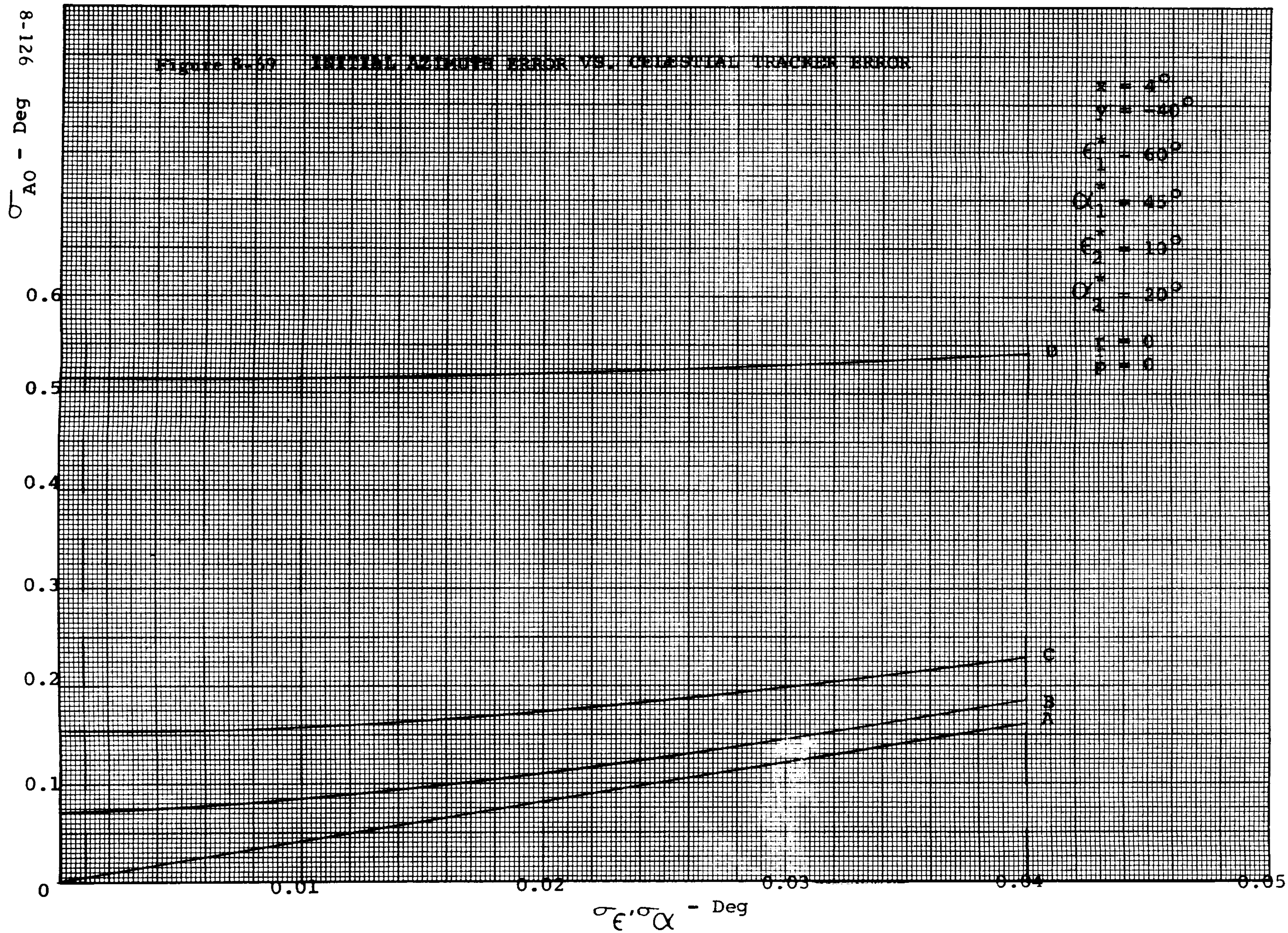

Figure 8-69 INITIAL AZIMUTH ERROR VS. CELESTIAL TRACKER ERROR

921-8

NON GYRO / INERTIAL CONCEPT

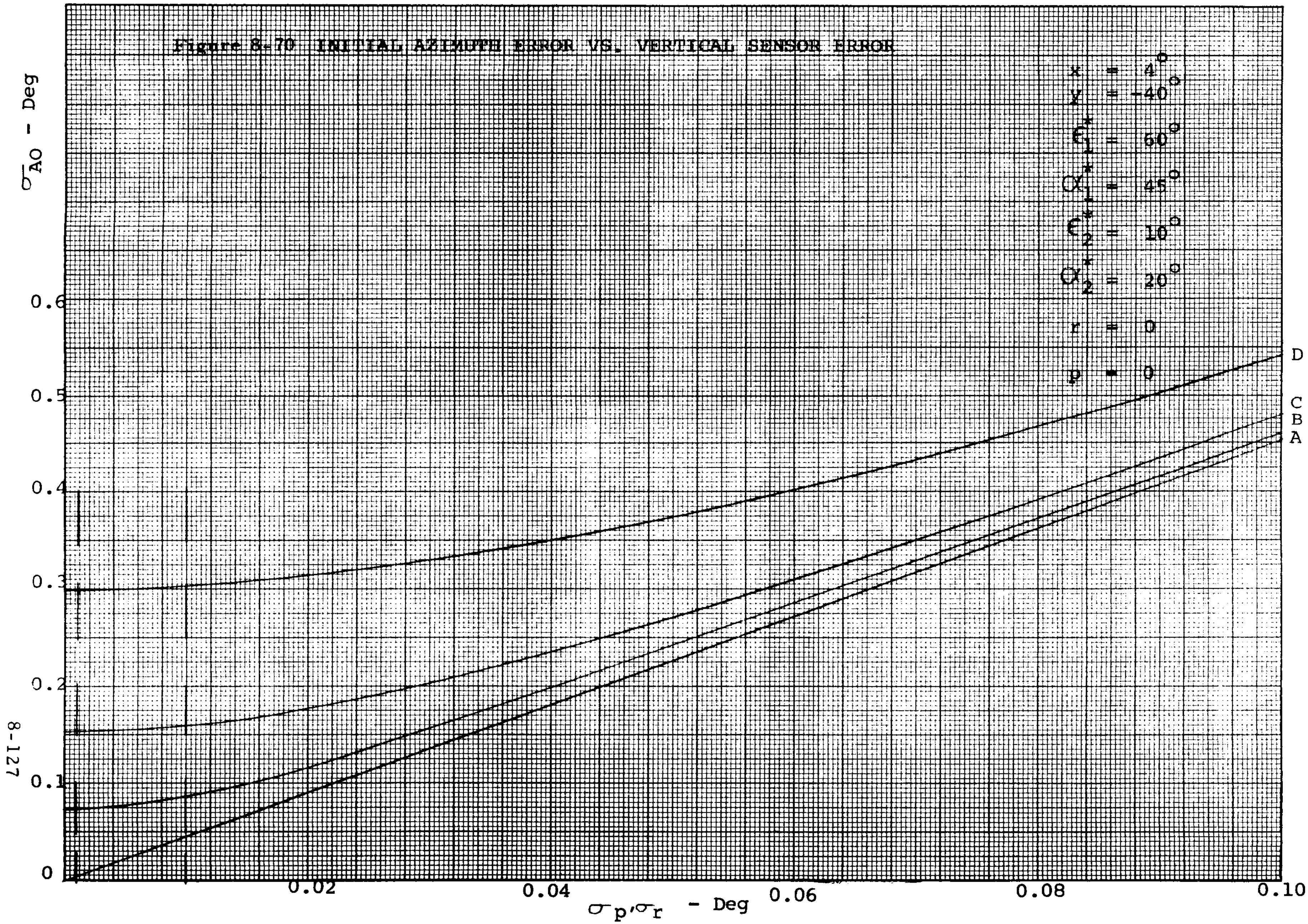

Figure 8-70 INITIAL AZIMUTH ERROR VS. VERTICAL SENSOR ERROR

NON GYRO / INERTIAL CONCEPT

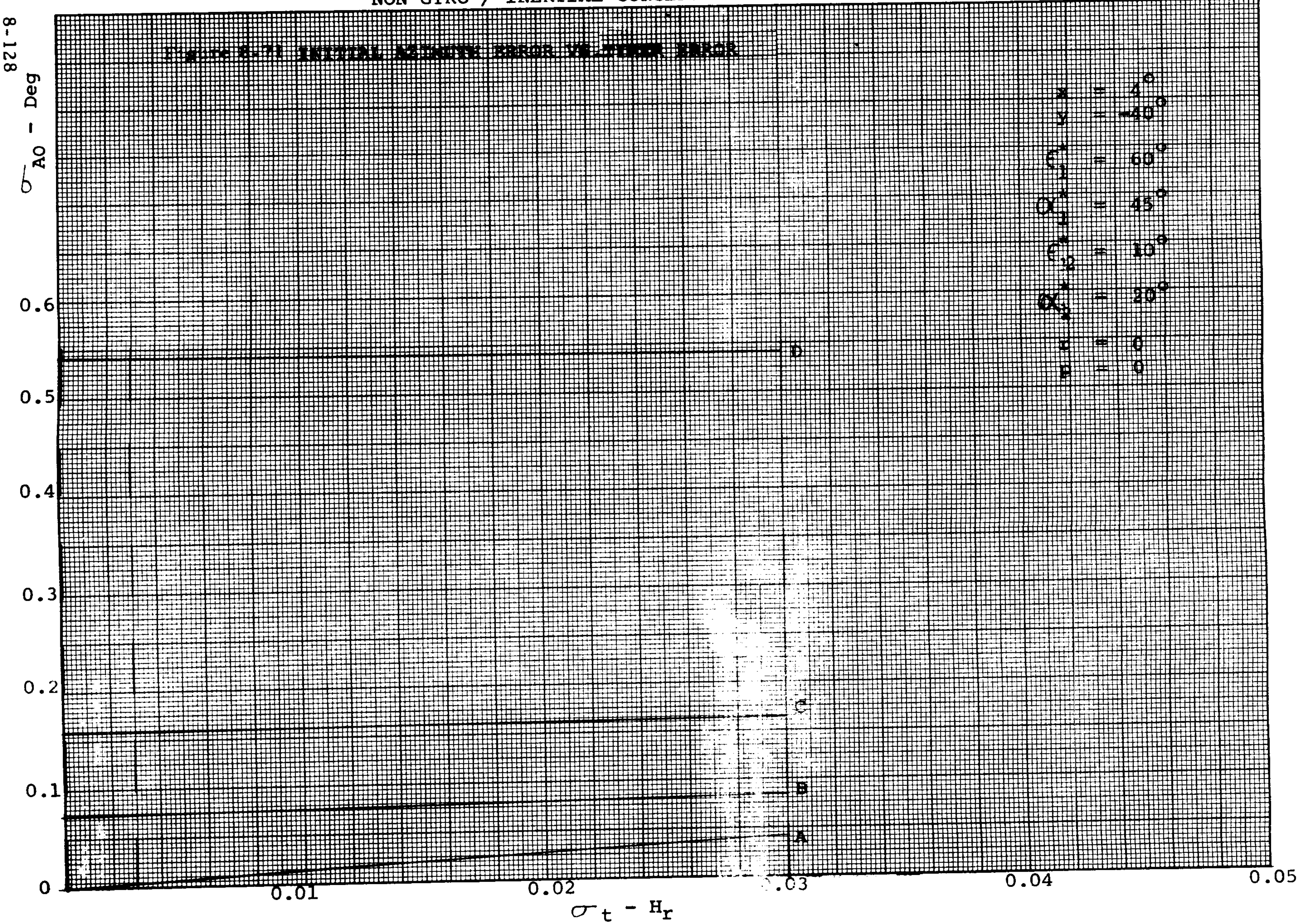

Figure 8-71 INITIAL AZIMUTH ERROR VS TIMER ERROR

NON GYRO / INERTIAL CONCEPT

Figure 8-72 INITIAL AZIMUTH ERROR VS. EPHEMERIS ERROR

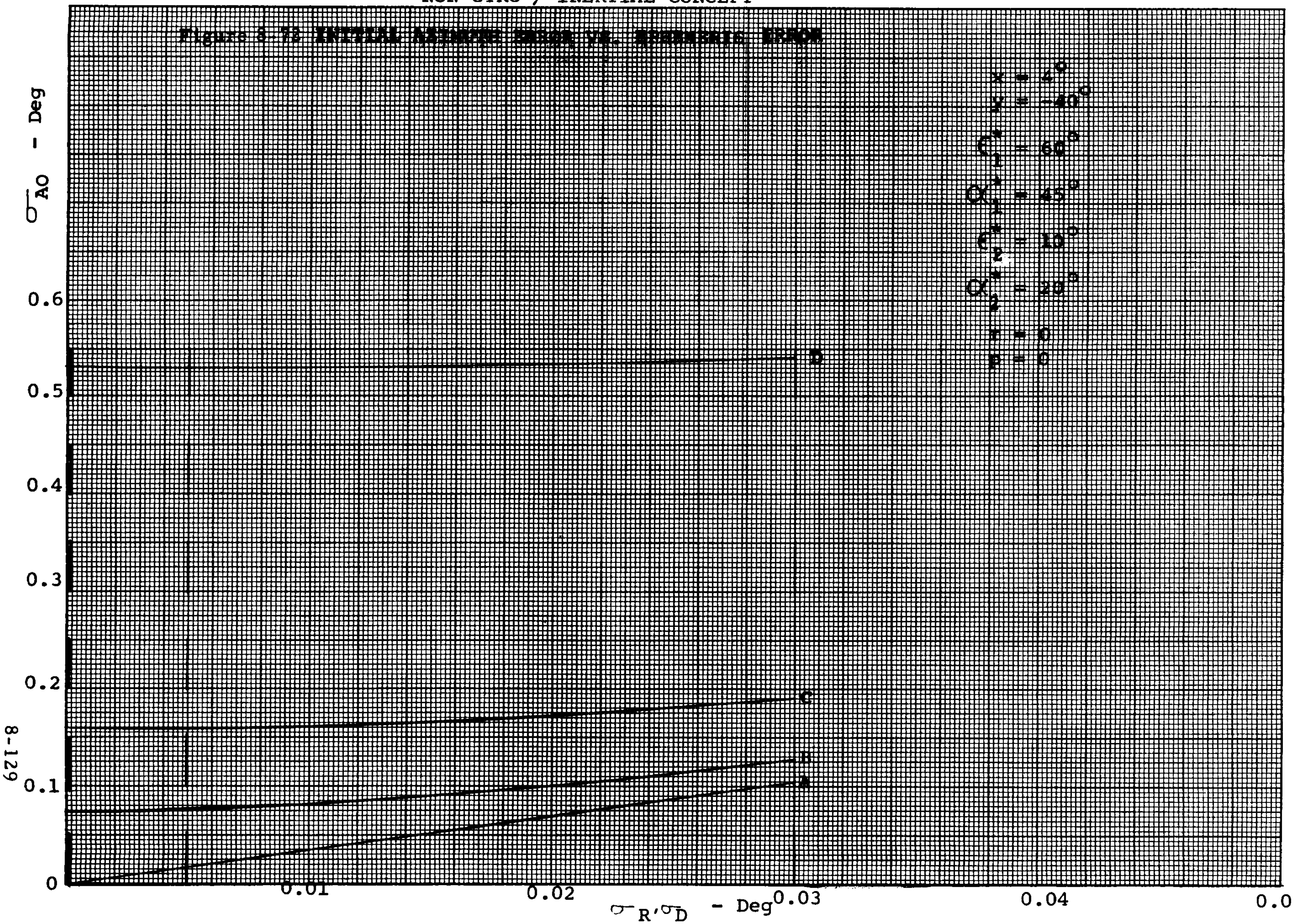

NON GYRO / INERTIAL CONCEPT

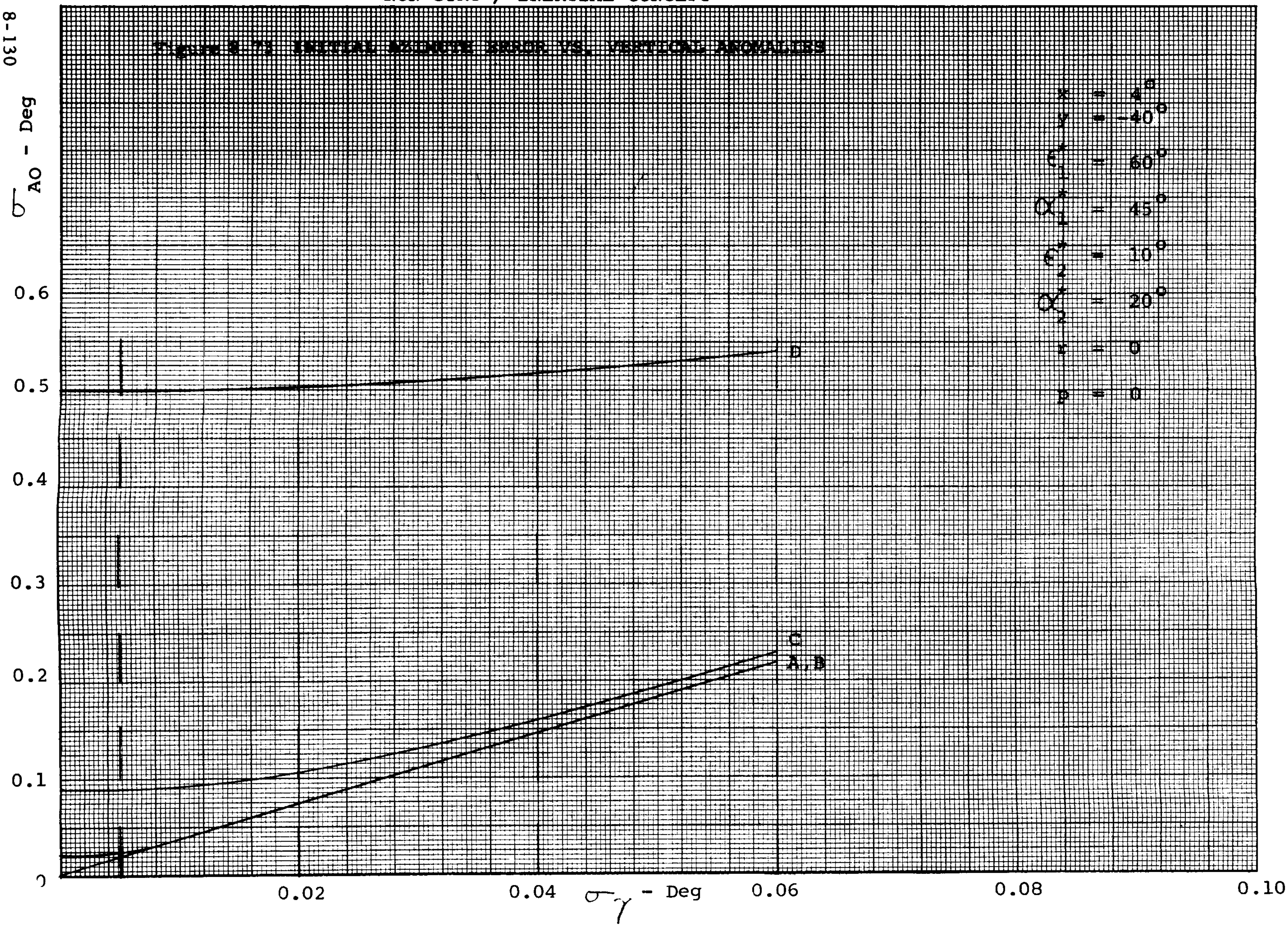

Figure 8-73 INITIAL AZIMUTH ERROR VS. VERTICAL ANOMALIES

NON GYRO / INERTIAL CONCEPT

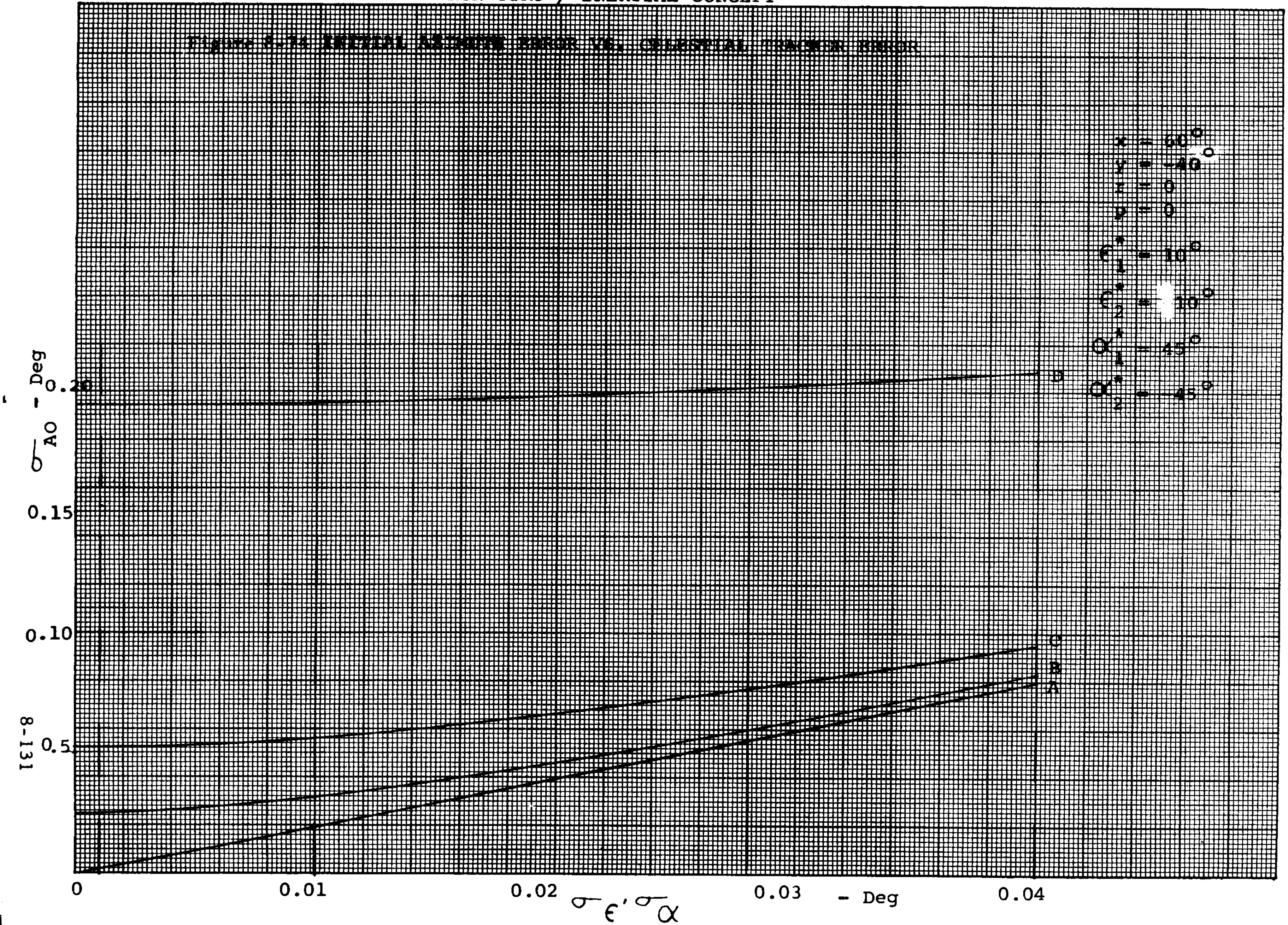

Figure 8-74 INERTIAL AZIMUTH ERROR VS. CELESTIAL TRACKER ERROR

NON GYRO / INERTIAL CONCEPT

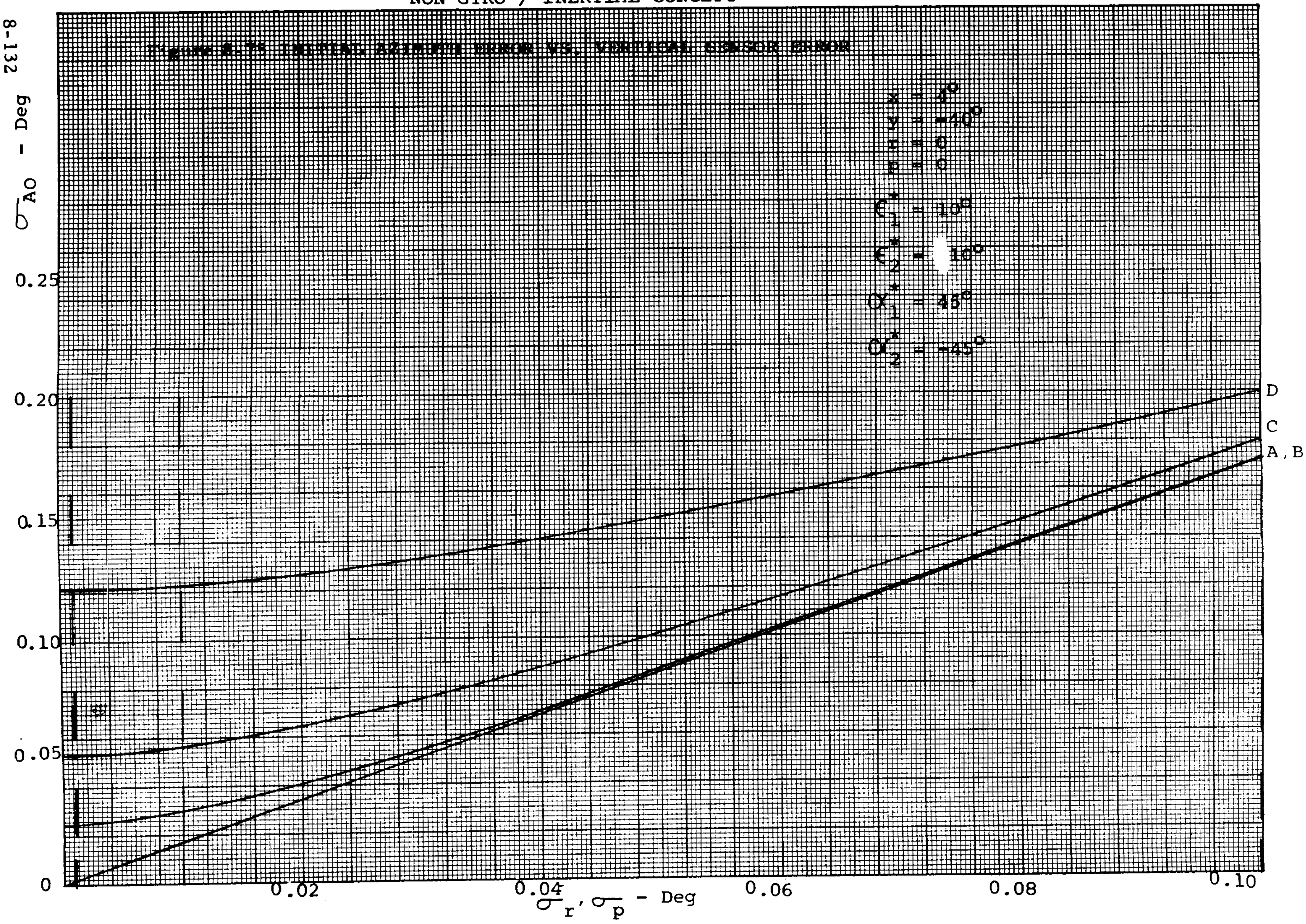

Figure 8.75 INITIAL AZIMUTH ERROR VS. VERTICAL SENSOR ERROR

NON GYRO / INERTIAL CONCEPT

Figure 8-76 INITIAL AZIMUTH ERROR VS. TIMER ERROR

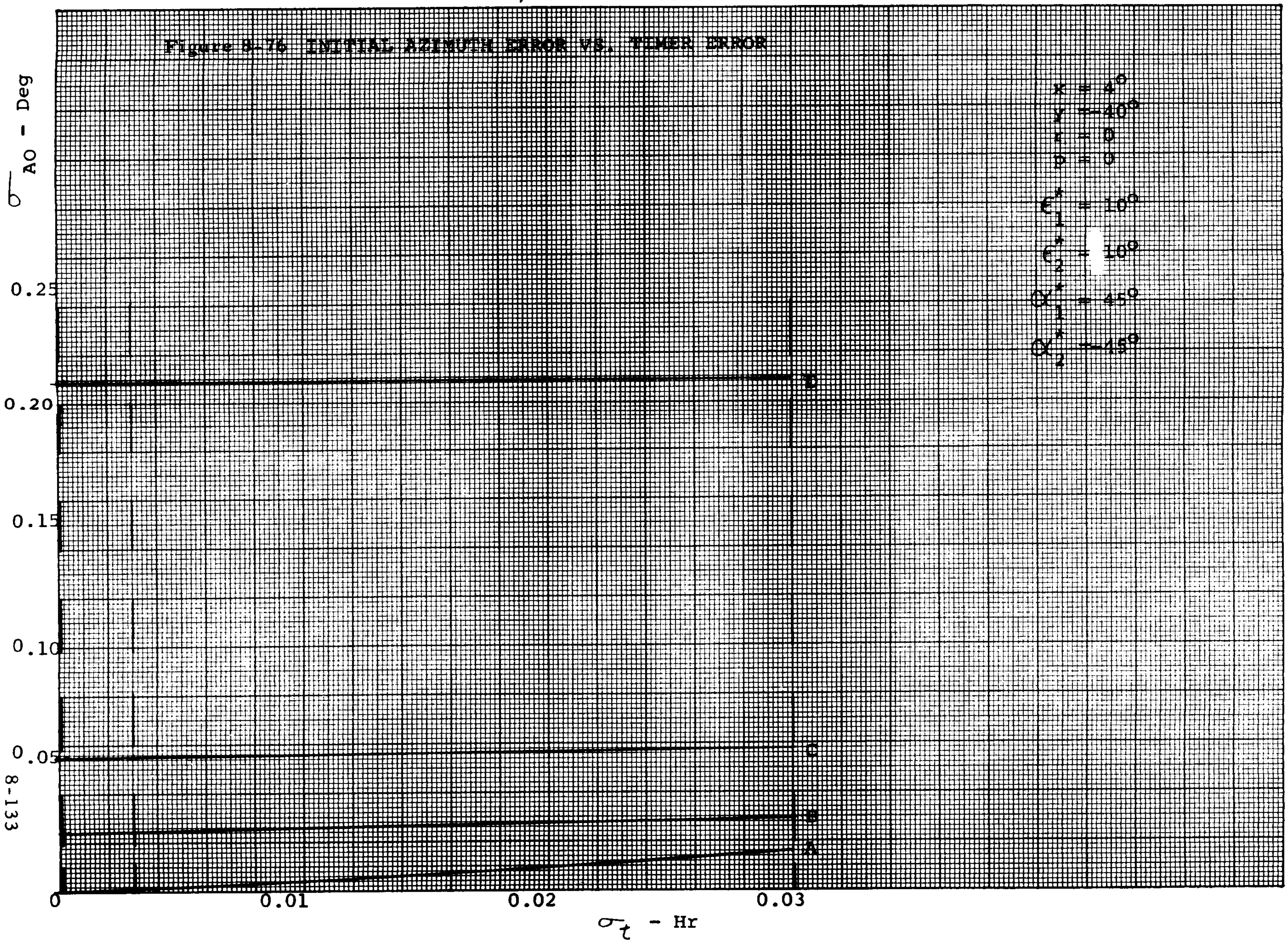

NON GYRO / INERTIAL CONCEPT

Figure 8.77 INITIAL AZIMUTH ERROR VS. EPHEMERIS ERROR

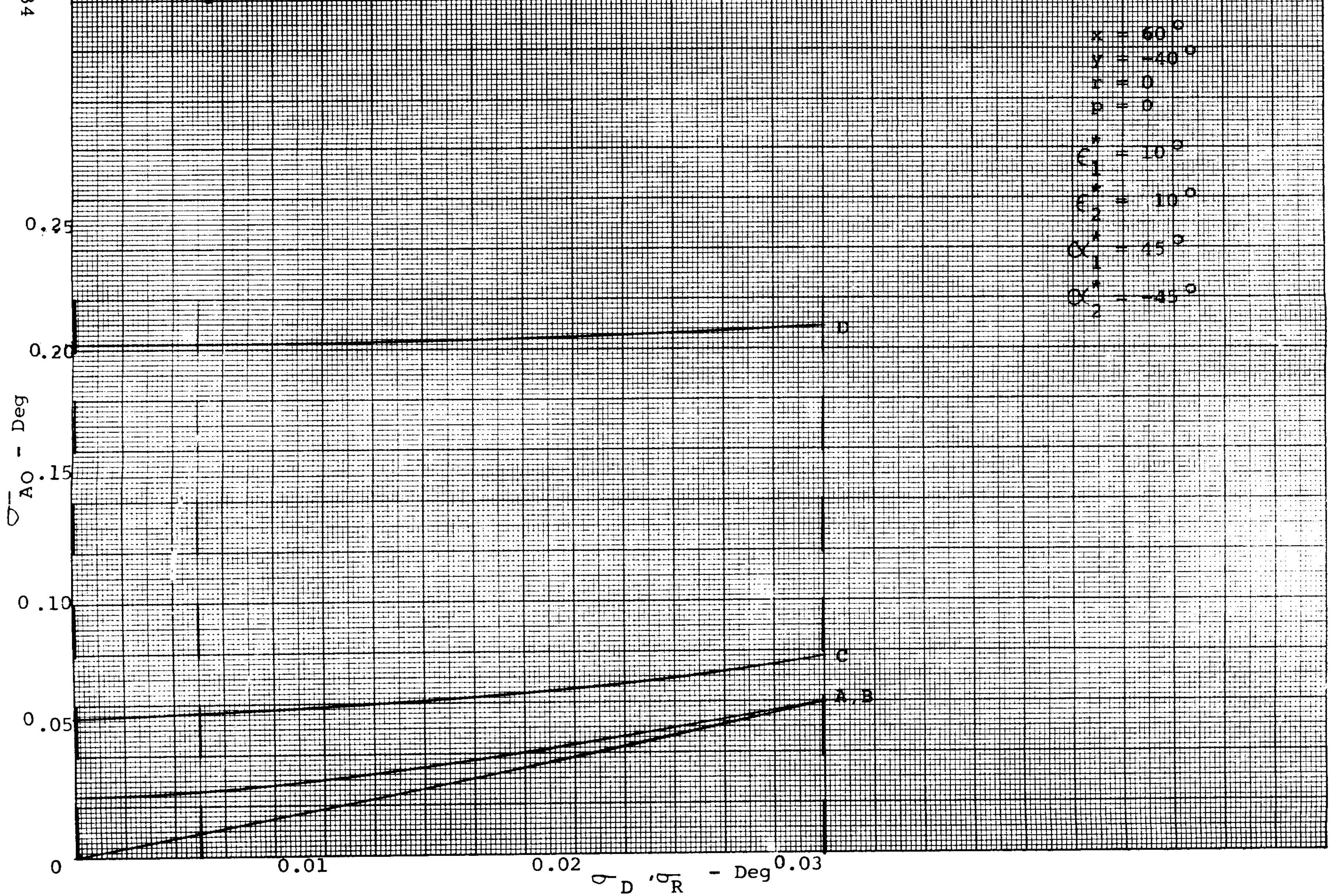

NON GYRO / INERTIAL CONCEPT

Figure 8-78 INITIAL AZIMUTH ERROR VS. VERTICAL ANOMALIES

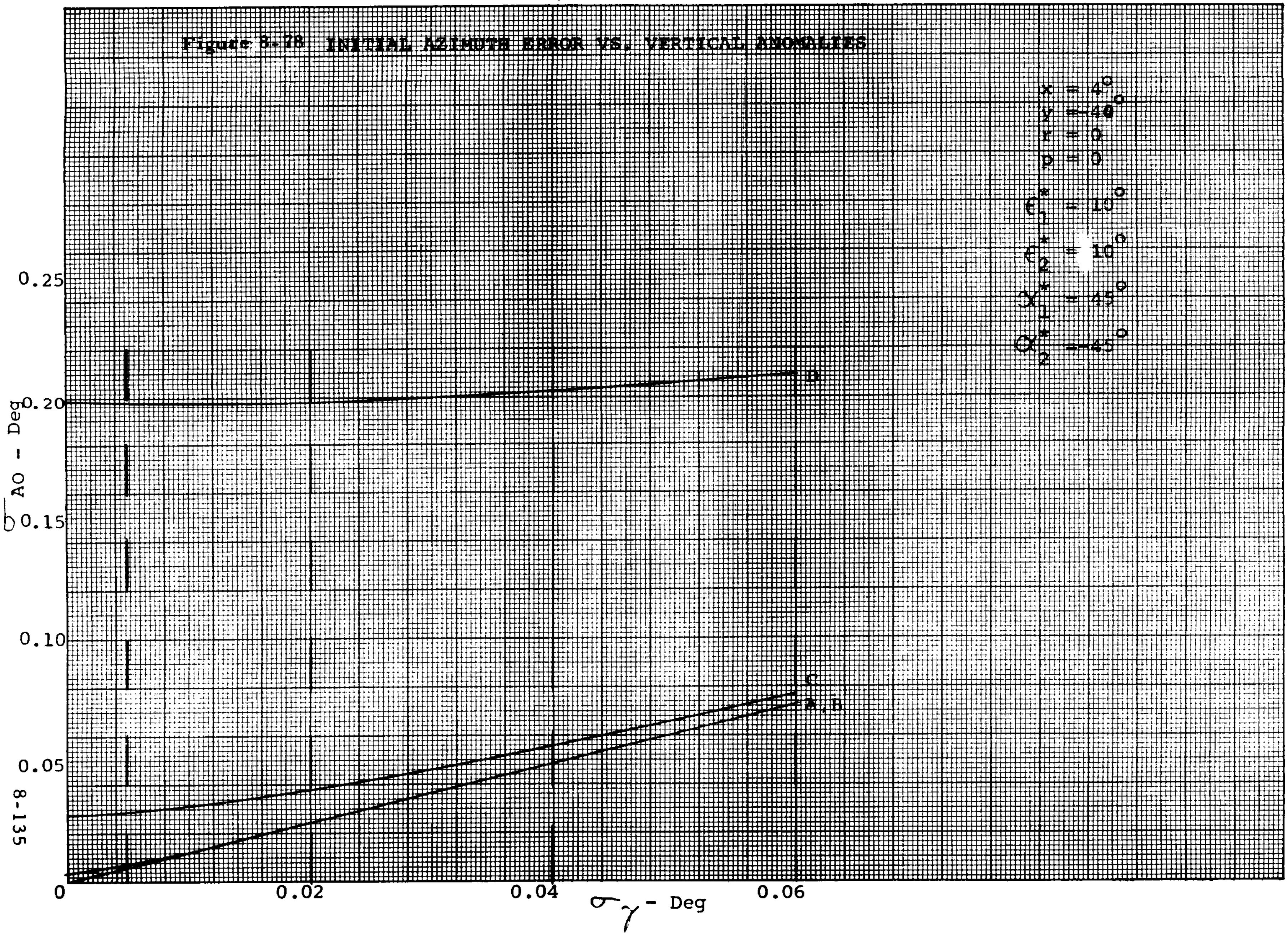

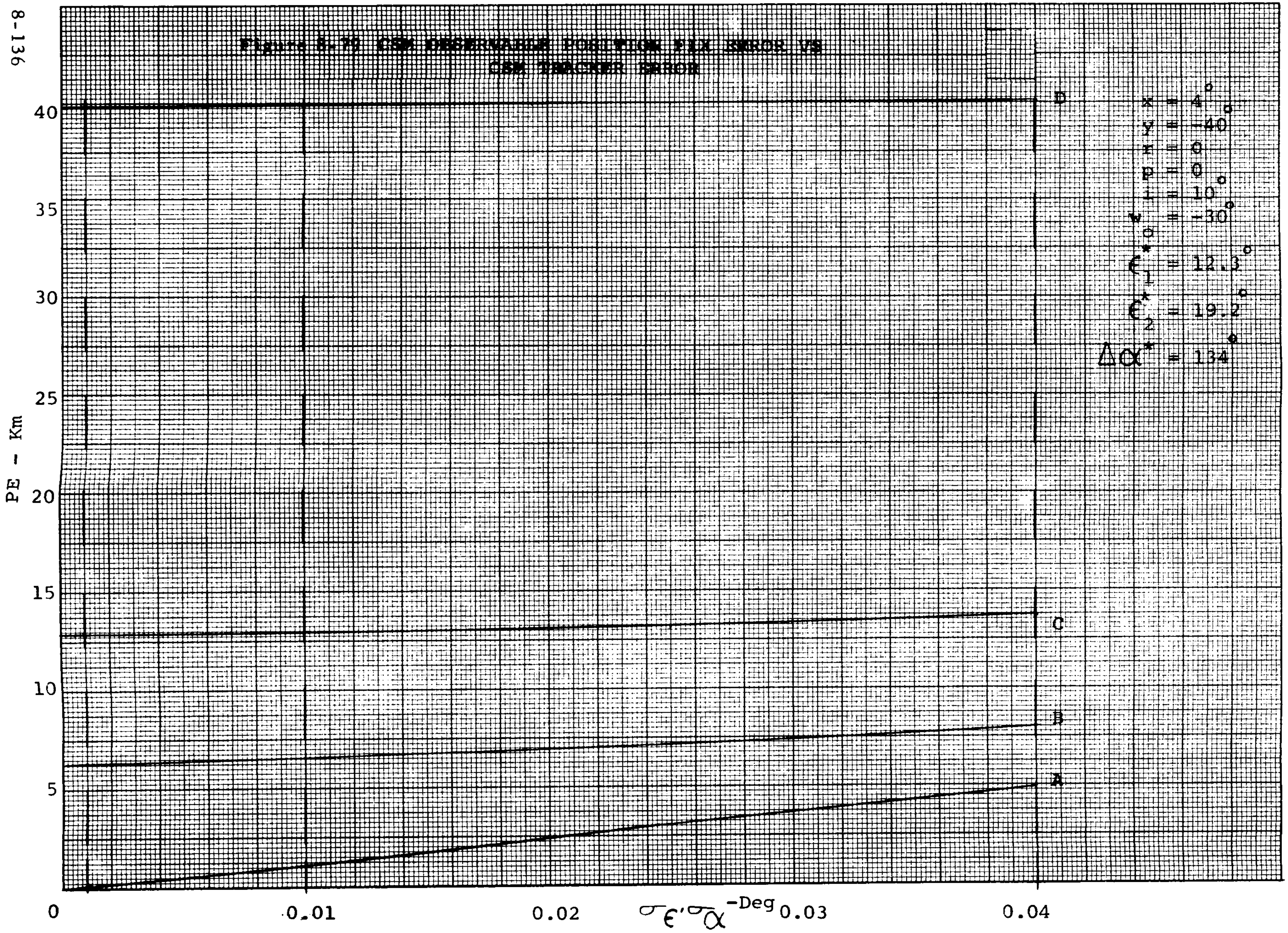

Figure 8-79 CSM OBSERVABLE POSITION FIX ERROR VS CSM TRACKER ERROR

Figure 8-30

CSM OBSERVABLE POSITION FIX ERROR VS. VERTICAL SENSOR ERROR

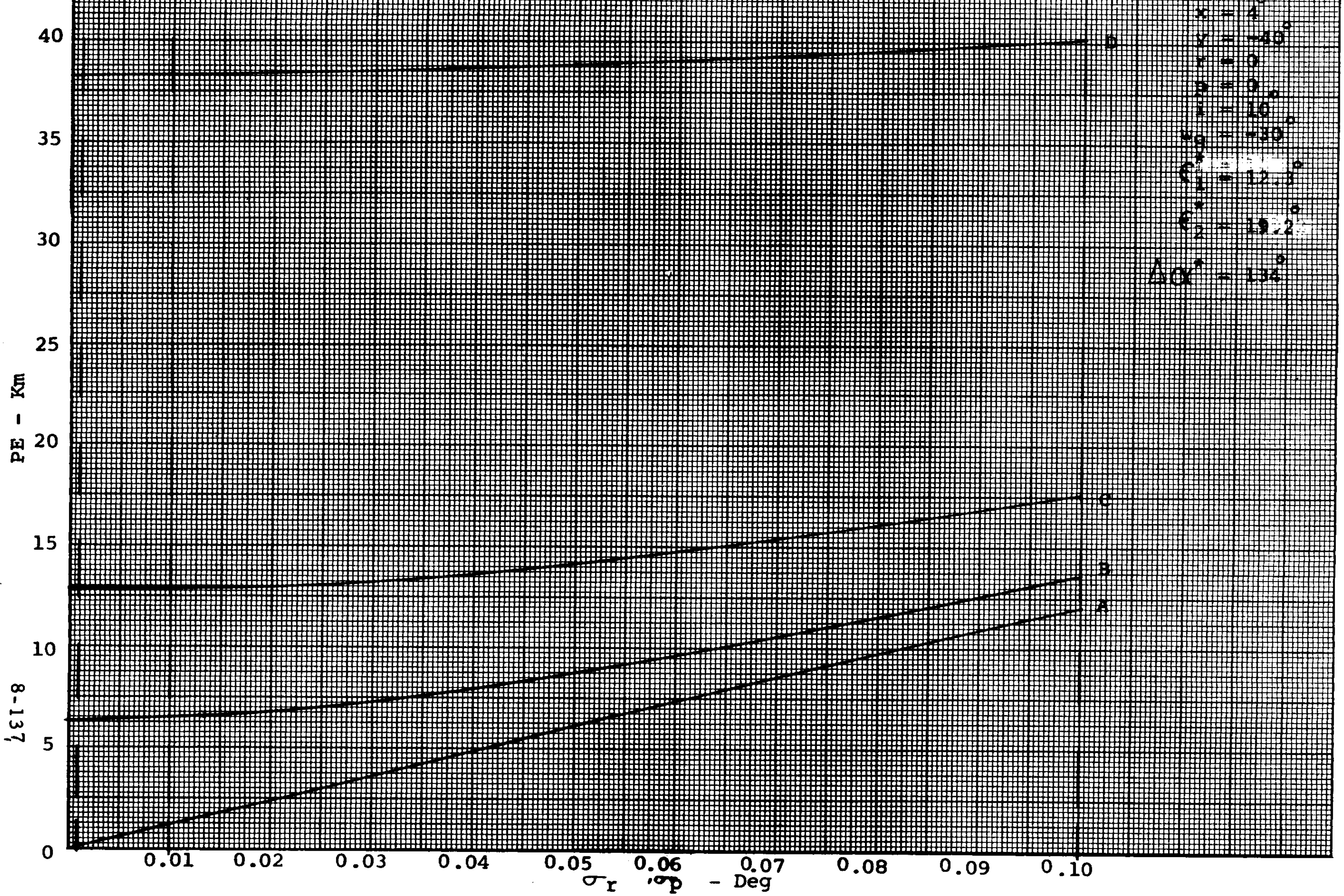

Figure 8-81

CSM OBSERVABLE POSITION FIX ERROR VS. VERTICAL ANOMALY ERROR

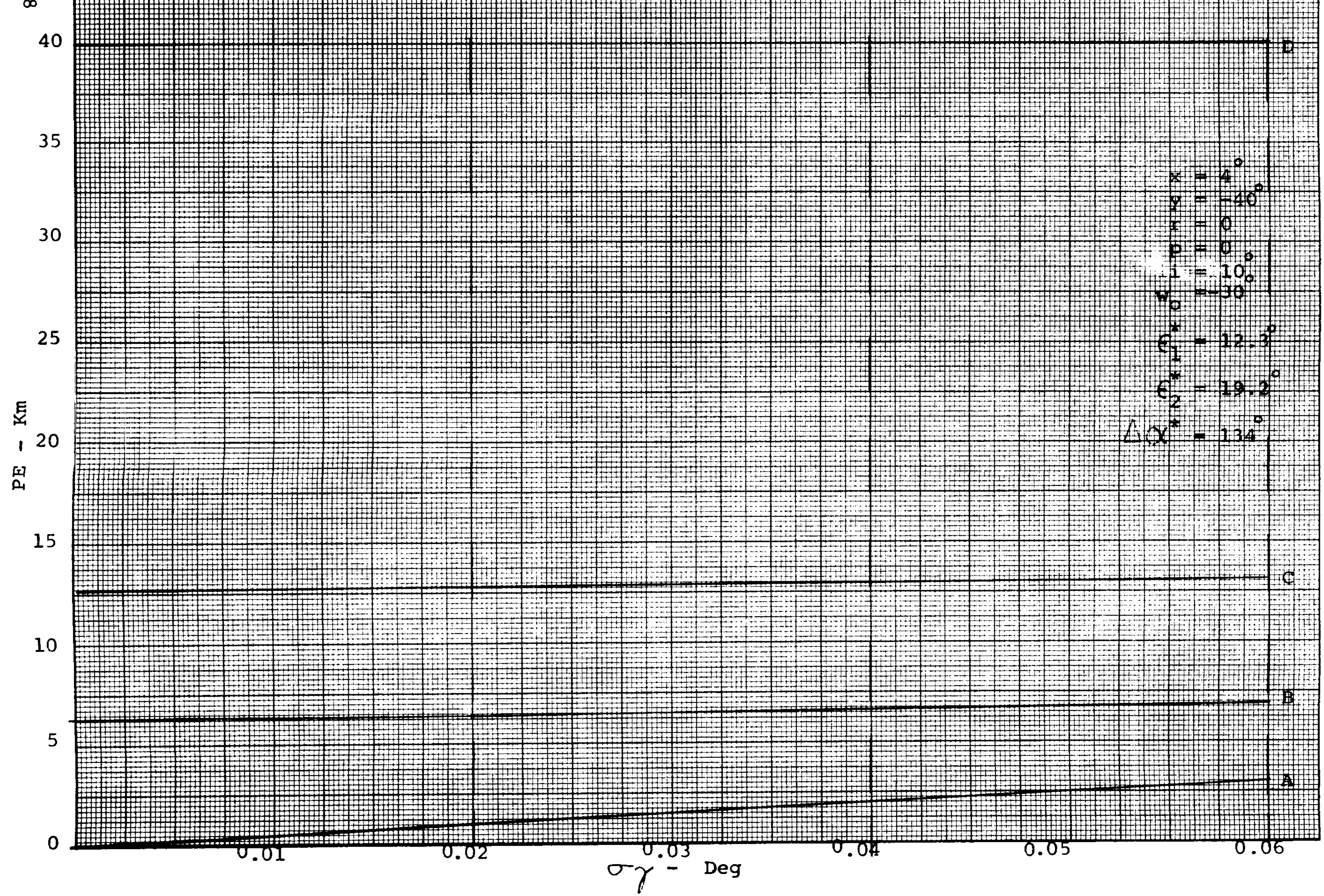

Figure 8-82

CSM OBSERVABLE POSITION FIX ERROR VS. CSM ORBIT ERROR

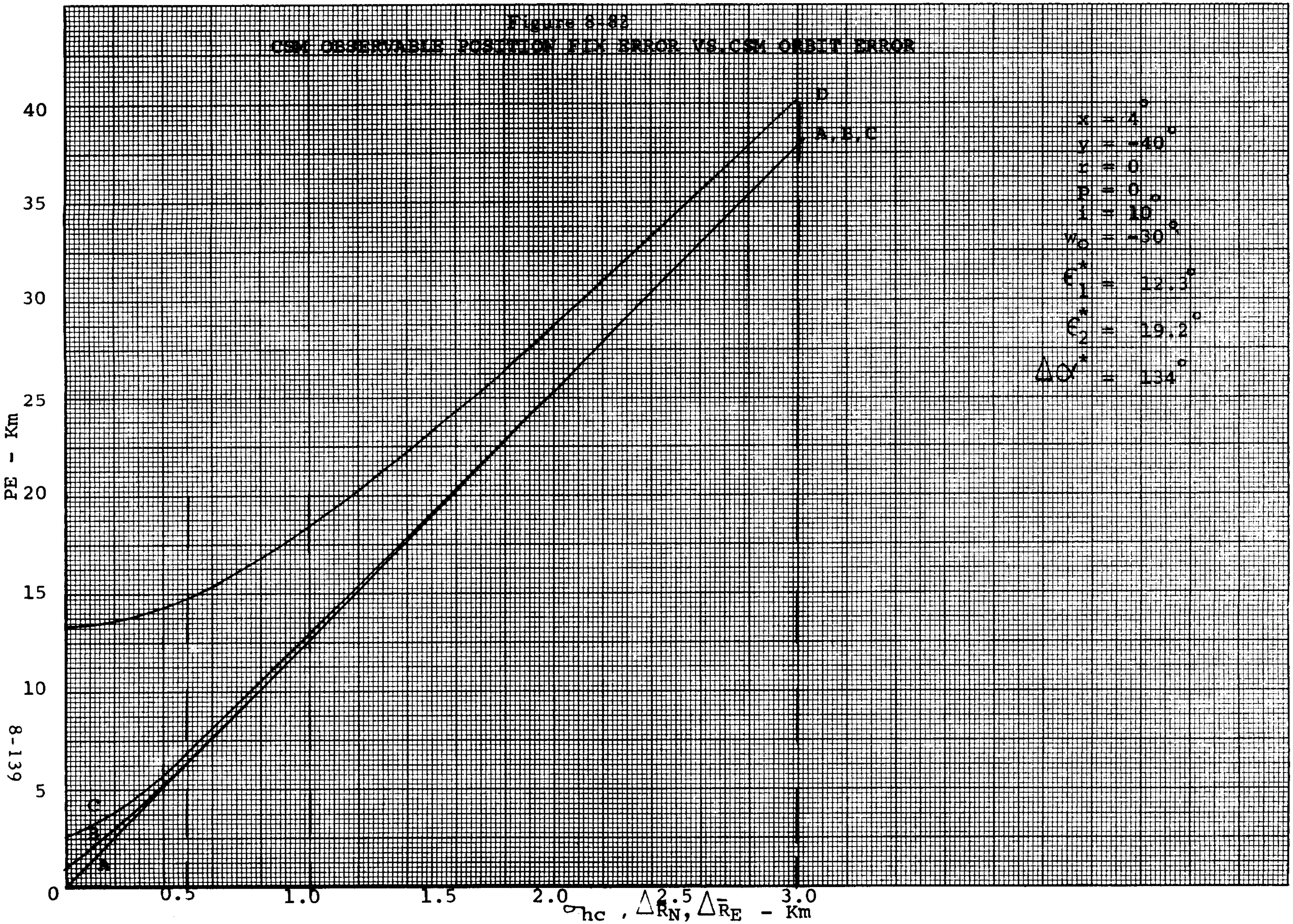

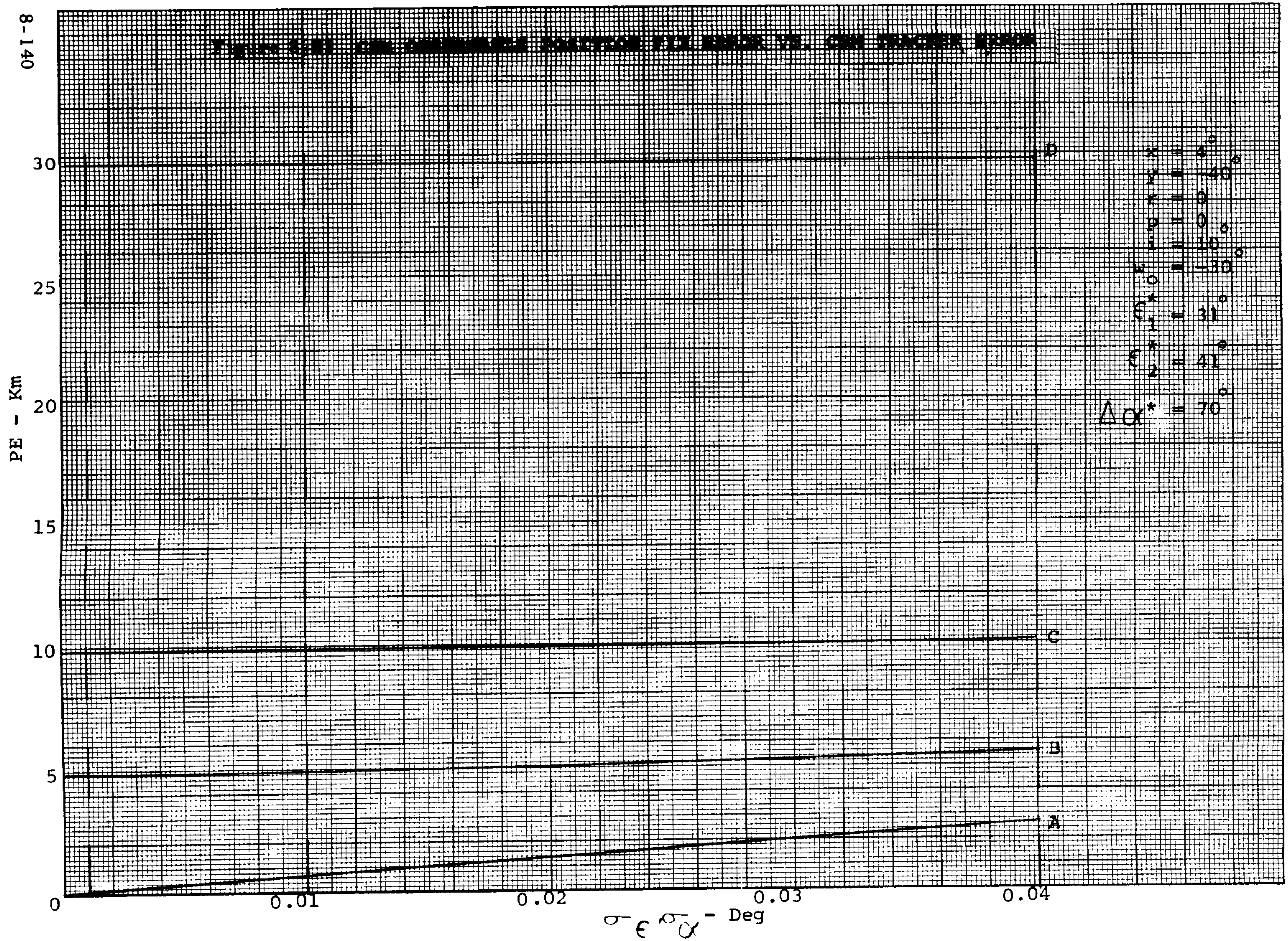

PE - Km
30
25
20
15
10
5
0
0.01
0.02
0.03
0.04
$\sigma_\epsilon \sigma_\alpha$ - Deg
D
C
B
A
$x = 4^\circ$
$y = -40^\circ$
$\kappa = 0$
$p = 0$
$i = 10^\circ$
$\omega_o = -30^\circ$
$\epsilon_1^* = 31^\circ$
$\epsilon_2^* = 41^\circ$
$\Delta\alpha^* = 70^\circ$

Figure 8-84 CSM OBSERVABLE POSITION FIX ERROR VS. VERTICAL SENSOR ERROR

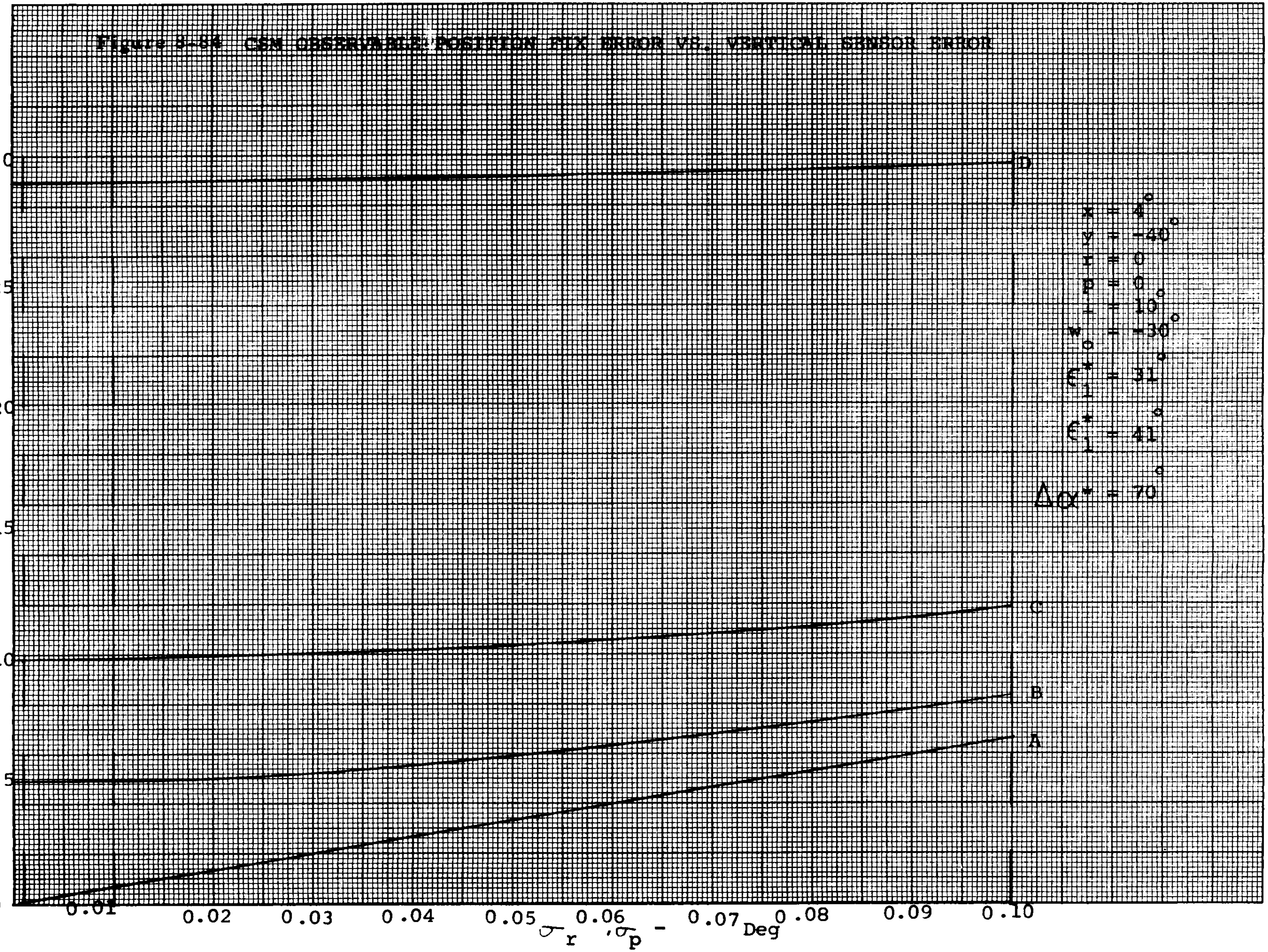

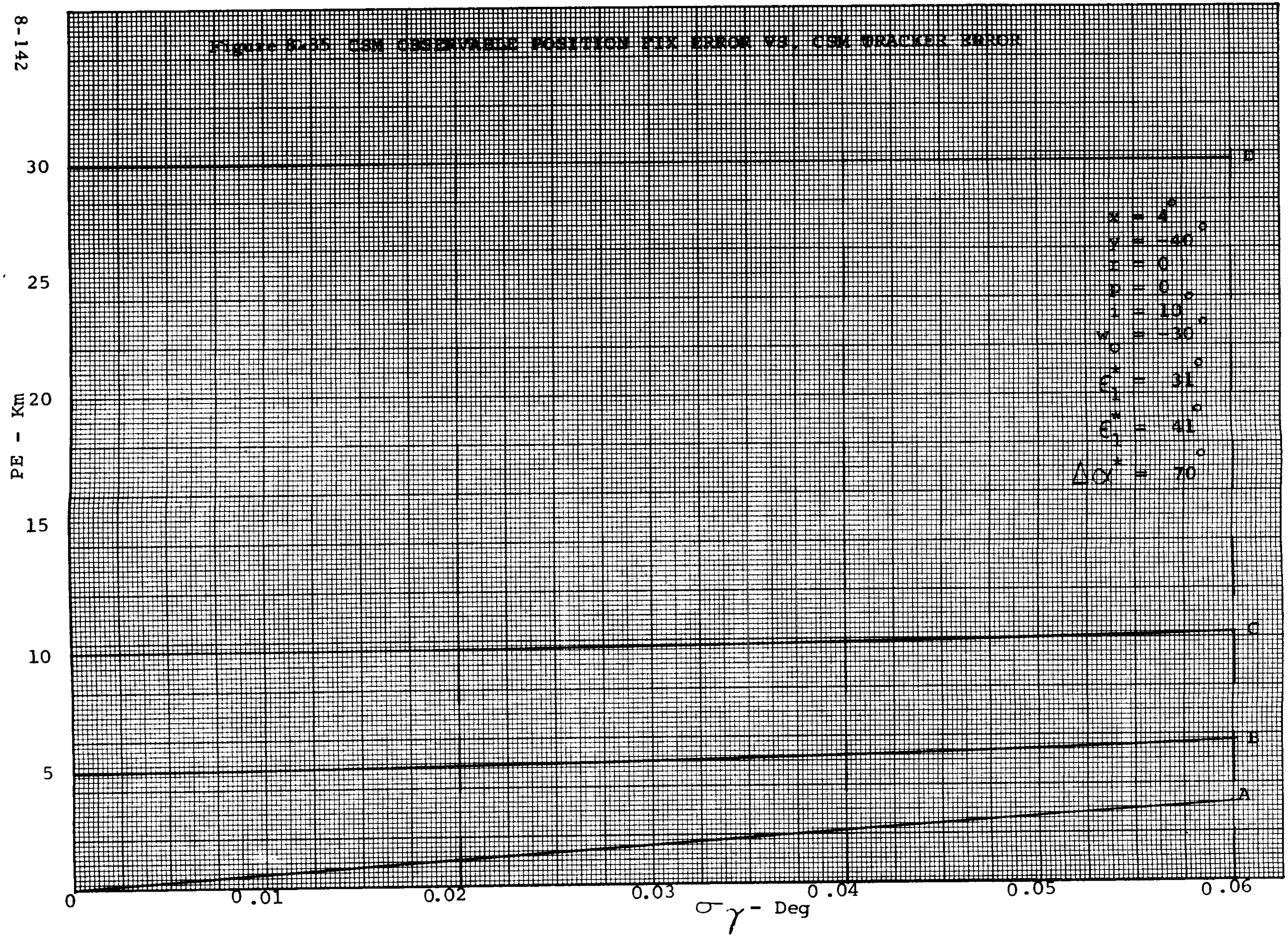

Figure 8-85 CSM OBSERVABLE POSITION FIX ERROR VS. CSM TRACKER ERROR

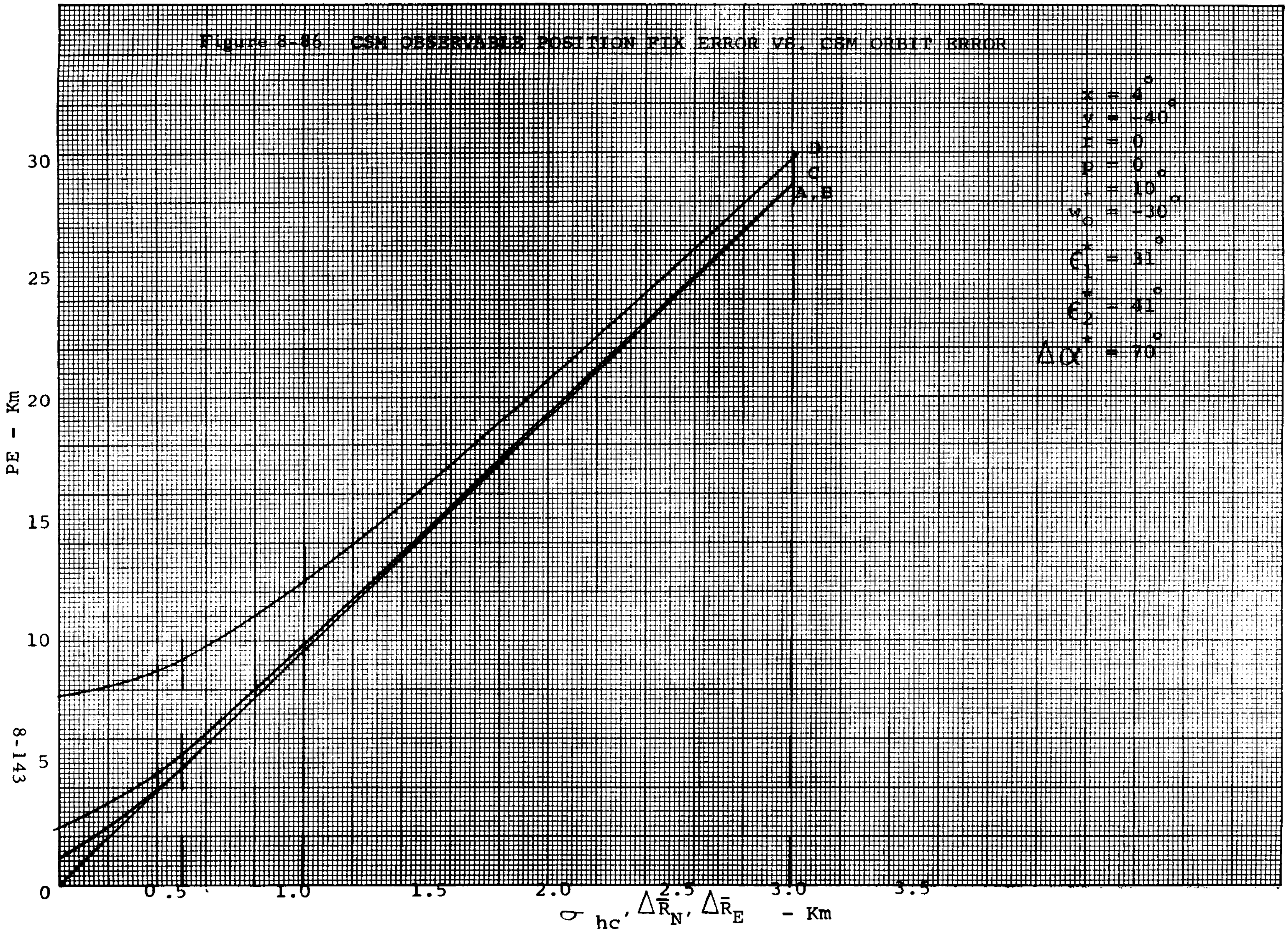
Figure 8-86 CSM OBSERVABLE POSITION FIX ERROR VS. CSM ORBIT ERROR
x = 4°
y = -40°
r = 0
p = 0°
i = 10°
w_o = -30°
ϵ_1^* = 31°
ϵ_2^* = 41°
$\Delta\alpha^*$ = 70°
D
C
A, B
30
25
20
15
10
5
0
PE - Km
0.5
1.0
1.5
2.0
2.5
3.0
3.5
$\sigma_{hc}, \Delta\bar{R}_N, \Delta\bar{R}_E$ - Km

Figure 8-87

CSM OBSERVABLE INITIAL AZIMUTH ALIGNMENT ERROR VS. CSM TRACKER ERROR

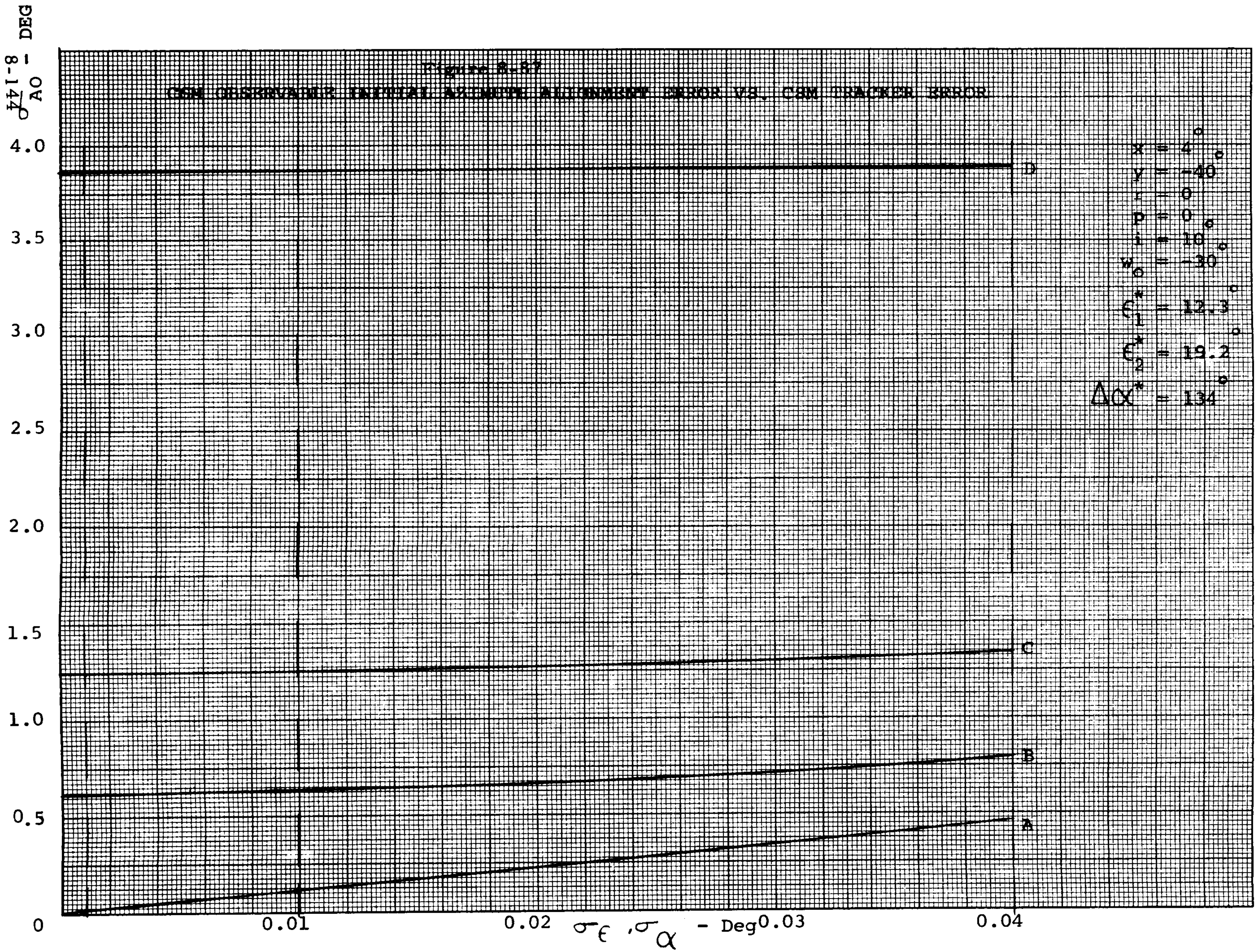

Figure 8-38

CSM OBSERVABLE INITIAL AZIMUTH ALIGNMENT ERROR VS. VERTICAL SENSOR ERROR

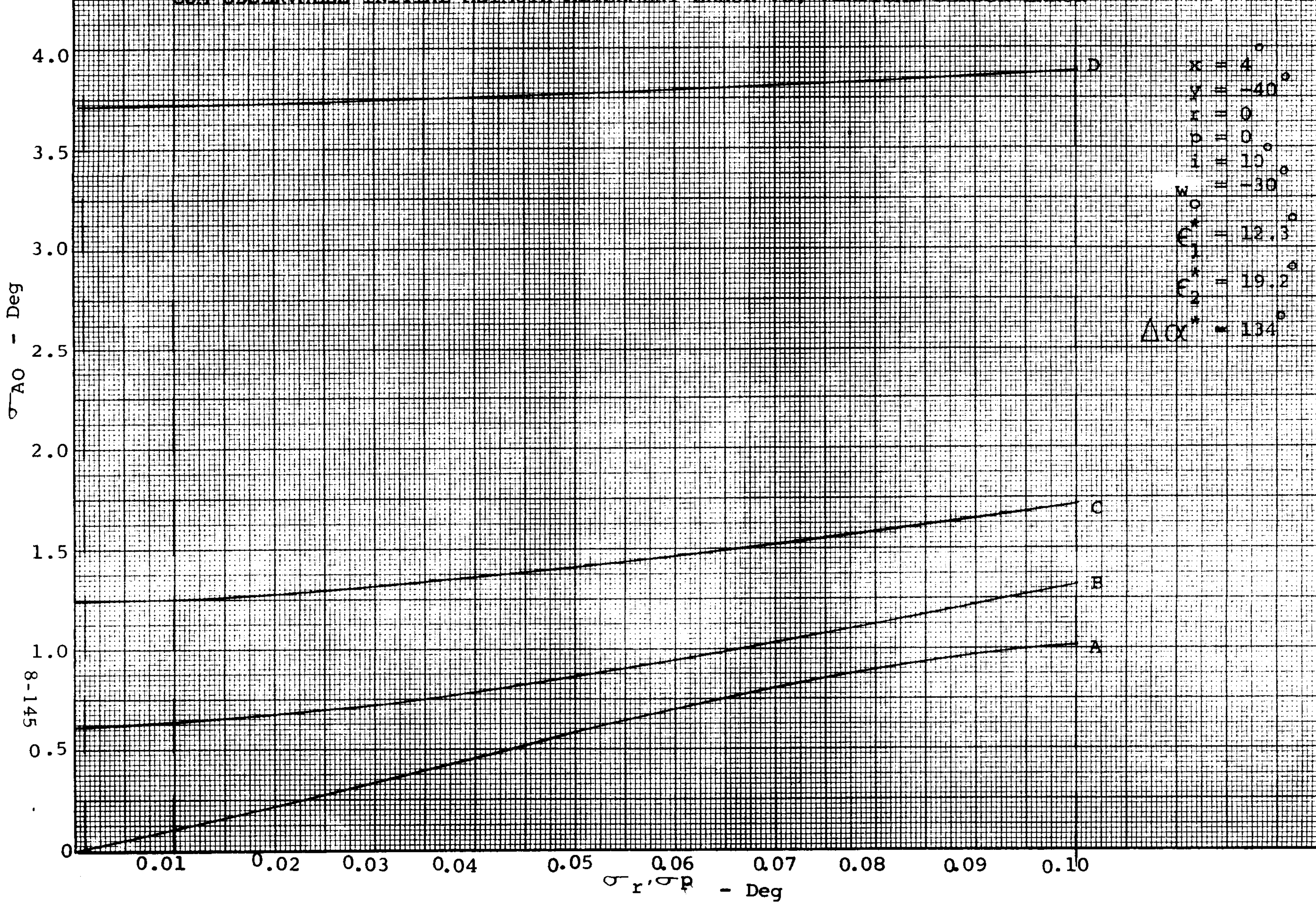

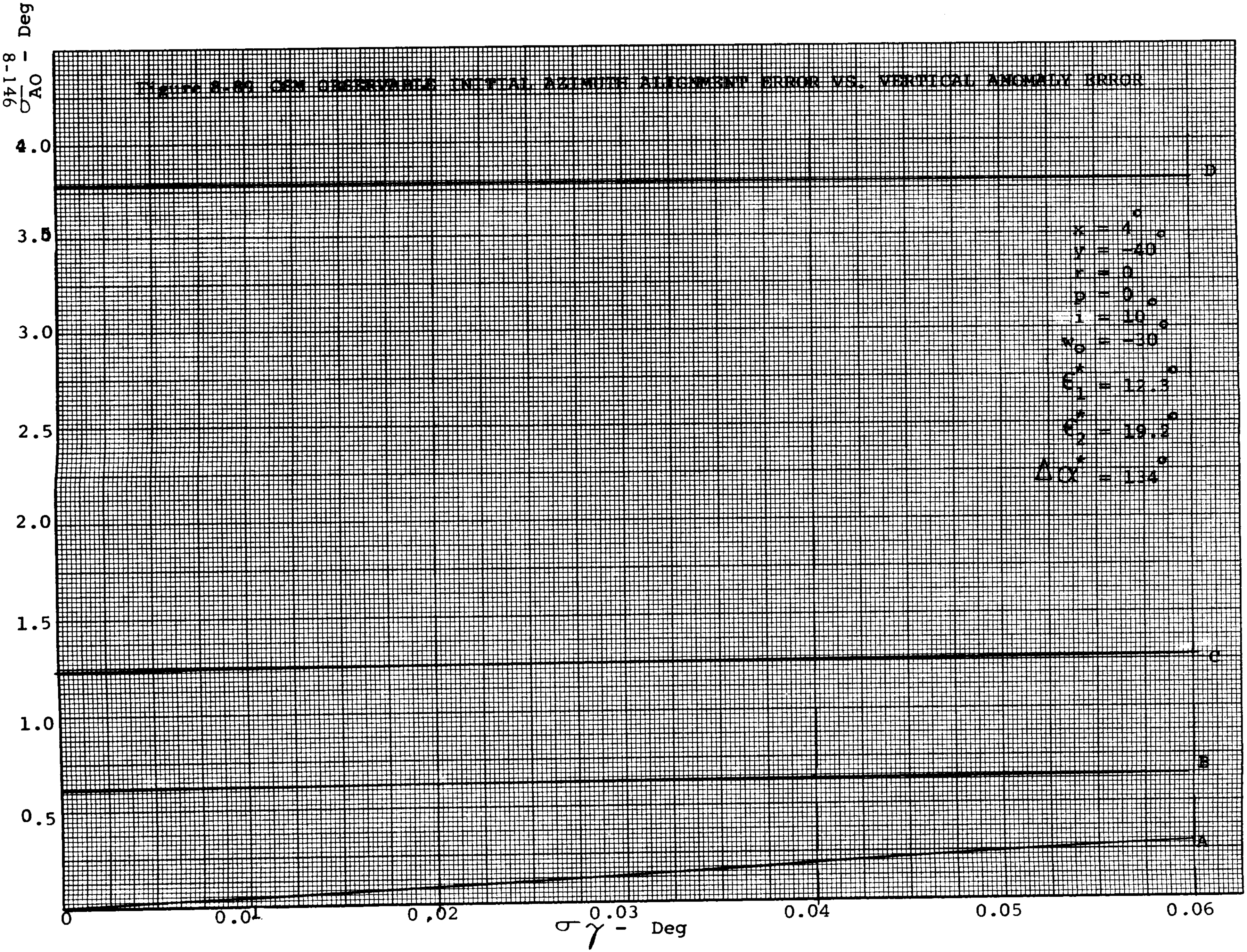

Figure 8.80 CSM OBSERVABLE INITIAL AZIMUTH ALIGNMENT ERROR VS. VERTICAL ANOMALY ERROR

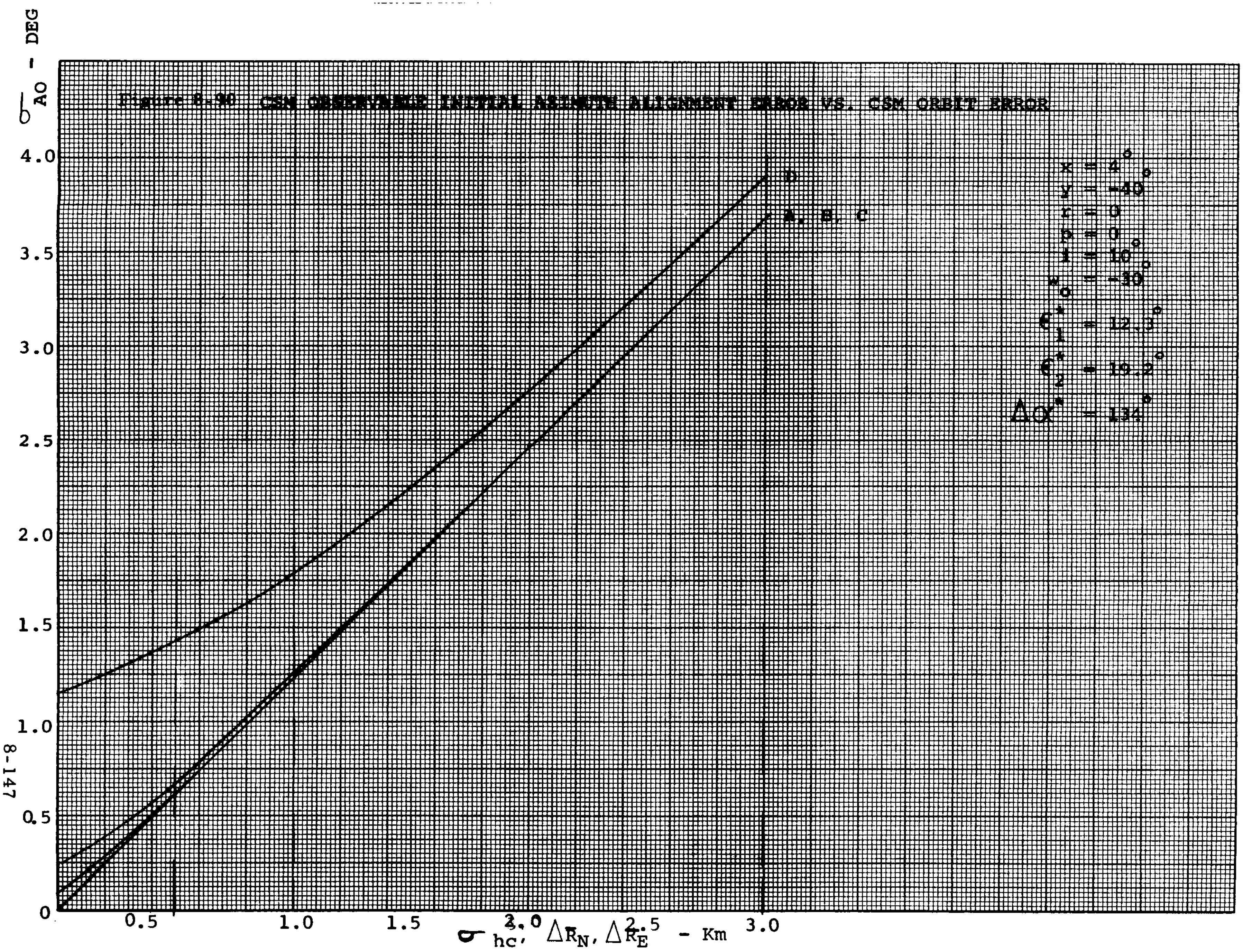
Figure 8-90 CSM OBSERVABLE INITIAL AZIMUTH ALIGNMENT ERROR VS. CSM ORBIT ERROR
σ_{AO} - DEG
4.0
3.5
3.0
2.5
2.0
1.5
1.0
0.5
0
0.5
1.0
1.5
2.0
2.5
3.0
$\sigma_{hc}, \Delta R_N, \Delta R_E$ - Km
D
A, B, C
$x = 4^\circ$
$y = -40^\circ$
$r = 0$
$p = 0$
$i = 10^\circ$
$w_o = -30^\circ$
$\epsilon_1^* = 12.3^\circ$
$\epsilon_2^* = 19.2^\circ$
$\Delta\alpha^* = 134^\circ$

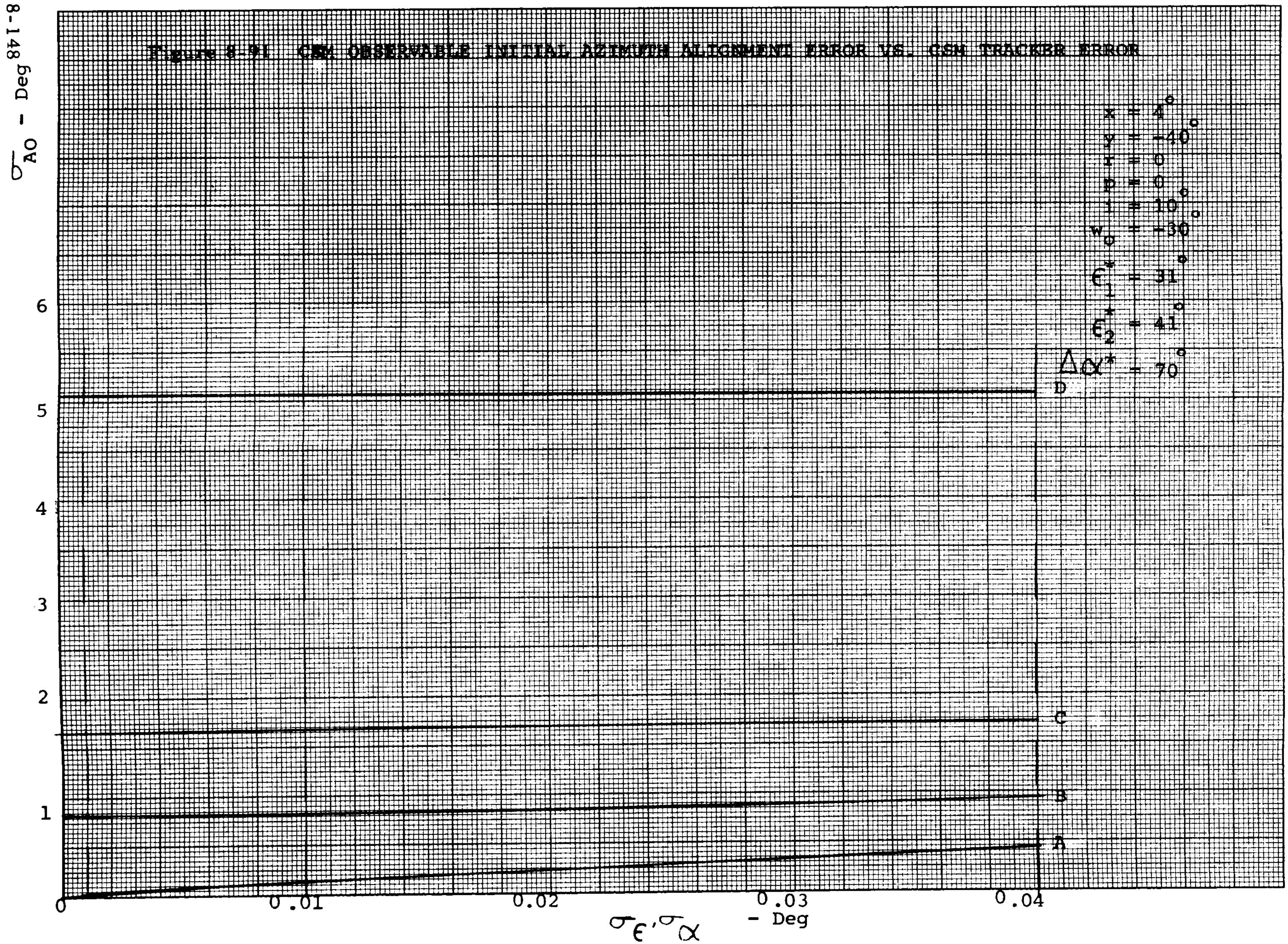
Figure 8-91 CSM OBSERVABLE INITIAL AZIMUTH ALIGNMENT ERROR VS. CSM TRACKER ERROR
x = 4°
y = -40°
r = 0
p = 0
i = 10°
w_o = -30°
ε₁* = 31°
ε₂* = 41°
Δα* = 70°
A
B
C
D
σ_AO - Deg
σ_ε, σ_α - Deg
0
0.01
0.02
0.03
0.04
1
2
3
4
5
6

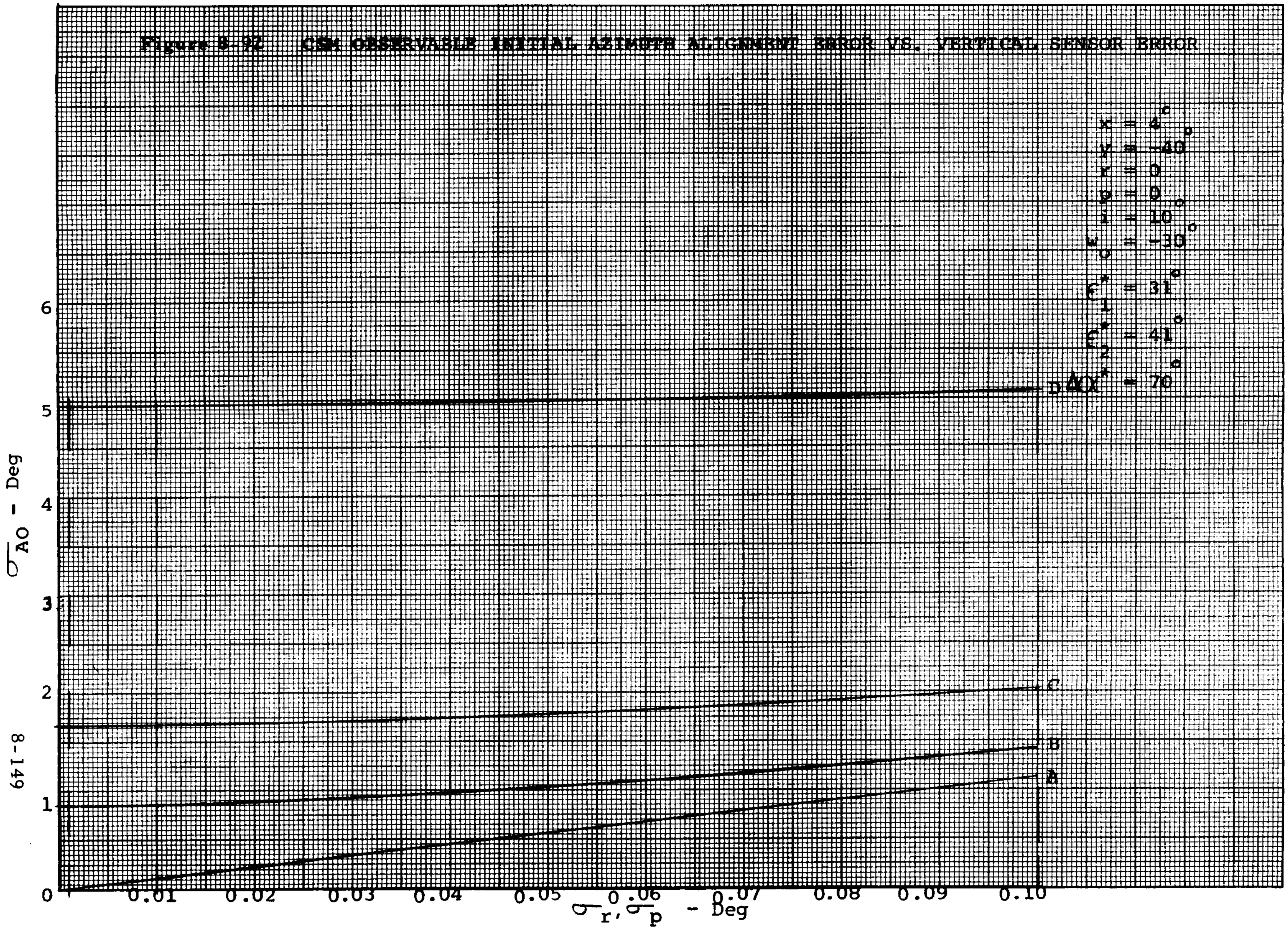

Figure 8-92 CSM OBSERVABLE INITIAL AZIMUTH ALIGNMENT ERROR VS. VERTICAL SENSOR ERROR

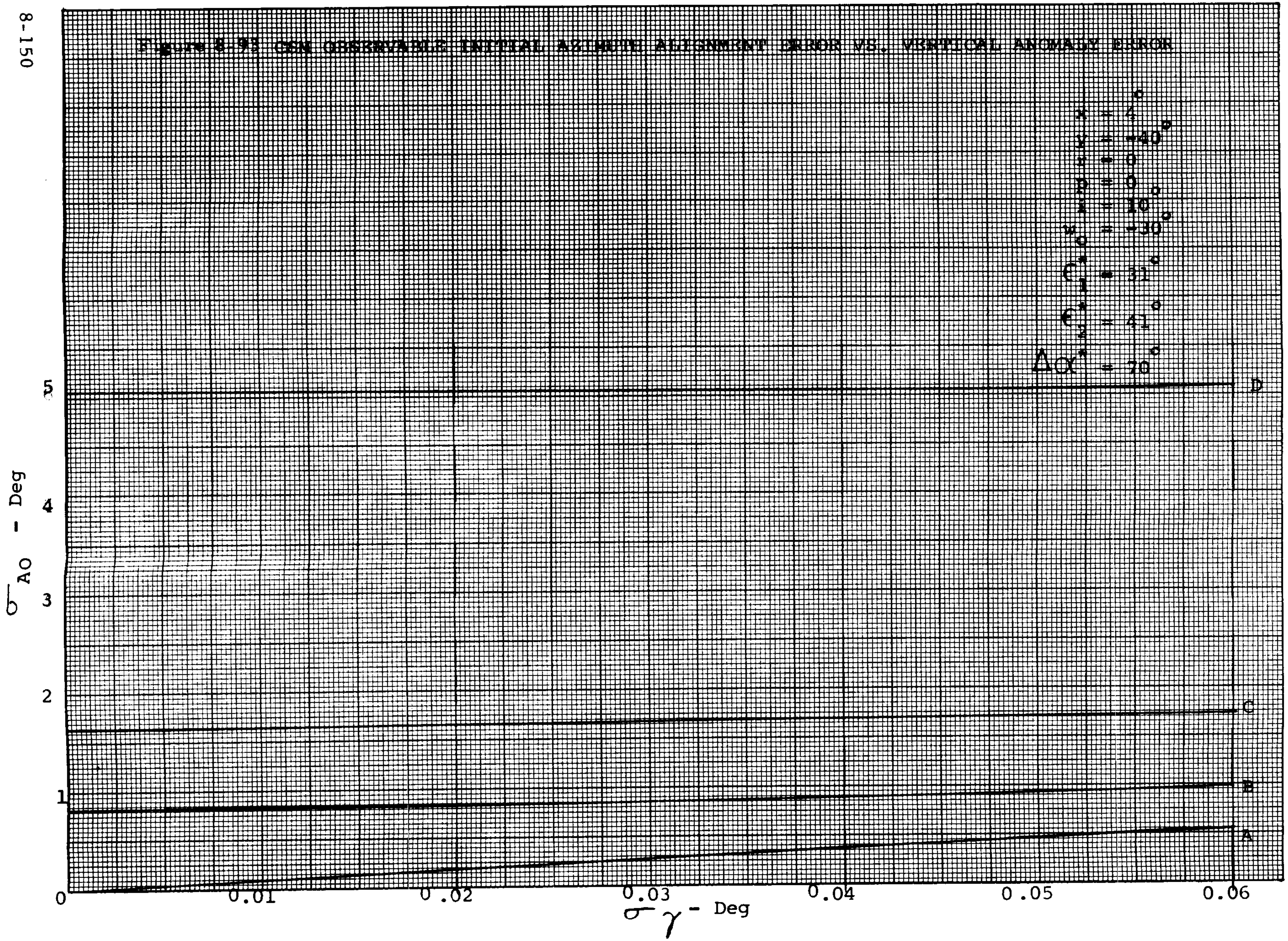

Figure 8-93 CSM OBSERVABLE INITIAL AZIMUTH ALIGNMENT ERROR VS. VERTICAL ANOMALY ERROR

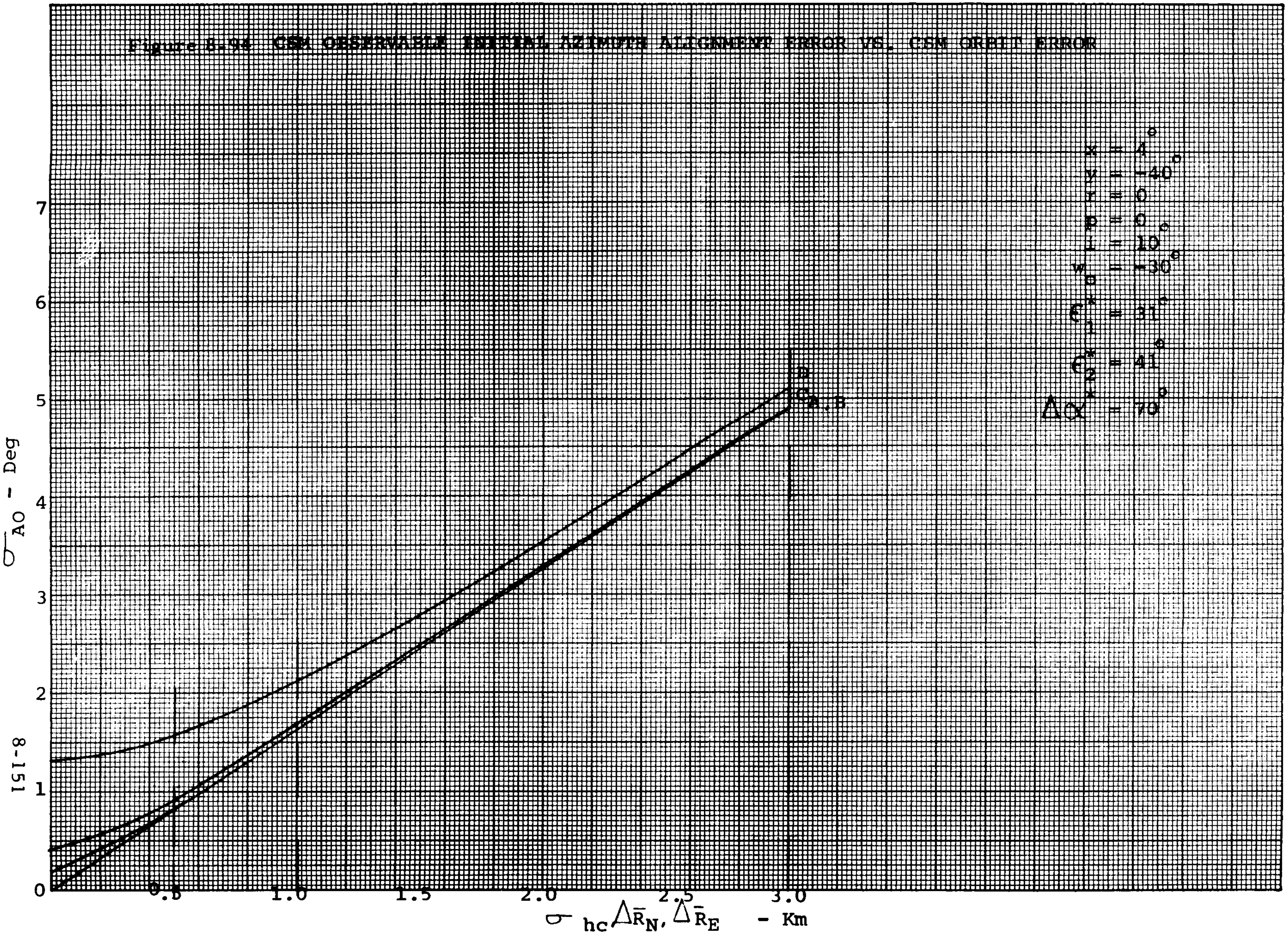

Figure 8.94 CSM OBSERVABLE INITIAL AZIMUTH ALIGNMENT ERROR VS. CSM ORBIT ERROR

Figure 8-95. POSITION FIX ERROR VS. CSM RANGING ERROR

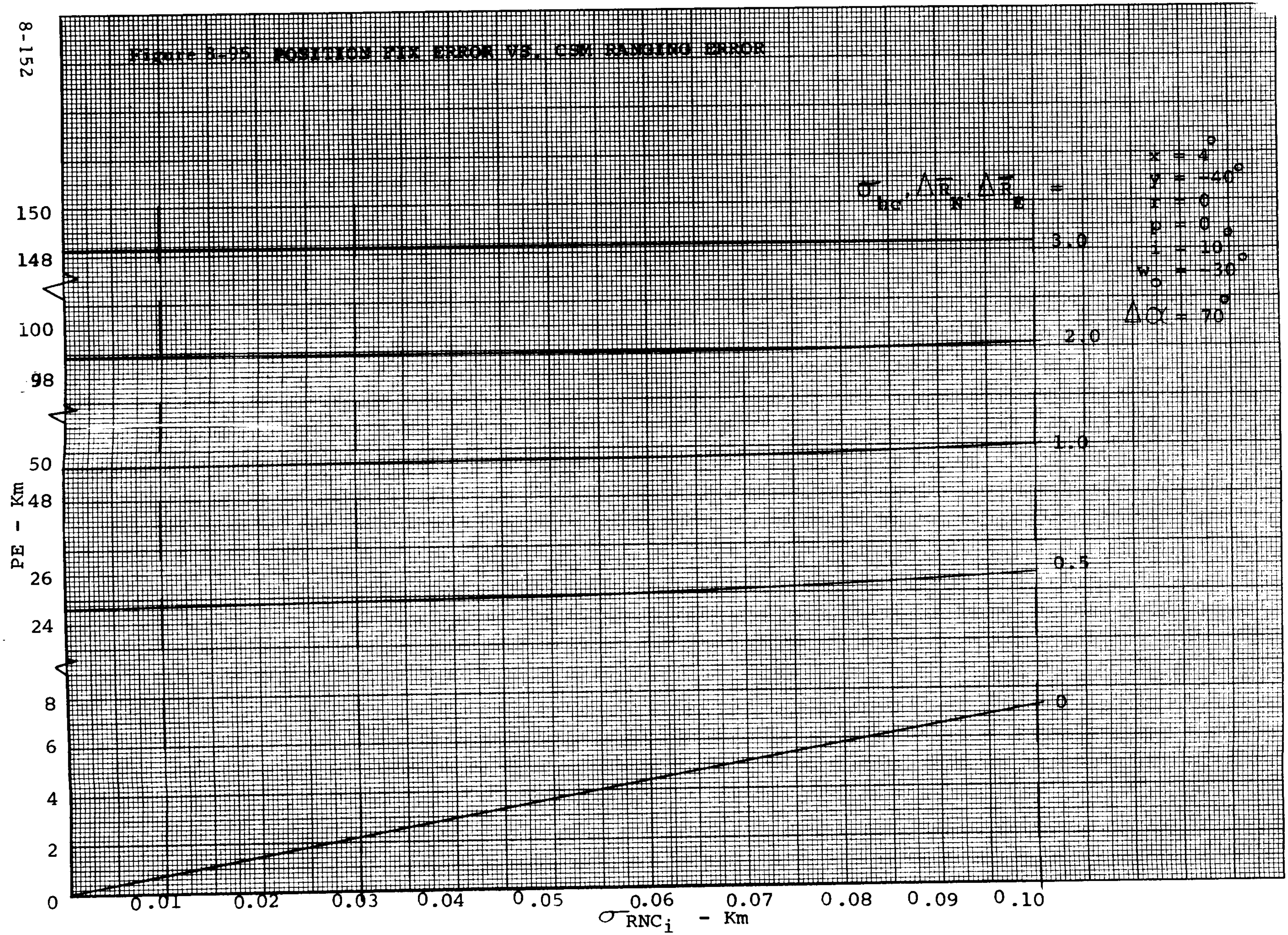

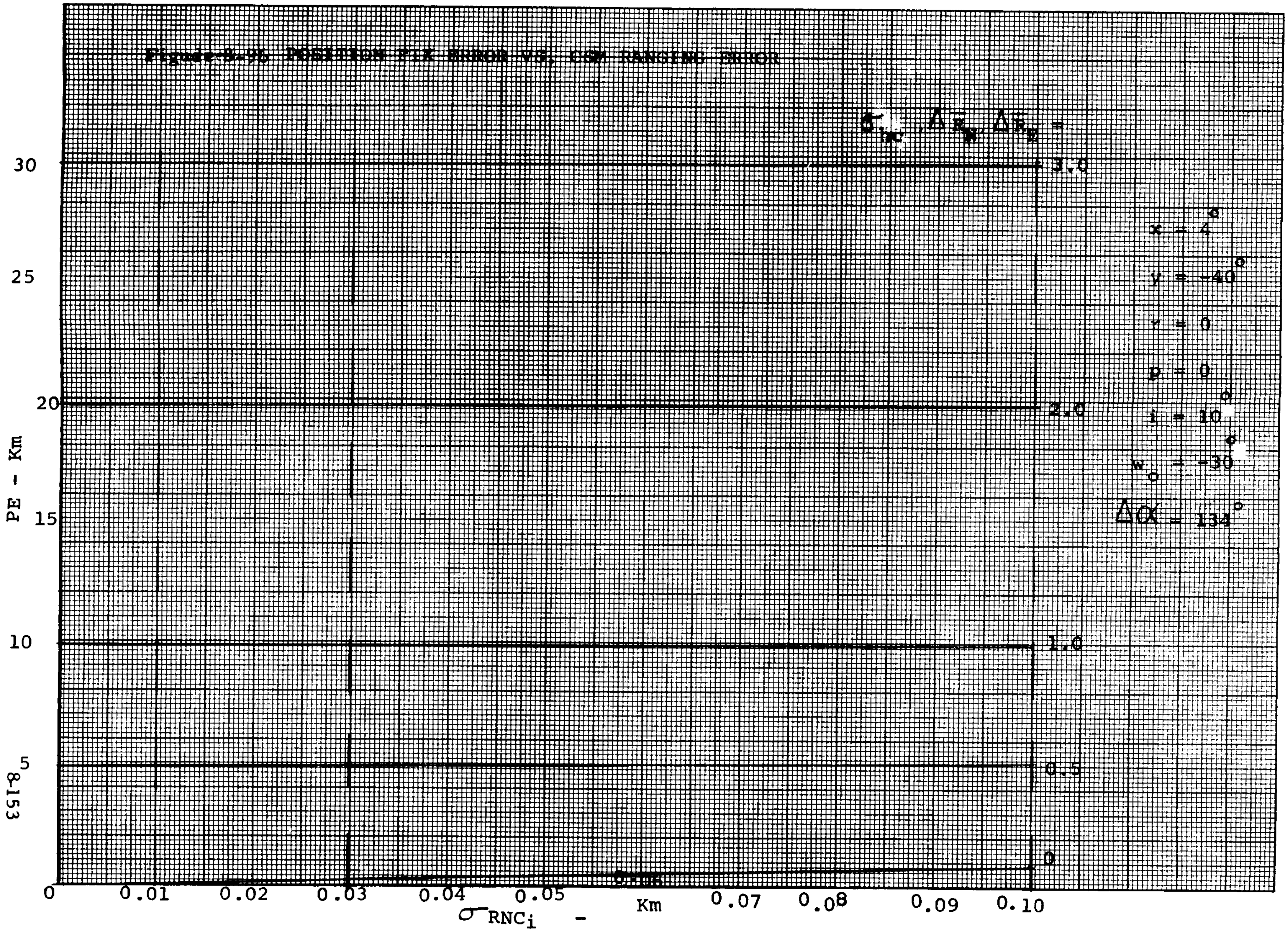

Figure 8-96 POSITION FIX ERROR VS. CSM RANGING ERROR

Figures 8-97 to 8-102 appear on pages 8-24 to 8-29.

Figure 8-103 NON-GYRO CONCEPT/PE VERSUS ODOMETER ERROR

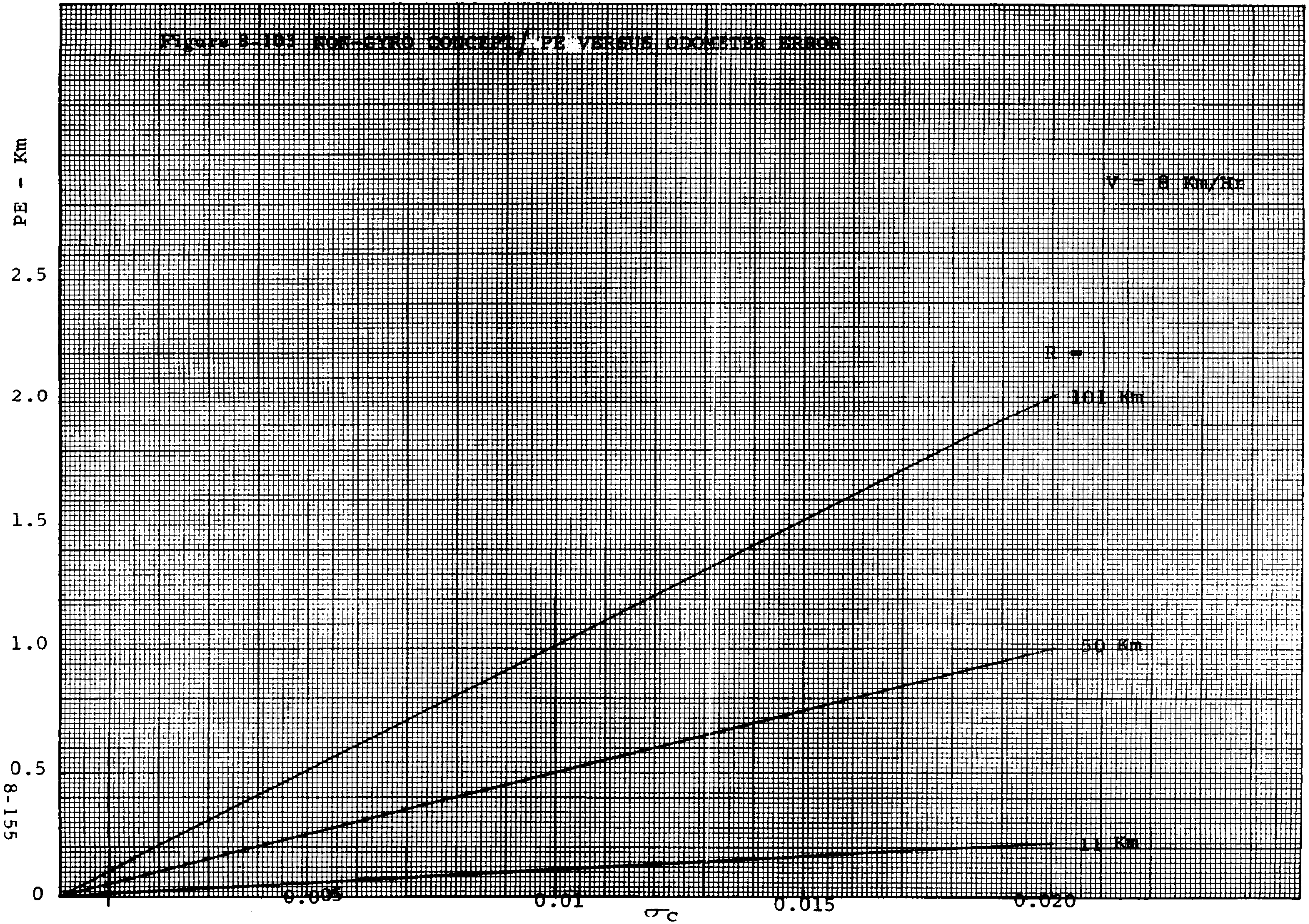

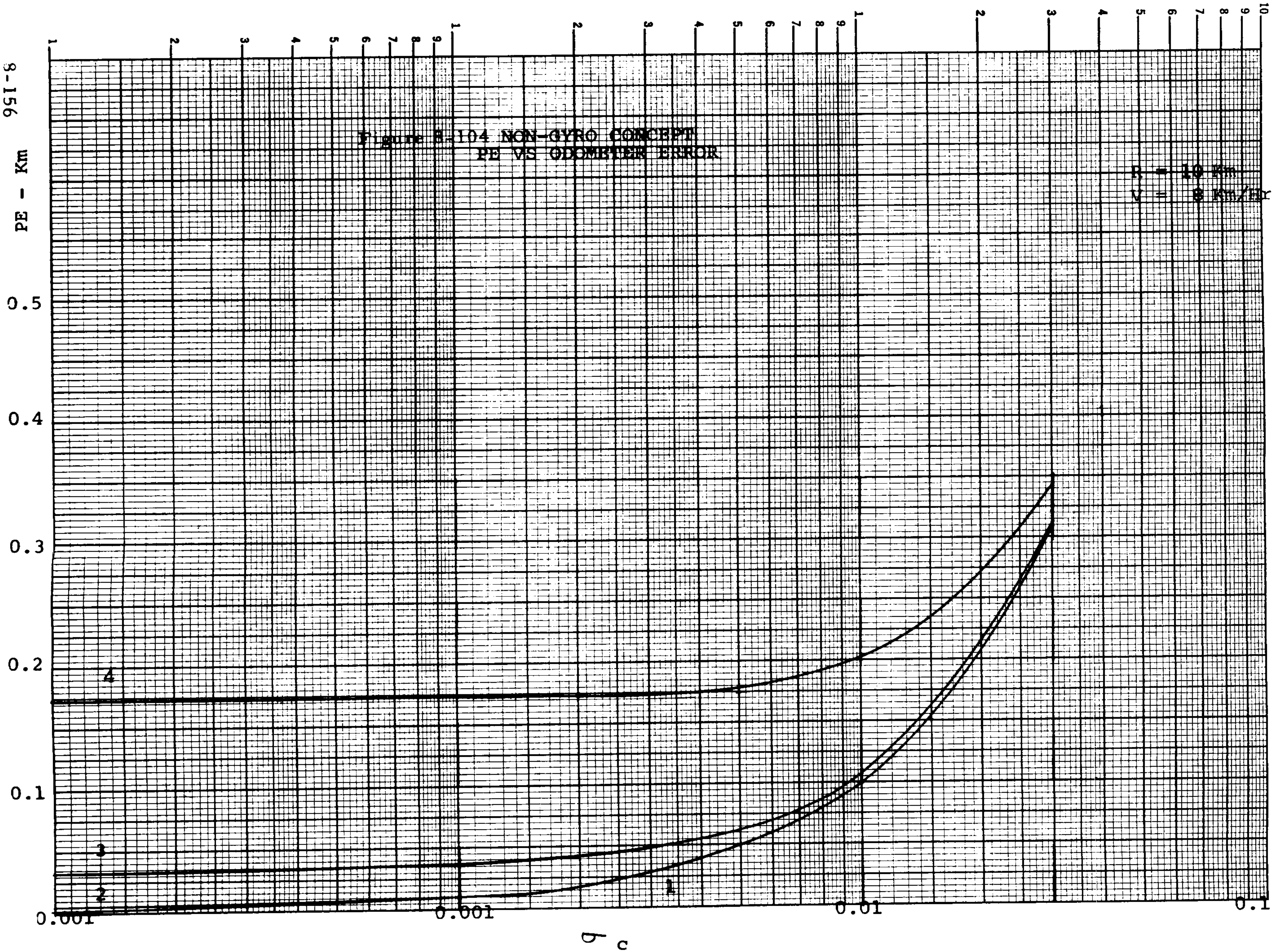

Figure 8-104 NON-GYRO CONCEPT
PE VS ODOMETER ERROR

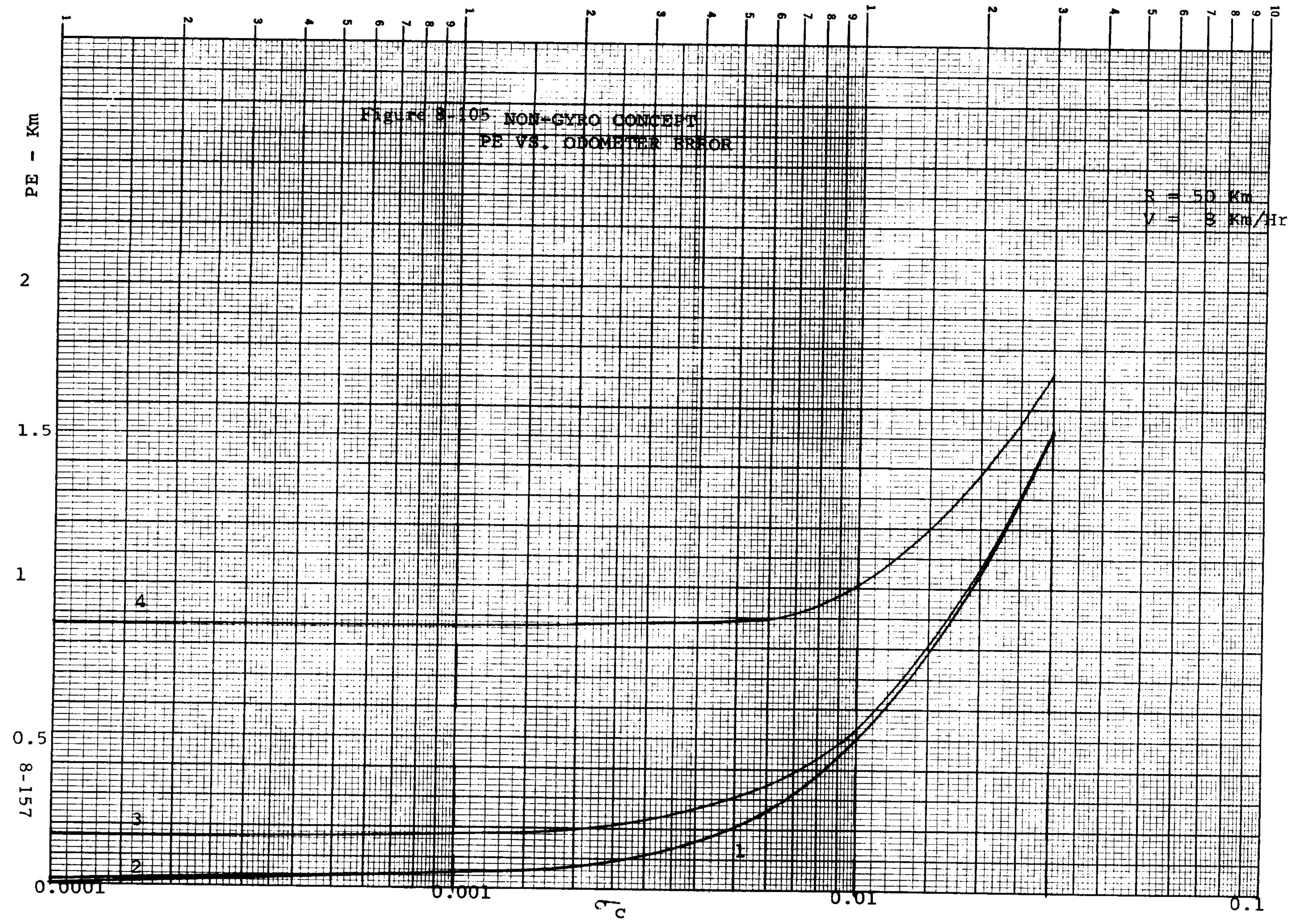

Figure 8-105 NON-GYRO CONCEPT PE VS. ODOMETER ERROR

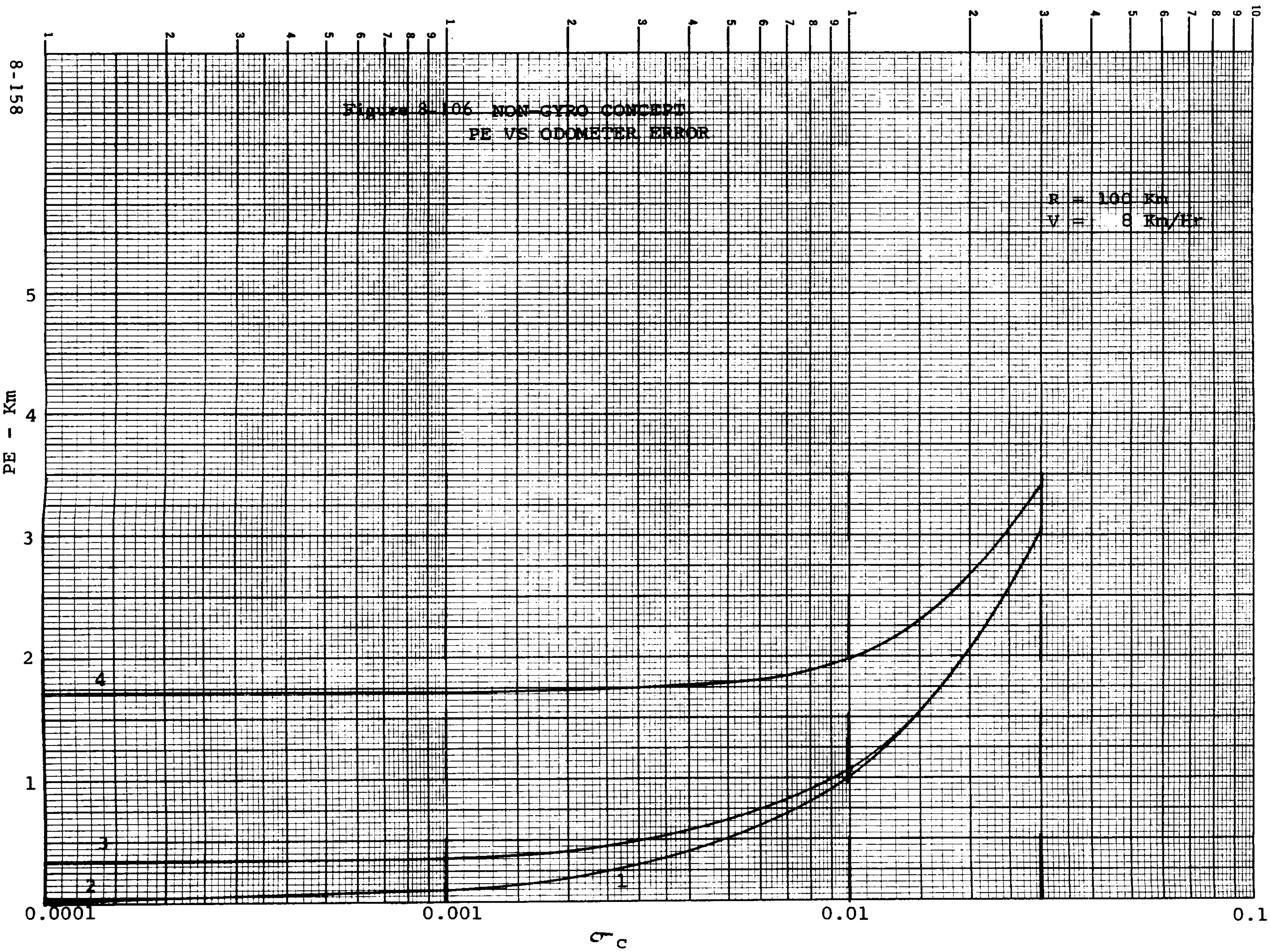

Figure 8-106 NON-GYRO CONCEPT
PE VS ODOMETER ERROR

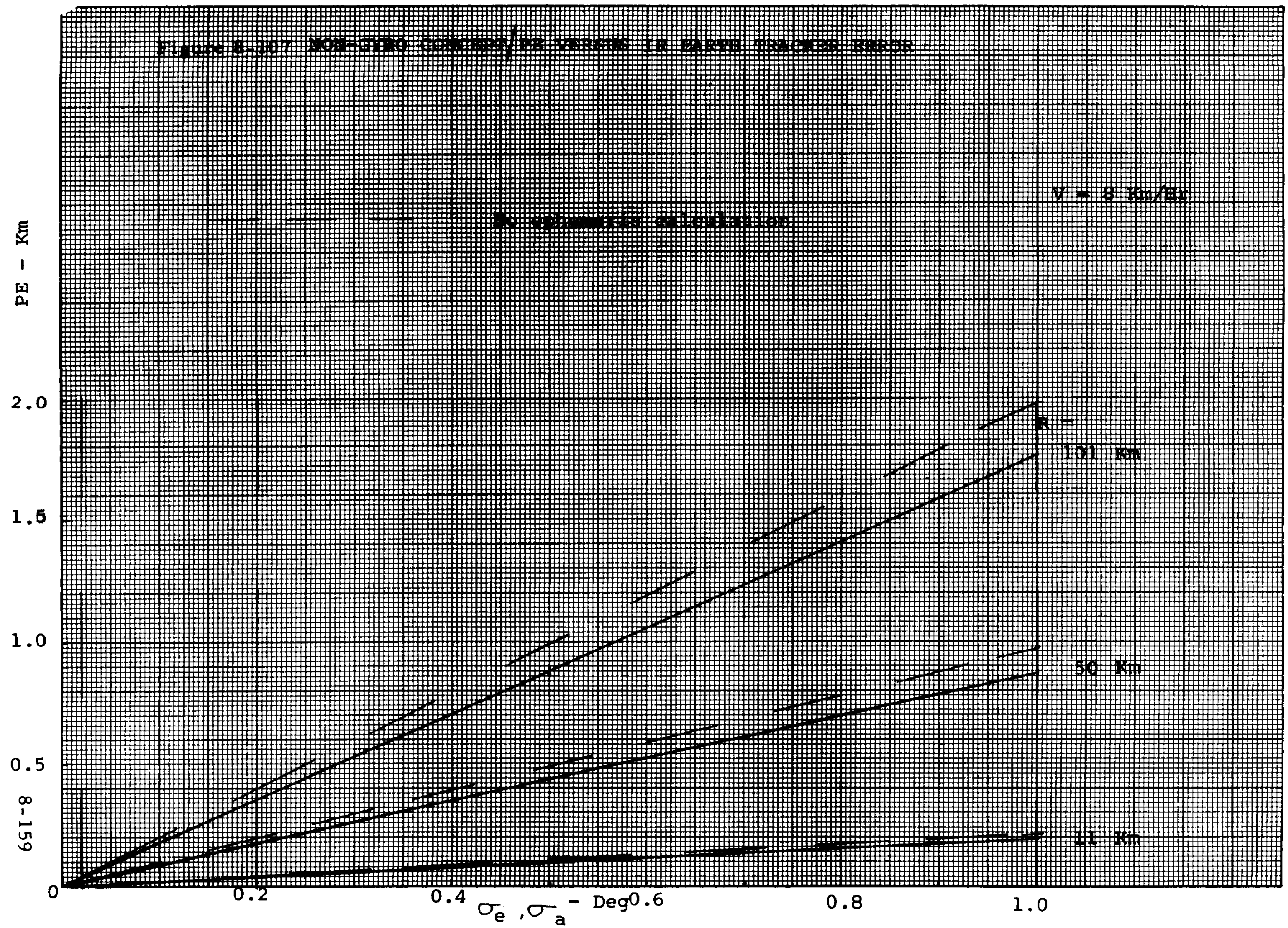

Figure 8-107 NON-GYRO CONCEPT/PE VERSUS IR EARTH TRACKER ERROR

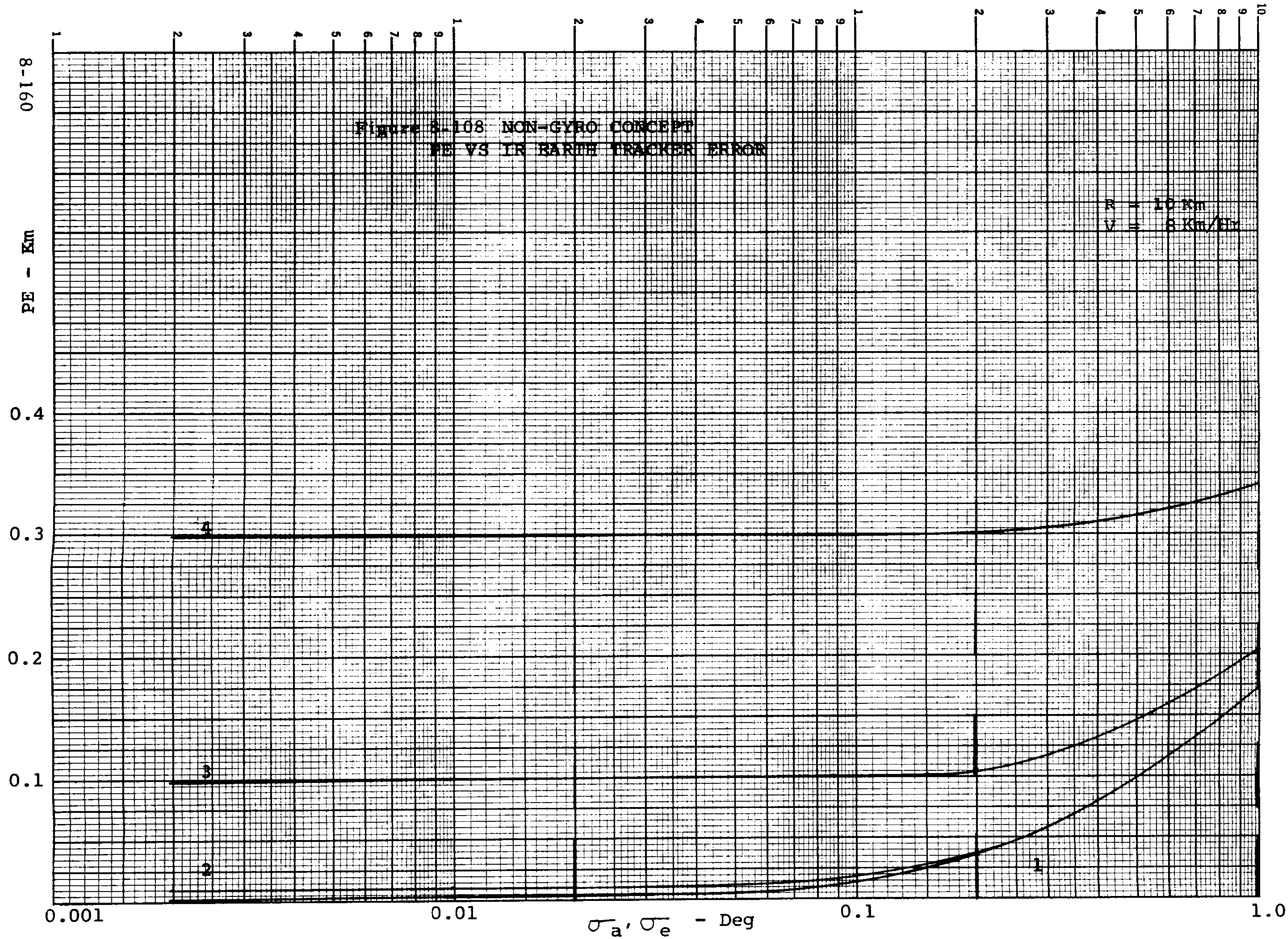

Figure 8-108 NON-GYRO CONCEPT
PE VS IR EARTH TRACKER ERROR
R = 10 Km
V = 8 Km/Hr
PE - Km
0.4
0.3
0.2
0.1
4
3
2
1
0.001
0.01
0.1
1.0
σ_a, σ_e - Deg

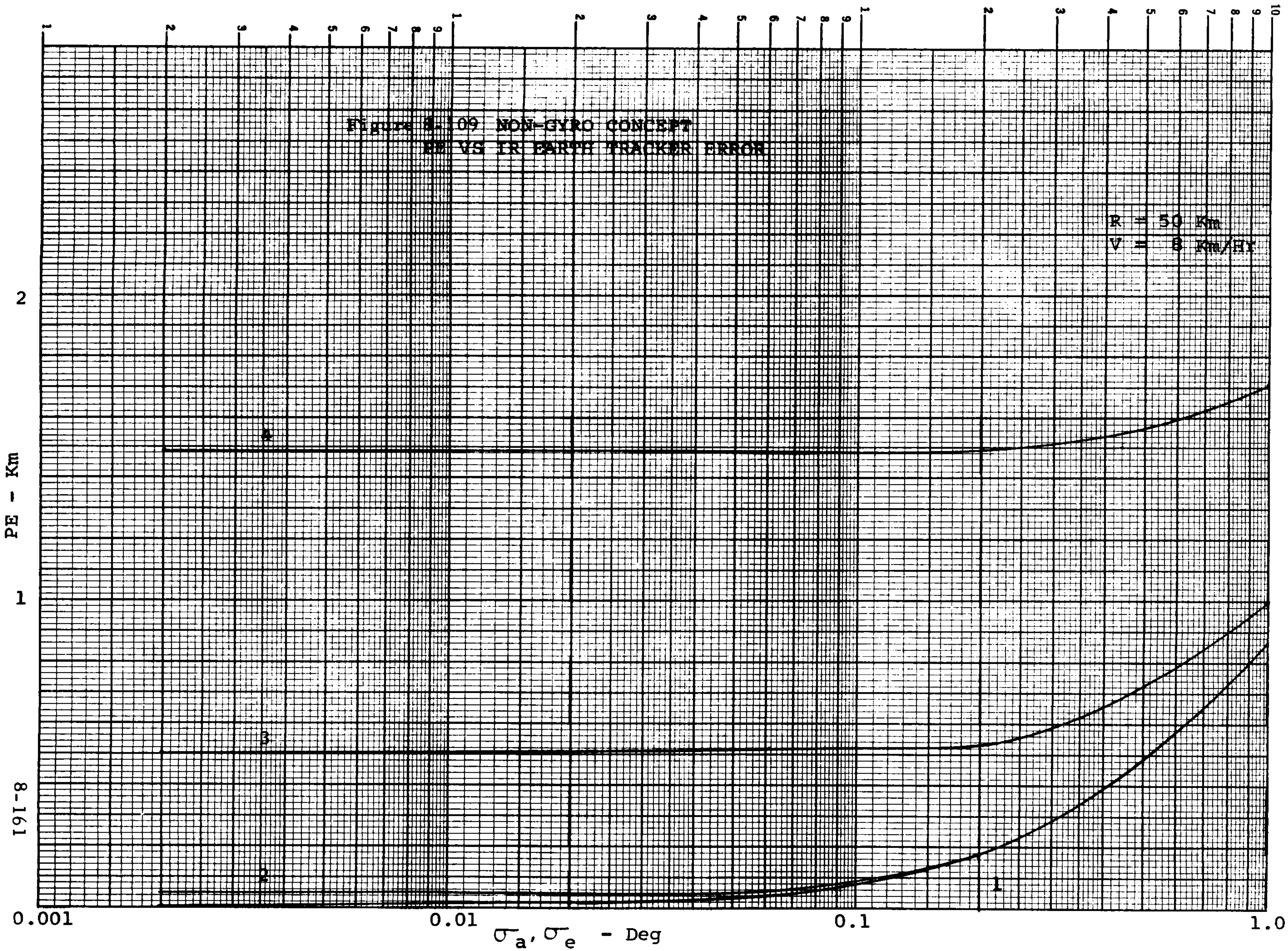

Figure 8-109 NON-GYRO CONCEPT
PE VS IR EARTH TRACKER ERROR

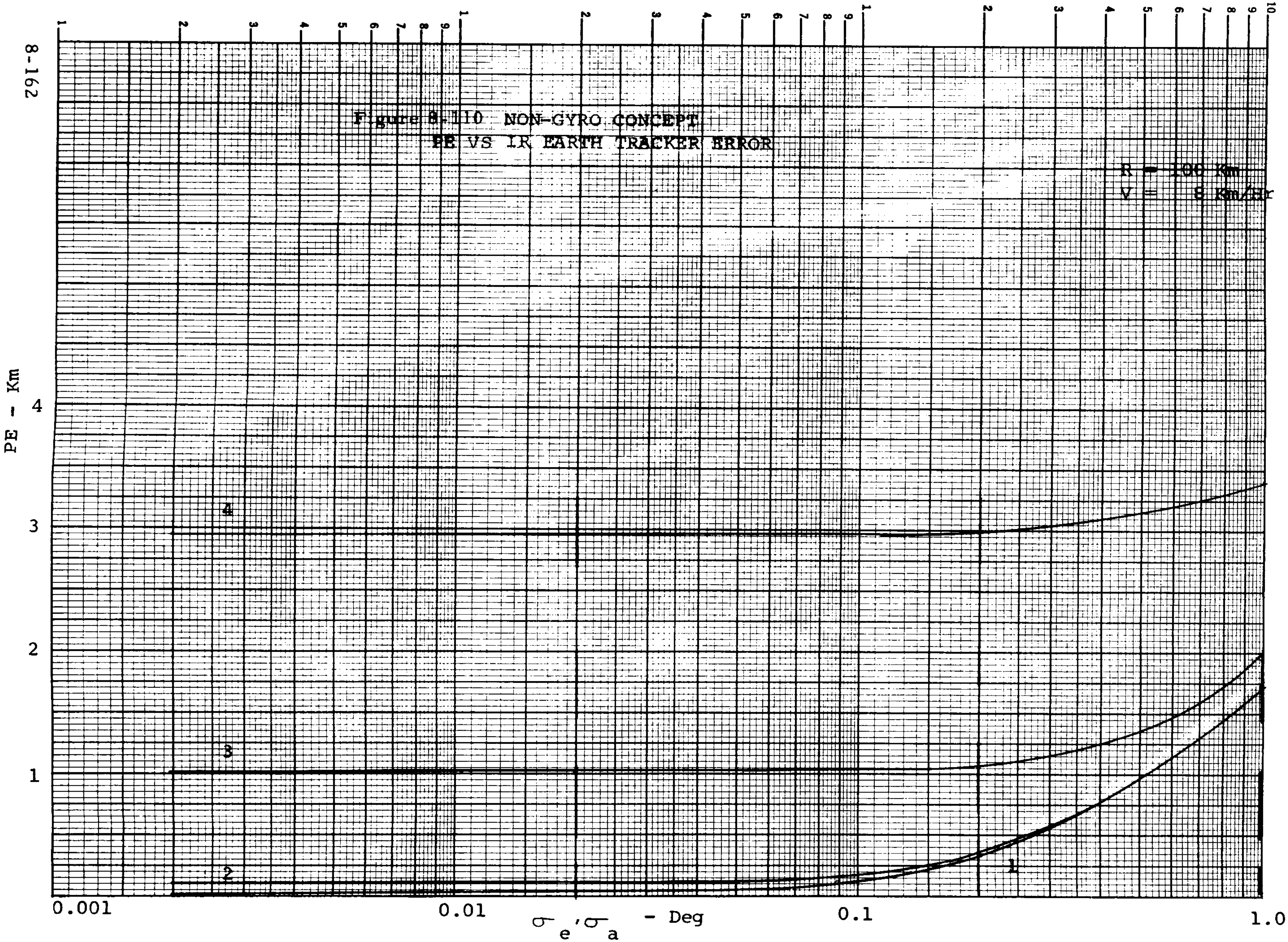

Figure 8.110 NON-GYRO CONCEPT
PE VS IR EARTH TRACKER ERROR

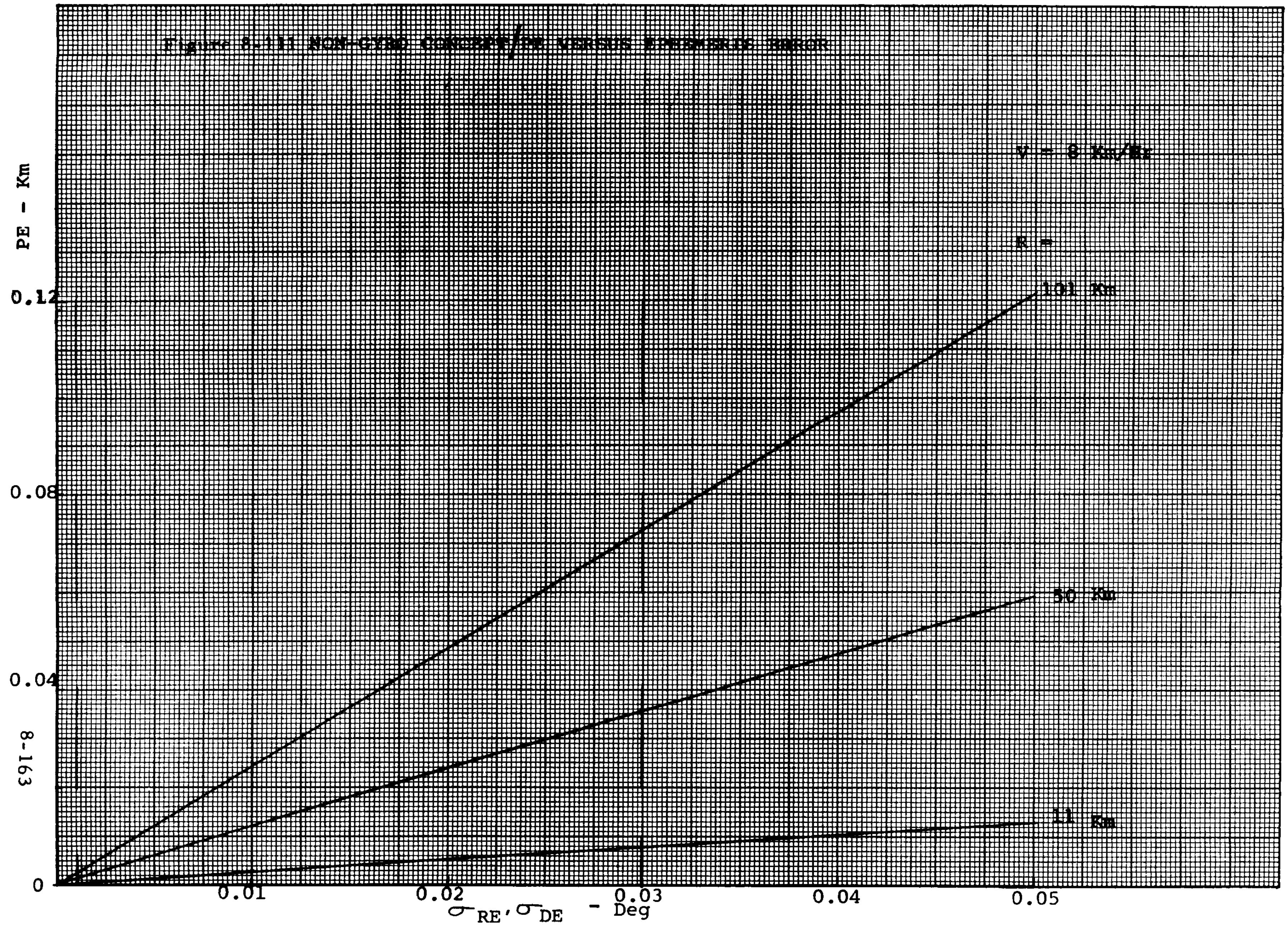

Figure 8-111 NON-GYRO CONCEPT PE VERSUS EPHEMERIS ERROR

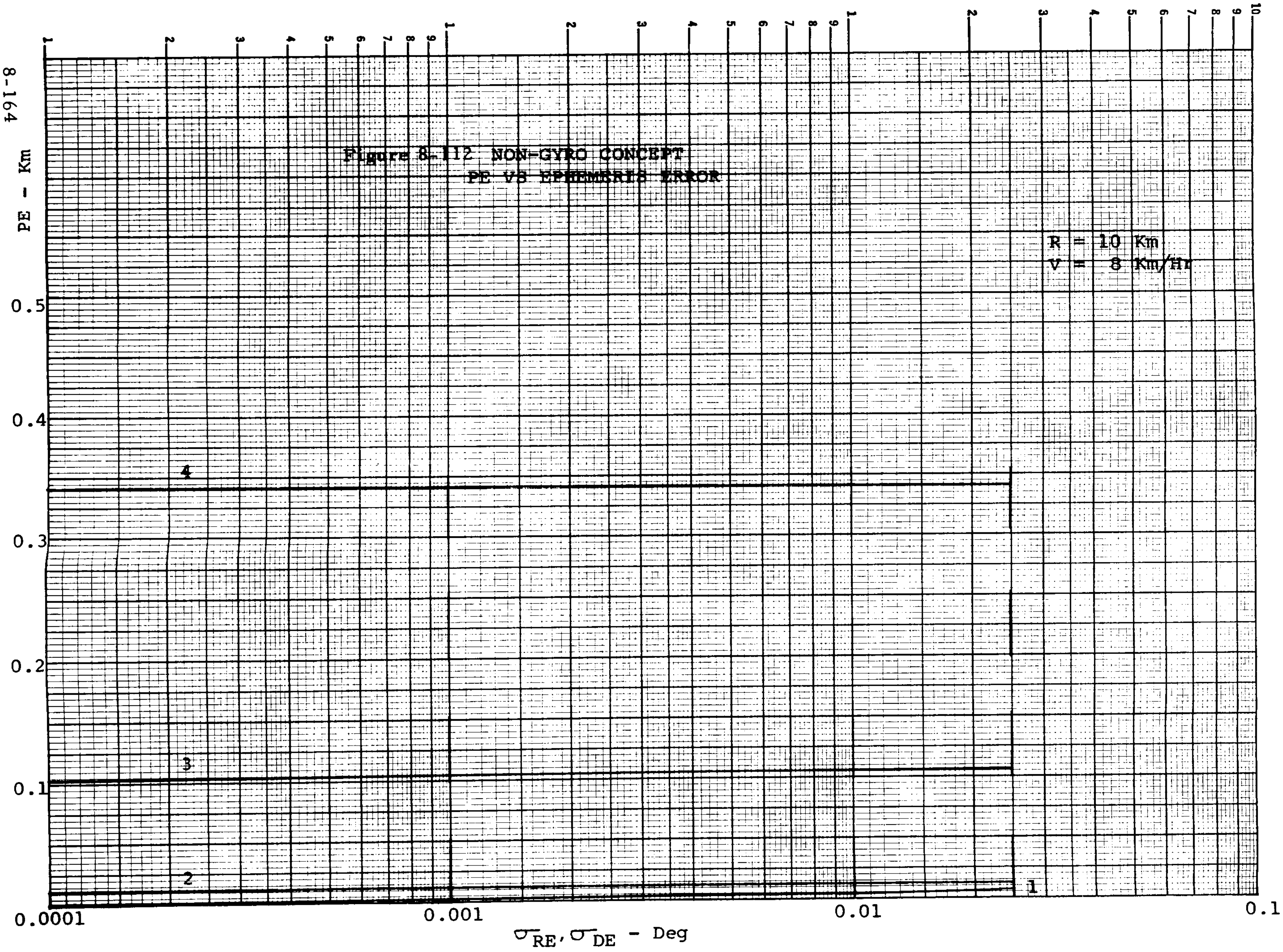

Figure 8-112 NON-GYRO CONCEPT
PE VS EPHEMERIS ERROR
R = 10 Km
V = 8 Km/Hr
PE - Km
0.5
0.4
0.3
0.2
0.1
0.0001
0.001
0.01
0.1
σ_{RE}, σ_{DE} - Deg
1
2
3
4

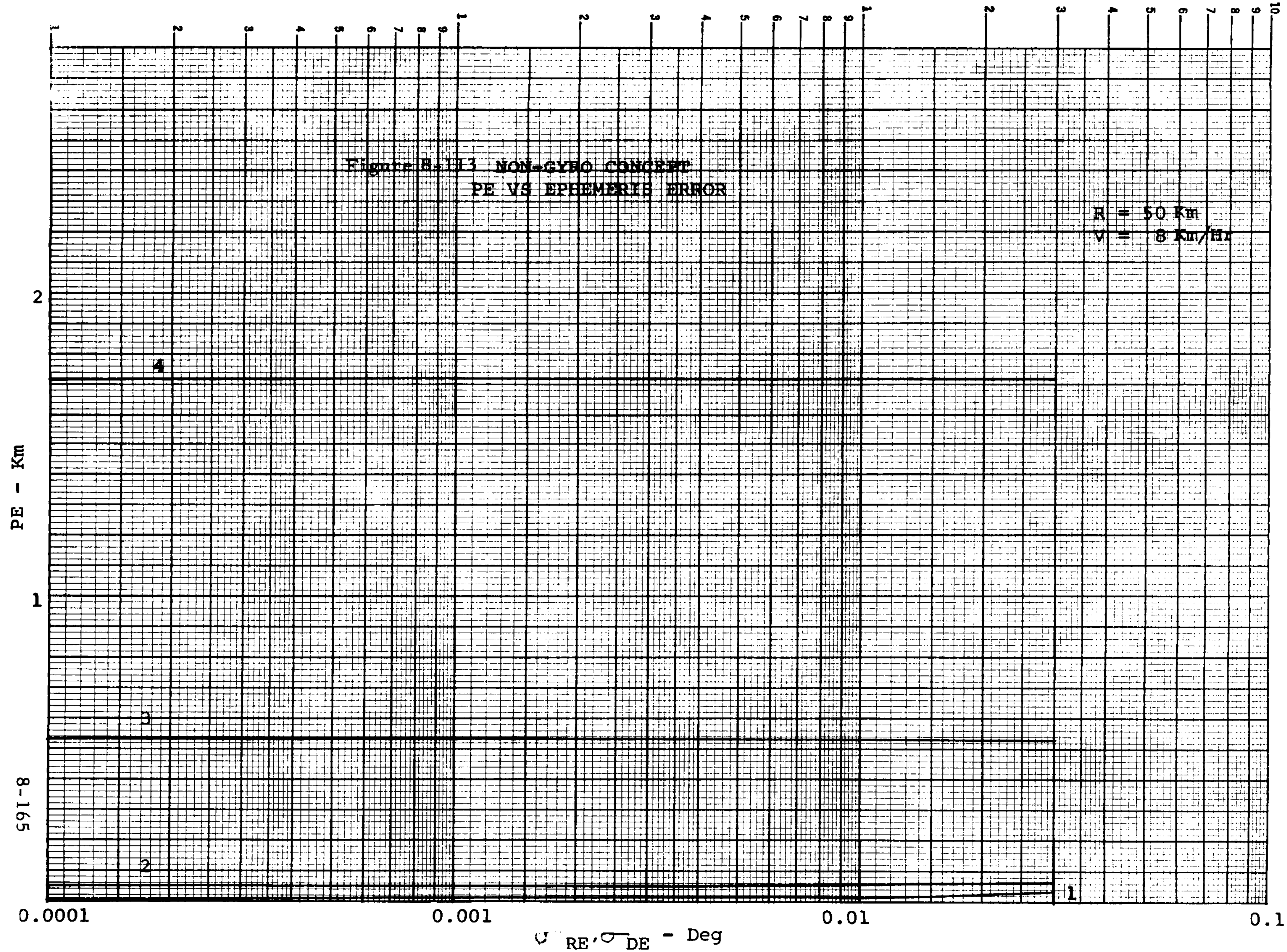

Figure 8.113 NON-GYRO CONCEPT
PE VS EPHEMERIS ERROR
R = 50 Km
V = 8 Km/Hr
PE - Km
σ_{RE}, σ_{DE} - Deg
0.0001
0.001
0.01
0.1

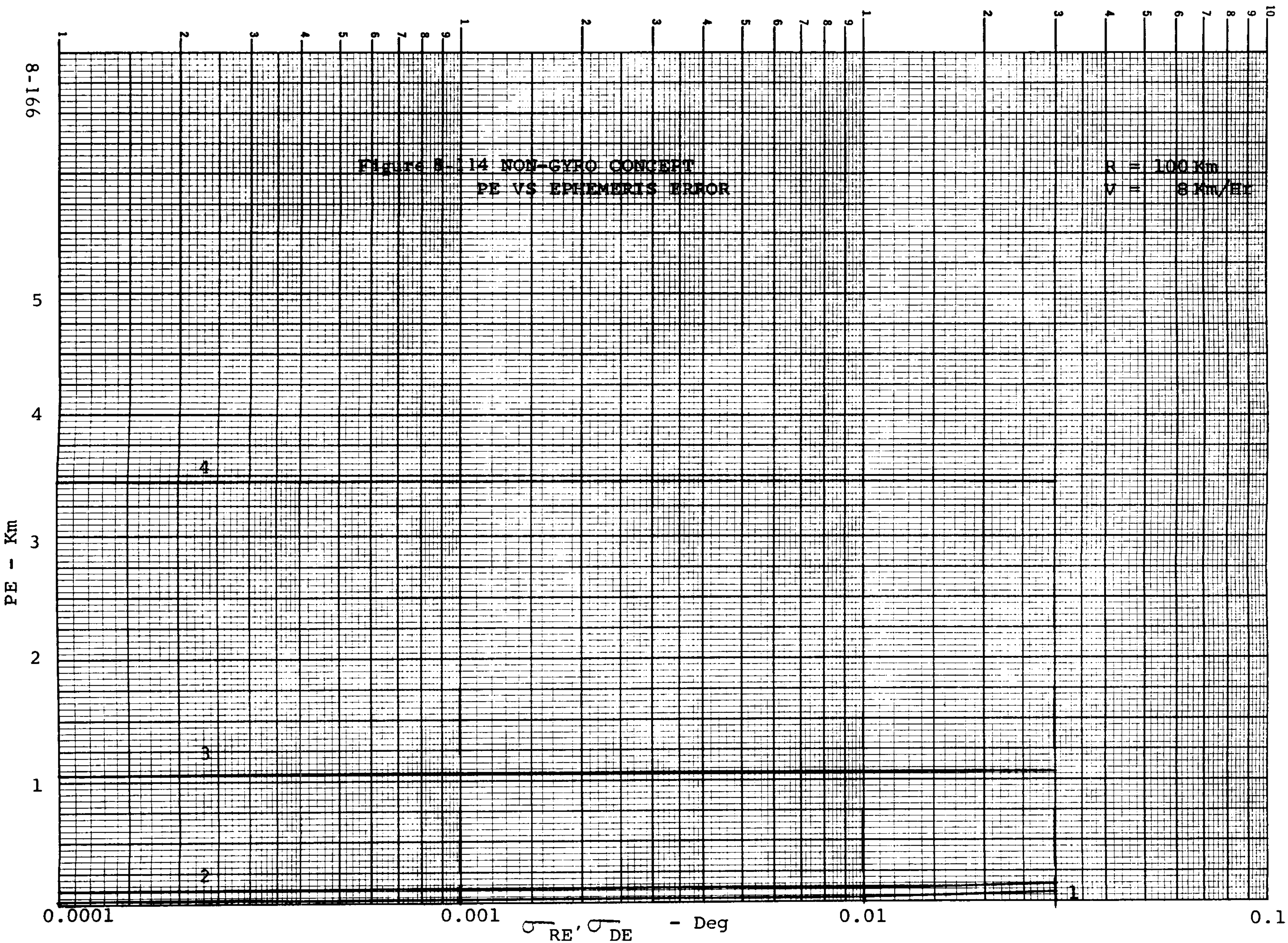

Figure 8.14 NON-GYRO CONCEPT
PE VS EPHEMERIS ERROR

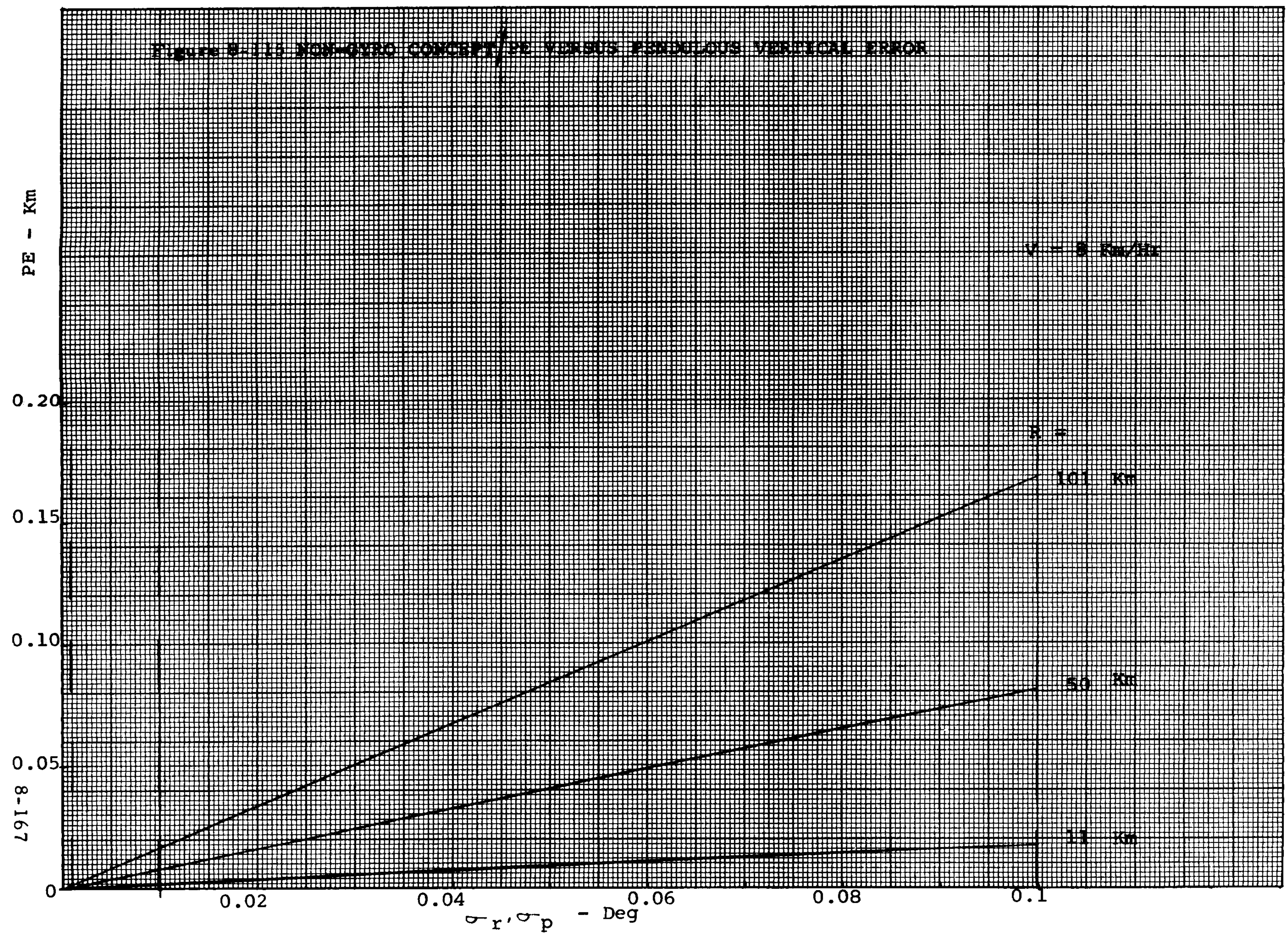

Figure 8-115 NON-GYRO CONCEPT/PE VERSUS PENDULOUS VERTICAL ERROR

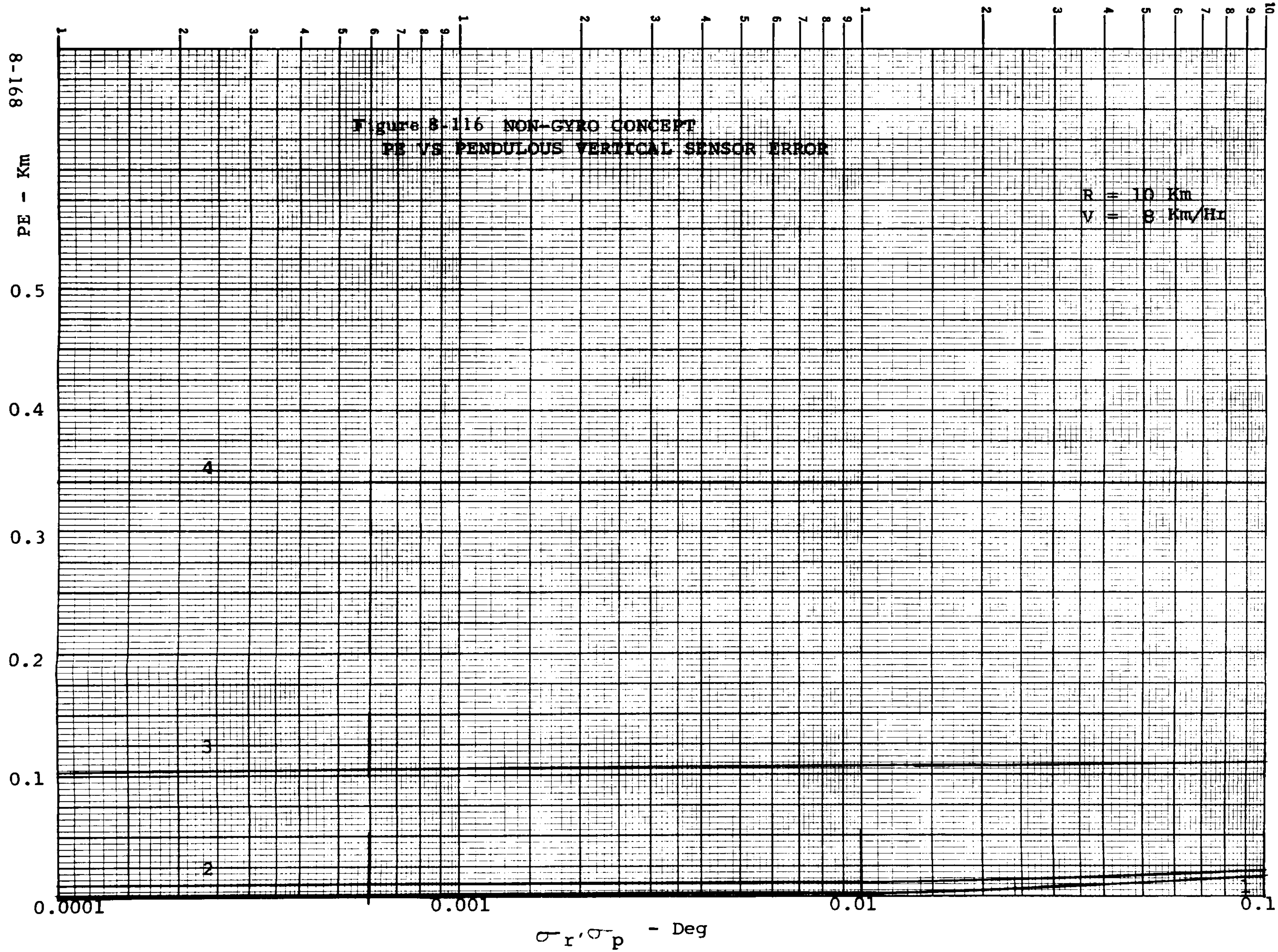

Figure 8-116 NON-GYRO CONCEPT
PE VS PENDULOUS VERTICAL SENSOR ERROR
R = 10 Km
V = 8 Km/Hr
PE - Km
0.5
0.4
0.3
0.2
0.1
0.0001
0.001
0.01
0.1
σ_r, σ_p - Deg
4
3
2
1

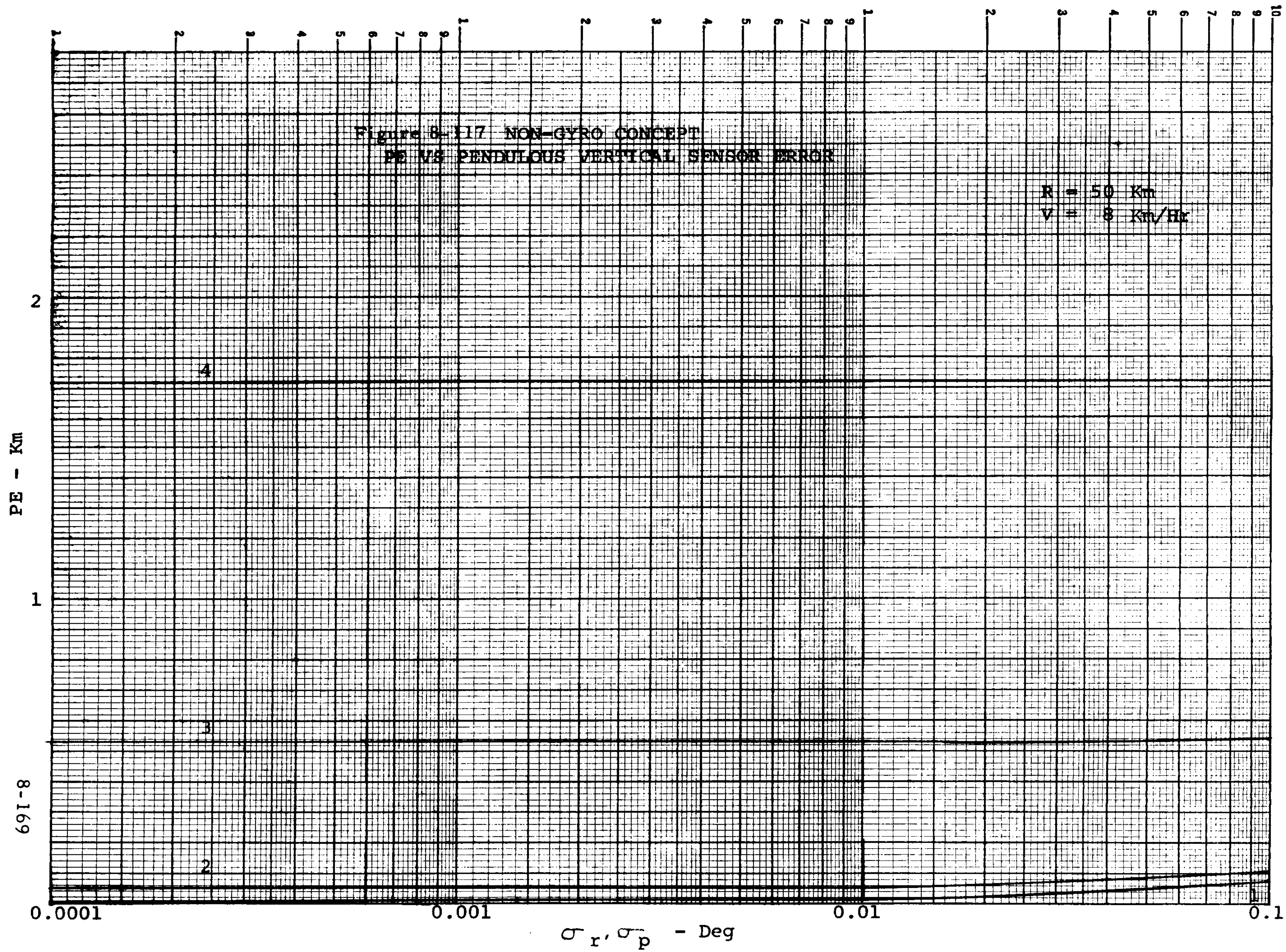
Figure 8-117 NON-GYRO CONCEPT
PE VS PENDULOUS VERTICAL SENSOR ERROR
R = 50 Km
V = 8 Km/Hr
PE - Km
2
1
4
3
2
1
0.0001
0.001
0.01
0.1
σ_r, σ_p - Deg

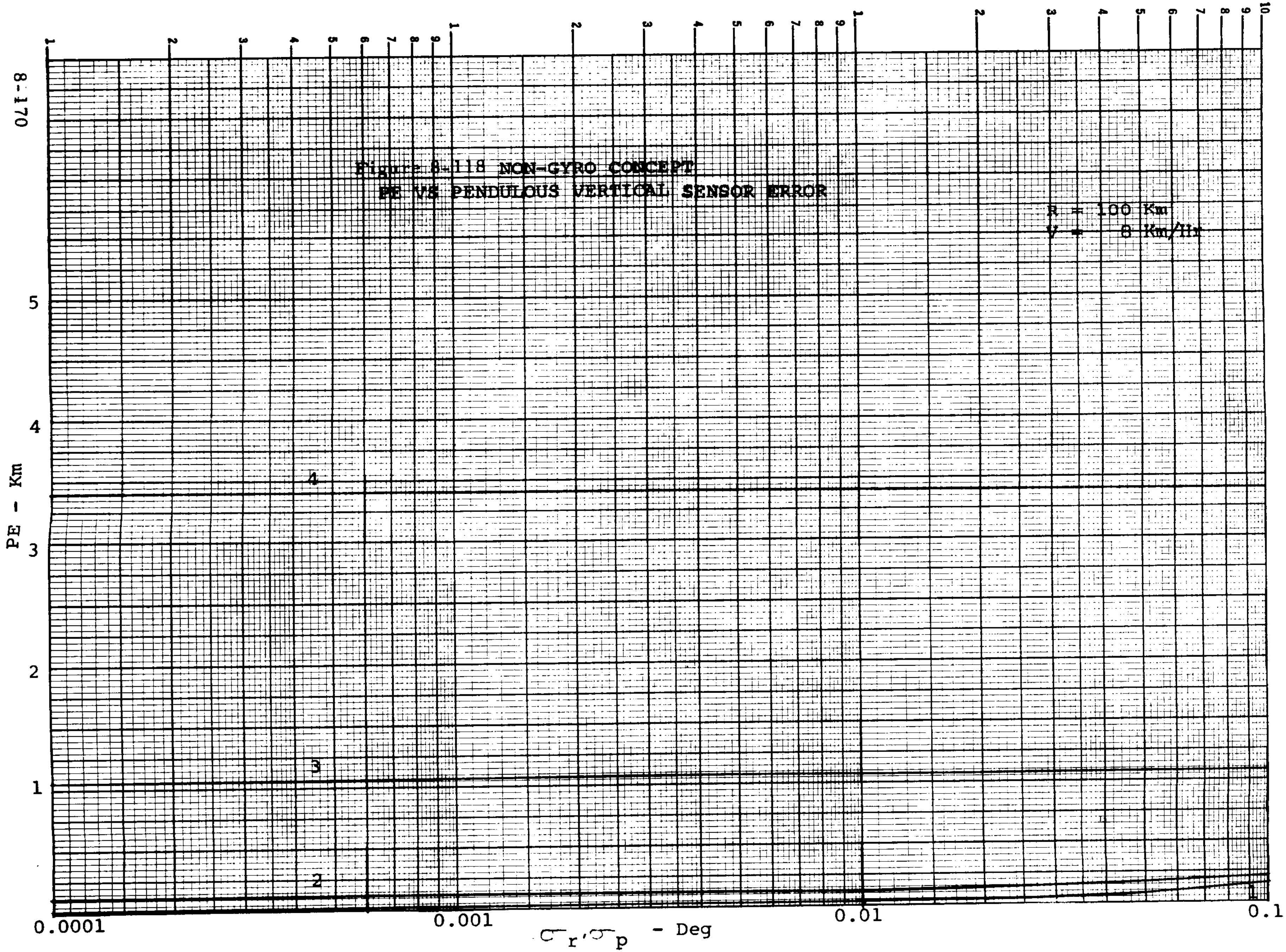

Figure 8-118 NON-GYRO CONCEPT
PE VS PENDULOUS VERTICAL SENSOR ERROR

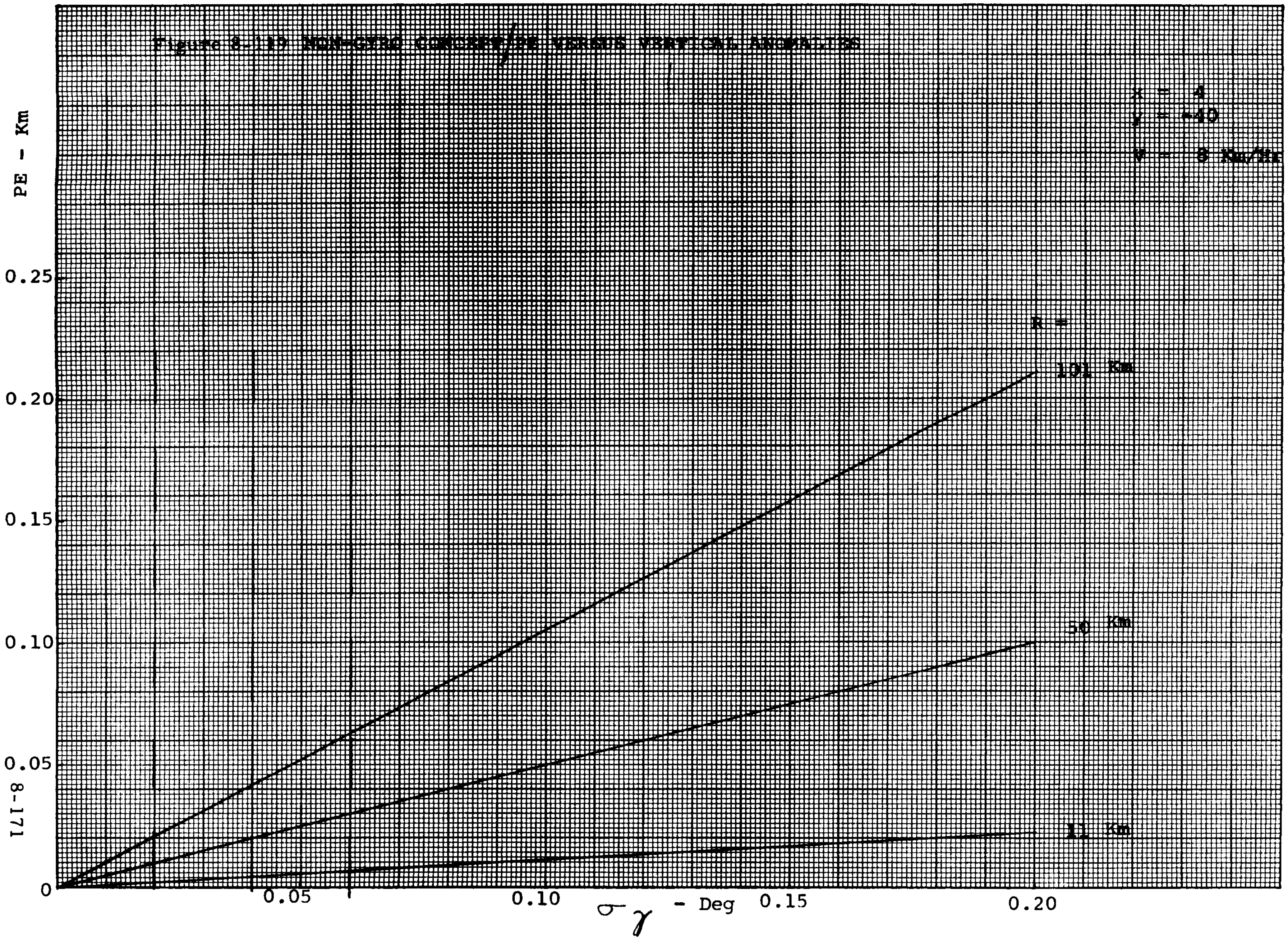

Figure 8-119 NON-GYRO CONCEPT/PE VERSUS VERTICAL ANOMALIES

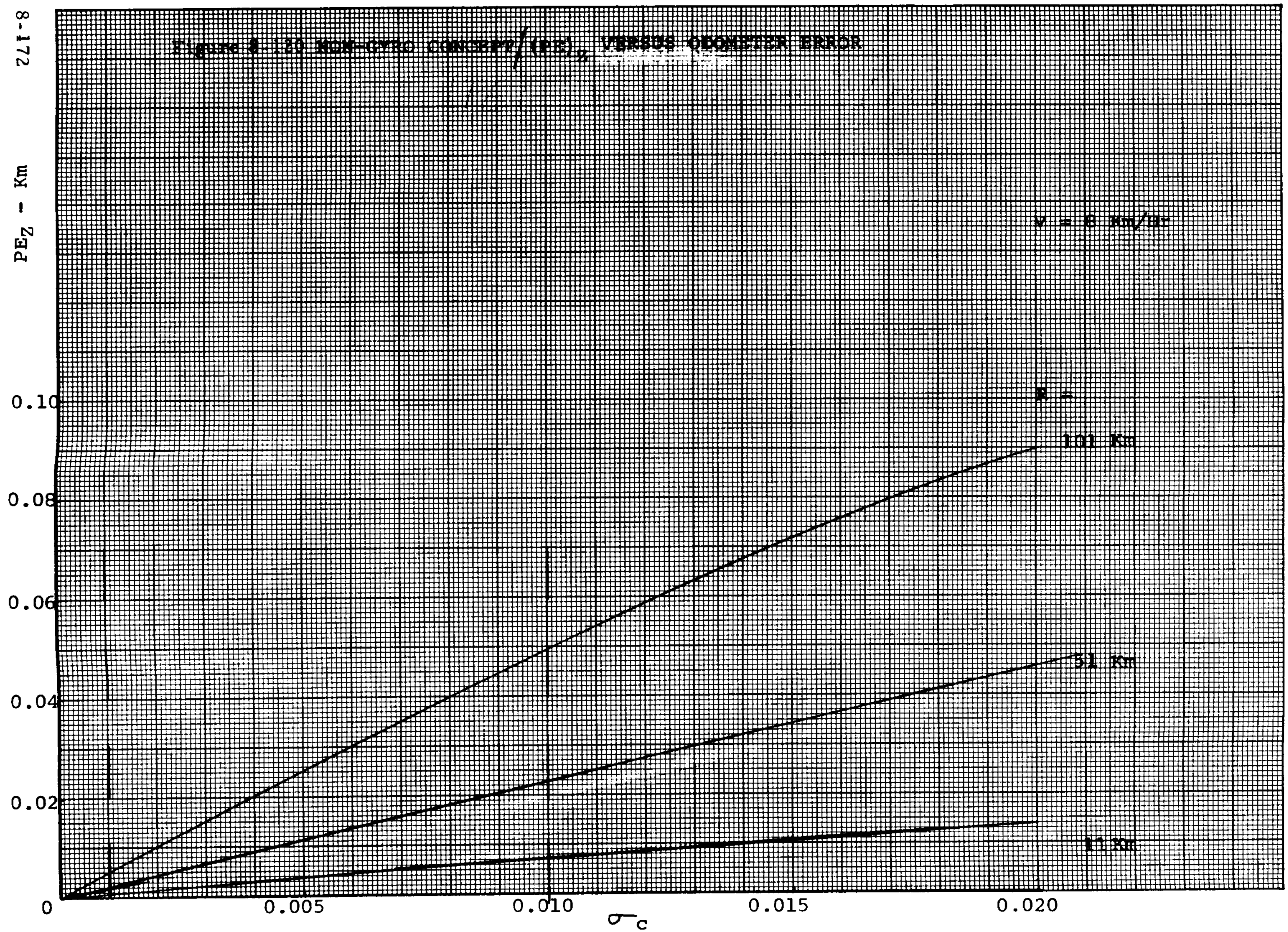

Figure 8-120 NON-GYRO CONCEPT $(PE)_Z$ VERSUS ODOMETER ERROR

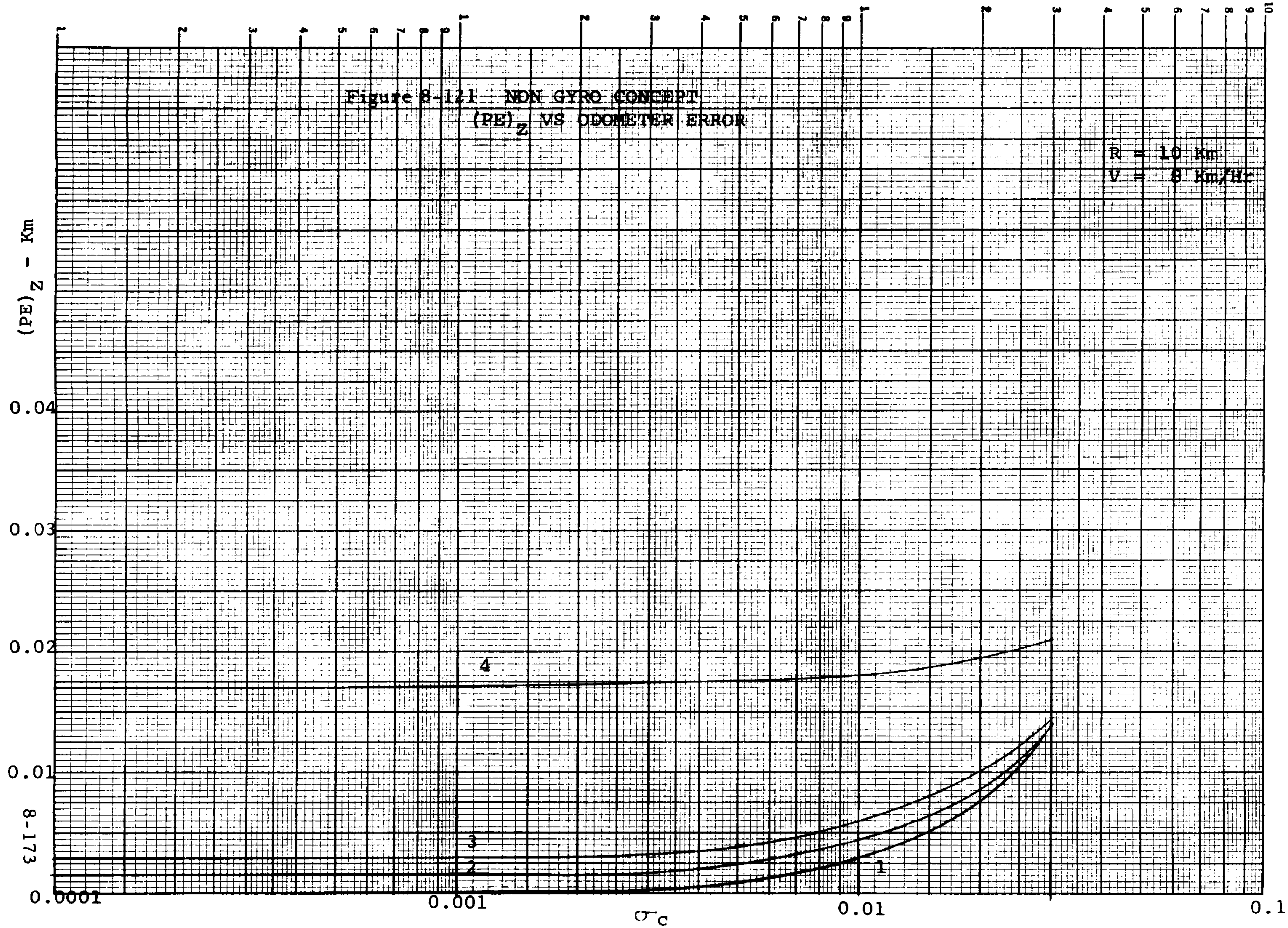

Figure 8-121 NON GYRO CONCEPT
$(PE)_Z$ VS ODOMETER ERROR

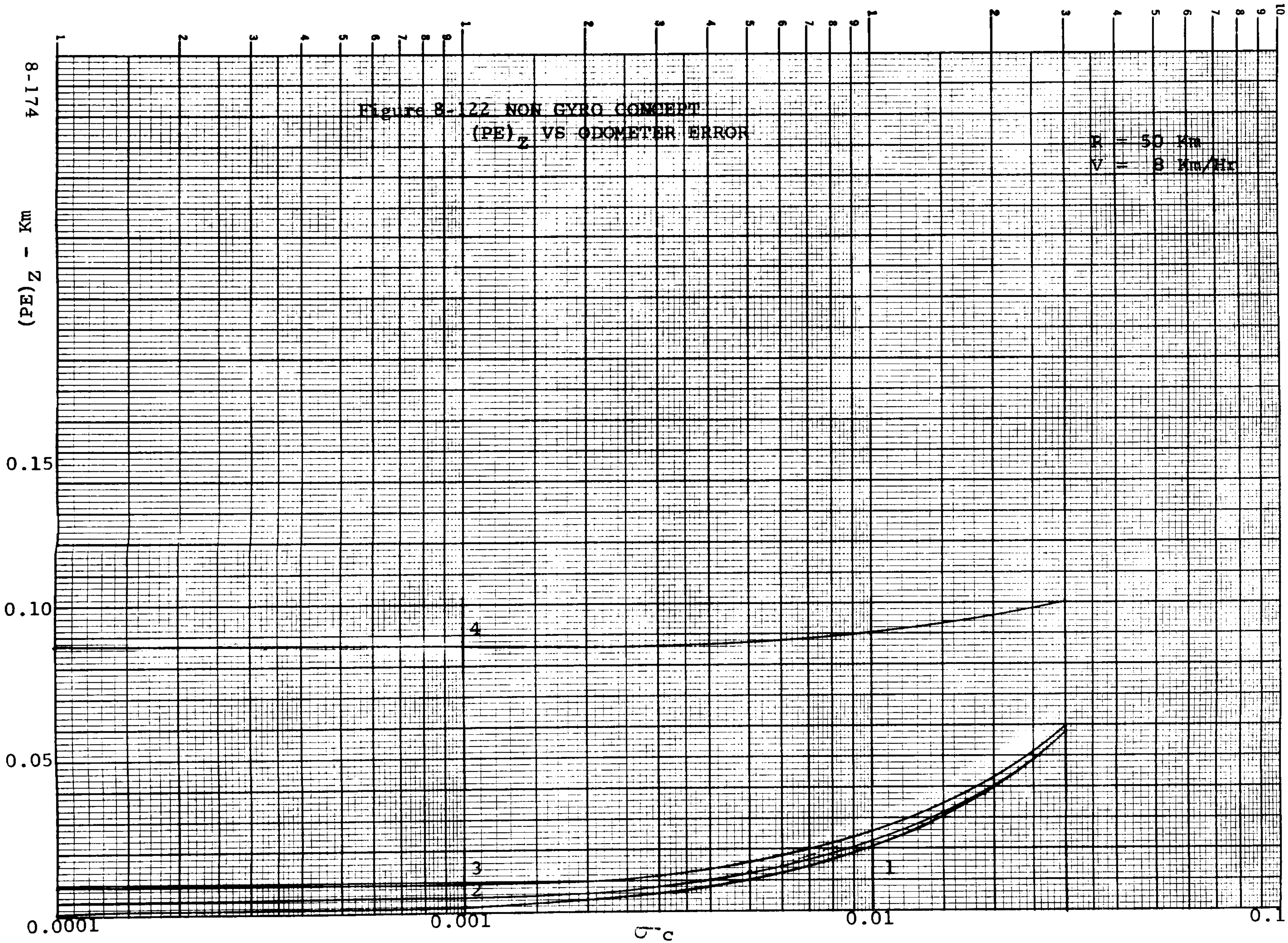

Figure 8-122 NON GYRO CONCEPT
(PE)Z VS ODOMETER ERROR
R = 50 Km
V = 8 Km/Hr
(PE)Z - Km
0.15
0.10
0.05
0.0001
0.001
0.01
0.1
σc
1
2
3
4

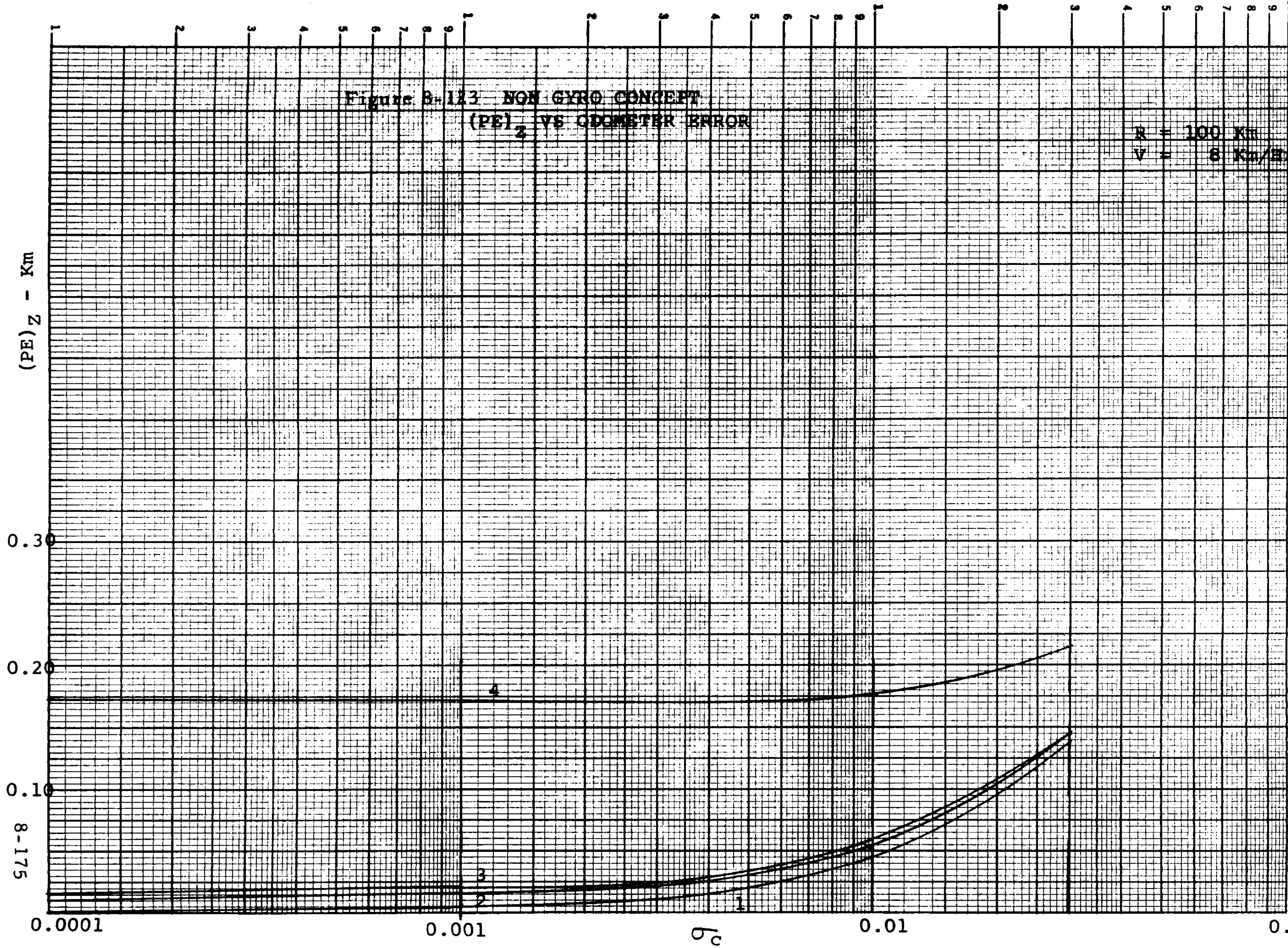

Figure 8-123 NON GYRO CONCEPT
(PE)$_Z$ VS ODOMETER ERROR

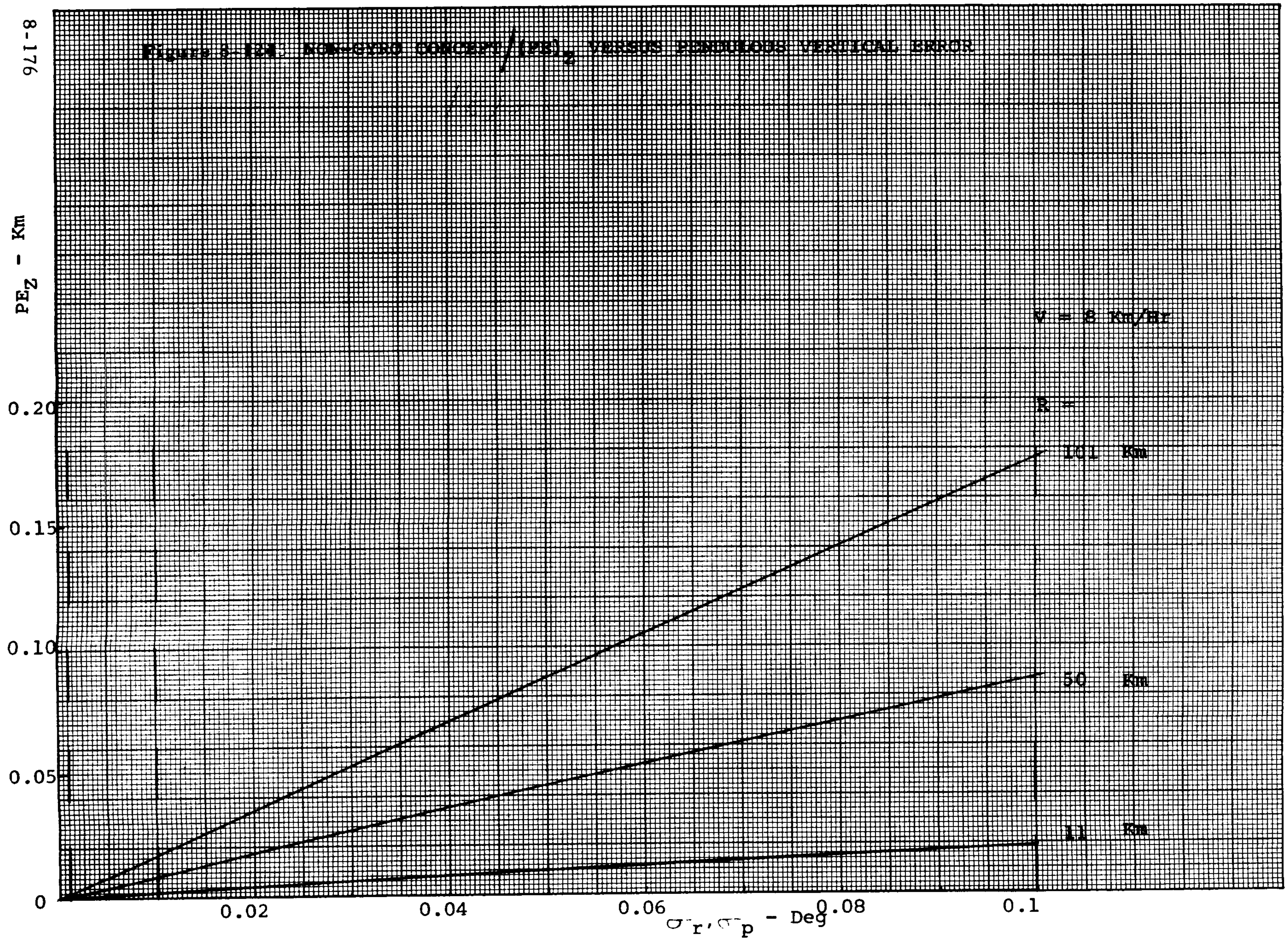

Figure 8-124. NON-GYRO CONCEPT/$(PE)_Z$ VERSUS PENDULOUS VERTICAL ERROR

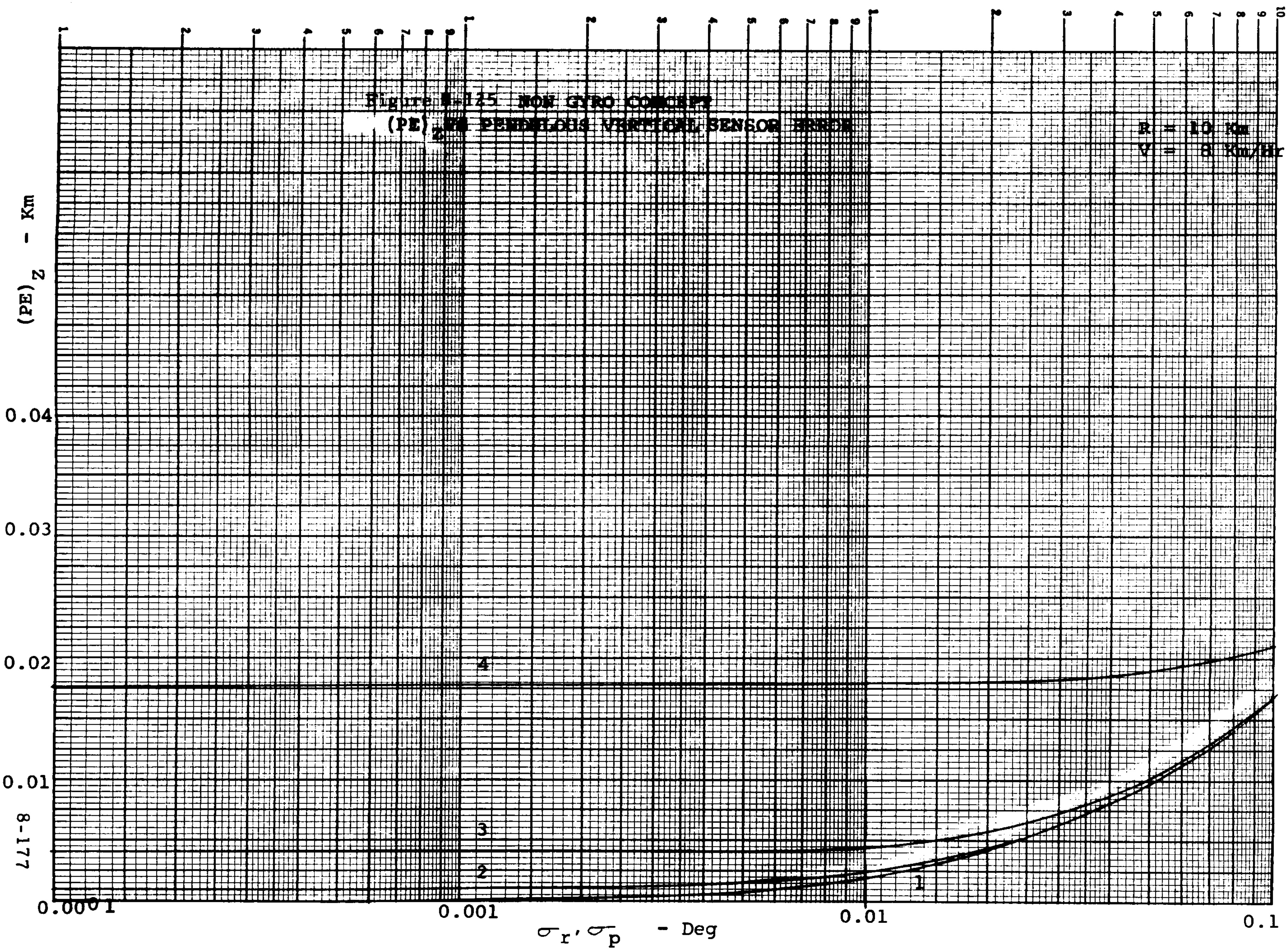

Figure 8-125 NON GYRO CONCEPT
$(PE)_Z$ VS PENDULOUS VERTICAL SENSOR ERROR

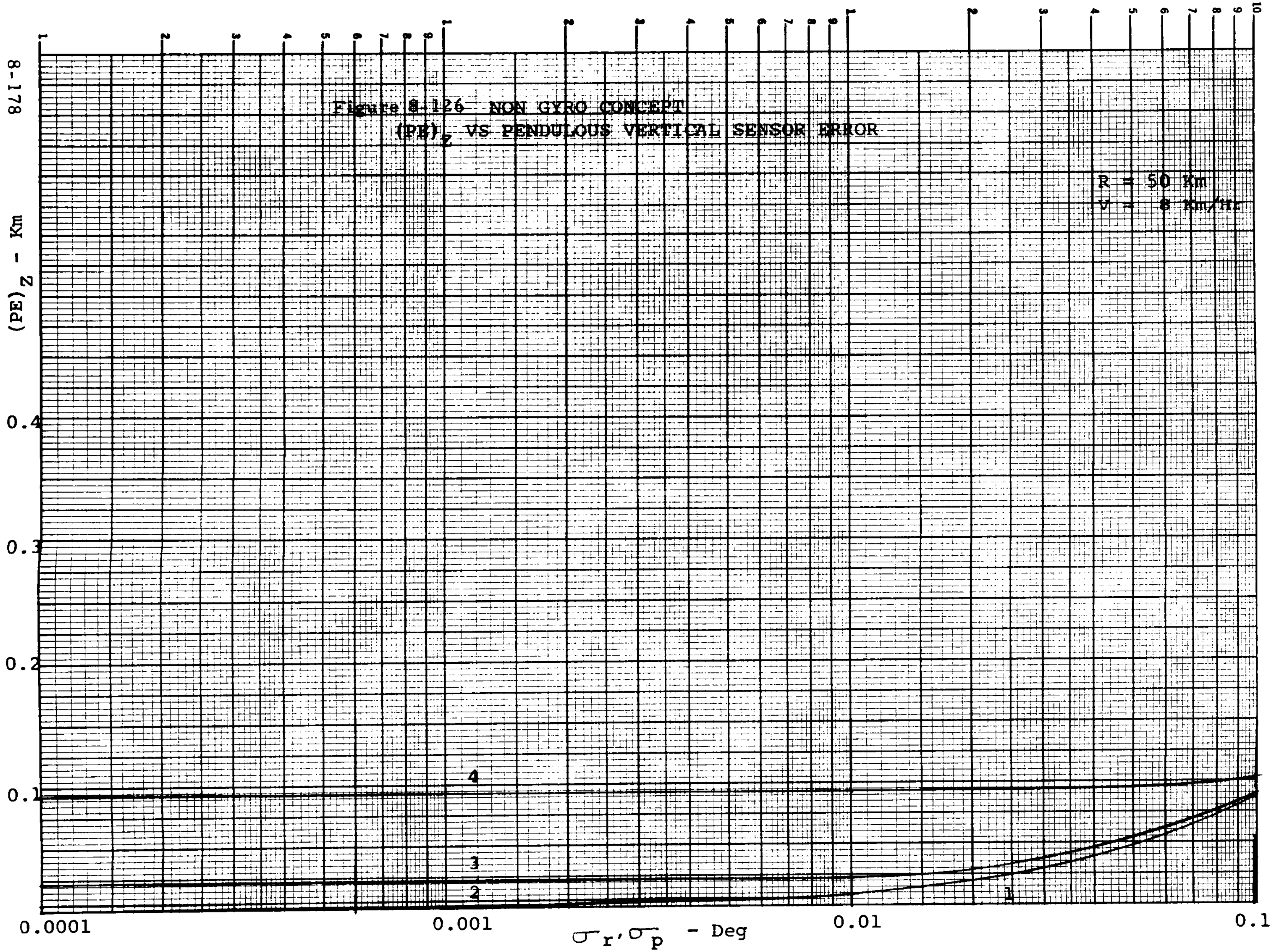

Figure 8-126 NON GYRO CONCEPT
$(PE)_z$ VS PENDULOUS VERTICAL SENSOR ERROR

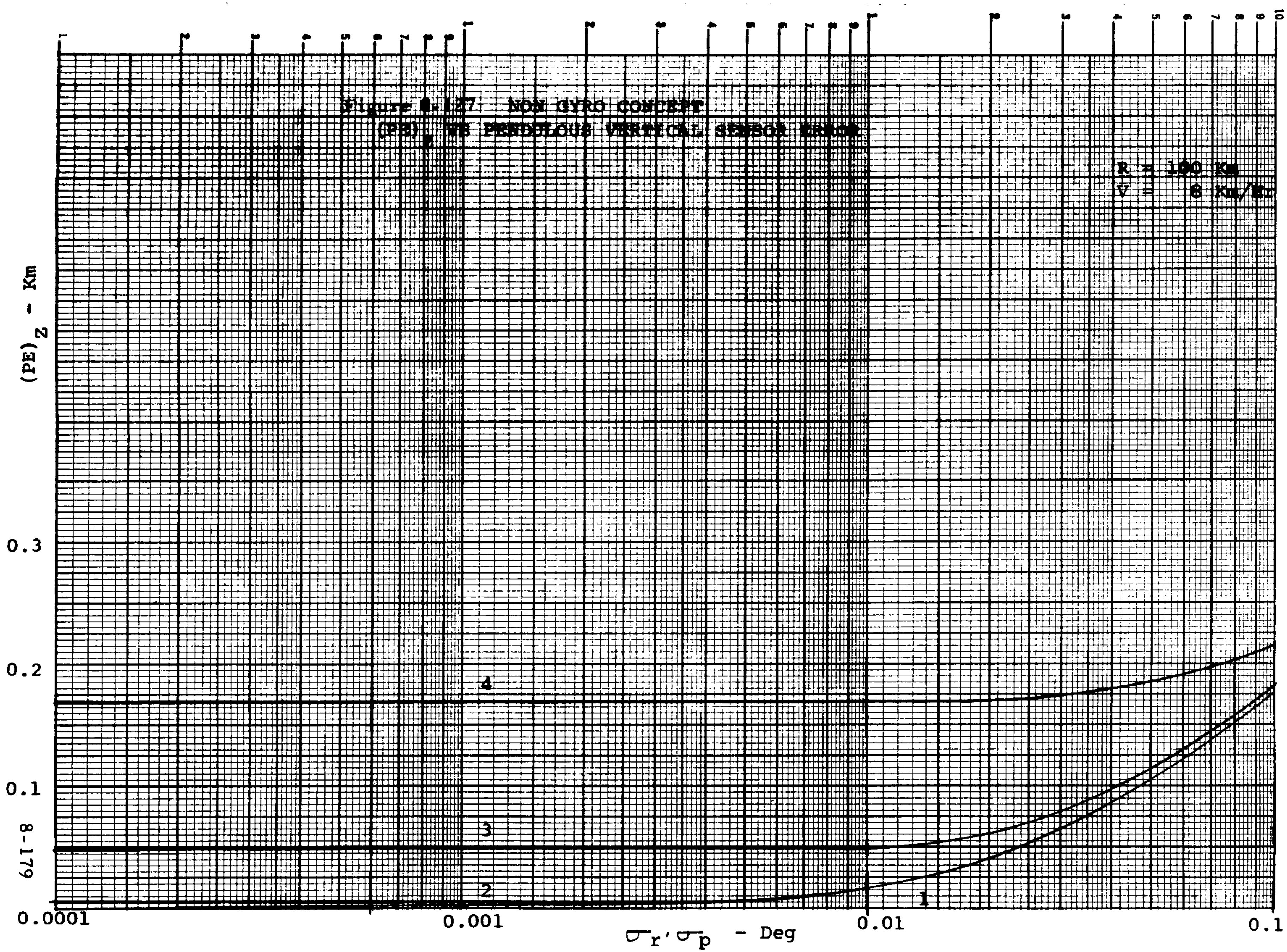

Figure 8.127 NON GYRO CONCEPT
(PE)$_z$ VS PENDULOUS VERTICAL SENSOR ERROR

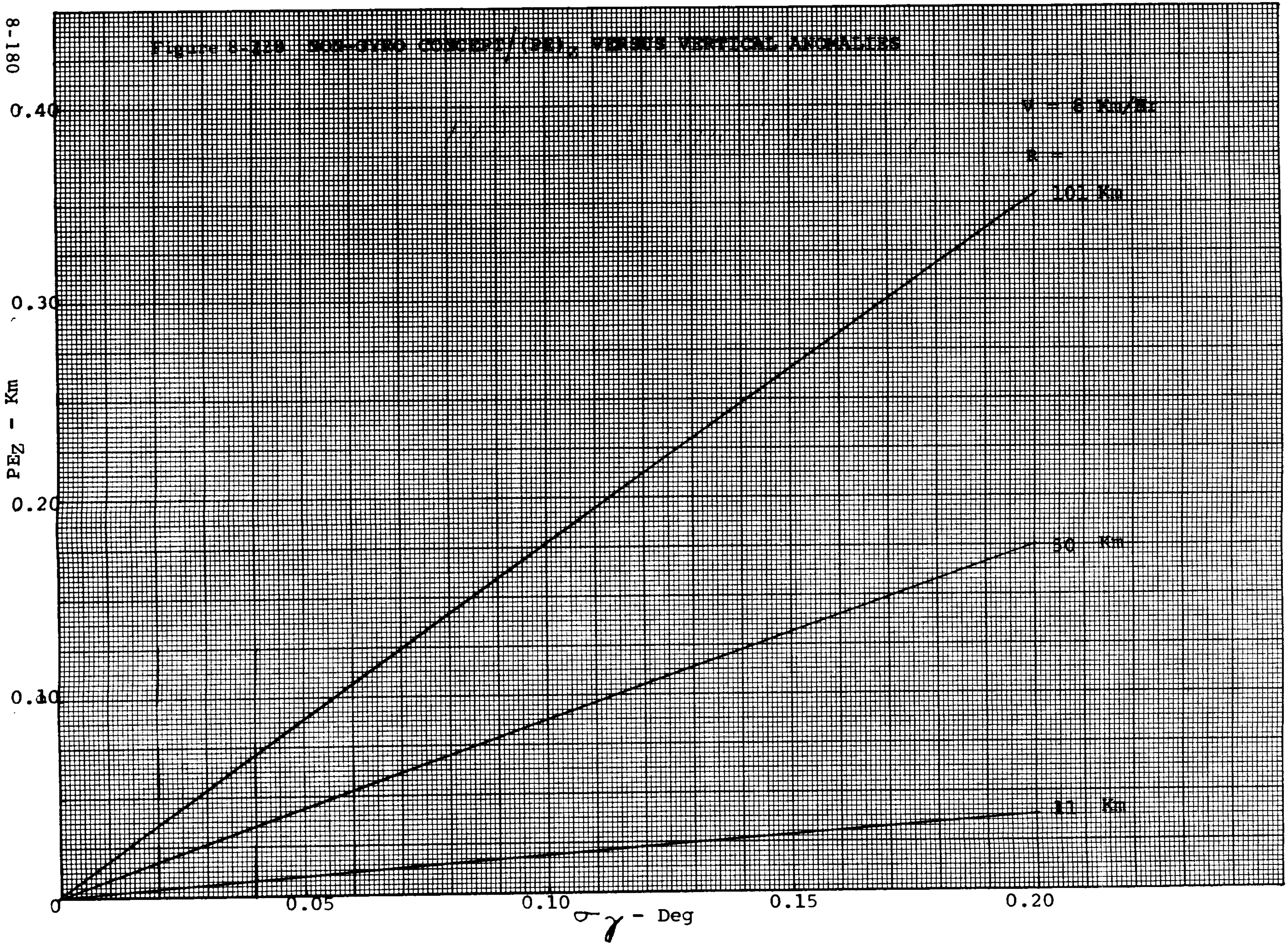

Figure 8-229 NON-GYRO CONCEPT/$(PE)_z$ VERSUS VERTICAL ANOMALIES

Figure 8-129 PLOT 1 MISSION I 1972 LEG C

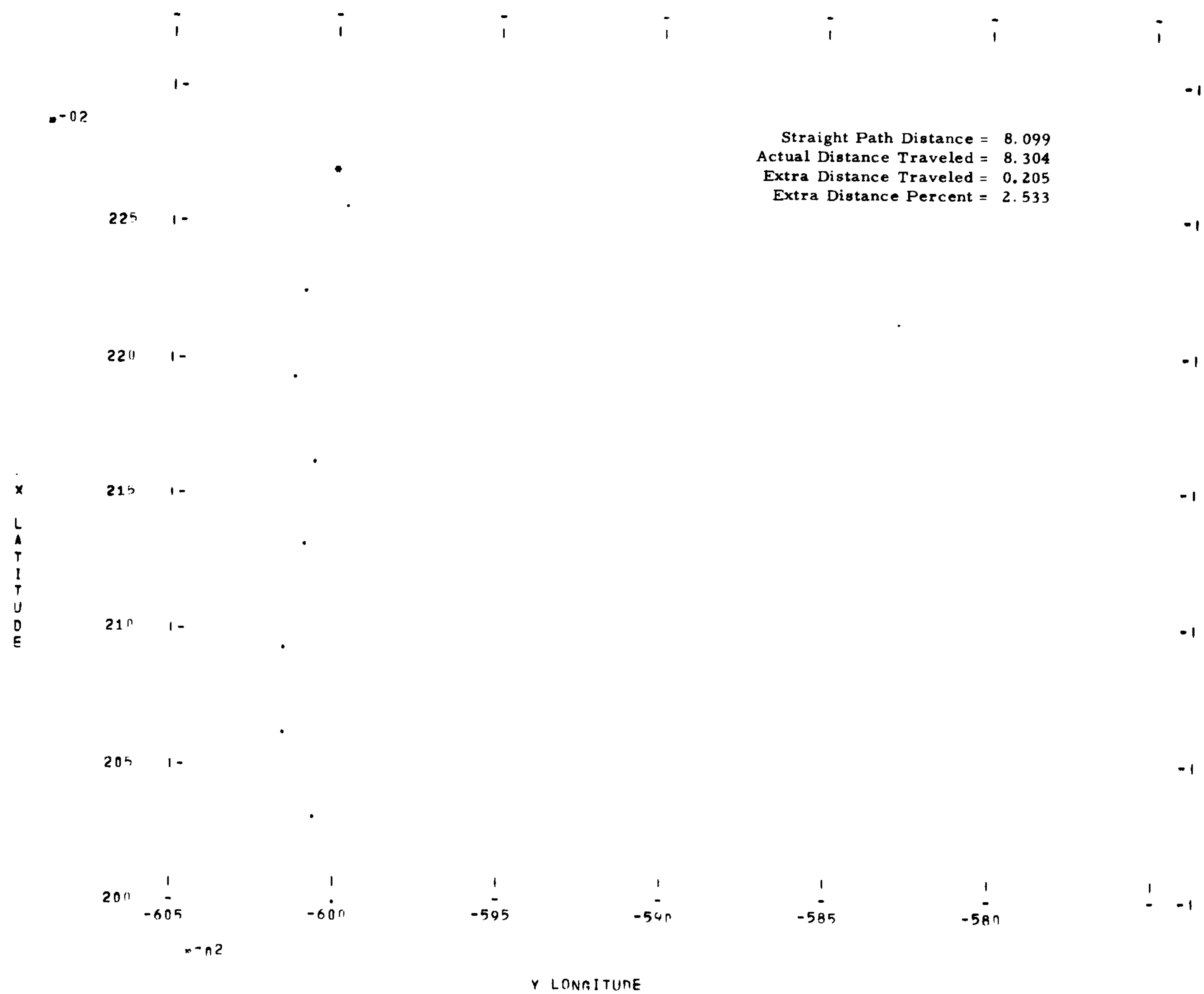

Figure 8-130 PLOT 18 MISSION I 1972 LEG C

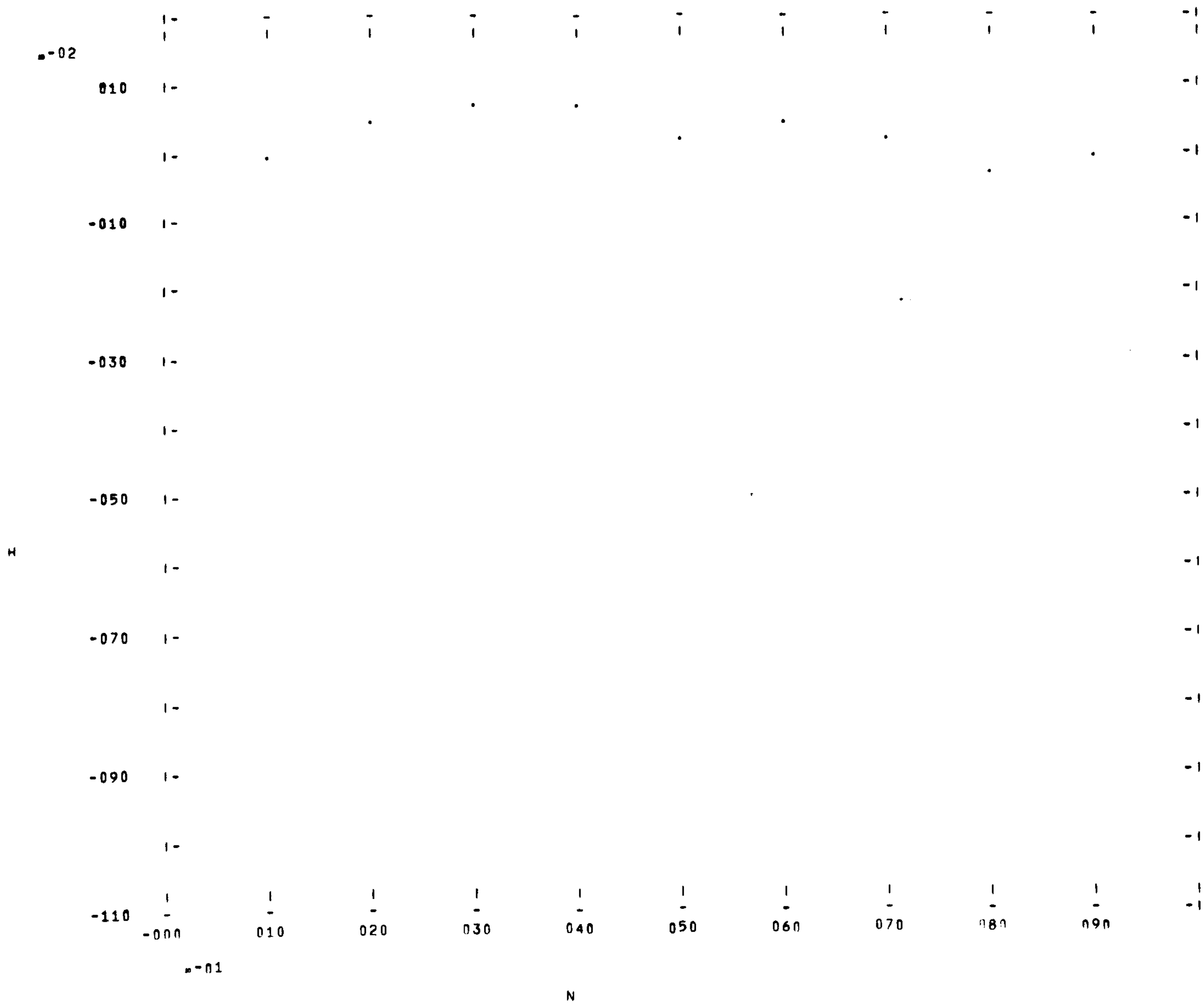

Figure 8-131 PLOT 1 MISSION II 1976 LEG E

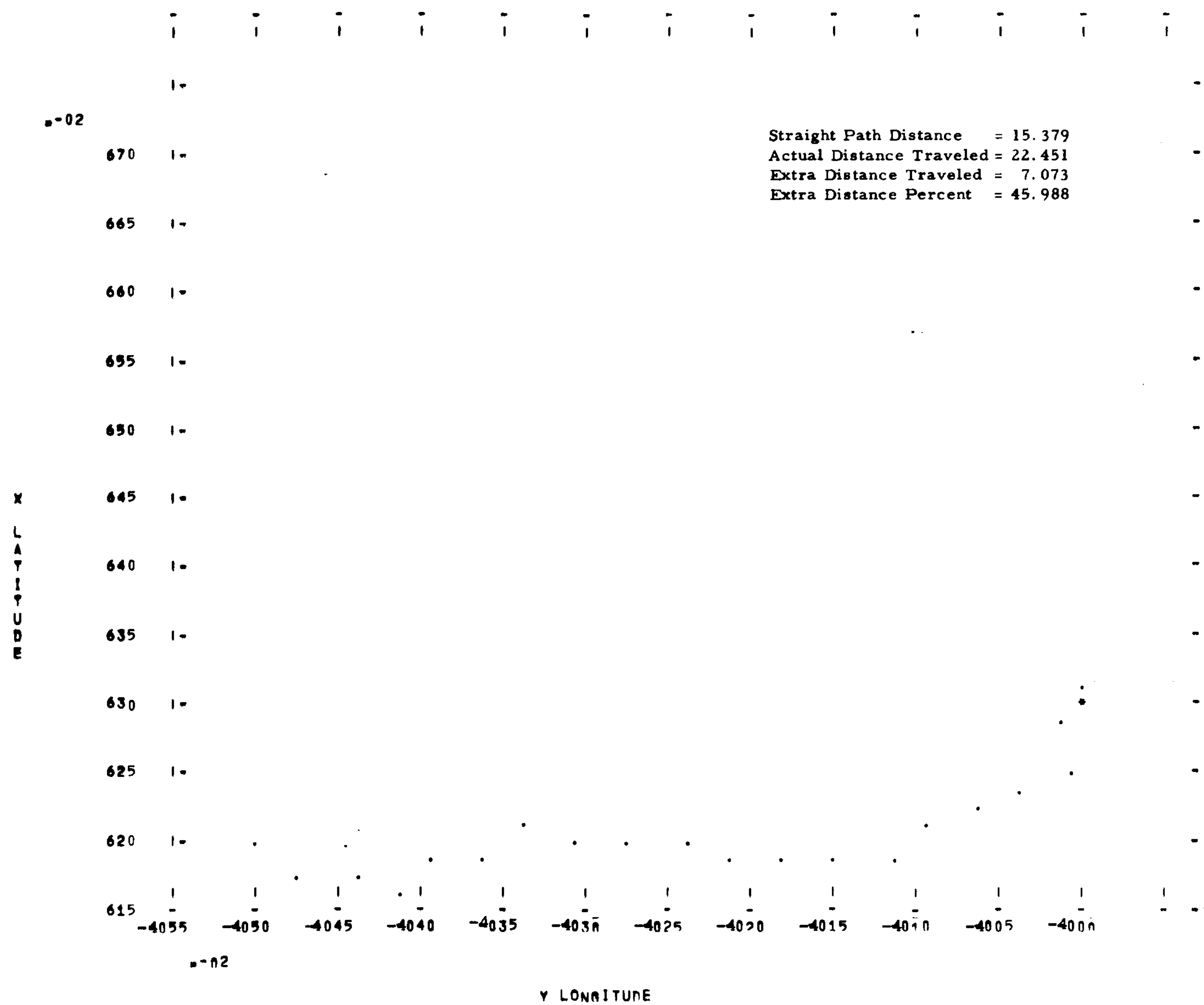

Figure 8-132 PLOT 18 MISSION II 1976 LEG E

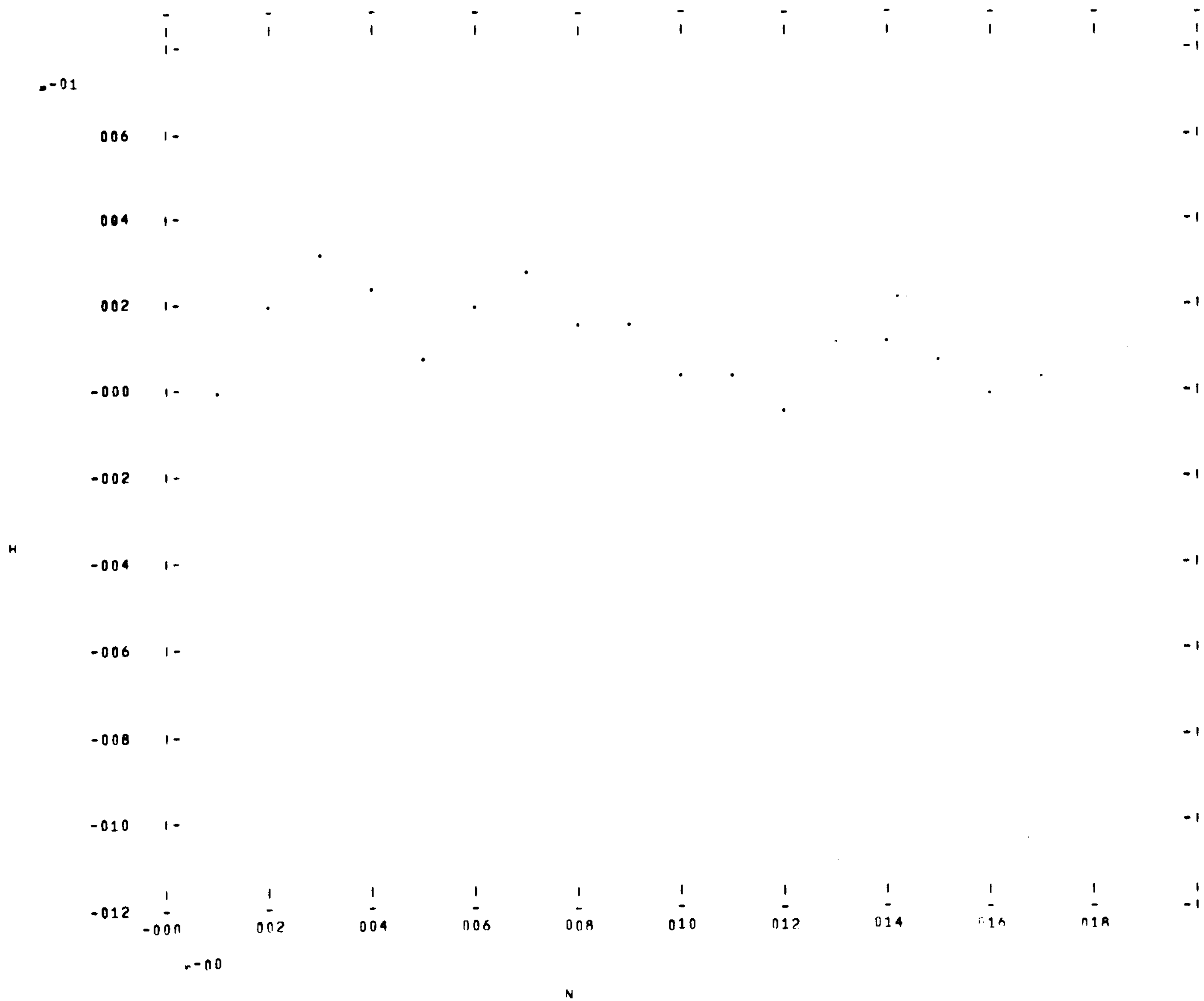

4

Figure 8-133 PLOT 1 MISSION III 1978 LEG A

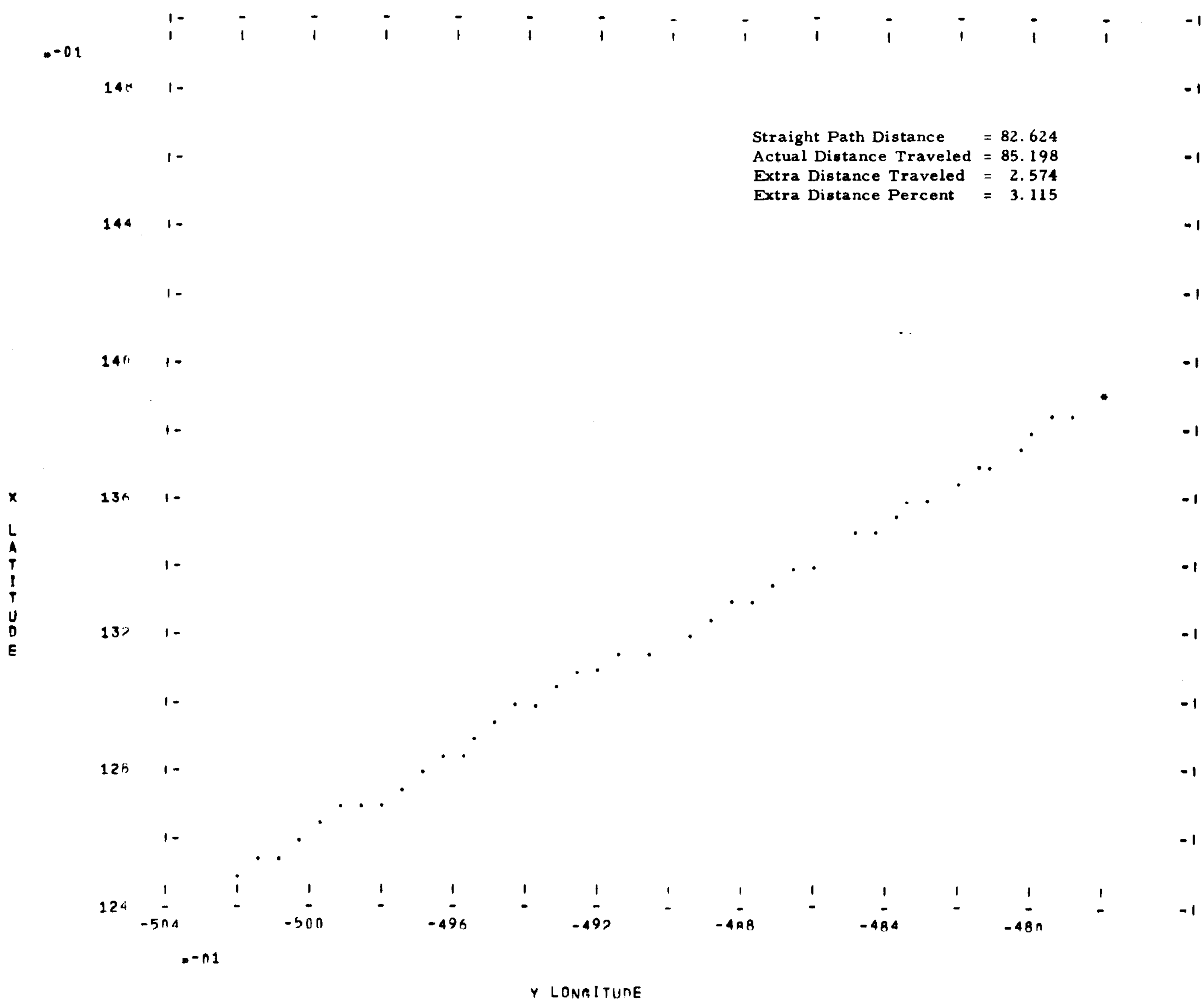

Straight Path Distance = 82.624
Actual Distance Traveled = 85.198
Extra Distance Traveled = 2.574
Extra Distance Percent = 3.115

Figure 8-134 PLOT 18 MISSION III 1978 LEG A

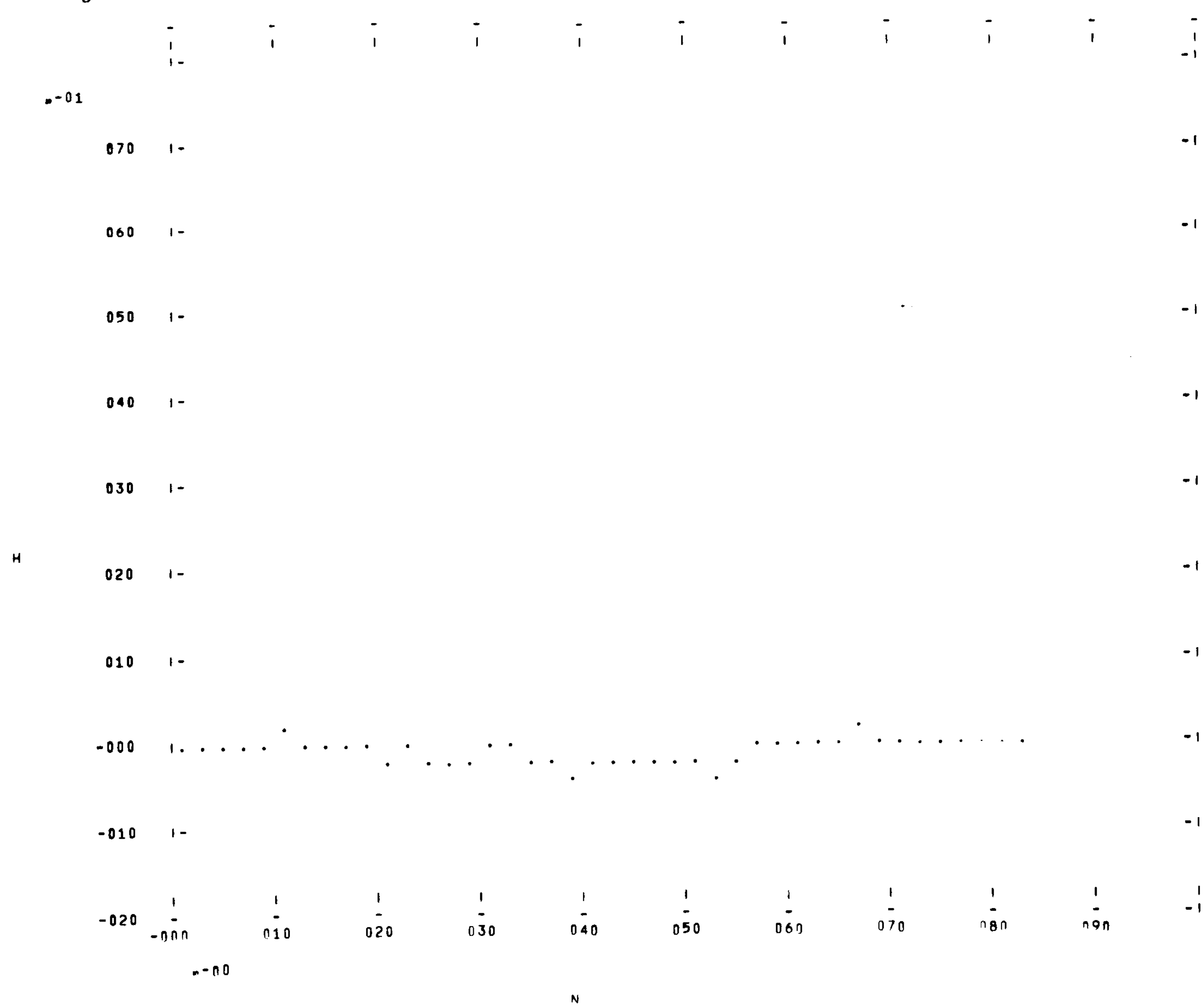

Figure 8-135 PLOT 1 MISSION III 1978 LEG A

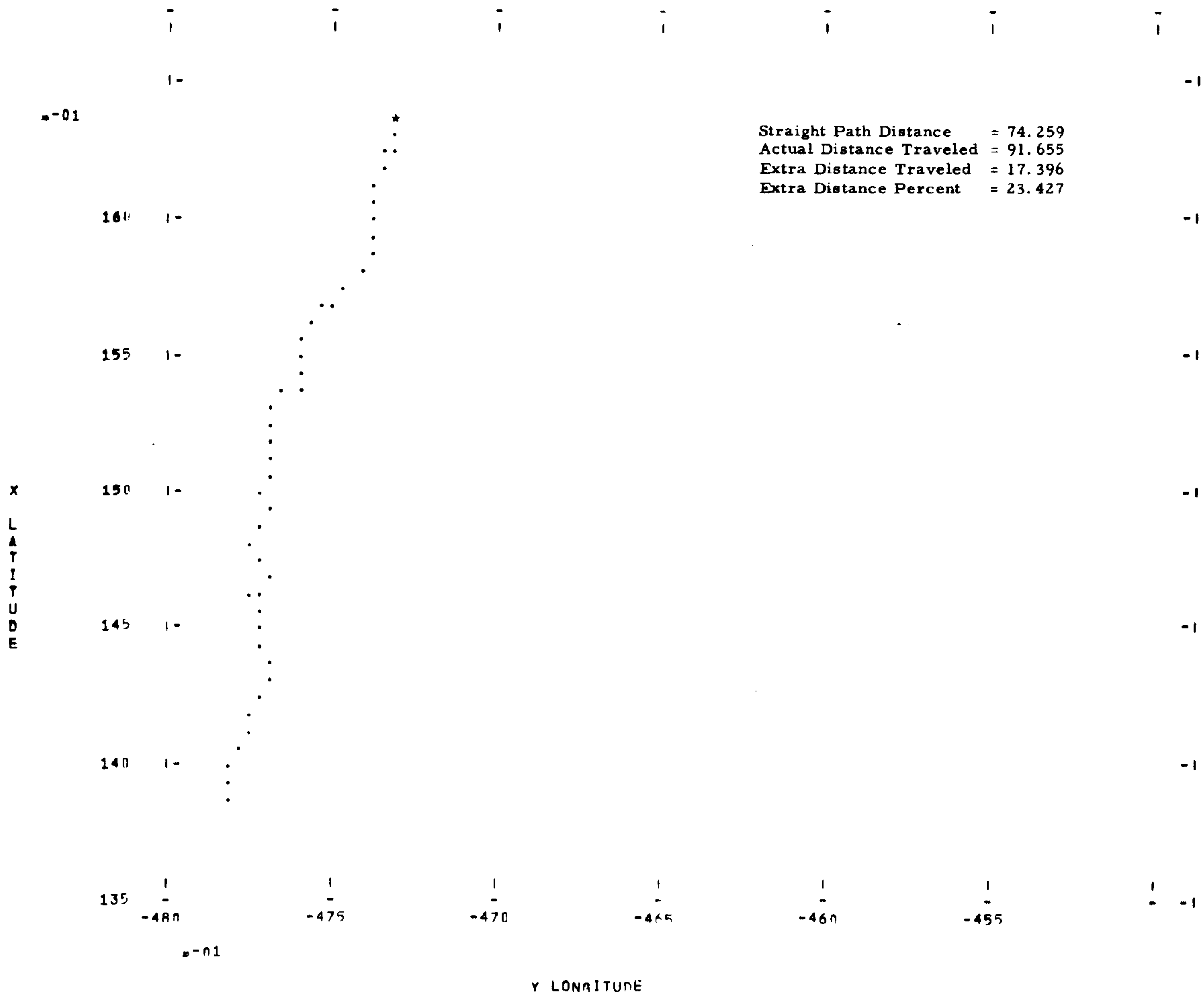

Figure 8-136 PLOT 18 MISSION III 1978 LEG B

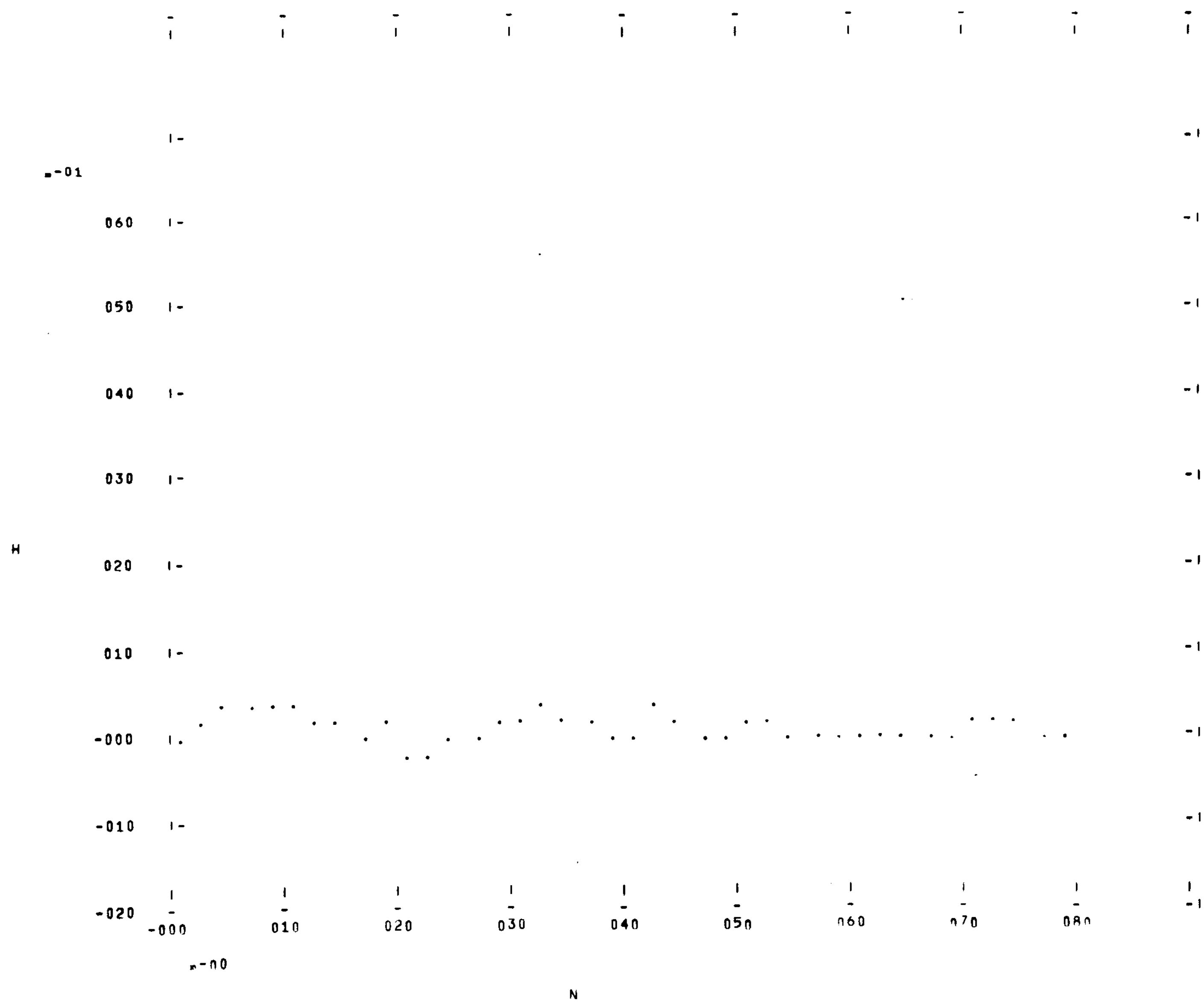

Figure 8-137 PLOT 1 MISSION IIII 1980 LEG C

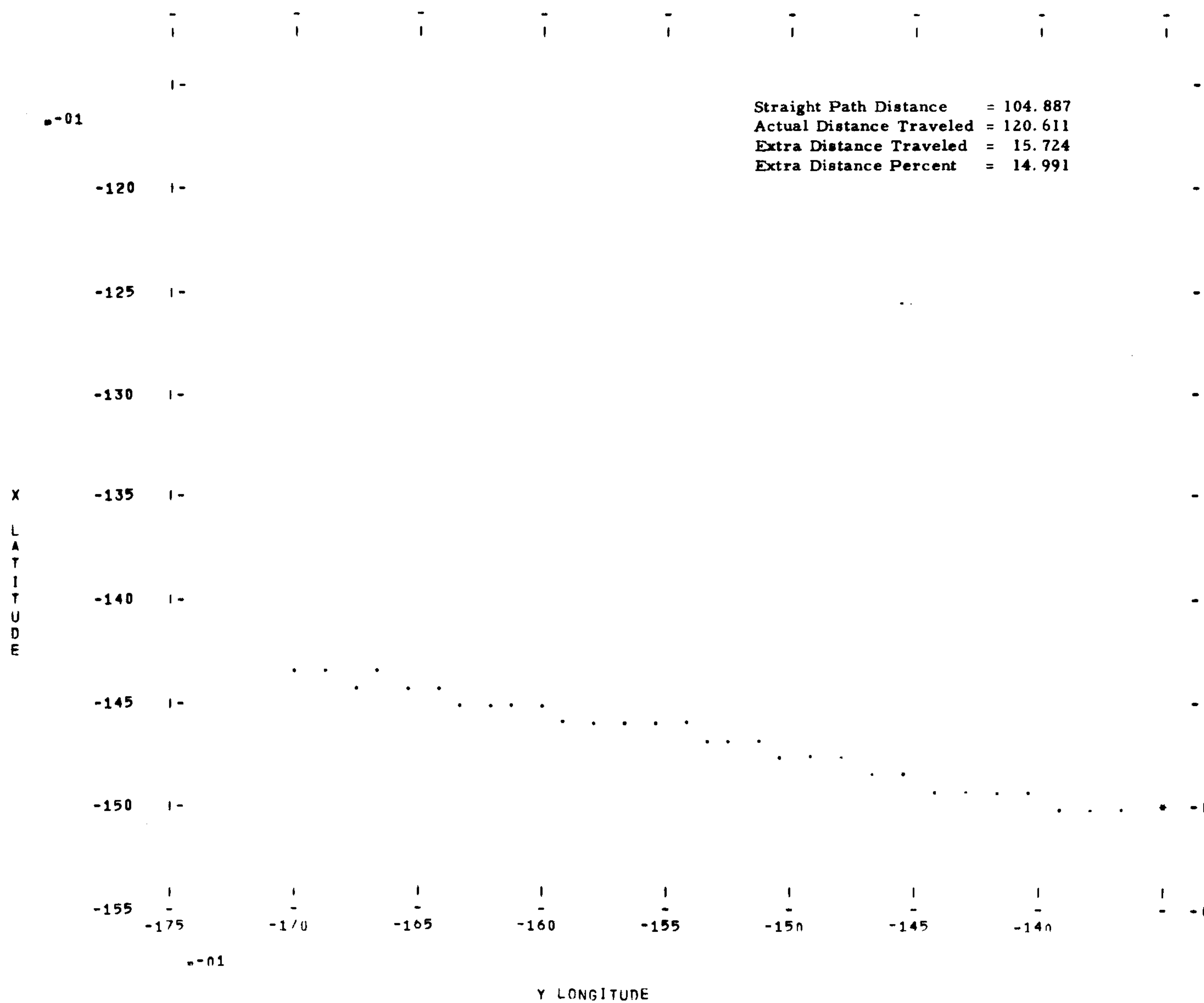

Figure 8-138 PLOT 18 MISSION IIII 1960 LEG C

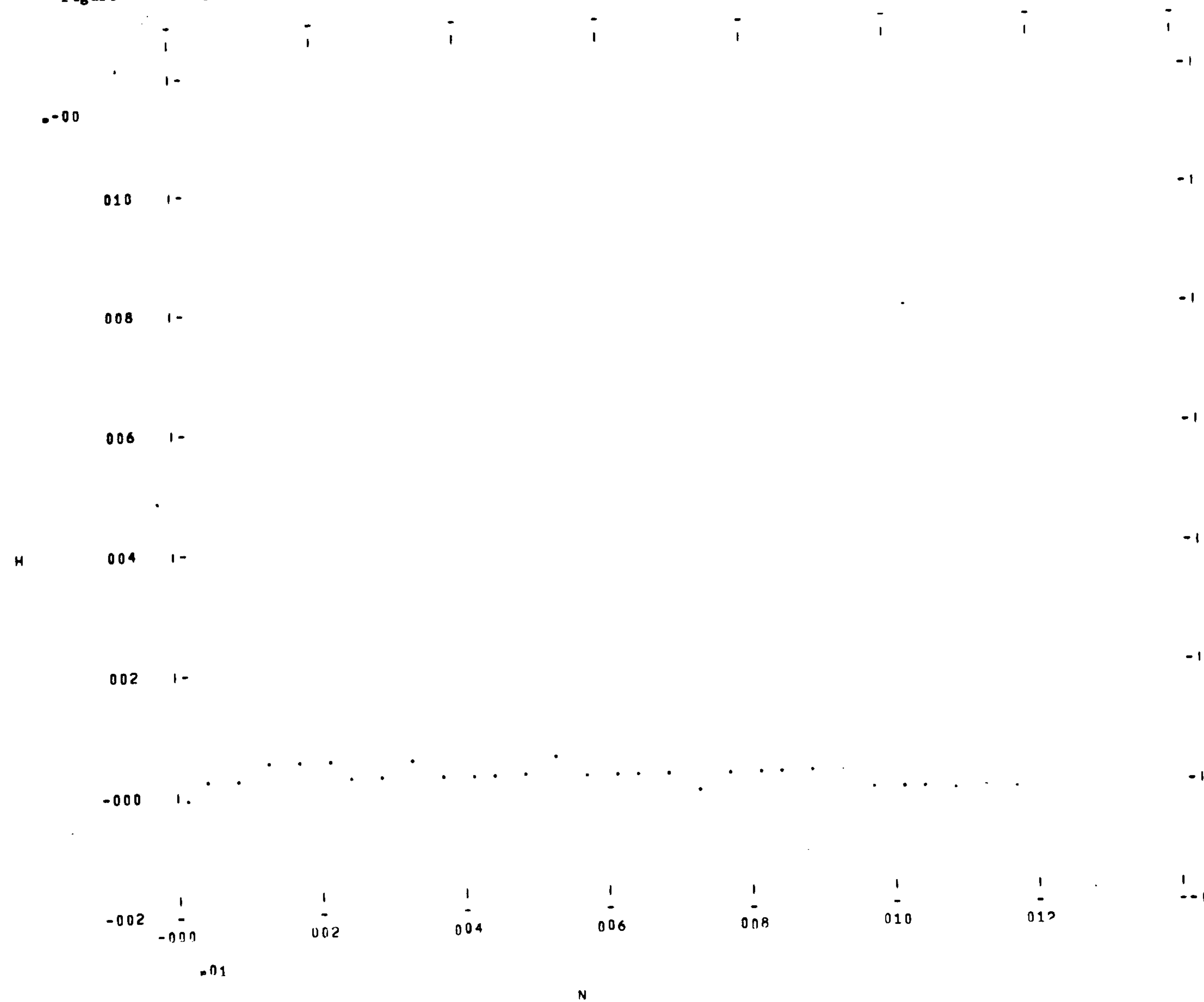

Figure 8-139 PLOT 1 MISSION IIII 1980 LEG E

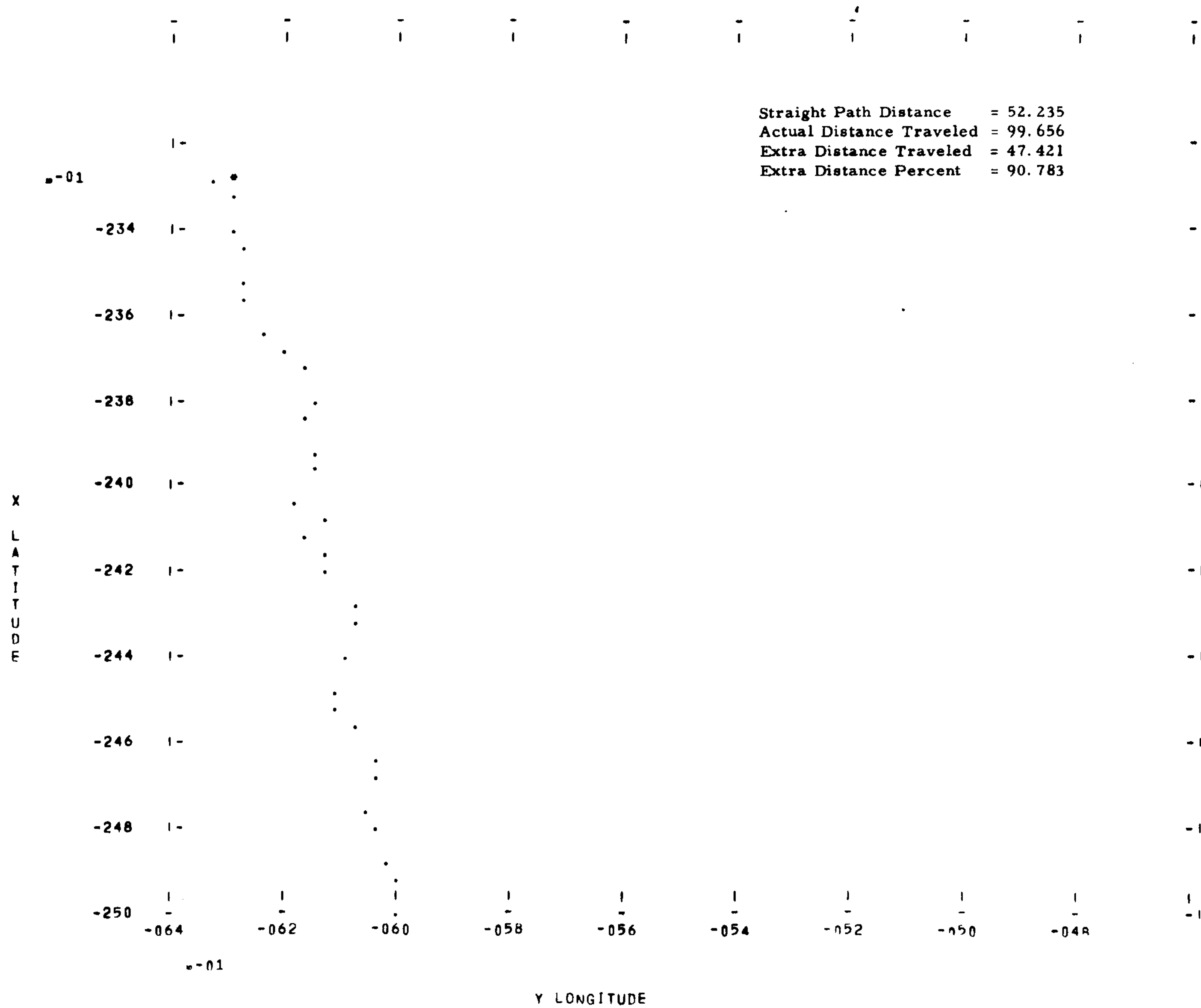

Figure 8-140 PLOT 18 MISSION IIII 1980 LEG F

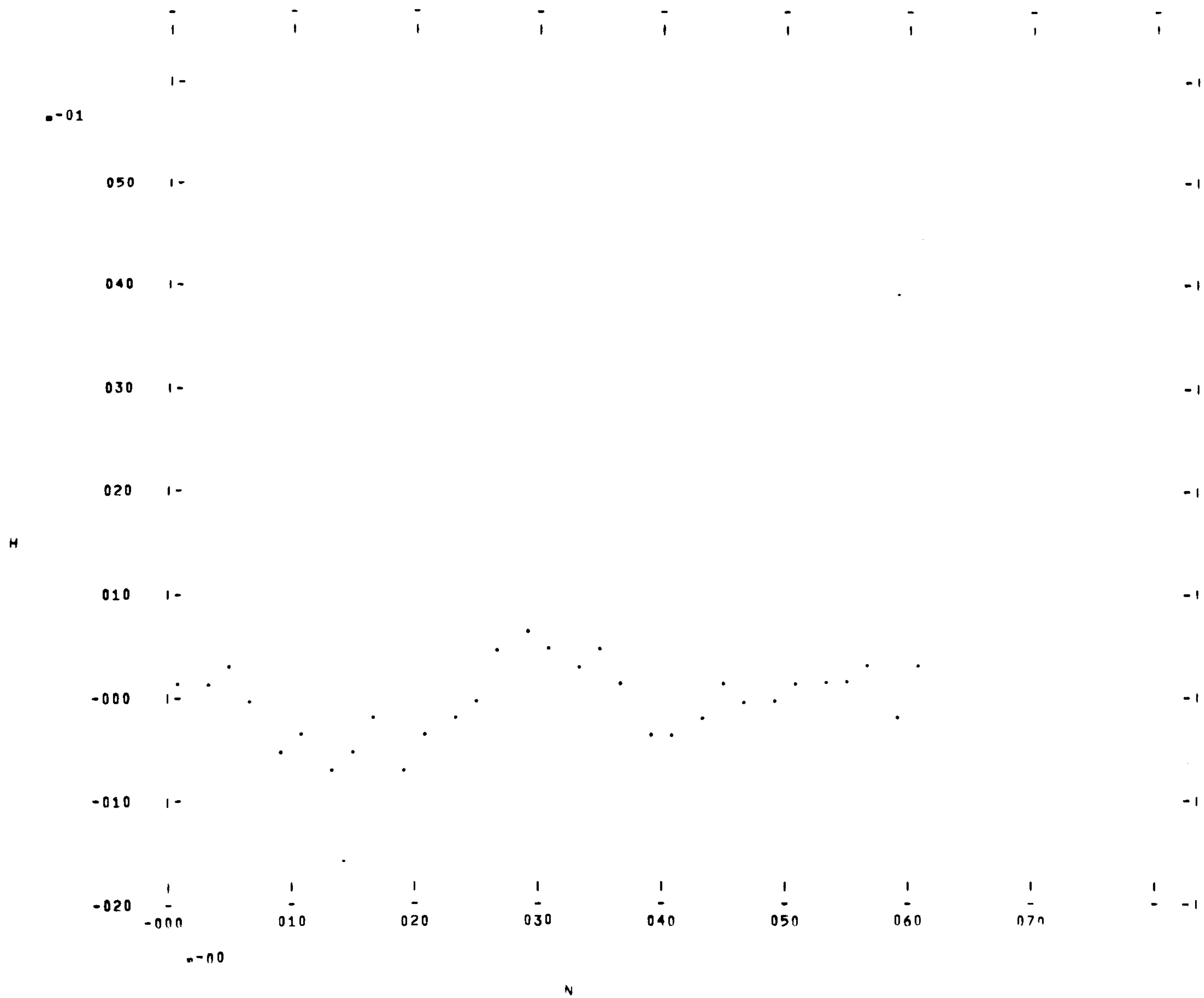

Figure 8-141 PLOT 1 MISSION V 1980 LEG A

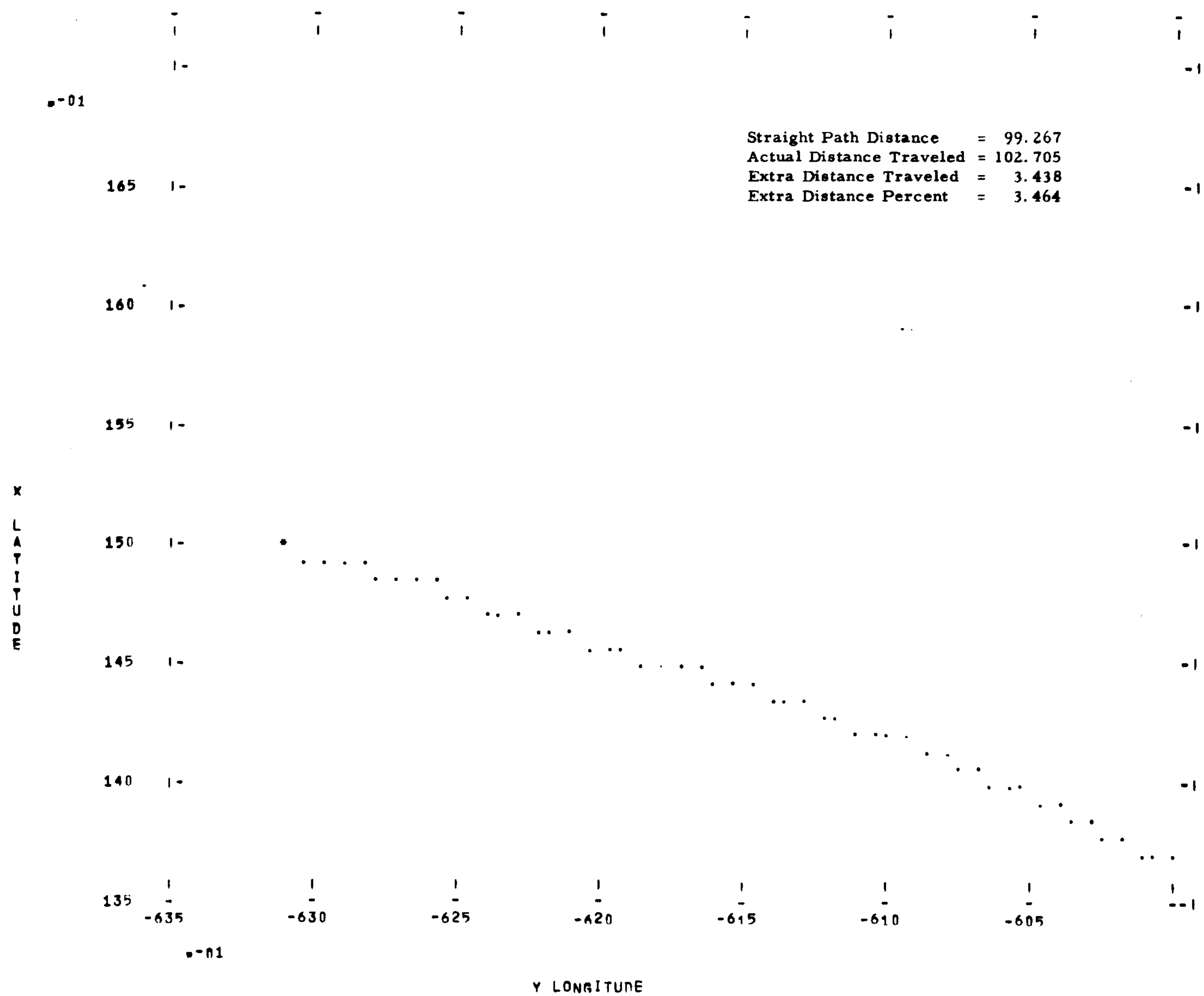

Figure 8-142 PLOT 18 MISSION V 1980 LEG A

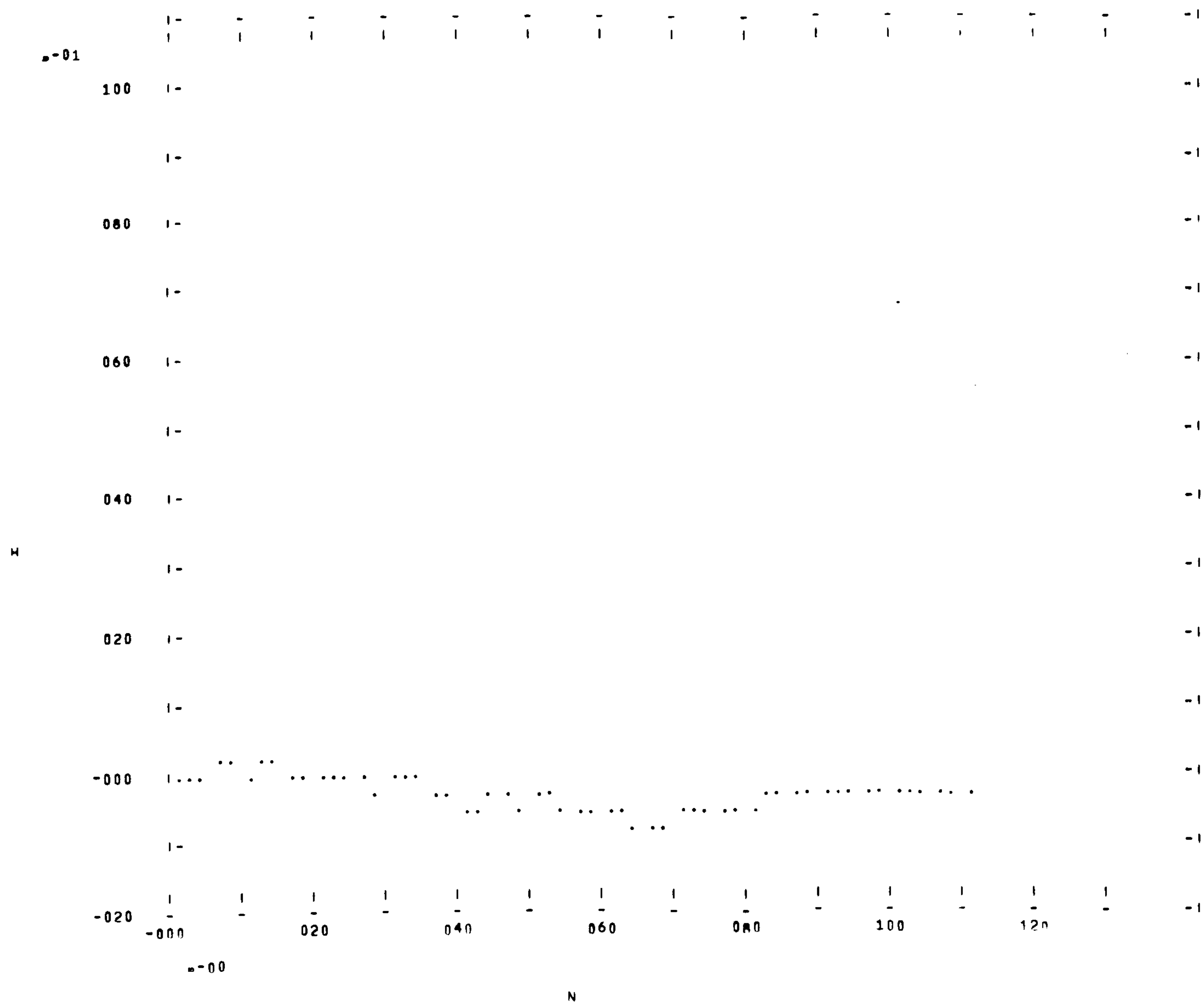

Figure 8-143 PLOT 1 MISSION V 1980 LEG B

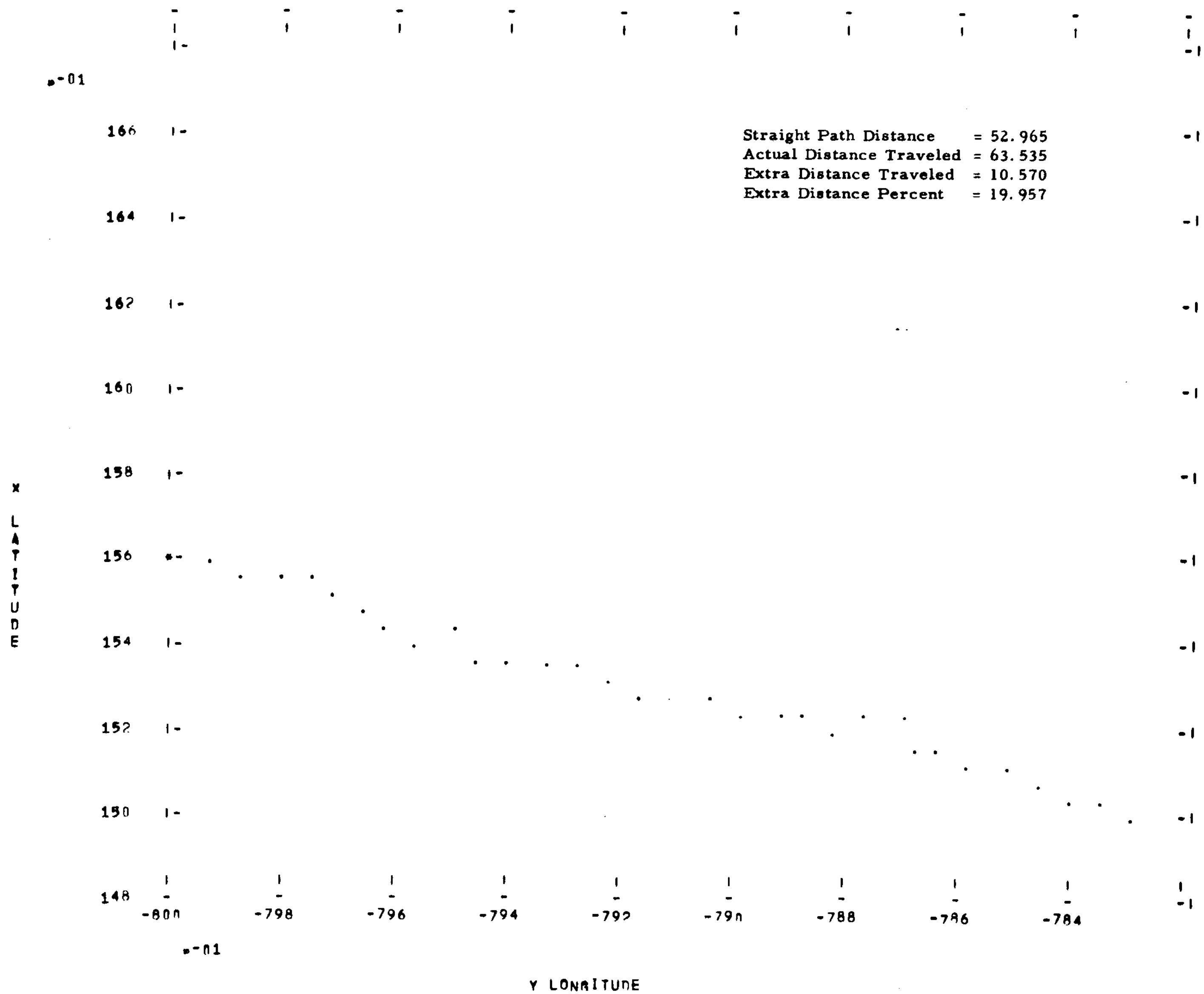

Figure 8-144 PLOT 18 MISSION V 1980 LEG B

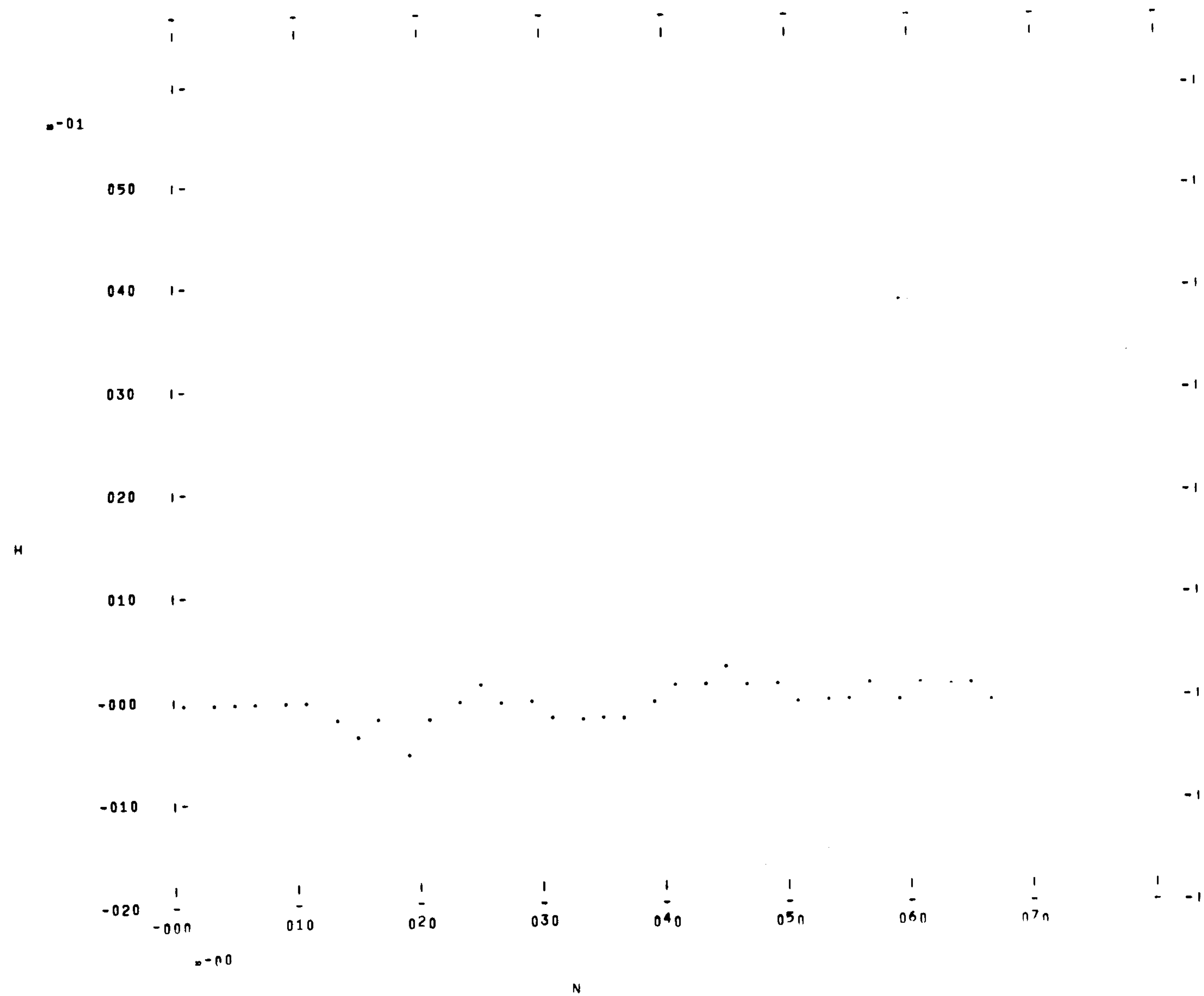

Figure 8-145 PLOT 1 MISSION V 1980 LEG C

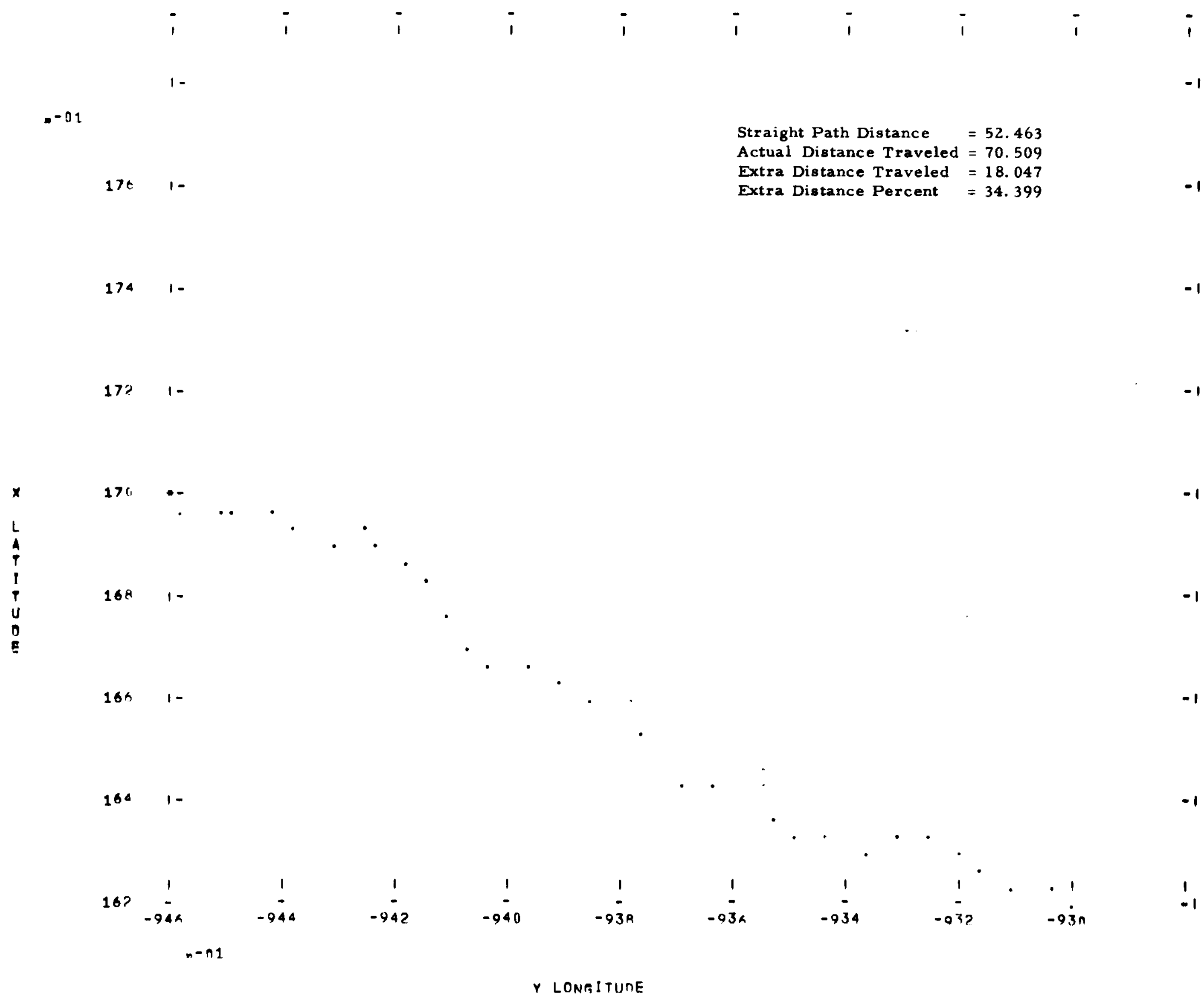

Figure 8-146 PLOT 18 MISSION V 1980 LEG C

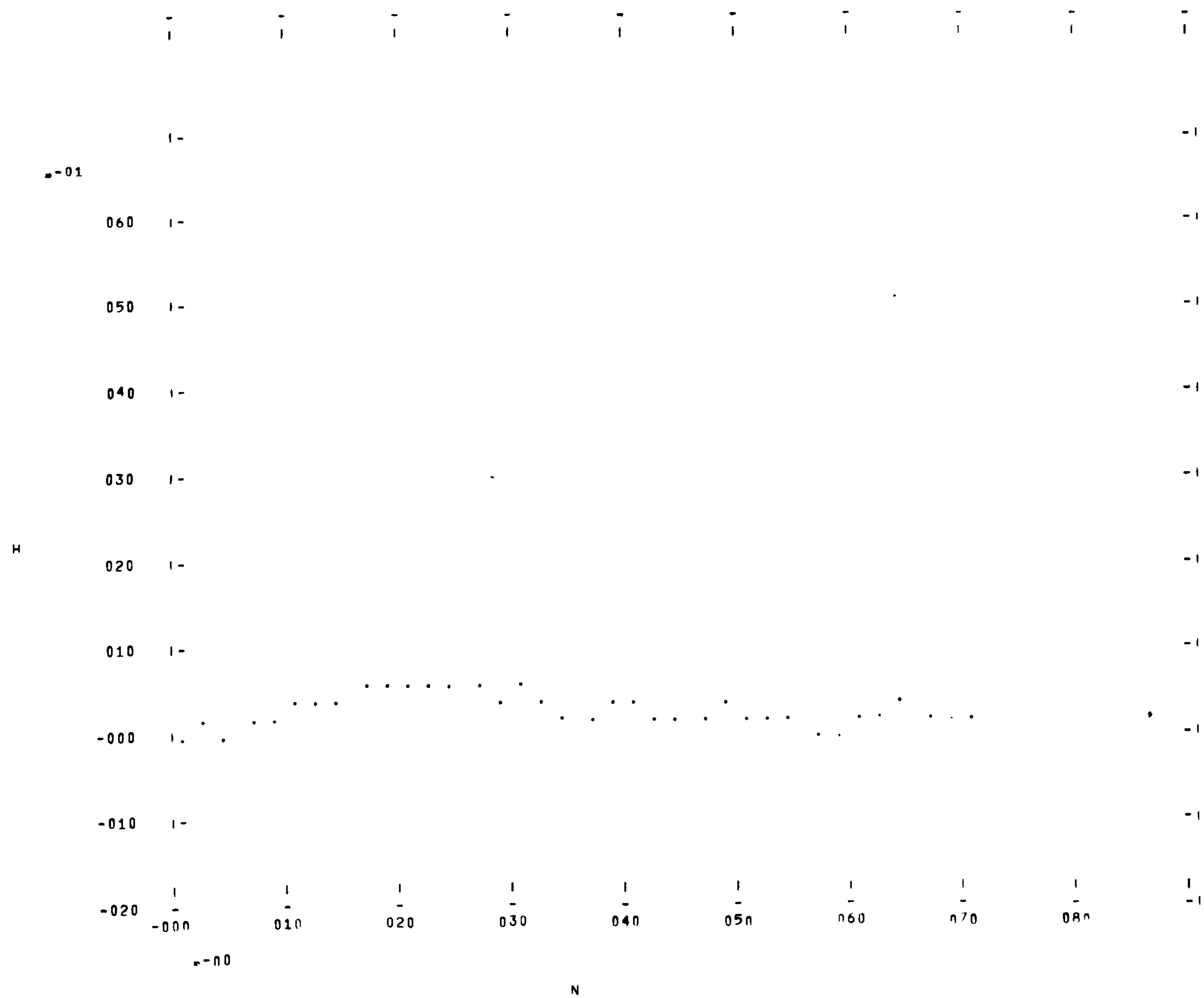

Figure 8-147 PLOT 1 MISSION VI 1984 LEG B

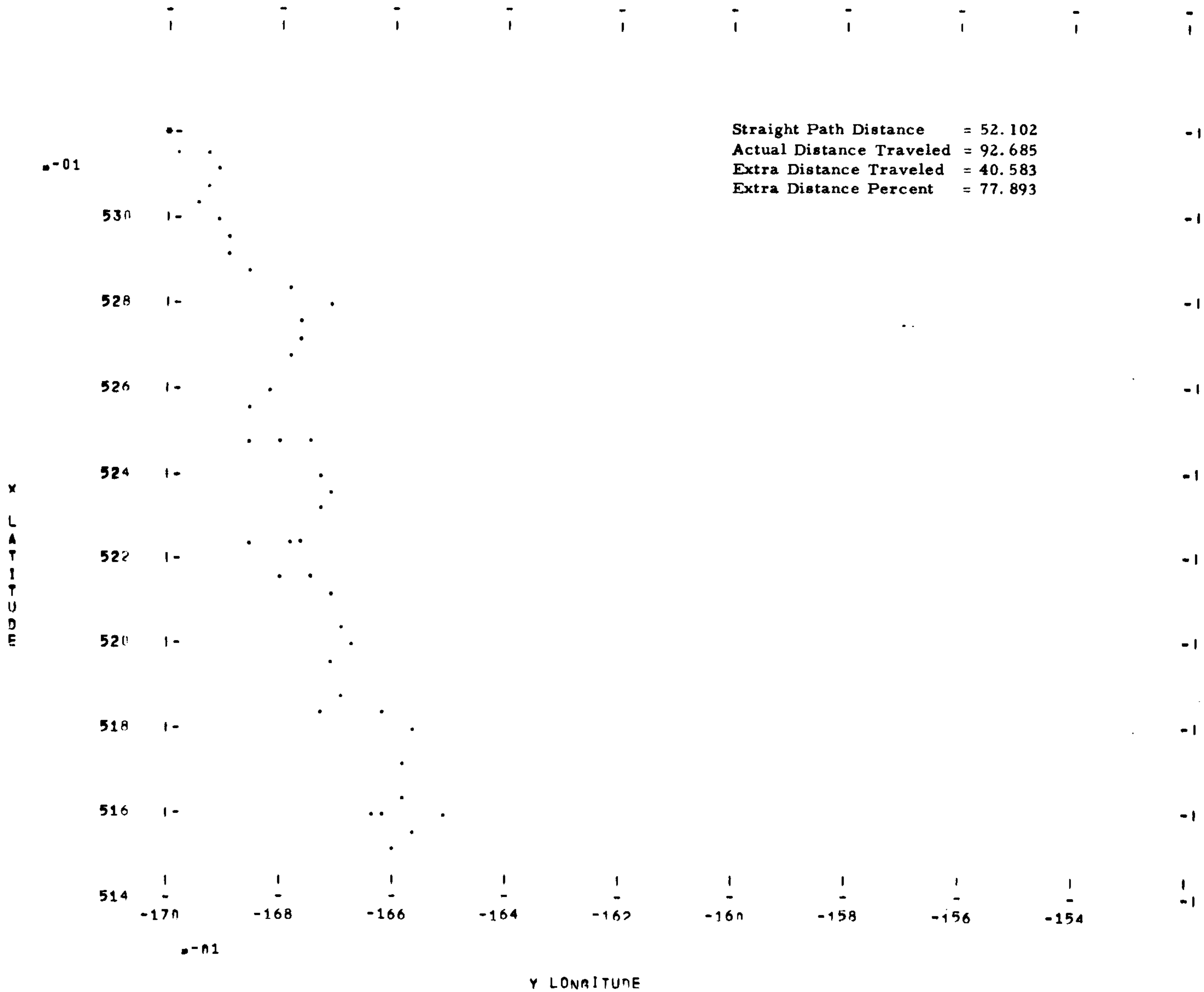

Figure 8-148 PLOT 18 MISSION VI 1984 LEG B

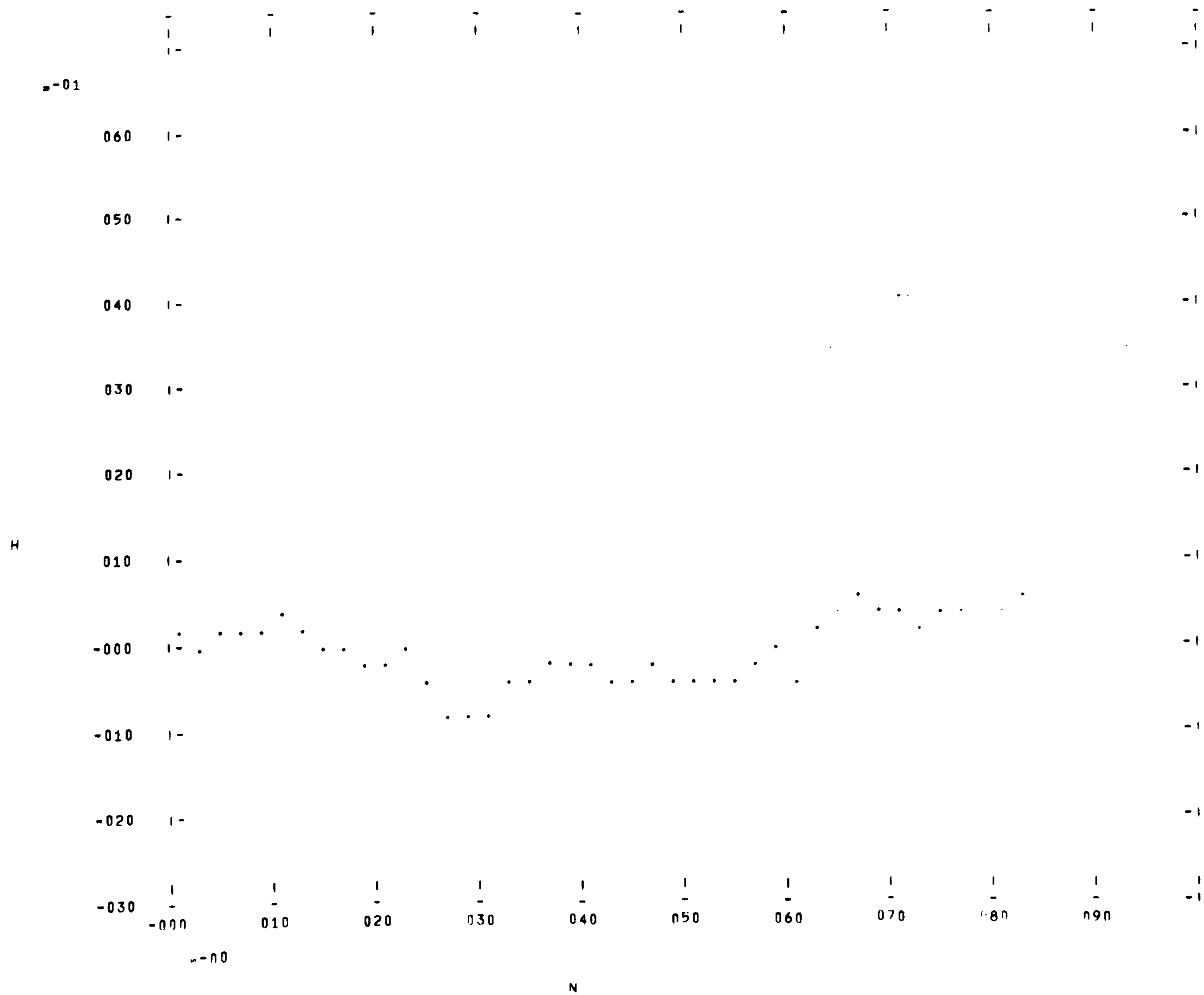

Figure 8-149 PLOT 13 MISSION I 1972 LEG C

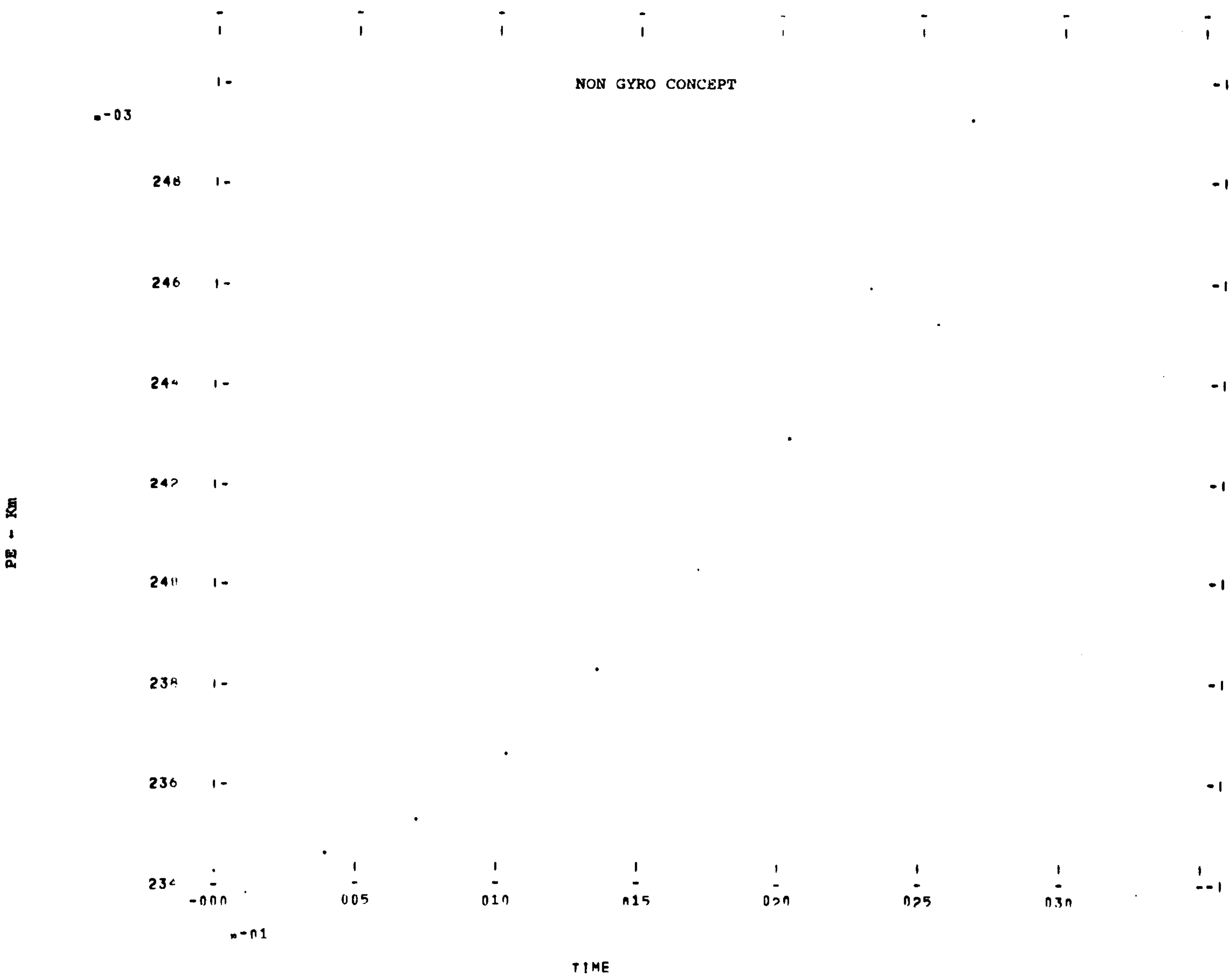

Figure 8-150 PLOT 12 MISSION I 1972 LEG C

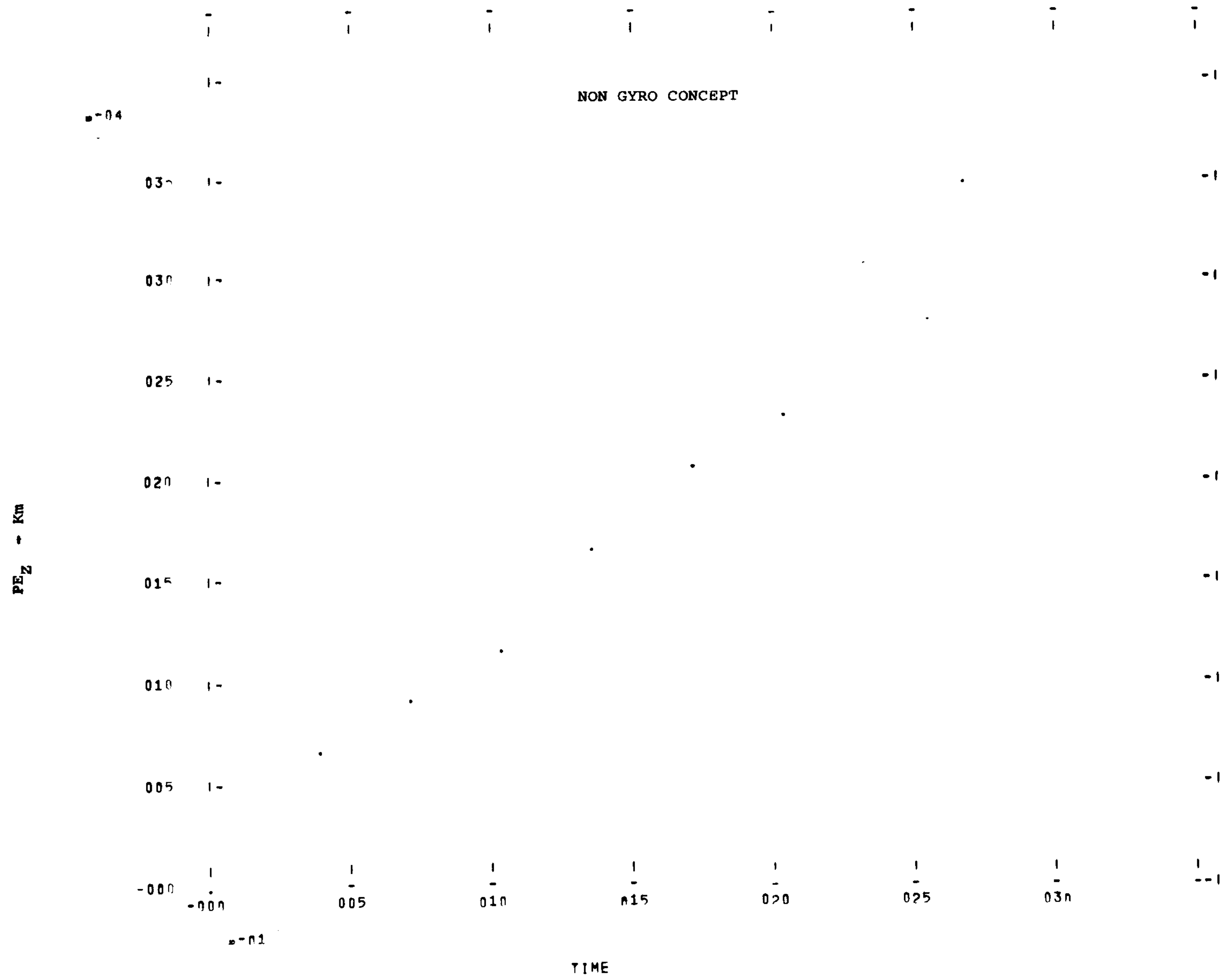

Figure 8-151 PLOT 13 MISSION II 1976 LEG E

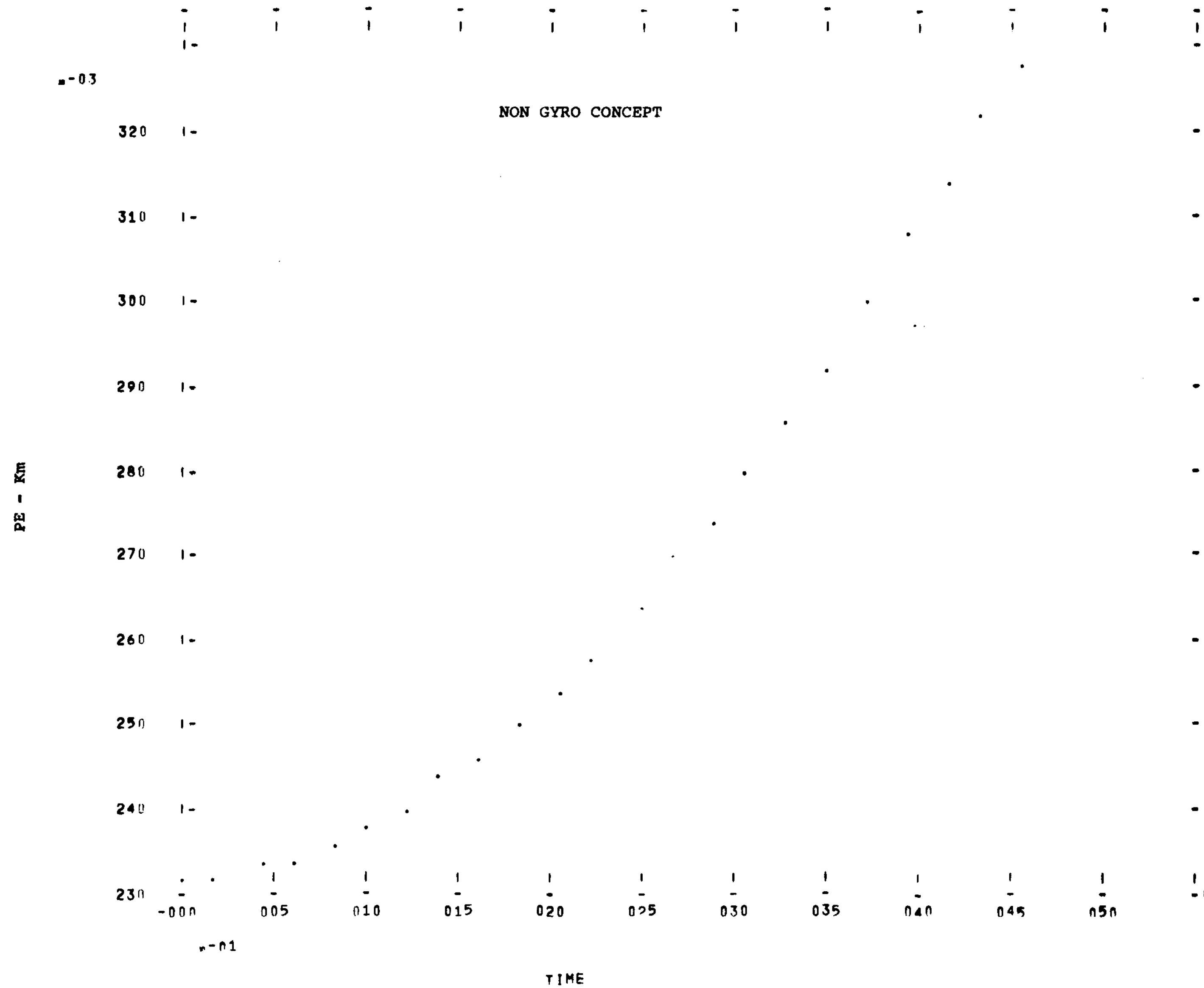

Figure 8-152 PLOT 12 MISSION II 1976 LEG E

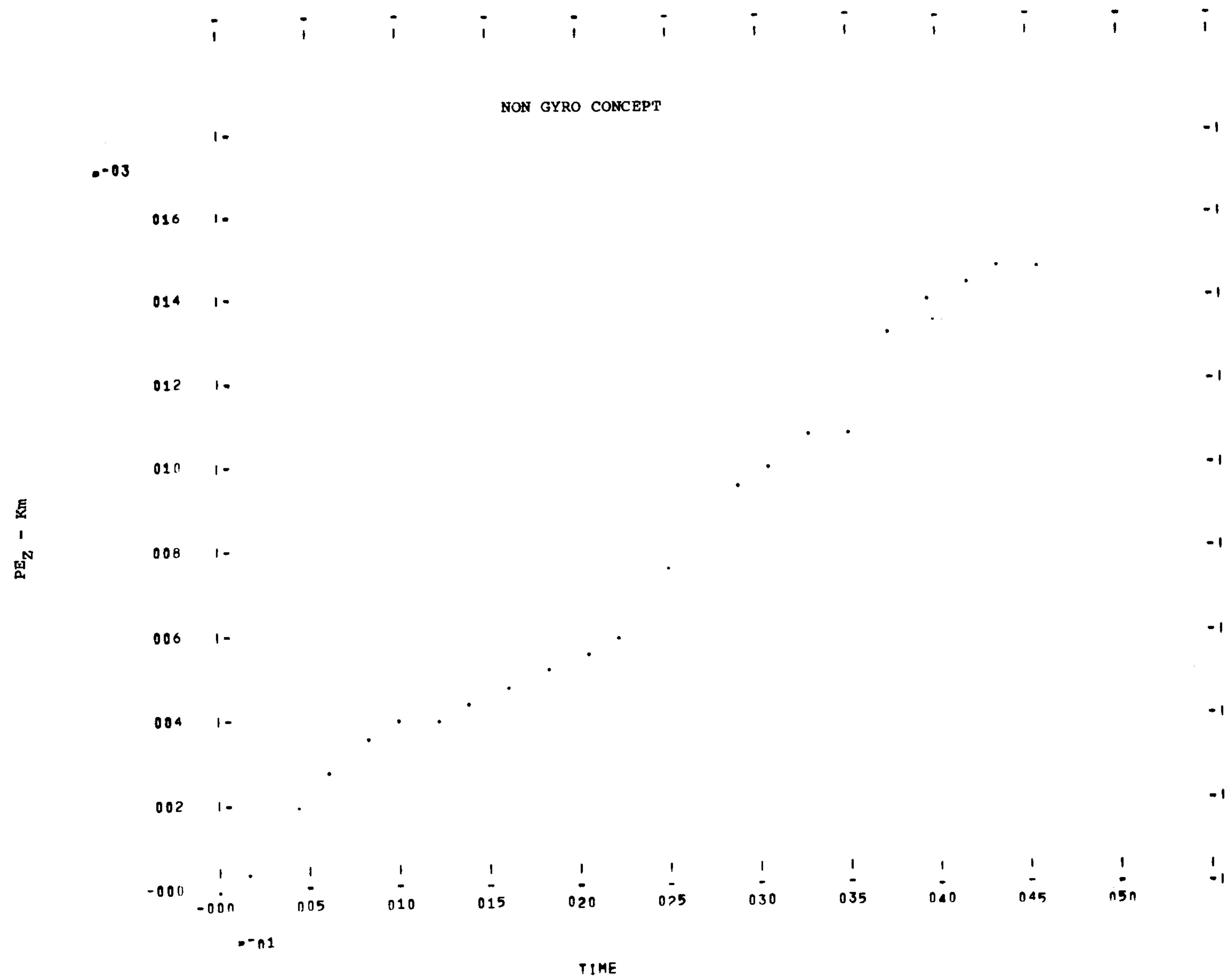

Figure 8-153 PLOT 13 MISSION III 1978 LEG A

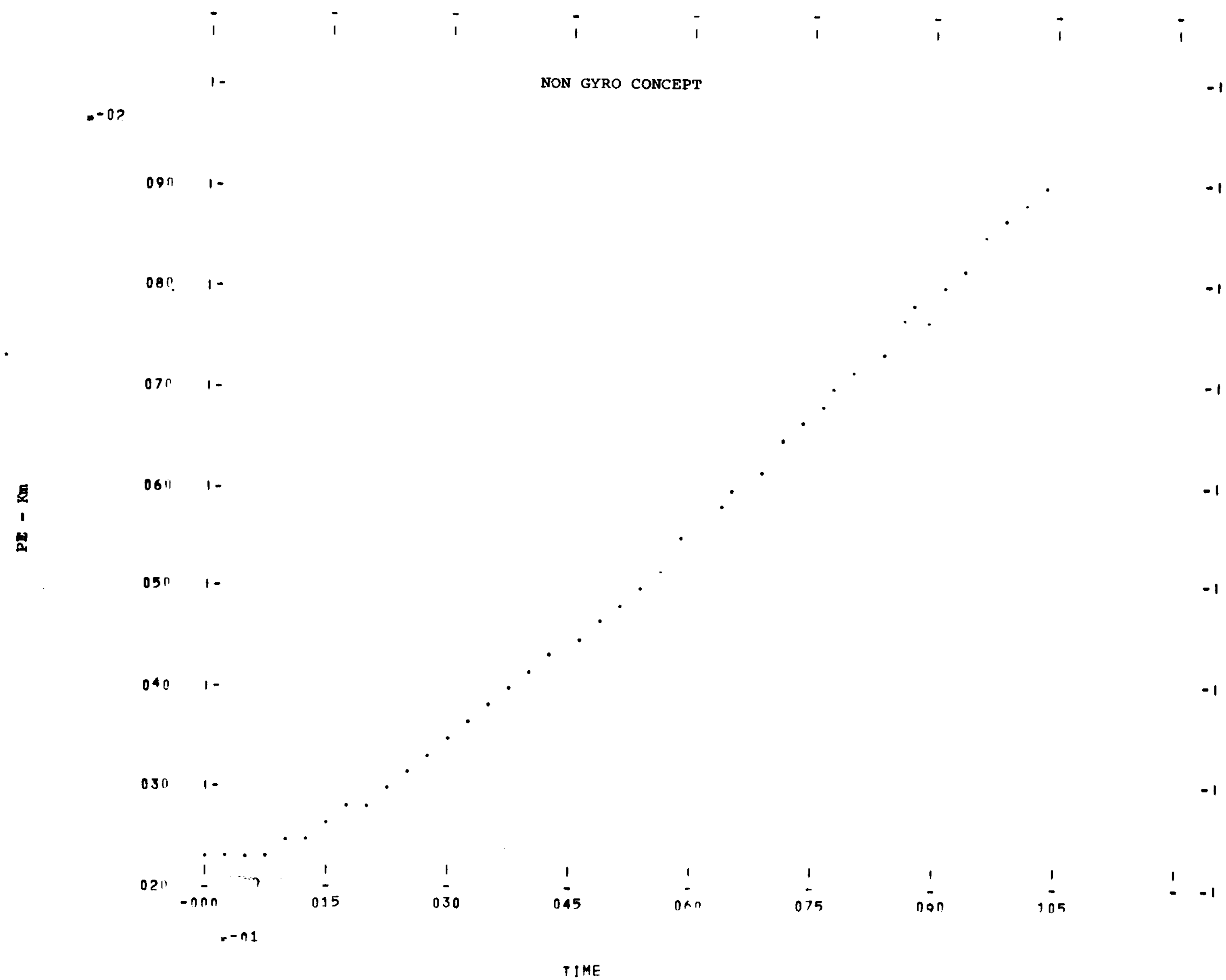

Figure 8-154 PLOT 12 MISSION III 1978 LEG A

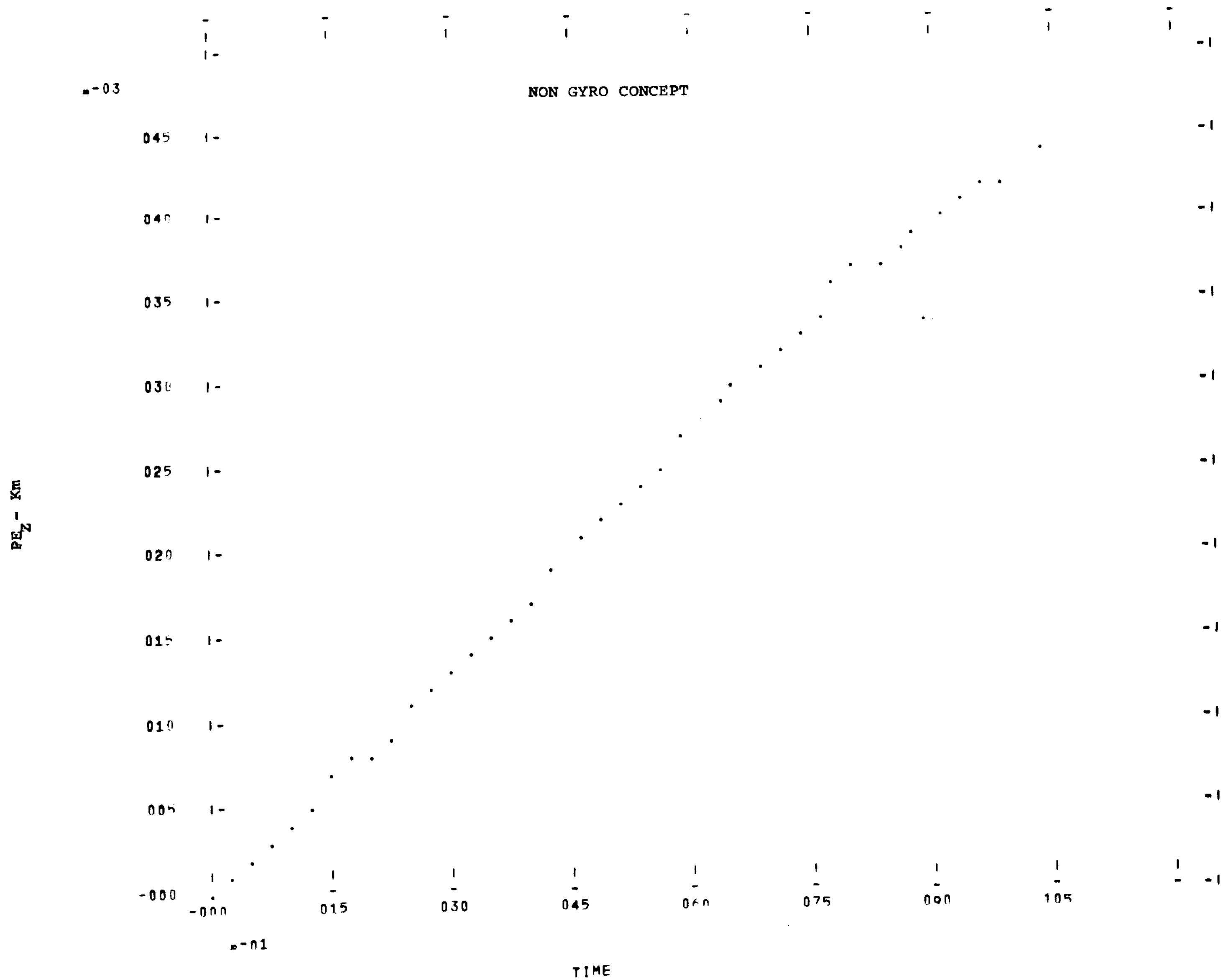

Figure 8-155 PLOT 13 MISSION III 1978 LEG B

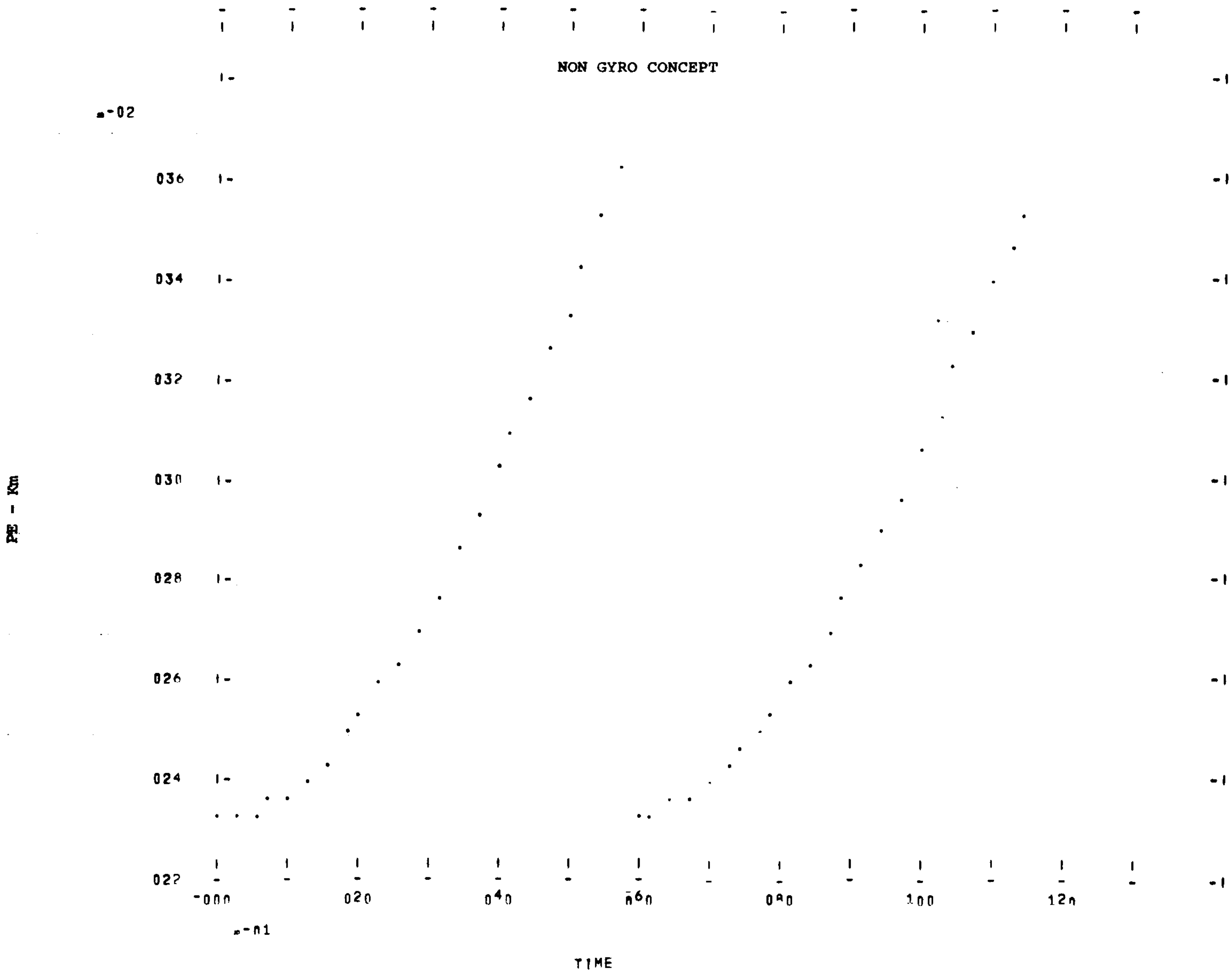

Figure 8-156 PLOT 12 MISSION III 1978 LEG B

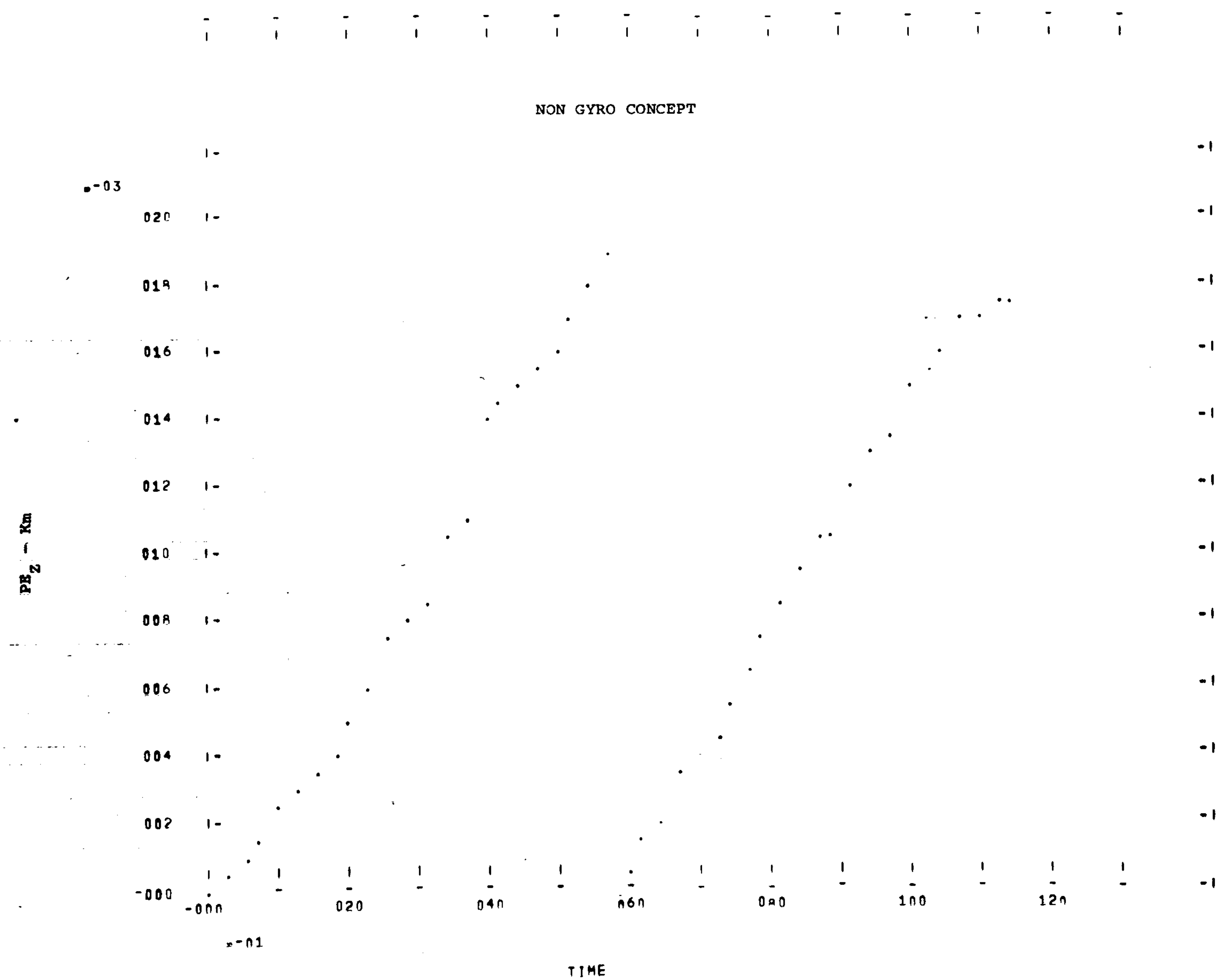

Figure 8-157 PLOT 13 MISSION IIII 1980 LEG C

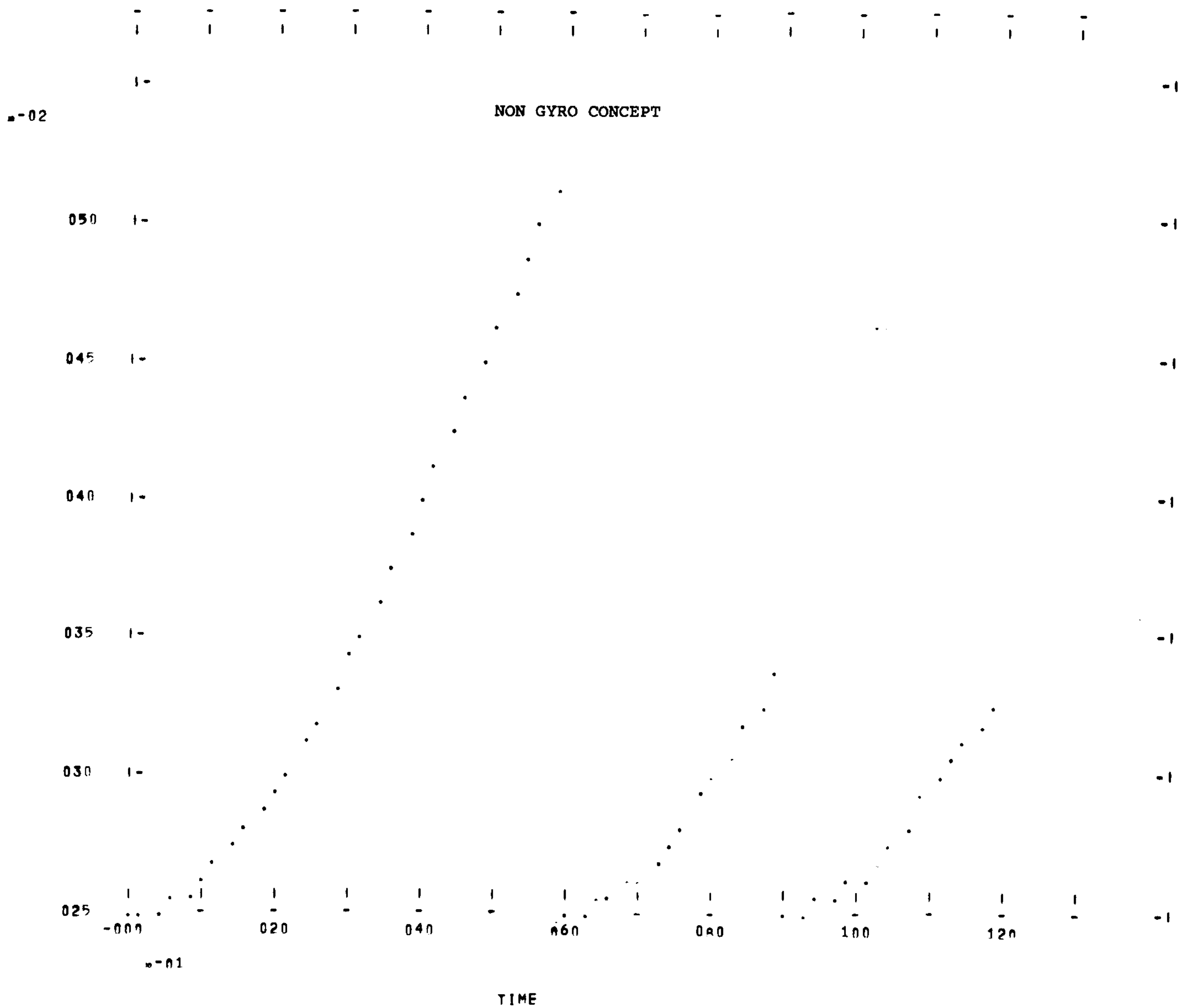

Figure 8-158 PLOT 12 MISSION IIII 1980 LEG C

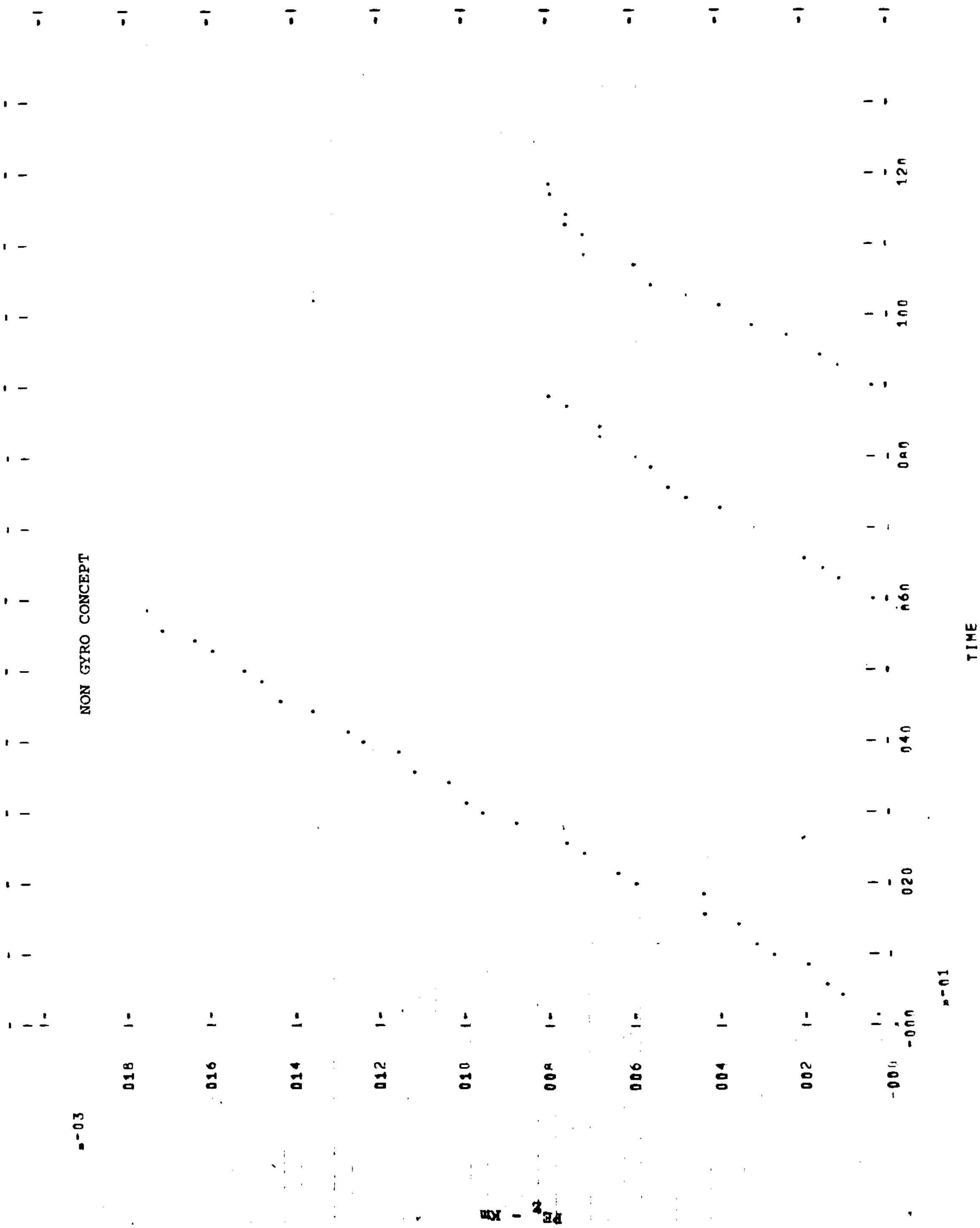

Figure 8-159 PLOT 13 MISSION IIII 1980 LEG F

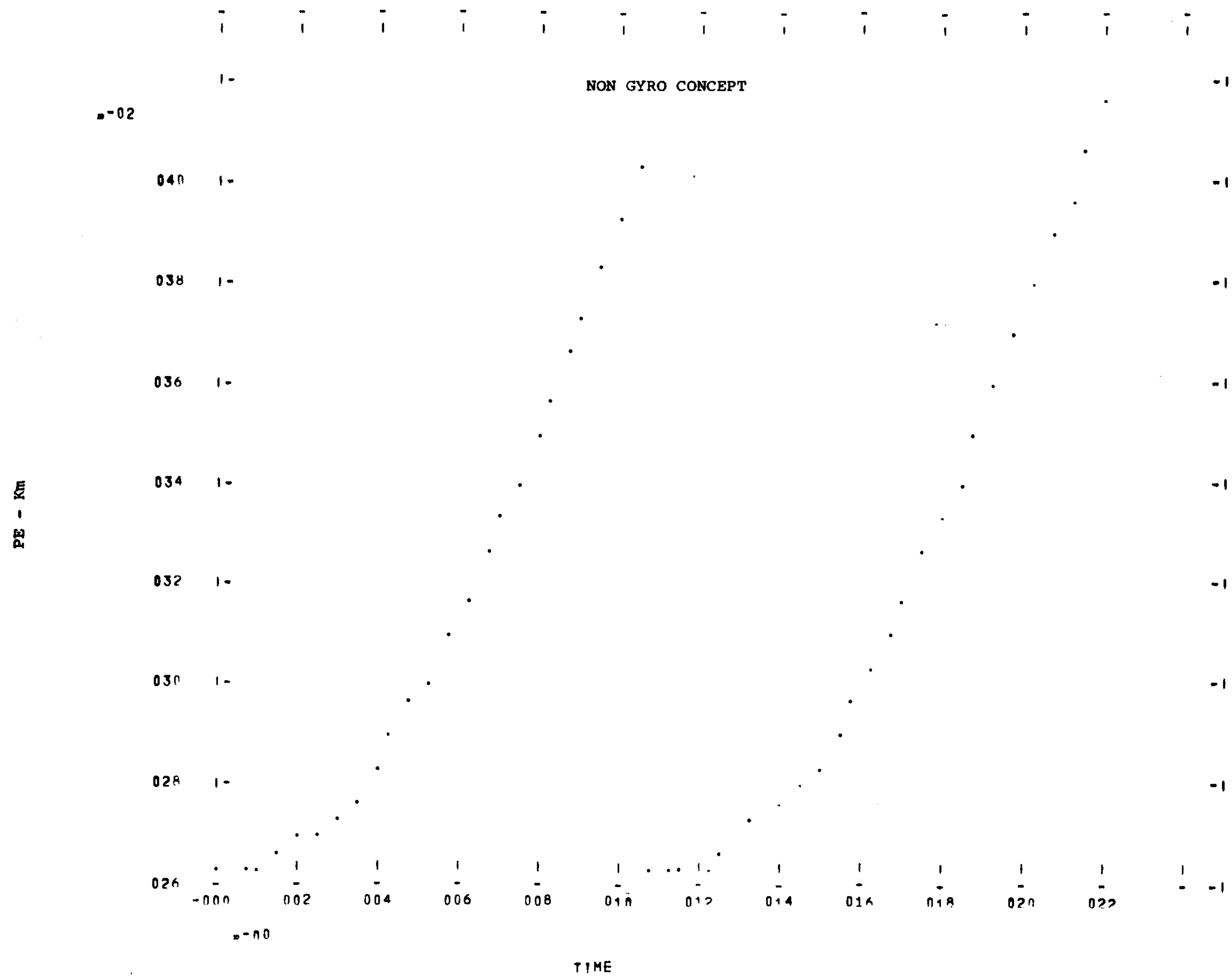

Figure 8-160 PLOT 12 MISSION IIII 1980 LEG F

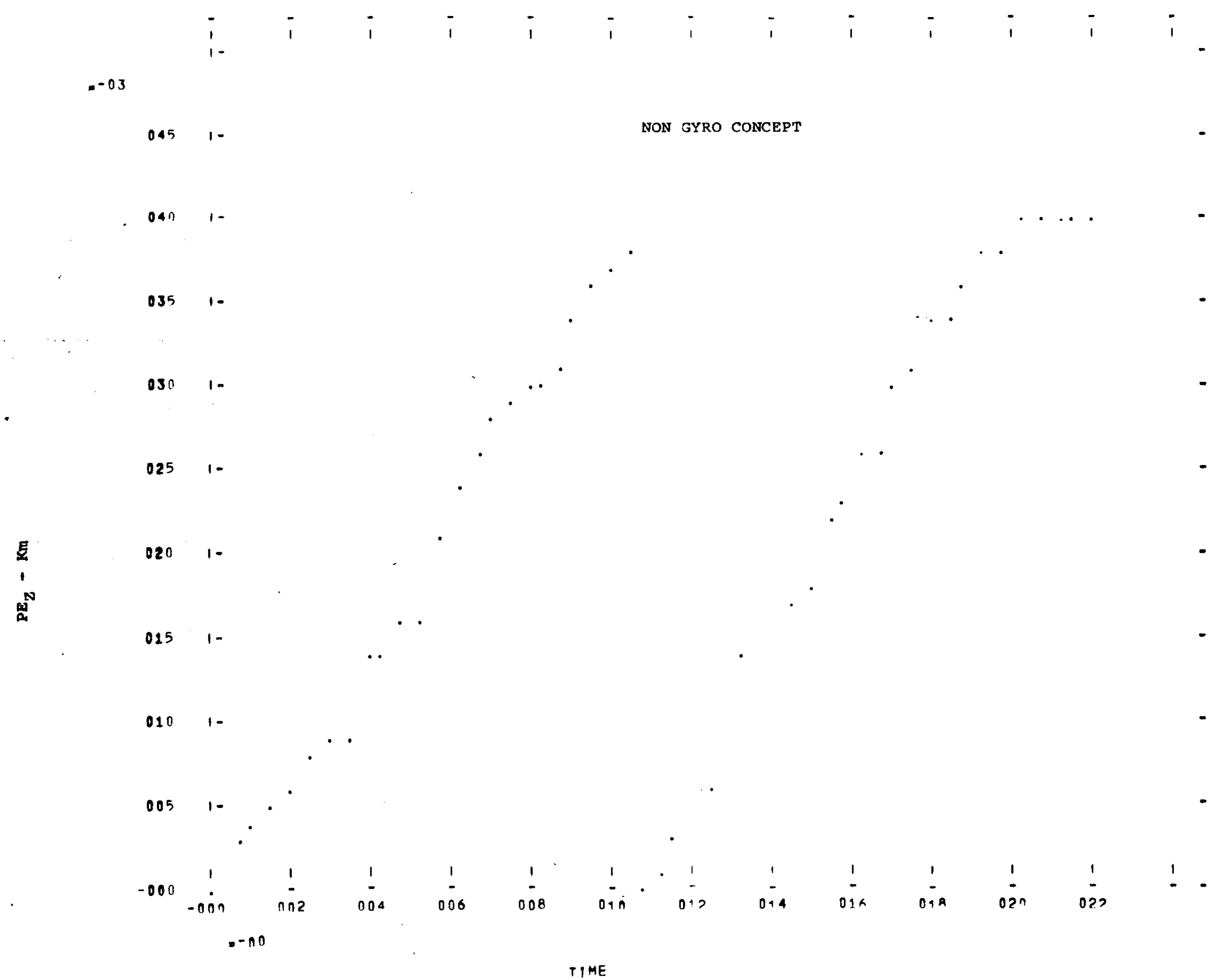

Figure 8-161 PLOT 13 MISSION V 1980 LEG A

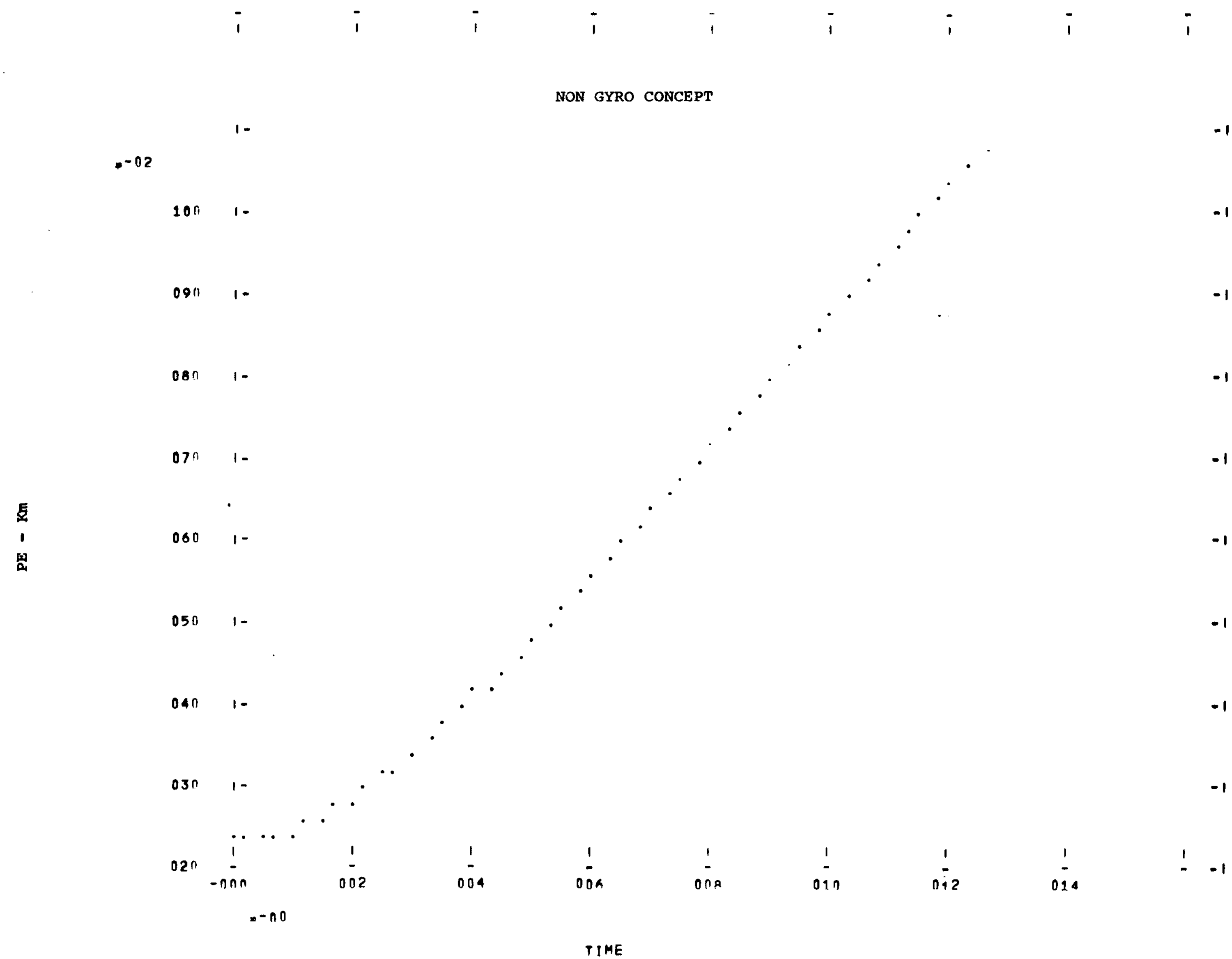

Figure 8-162 PLOT 12 MISSION V 1980 LEG A

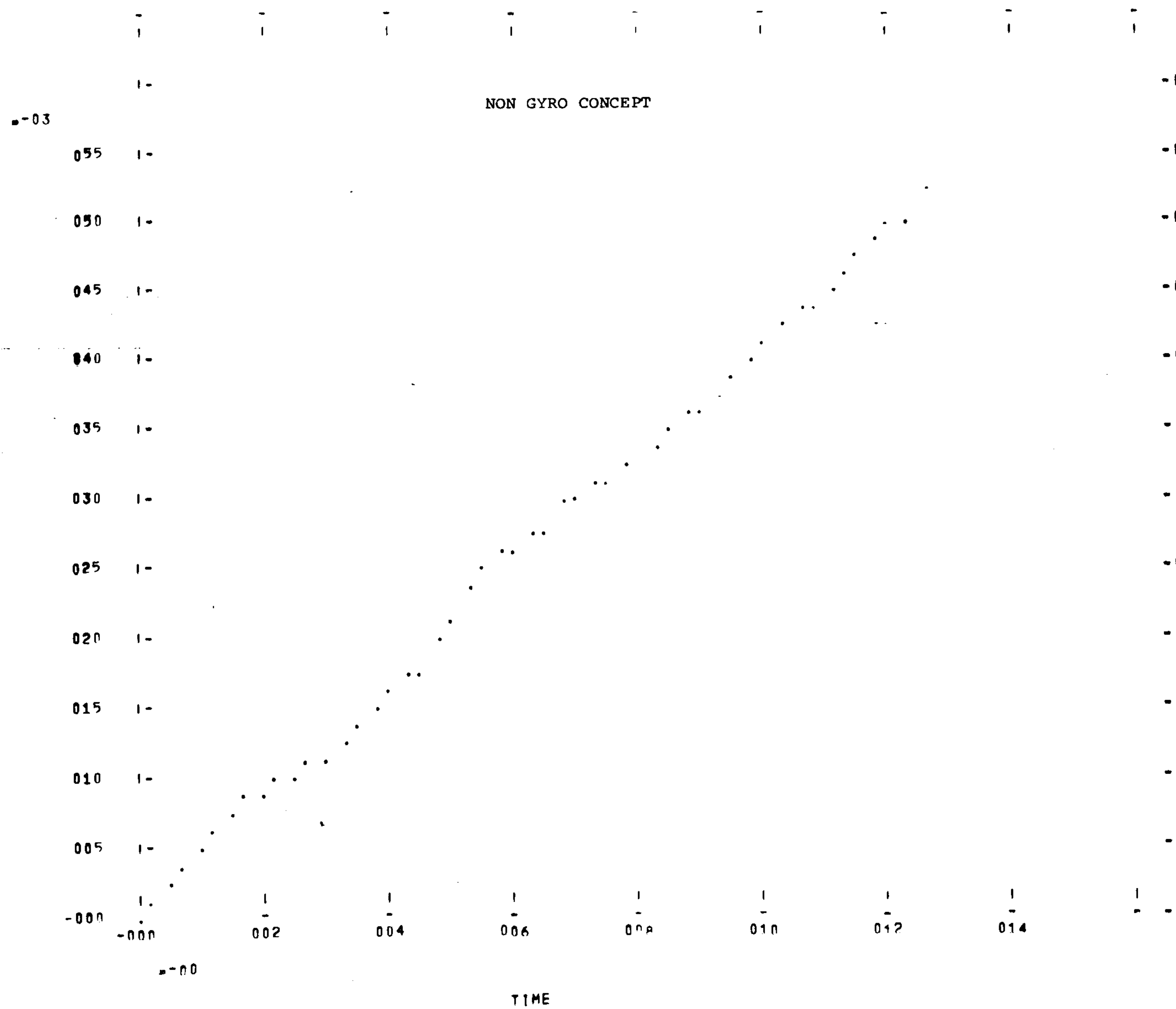

Figure 8-163a PLOT 13 MISSION V 1980 LEG 8

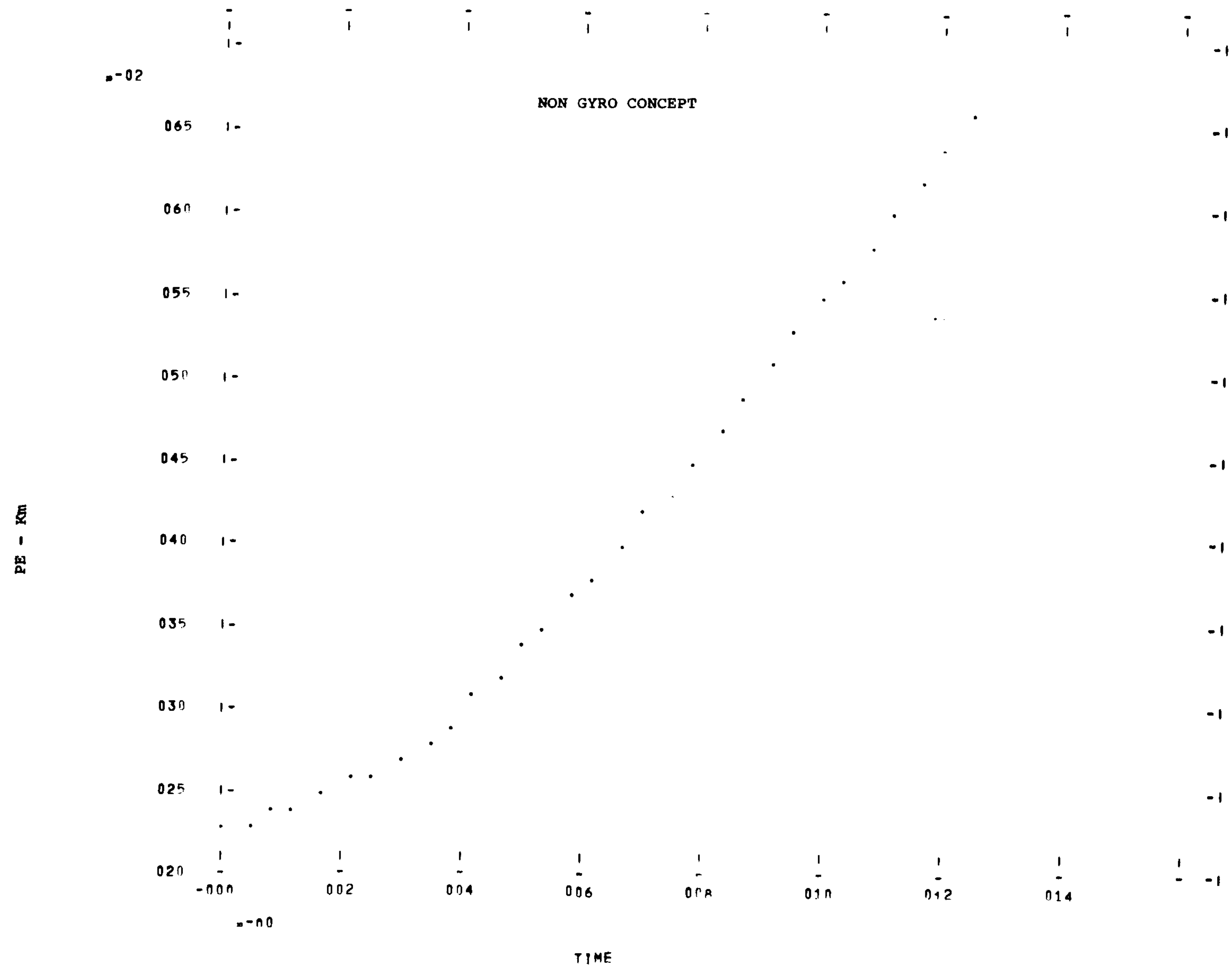

Figure 8-163b PLOT 12 MISSION V 1980 LEG B

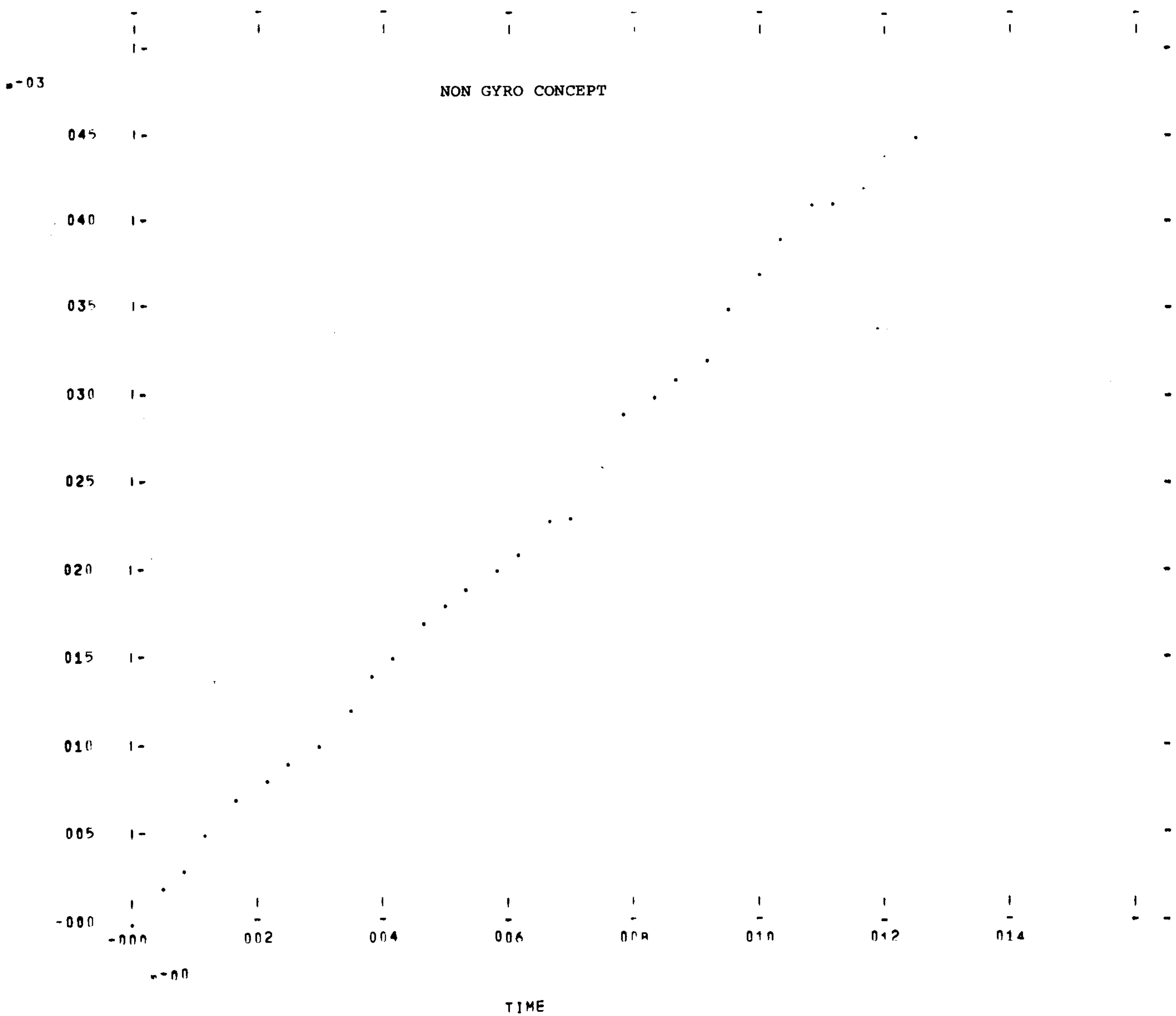

Figure 8-164a PLOT 13 MISSION VI 1984 LEG B

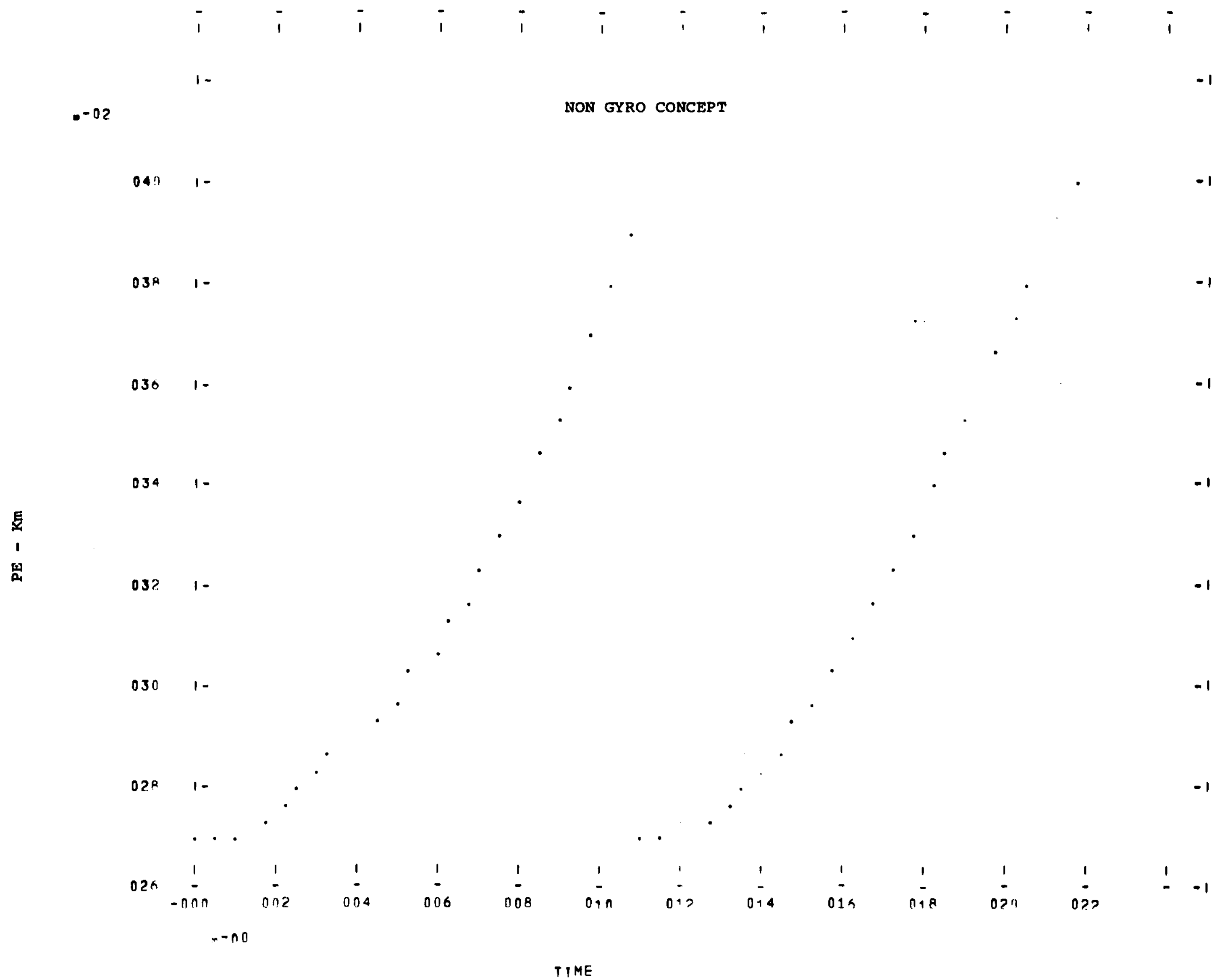

Figure 8-164b PLOT 12 MISSION VI 1984 LEG B

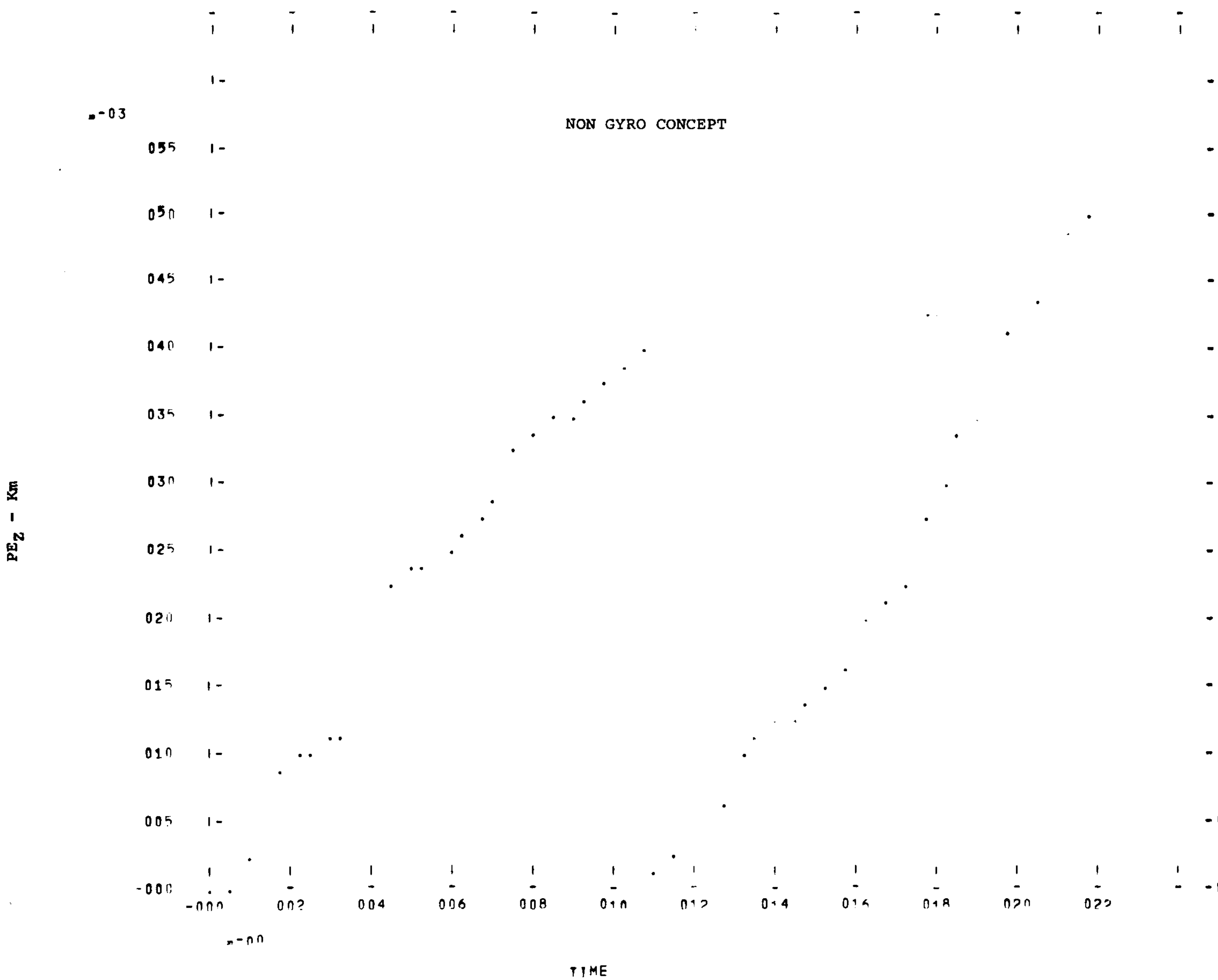

Figure 8-165 INERTIAL CONCEPT
PE VERSUS ACCELEROMETER ERROR

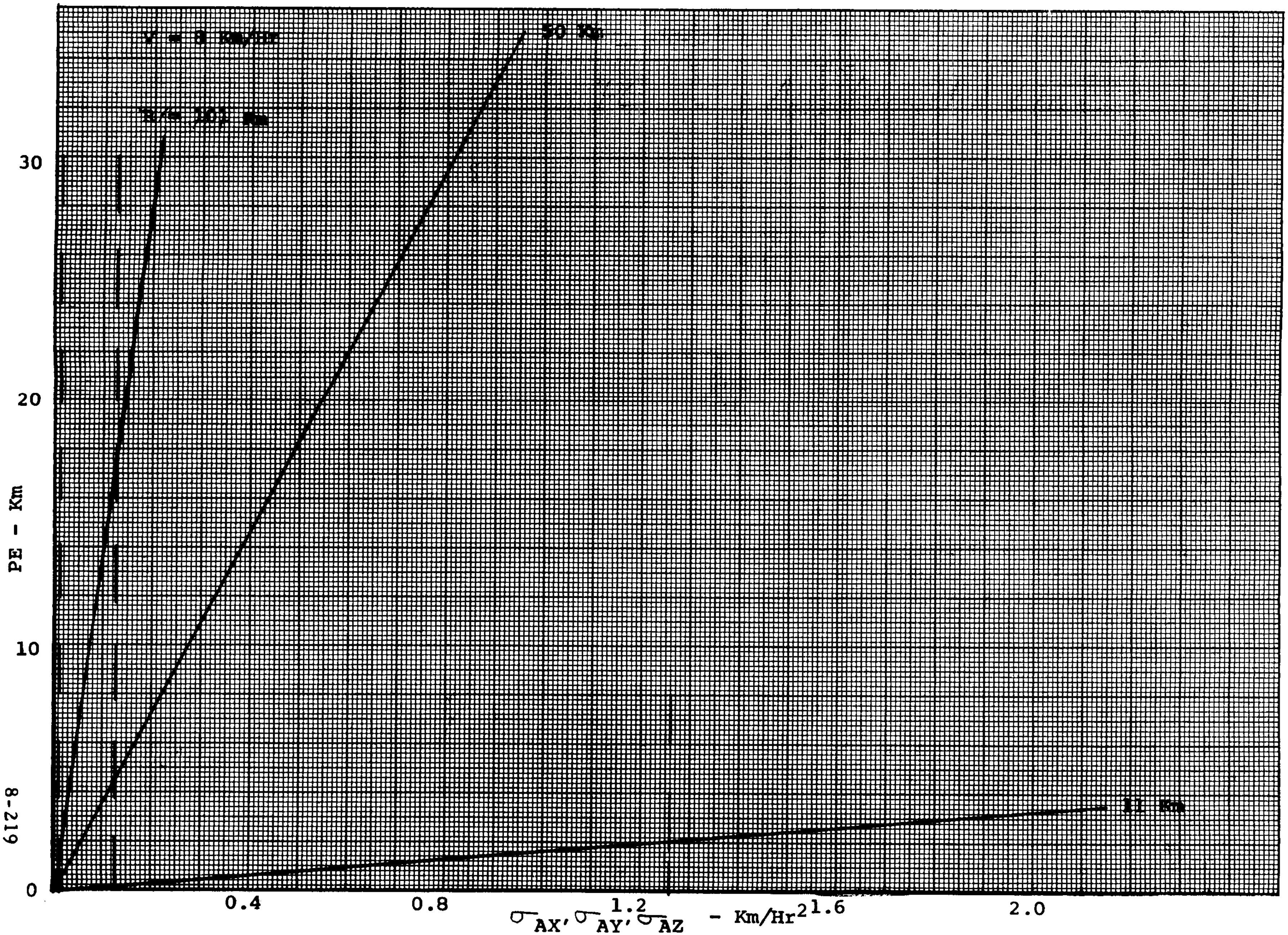

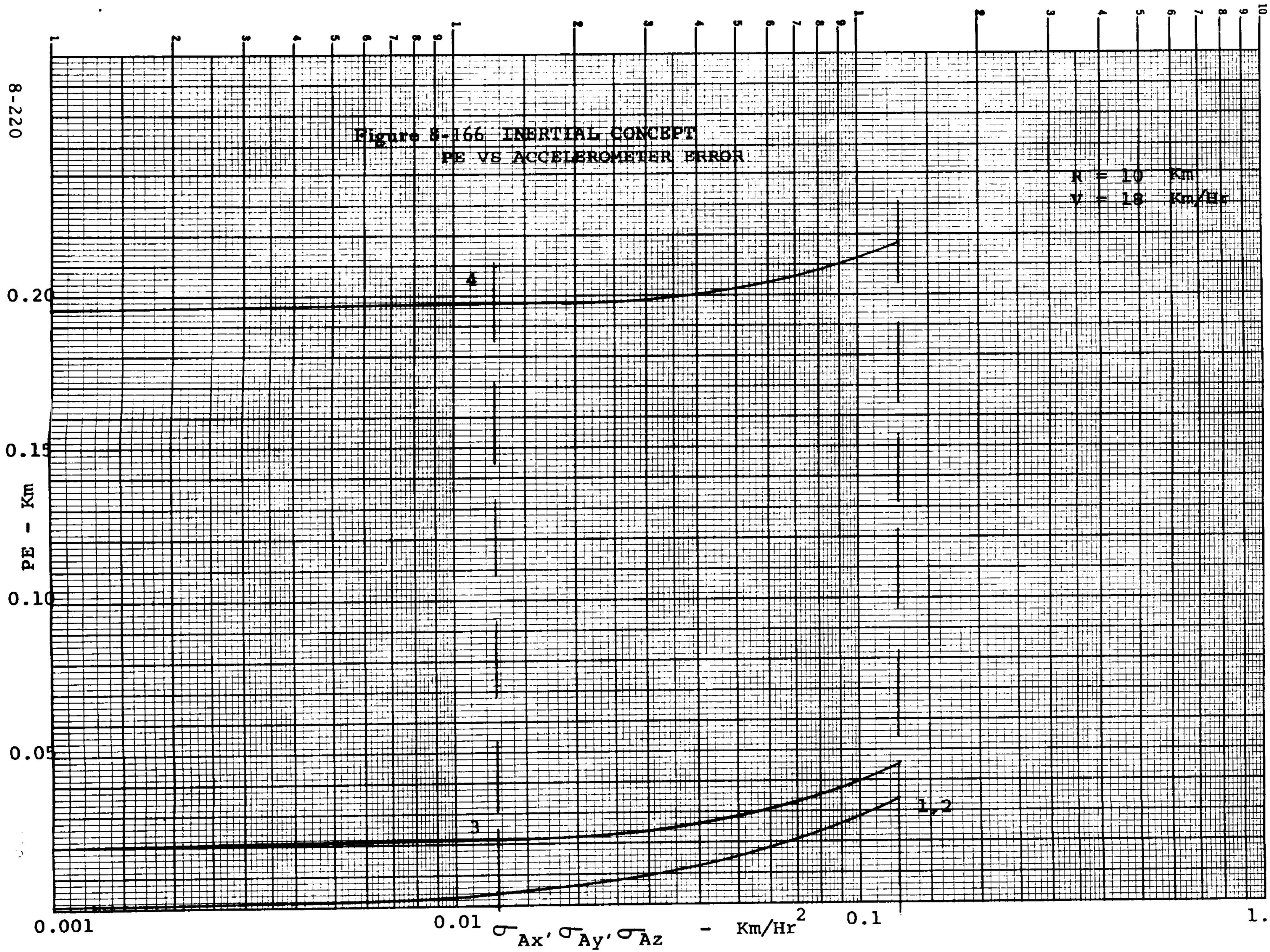
Figure 8-166 INERTIAL CONCEPT
PE VS ACCELEROMETER ERROR
R = 10 Km
V = 18 Km/Hr
4
3
1,2
PE - Km
0.20
0.15
0.10
0.05
0.001
0.01
0.1
1.0
$\sigma_{Ax}, \sigma_{Ay}, \sigma_{Az}$ - Km/Hr^2

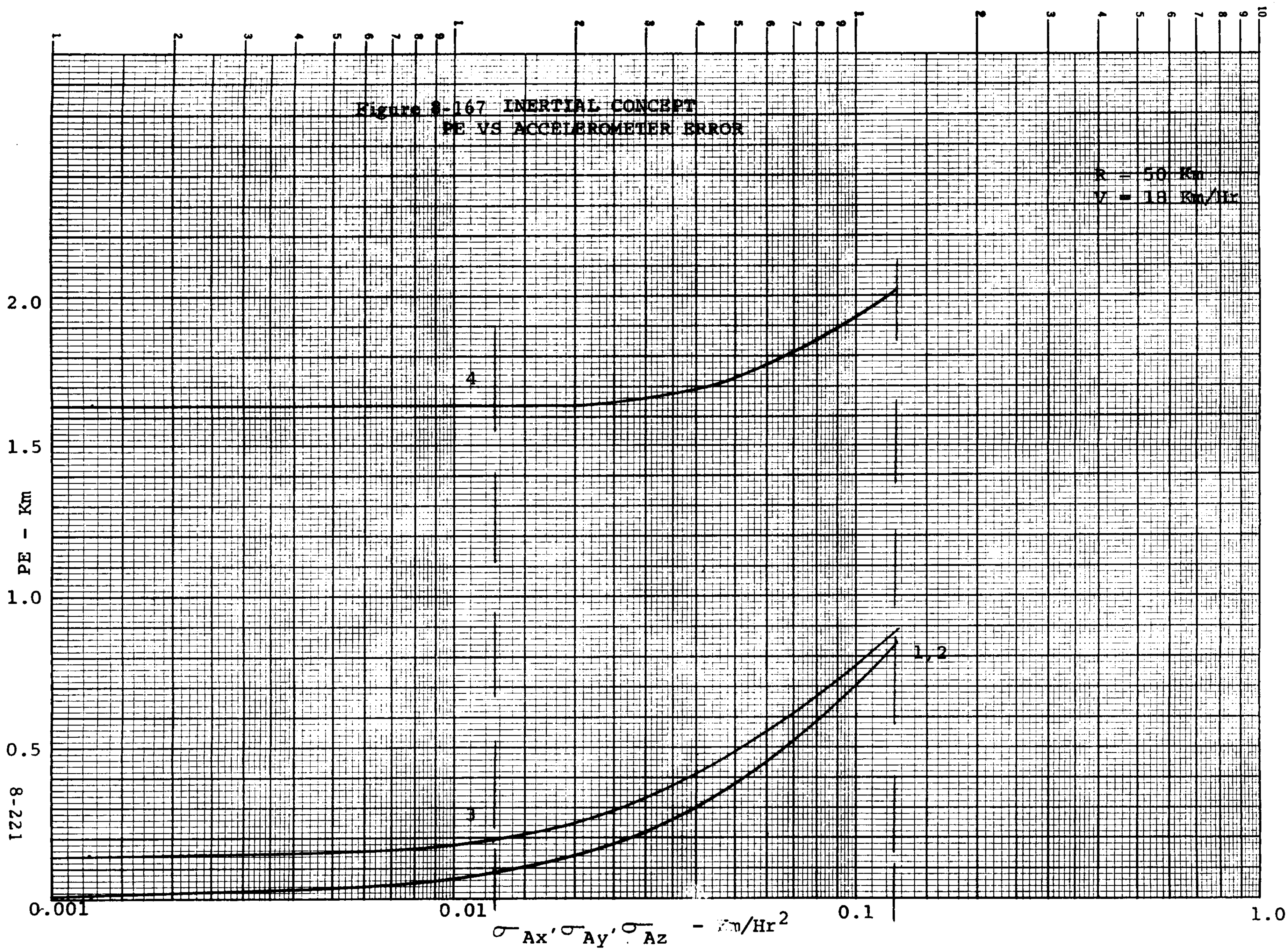

Figure 8-167 INERTIAL CONCEPT
PE VS ACCELEROMETER ERROR

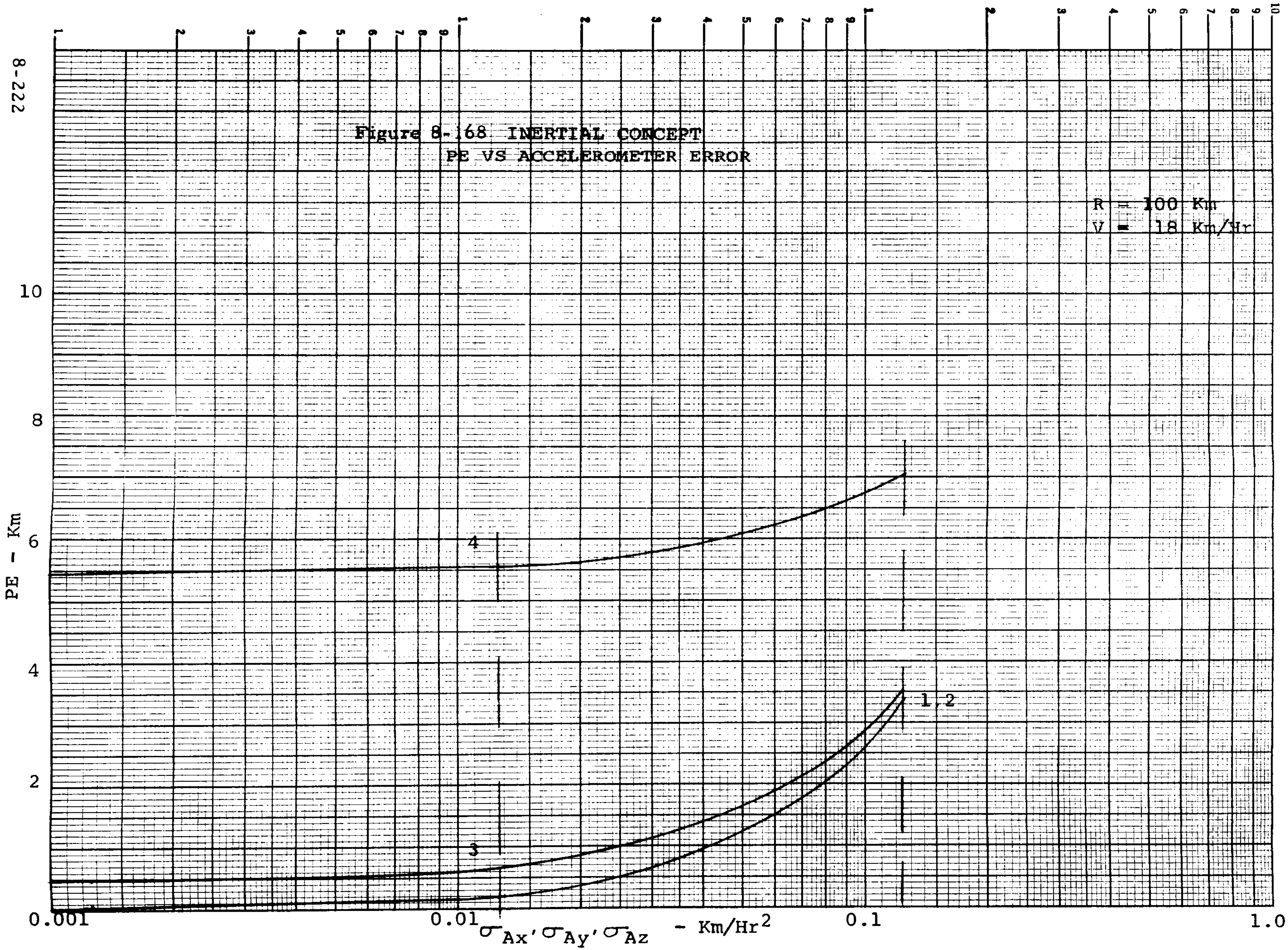

Figure 8-168 INERTIAL CONCEPT
PE VS ACCELEROMETER ERROR

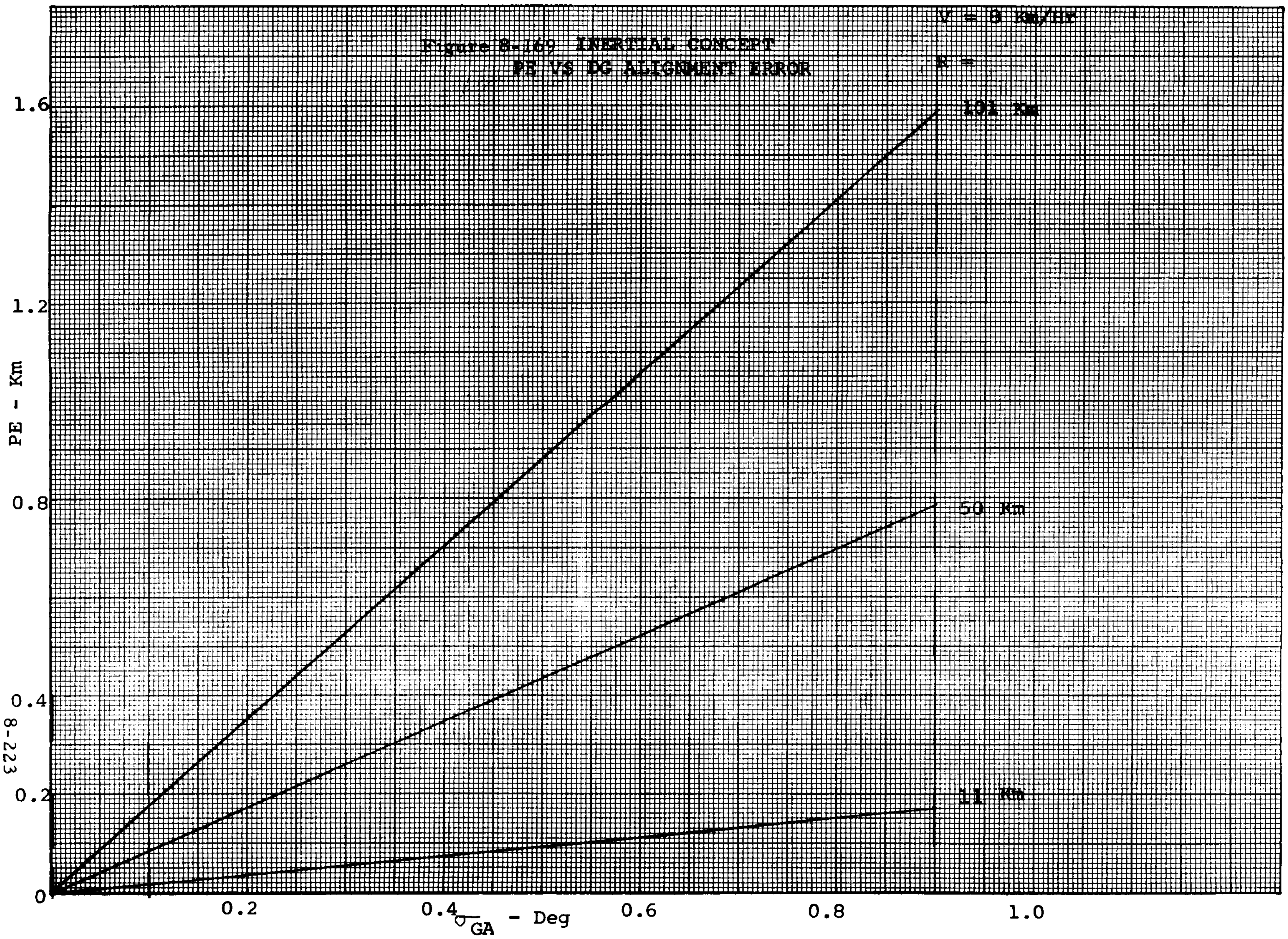
Figure 8-169 INERTIAL CONCEPT
PE VS DG ALIGNMENT ERROR
V = 3 Km/Hr
R =
101 Km
50 Km
11 Km
PE - Km
1.6
1.2
0.8
0.4
0.2
0
0.2
0.4
0.6
0.8
1.0
σ_{GA} - Deg

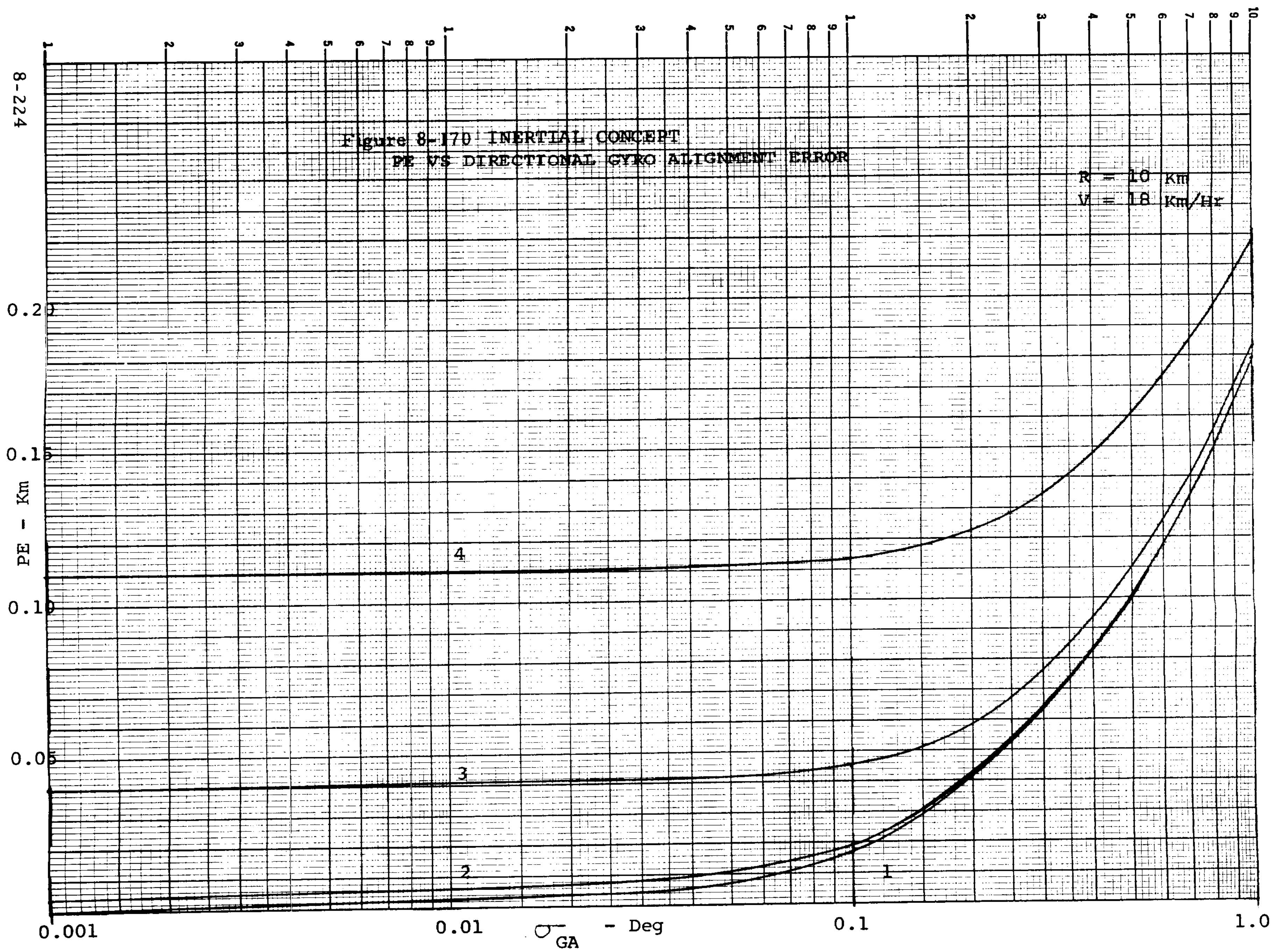
Figure 8-170 INERTIAL CONCEPT
PE VS DIRECTIONAL GYRO ALIGNMENT ERROR
R = 10 Km
V = 18 Km/Hr
0.20
0.15
0.10
0.05
PE - Km
4
3
2
1
0.001
0.01
0.1
1.0
σ_{GA} - Deg

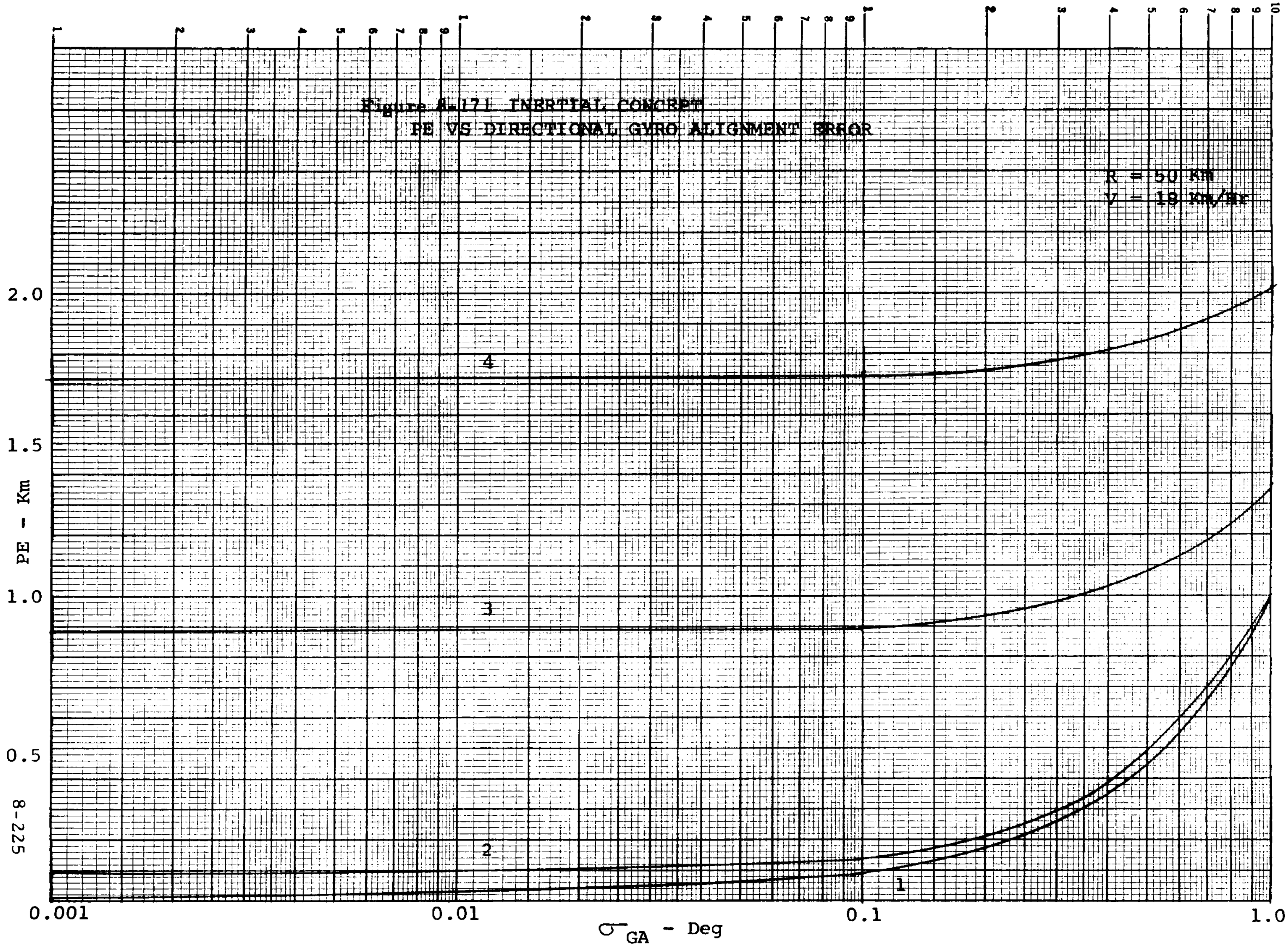

Figure 8-171 INERTIAL CONCEPT
PE VS DIRECTIONAL GYRO ALIGNMENT ERROR

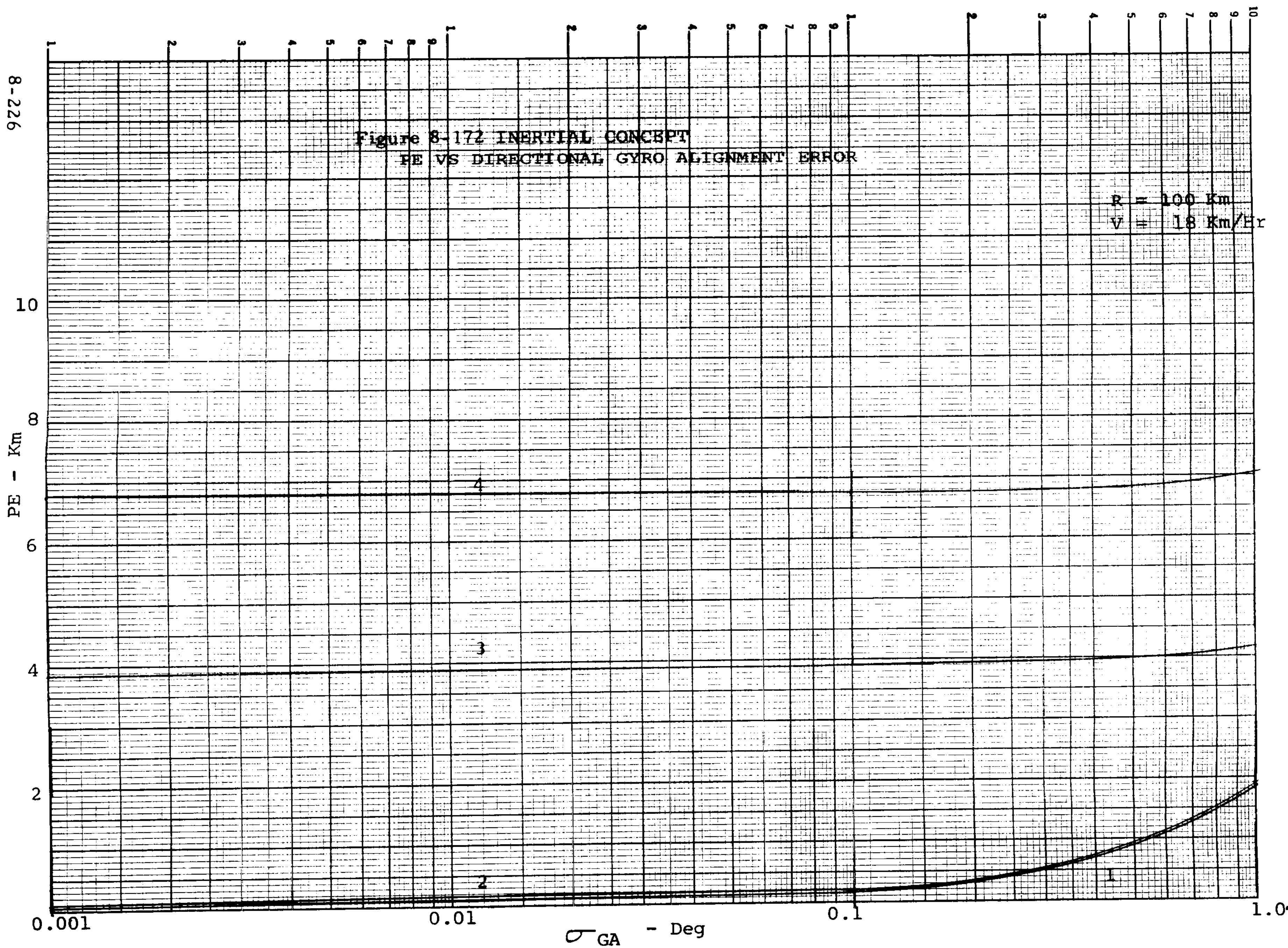
Figure 8-172 INERTIAL CONCEPT
PE VS DIRECTIONAL GYRO ALIGNMENT ERROR
R = 100 Km
V = 18 Km/Hr
PE - Km
10
8
6
4
2
0.001
0.01
0.1
1.0
σ_{GA} - Deg
1
2
3
4

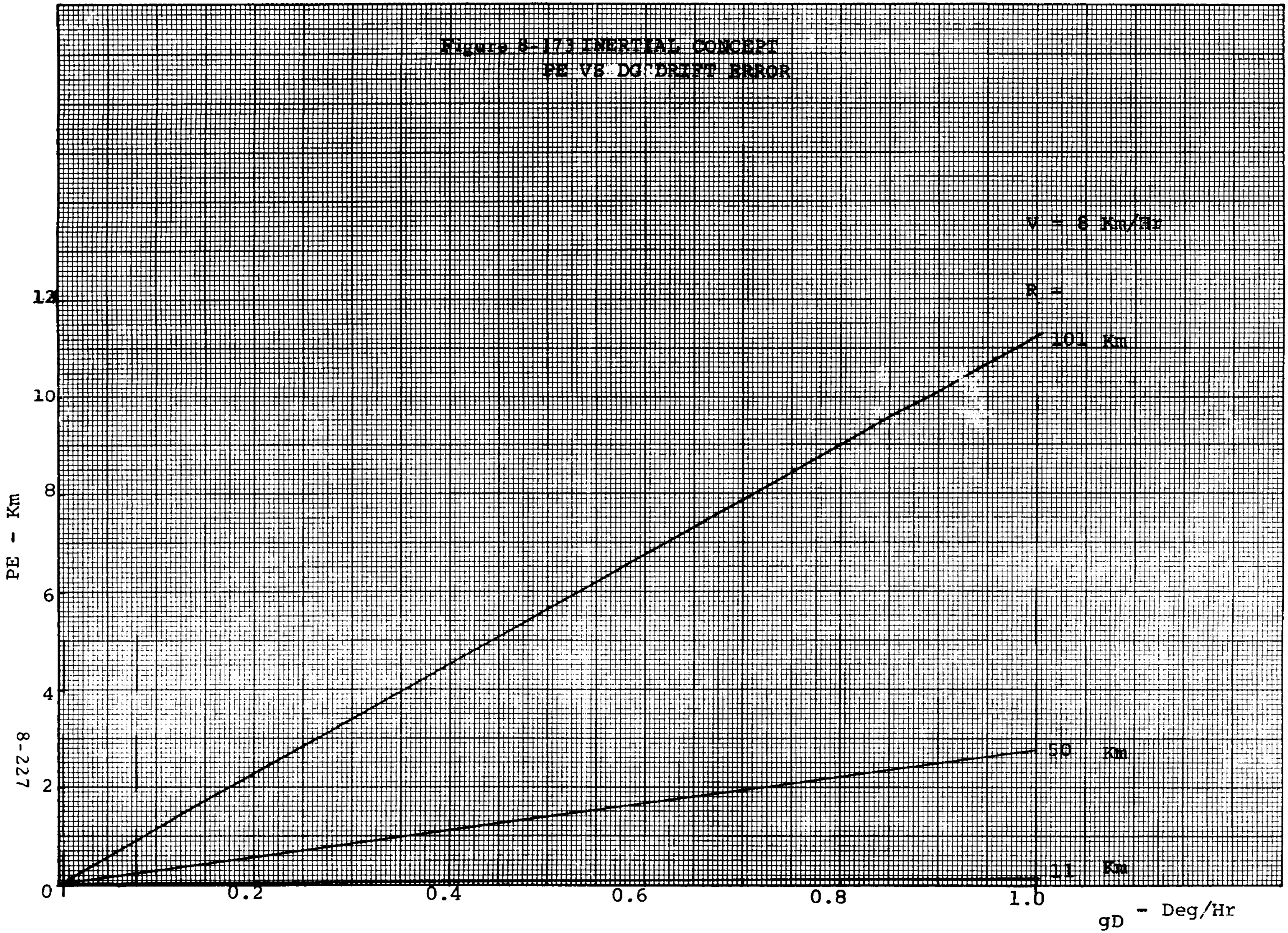

Figure 8-173 INERTIAL CONCEPT
PE VS DG DRIFT ERROR

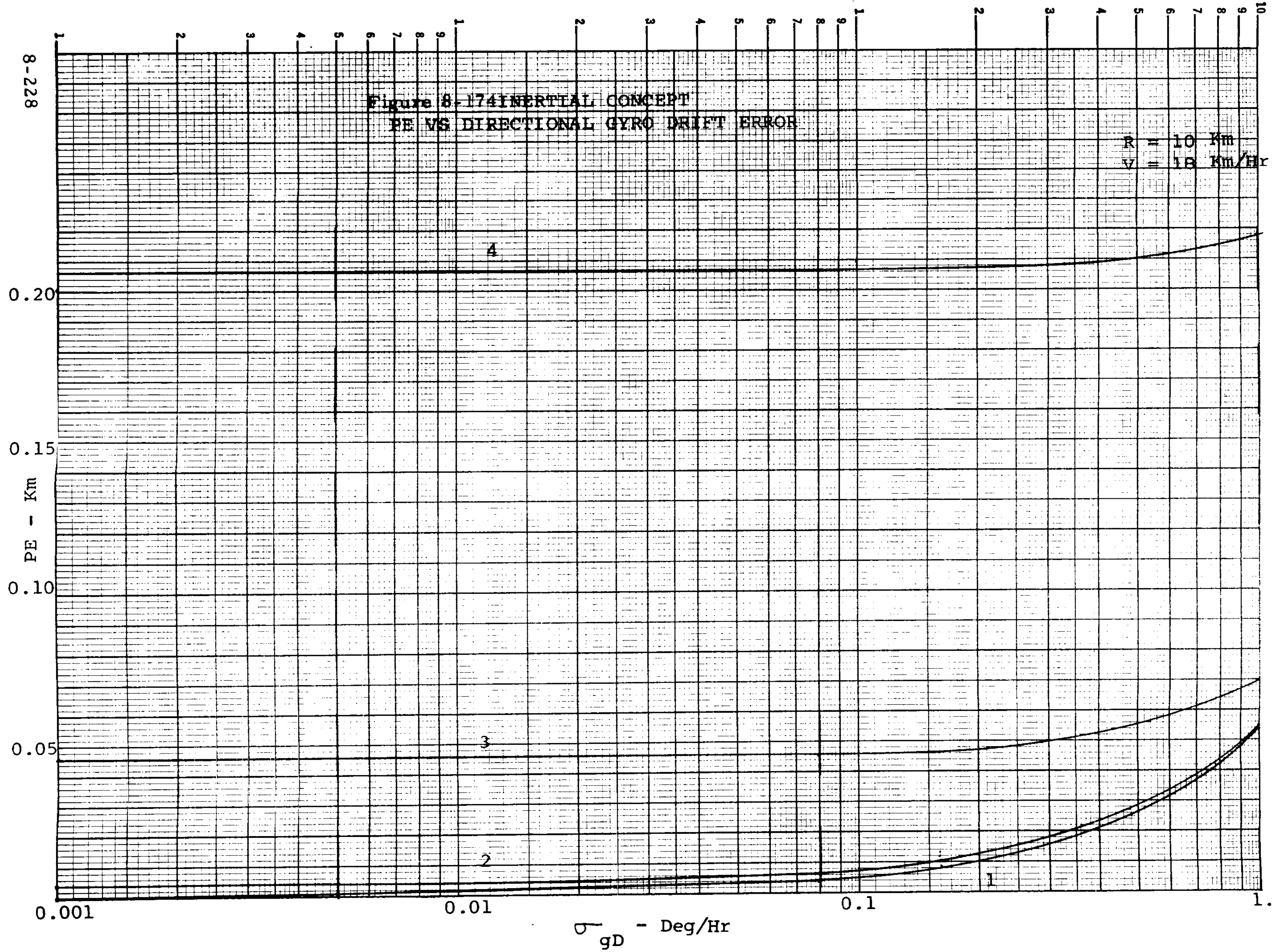
Figure 8-174 INERTIAL CONCEPT
PE VS DIRECTIONAL GYRO DRIFT ERROR
R = 10 Km
V = 18 Km/Hr
4
3
2
1
0.20
0.15
0.10
0.05
PE - Km
0.001
0.01
0.1
1.0
σ gD - Deg/Hr

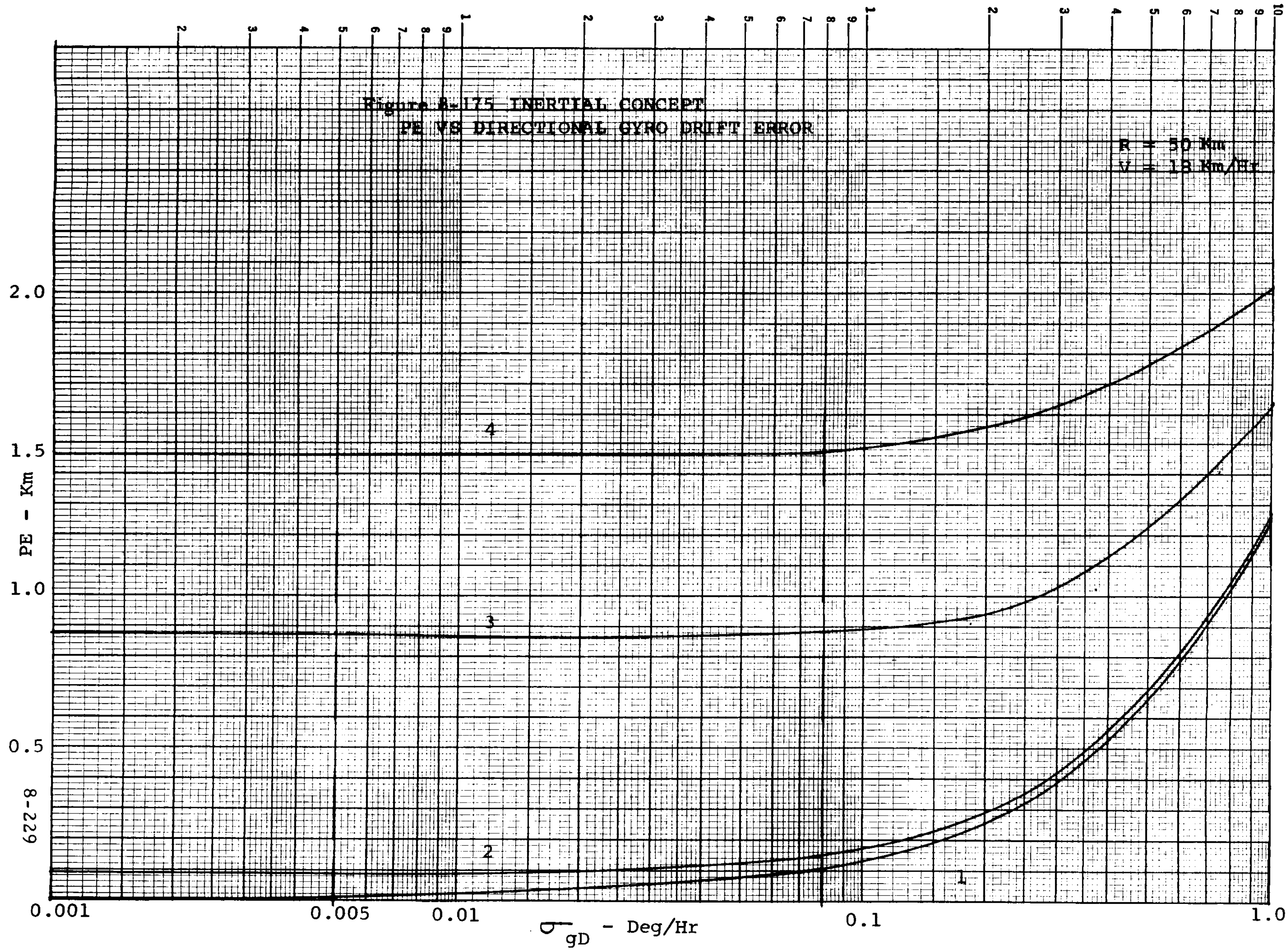

Figure 8-175 INERTIAL CONCEPT
PE VS DIRECTIONAL GYRO DRIFT ERROR

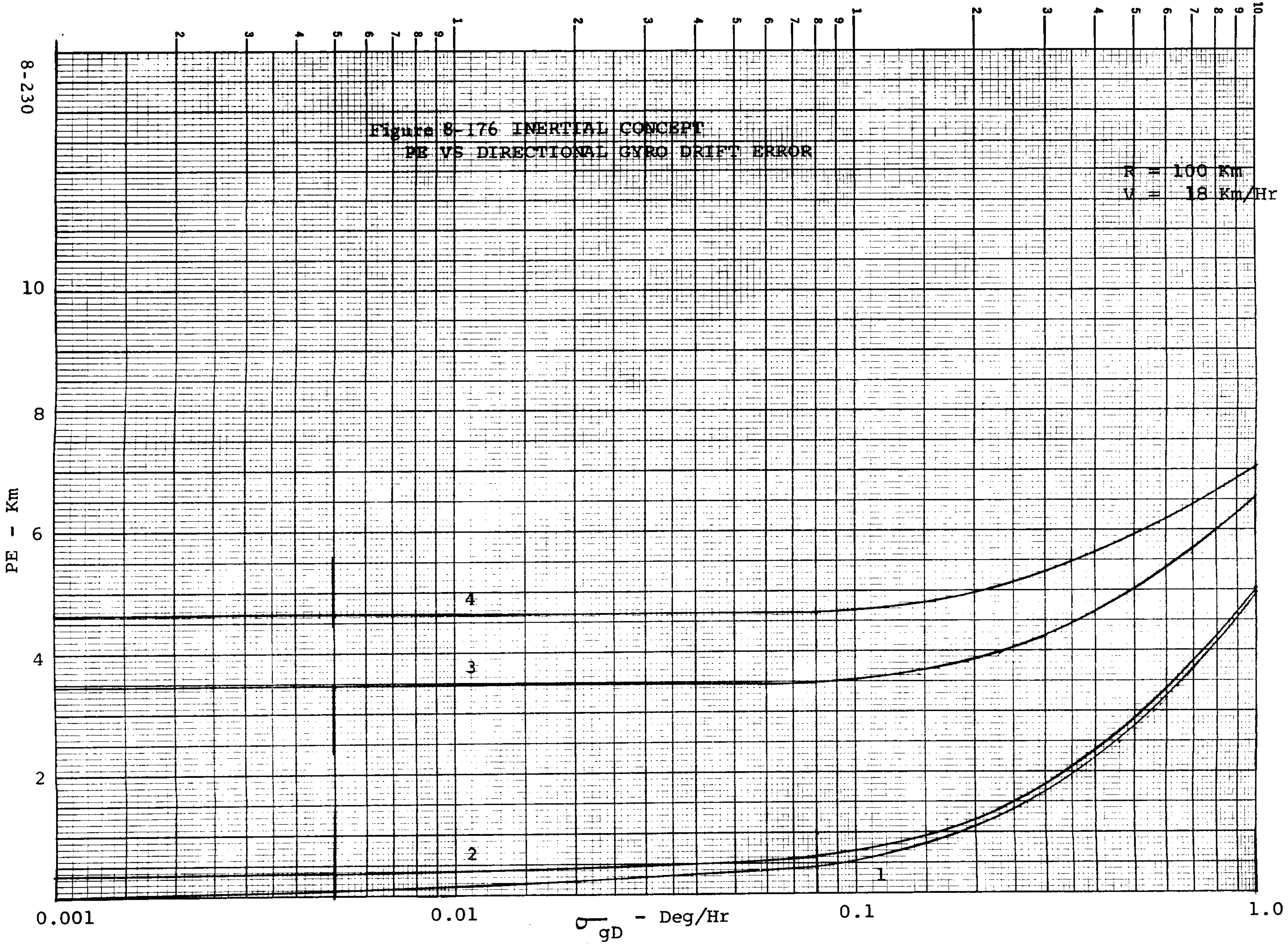
Figure 8-176 INERTIAL CONCEPT
PE VS DIRECTIONAL GYRO DRIFT ERROR
R = 100 Km
V = 18 Km/Hr
PE - Km
10
8
6
4
2
4
3
2
1
0.001
0.01
0.1
1.0
σ_{gD} - Deg/Hr

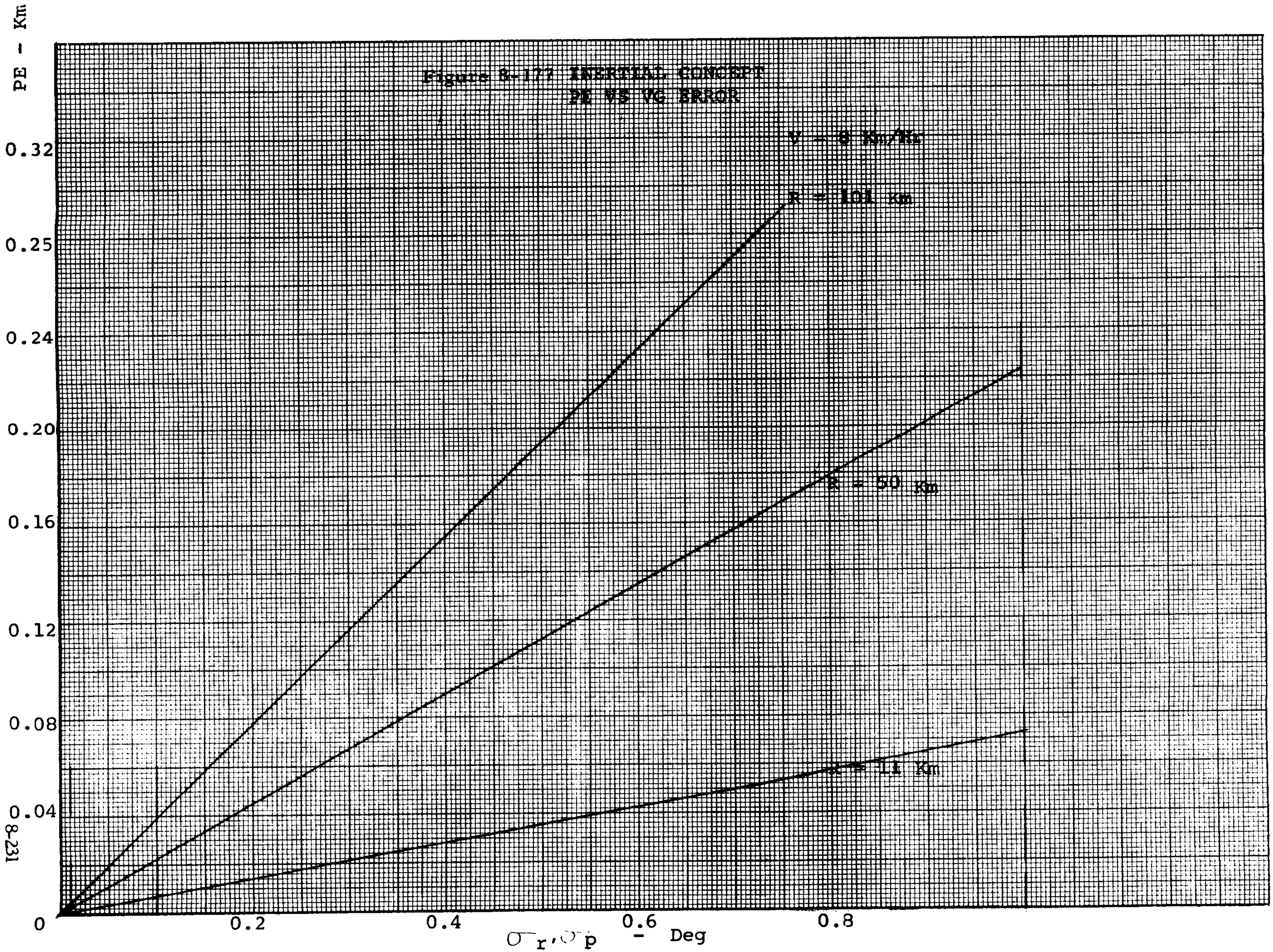

Figure 8-177 INERTIAL CONCEPT
PE VS VG ERROR

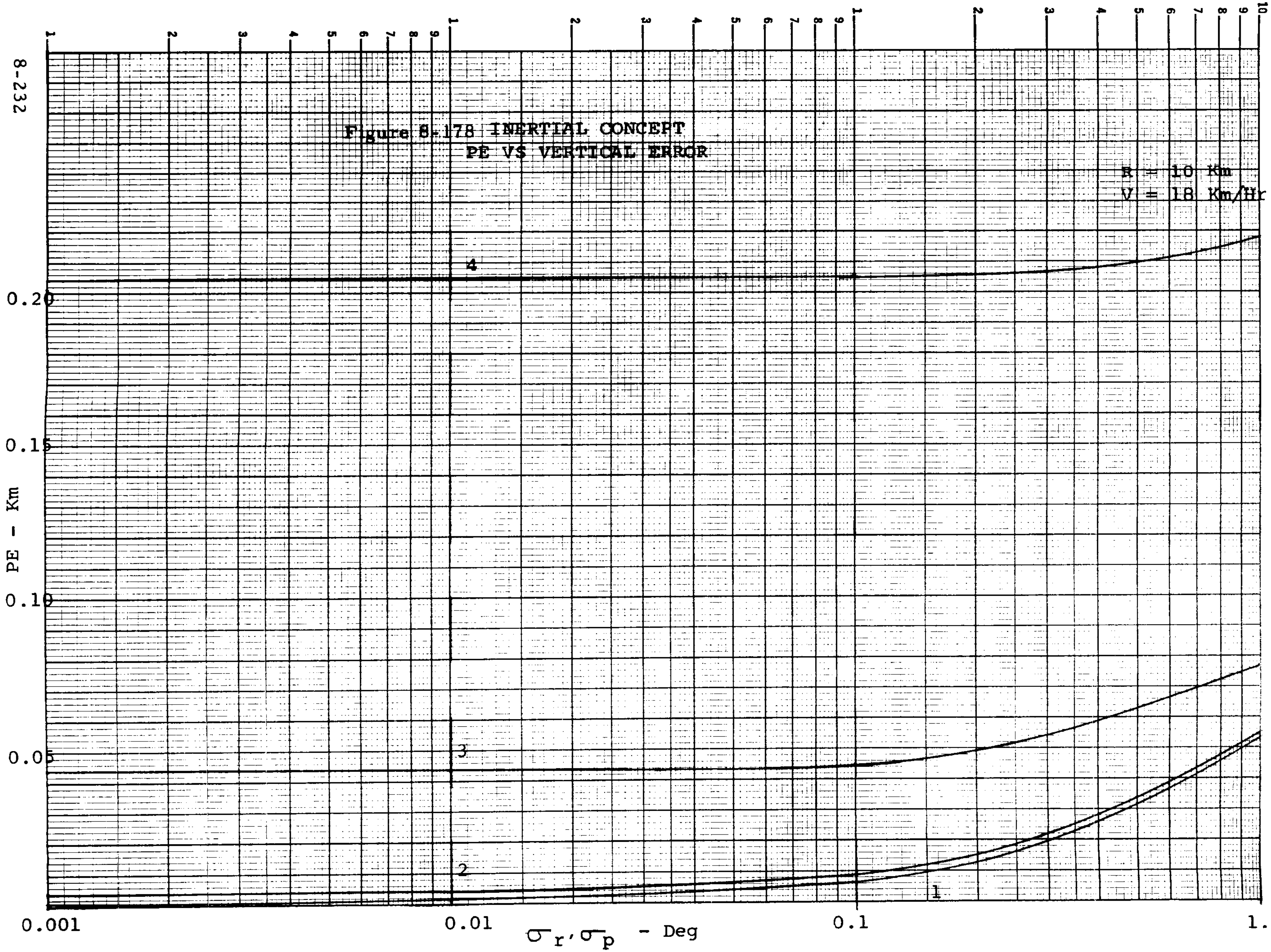

Figure 8-178 INERTIAL CONCEPT
PE VS VERTICAL ERROR

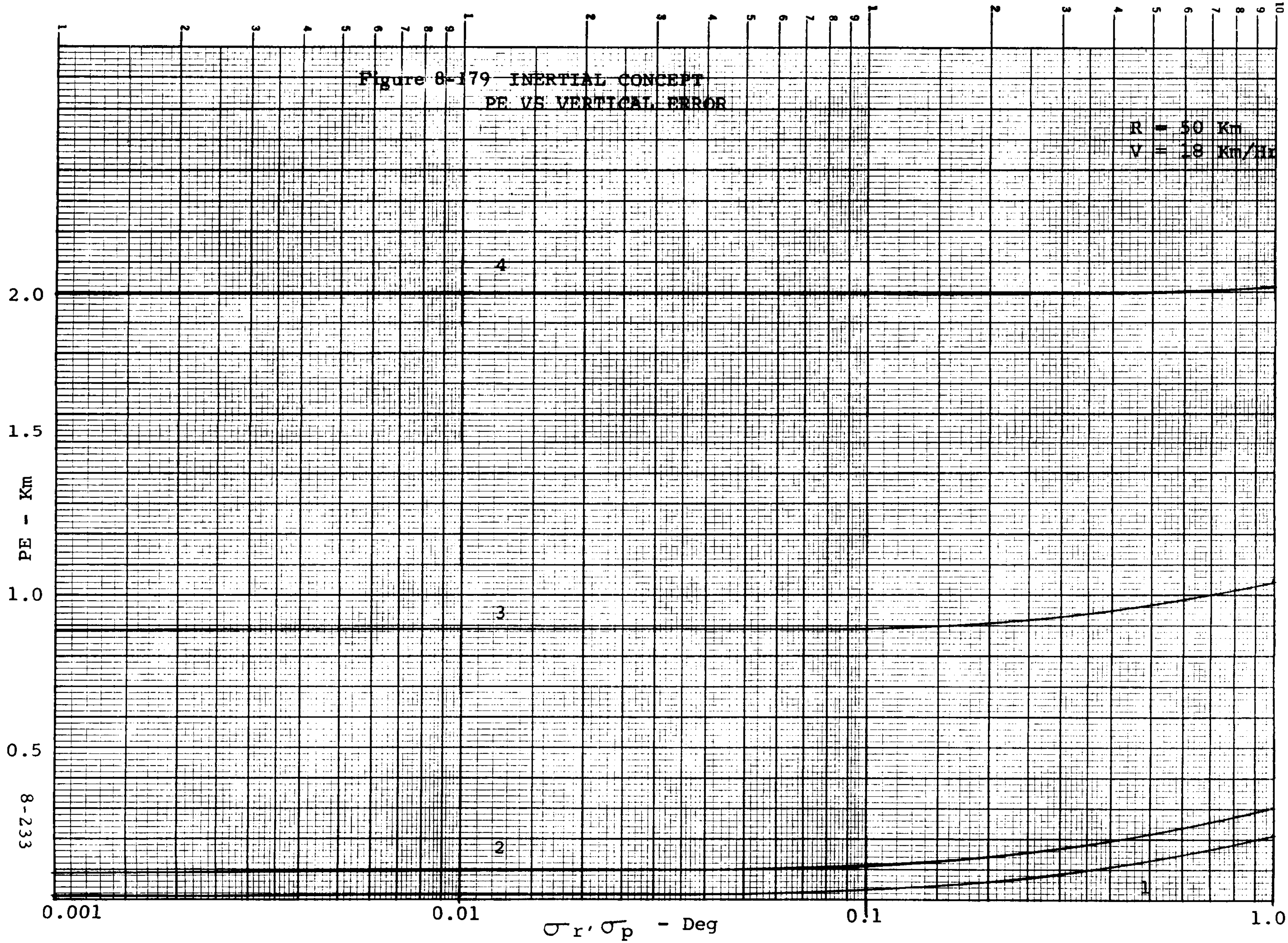

Figure 8-179 INERTIAL CONCEPT
PE VS VERTICAL ERROR

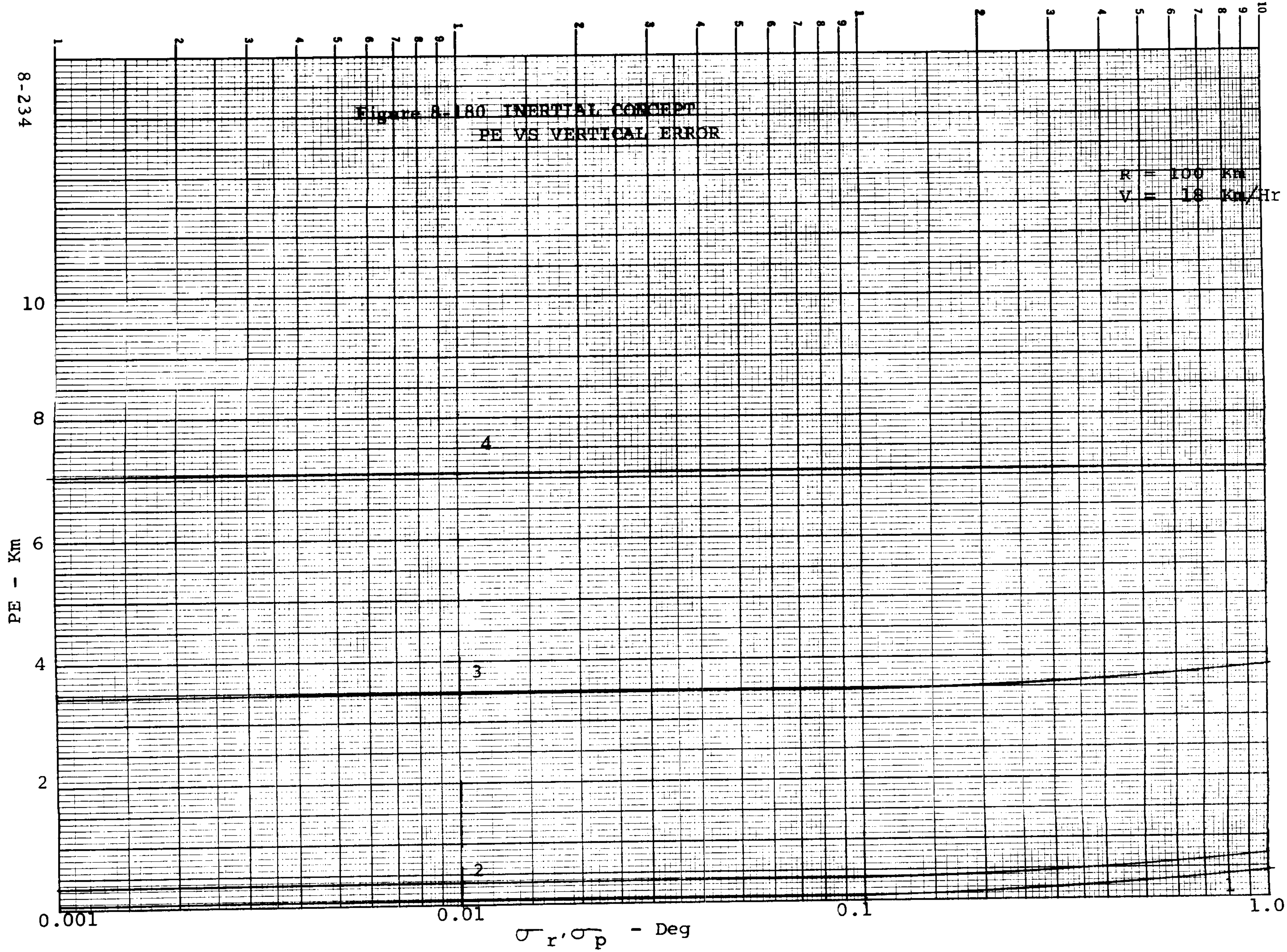
Figure 8-180 INERTIAL CONCEPT
PE VS VERTICAL ERROR
R = 100 Km
V = 18 Km/Hr
4
3
2
PE - Km
10
8
6
4
2
0.001
0.01
0.1
1.0
σ_r, σ_p - Deg

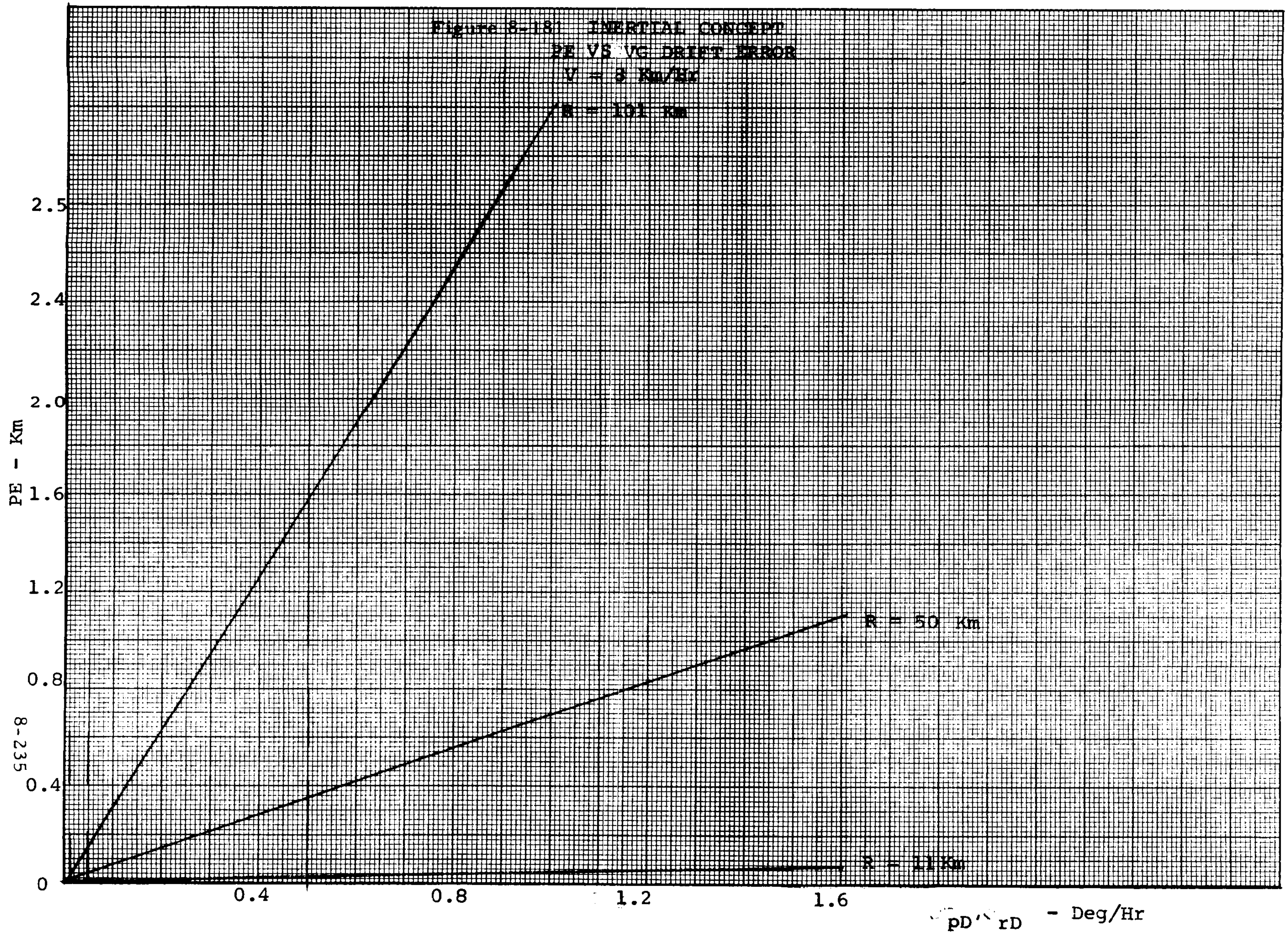

Figure 8-181 INERTIAL CONCEPT
PE VS VG DRIFT ERROR
V = 8 Km/Hr

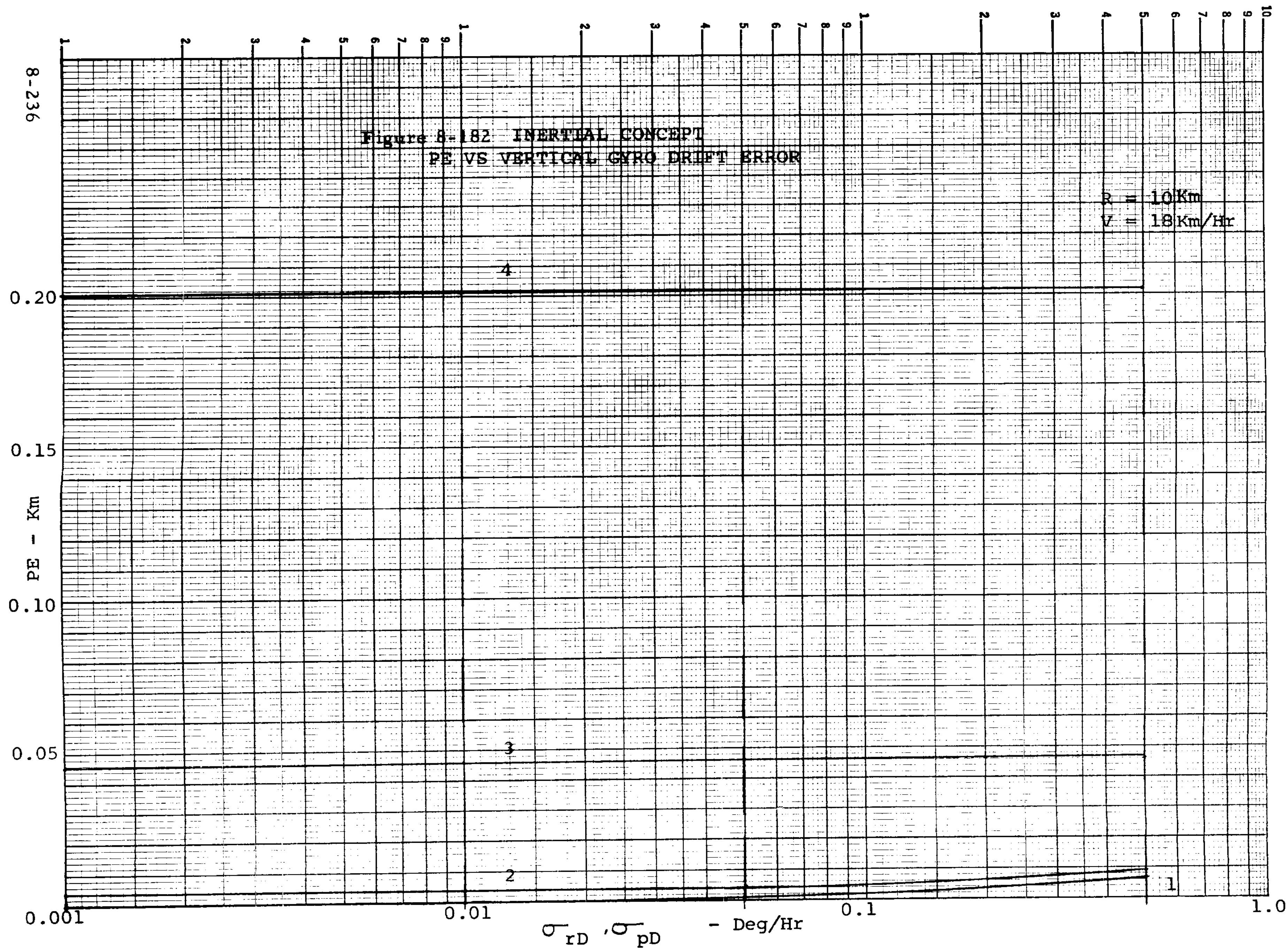

Figure 8-182 INERTIAL CONCEPT
PE VS VERTICAL GYRO DRIFT ERROR

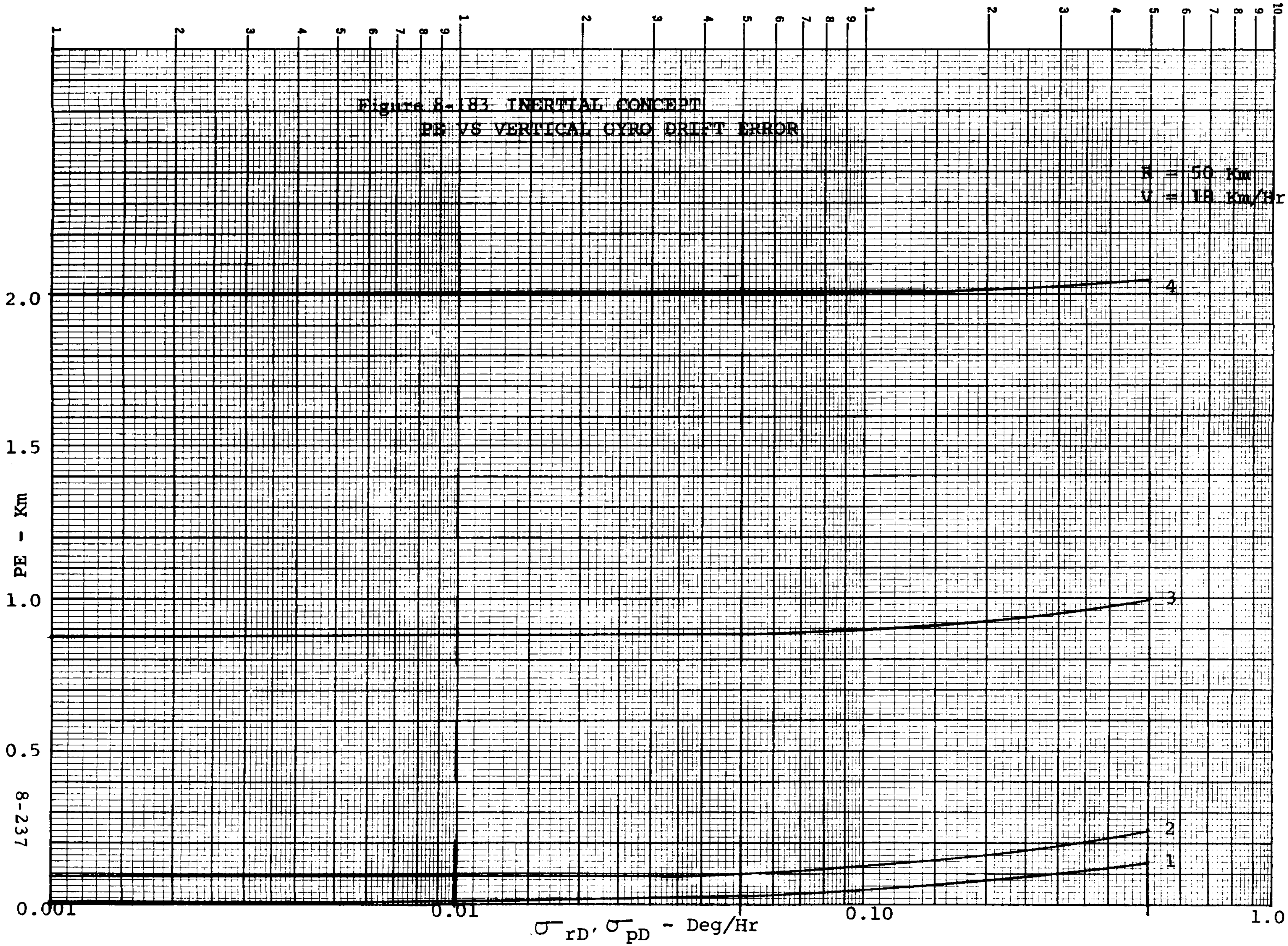

Figure 8-183 INERTIAL CONCEPT
PE VS VERTICAL GYRO DRIFT ERROR

Figure 8-184 INERTIAL CONCEPT
PE VS VERTICAL GYRO DRIFT ERROR

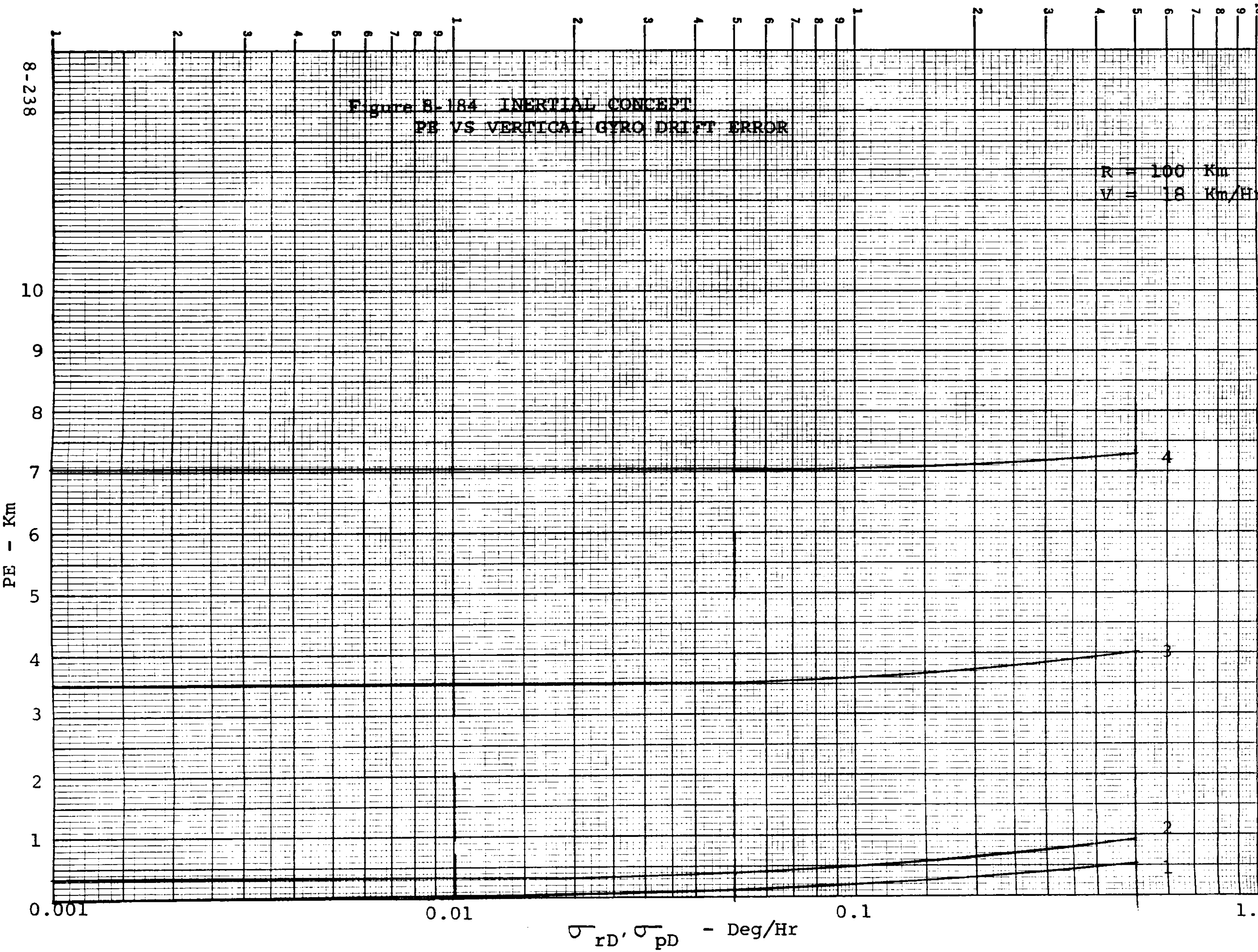

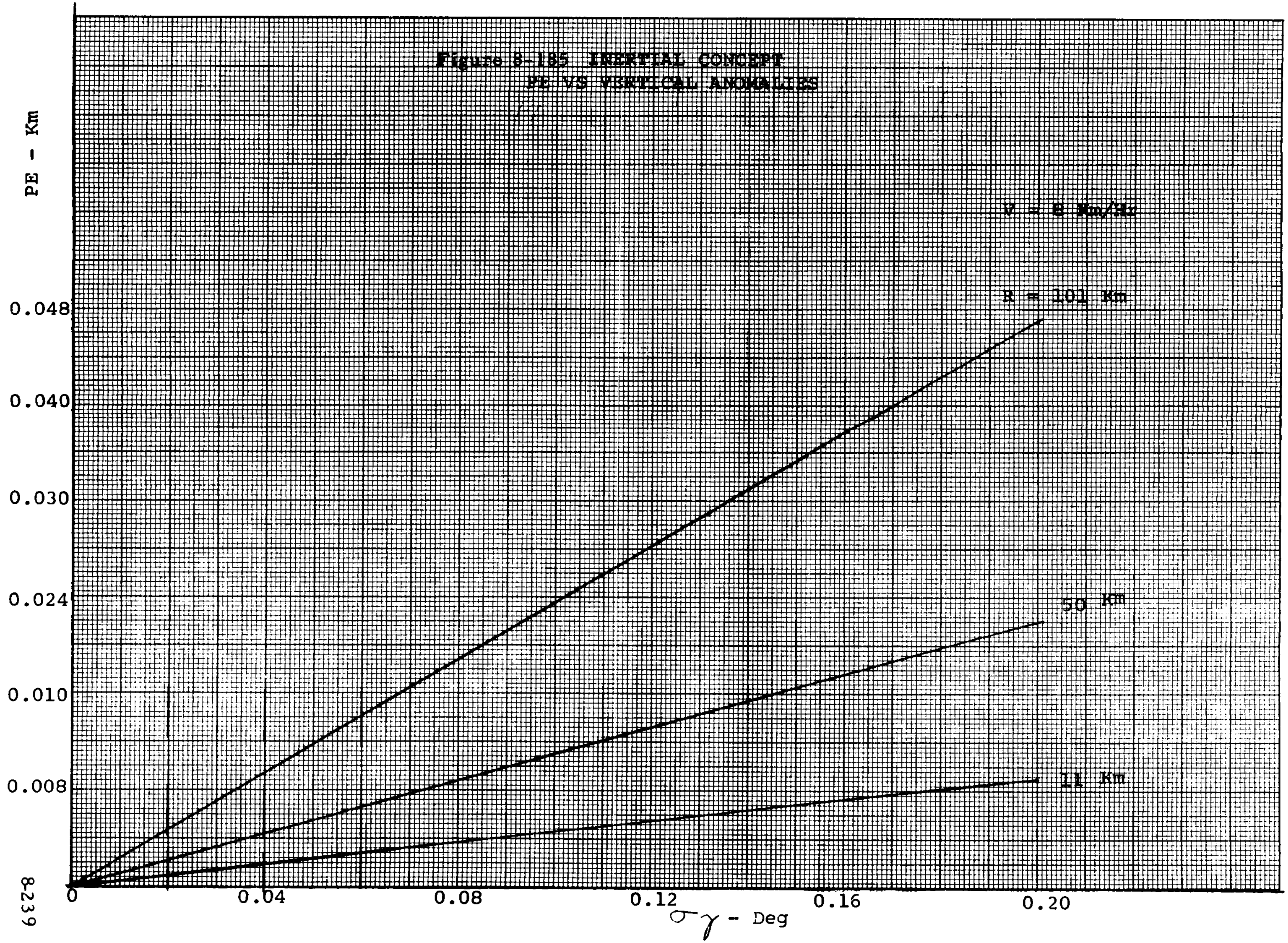

Figure 8-185 INERTIAL CONCEPT
PE VS VERTICAL ANOMALIES

Figure 8-186 INERTIAL CONCEPT/(PE)$_Z$ VERSUS ACCELEROMETER ERROR

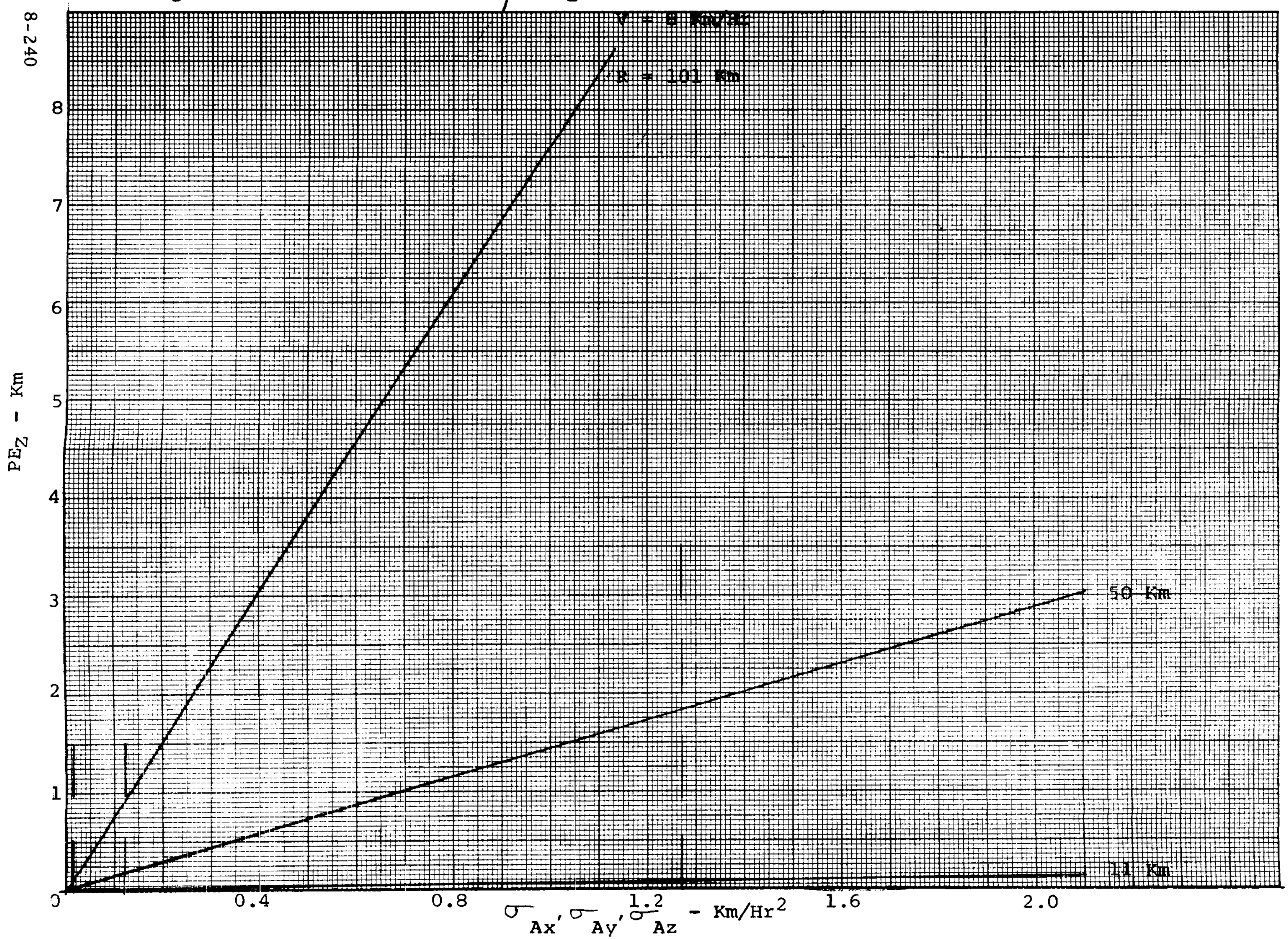

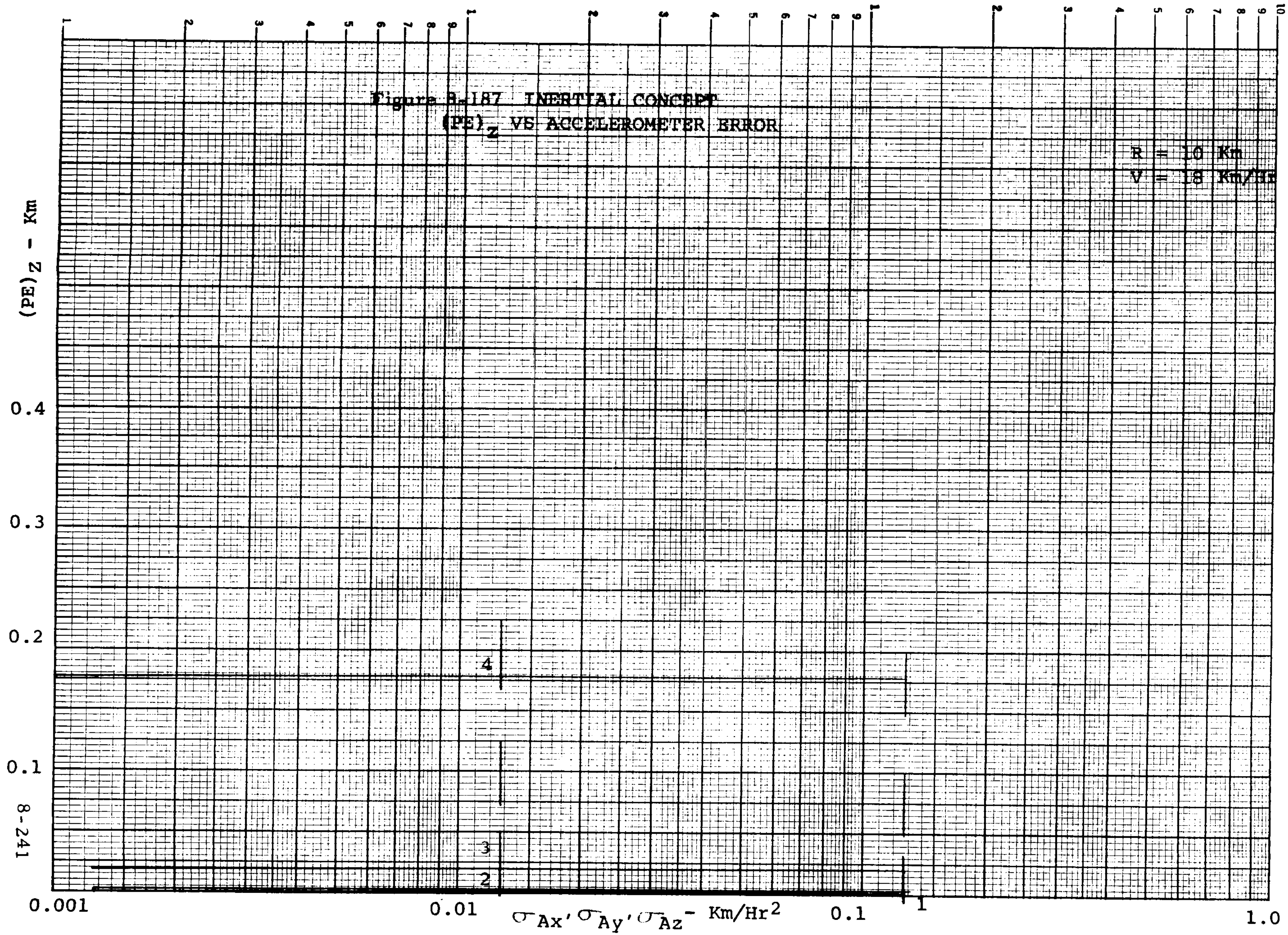

Figure 8-187 INERTIAL CONCEPT
$(PE)_Z$ VS ACCELEROMETER ERROR

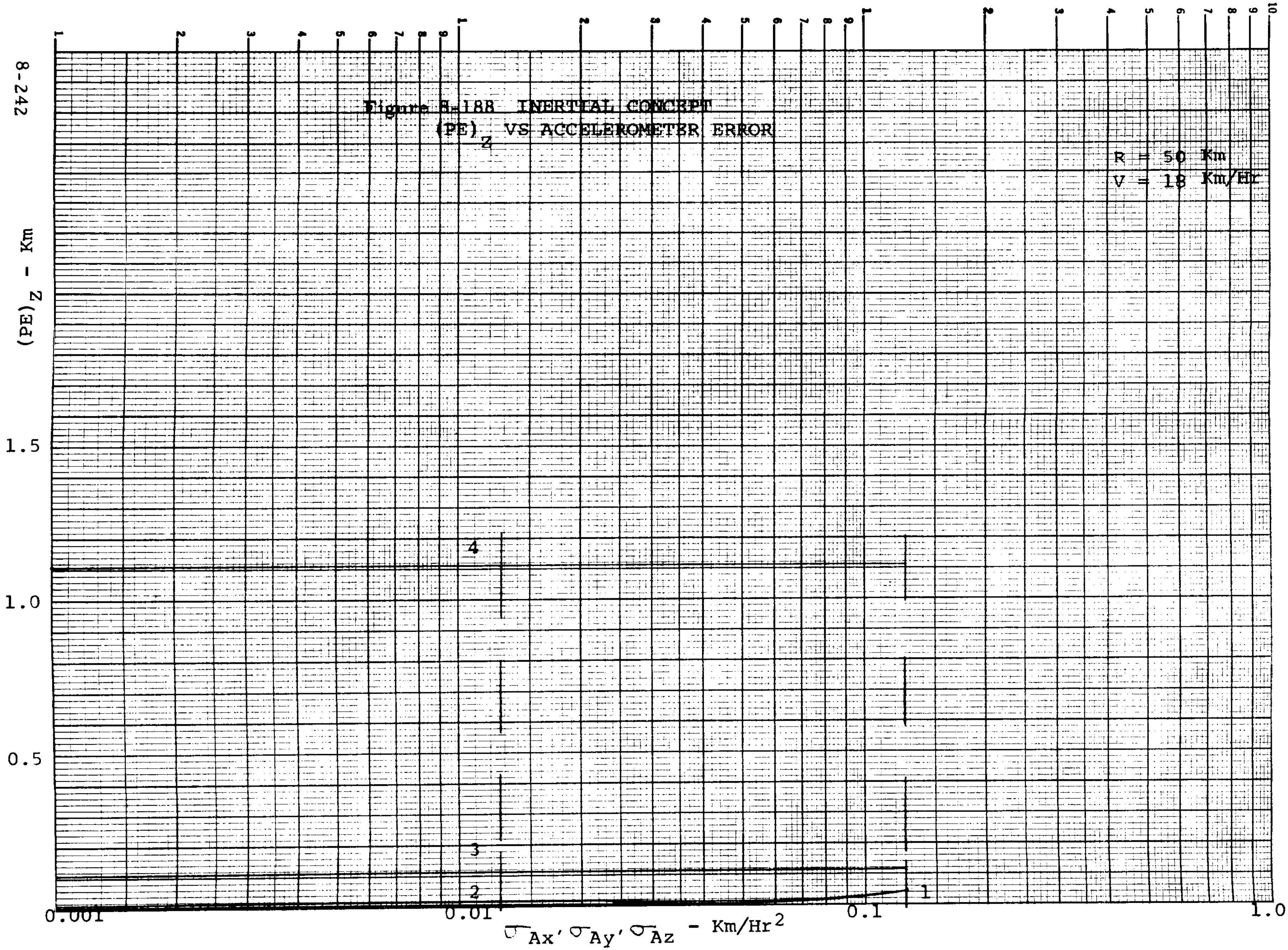

Figure 8-188 INERTIAL CONCEPT
(PE)$_Z$ VS ACCELEROMETER ERROR

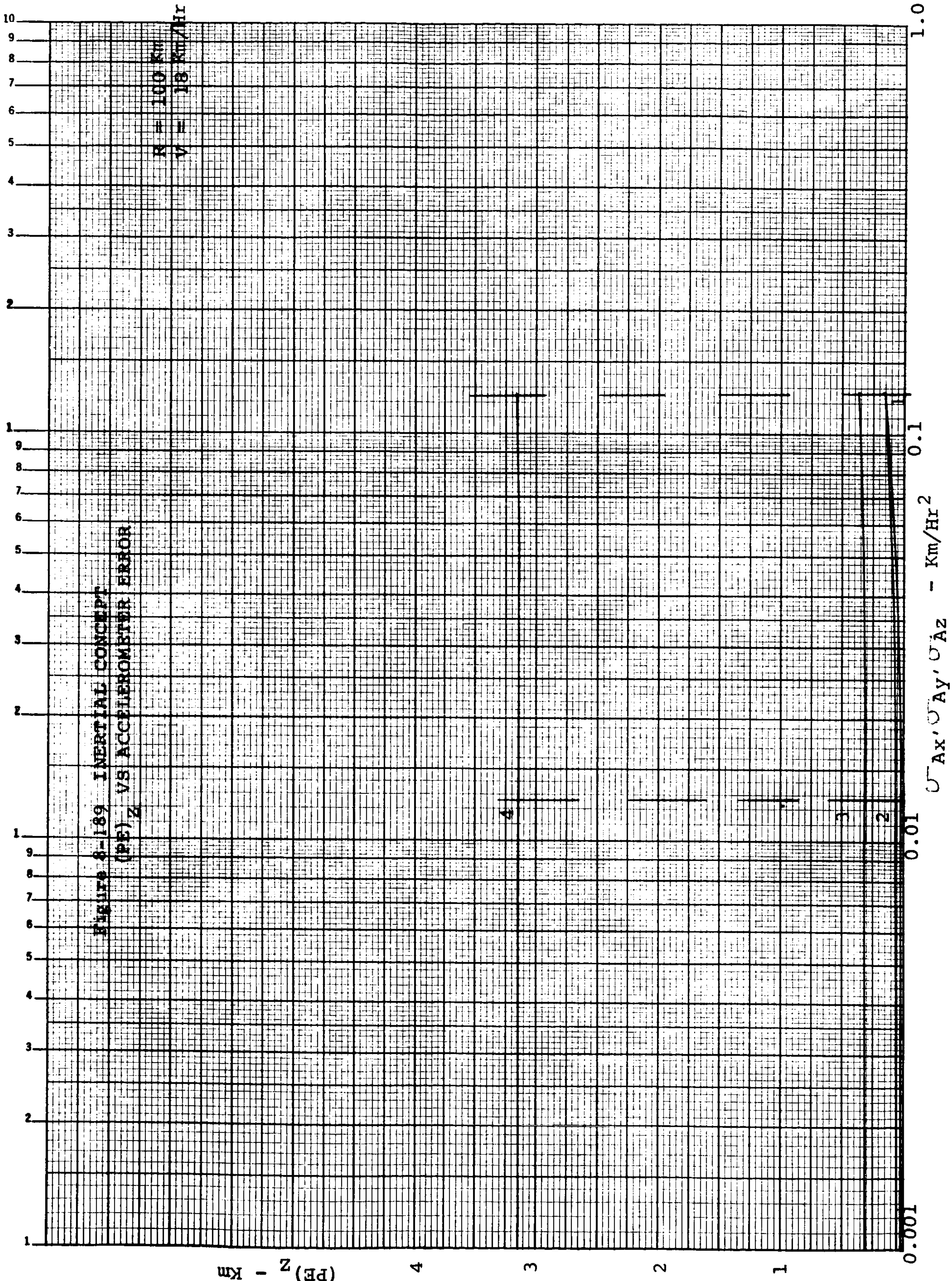

Figure 8-189 INERTIAL CONCEPT $(PE)_Z$ VS ACCELEROMETER ERROR

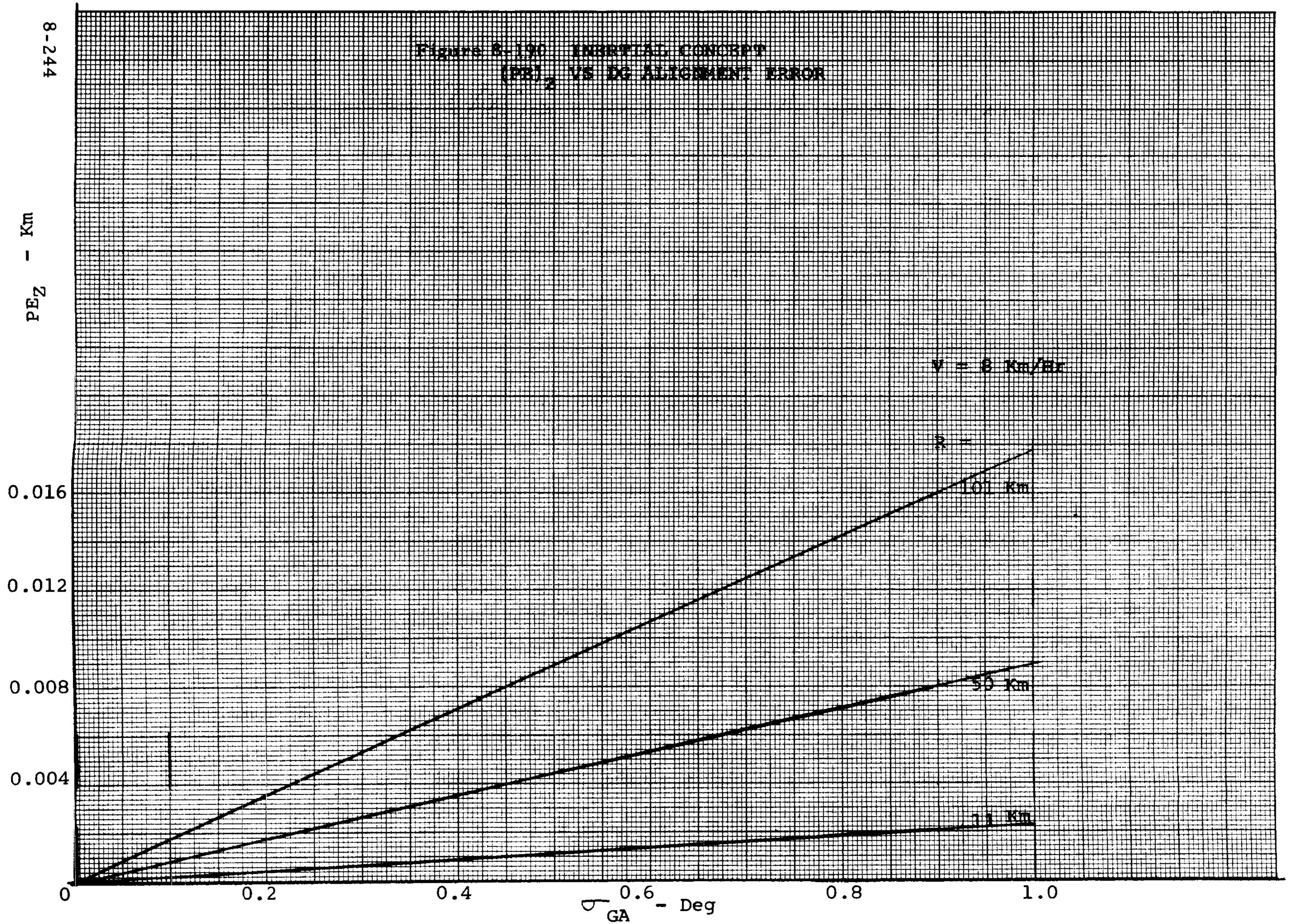

Figure 8-190 INERTIAL CONCEPT
$(PE)_Z$ VS DG ALIGNMENT ERROR

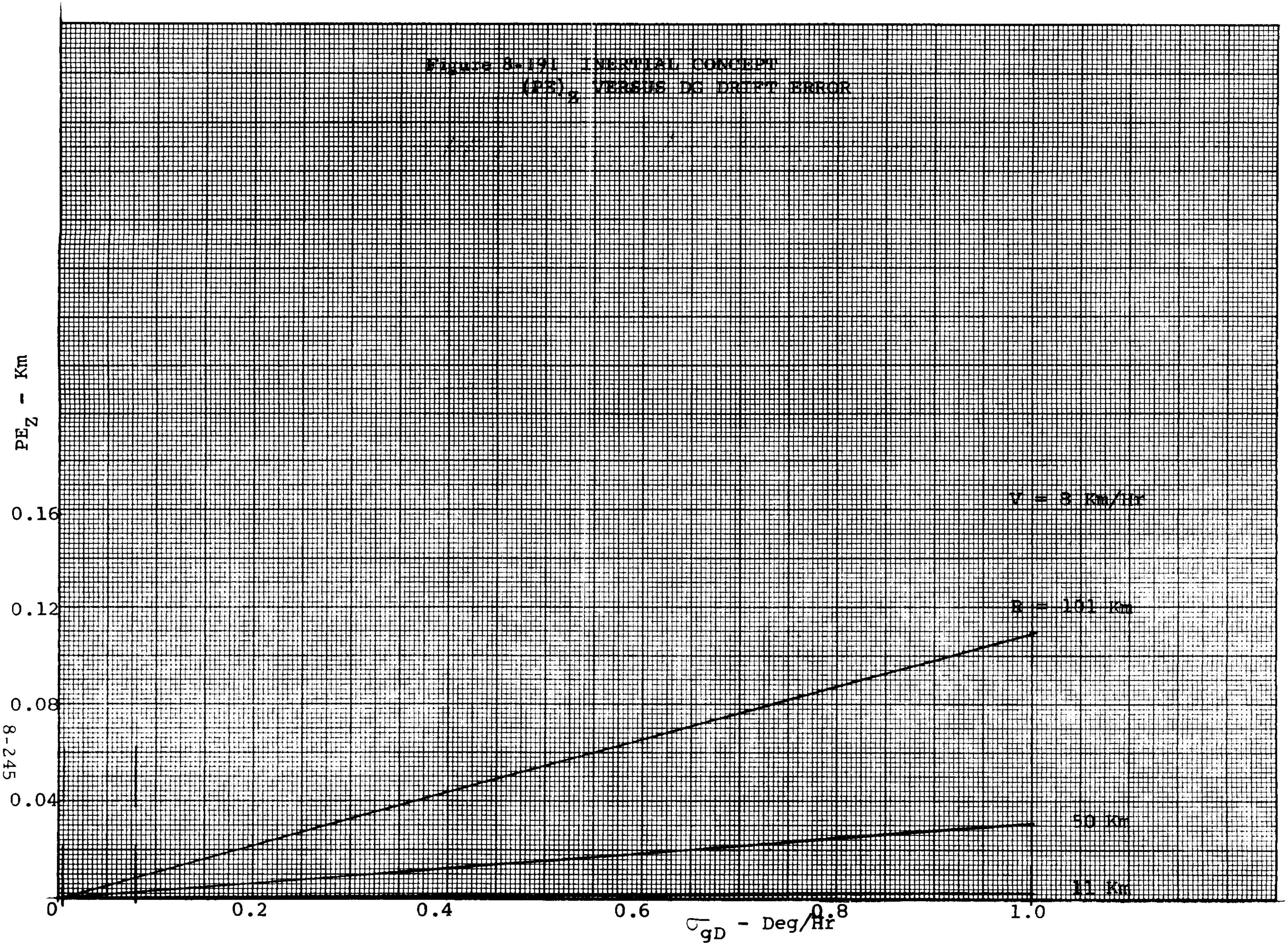

Figure 8-191 INERTIAL CONCEPT
$(PE)_Z$ VERSUS DG DRIFT ERROR

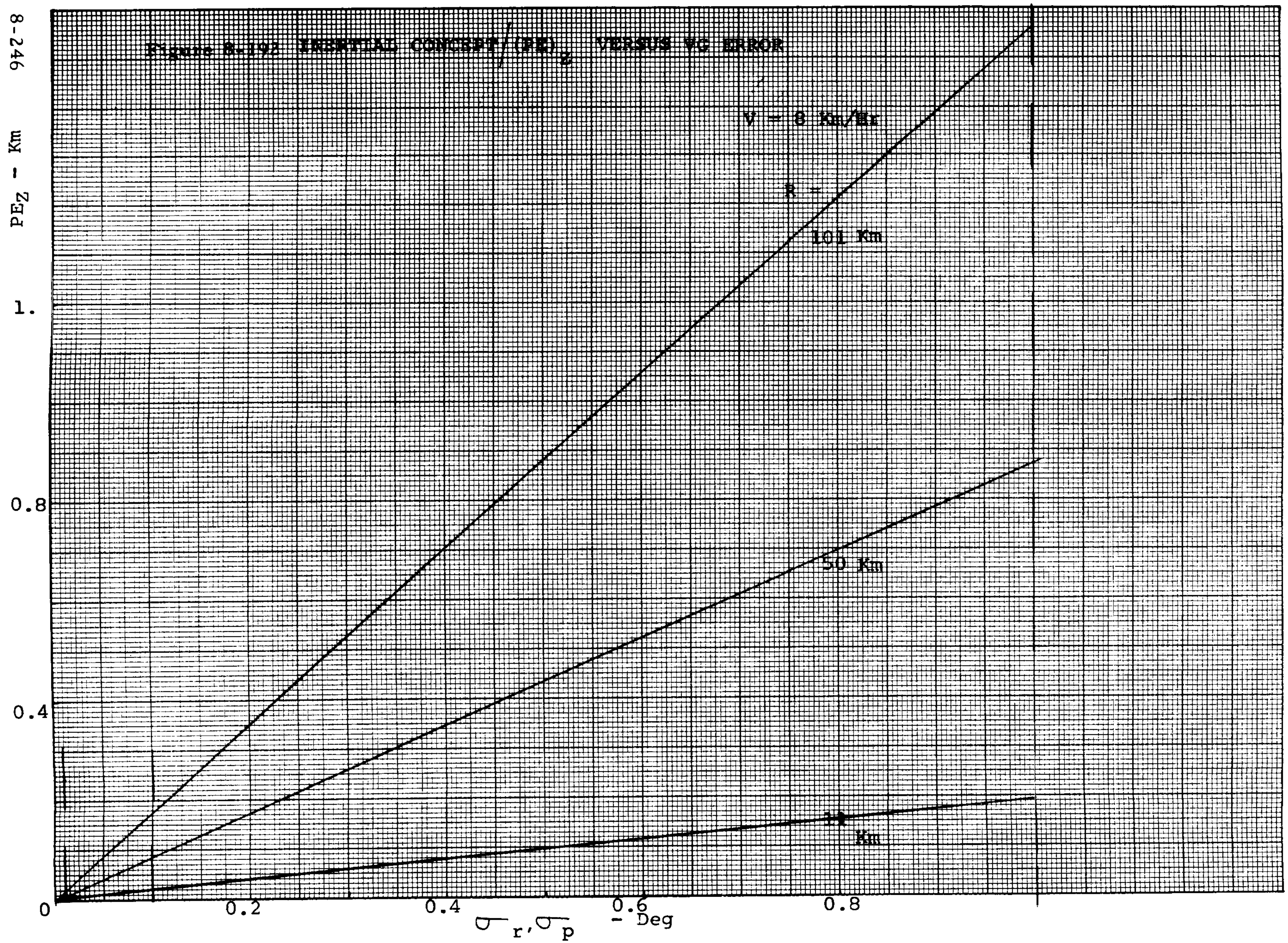

Figure 8-192 INERTIAL CONCEPT/$(PE)_Z$ VERSUS VG ERROR

Figure 8-193 INERTIAL CONCEPT
$(PE)_Z$ VS VERTICAL ERROR

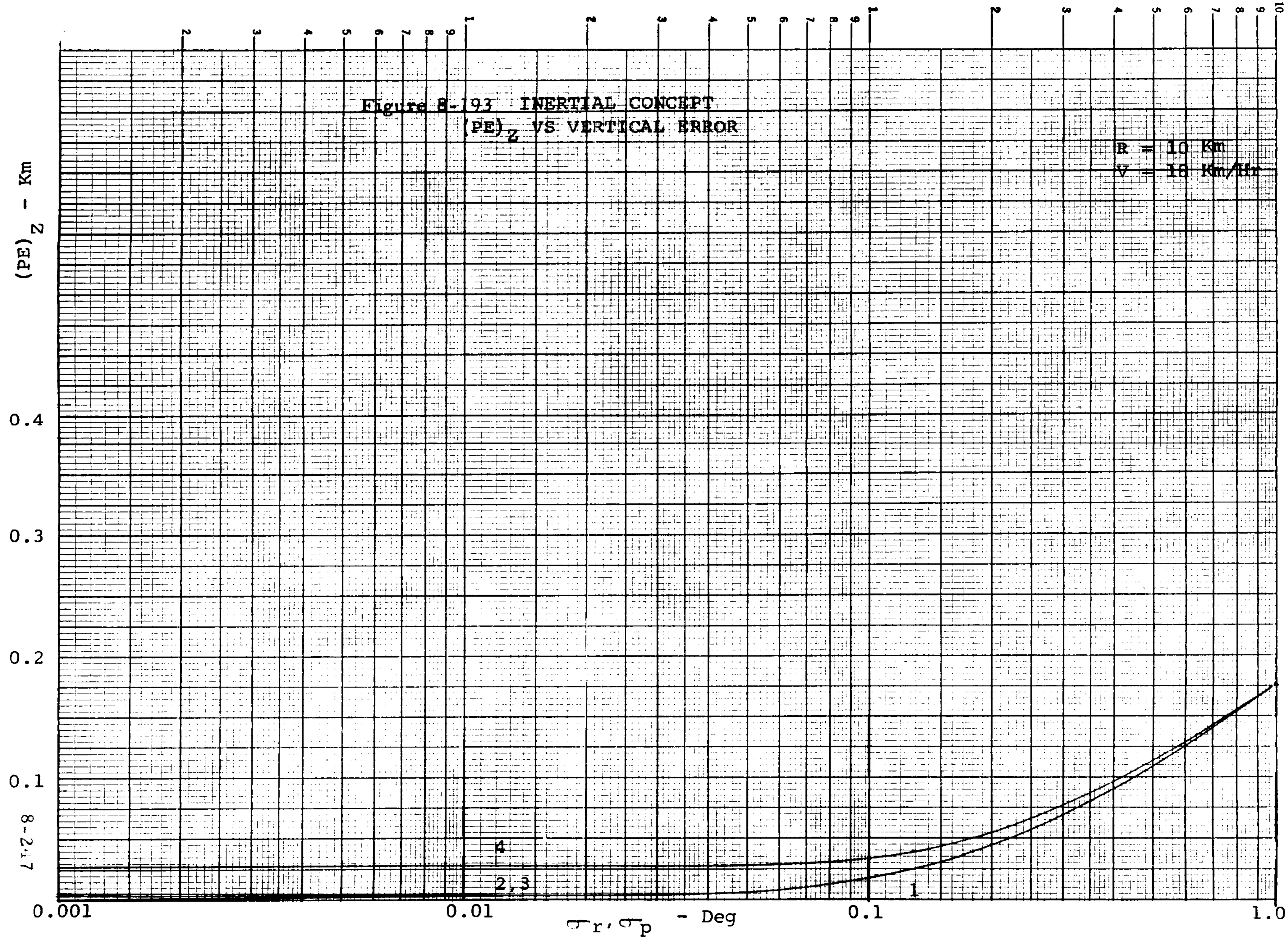

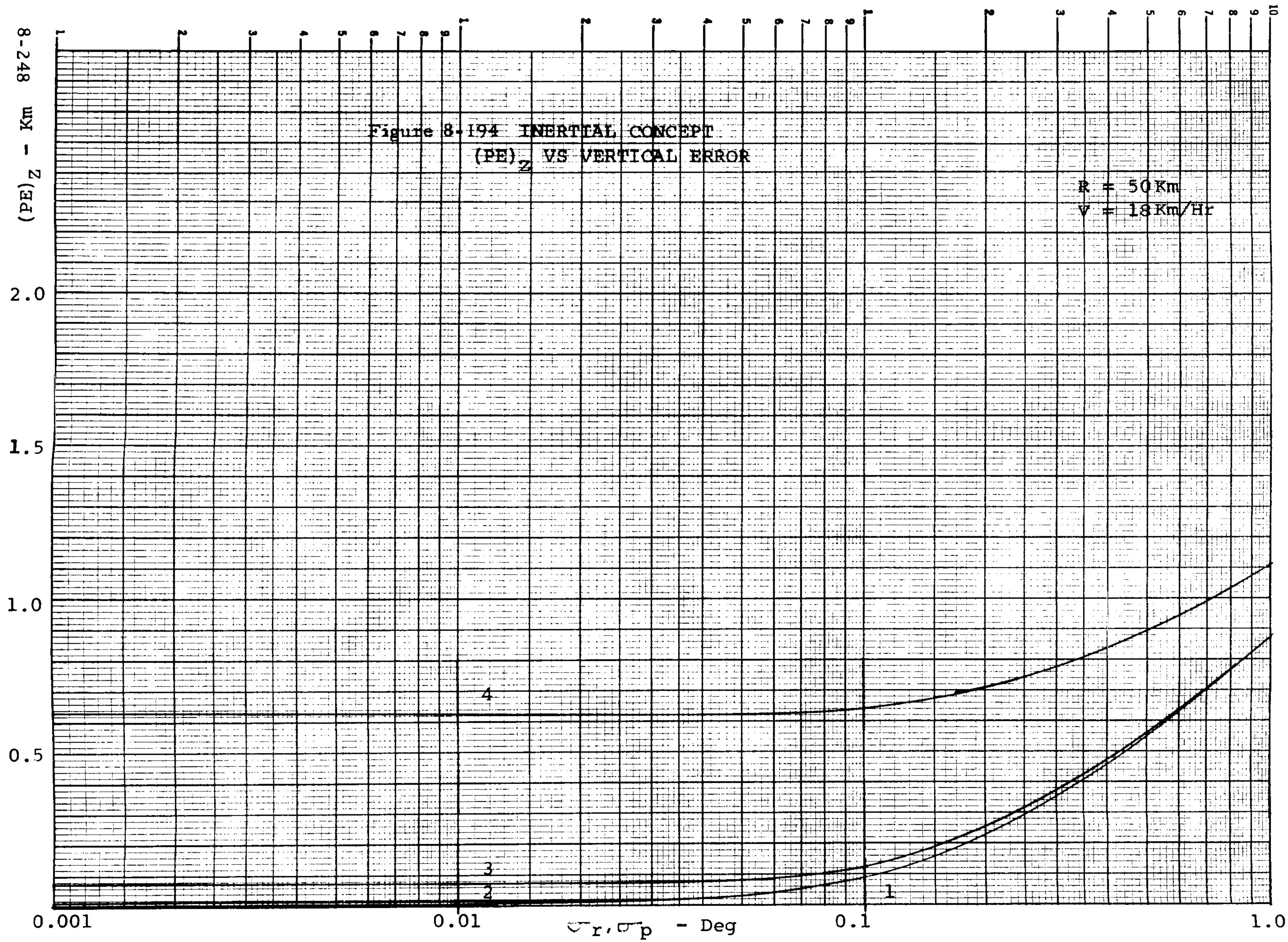

Figure 8-194 INERTIAL CONCEPT
$(PE)_Z$ VS VERTICAL ERROR

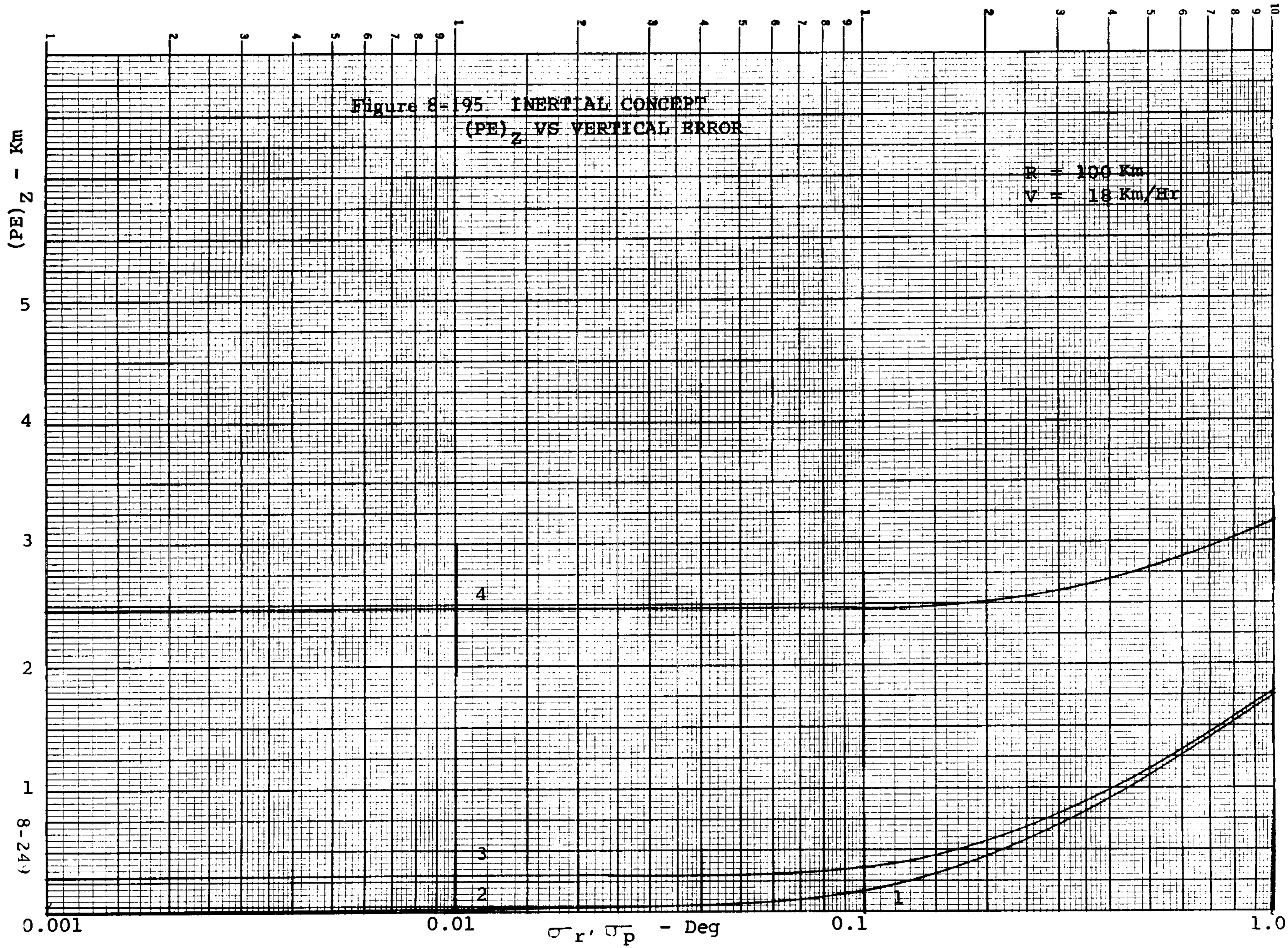

Figure 8-195 INERTIAL CONCEPT
$(PE)_Z$ VS VERTICAL ERROR
R = 100 Km
V = 18 Km/Hr
$(PE)_Z$ - Km
σ_r, σ_p - Deg
0.001
0.01
0.1
1.0
1
2
3
4
5

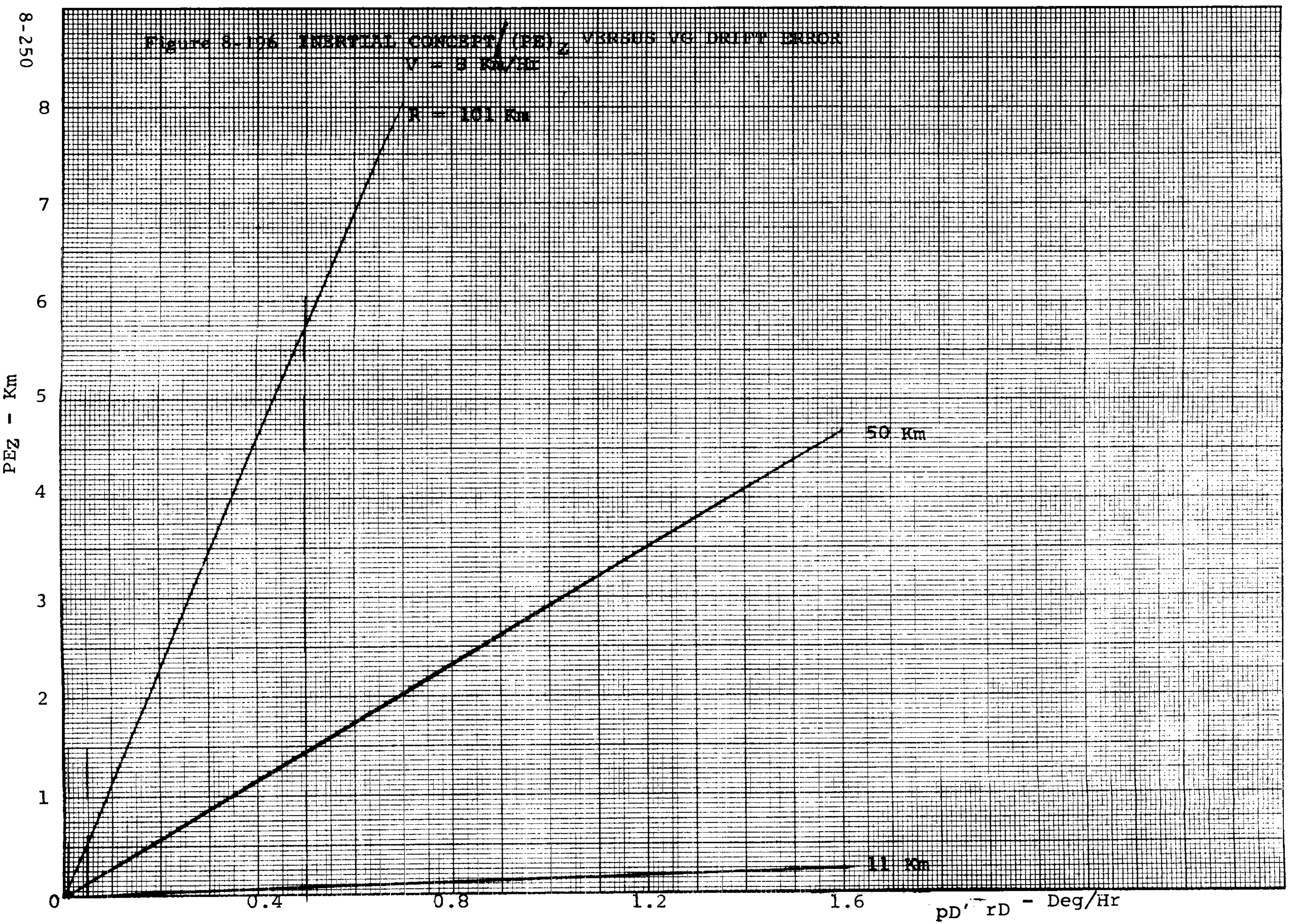

Figure 8-196 INERTIAL CONCEPT (PE)$_Z$ VERSUS VG DRIFT ERROR

Figure 8-197 INERTIAL CONCEPT
$(PE)_Z$ VS VERTICAL GYRO DRIFT ERROR

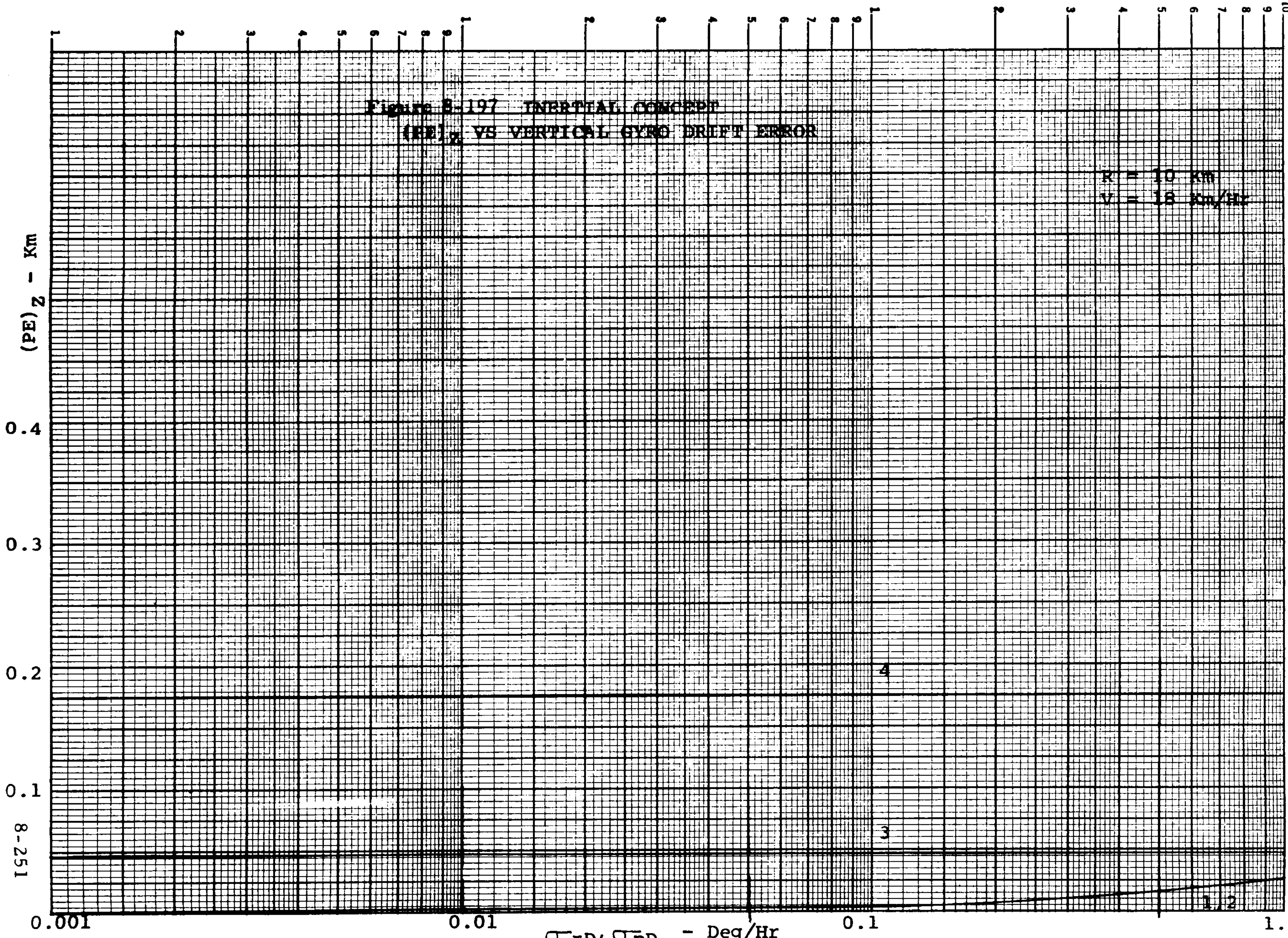

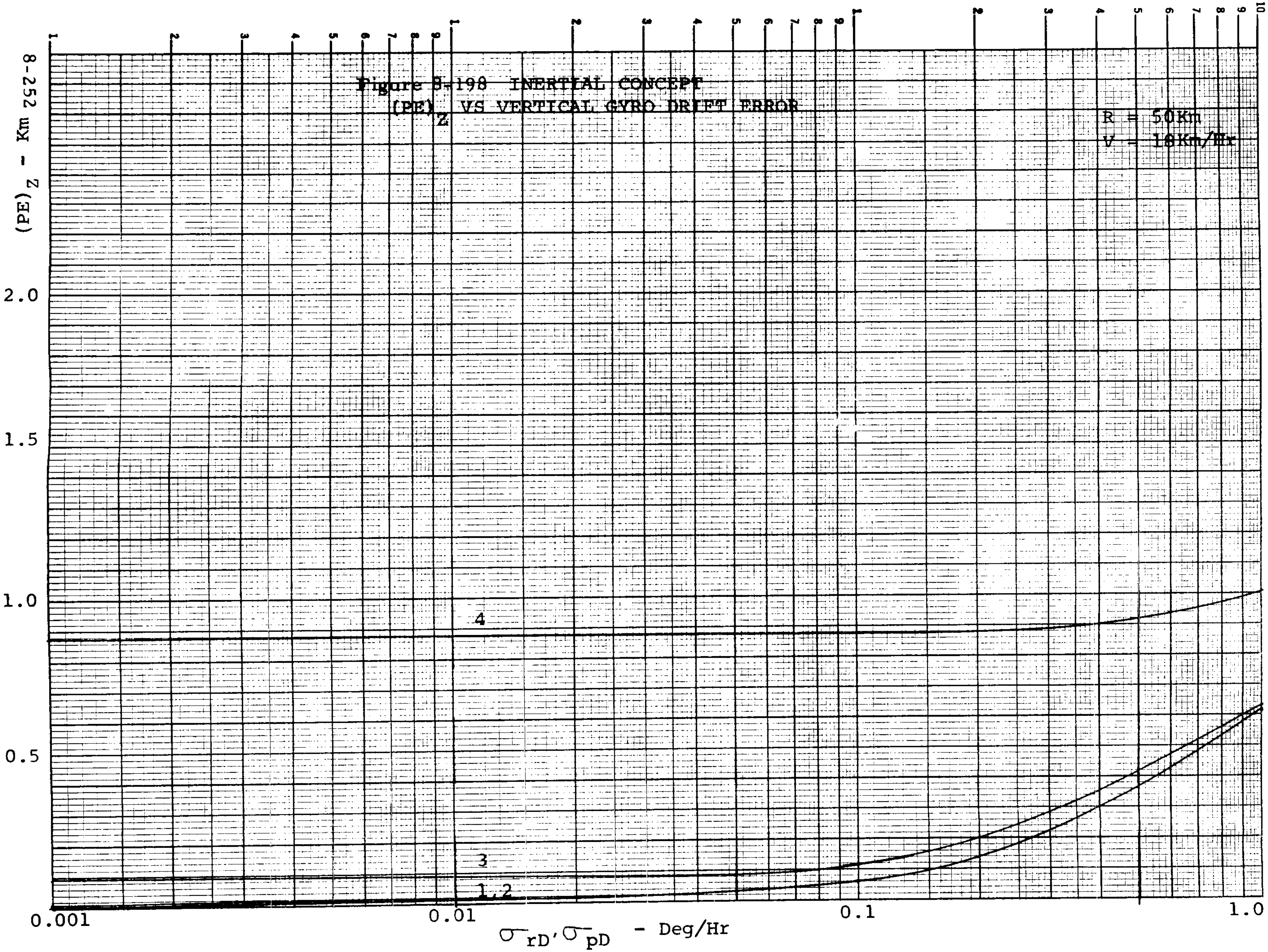

Figure 8-198 INERTIAL CONCEPT
$(PE)_Z$ VS VERTICAL GYRO DRIFT ERROR

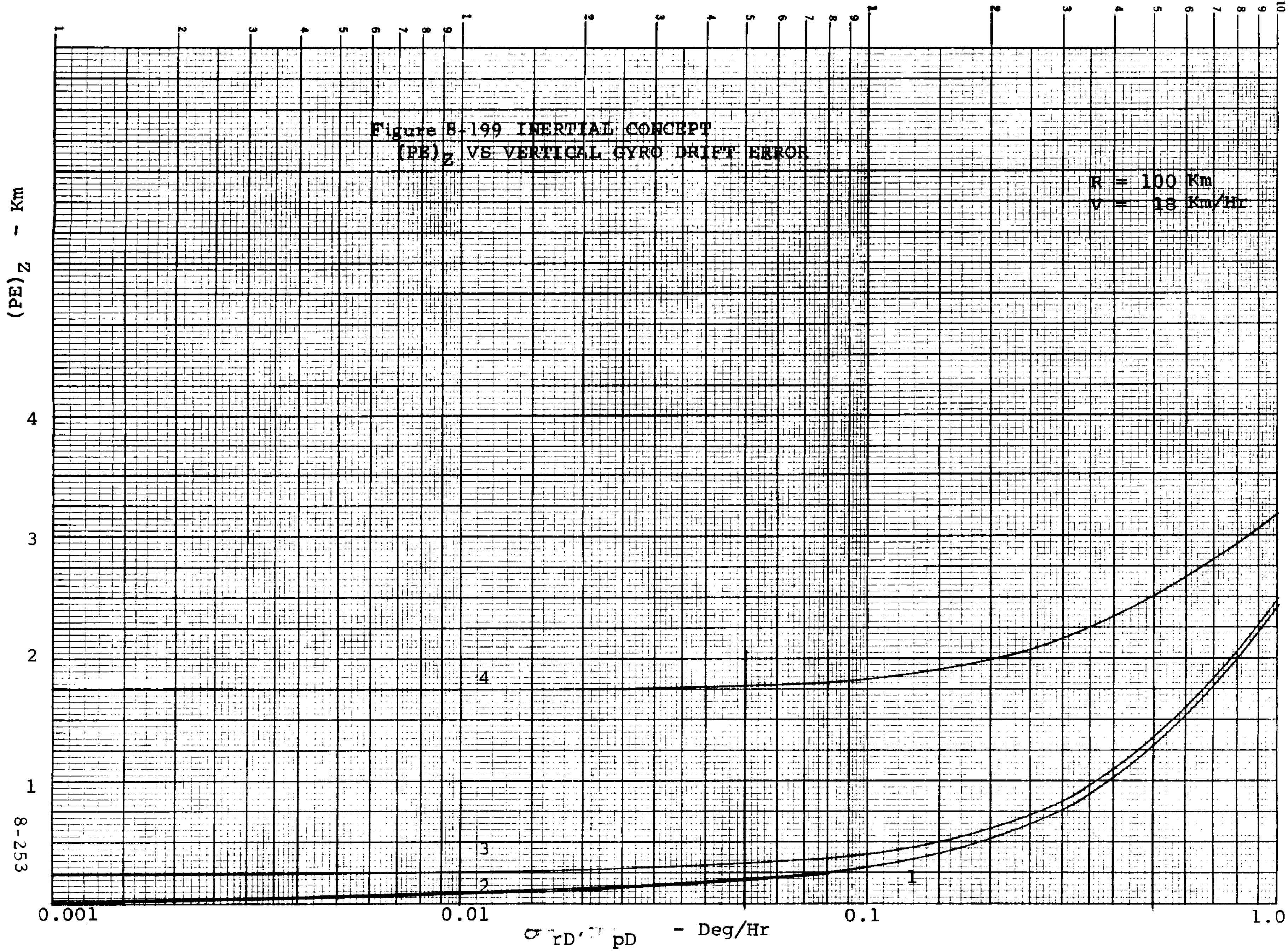

Figure 8-199 INERTIAL CONCEPT
(PE)z VS VERTICAL GYRO DRIFT ERROR

Figure 8-200 INERTIAL CONCEPT
$(PE)_Z$ VERSUS VERTICAL ANOMALIES

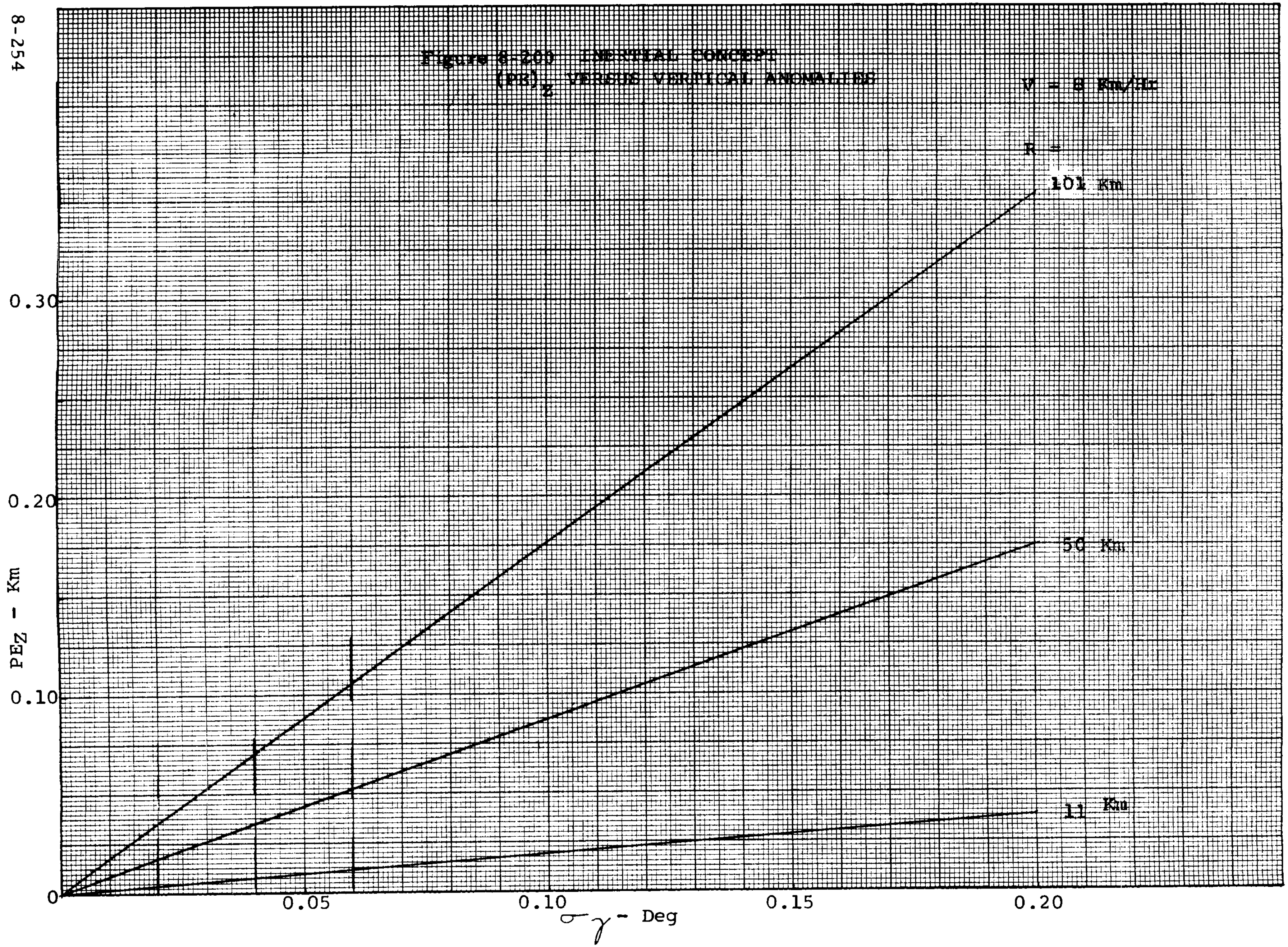

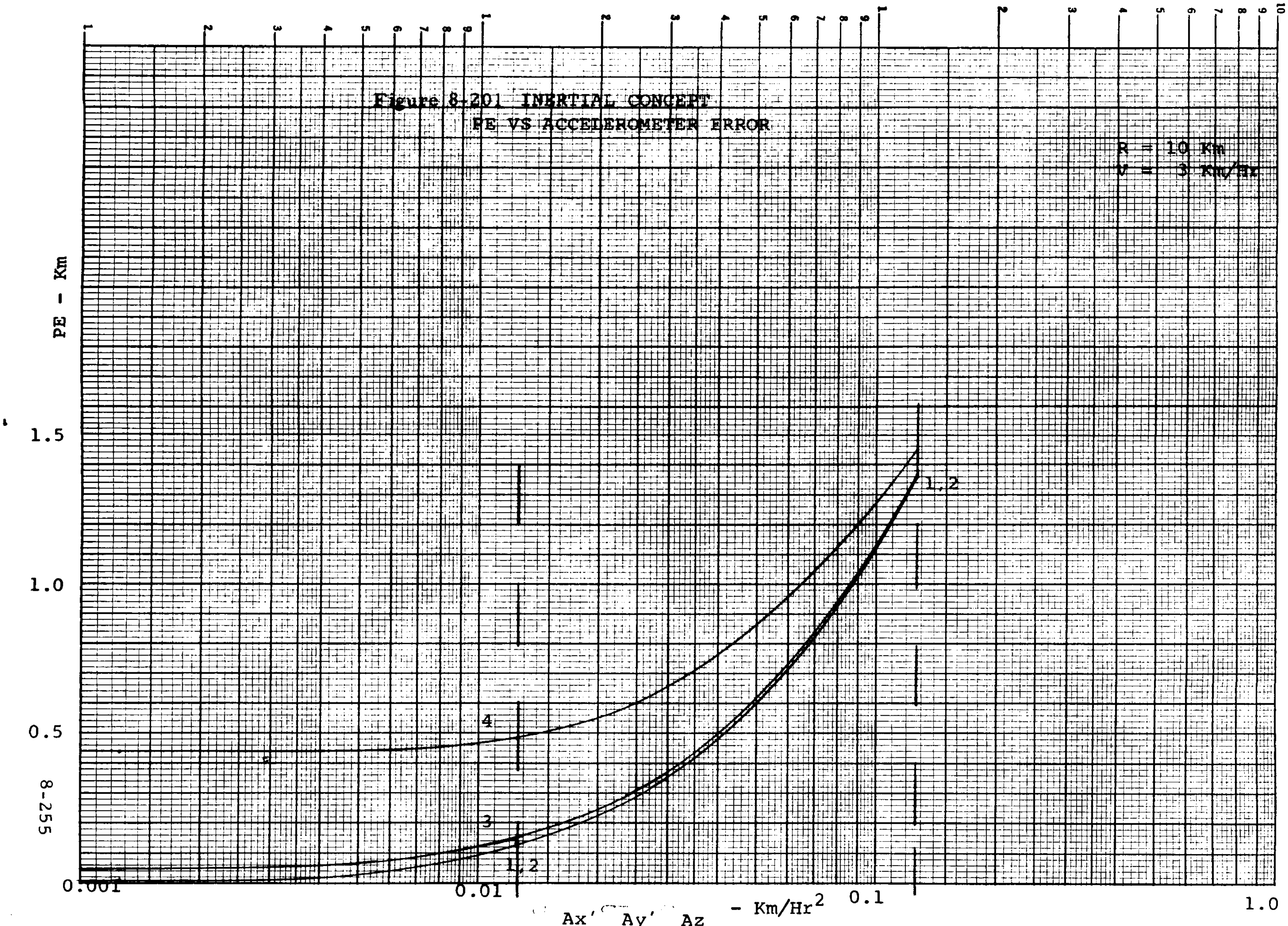
Figure 8-201 INERTIAL CONCEPT
PE VS ACCELEROMETER ERROR
R = 10 Km
V = 3 Km/Hr
PE - Km
1.5
1.0
0.5
4
3
1,2
1,2
0.001
0.01
0.1
1.0
Ax' Ay' Az - Km/Hr2

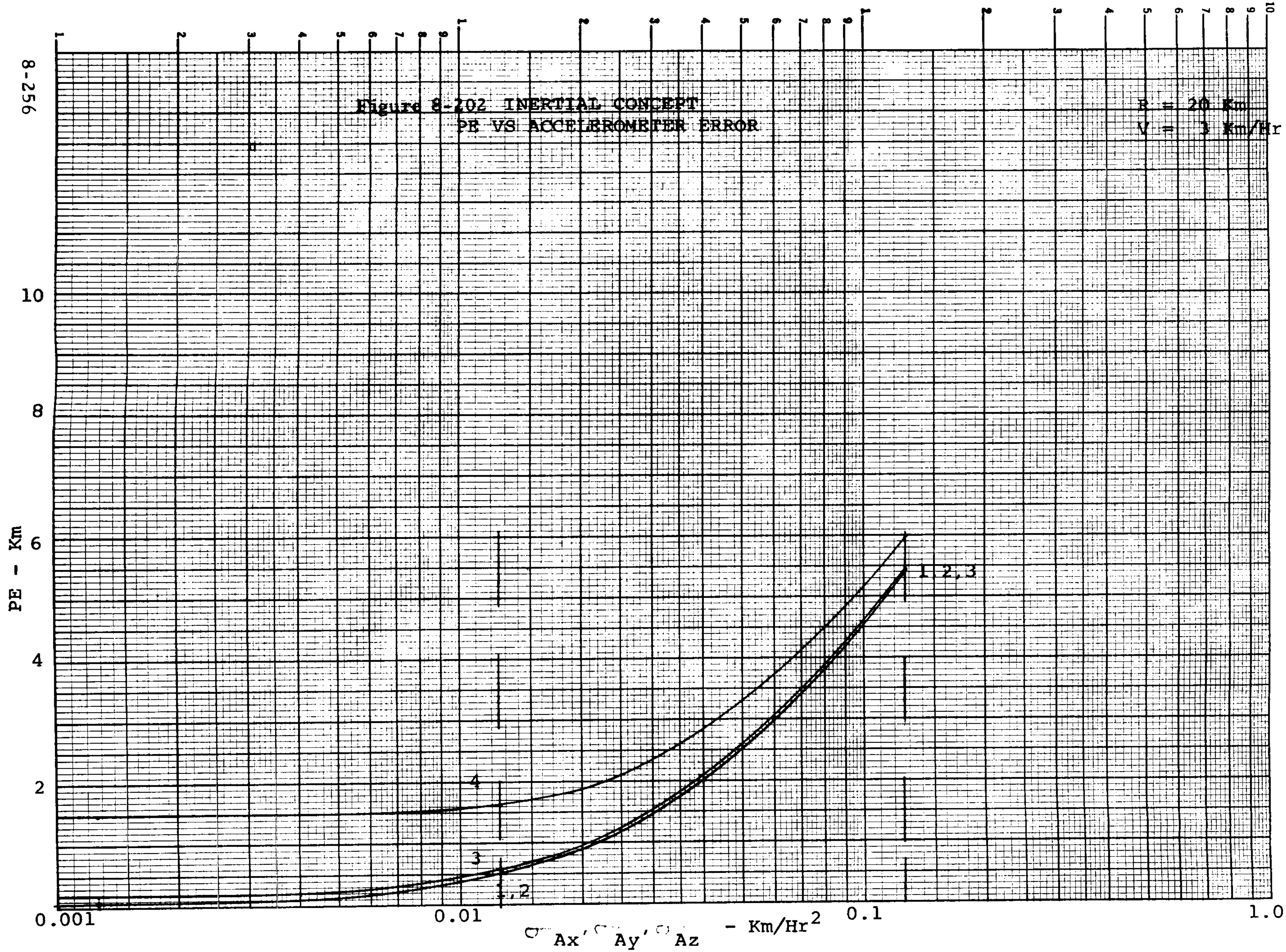

Figure 8-202 INERTIAL CONCEPT PE VS ACCELEROMETER ERROR

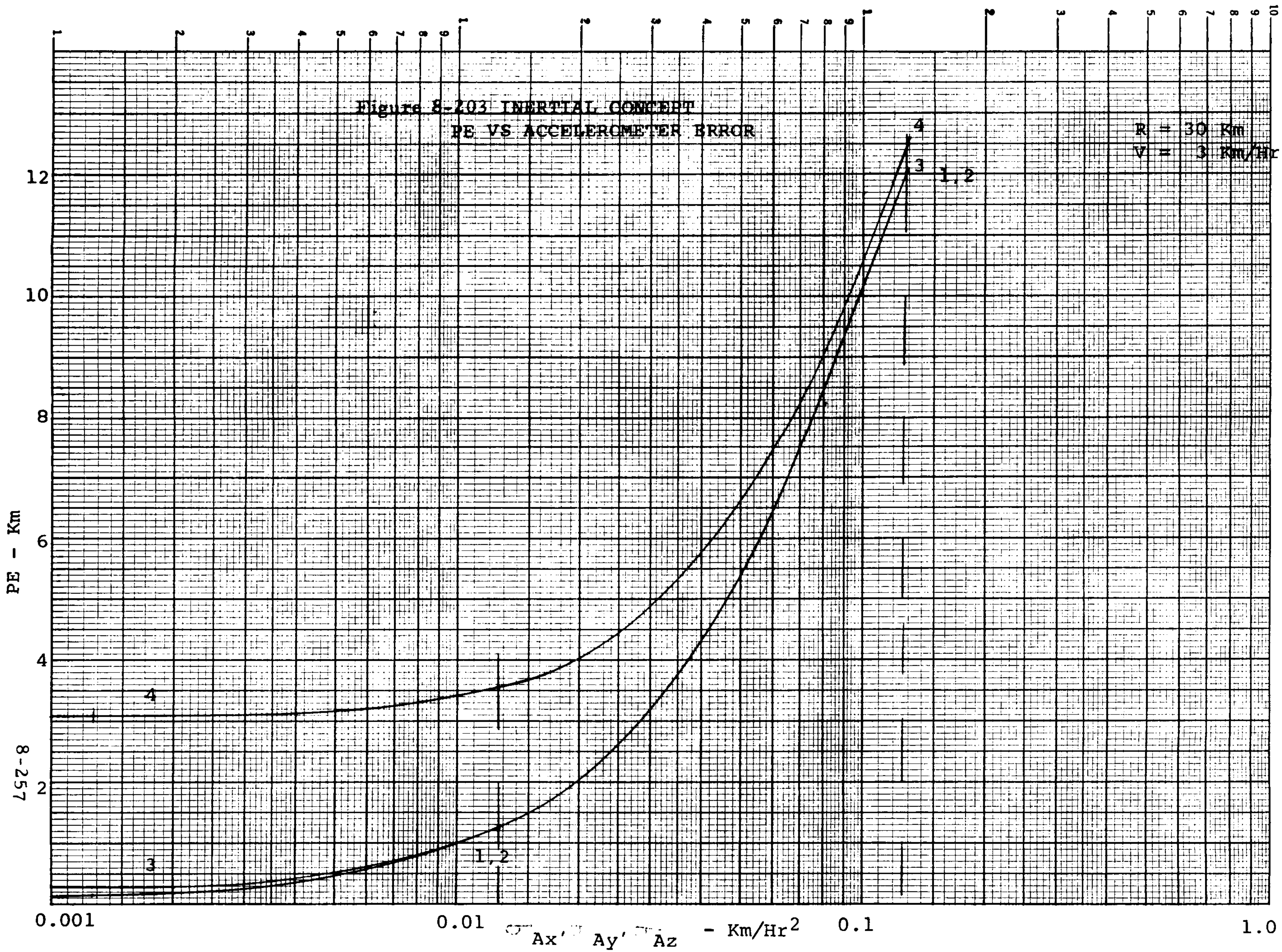

Figure 8-203 INERTIAL CONCEPT
PE VS ACCELEROMETER ERROR

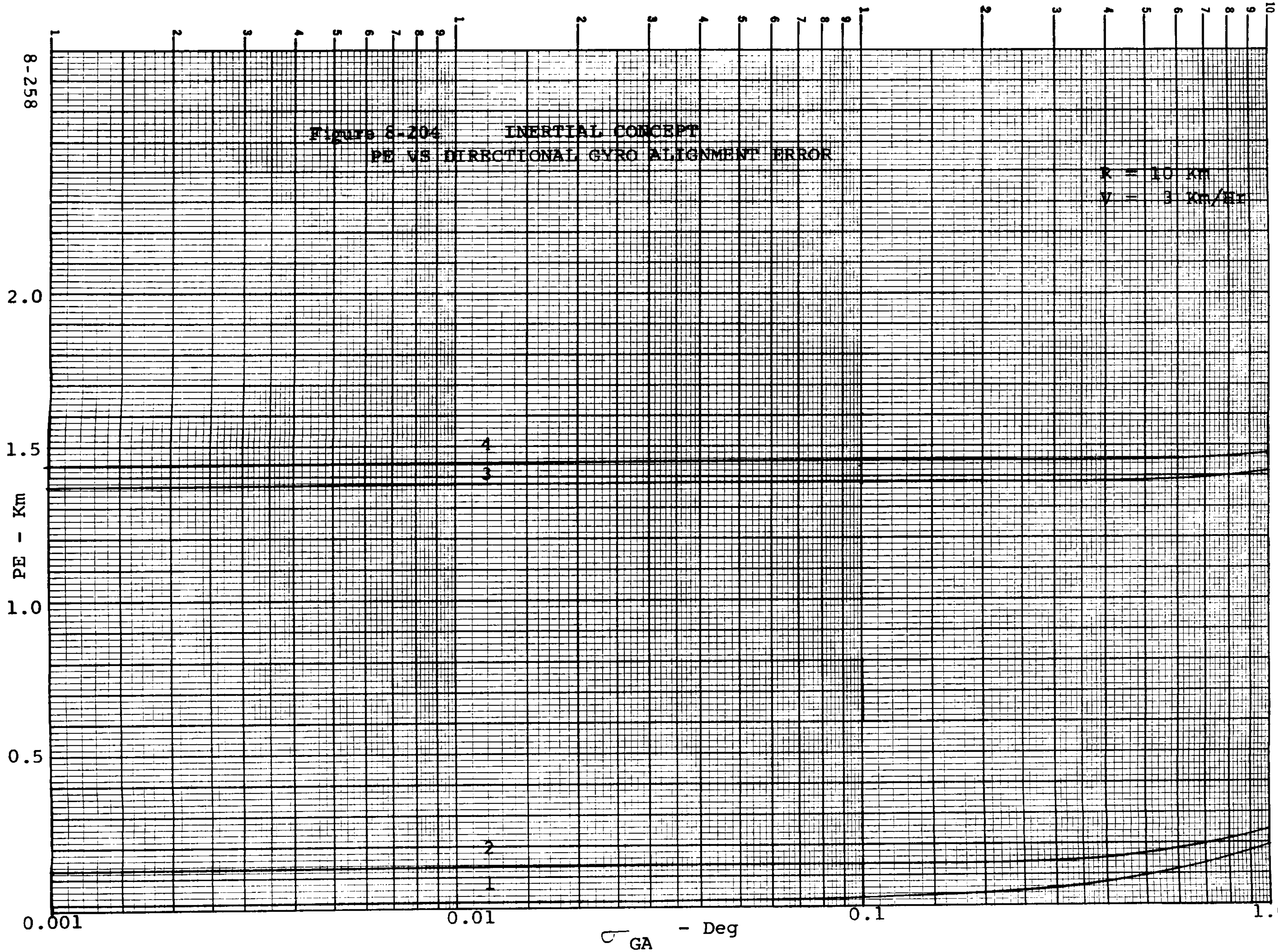

Figure 8-204 INERTIAL CONCEPT
PE VS DIRECTIONAL GYRO ALIGNMENT ERROR

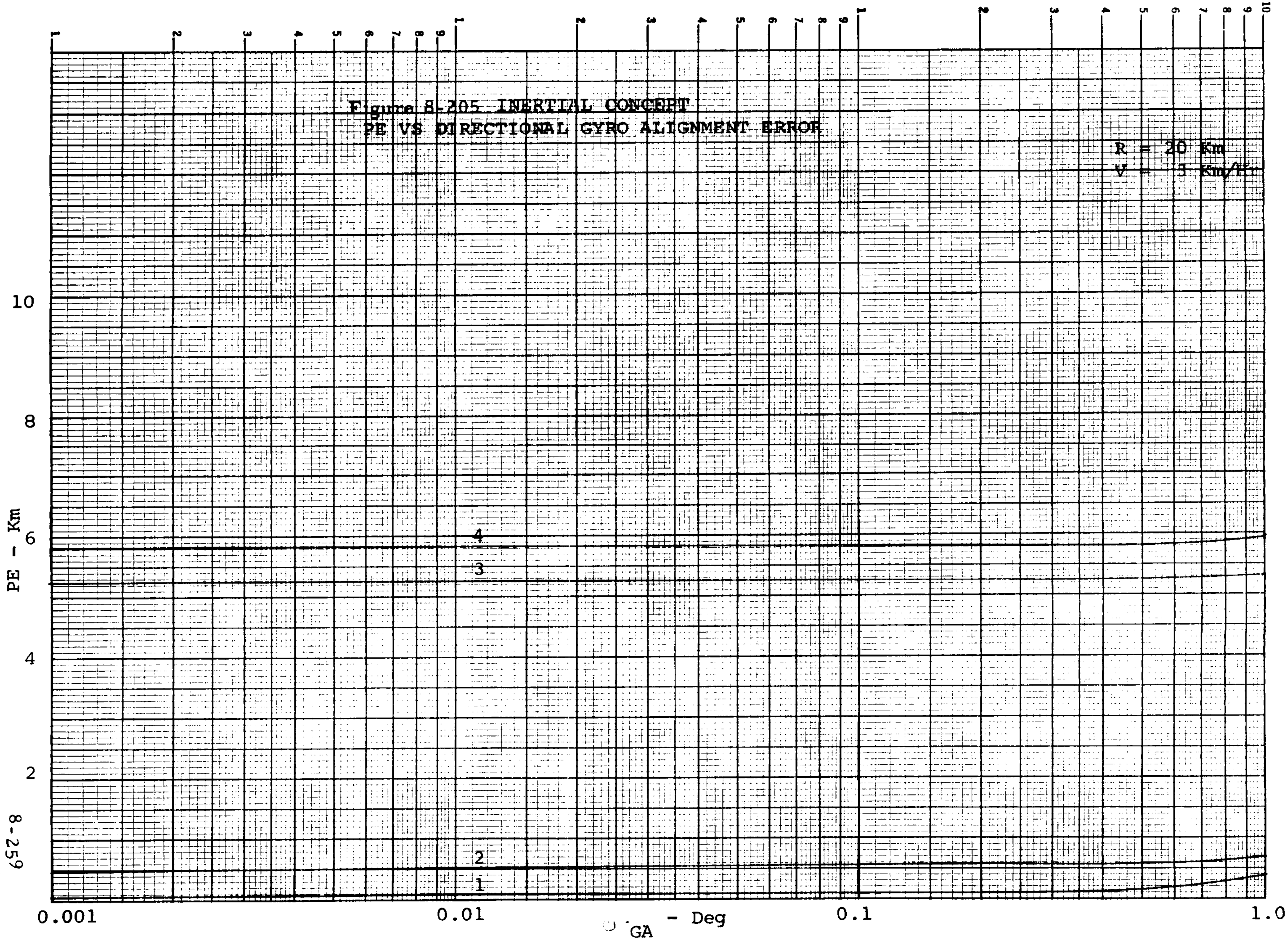

Figure 8-205 INERTIAL CONCEPT
PE VS DIRECTIONAL GYRO ALIGNMENT ERROR
R = 20 Km
V = 5 Km/Hr
PE - Km
10
8
6
4
2
4
3
2
1
0.001
0.01
0.1
1.0
GA - Deg

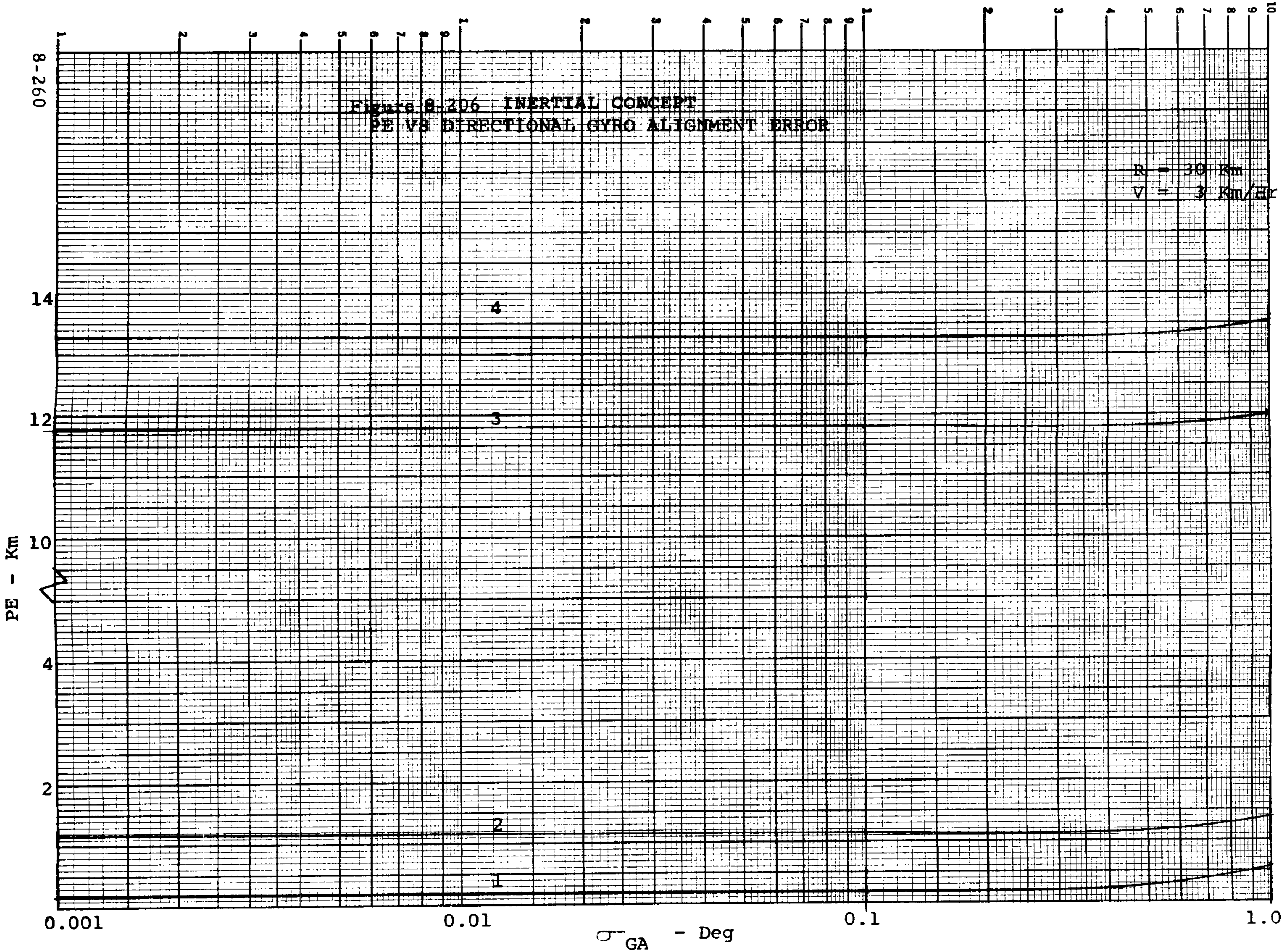
Figure 8-206 INERTIAL CONCEPT
PE VS DIRECTIONAL GYRO ALIGNMENT ERROR
R = 30 Km
V = 3 Km/Hr
4
3
2
1
PE - Km
14
12
10
4
2
0.001
0.01
0.1
1.0
σ_{GA} - Deg

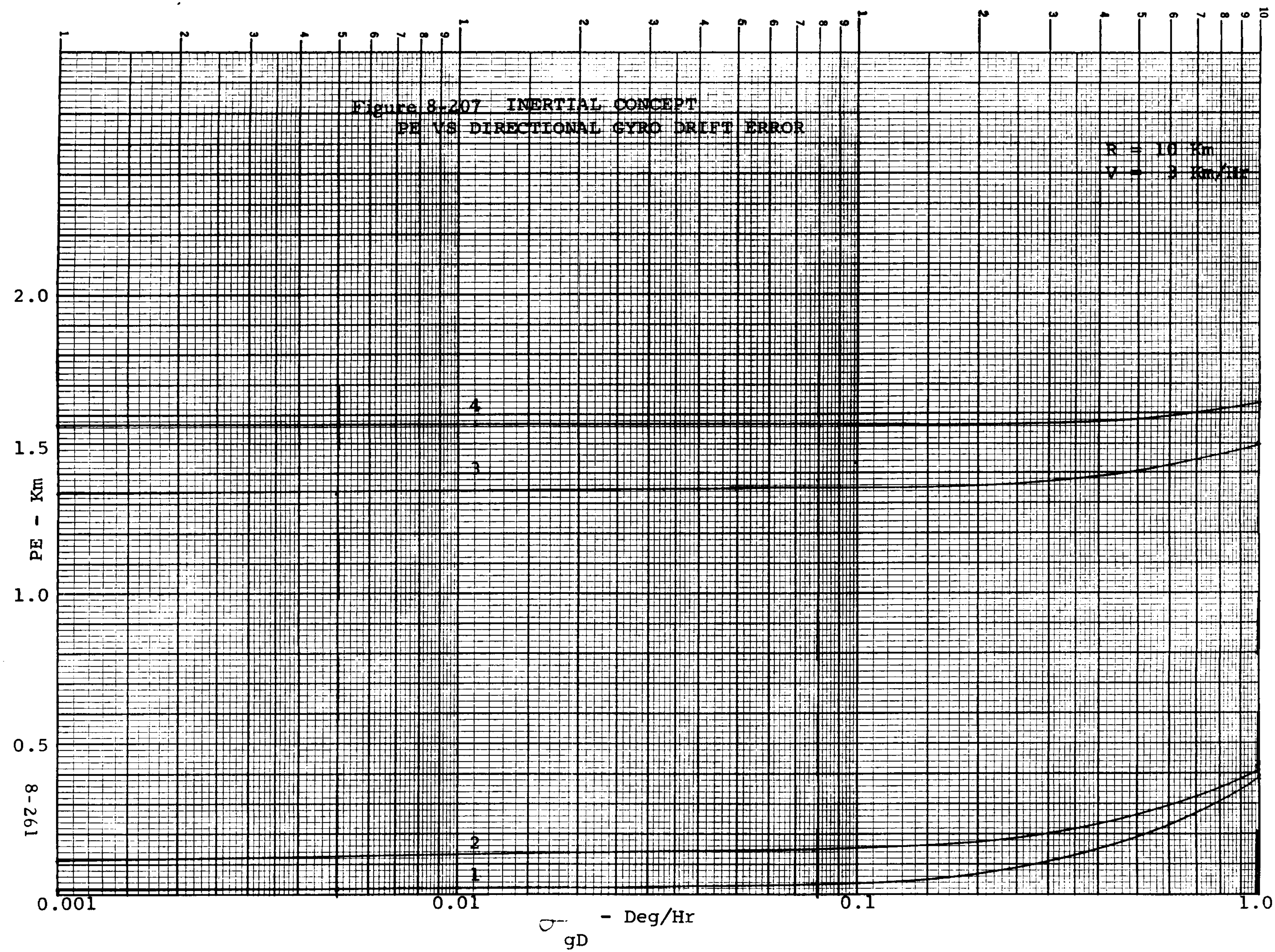

Figure 8-207 INERTIAL CONCEPT
PE VS DIRECTIONAL GYRO DRIFT ERROR

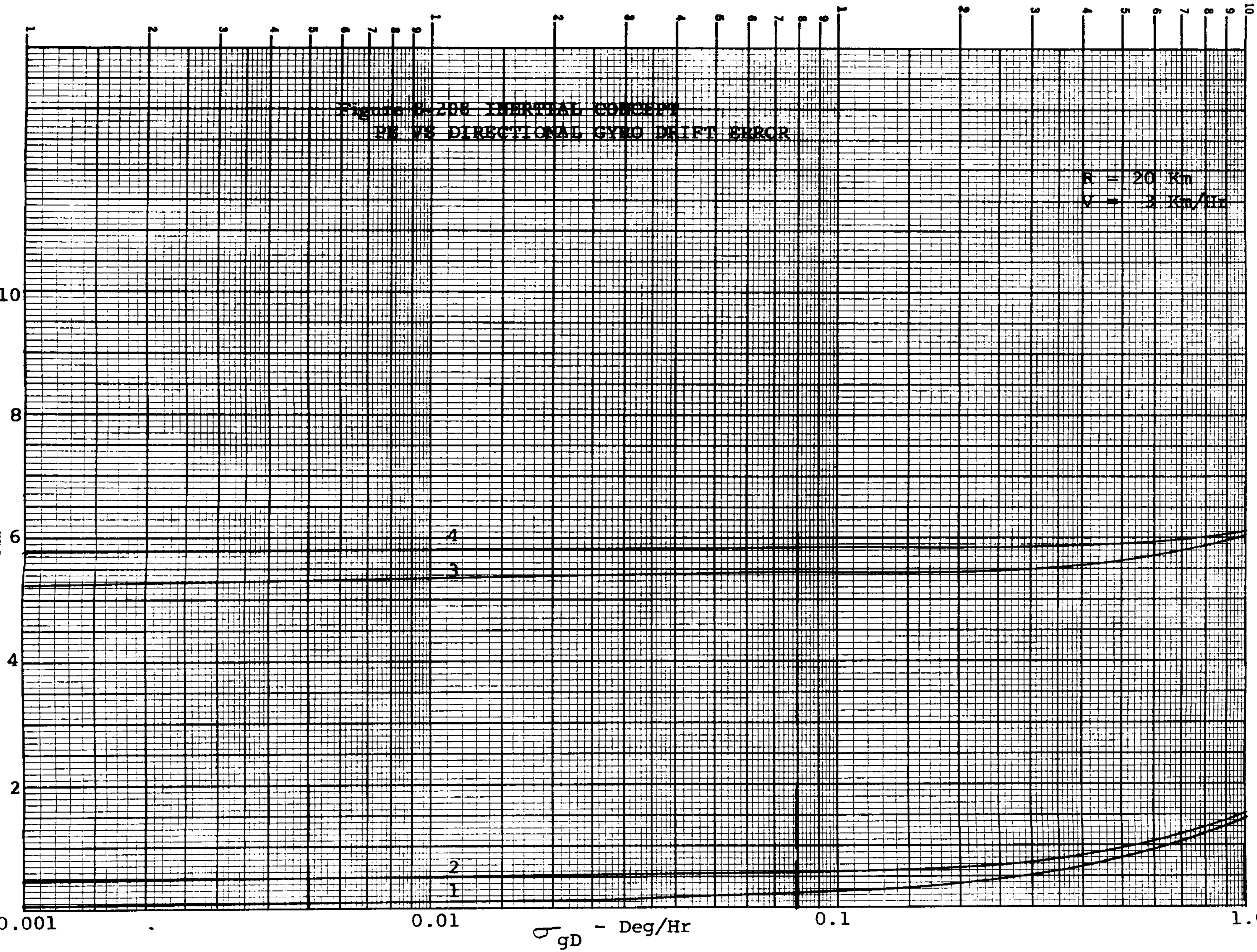

Figure 8-208 INERTIAL CONCEPT
PE VS DIRECTIONAL GYRO DRIFT ERROR

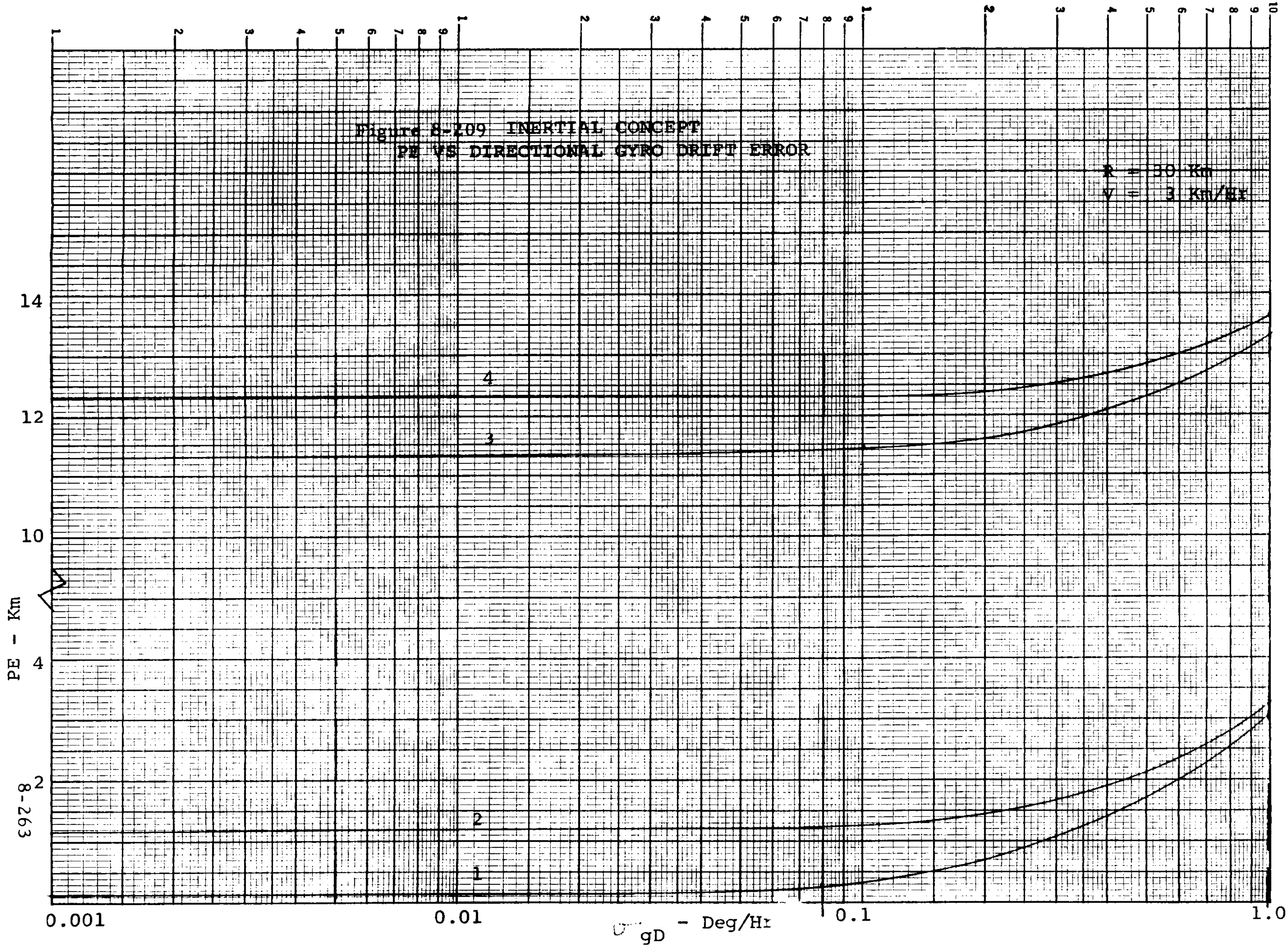

Figure 8-209 INERTIAL CONCEPT
PE VS DIRECTIONAL GYRO DRIFT ERROR

Figure 8-200 INERTIAL CONCEPT
PE VS VERTICAL ERROR

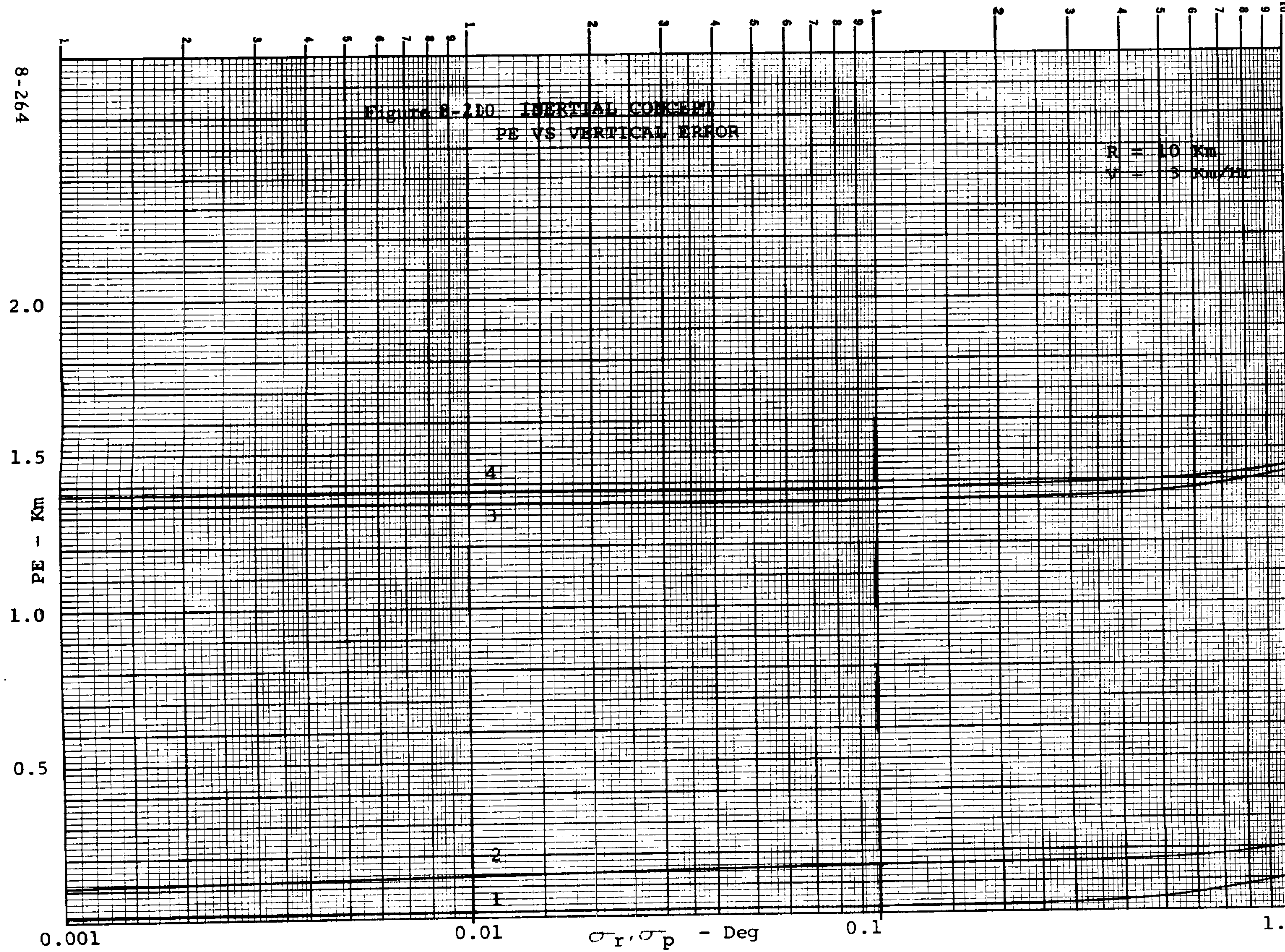

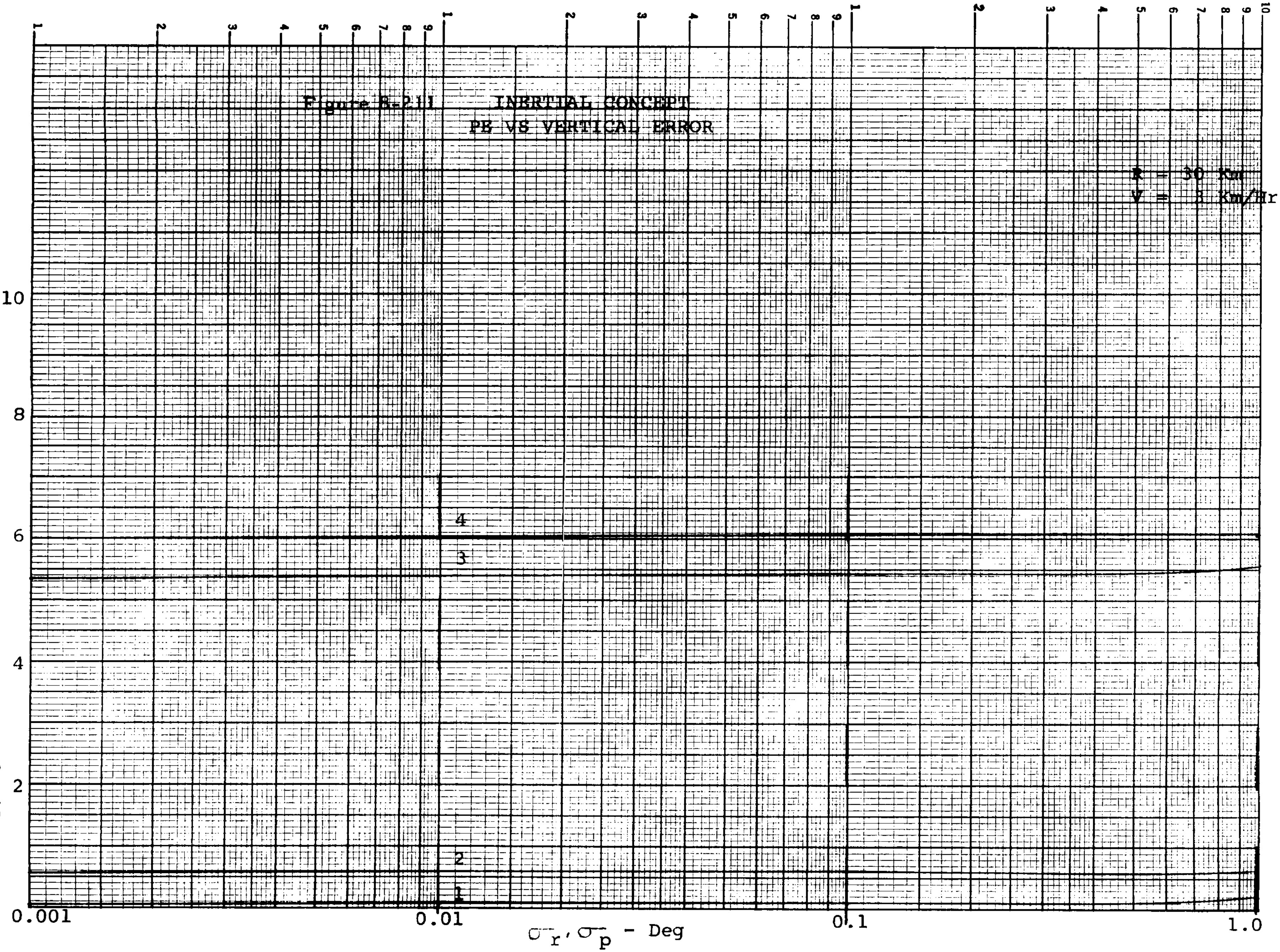
Figure 8-211 INERTIAL CONCEPT
PE VS VERTICAL ERROR
R = 30 Km
V = 1 Km/Hr
PE - Km
σ_r, σ_p - Deg
0.001
0.01
0.1
1.0
10
8
6
4
2
4
3
2
1

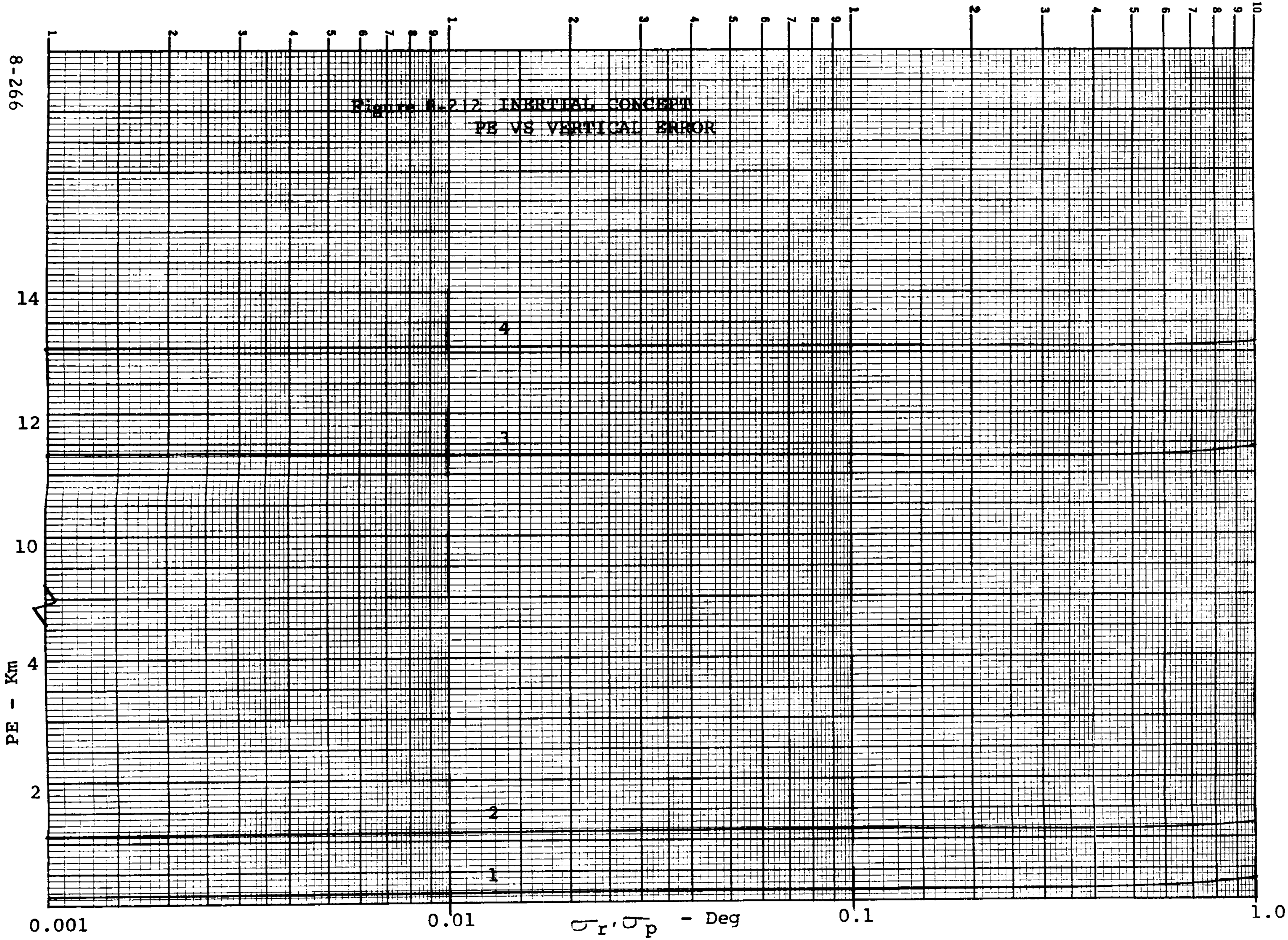

Figure 8.212 INERTIAL CONCEPT
PE VS VERTICAL ERROR

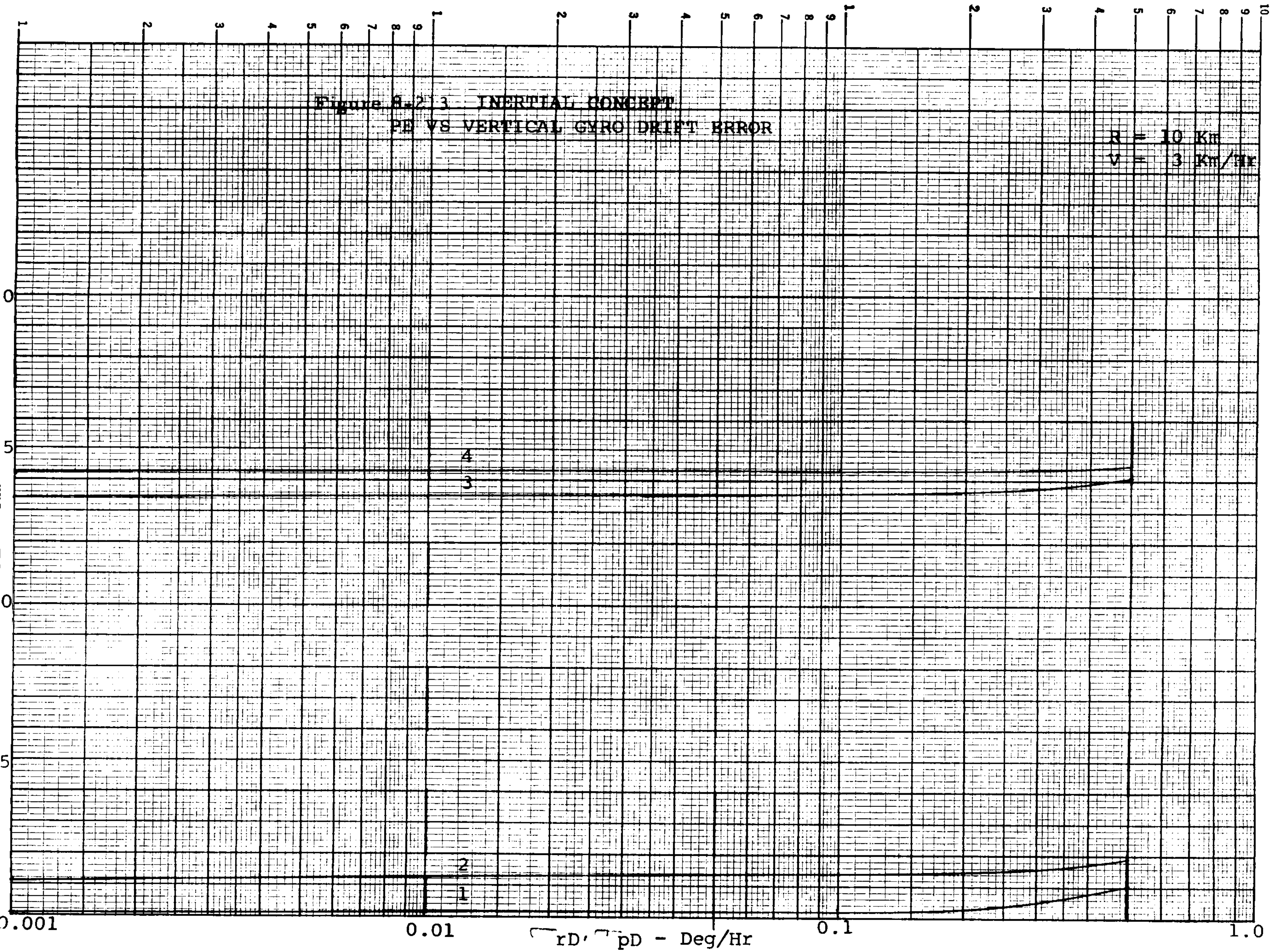

Figure 8.213 INERTIAL CONCEPT
PE VS VERTICAL GYRO DRIFT ERROR

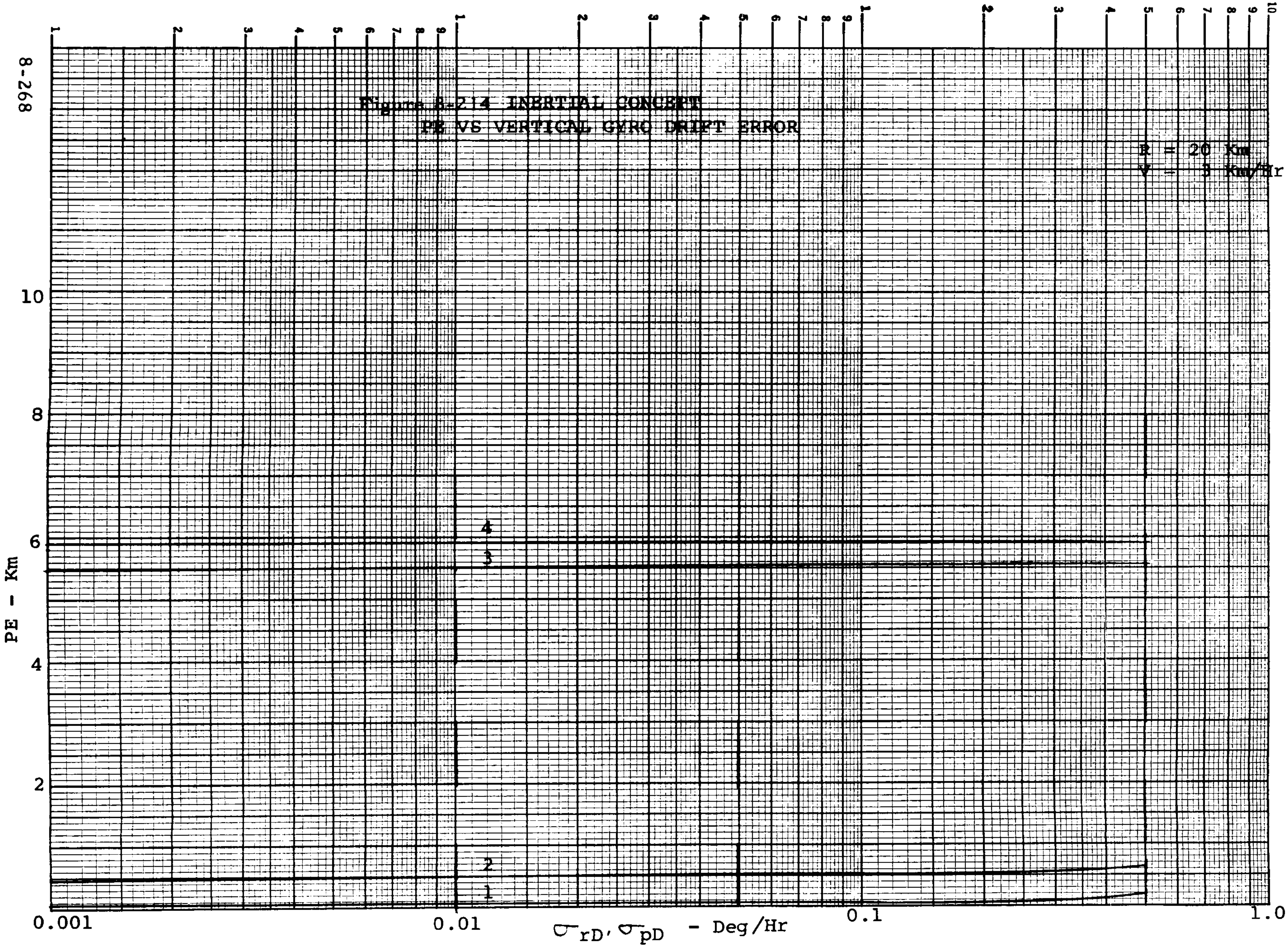

Figure 8-214 INERTIAL CONCEPT
PE VS VERTICAL GYRO DRIFT ERROR

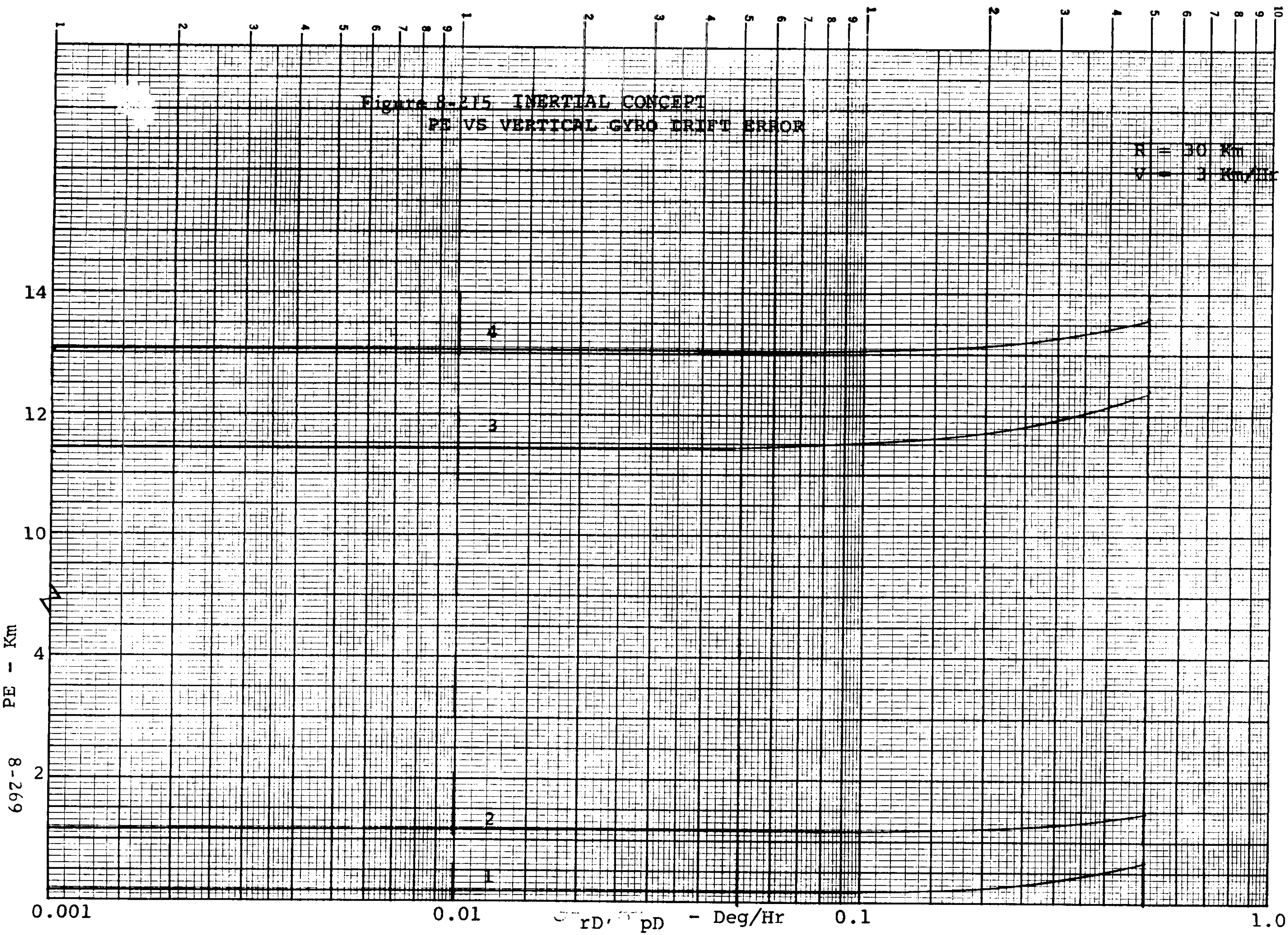

Figure 8-215 INERTIAL CONCEPT
PE VS VERTICAL GYRO DRIFT ERROR

Figure 8-216 PLOT 13 MISSION I 1972 LEG C

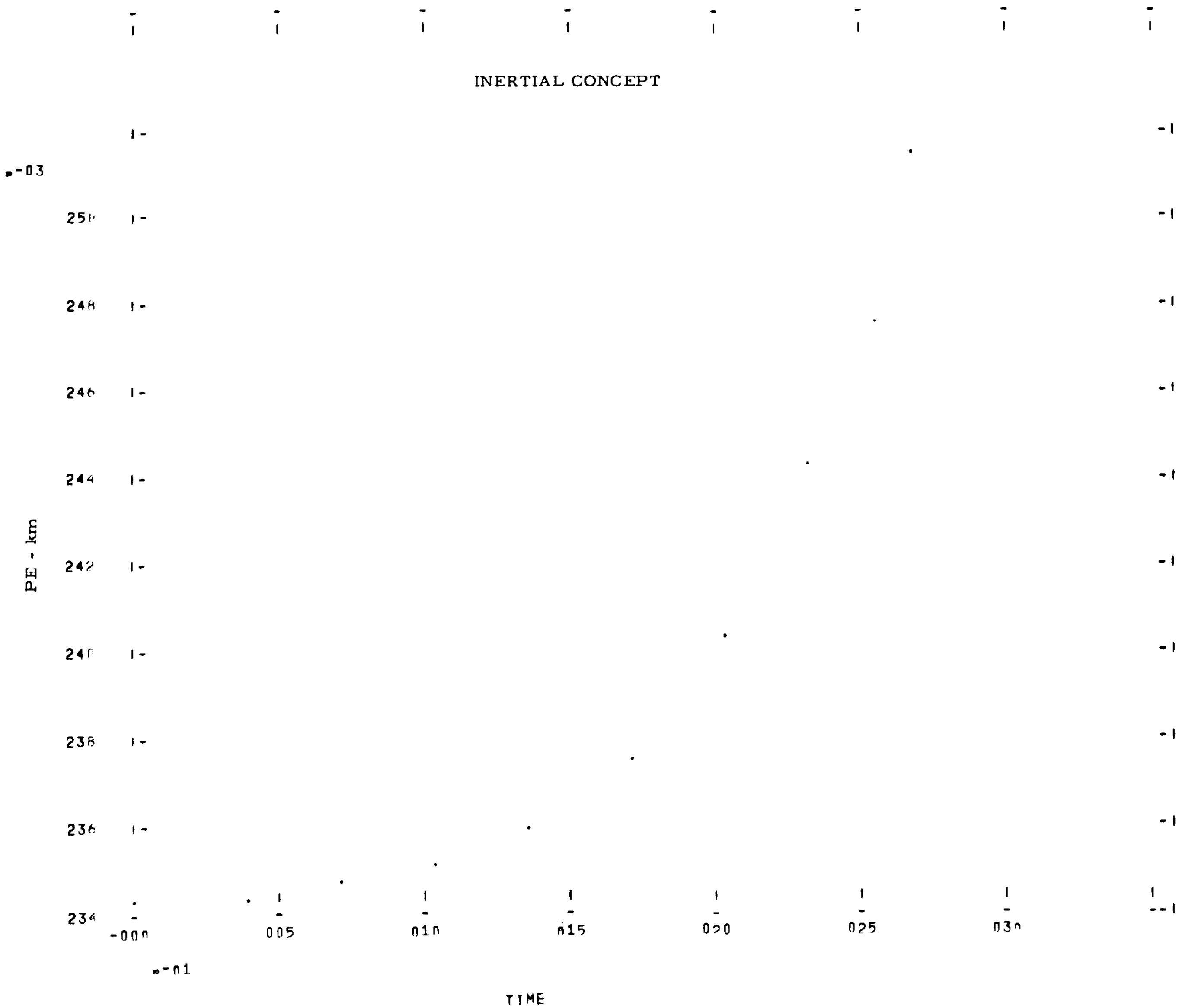

Figure 8-217 PLOT 12 MISSION I 1972 LEG C

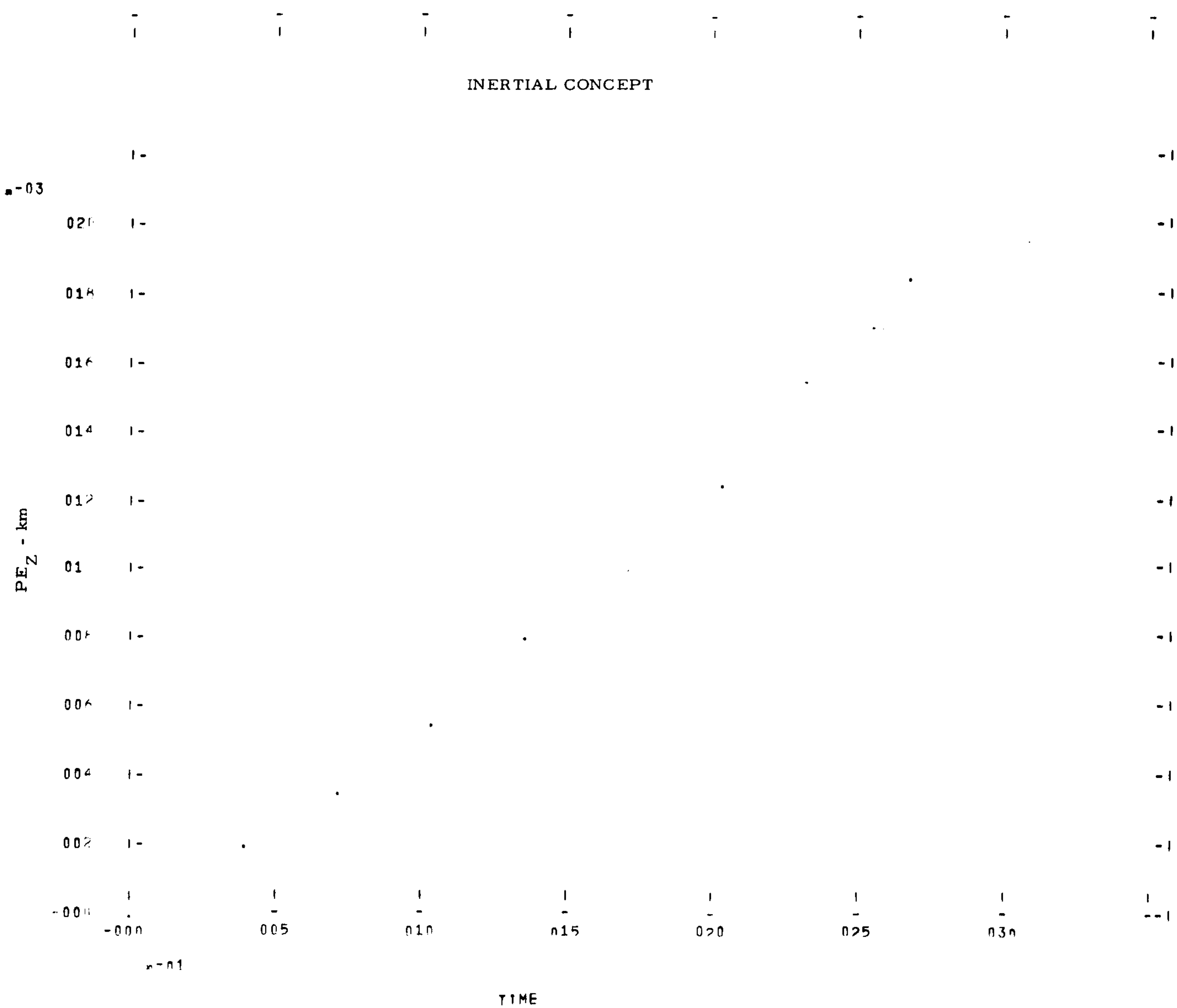

Figure 8-218 PLOT 13 MISSION II 1976 LEG E

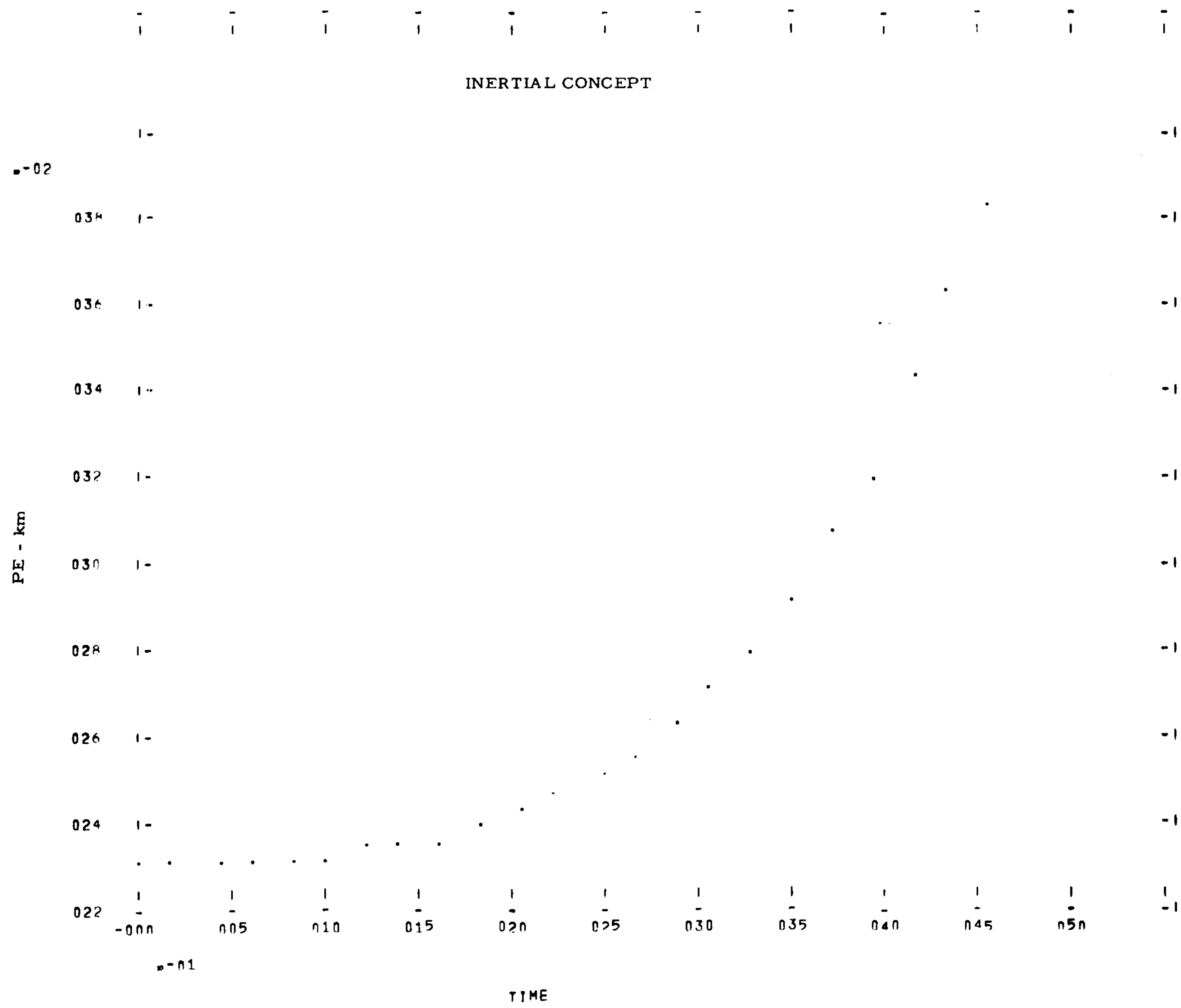

Figure 8-219 PLOT 12 MISSION II 1976 LEG E

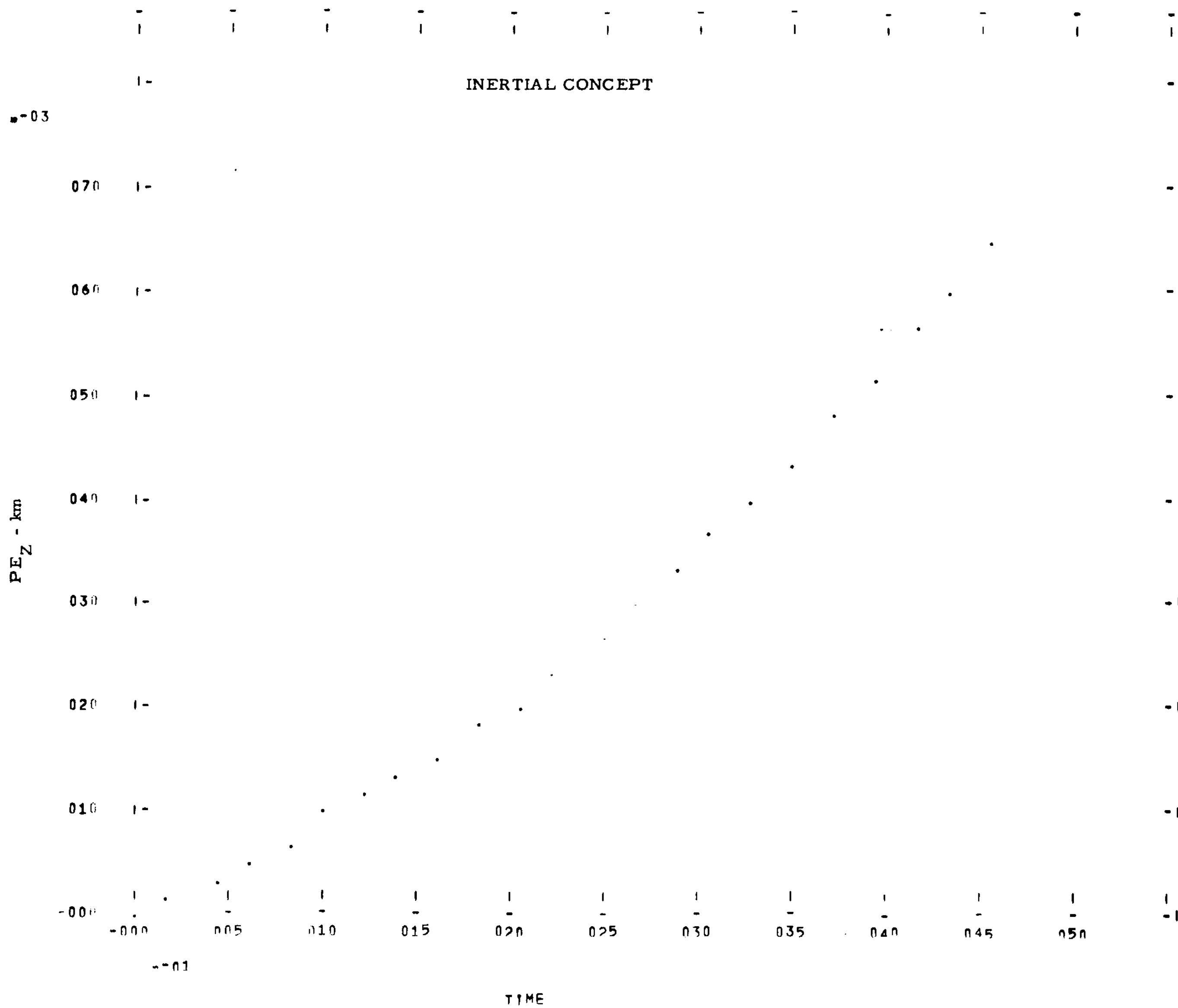

Figure 8-220 PLOT 13 MISSION III 1978 LEG 4

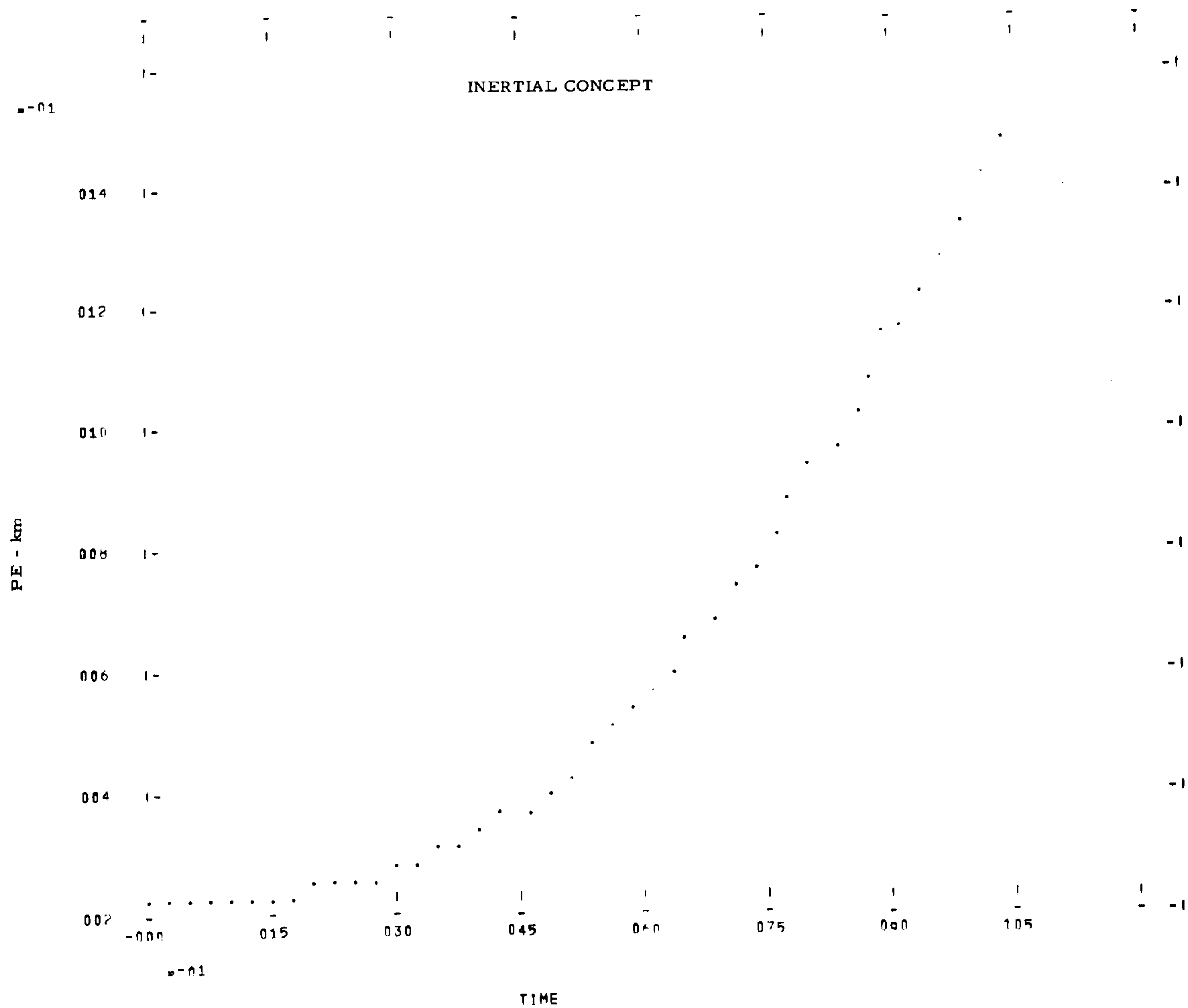

Figure 8-221 PLOT 12 MISSION III 1978 LEG A

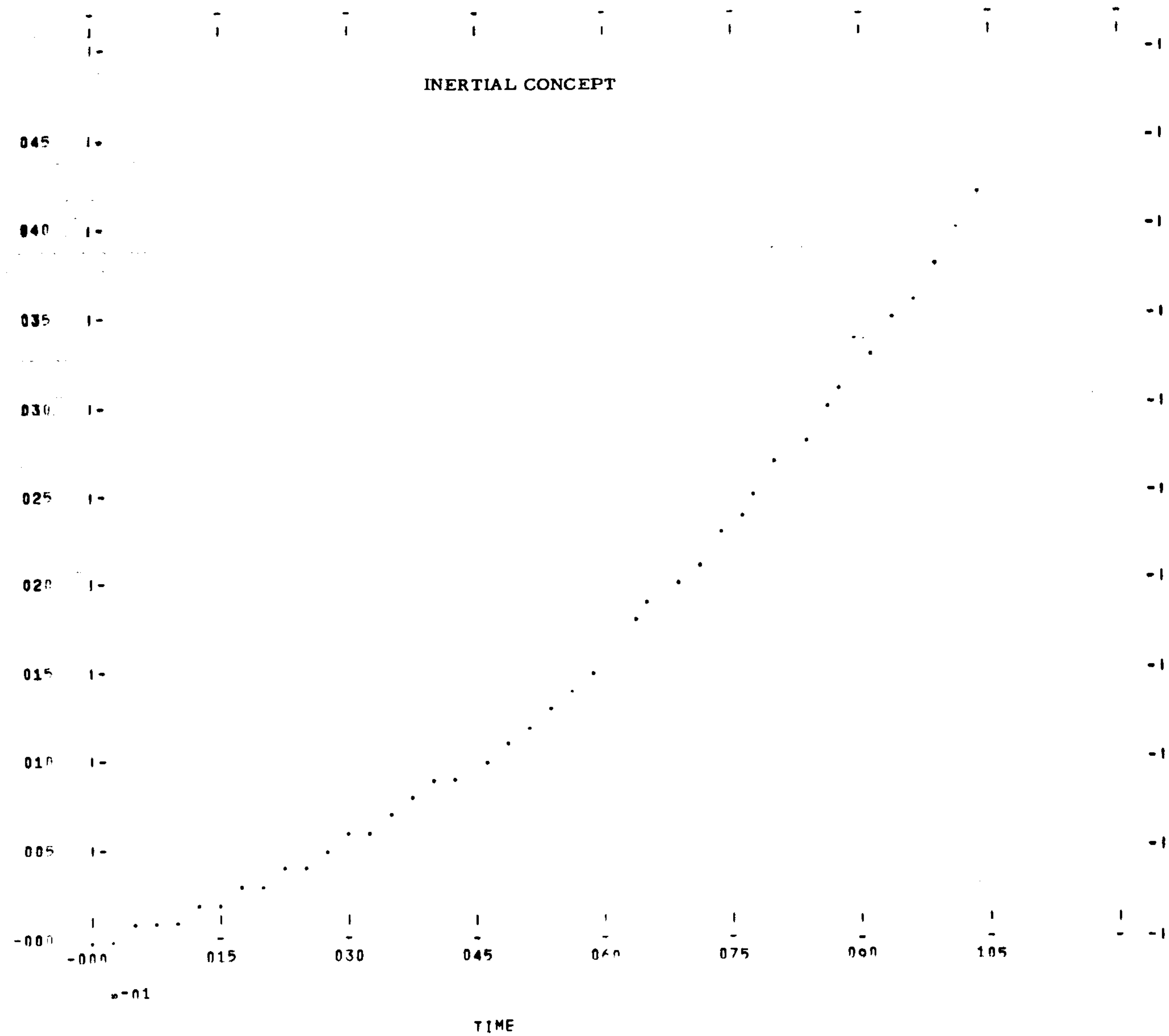

Figure 8-222 PLOT 13 MISSION III 1978 LEG B

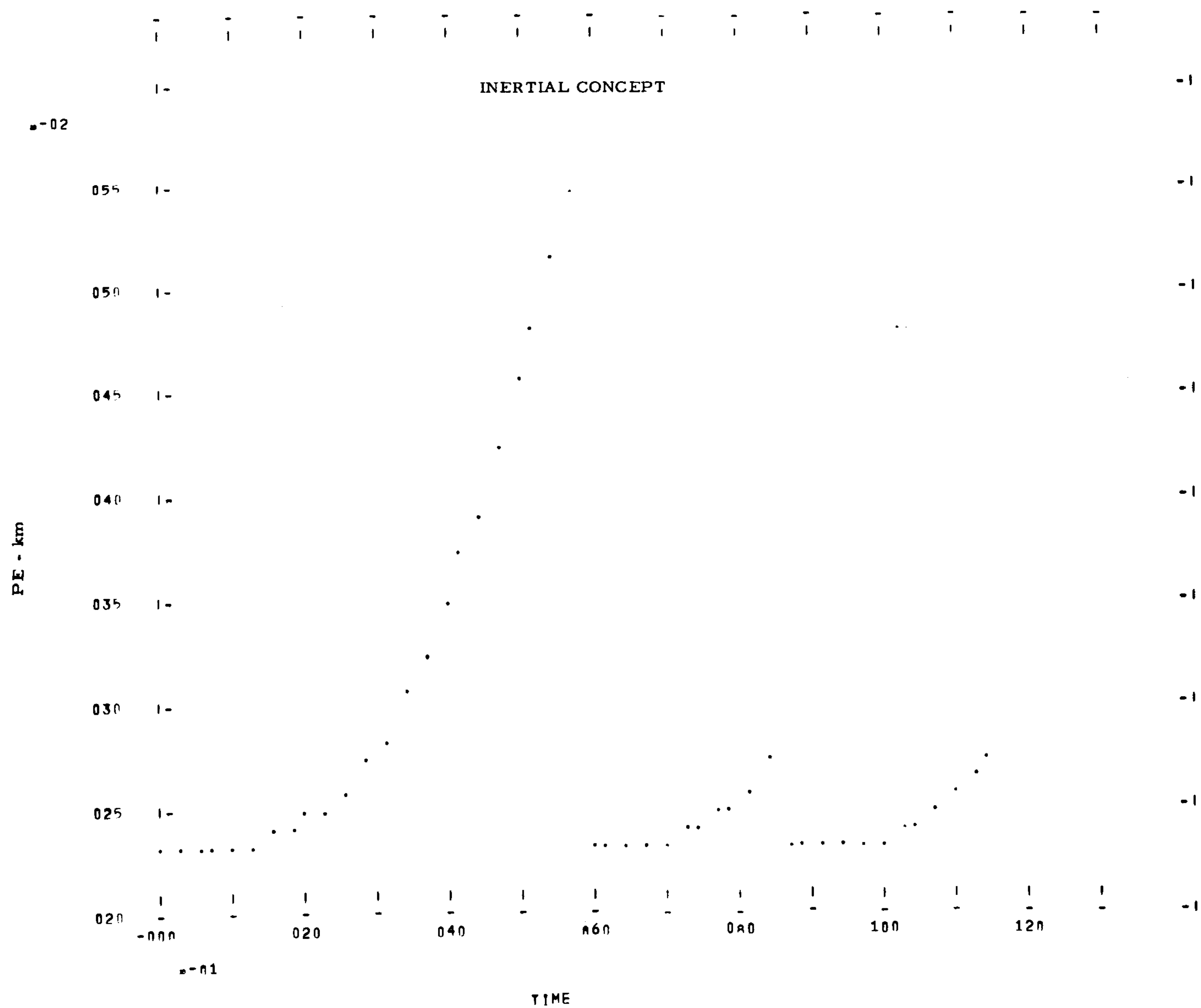

Figure 8-223 PLOT 12 MISSION III 1978 LEG B

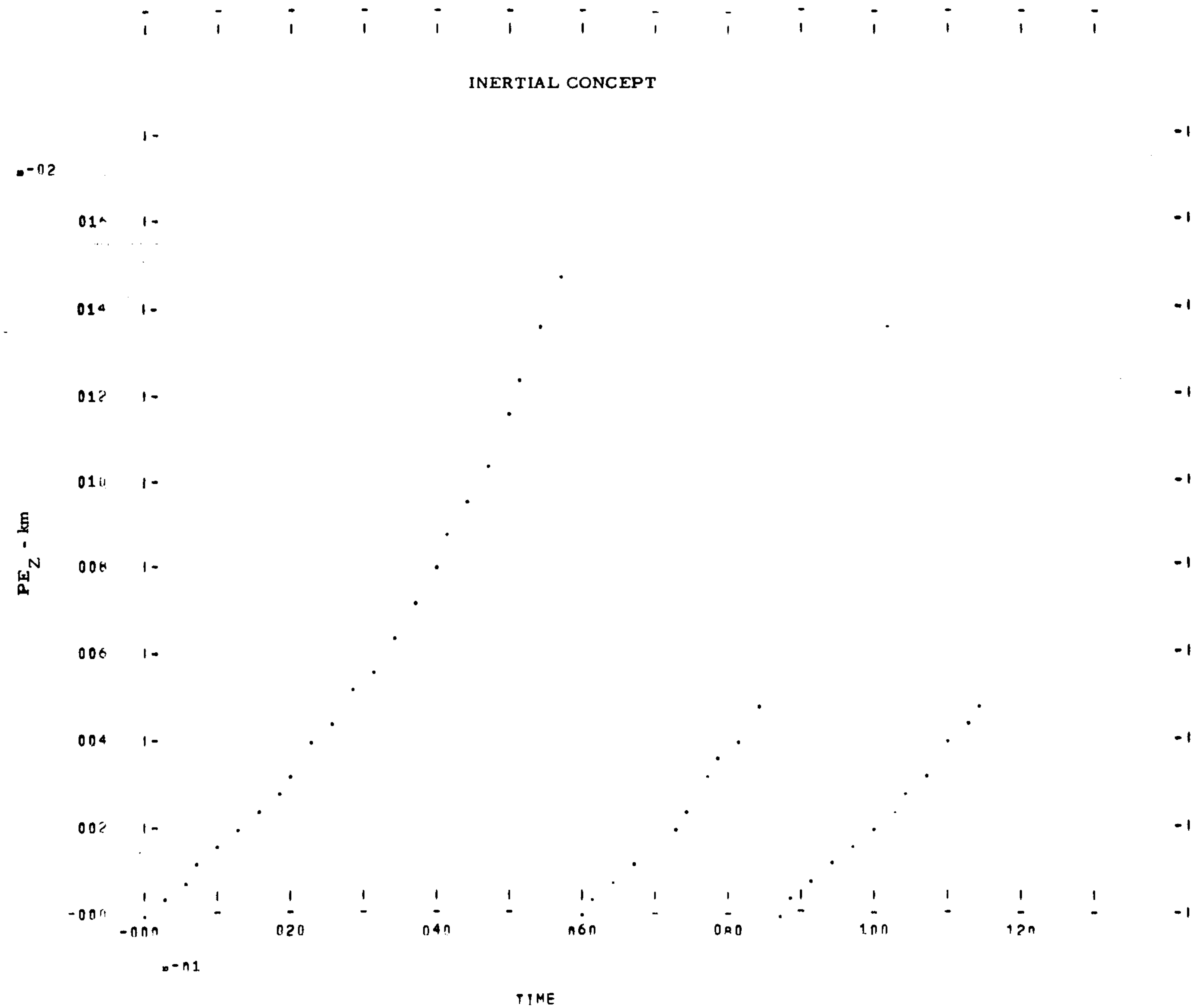

Figure 8-224 PLOT 13 MISSION IIII 1980 LEG C

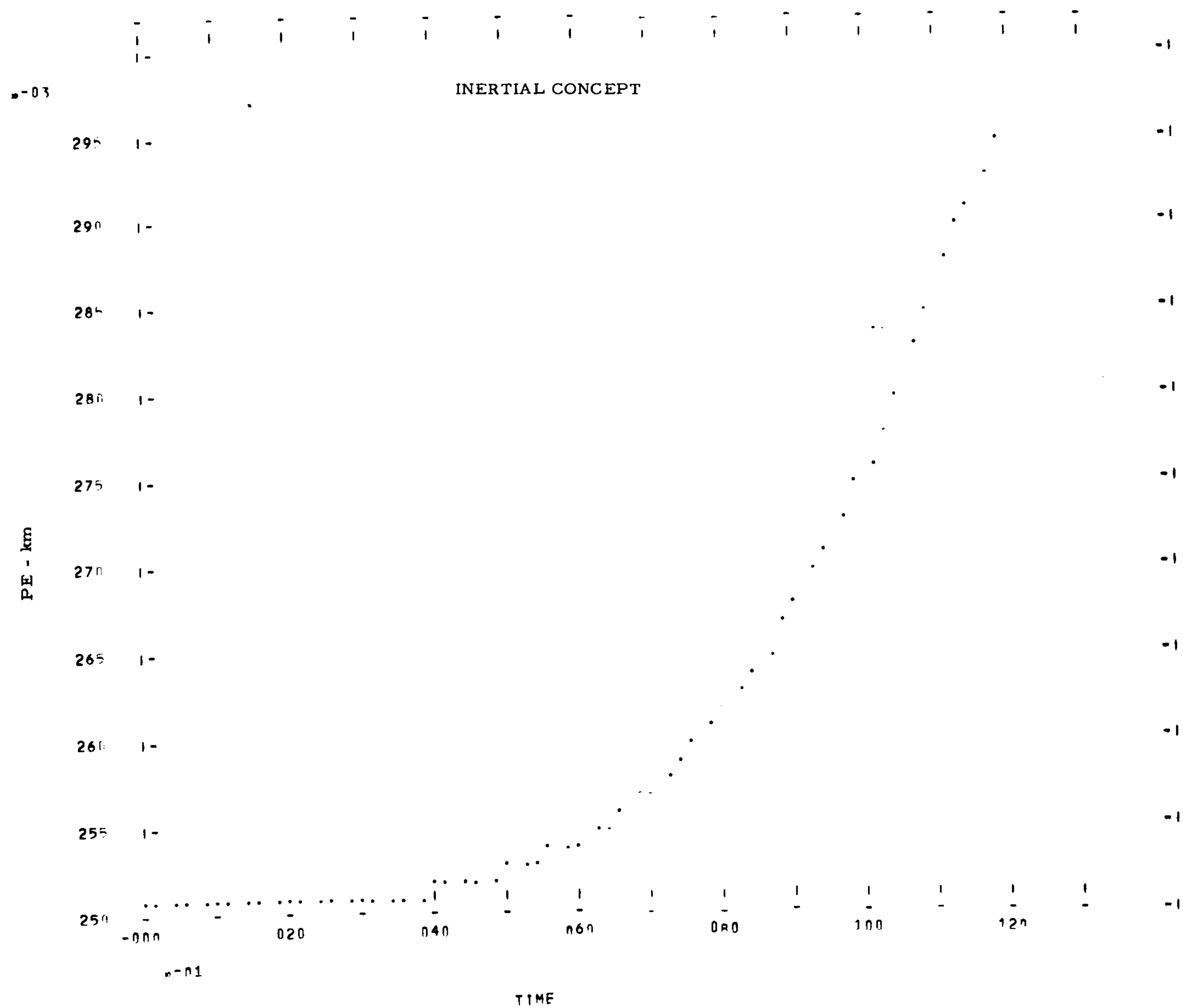

Figure 8-225 PLOT 12 MISSION IIII 1980 LEG C

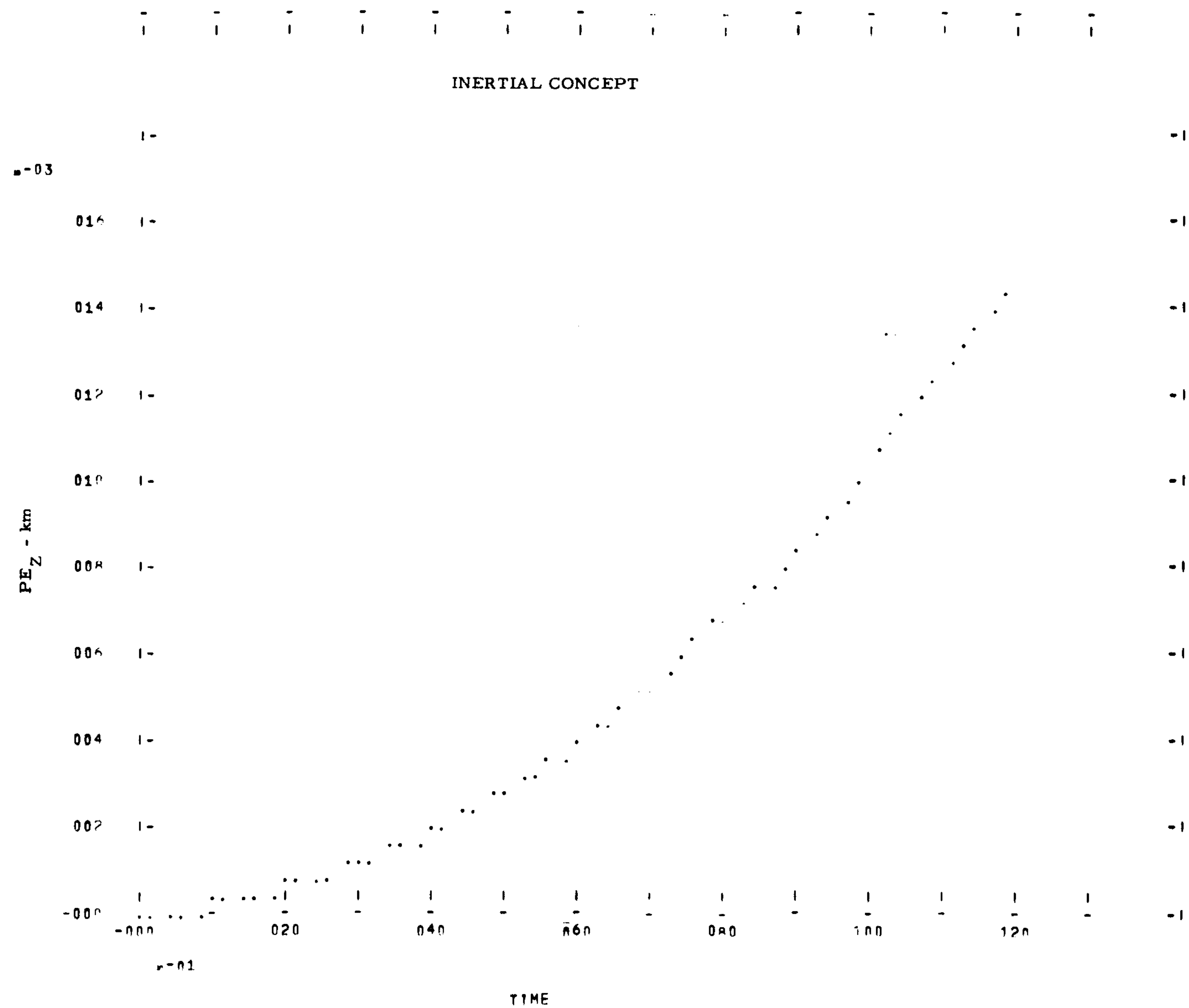

Figure 8-226 PLOT 13 MISSION IIII 1980 LEG F

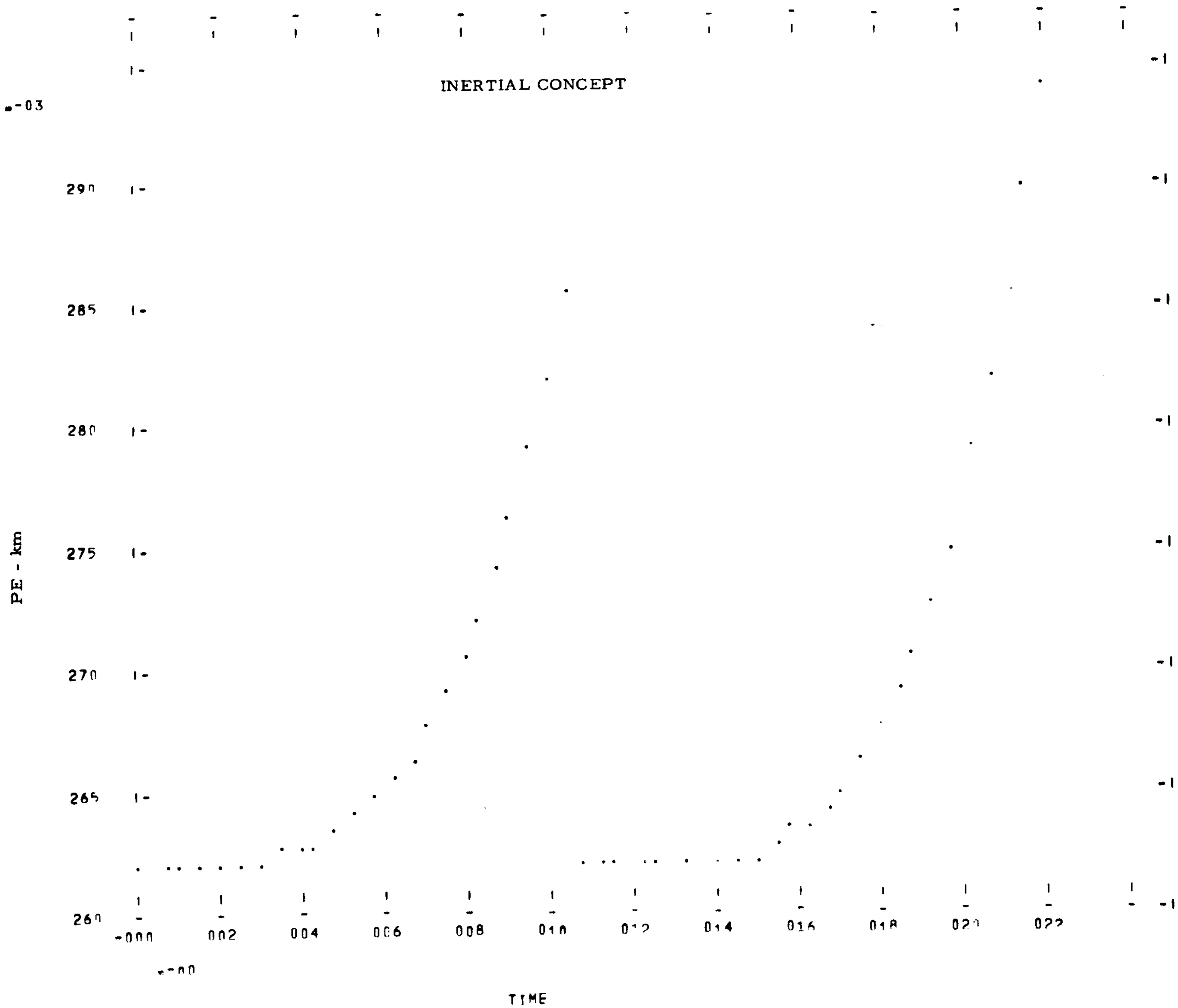

Figure 8-227 PLOT 12 MISSION IIII 1980 LEG F

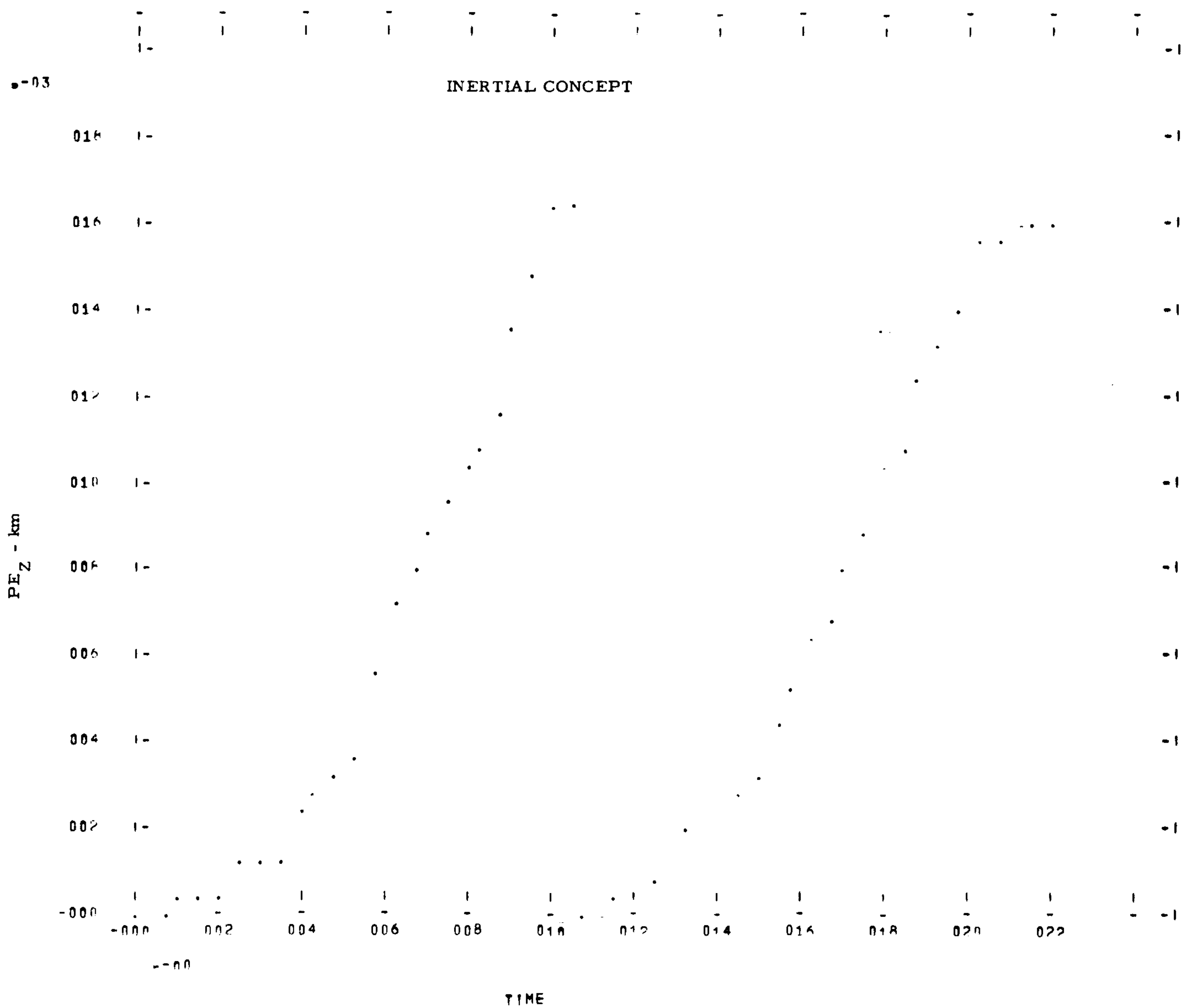

Figure 8-228 PLOT 13 MISSION V 1980 LEG A

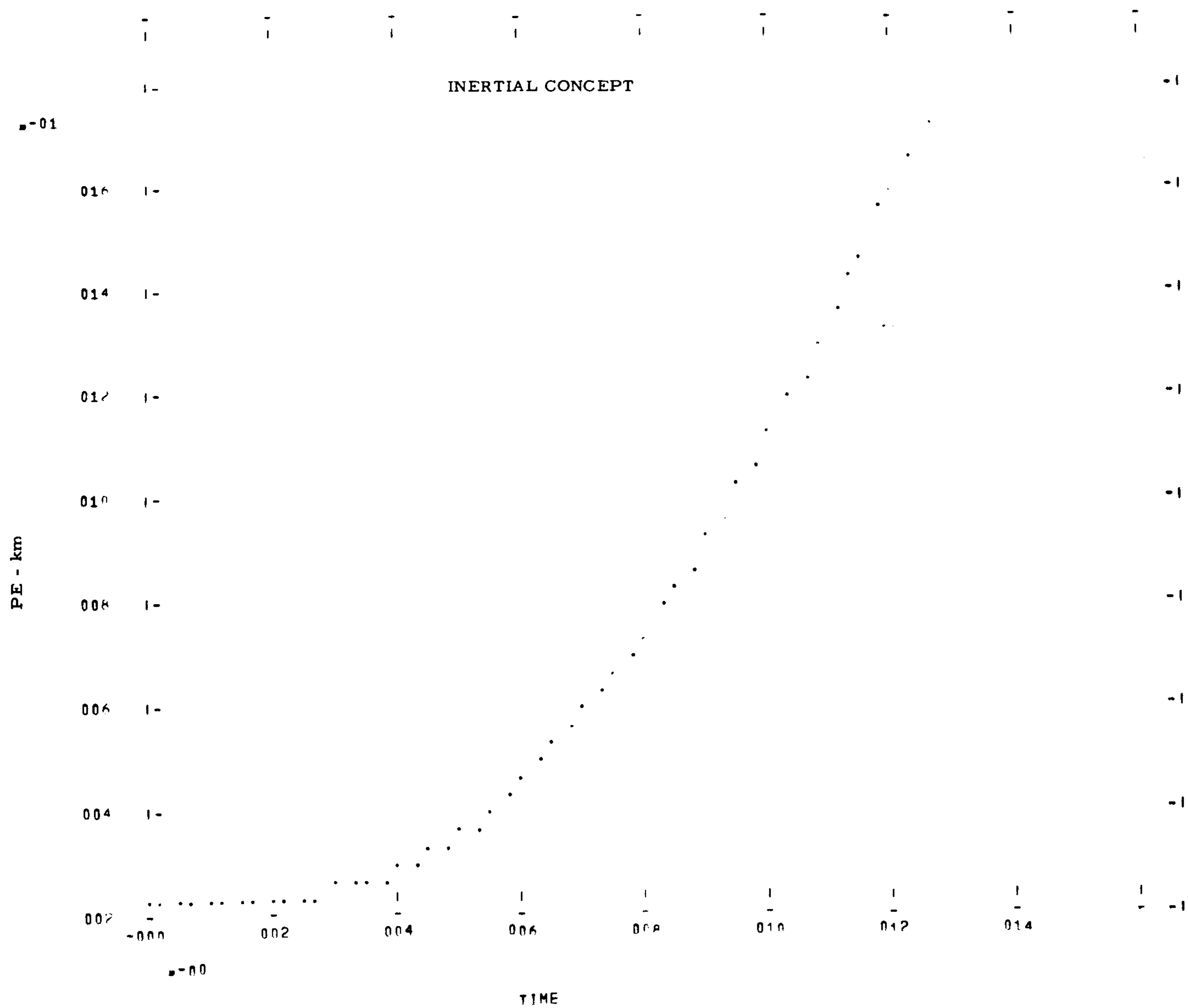

Figure 8-229 PLOT 12 MISSION V 1980 LEG A

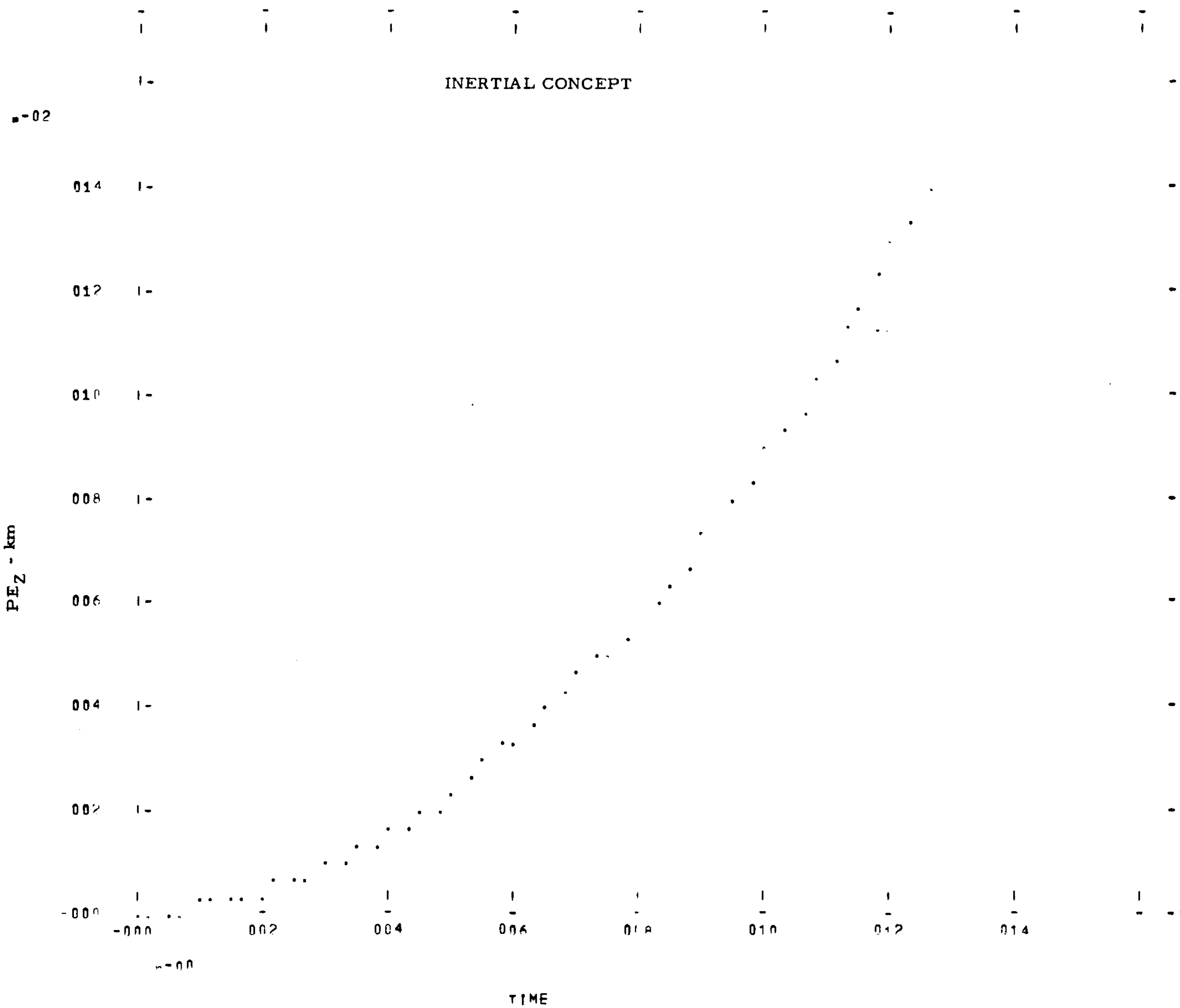

Figure 8-230 PLOT 13 MISSION V 1980 LEG B

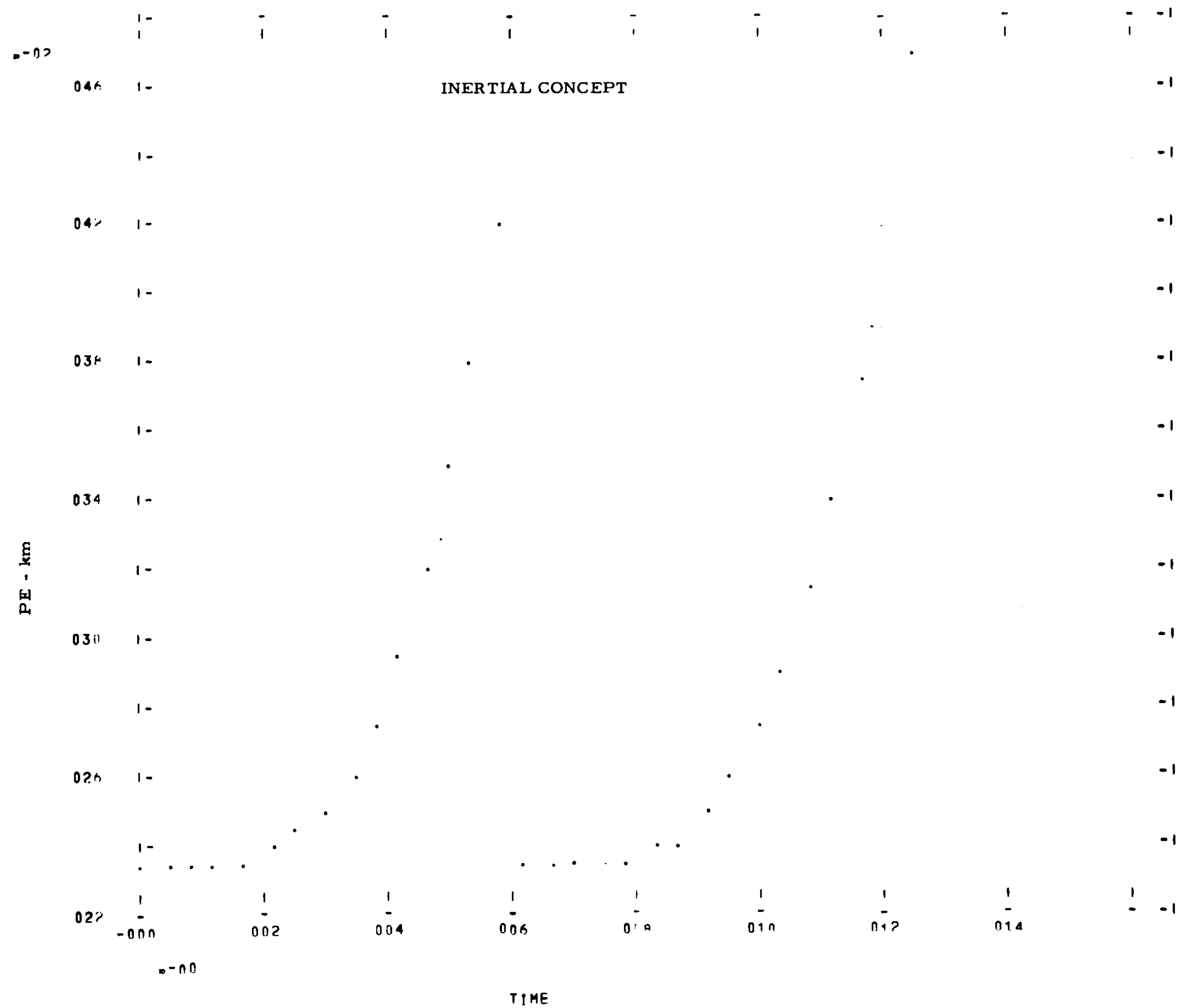

Figure 8-231 PLOT 12 MISSION V 1980 LEG B

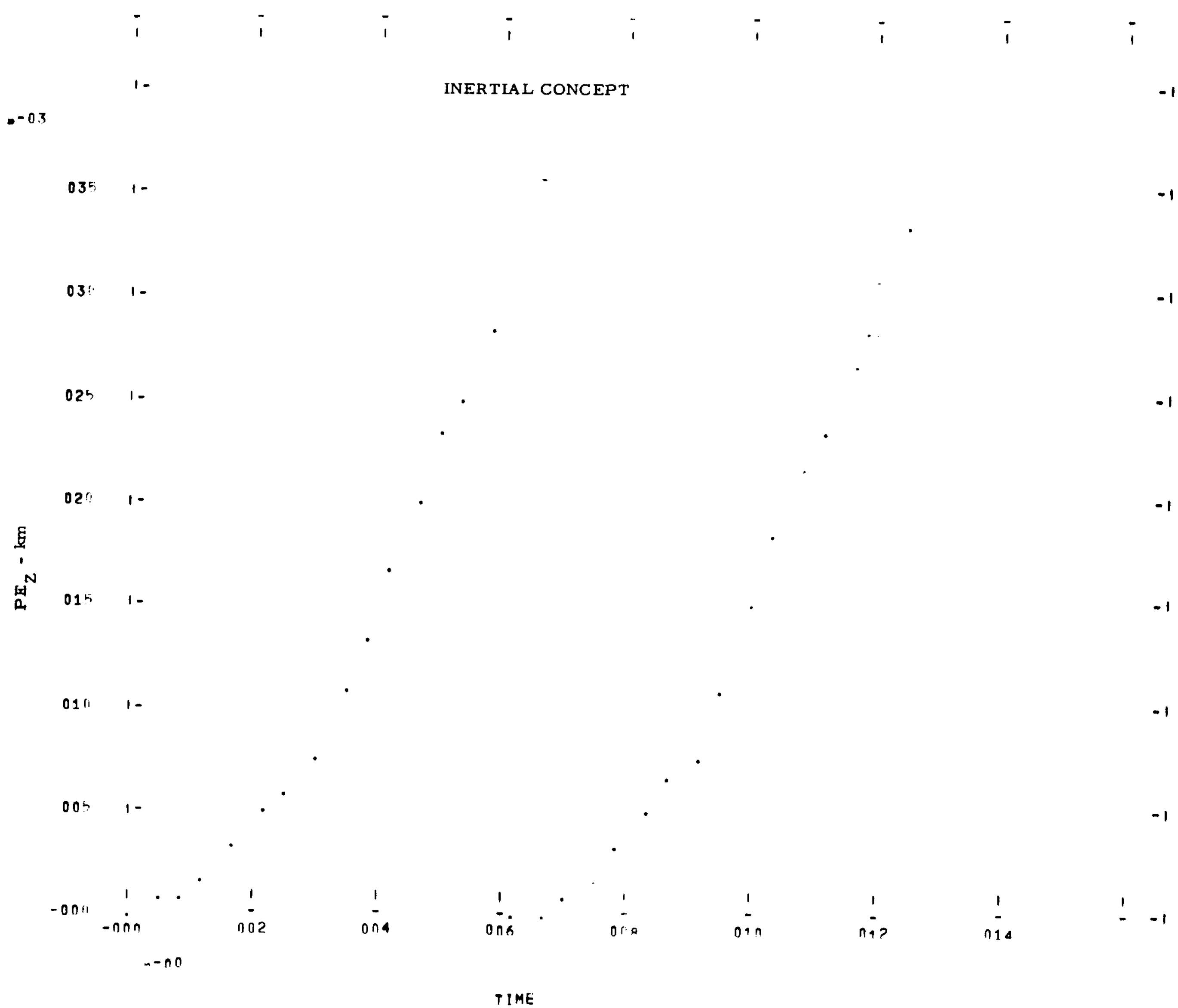

Figure 8-232 PLOT 13 MISSION V 1980 LEG C

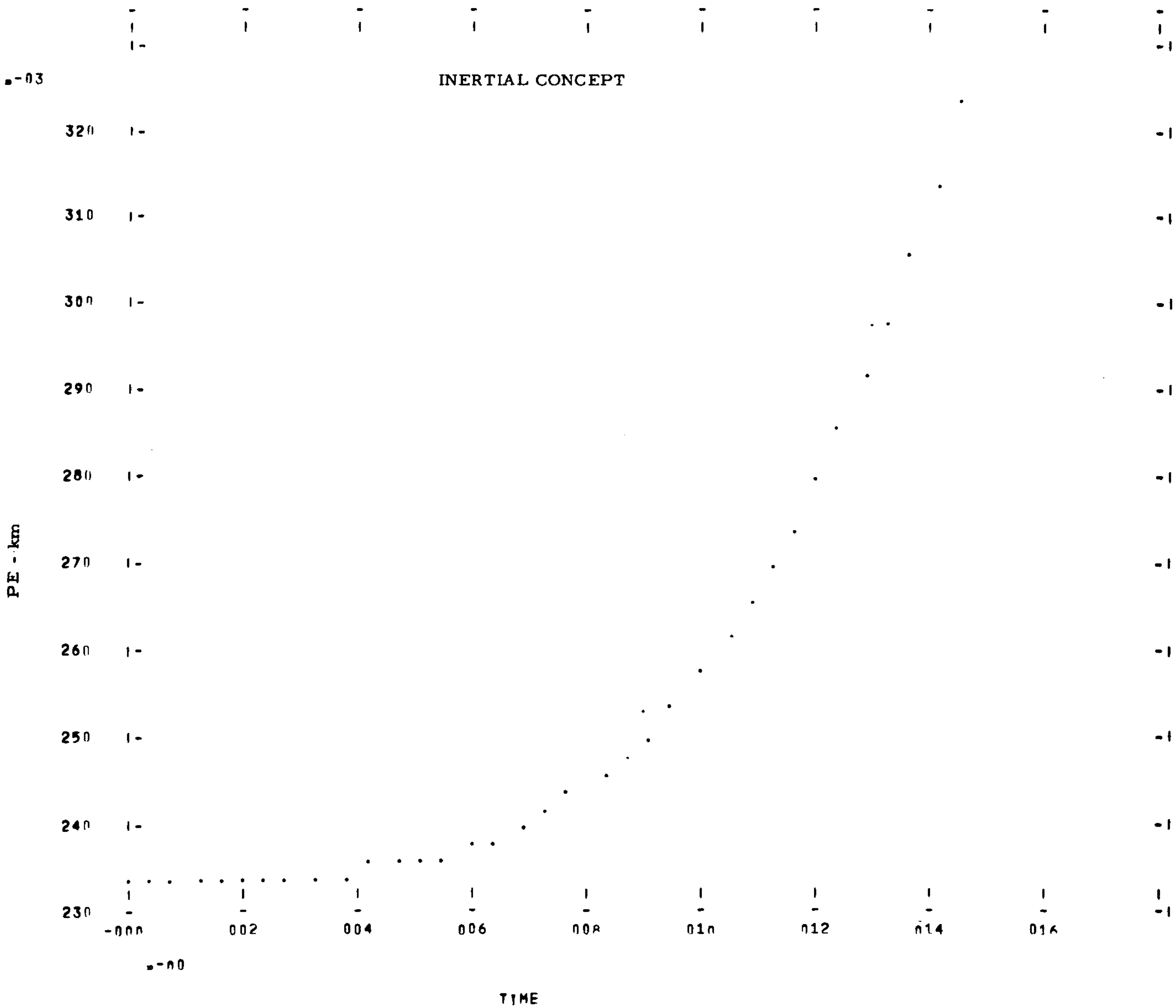

Figure 8-233 PLOT 12 MISSION V 1980 LEG C

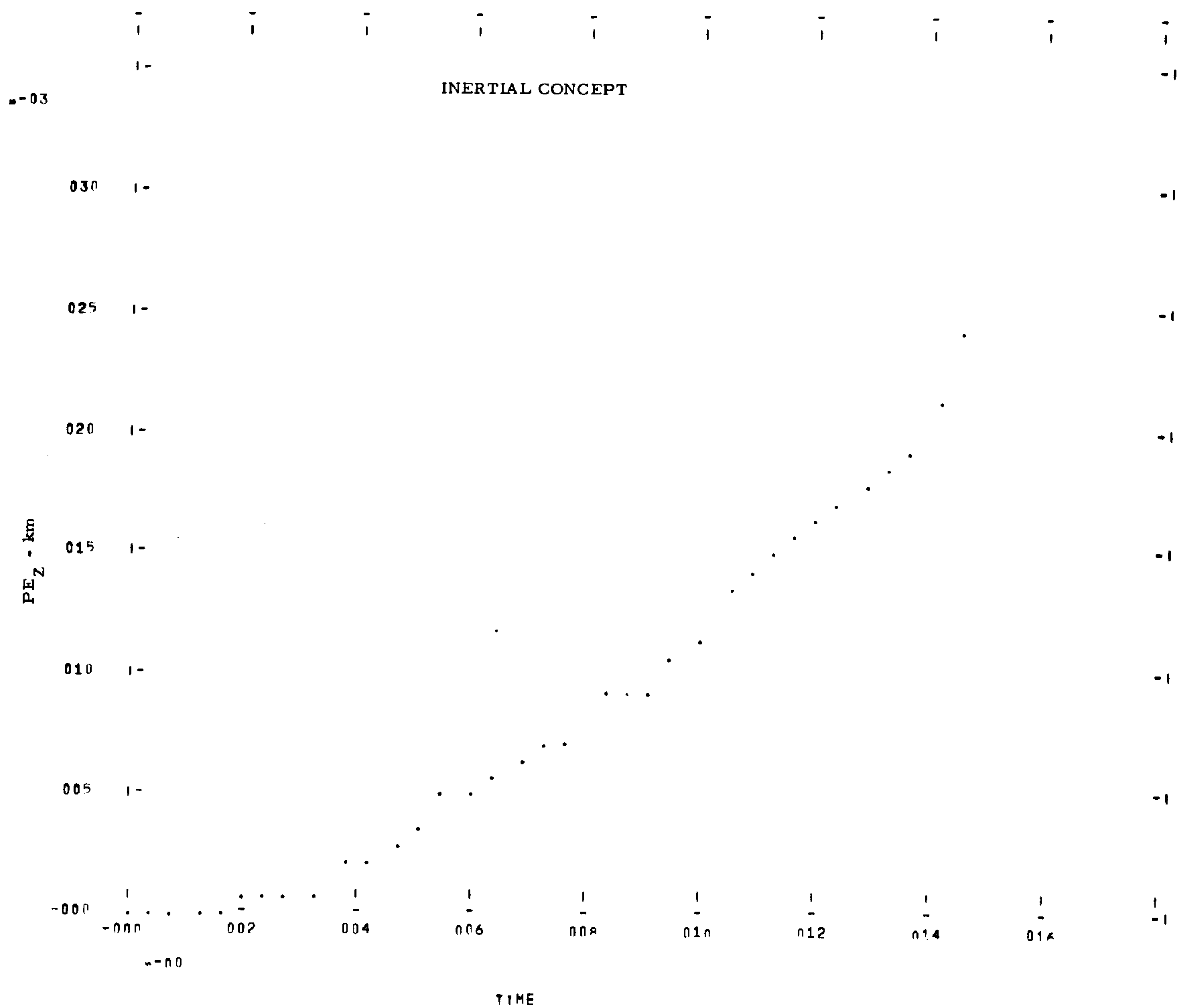

Figure 8-234 PLOT 13 MISSION VI 1984 LEG B

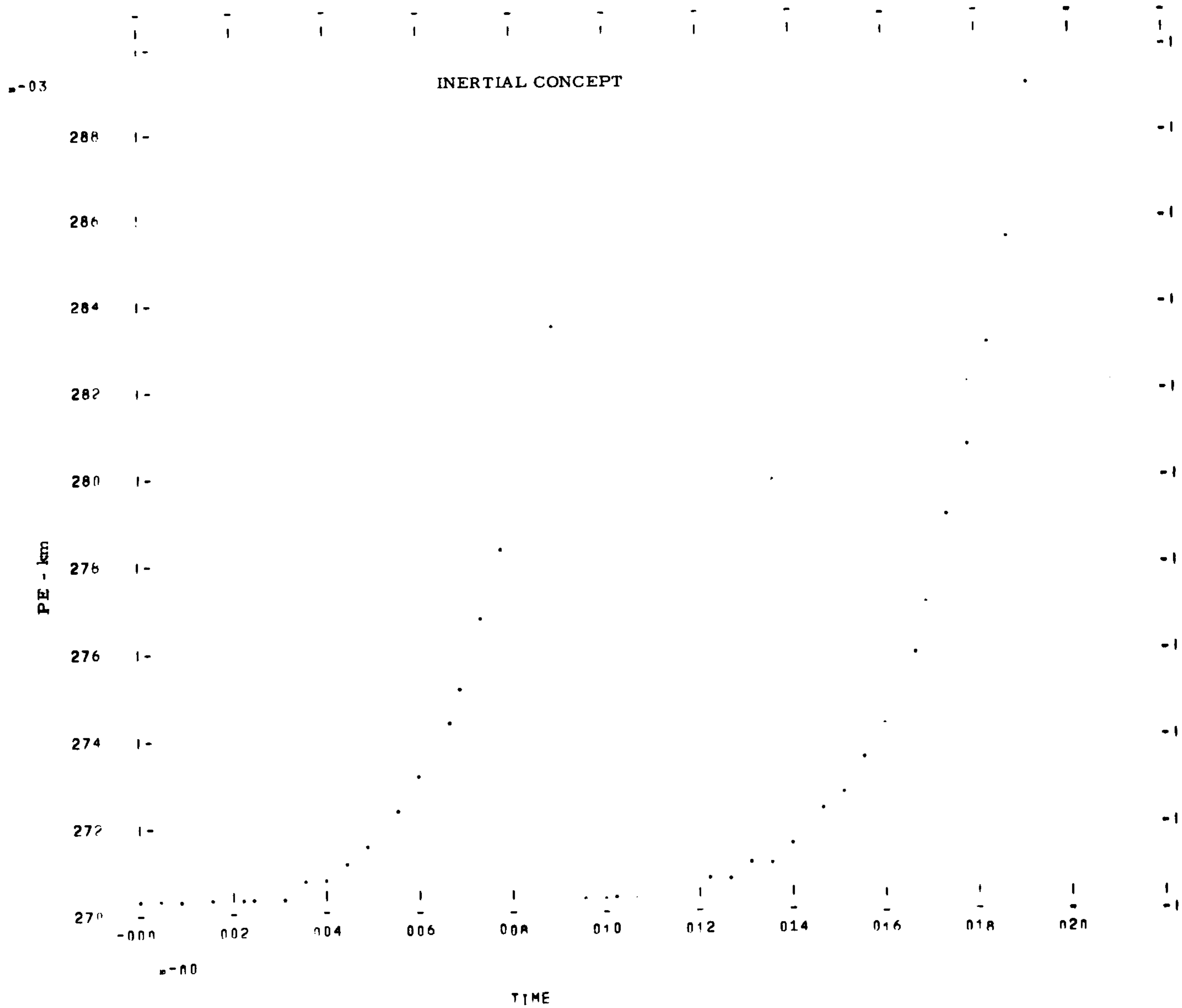

Figure 8-235 PLOT 12 MISSION VI 1984 LEG B

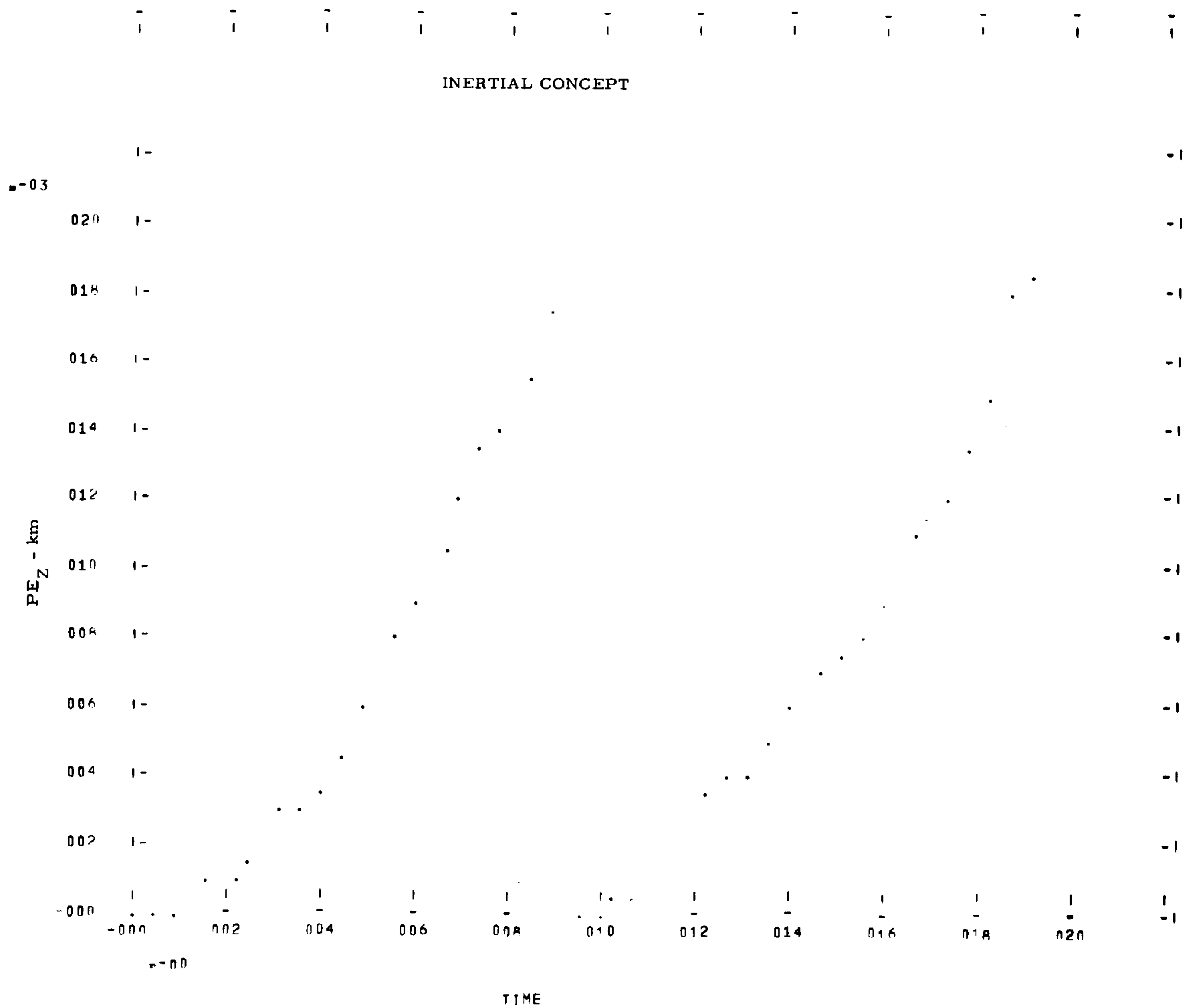

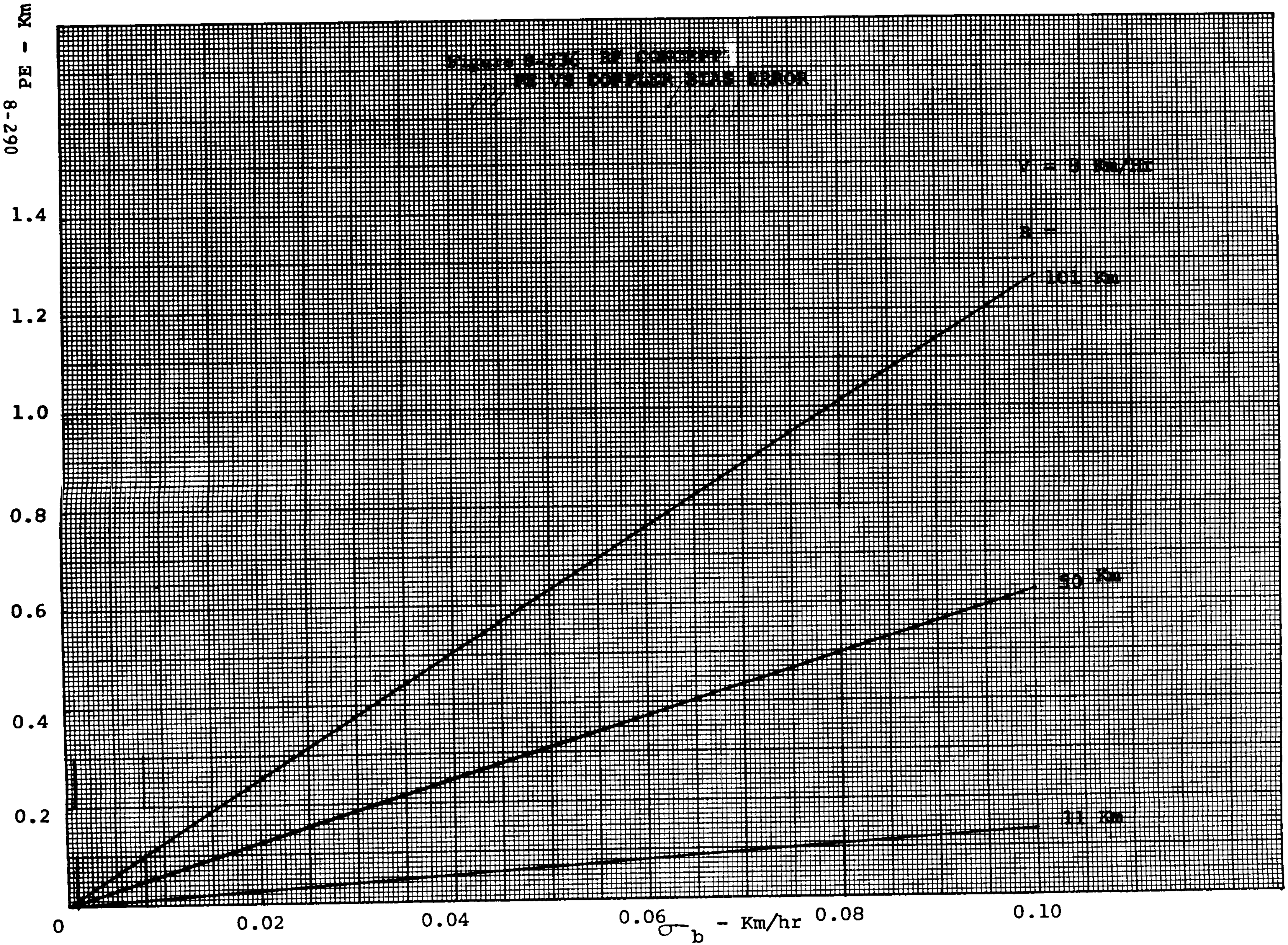
Figure 8-23C RF CONCEPT
PE VS DOPPLER BIAS ERROR
V = 3 Km/Hr
R =
101 Km
50 Km
11 Km
PE - Km
1.4
1.2
1.0
0.8
0.6
0.4
0.2
0
0.02
0.04
0.06
0.08
0.10
σ_b - Km/hr

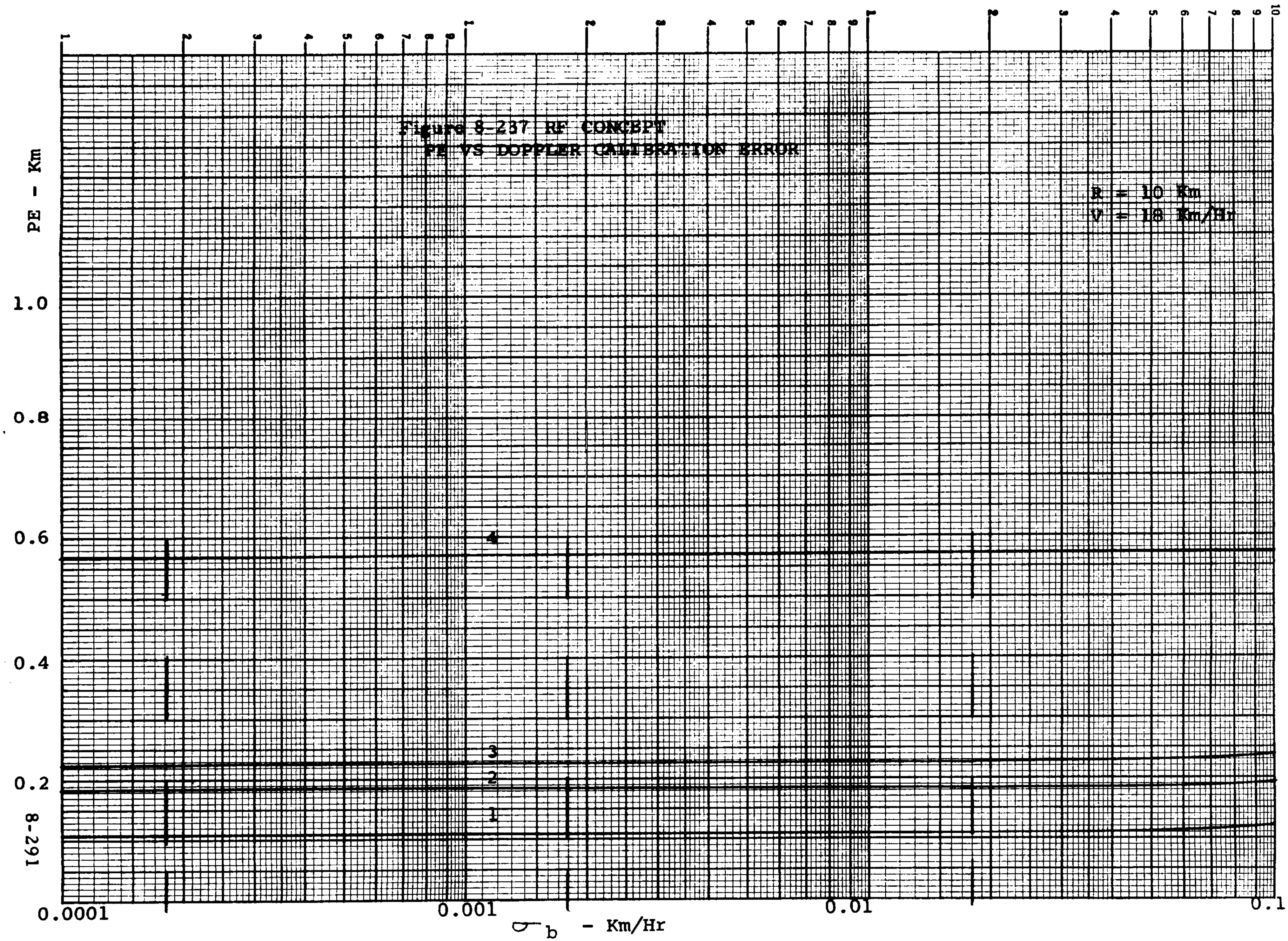

Figure 8-237 RF CONCEPT
PE VS DOPPLER CALIBRATION ERROR

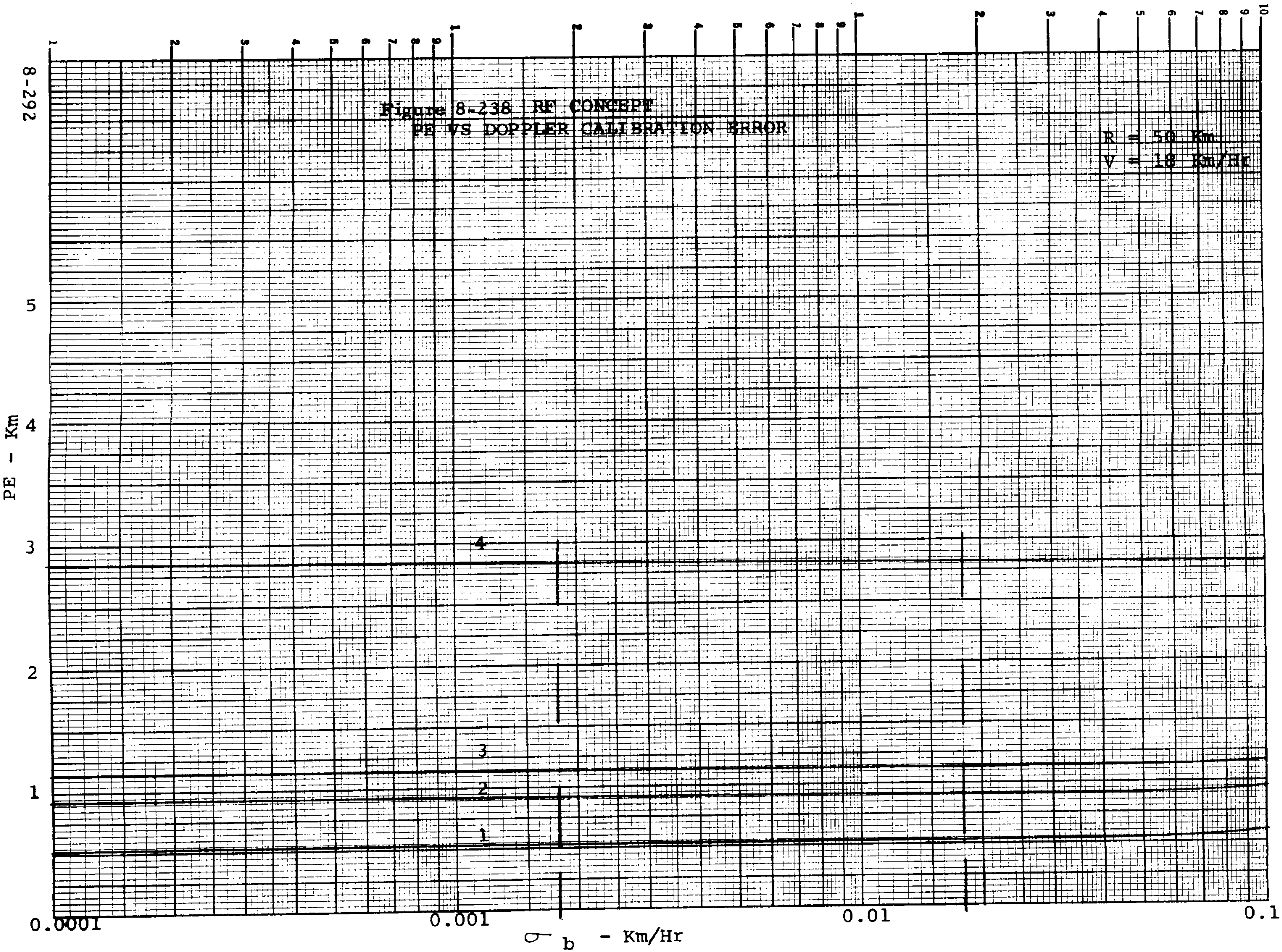

Figure 8-238 RF CONCEPT
PE VS DOPPLER CALIBRATION ERROR

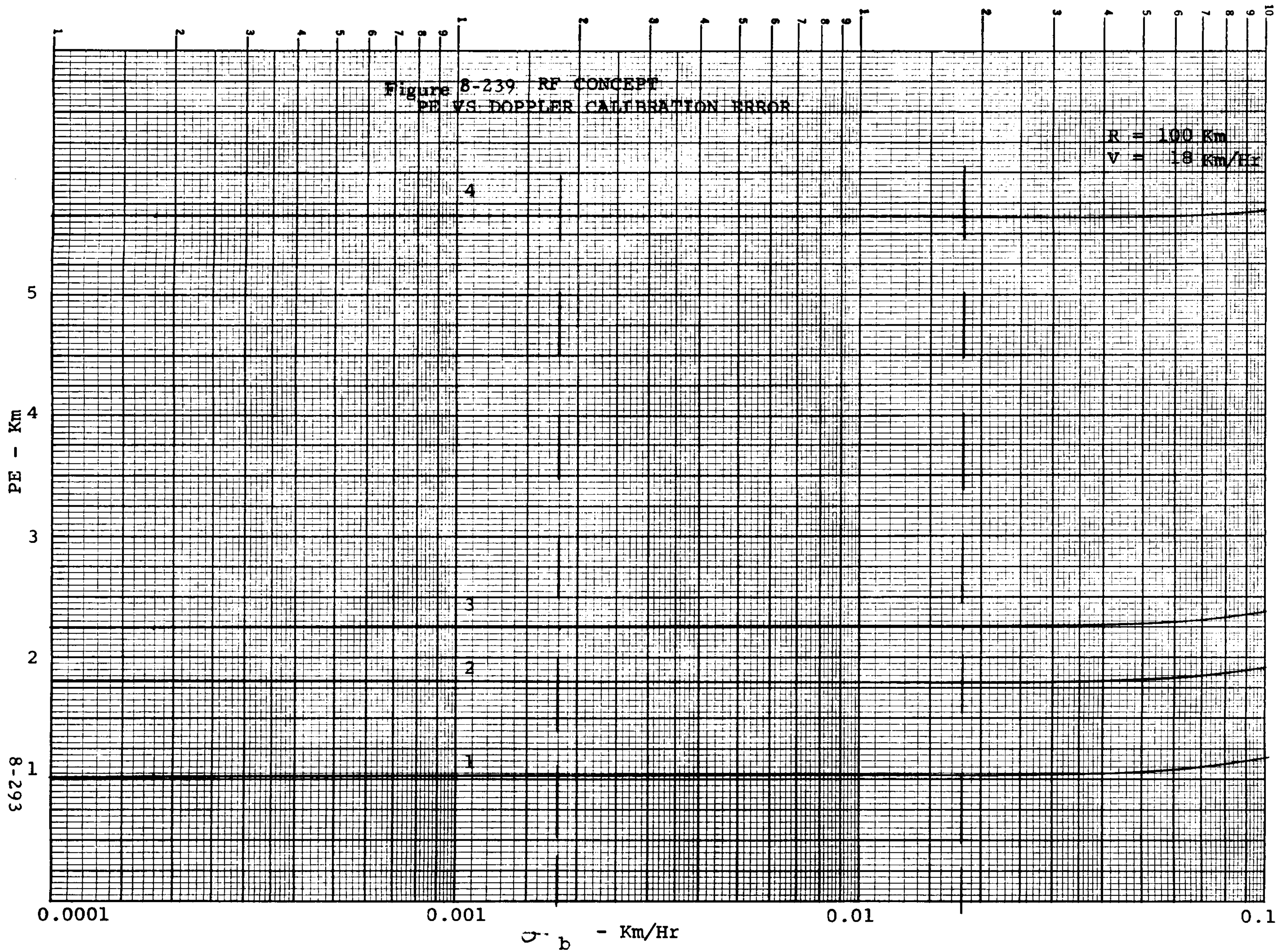

Figure 8-239 RF CONCEPT
PE VS DOPPLER CALIBRATION ERROR

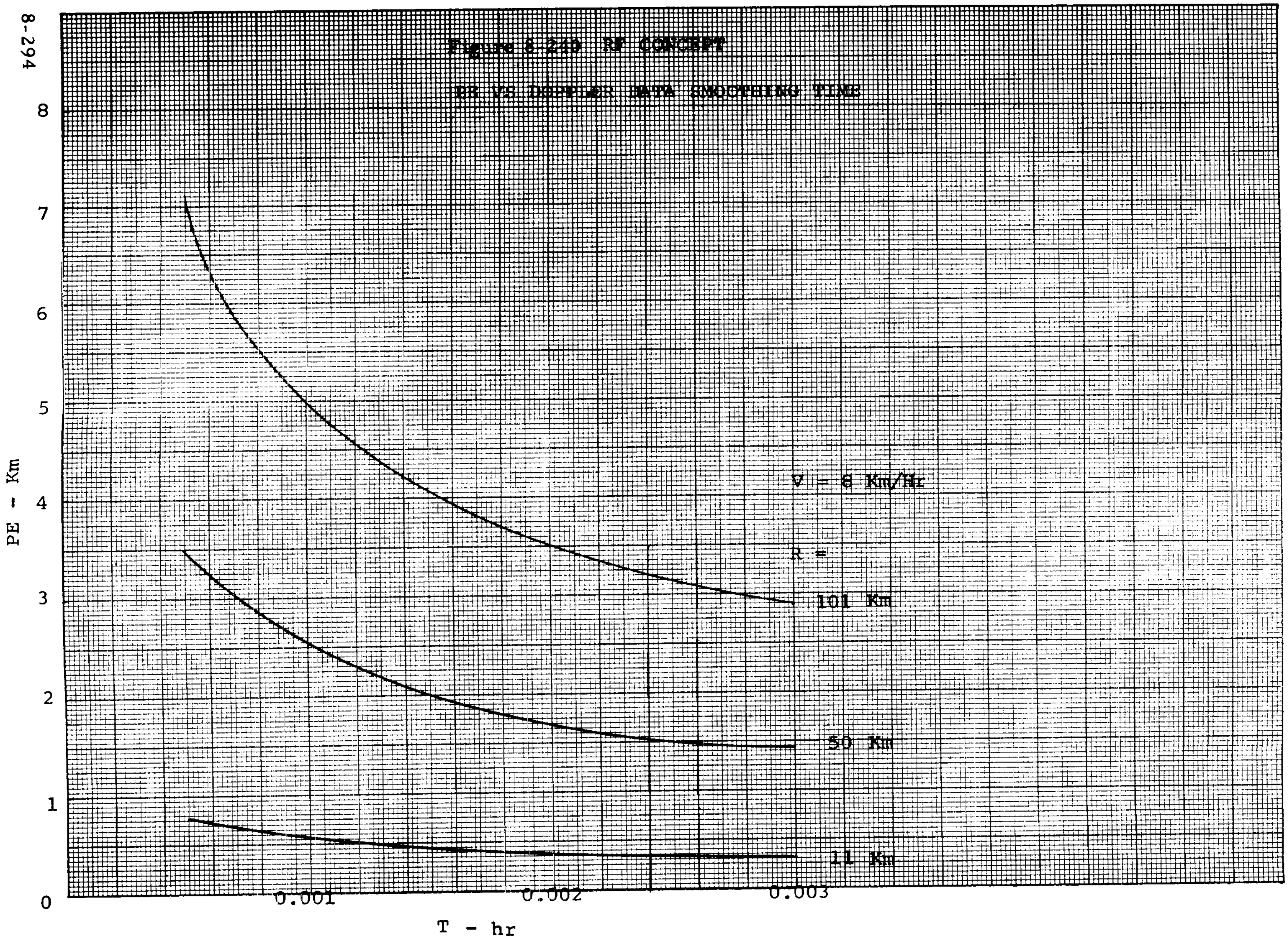

Figure 8-24D RF CONCEPT

PE VS DOPPLER DATA SMOOTHING TIME

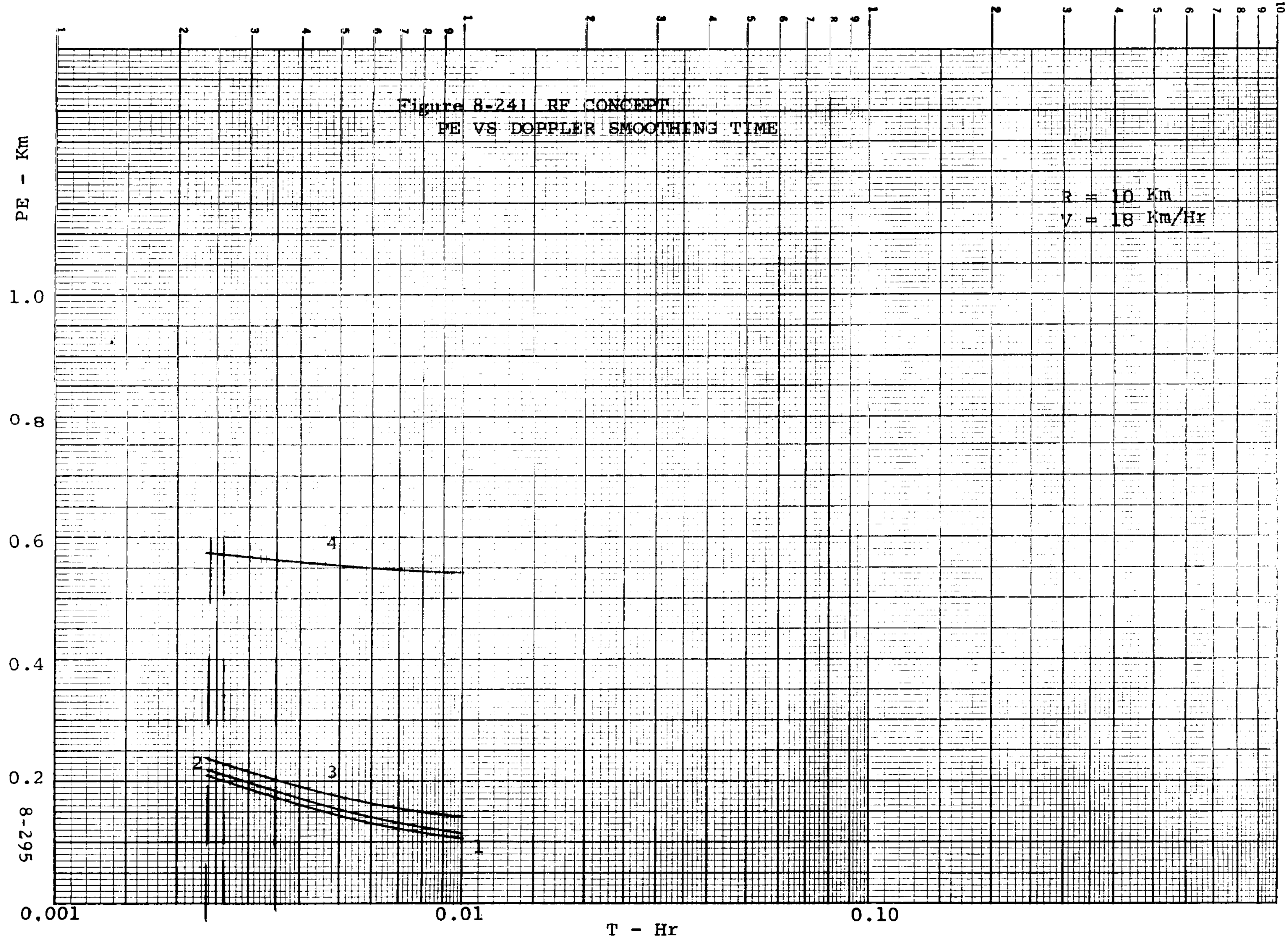

Figure 8-241 RF CONCEPT
PE VS DOPPLER SMOOTHING TIME
R = 10 Km
V = 18 Km/Hr
PE - Km
1.0
0.8
0.6
0.4
0.2
T - Hr
0.001
0.01
0.10
1
2
3
4

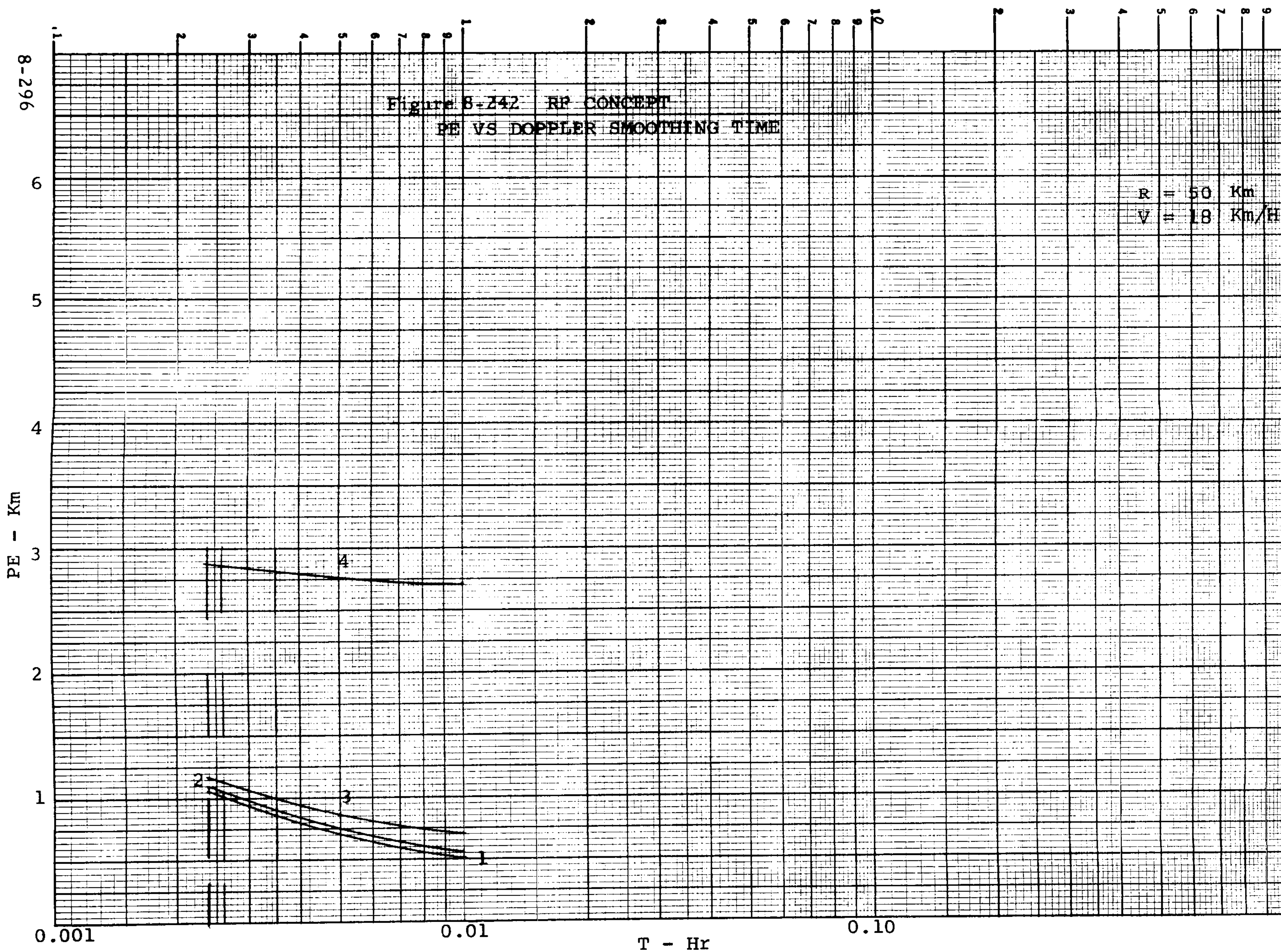

Figure 8-242 RP CONCEPT
PE VS DOPPLER SMOOTHING TIME
R = 50 Km
V = 18 Km/Hr
PE - Km
T - Hr
0.001
0.01
0.10
1
2
3
4
5
6

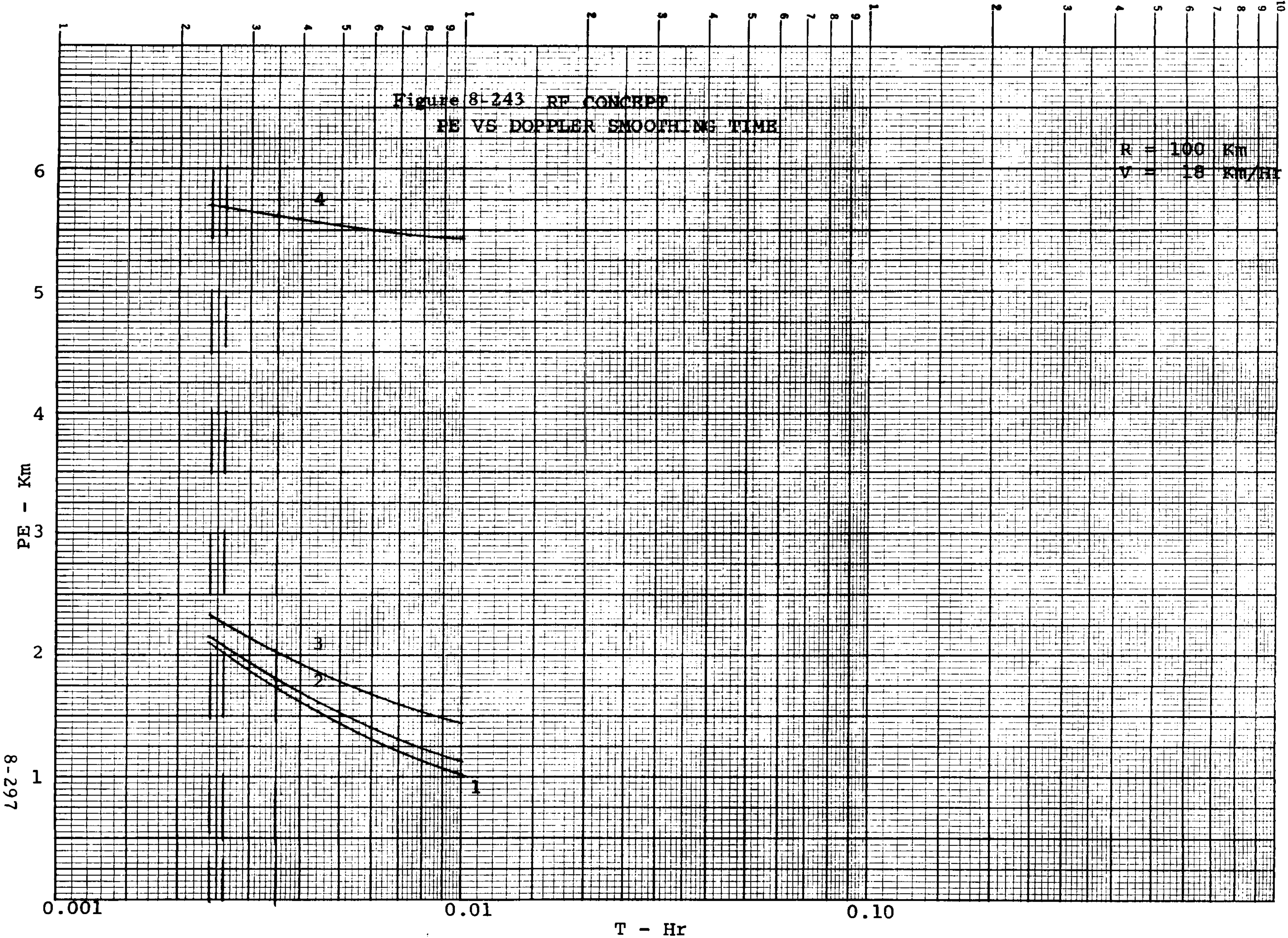

Figure 8-243 RF CONCEPT
PE VS DOPPLER SMOOTHING TIME

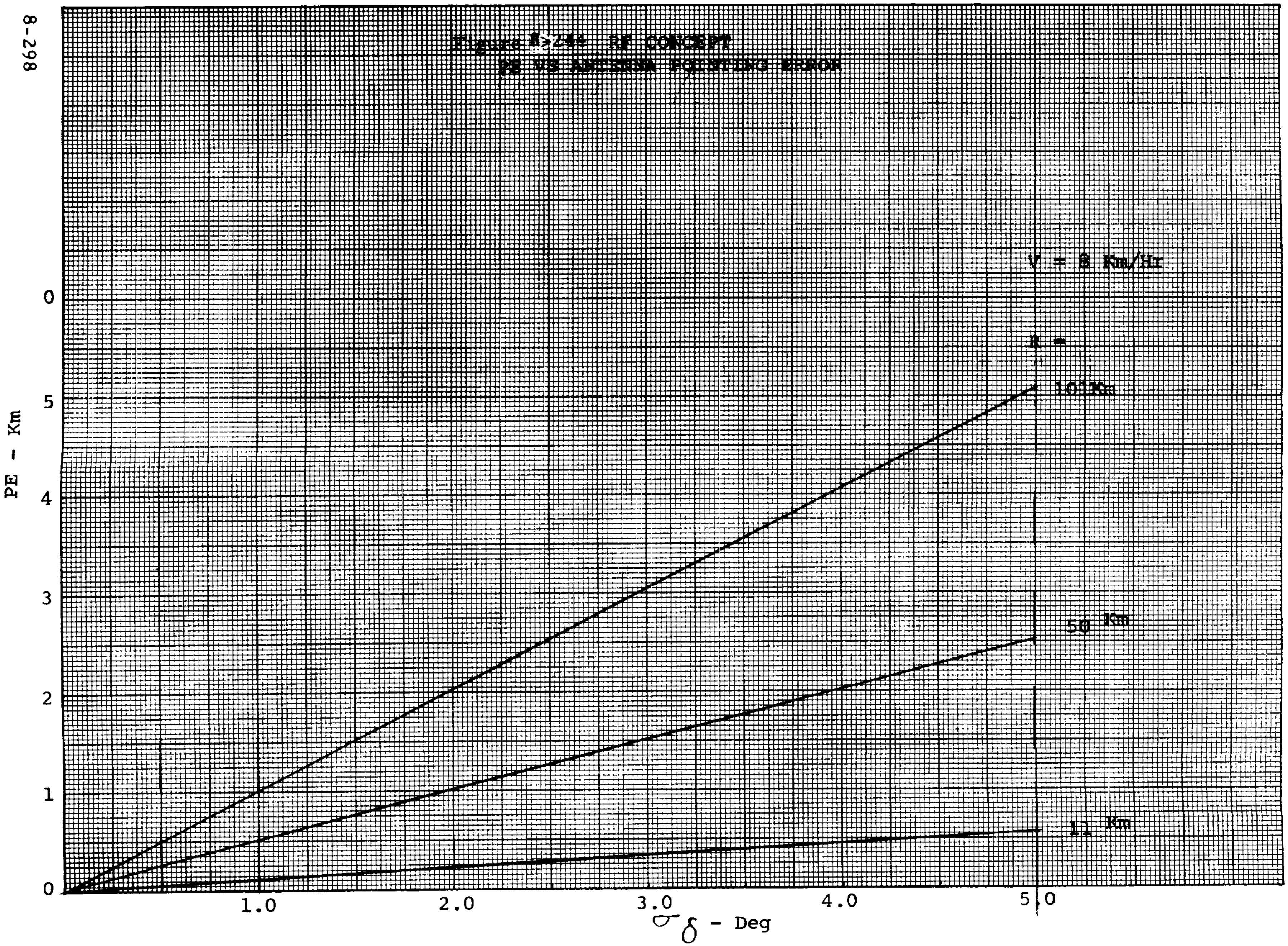

Figure 8-244 RF CONCEPT
PE VS ANTENNA POINTING ERROR

Figure 8-245 RF CONCEPT
PE VS DOPPLER ANTENNA POINTING ERROR

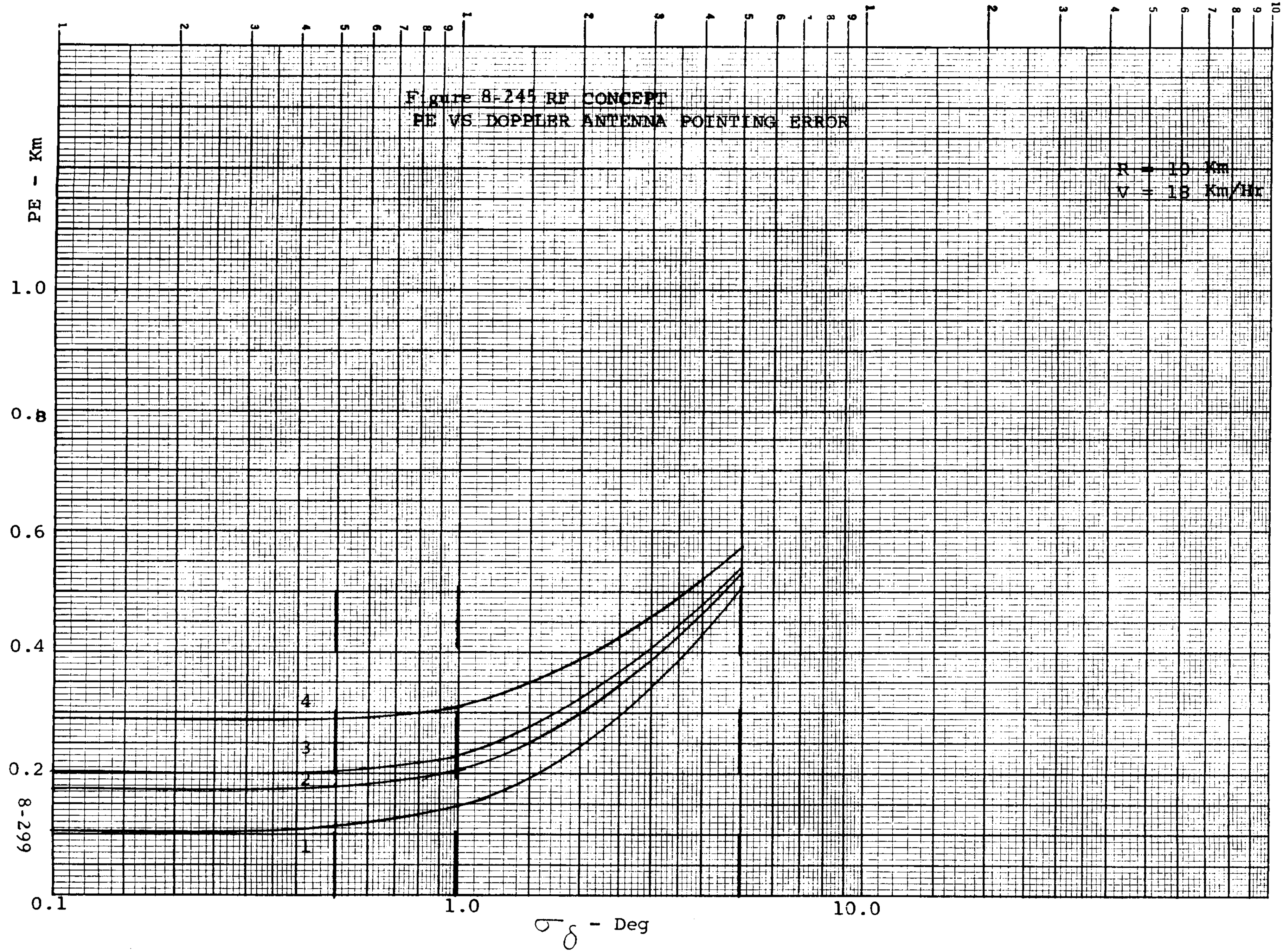

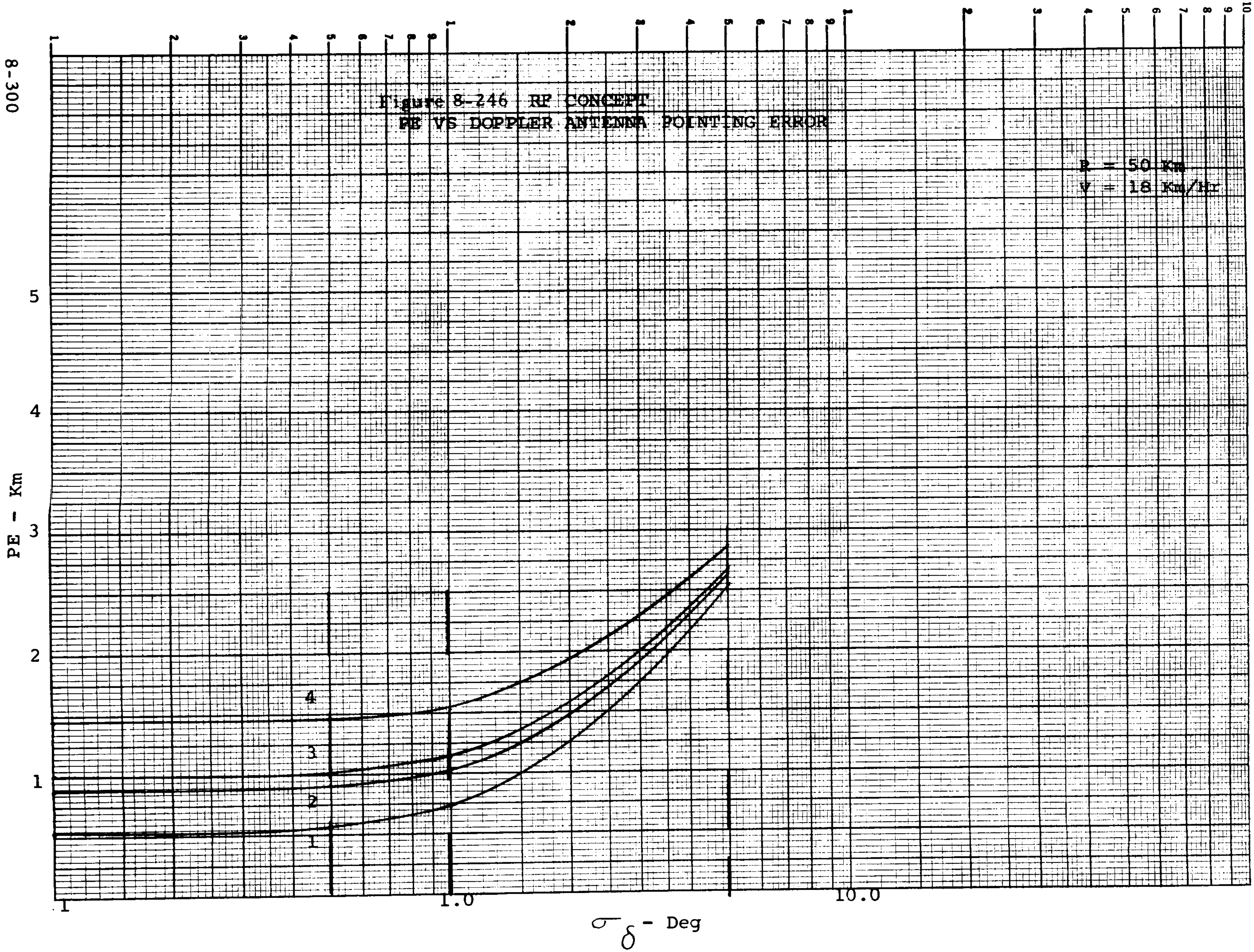

Figure 8-246 RF CONCEPT
PE VS DOPPLER ANTENNA POINTING ERROR

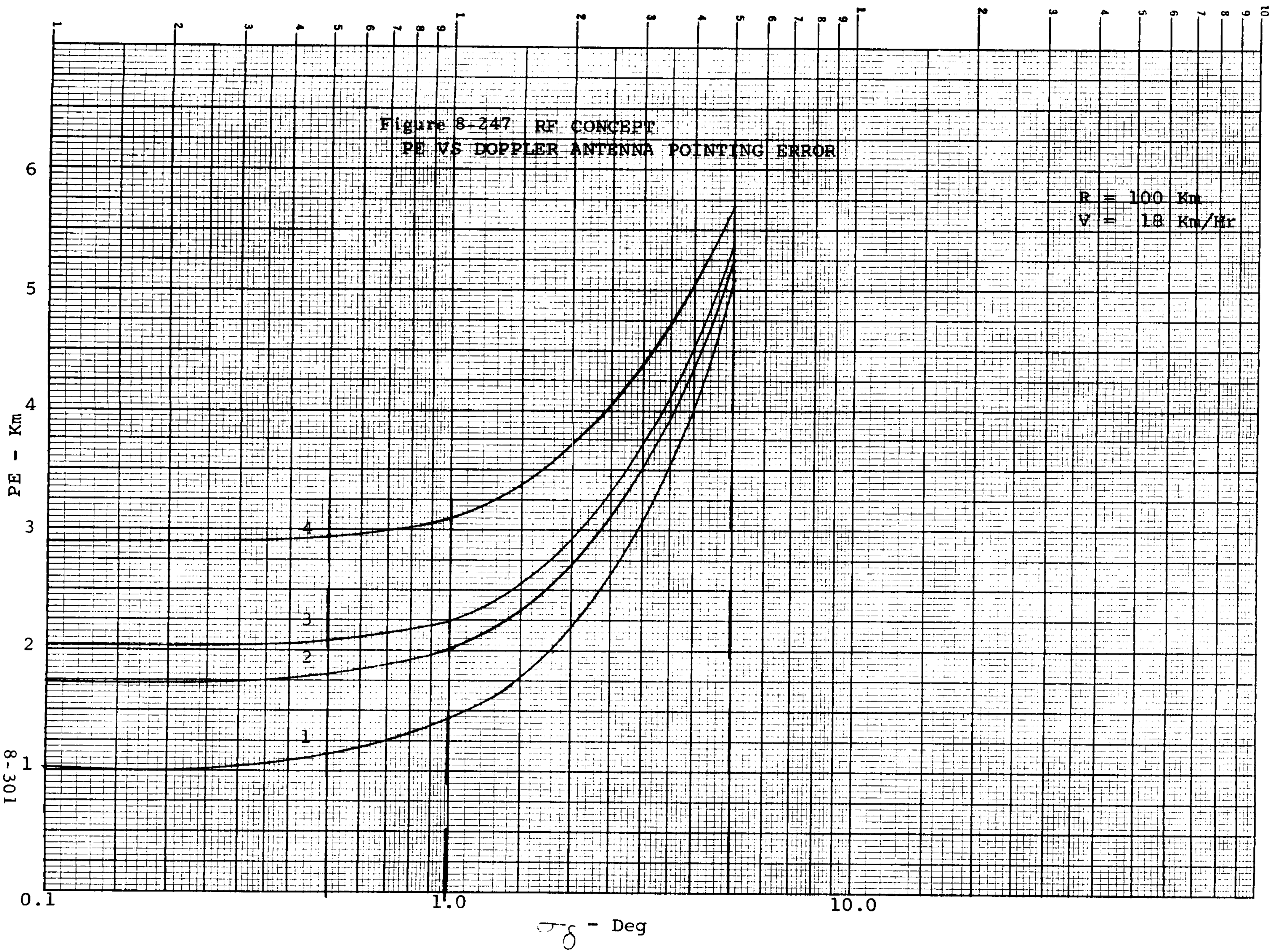

Figure 8-247 RF CONCEPT
PE VS DOPPLER ANTENNA POINTING ERROR

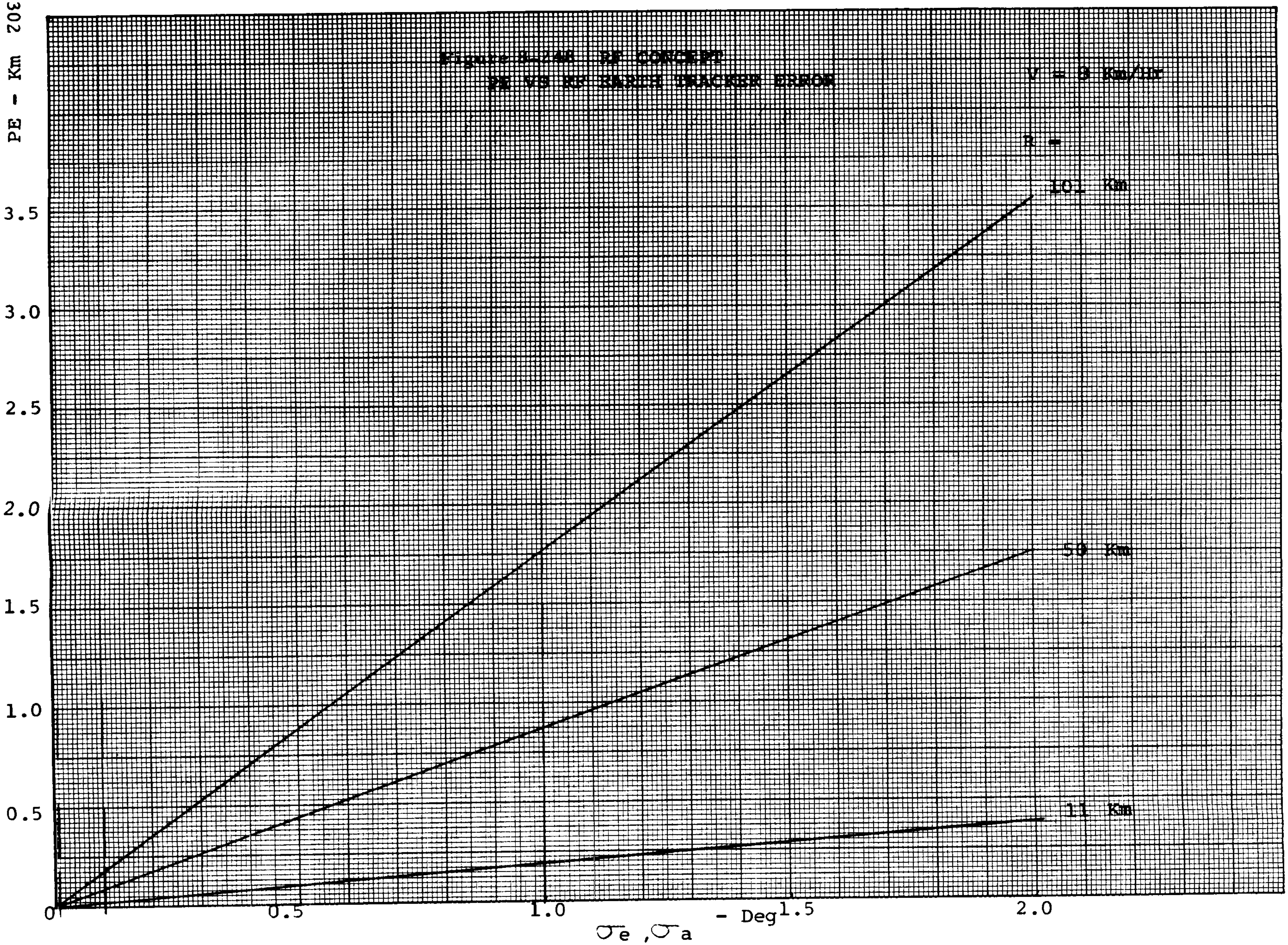

Figure 8-248 RF CONCEPT
PE VS RF EARTH TRACKER ERROR
V = 8 Km/Hr
R =
101 Km
50 Km
11 Km
PE - Km
3.5
3.0
2.5
2.0
1.5
1.0
0.5
0
0.5
1.0
1.5
2.0
σ_e, σ_a - Deg

Figure 8-249 RF CONCEPT
PE VS RF EARTH TRACKER ERROR

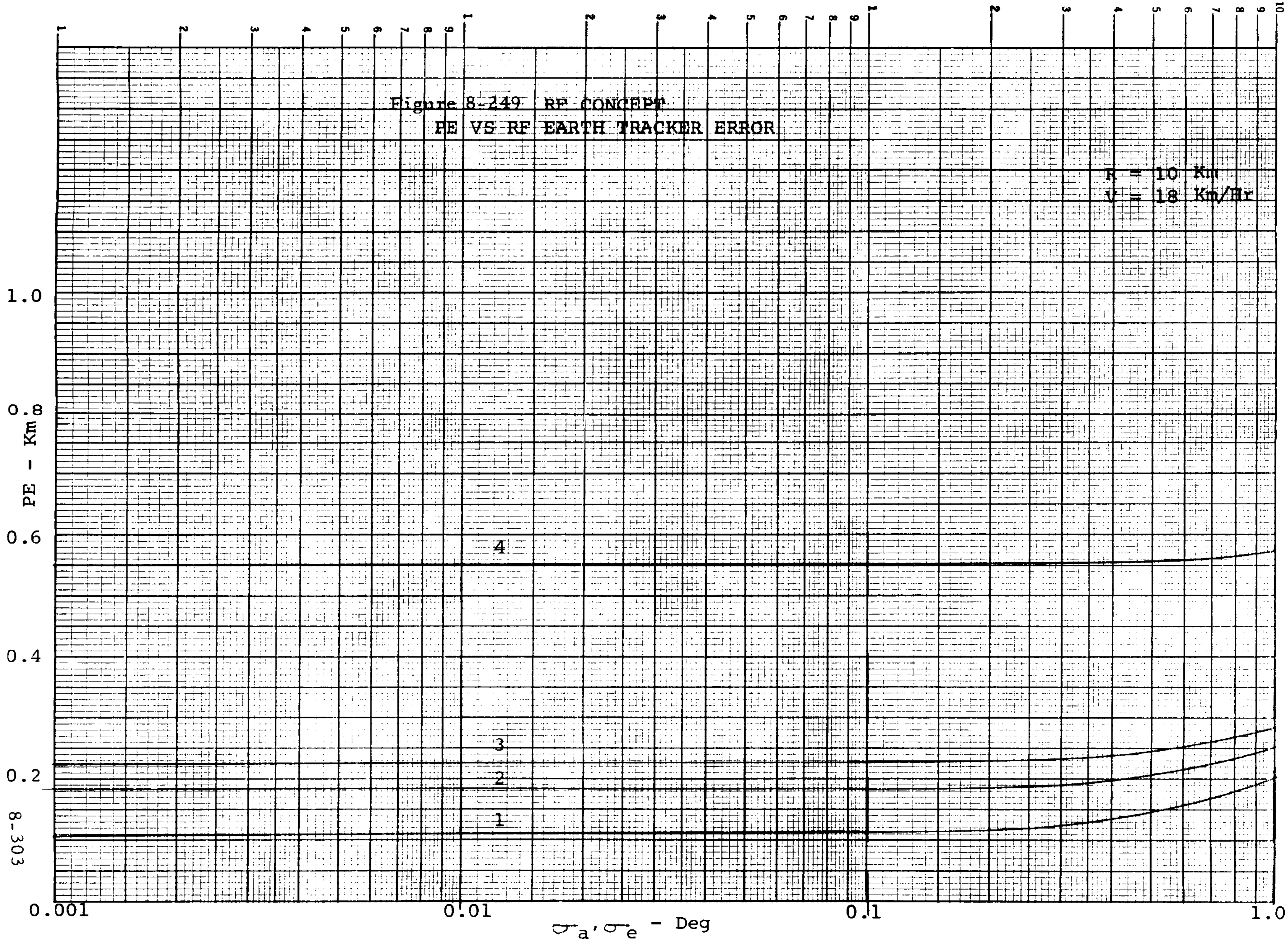

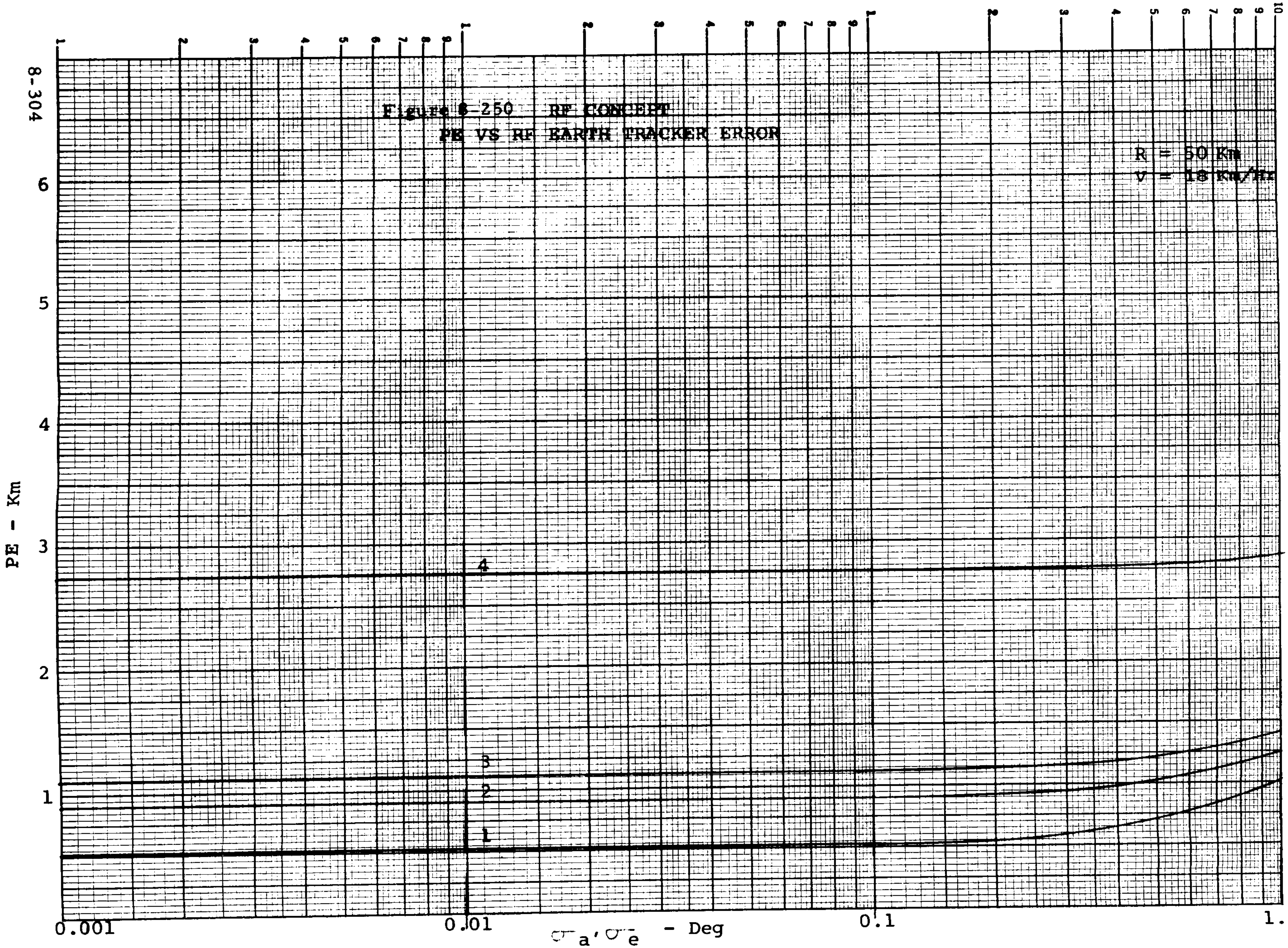

Figure 8-250 RF CONCEPT
PE VS RF EARTH TRACKER ERROR

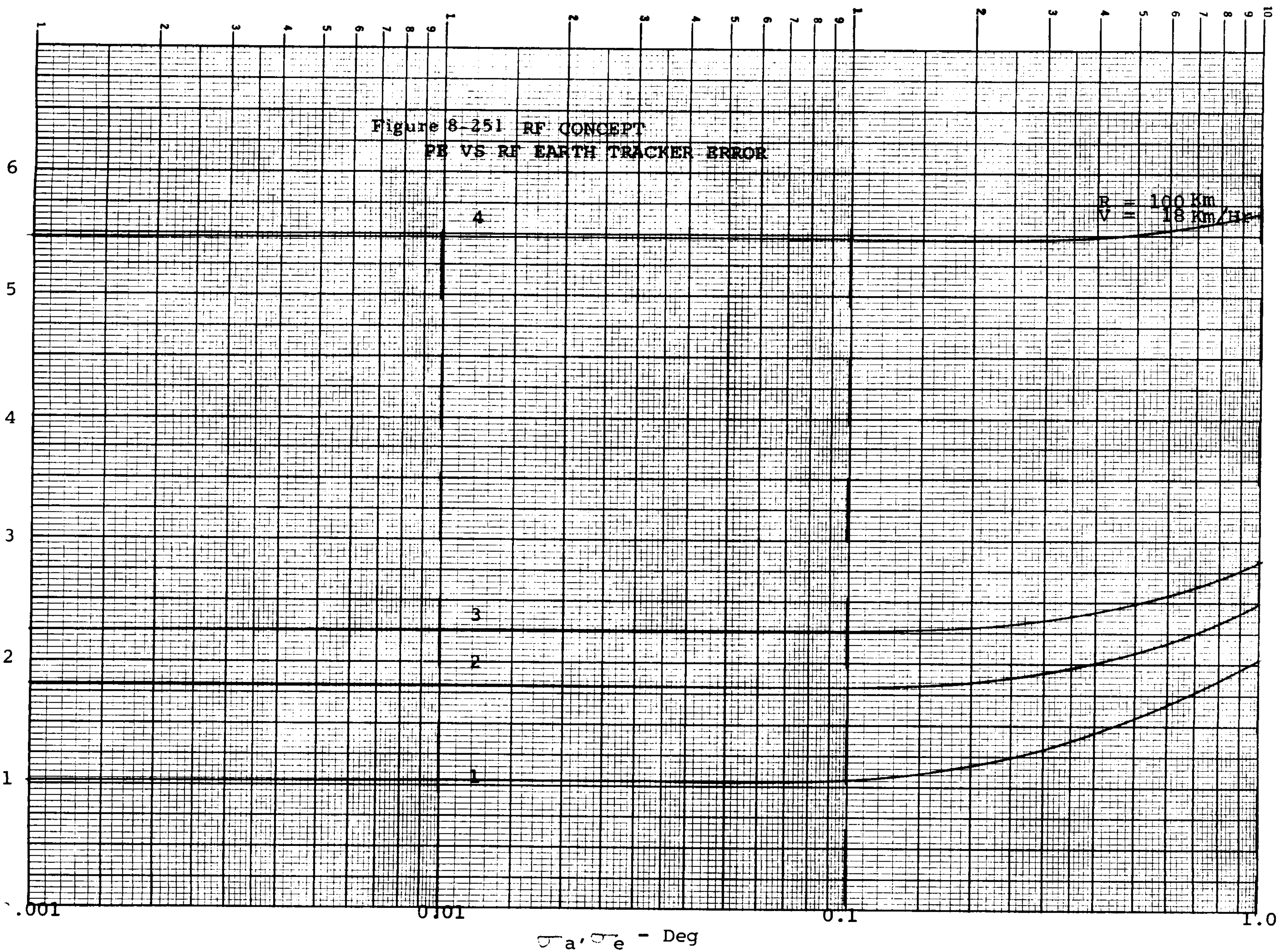
Figure 8-251 RF CONCEPT
PE VS RF EARTH TRACKER ERROR
R = 100 Km
V = 18 Km/Hr
4
3
2
1
6
5
4
3
2
1
PE - Km
.001
0.01
0.1
1.0
σ_a, σ_e - Deg

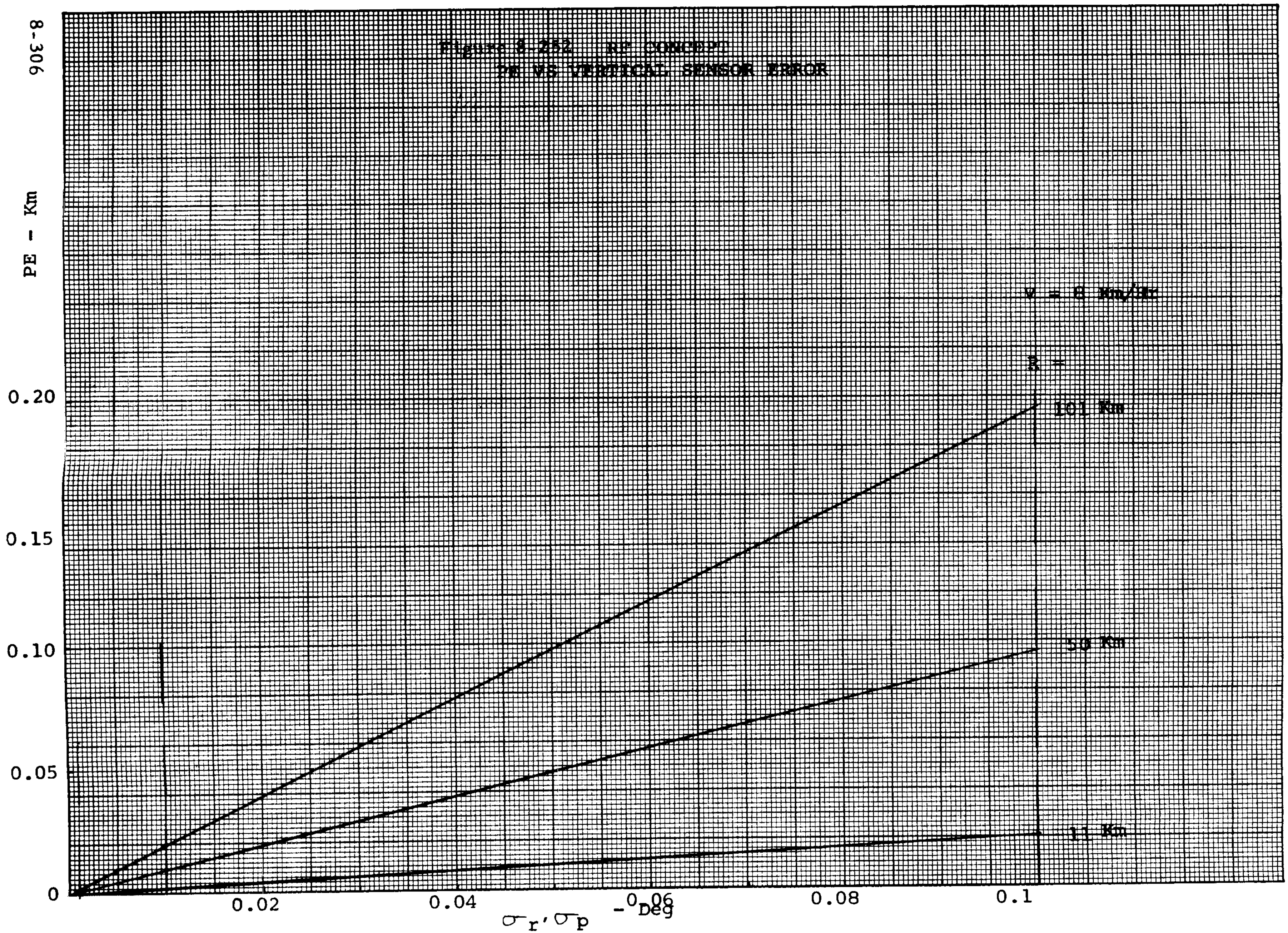

Figure 8-252 RF CONCEPT
PE VS VERTICAL SENSOR ERROR

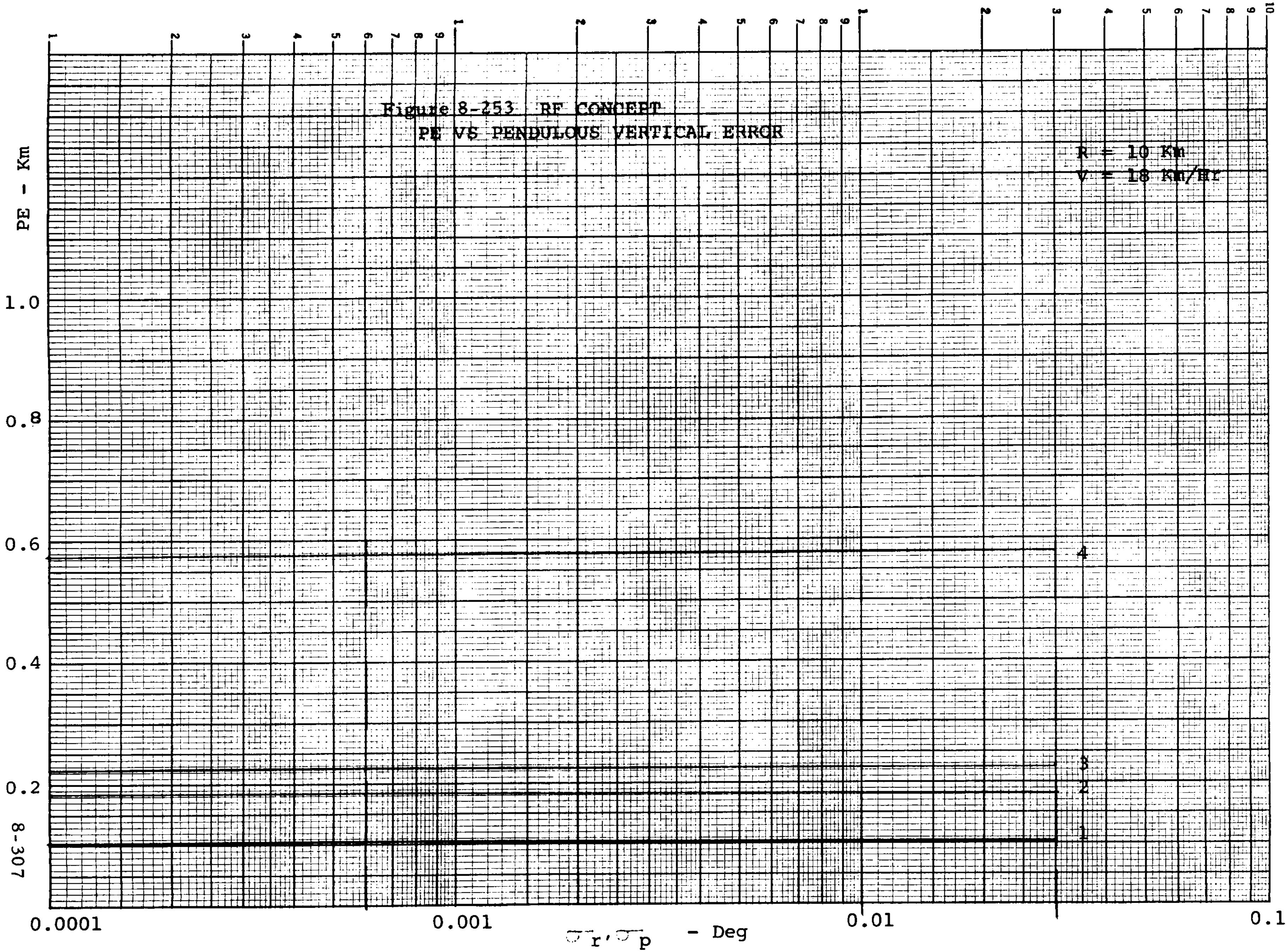

Figure 8-253 RF CONCEPT
PE VS PENDULOUS VERTICAL ERROR

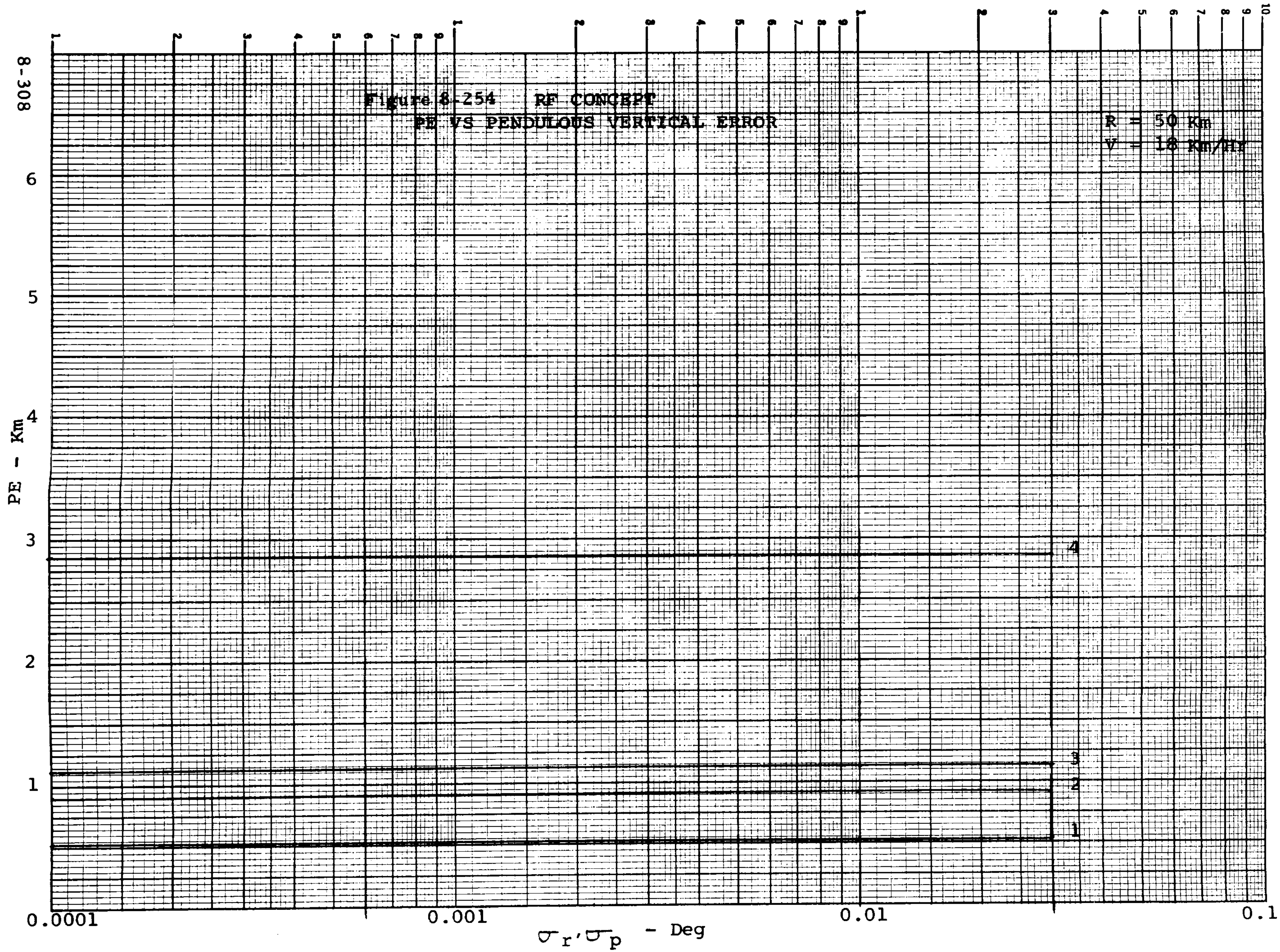
Figure 8-254 RF CONCEPT
PE VS PENDULOUS VERTICAL ERROR
R = 50 Km
V = 18 Km/Hr
PE - Km
σ_r, σ_p - Deg
0.0001
0.001
0.01
0.1
1
2
3
4
5
6
1
2
3
4

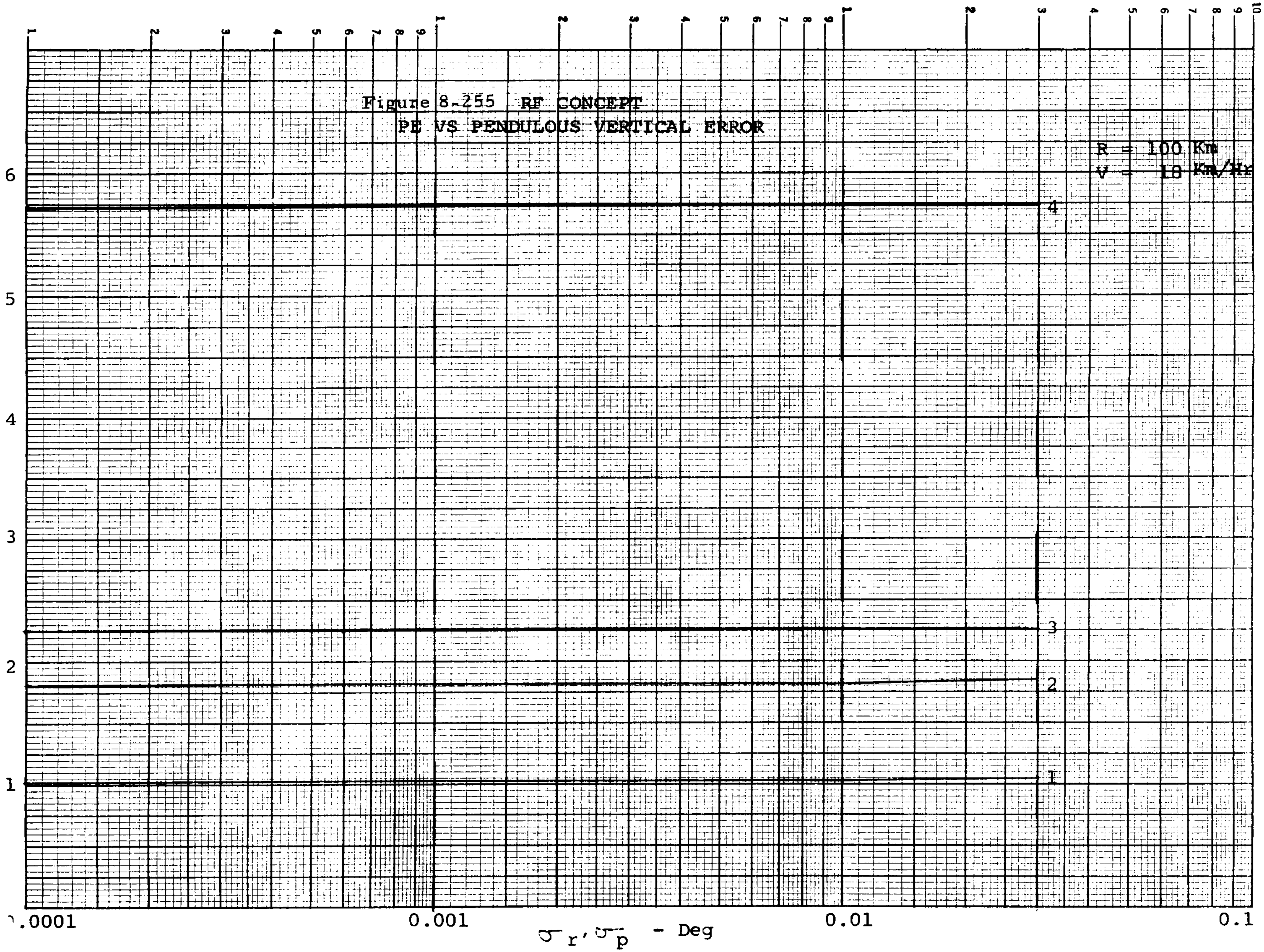
Figure 8-255 RF CONCEPT
PE VS PENDULOUS VERTICAL ERROR
R = 100 Km
V = 18 Km/Hr
4
3
2
1
PE - Km
6
5
4
3
2
1
.0001
0.001
0.01
0.1
σr, σp - Deg

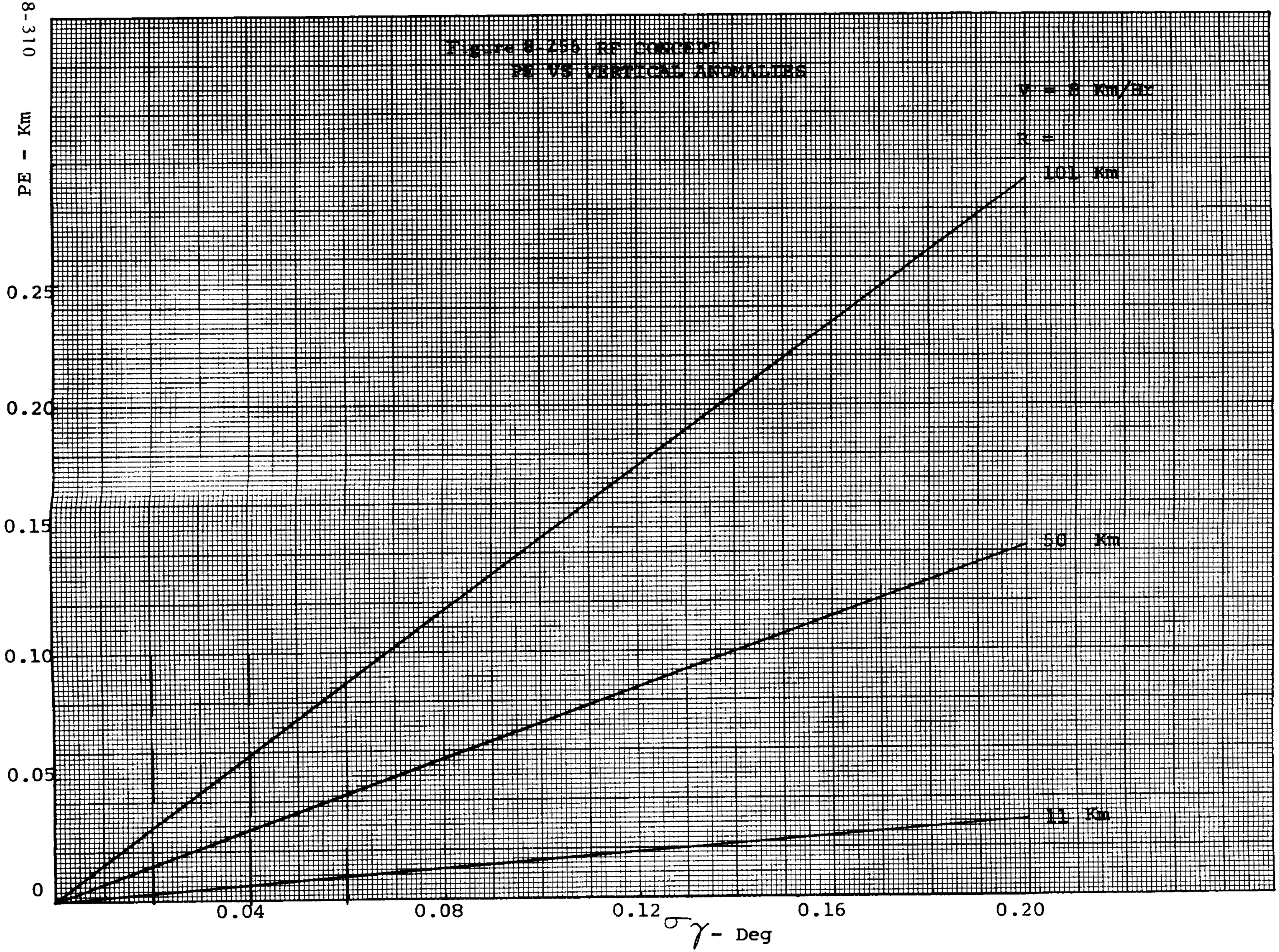

Figure 8-256 RF CONCEPT
PE VS VERTICAL ANOMALIES

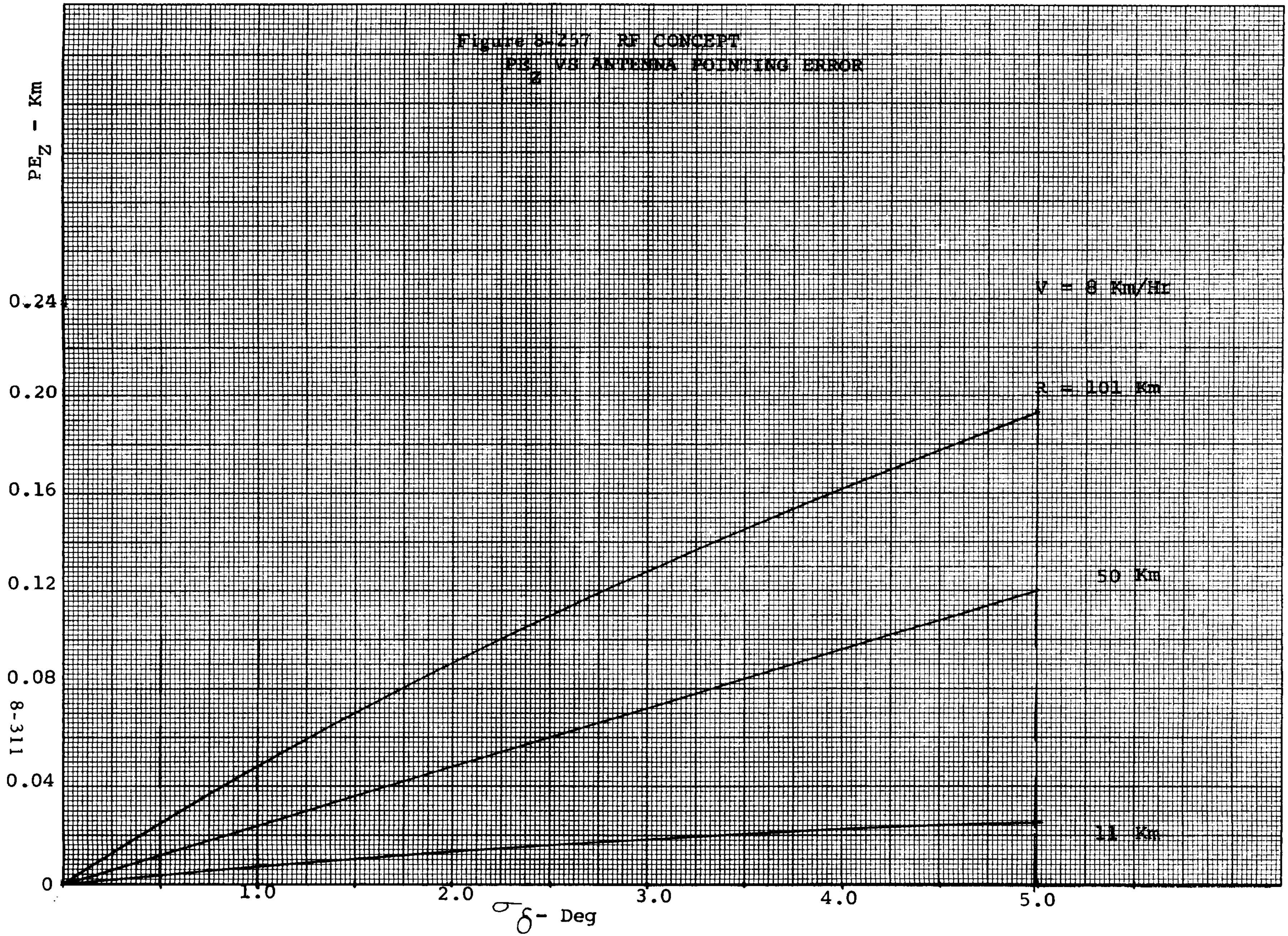

Figure 8-257 RF CONCEPT
PE_Z VS ANTENNA POINTING ERROR

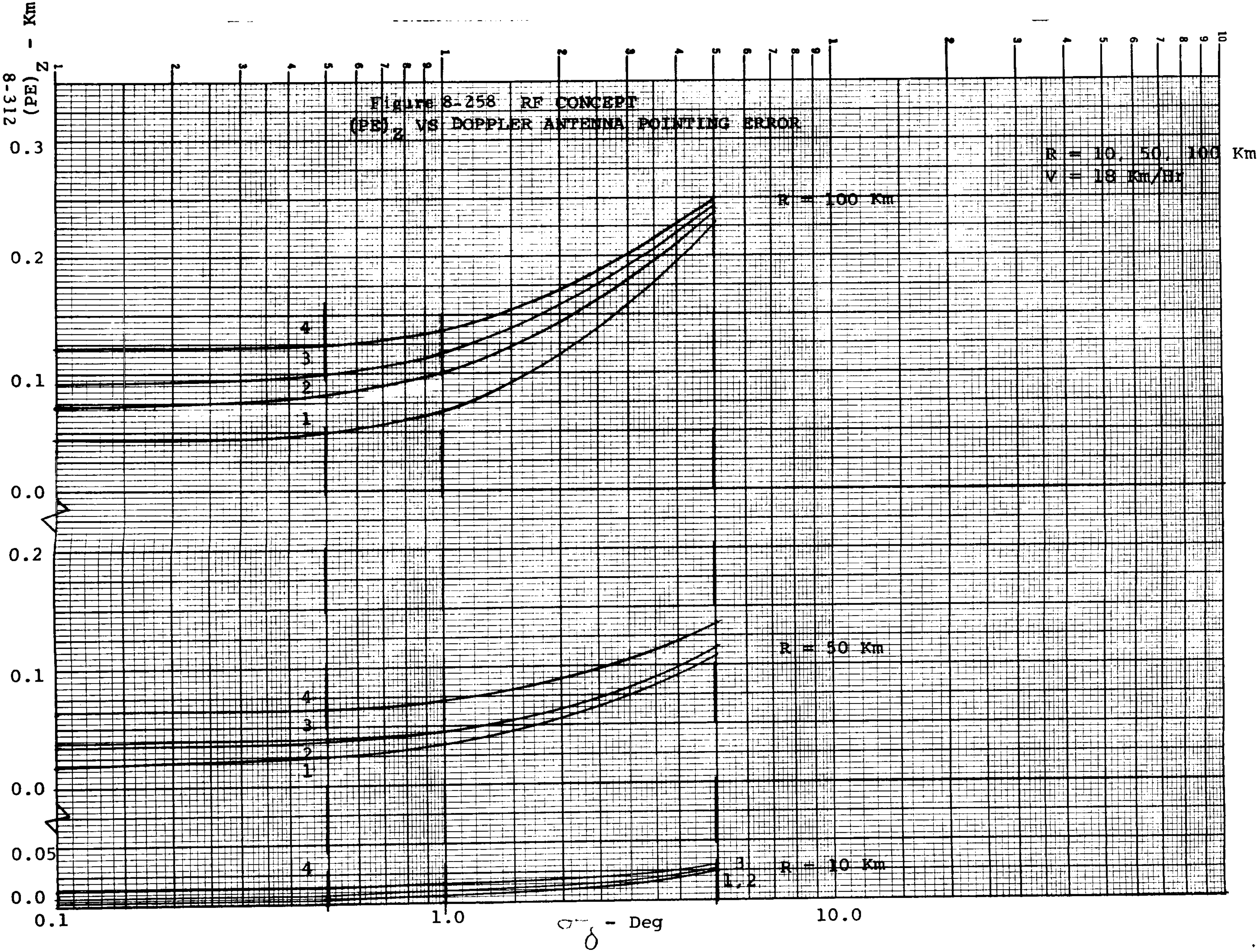

Figure 8-258 RF CONCEPT
$(PE)_Z$ VS DOPPLER ANTENNA POINTING ERROR

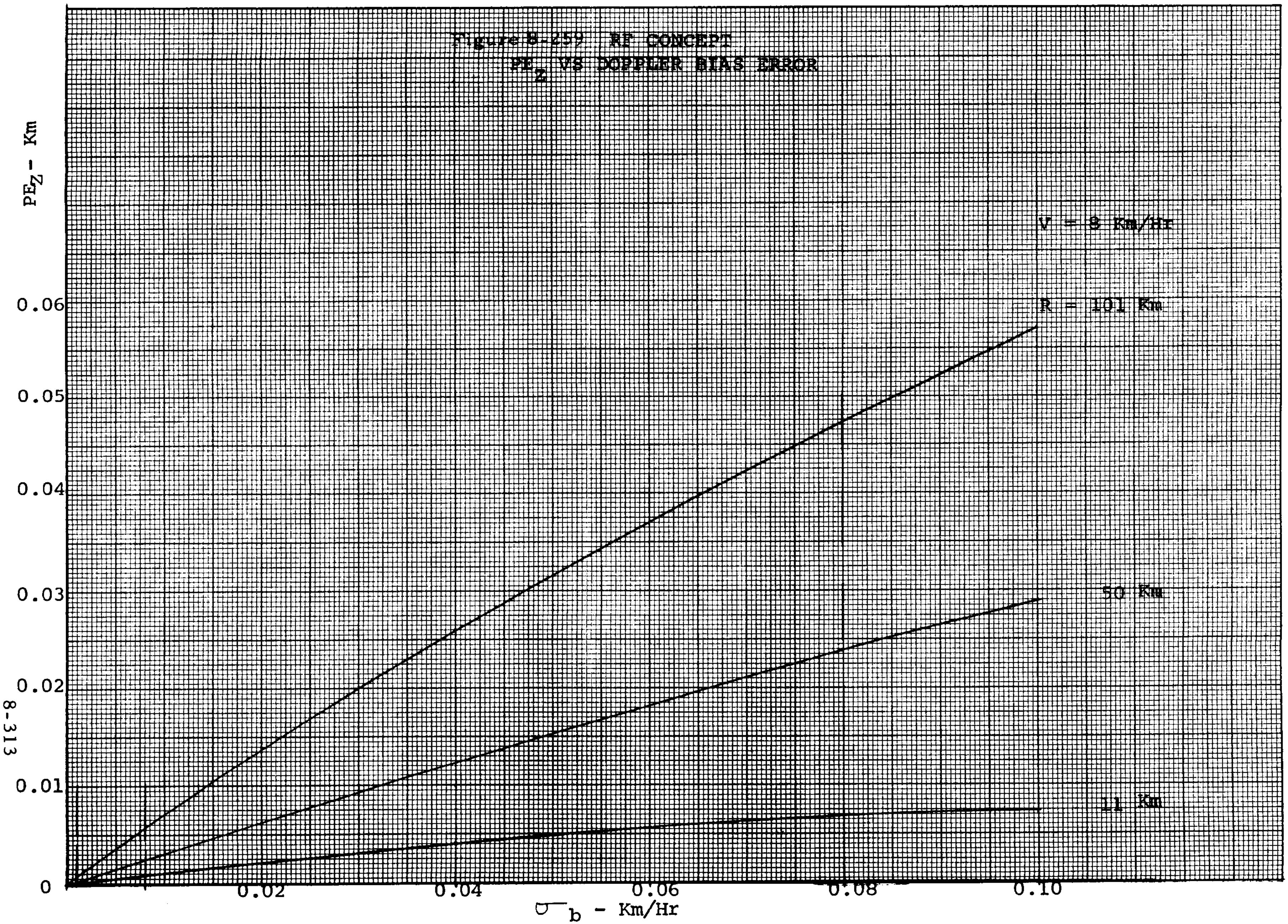

Figure 8-259 RF CONCEPT
PE_Z VS DOPPLER BIAS ERROR

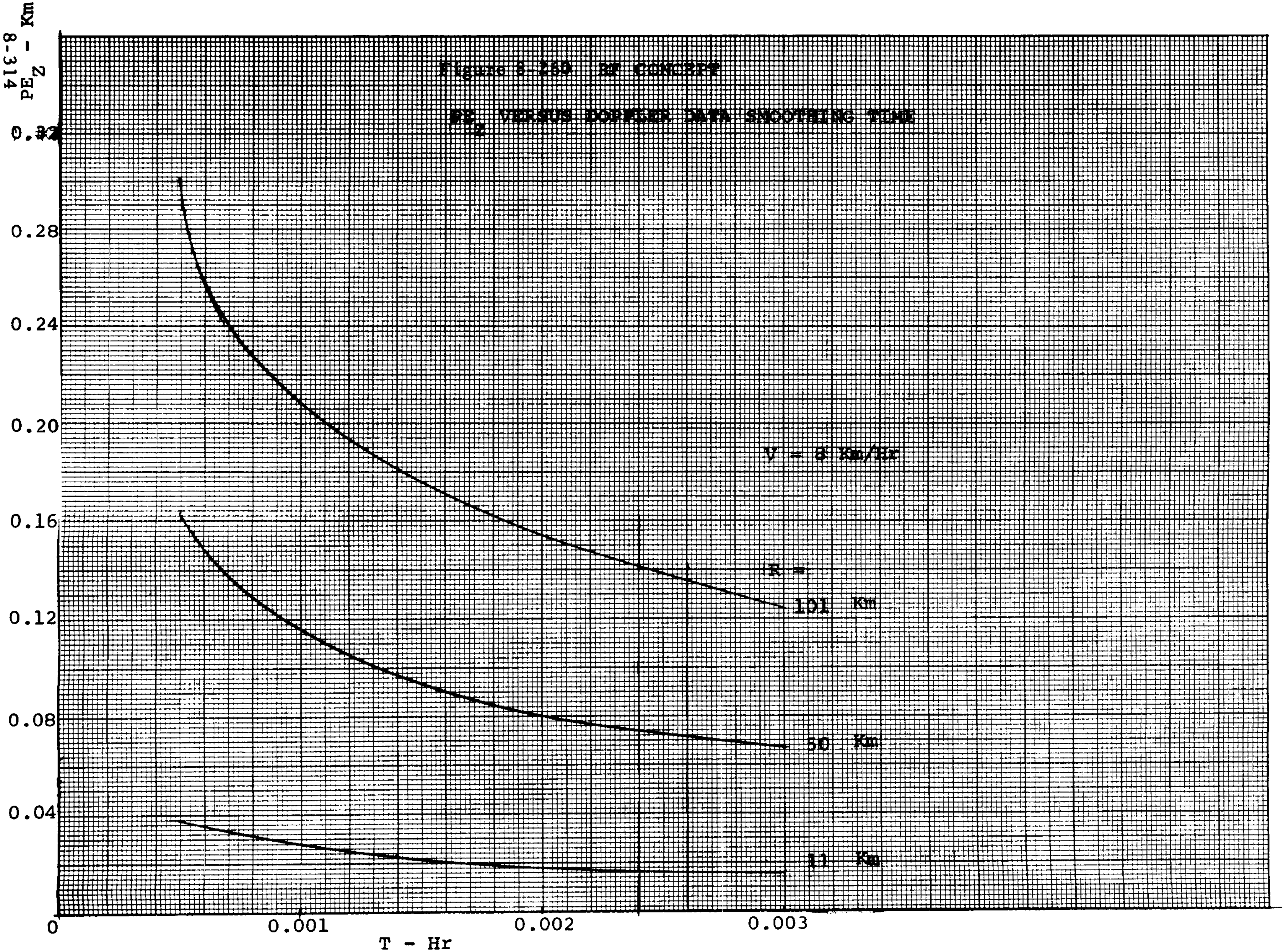

Figure 8-260 RF CONCEPT

PE_Z VERSUS DOPPLER DATA SMOOTHING TIME

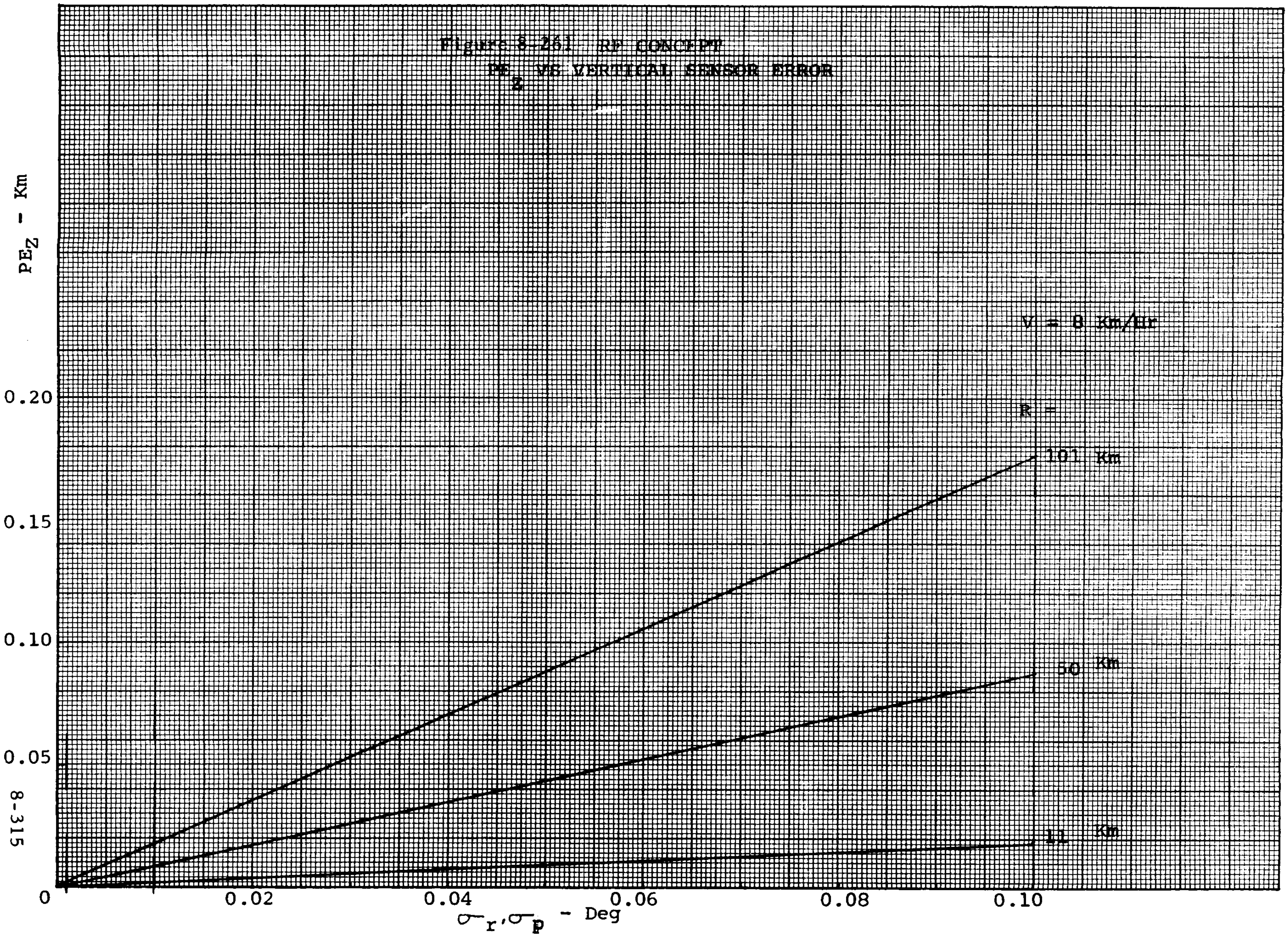
Figure 8-261 RF CONCEPT
PE_Z VS VERTICAL SENSOR ERROR
V = 8 Km/Hr
R =
101 Km
50 Km
11 Km
PE_Z - Km
0.20
0.15
0.10
0.05
0
0.02
0.04
0.06
0.08
0.10
σ_r, σ_p - Deg

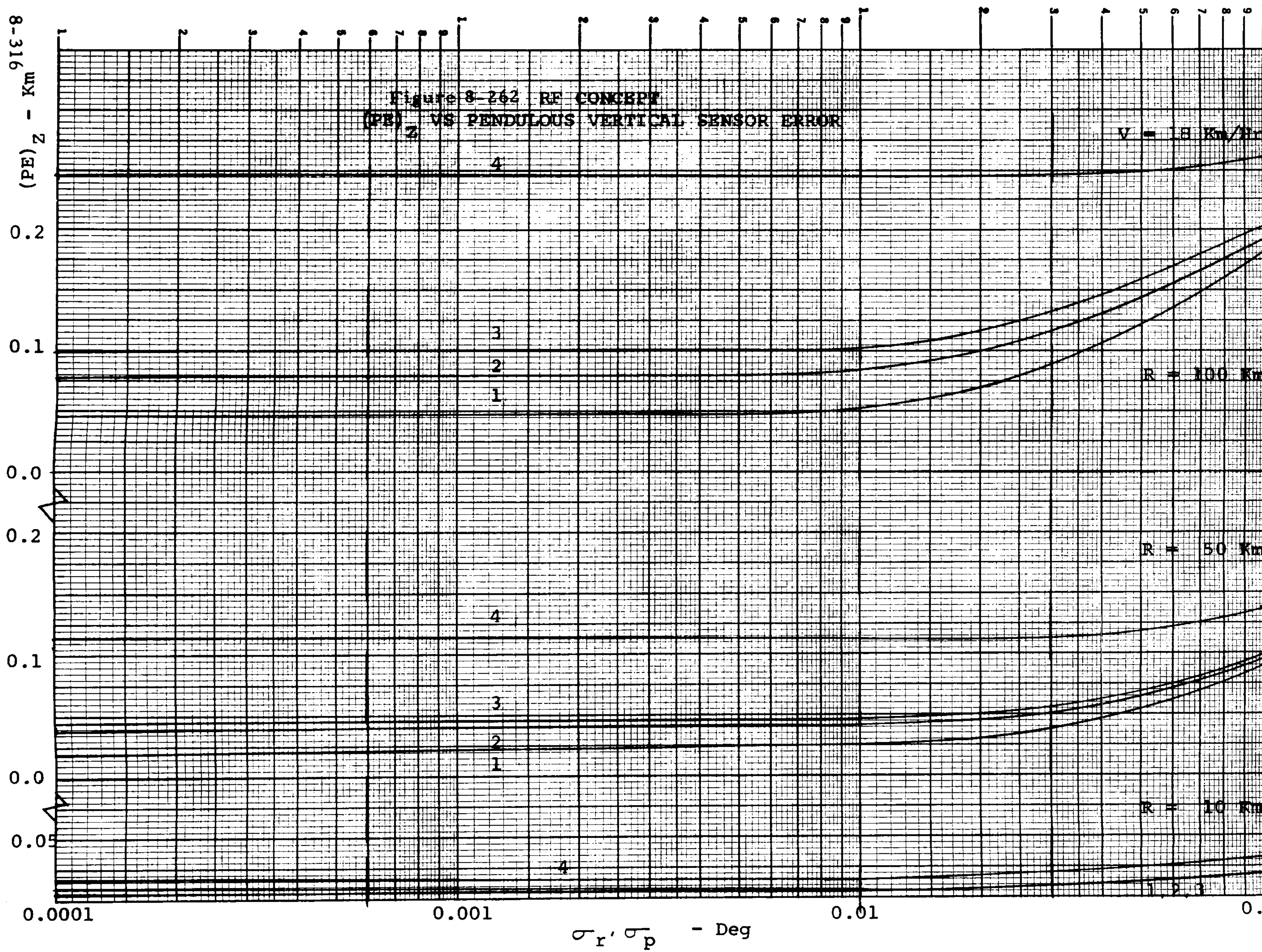

Figure 8-262 RF CONCEPT
$(PE)_Z$ VS PENDULOUS VERTICAL SENSOR ERROR

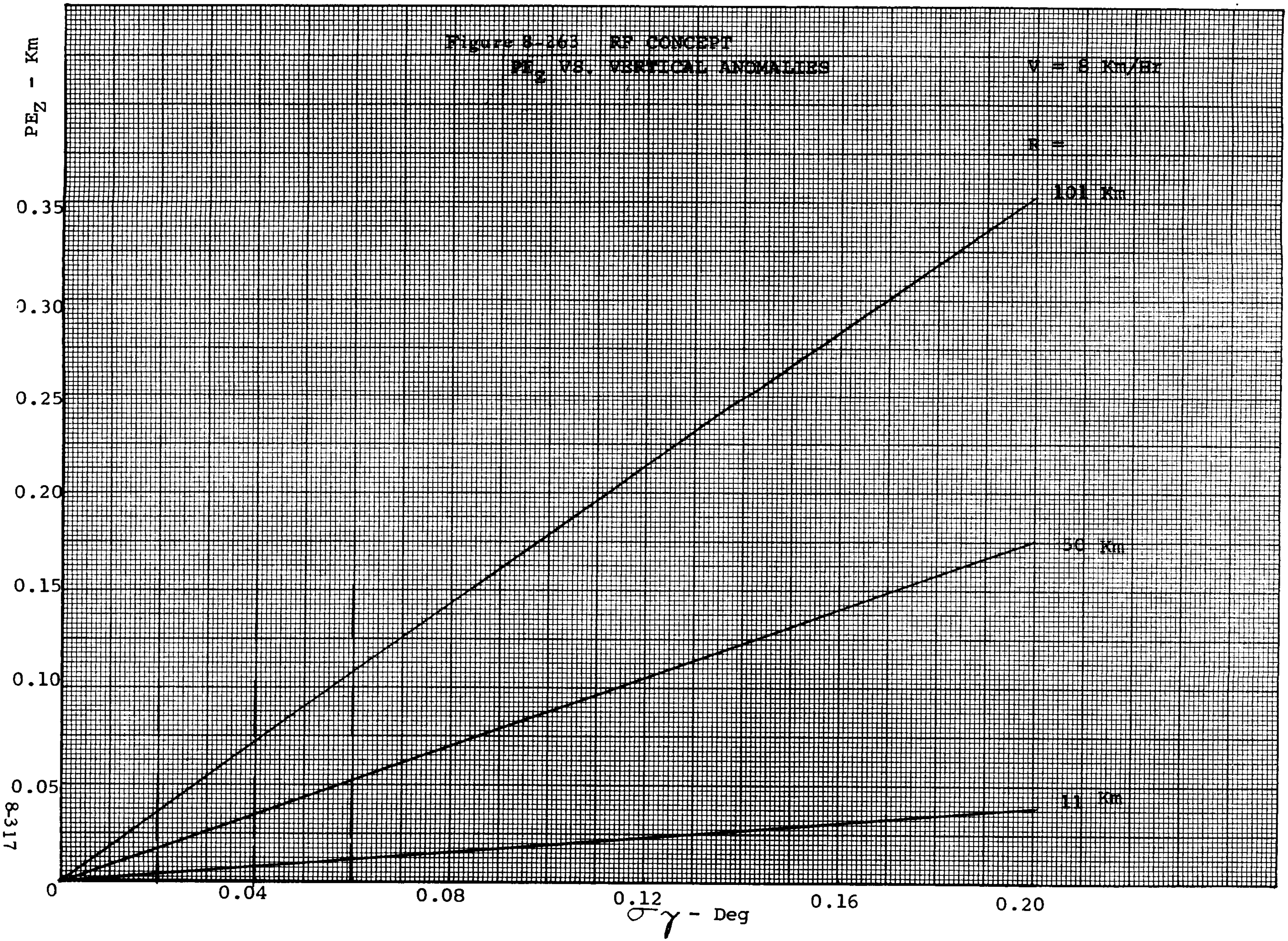

Figure 8-263 RF CONCEPT
PE_z VS. VERTICAL ANOMALIES

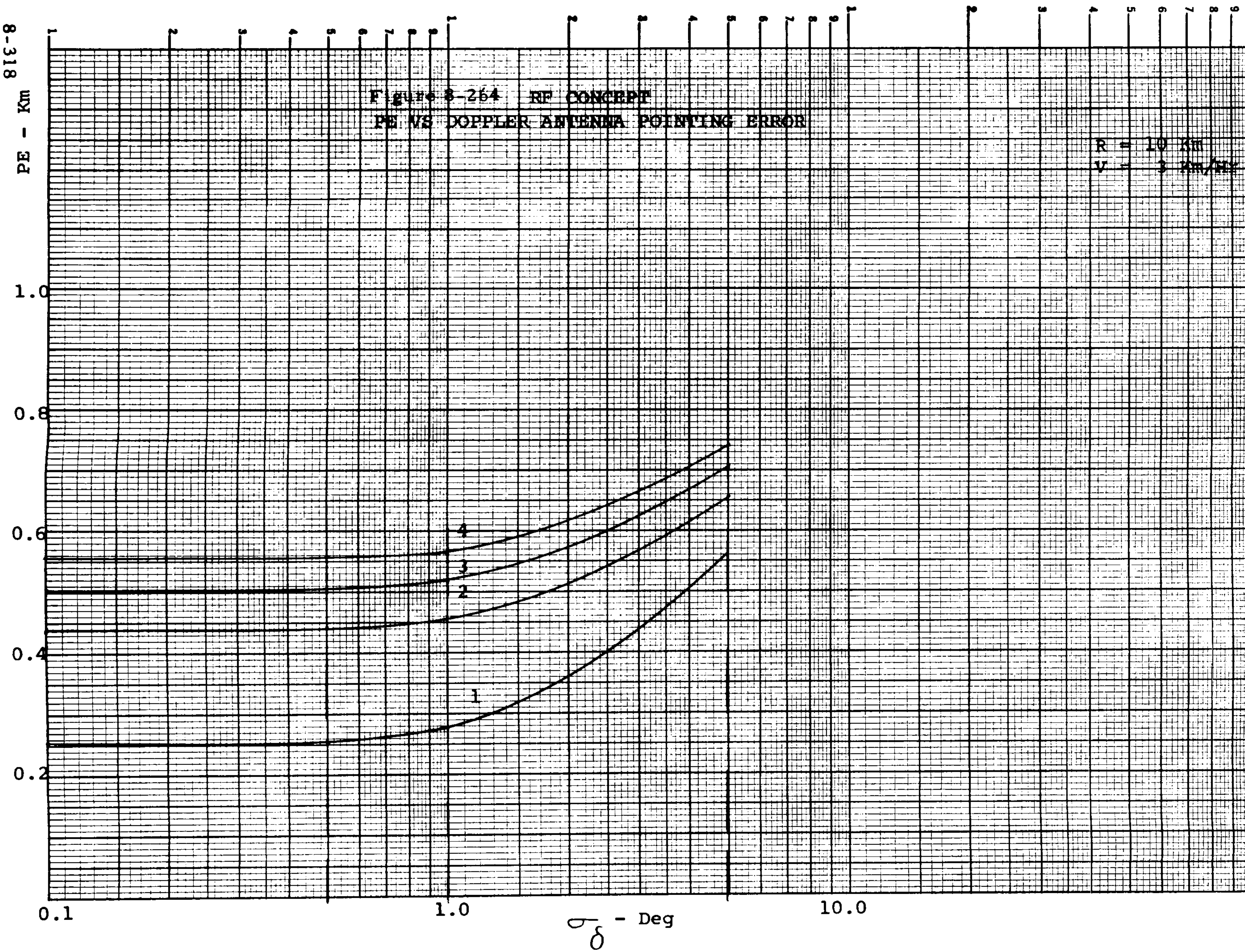

Figure 8-264 RF CONCEPT
PE VS DOPPLER ANTENNA POINTING ERROR

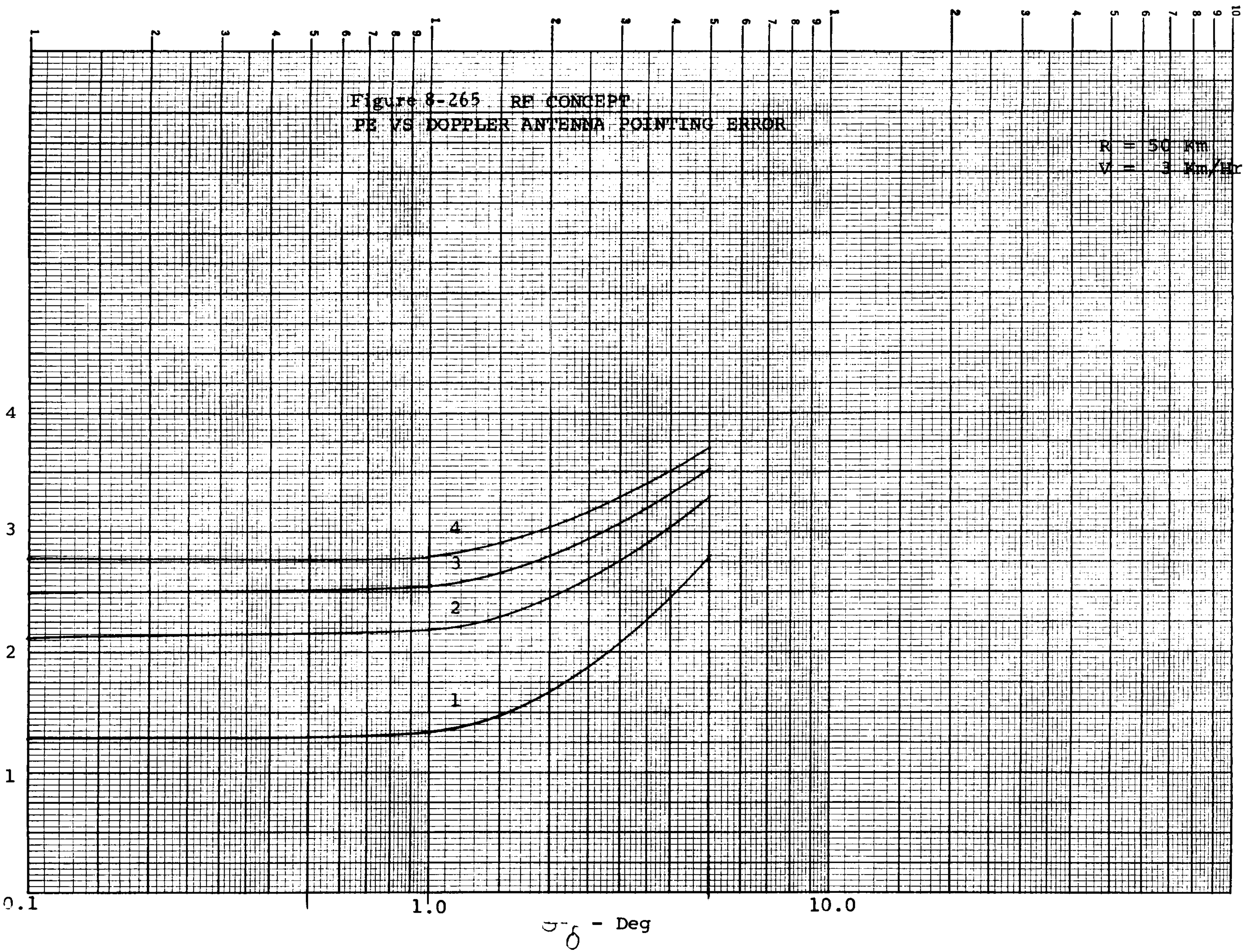

Figure 8-265 RF CONCEPT
PE VS DOPPLER ANTENNA POINTING ERROR

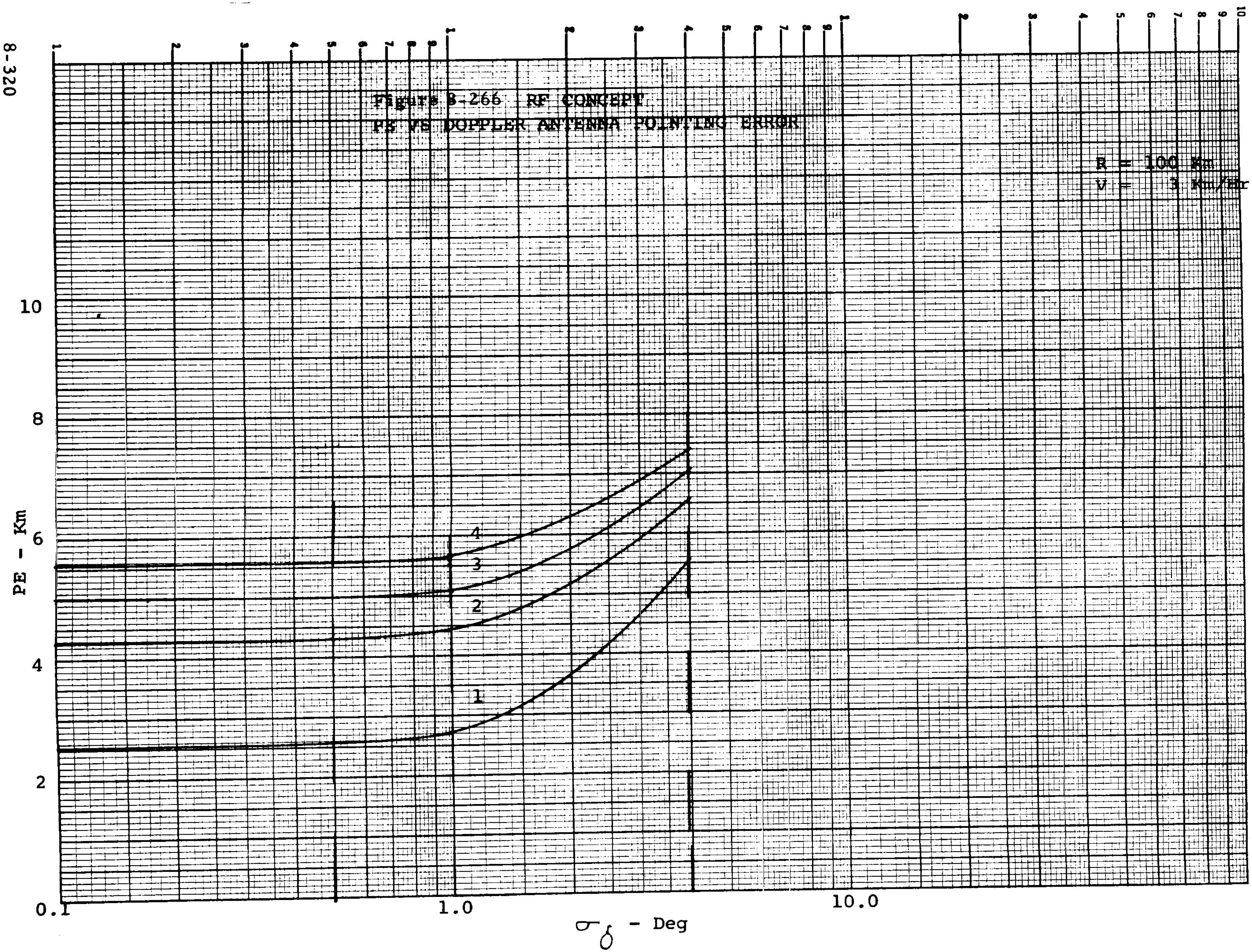

Figure 8-266 RF CONCEPT
PE VS DOPPLER ANTENNA POINTING ERROR

Figure 8-267 RF CONCEPT
PE VS DOPPLER CALIBRATION ERROR

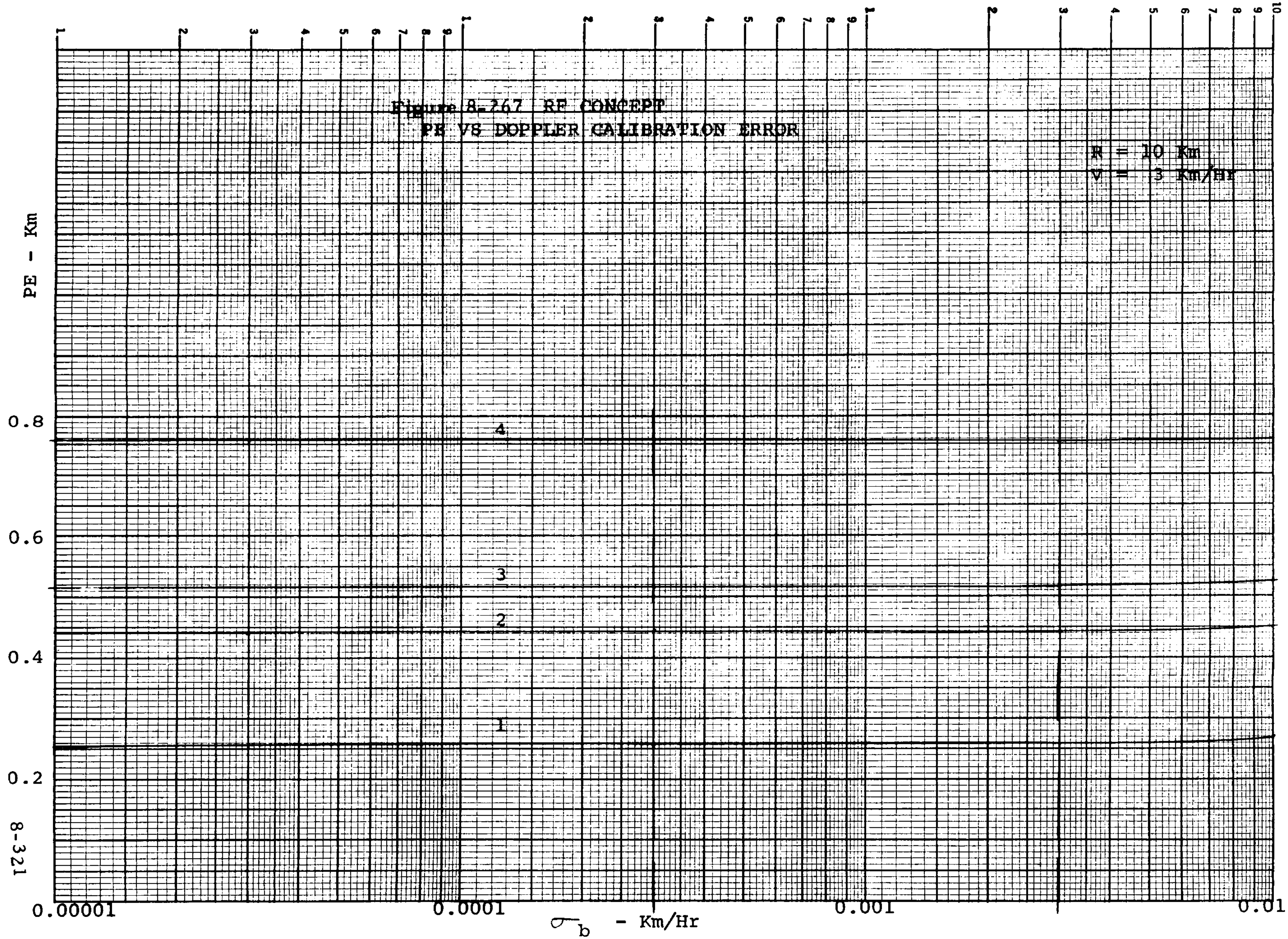

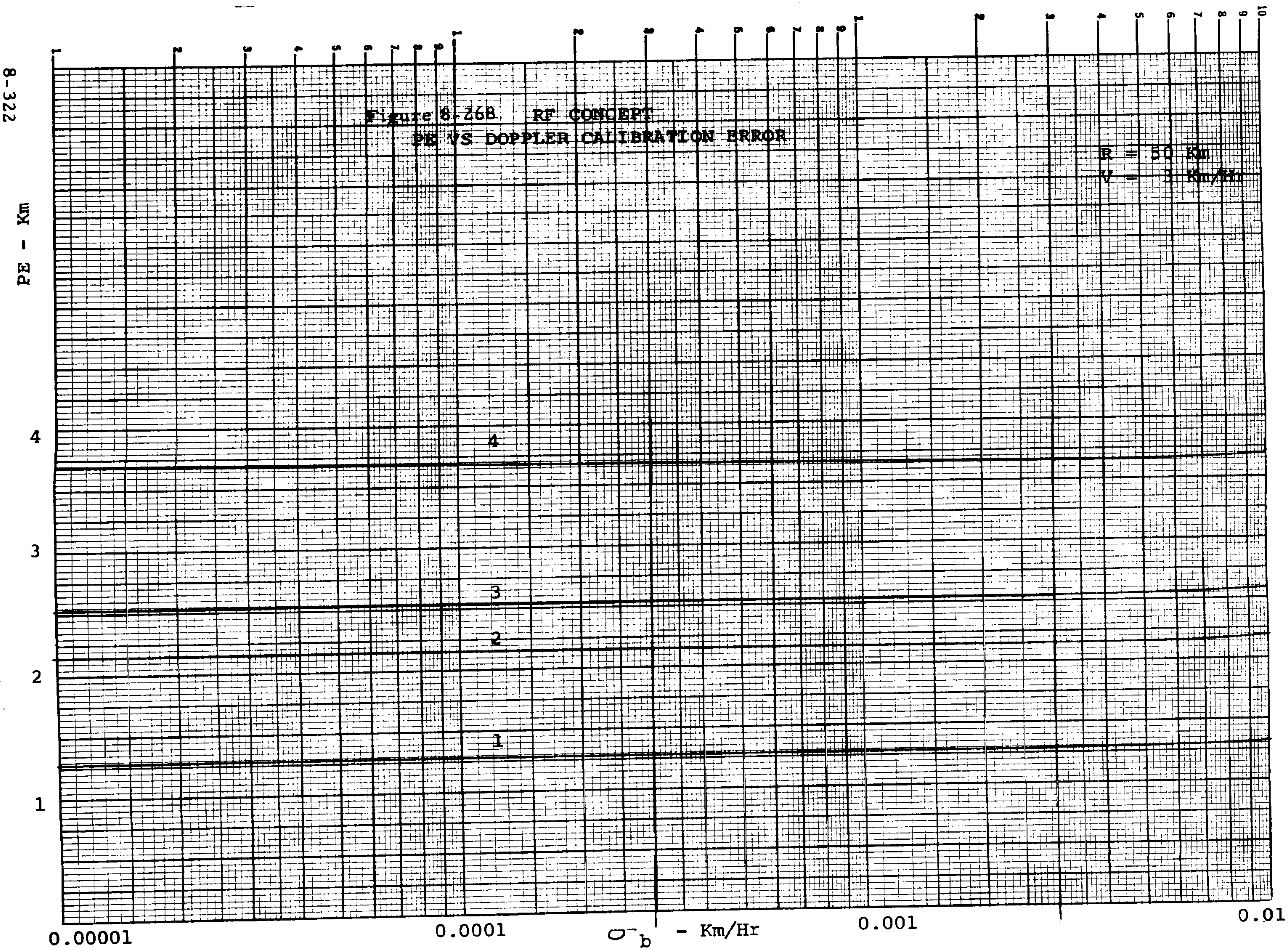

Figure 8-268 RF CONCEPT
PE VS DOPPLER CALIBRATION ERROR

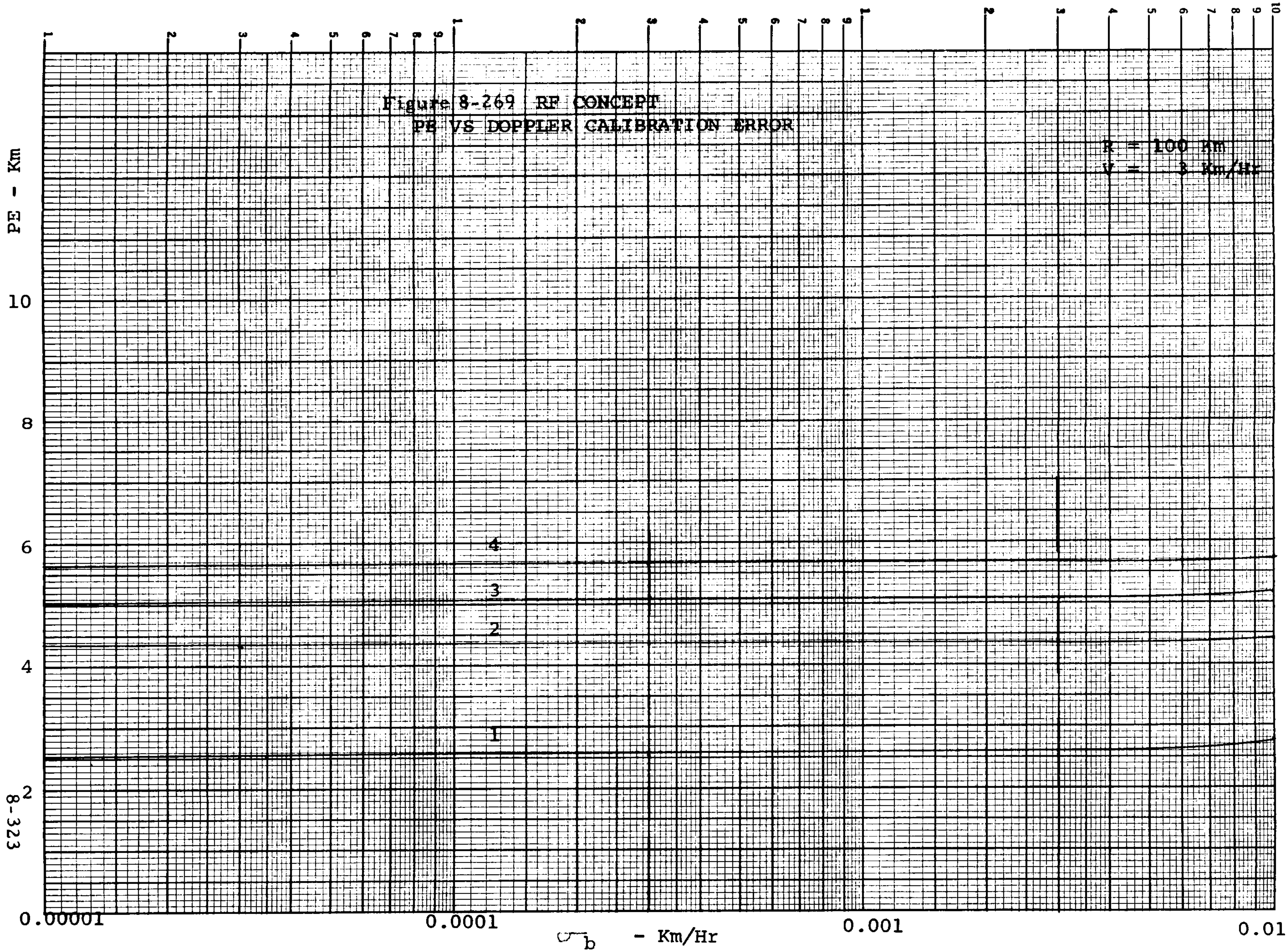

Figure 8-269 RF CONCEPT
PE VS DOPPLER CALIBRATION ERROR
R = 100 Km
V = 3 Km/Hr
PE - Km
10
8
6
4
2
4
3
2
1
0.00001
0.0001
0.001
0.01
σ_b - Km/Hr

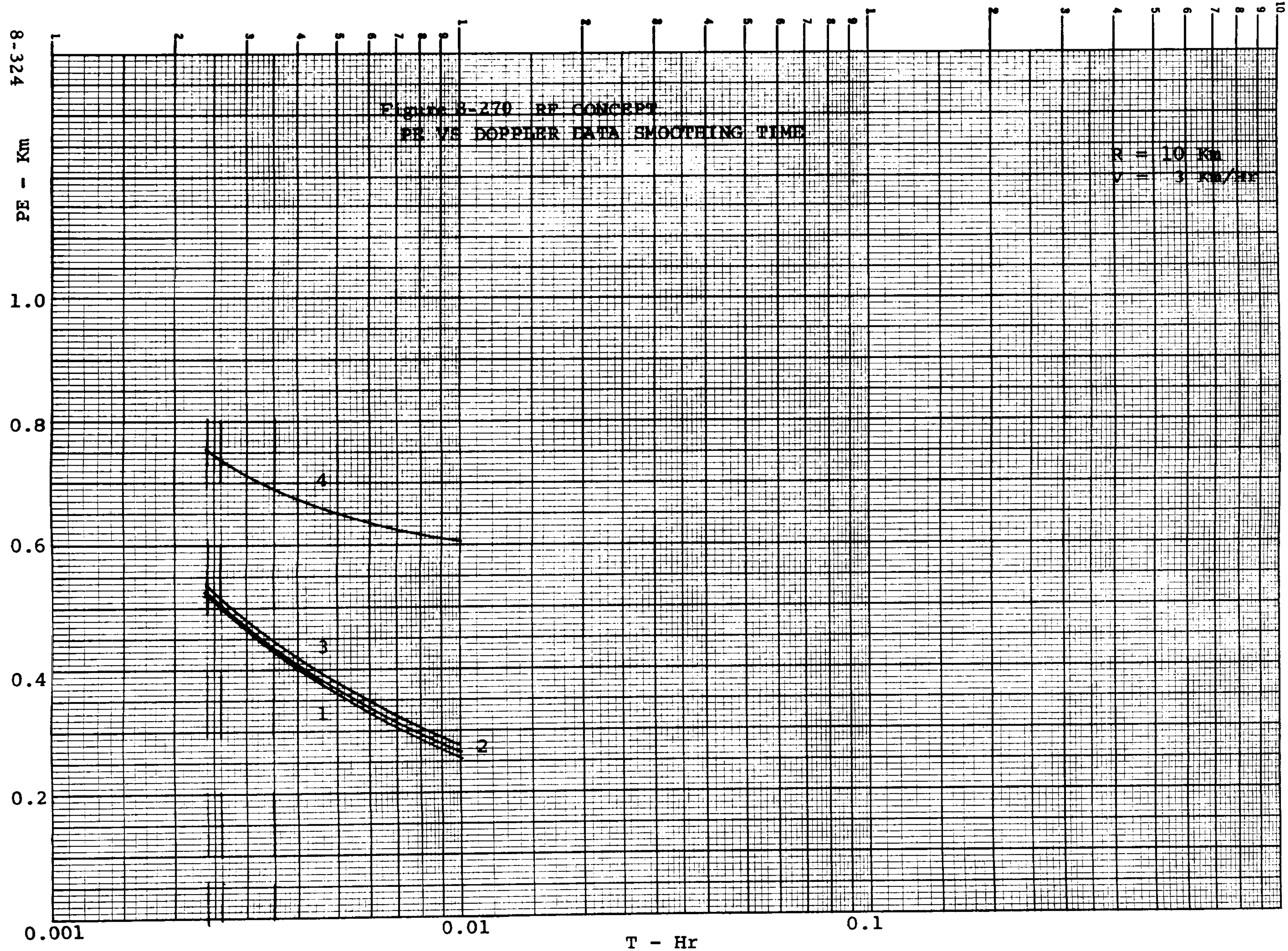
Figure 8-270 RF CONCEPT
PE VS DOPPLER DATA SMOOTHING TIME
R = 10 Km
V = 3 Km/Hr
PE - Km
1.0
0.8
0.6
0.4
0.2
0.001
0.01
0.1
T - Hr
4
3
1
2

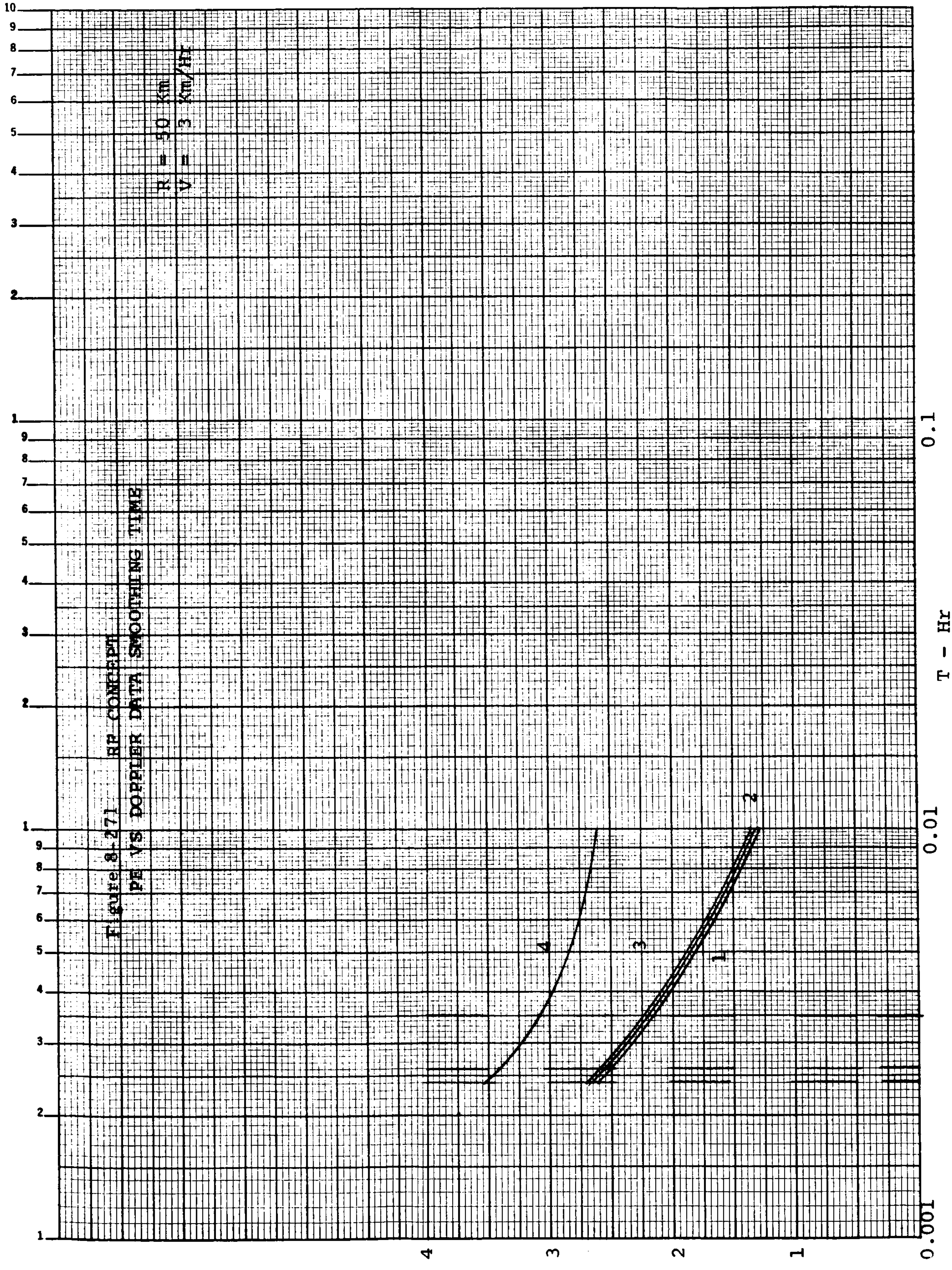

Figure 8-271 RP CONCEPT
PE VS DOPPLER DATA SMOOTHING TIME

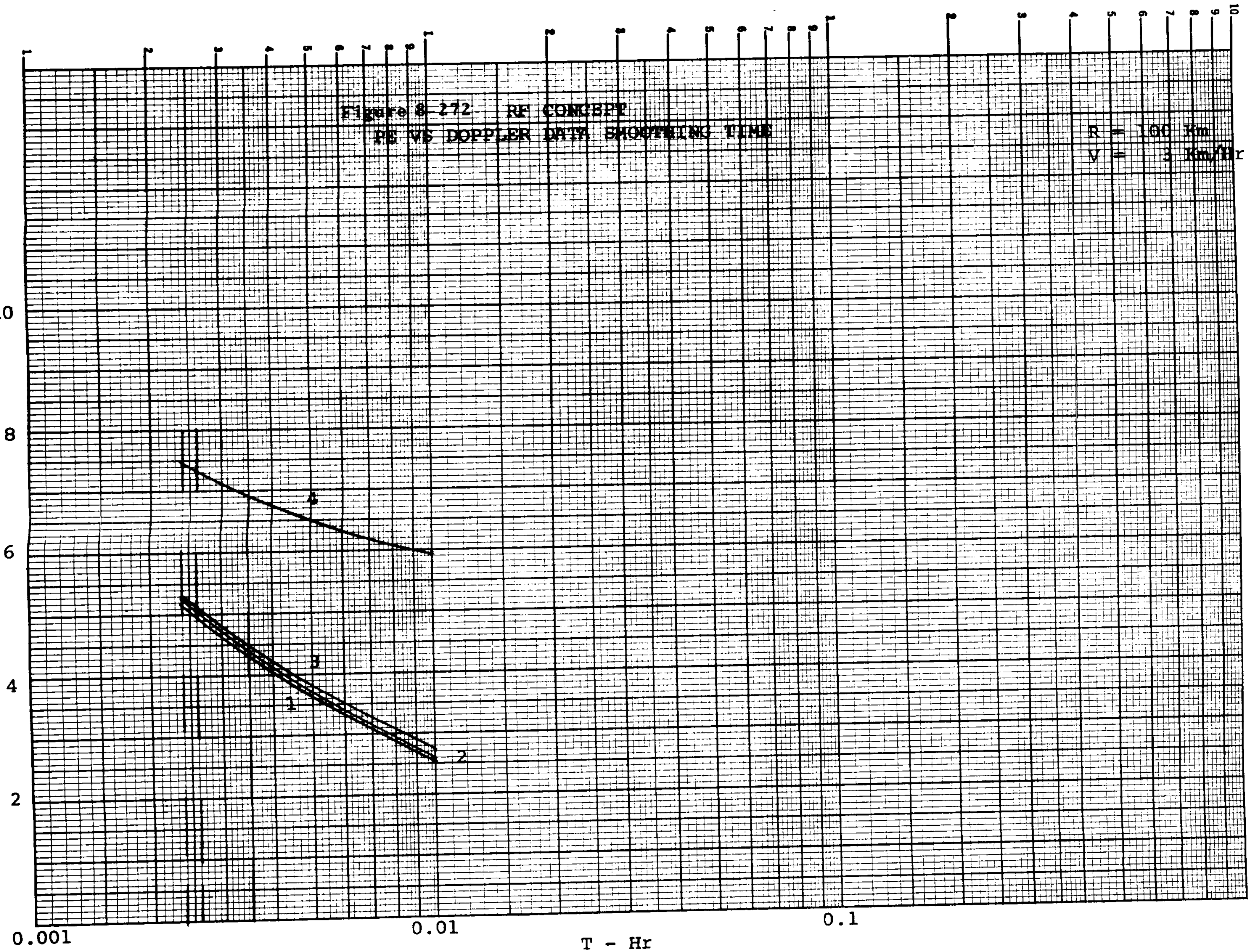

Figure 8-272 RF CONCEPT
PE VS DOPPLER DATA SMOOTHING TIME

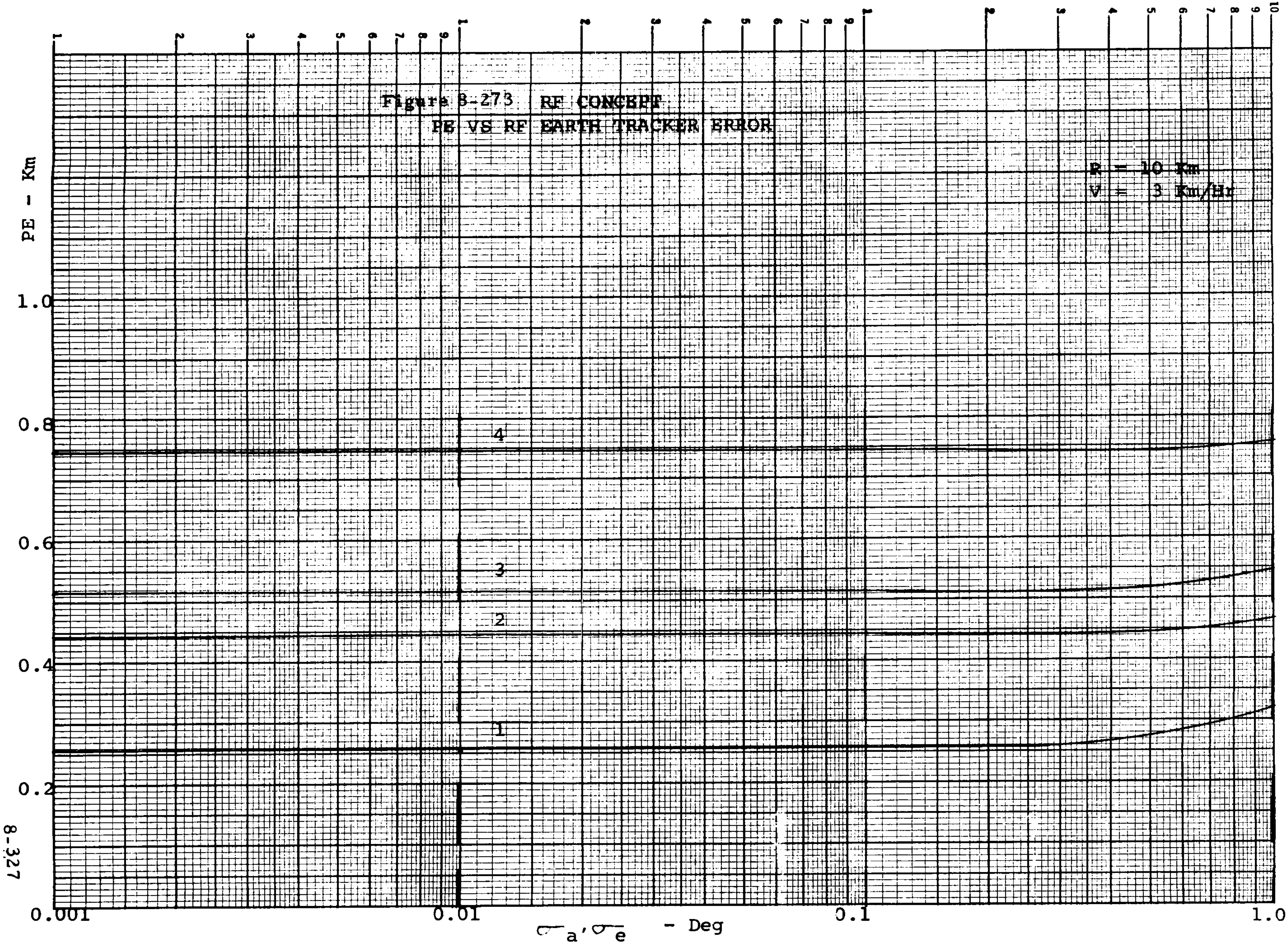

Figure 8-273 RF CONCEPT
PE VS RF EARTH TRACKER ERROR

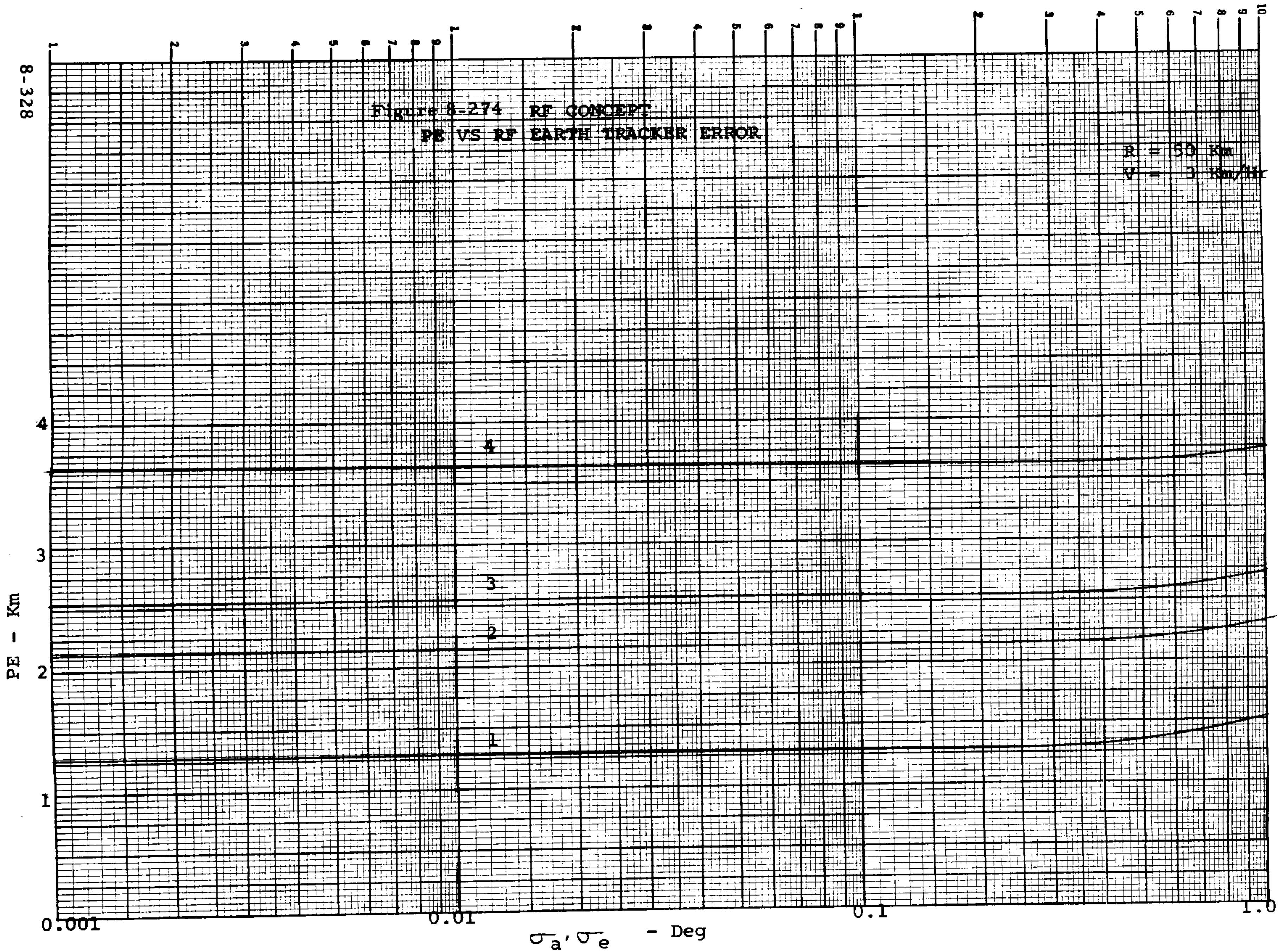

Figure 8-274 RF CONCEPT
PE VS RF EARTH TRACKER ERROR

Figure 8-275 RF CONCEPT
PE VS RF EARTH TRACKER ERROR

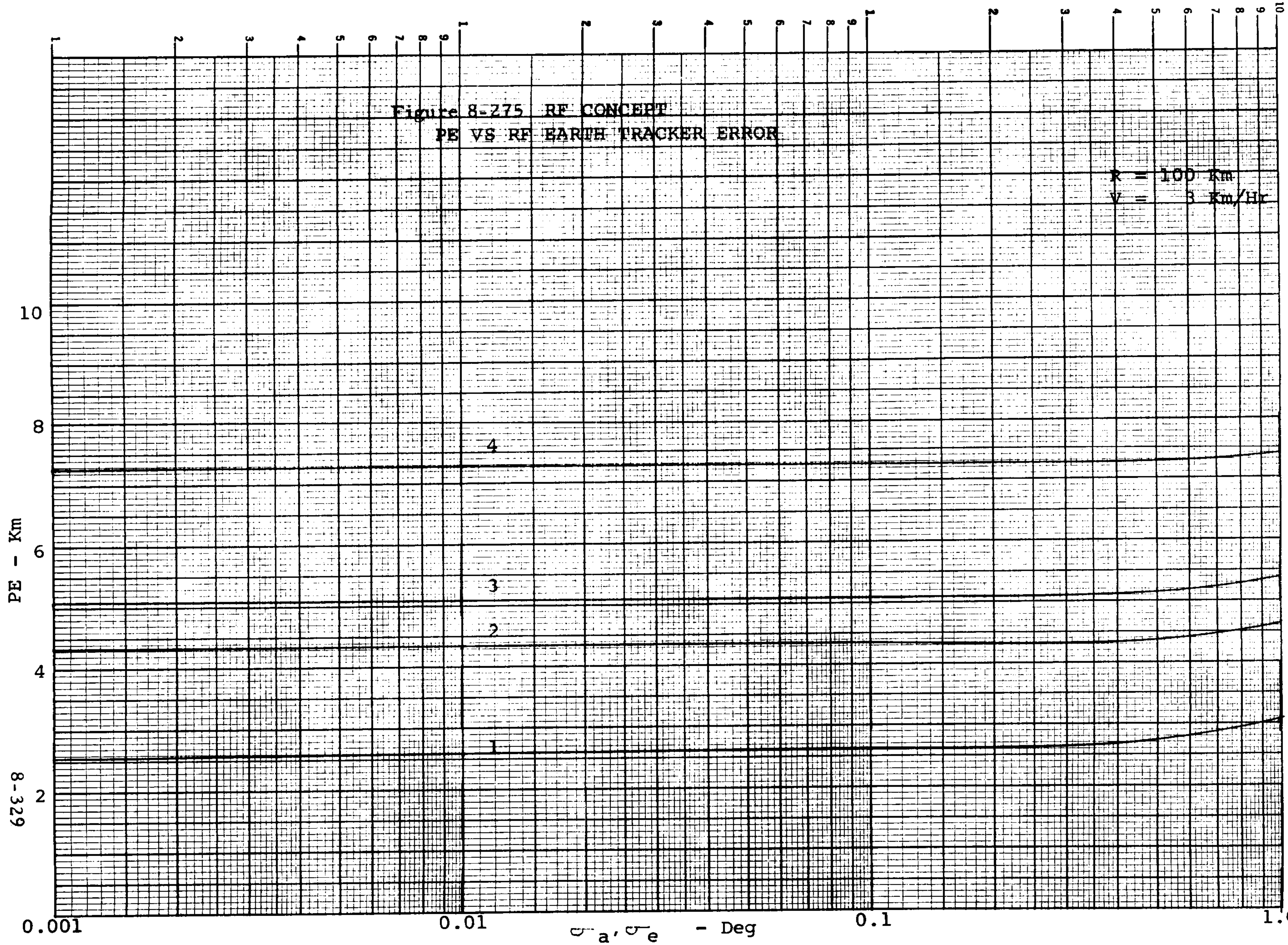

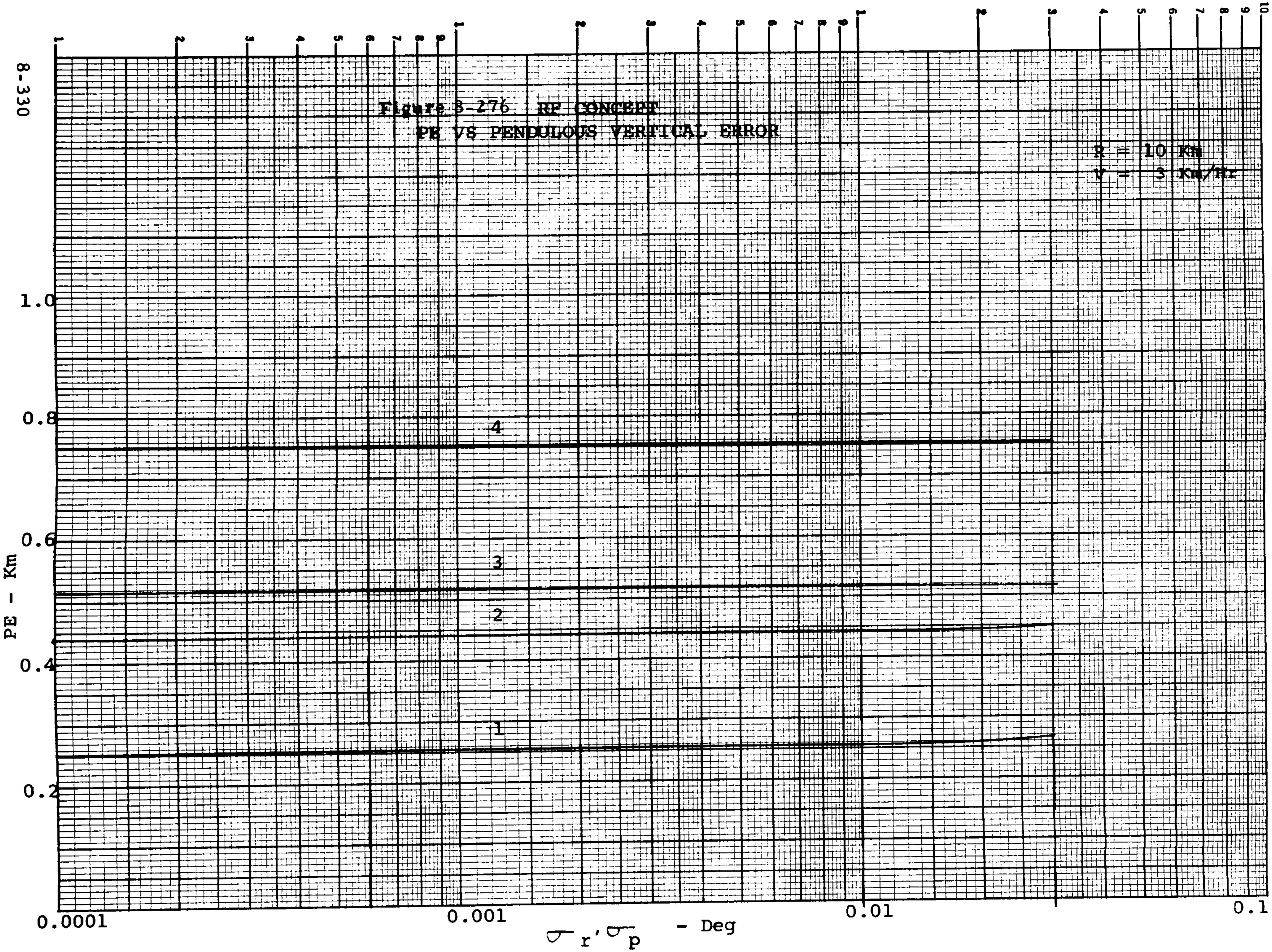

Figure 8-276 RF CONCEPT
PE VS PENDULOUS VERTICAL ERROR

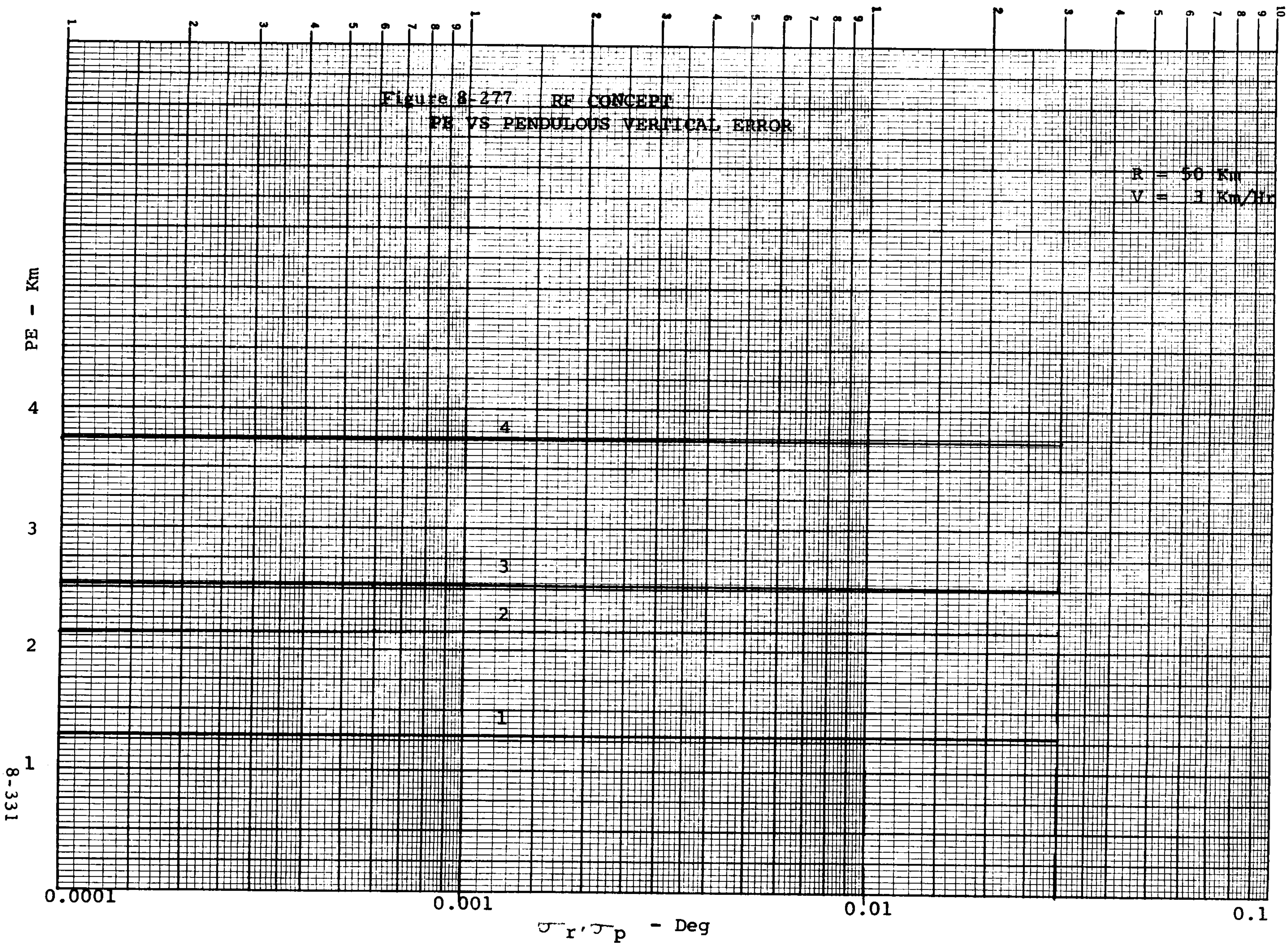

Figure 8-277 RF CONCEPT
PE VS PENDULOUS VERTICAL ERROR
R = 50 Km
V = 3 Km/Hr
PE - Km
4
3
2
1
0.0001
0.001
0.01
0.1
σ_r, σ_p - Deg

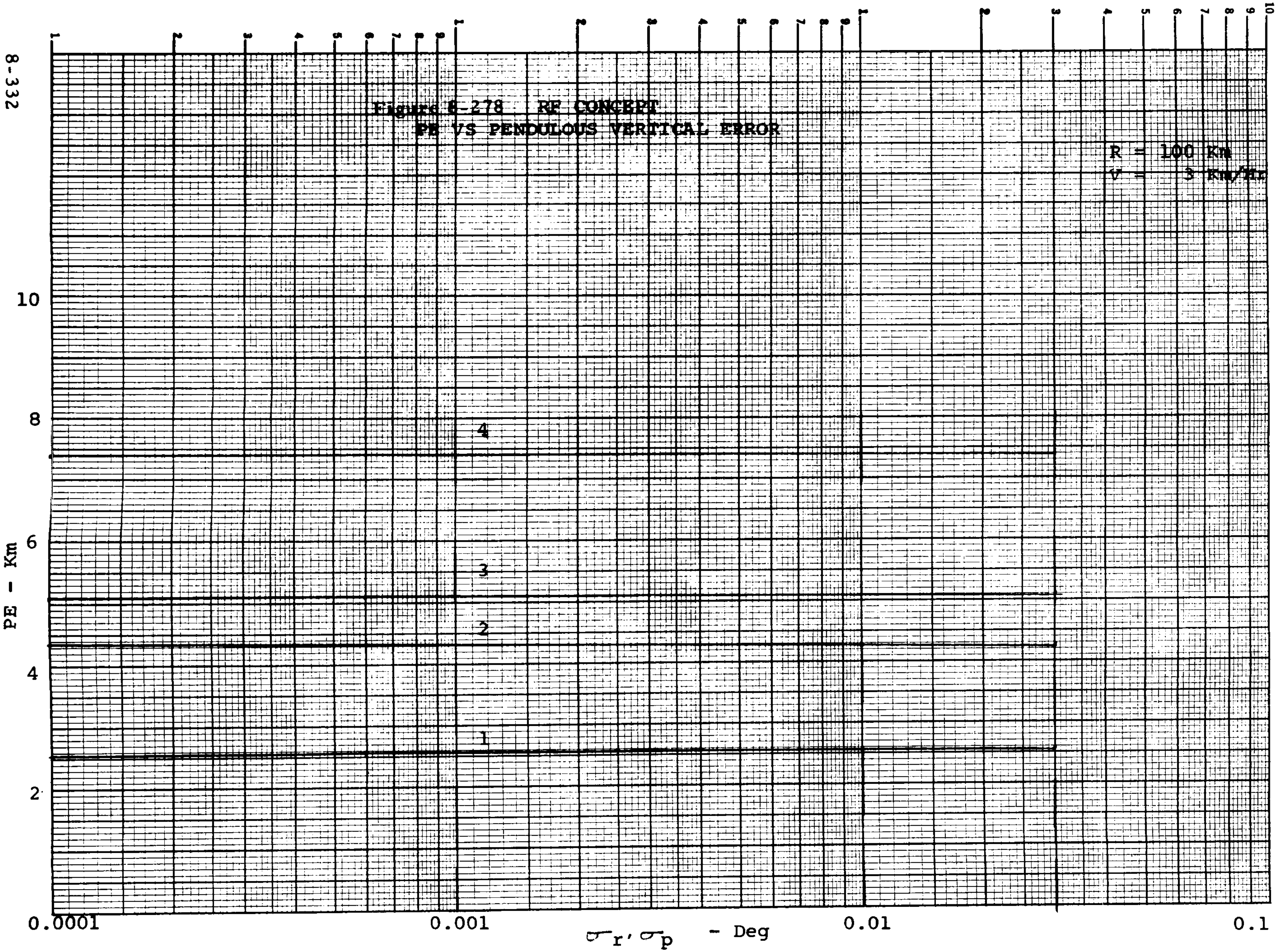
Figure 8-278 RF CONCEPT
PE VS PENDULOUS VERTICAL ERROR
R = 100 Km
V = 3 Km/Hr
PE - Km
10
8
6
4
2
4
3
2
1
0.0001
0.001
0.01
0.1
σ_r, σ_p - Deg

Figure 8-279 PLOT 13 MISSION I 1972 LEG C

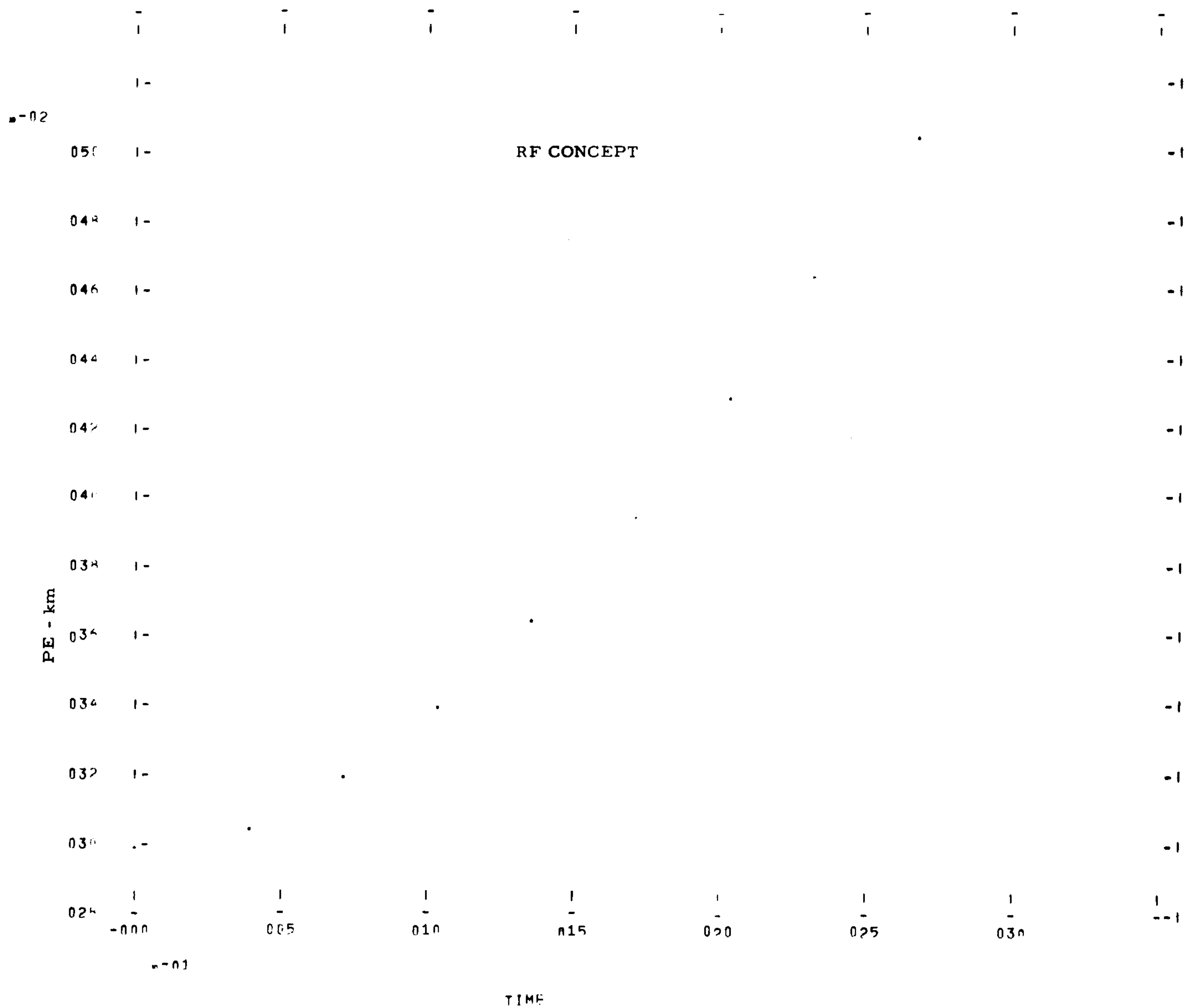

Figure 8-280 PLOT 12 MISSION I 1972 LEG C

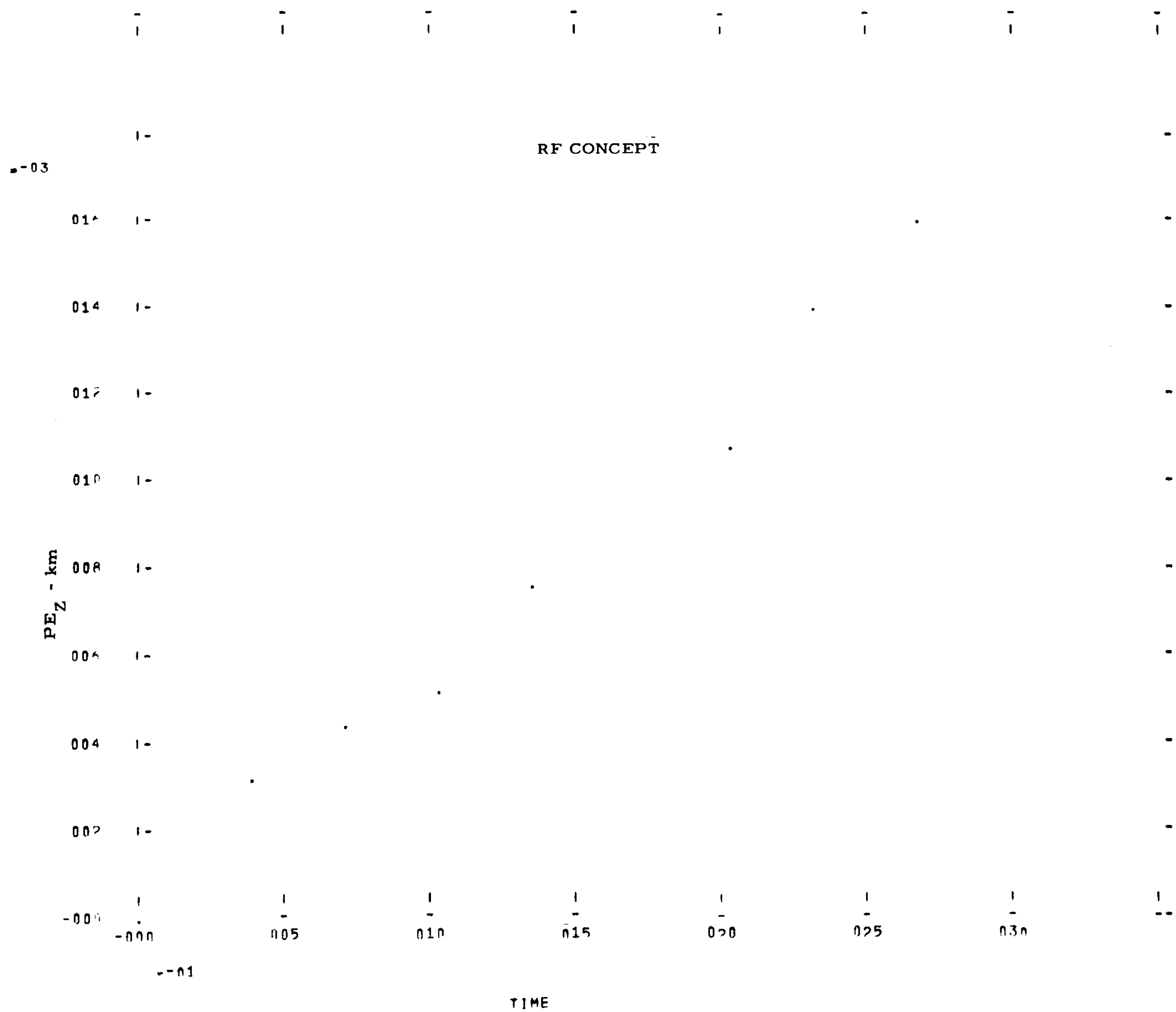

Figure 8-281 PLOT 13 MISSION II 1976 LEG E

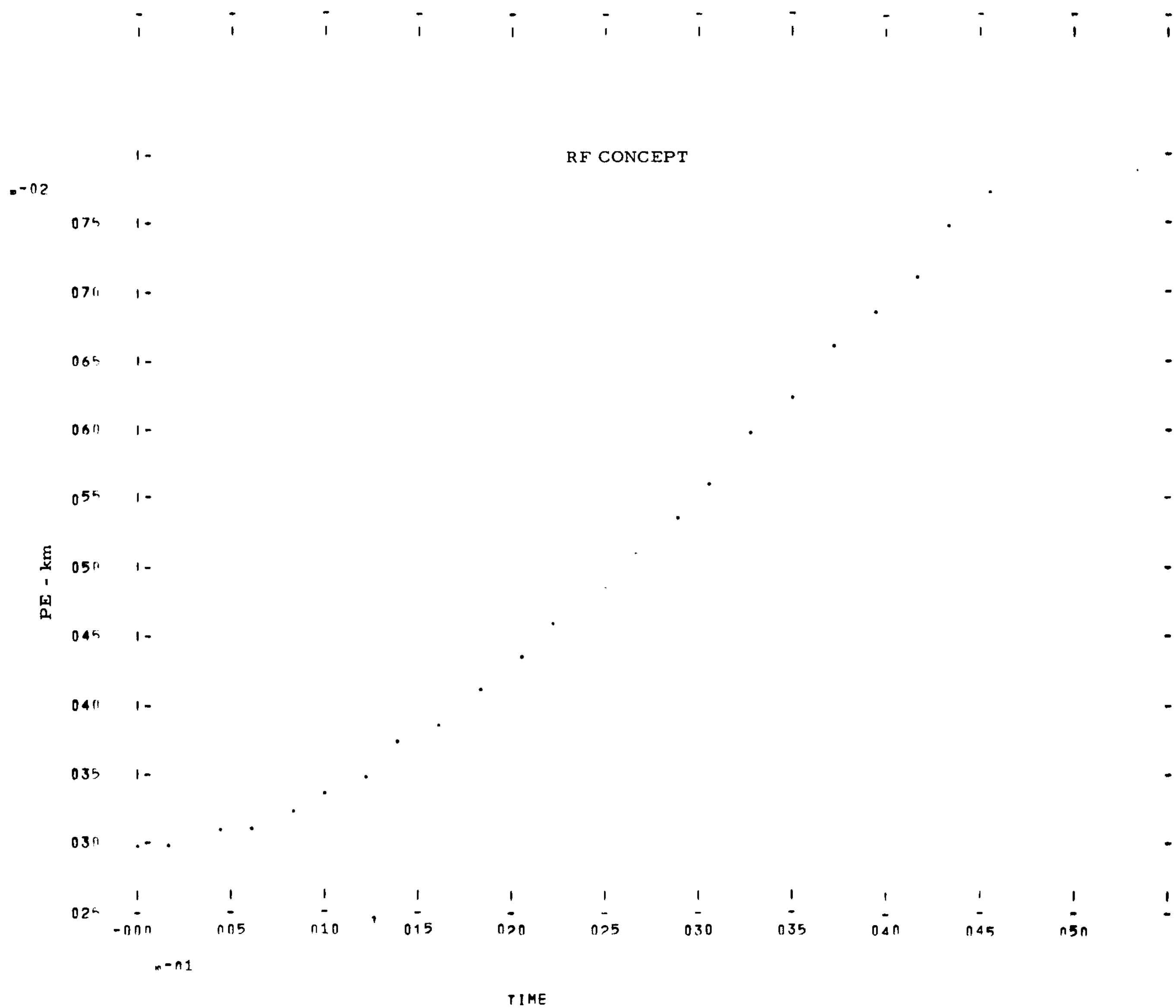

Figure 8-282 PLOT 12 MISSION II 1976 LEG E

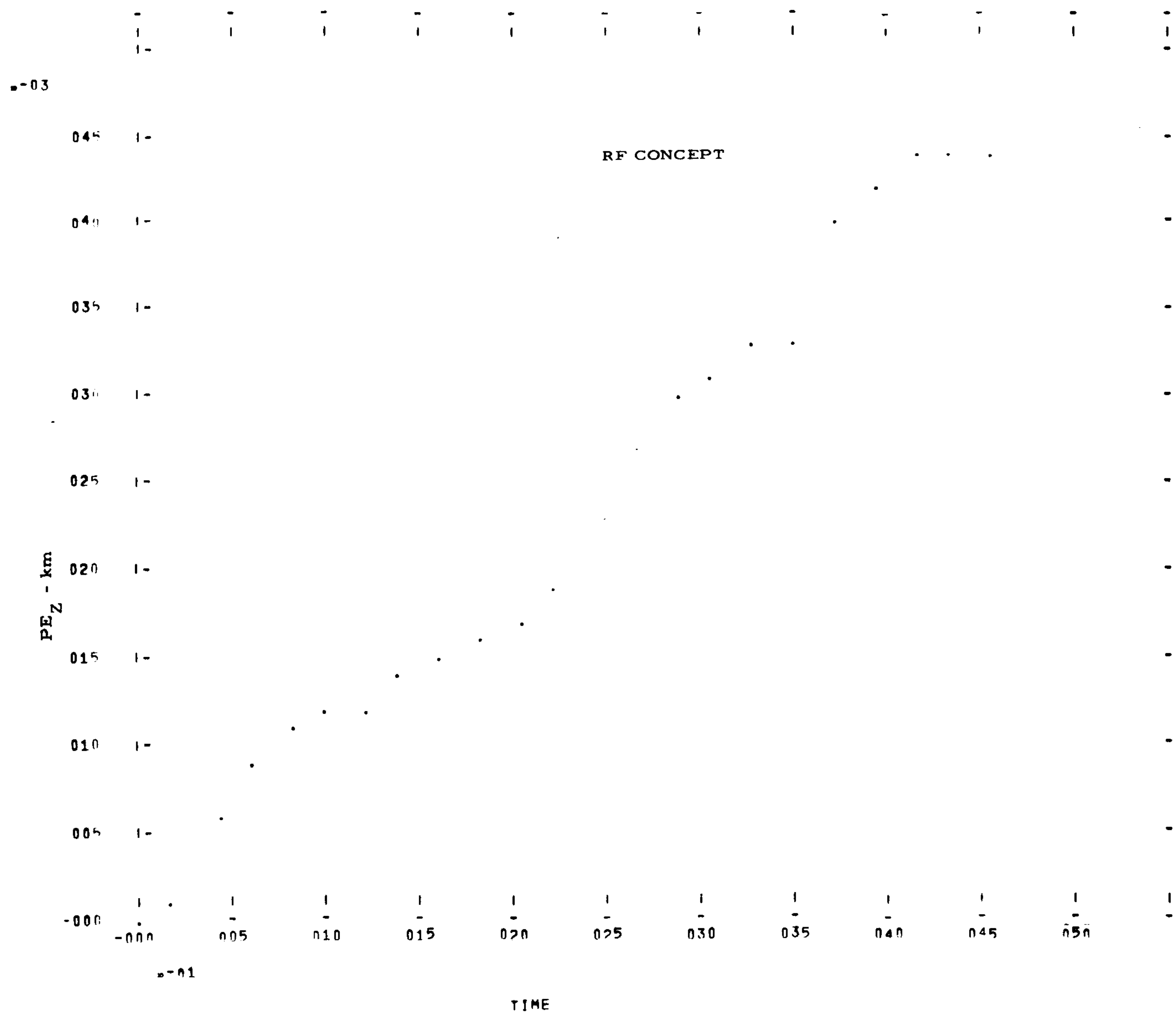

Figure 8-283 PLOT 13 MISSION III 1978 LEG A

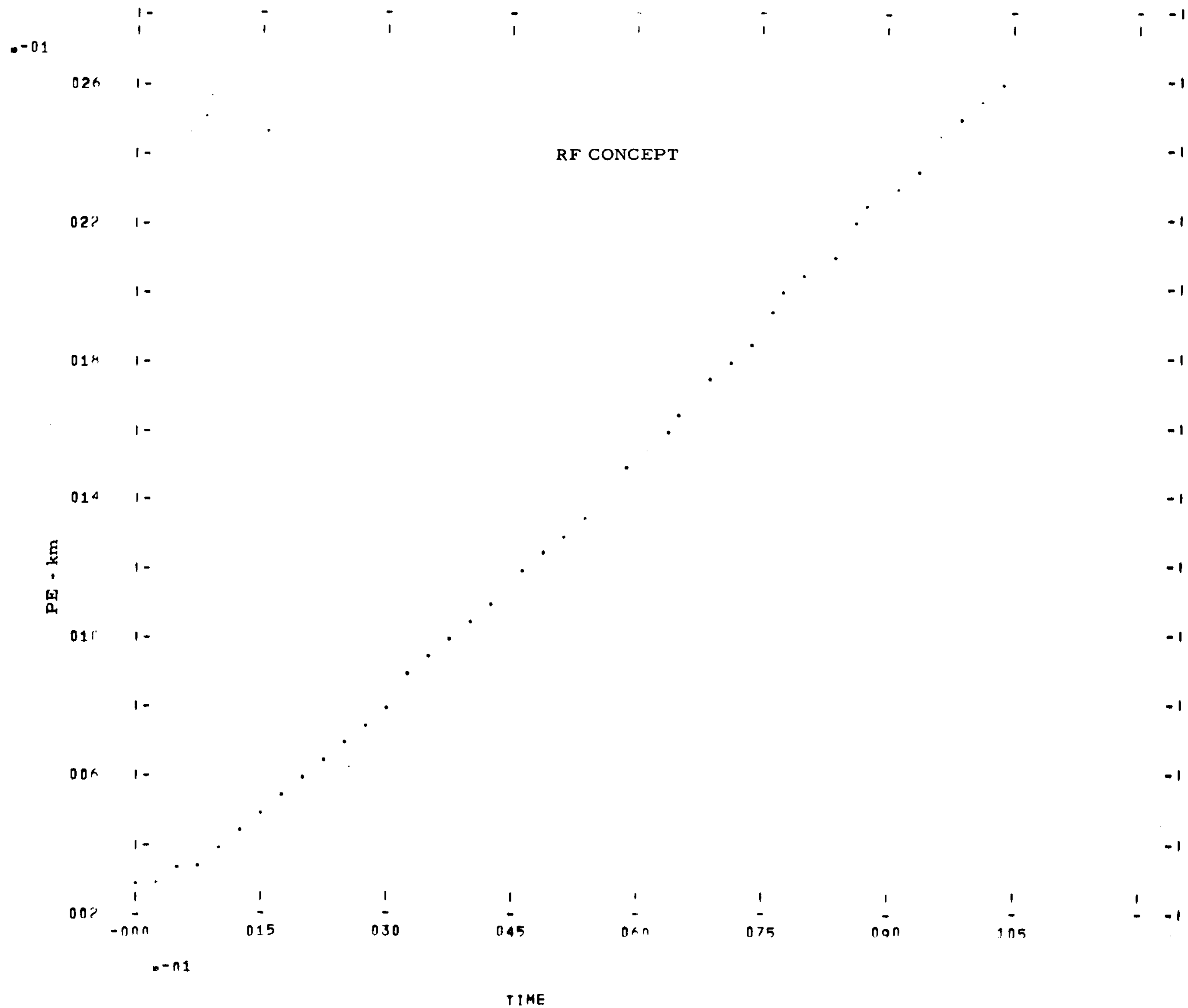

Figure 8-284 PLOT 12 MISSION III 1978 LEG A

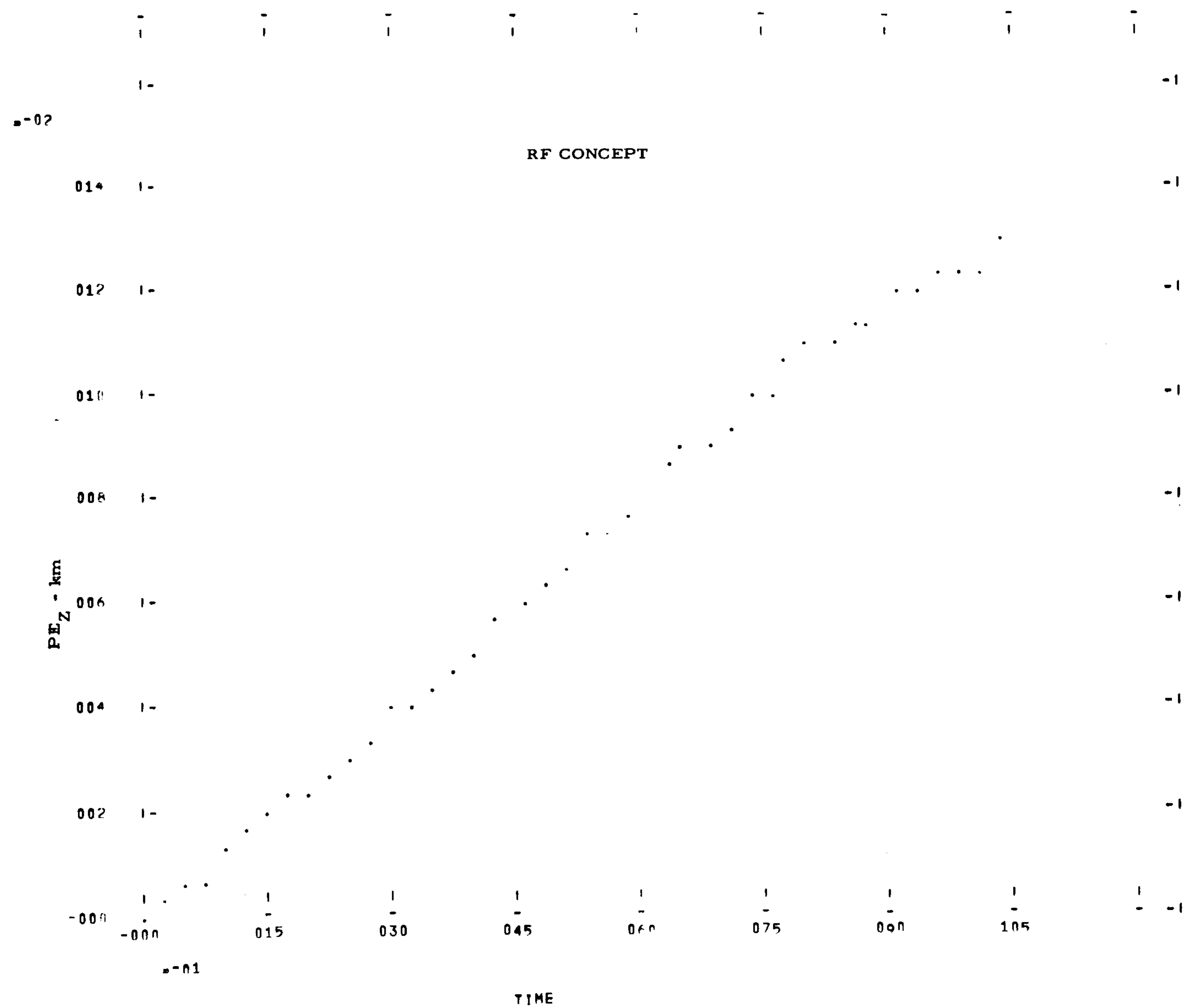

Figure 8-285 PLOT 13 MISSION III 1978 LEG R

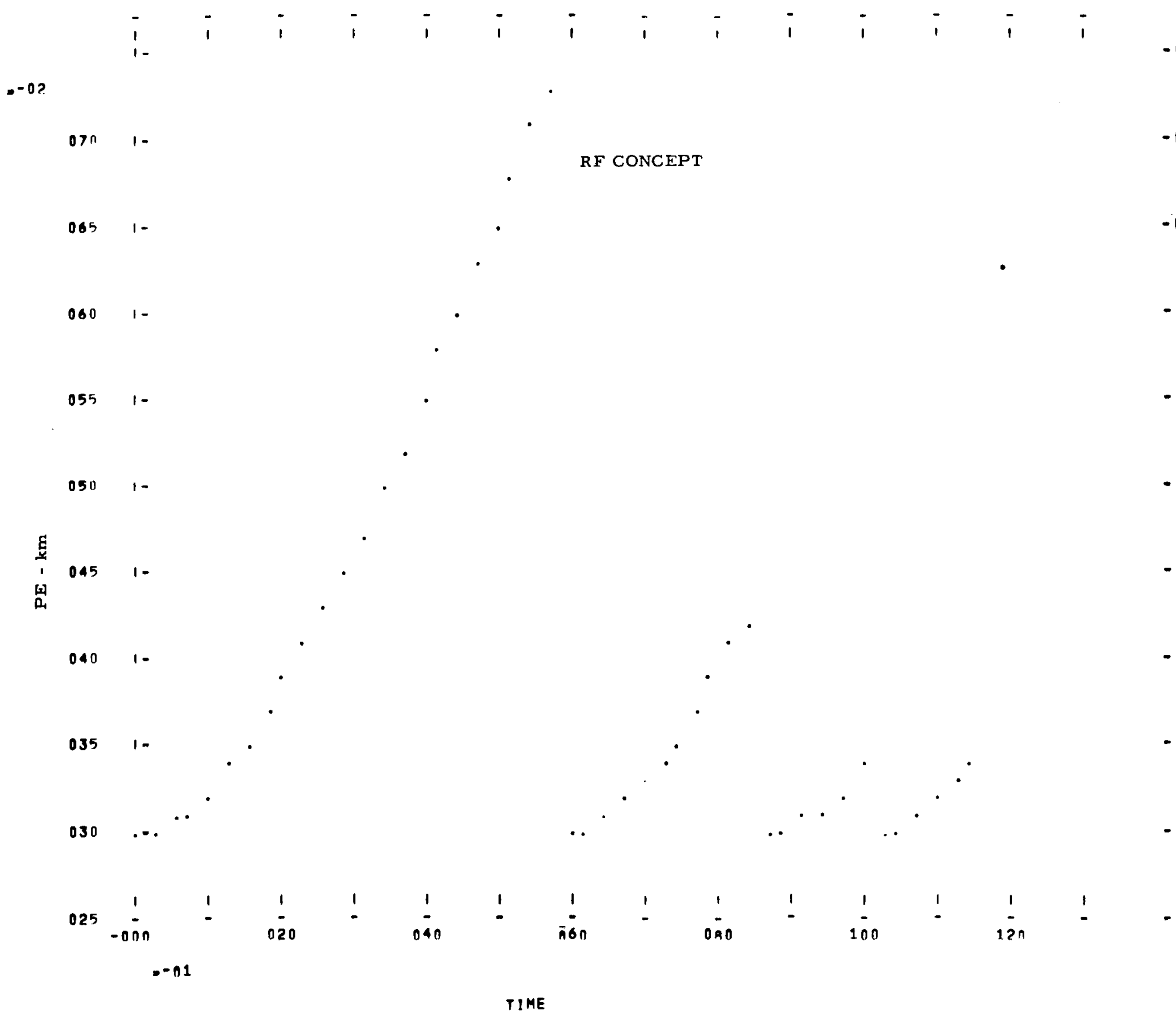

Figure 8-286 PLOT 12 MISSION III 1978 LEG B

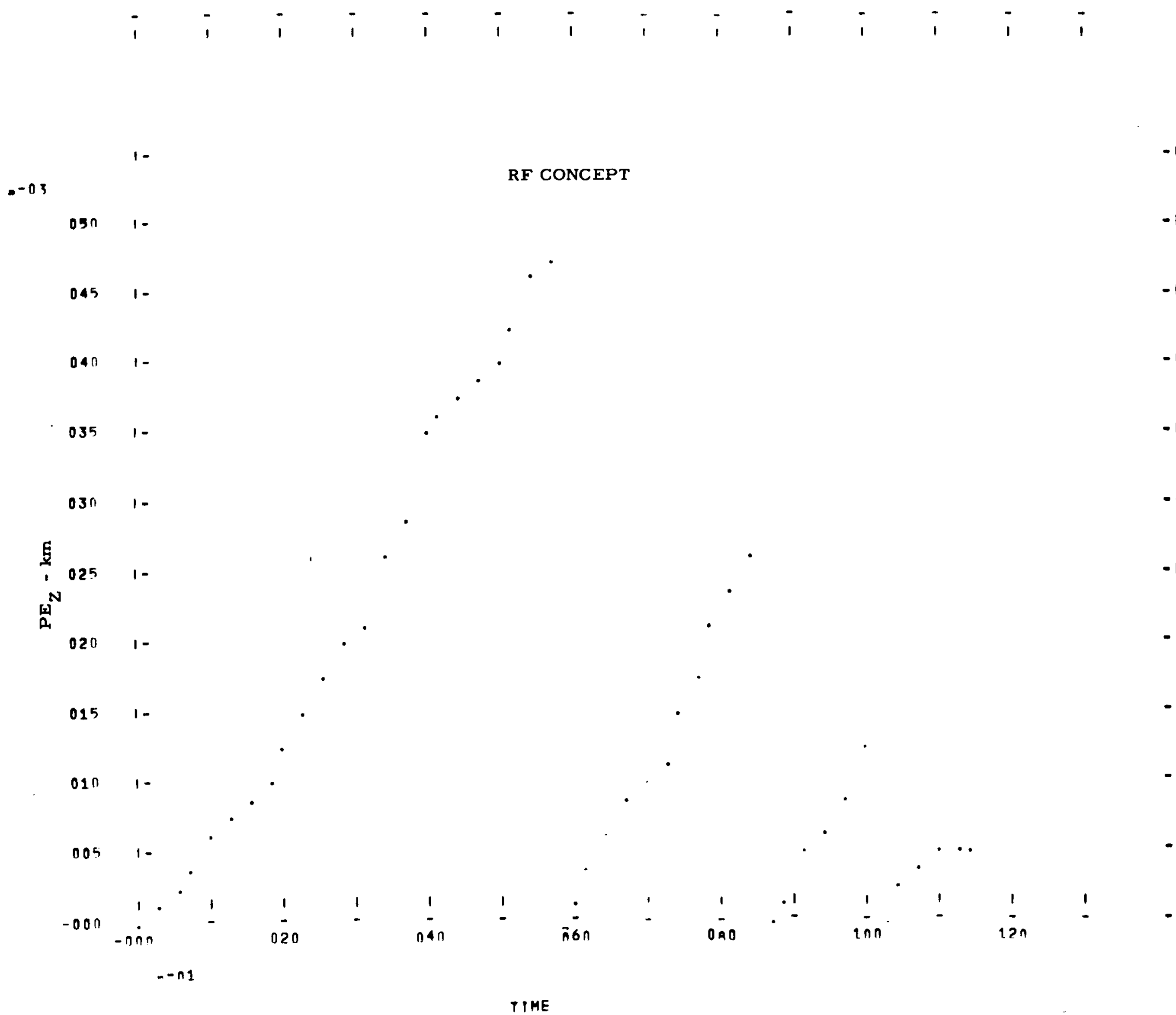

Figure 8-287 PLOT 13 MISSION IIII 1980 LEG C

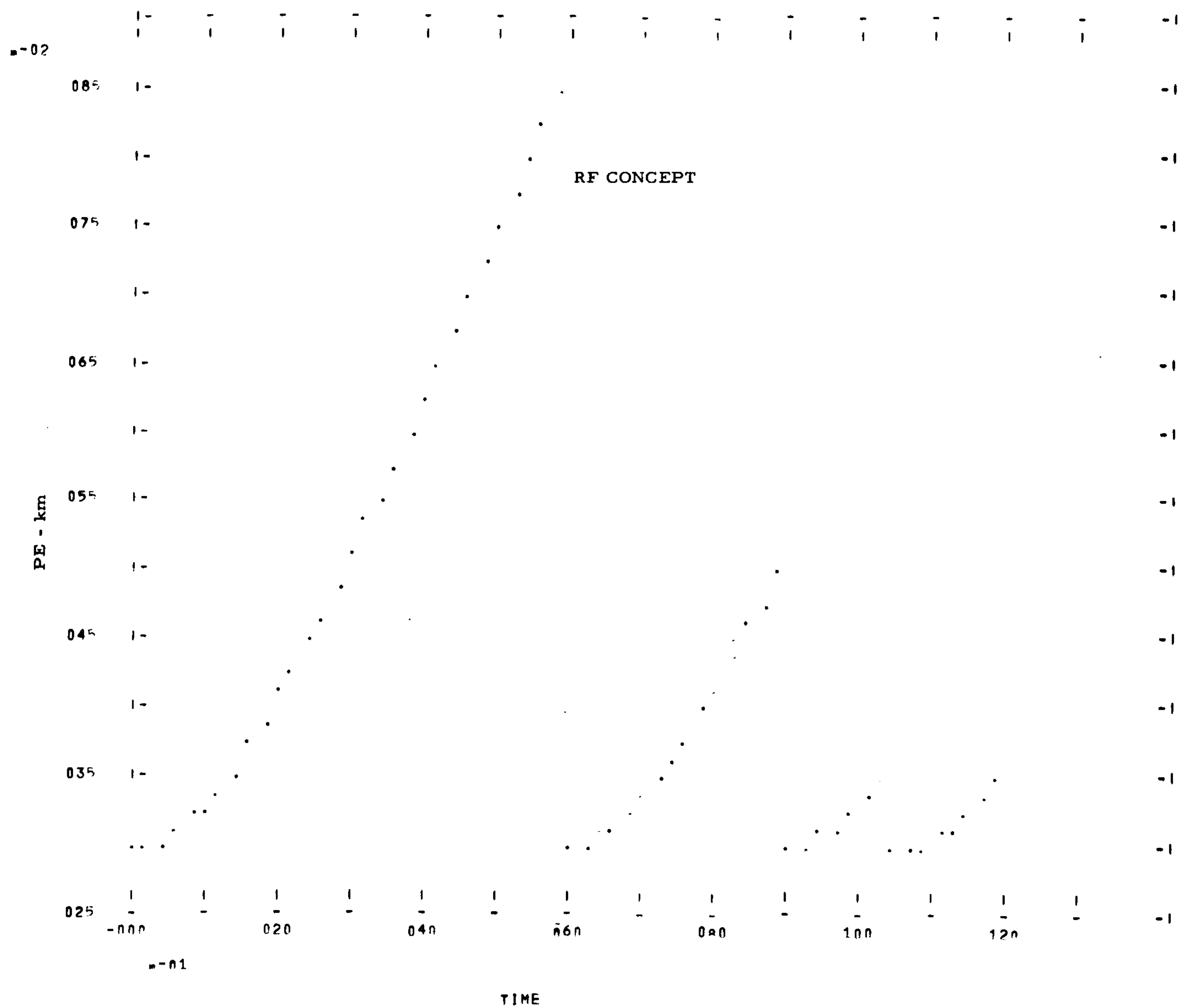

Figure 8-288 PLOT 12 MISSION IIII 1980 LEG C

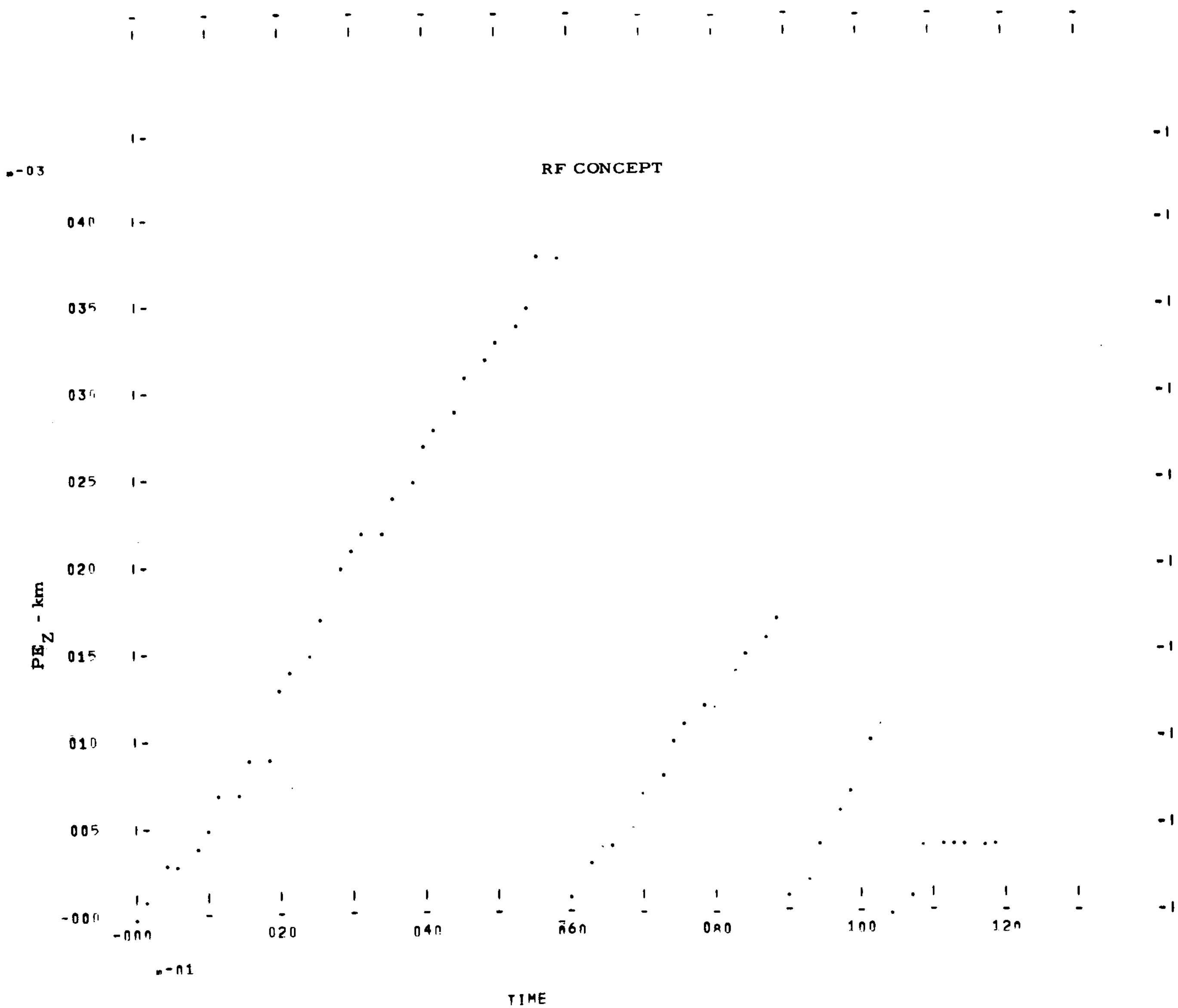

Figure 8-289 PLOT 13 MISSION IIII 1980 LEG F

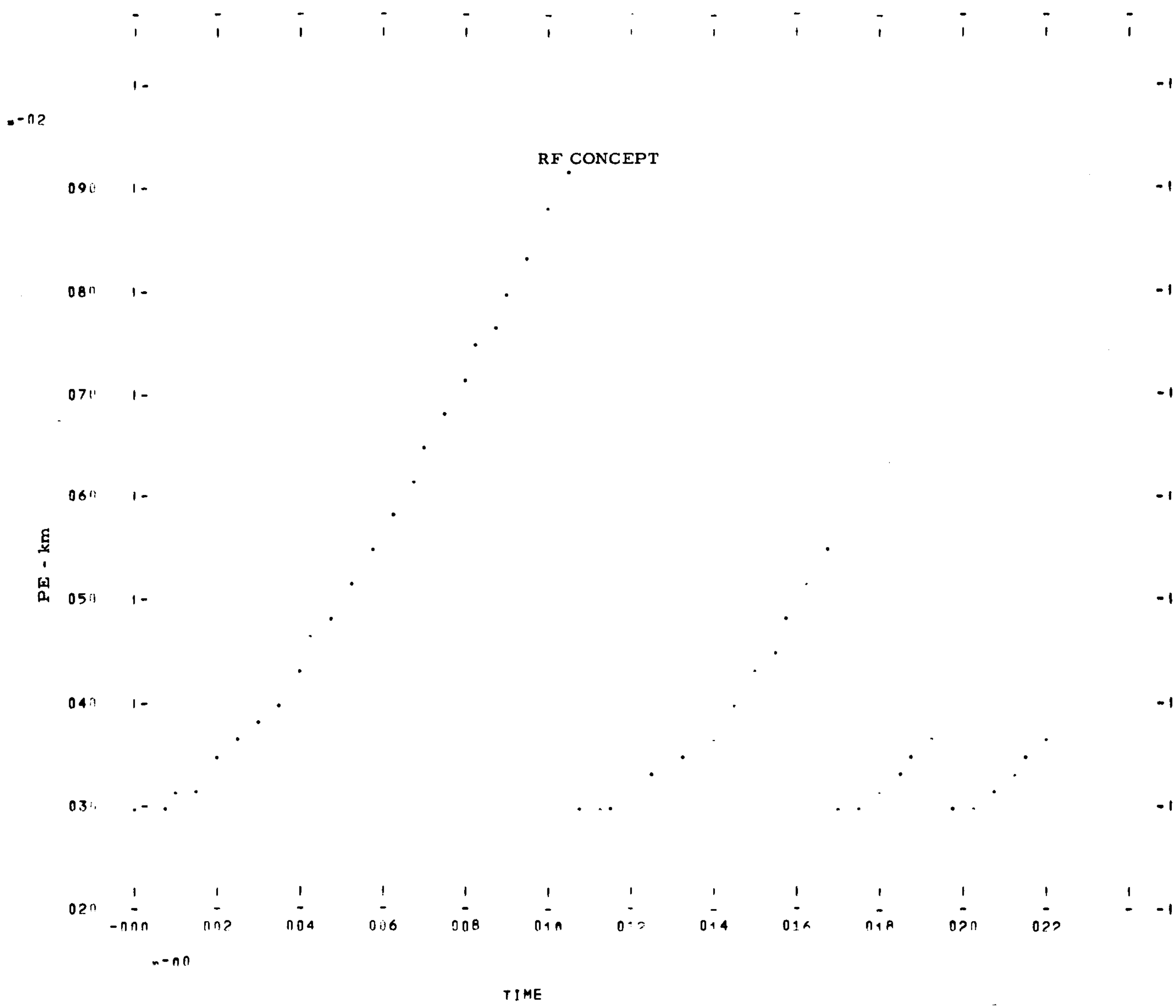

Figure 8-290 PLOT 12 MISSION IIII 1980 LEG F

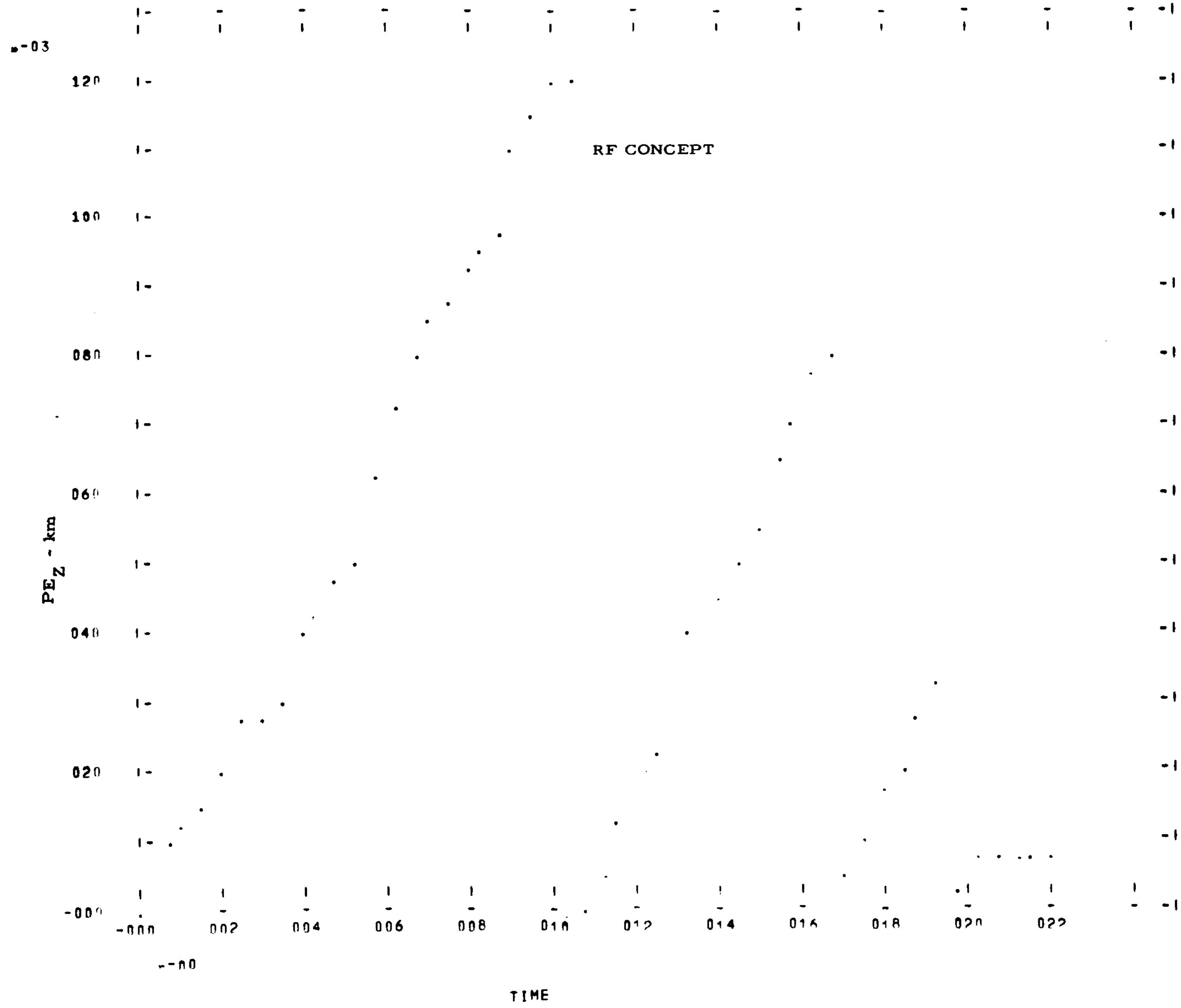

Figure 8-291 PLOT 13 MISSION V 1980 LEG A

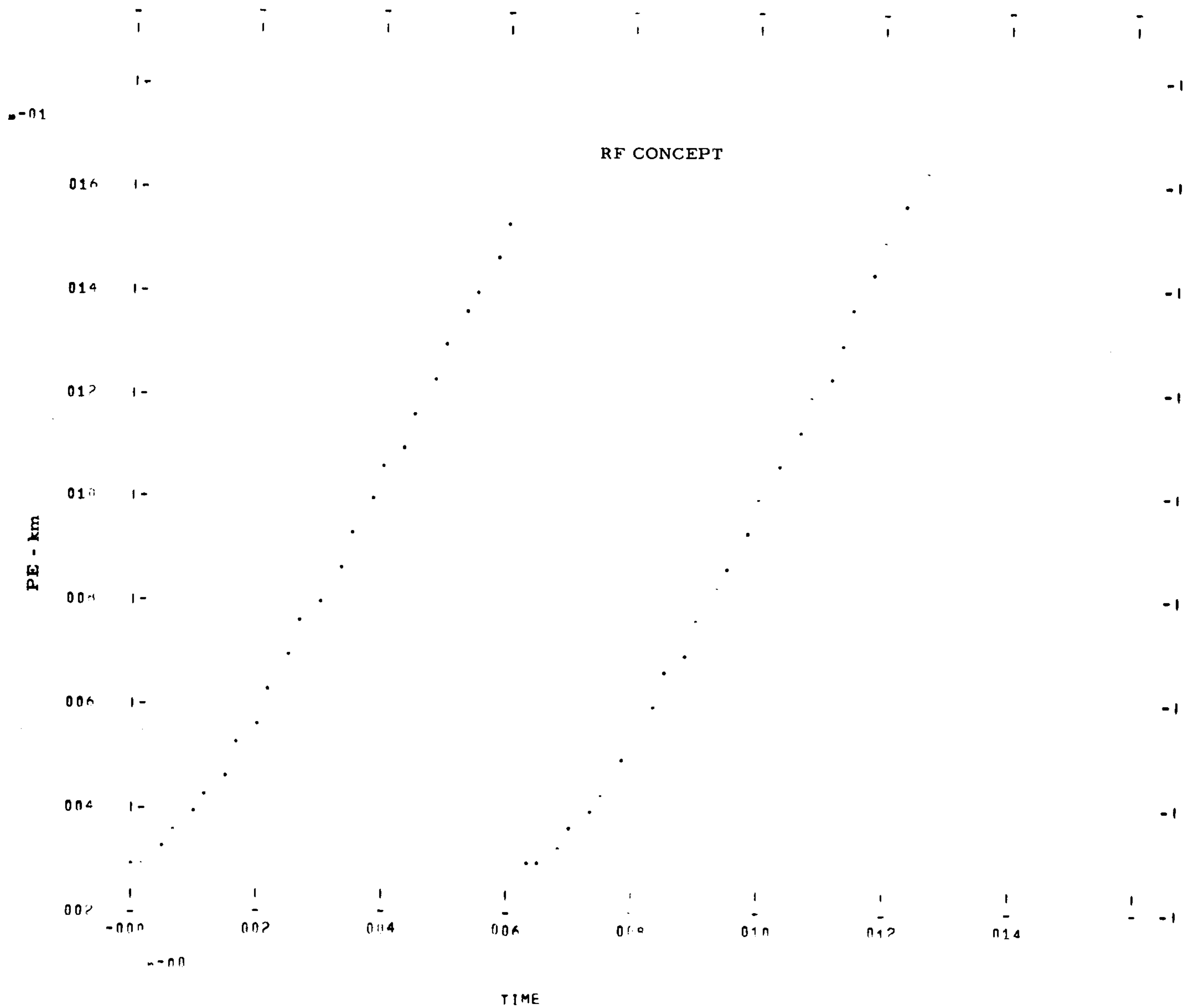

Figure 8-292 PLOT 12 MISSION V 1980 LEG A

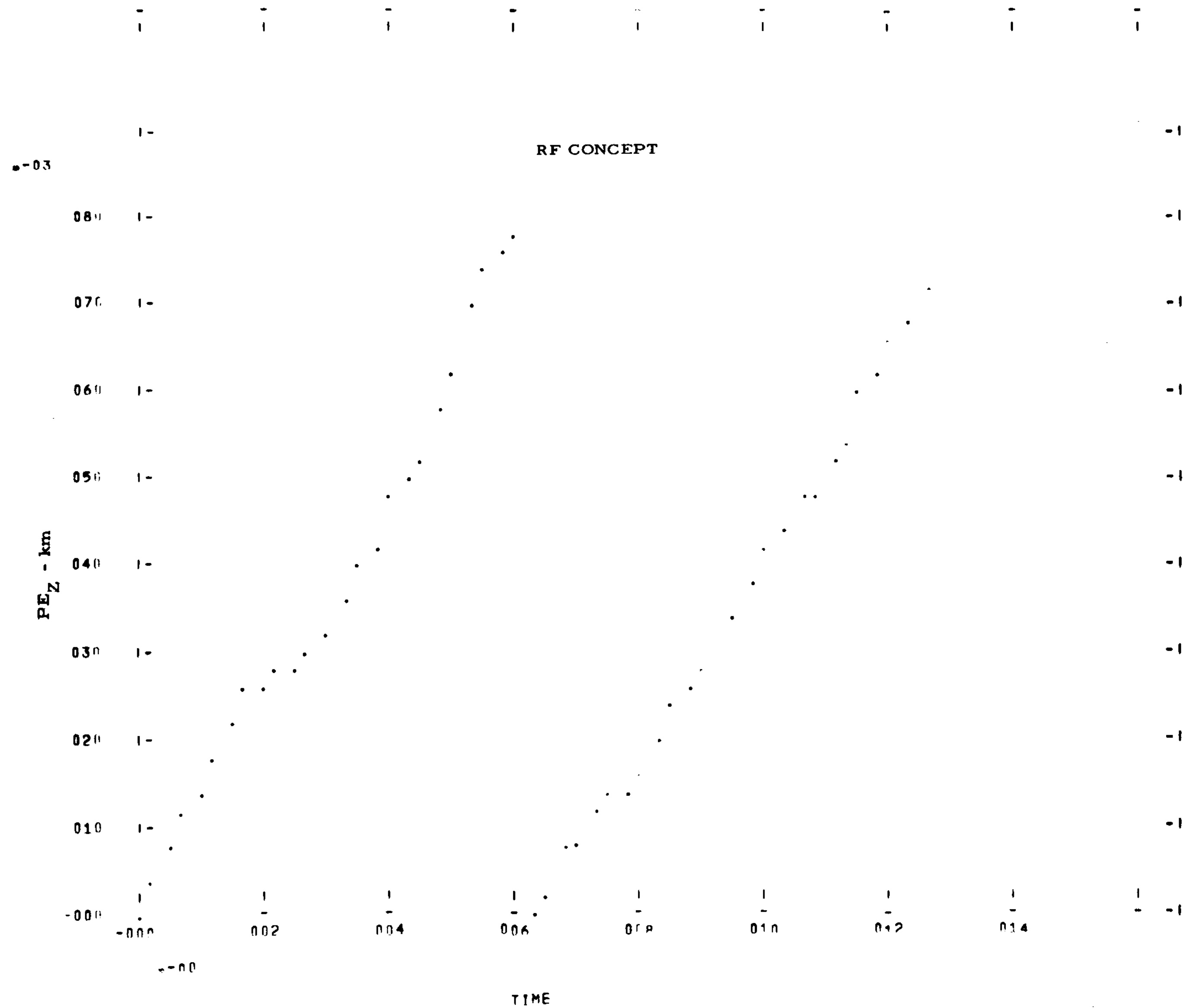

Figure 8-293 PLOT 13 MISSION V 1980 LEG B

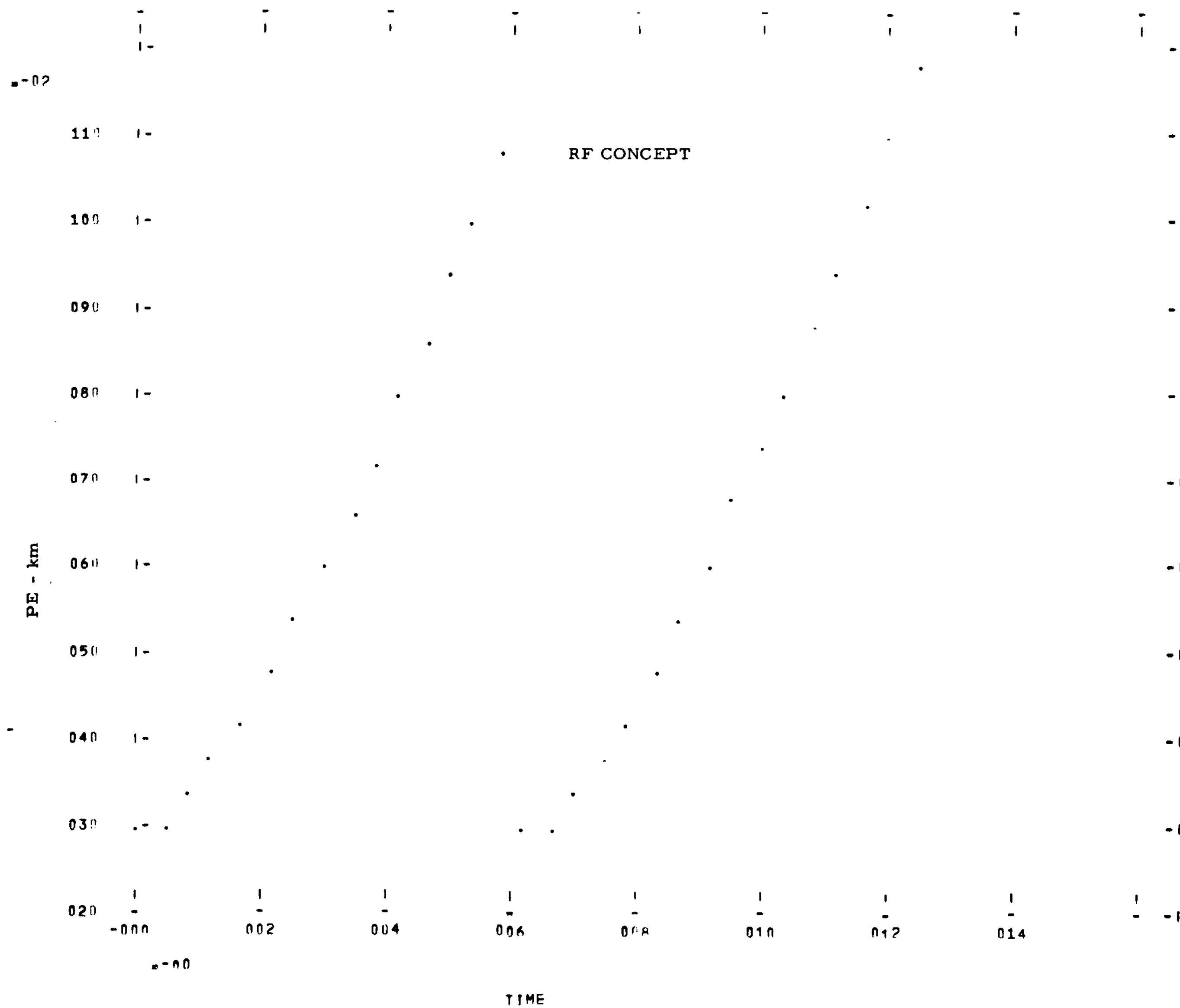

Figure 8-294 PLOT 12 MISSION V 1980 LEG B

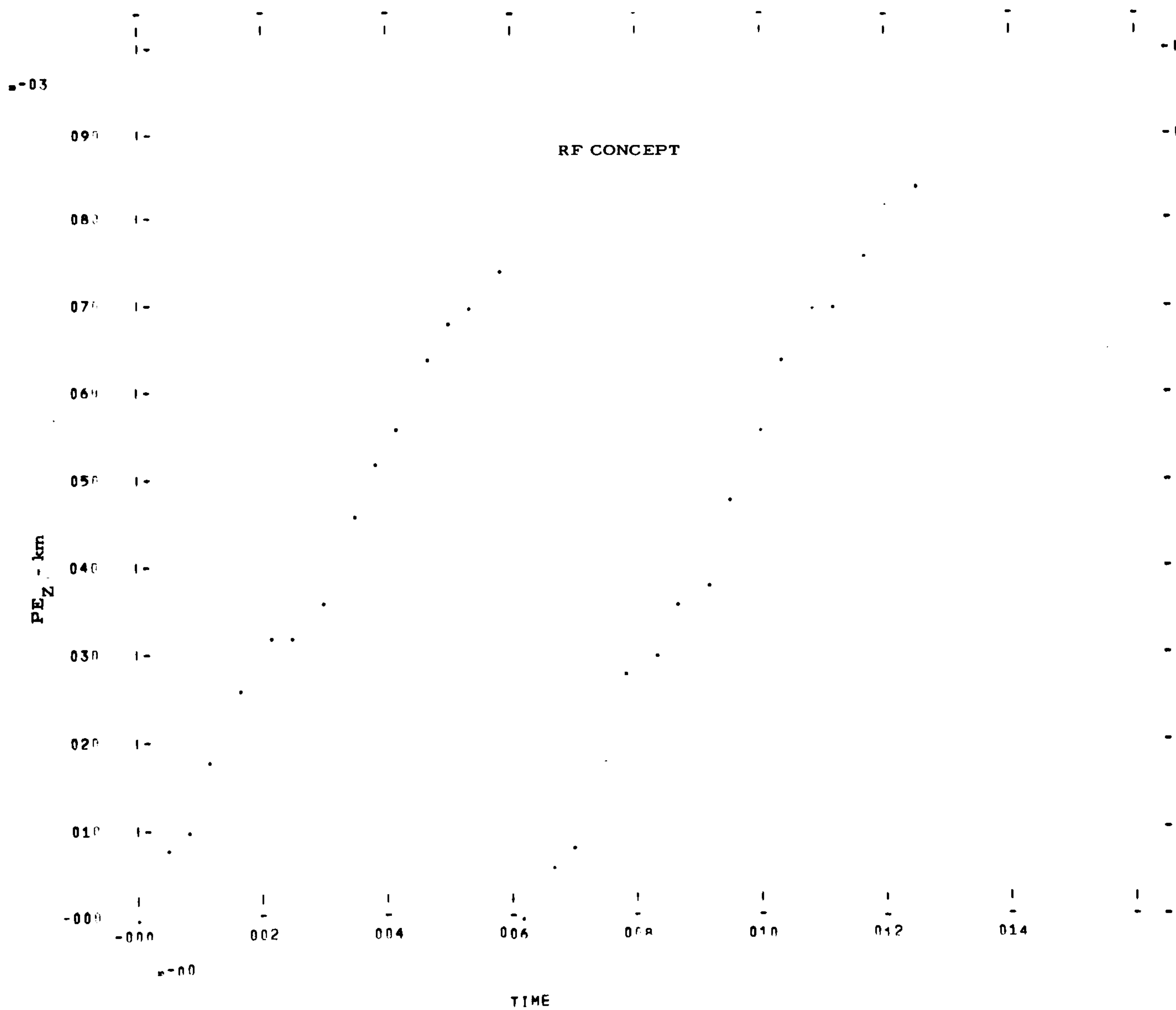

Figure 8-295 PLOT 13 MISSION VI 1984 LEG 8

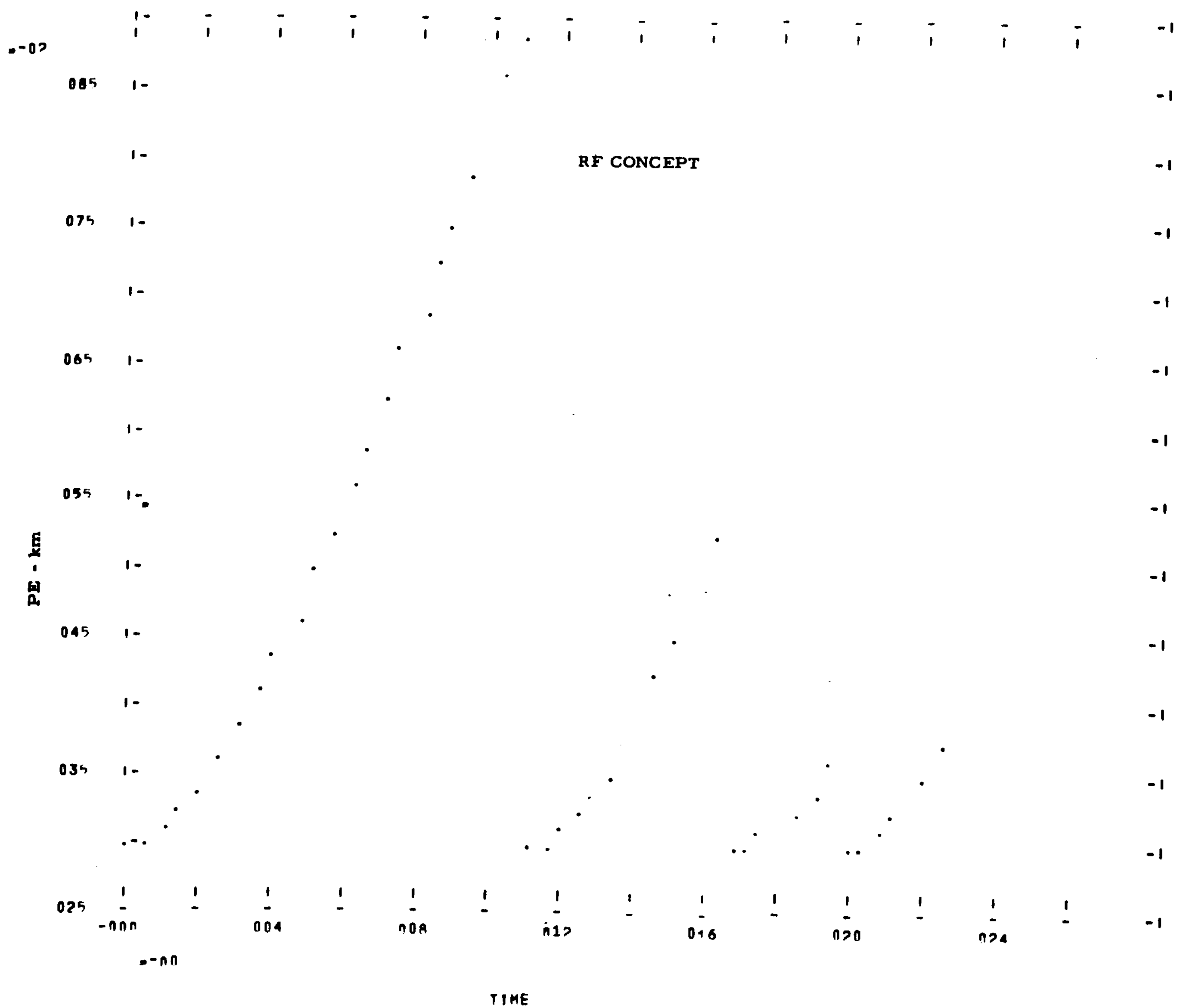

Figure 8-296 PLOT 12 MISSION VI 1984 LEG 8

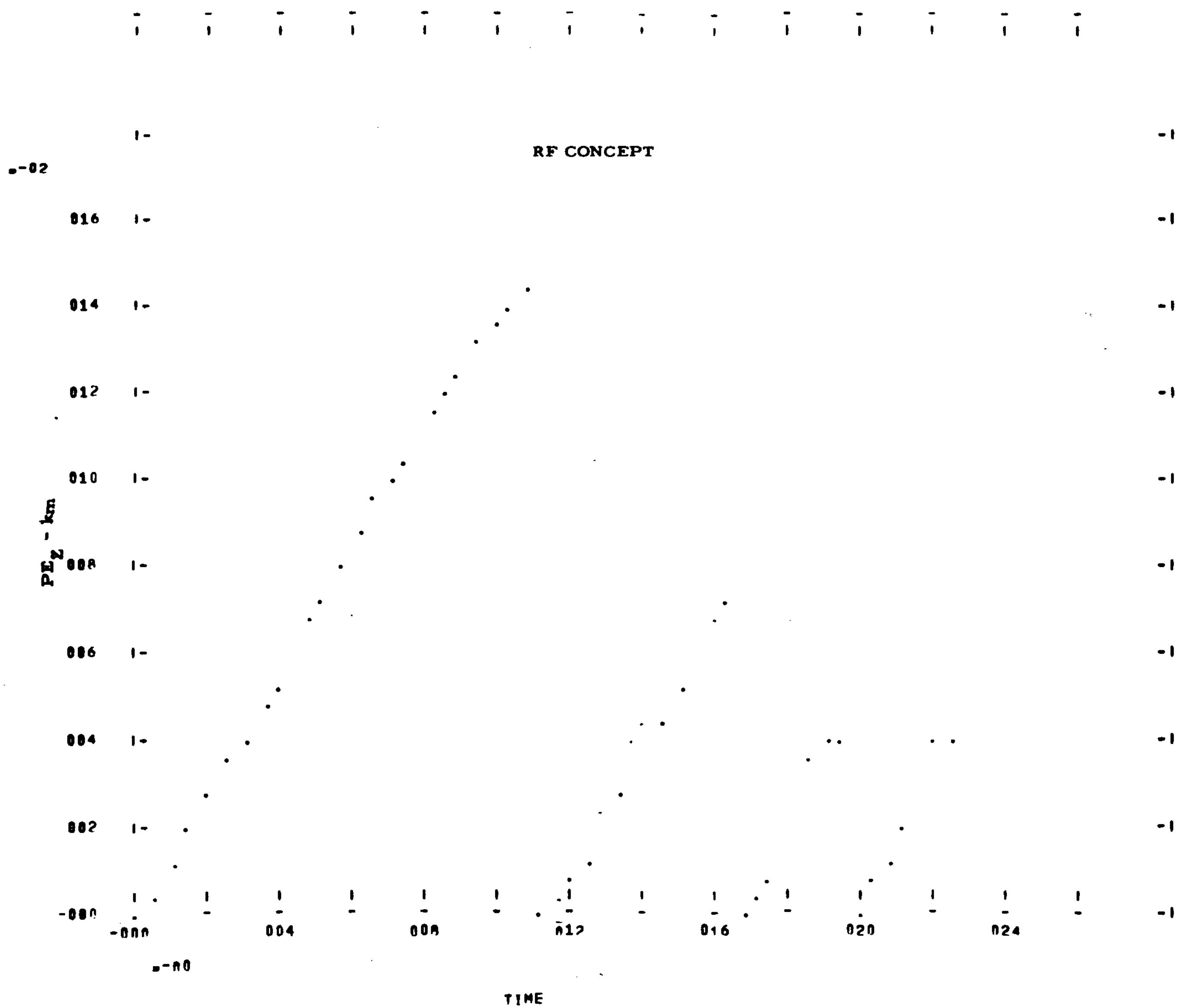

SECTION 9

SUMMARY OF RESULTS

Inherent to the problem of lunar surface navigation is the necessity for astronaut safety. Within the guidelines and framework of this study, safety is directly equated with navigation concept accuracy. Resolving this equation into analytical terms expresses a "safe" navigation system as that concept which allows the guidance or pilotage mode of homing to be effected.

Thus, the navigation error must be less than or equal to a homing range associated with each navigation concept. This navigation error may or may not fulfill one or more typical terminal requirements imposed by mission tasks, and it is at this point that tradeoff studies can be initiated.

Figure 9-1 shows plots of range of component accuracies required for the nongyro, inertial, and RF concepts to satisfy the lunar surface navigation accuracy requirements for the years from 1972 to 1984. The design point or accuracy type systems of the dead reckoning and position fix subconcepts of the selected surface navigation systems are plotted as a function of mission era, and represent the accuracy type concept required to meet the most demanding, but typical, navigation requirement of the era. The accuracy type systems are defined as nominal (NOM), state of the art (SOA) and projected state of the art (Proj. SOA). The definitions of these accuracy type or design point systems are:

NOM: The nominal accuracy type system is comprised of components with accuracies corresponding to the component accuracies of present day state-of-the-art instrumented concepts. These components are the types which have been used in operational navigation systems.

Figure 9-1 ACCURACY TYPE / DESIGN POINT REQUIREMENTS

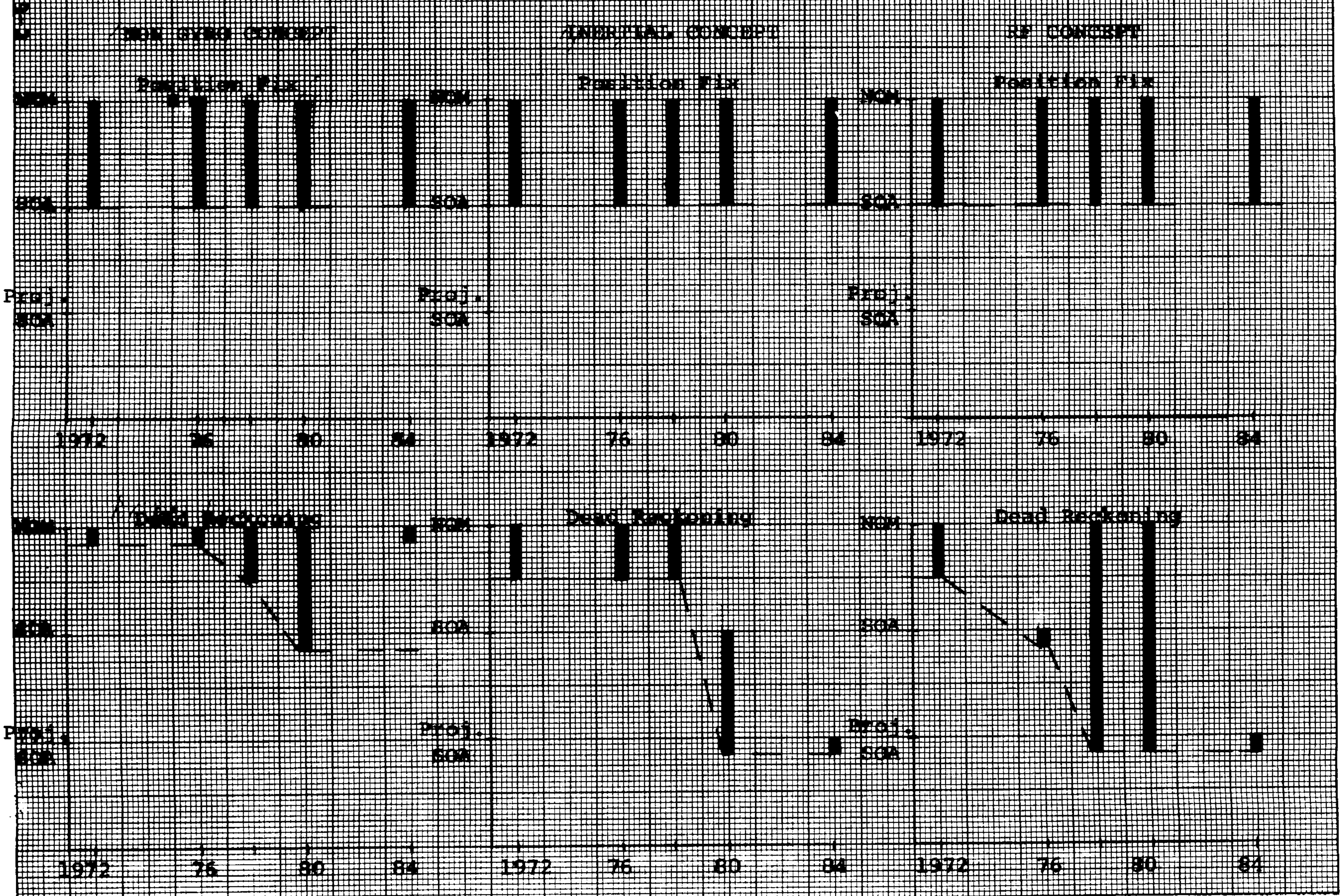

SOA: The state-of-the-art accuracy-type system consists of components with accuracies corresponding to state of the art laboratory-tested components. These components have generally an order of magnitude less error than the NOM components but represent components which are functional in a tightly controlled, ideal, laboratory-type environment.

Proj. SOA: The projected state-of-the-art accuracy components are representative of future attainable accuracies and are approximately an order of magnitude more accurate than the SOA type.

The position fix design point accuracy requirements are constant throughout the lunar exploration era. However, since ranges and durations increase with each lunar exploration mission, the dead reckoning requirements become more stringent. The nongyro dead reckoning subconcept requires no component state-of-the-art advancement, but by 1980 present-day ideal SOA accuracy-type components must be capable of functional system implementation in an uncontrolled environment. By 1980, however, the inertial dead reckoning concept will require operational projected state-of-the-art accuracy components, while the RF concept requires functional projected state-of-the-art components by 1978. The typical component error requirements for each concept and component are listed in Tables 9-1, 9-2, and 9-3. The asterisk notation indicates component accuracy requirements which cannot be met by NOM components.

The principal error contributors of each concept are listed in Table 9-4. The primary dead reckoning error contributors are the distance sensors and heading reference. Vertical error contributions to horizontal or planar dead reckoning error are secondary.

TABLE 9-1

NONGYRO CONCEPT, 3σ REQUIREMENT TABLE

	Component or Aid	Error	Units	Requirement vs Mission Era				
				1972	1976	1978	1980	1984
Position Fix	Star Tracker	Null	deg	0.004*	0.004*	0.004*	0.004*	0.004*
	Static Pendulous Vertical	Null	deg	0.001*	0.001*	0.001*	0.001*	0.001*
	Ephemeris	Uncertainty	deg	0.005	0.005	0.005	0.005	0.005
	Timer	Null	hr	0.00003	0.00003	0.00003	0.00003	0.00003
	Allowable Vertical Anomaly		deg	0.005	0.005	0.005	0.005	0.005
Dead Reckoning	Odometer	(1) Slip (2) Calibration	—	0.01	0.01	0.005*	0.001*	0.005*
	Pendulous Vertical	Null	deg	0.01	0.01	0.01	0.01	0.01
	Ephemeris	Uncertainty	deg	0.01	0.01	0.01	0.01	0.01
	IR Earth Tracker	Null	deg	0.2	0.2	0.2	0.2	0.2
	Timer	Null	hr	0.00003	0.00003	0.00003	0.00003	0.00003

TABLE 9-2

INERTIAL CONCEPT, 3σ REQUIREMENT TABLE

	Component or Aid	Error	Units	Requirement vs Mission Era				
				1972	1976	1978	1980	1984
Position Fix	Star Tracker	Null	deg	0.004*	0.004*	0.004*	0.004*	0.004*
	Static Pendulous Vertical	Null	deg	0.001*	0.001*	0.001*	0.001*	0.001*
	Ephemeris	Uncertainty	deg	0.005	0.005	0.005	0.005	0.005
	Timer	Null	hr	0.00003	0.00003	0.00003	0.00003	0.00003
	Allowable Vertical Anomaly		deg	0.005	0.005	0.005	0.005	0.005
Dead Reckoning	Accelerometers	Null	Earth g's	$*10^{-7}$	$*10^{-7}$	$*10^{-7}$	$*10^{-8}$	$*10^{-8}$
	Directional Gyro	Null	deg	0.1	0.1	0.1	*0.0001	*0.0001
		Drift	deg/hr	0.08	0.08	0.08	*0.001	*0.001
	Vertical Gyro	Null	deg	0.1	0.1	0.1	*0.001	*0.001
		Drift	deg/hr	0.05	0.05	0.05	*0.001	*0.001

TABLE 9-3

RF CONCEPT, 3σ REQUIREMENT TABLE

	Component or Aid	Error	Units	Requirement vs Mission Era				
				1972	1976	1978	1980	1984
Position Fix	Earth-Based RF Tracking (DSIF, MSFN)	Vehicle Position	km	0.300	0.300	0.300	0.300	0.300
Dead Reckoning	Doppler Radar	Null		*0.01	*0.005	*0.003	*0.001	*0.001
	Doppler Radar Antenna	Null	deg	1.0	*0.5	*0.1	*0.1	*0.1
	Pendulous Vertical	Null	deg	0.01	*0.0006	*0.0001	*0.0001	*0.0001
	RF Earth Tracker	Null	deg	0.2	*0.02	*0.002	*0.002	*0.002
	Ephemeris	Uncertainty	deg	0.01	*0.001	*0.001	*0.001	*0.001
	Timer	Null	hr	0.00003	0.00003	0.00003	0.00003	0.00003

TABLE 9-4

CRITICAL ERROR SOURCE

Subconcept	Position Fix		Dead Reckoning		
			Planar		Vertical
Weighting / Concept	Primary	Secondary	Primary	Secondary	Equally
Nongyro	Vertical Anomaly Vertical Sensor	Celestial Tracker Ephemeris	Odometer IR Earth Tracker	Pendulous Vertical	Pendulous Vertical Odometer Vertical Anomaly
Inertial	Vertical Anomaly	Celestial Tracker	Accelerometers Directional Gyro	Vertical Gyro	Vertical Gyro Accelerometers Vertical Anomaly
	Vertical Sensor	Ephemeris			
RF	Celestial Mechanics Tracking Equipment		Doppler Radar RF Earth Tracker		Pendulous Vertical Doppler Radar Vertical Anomaly

SECTION 10

CONCLUSIONS AND RECOMMENDATIONS

The data presented in Sections 8 and 9 of this report indicate that the principal component error sources for which research and development are required are the distance sensing devices. These are comprised of the odometer, accelerometers, and doppler radar of the dead reckoning subconcepts. Also, since celestial position fix error is a heavily weighted function of the deflection of lunar local vertical, a study should be undertaken to define, analyze, and derive compensation for this error source. With the preceding general recommendations as a background, the more specific recommendations are as follows:

1. Solution of the lunar navigation problem for the postulated era requires the implementation of concepts utilizing SOA components with the accuracy capabilities emphasized throughout the study. However, in most applications SOA accuracies are attainable in ideal environments and usually over limited ranges of measurement with typical low reliability, high cost, high weight, and high volume. In addition to the accuracy/safety aspect, to fully assess the lunar surface navigation problem, the additional weighting factors of cost, reliability, weight, volume, and power must be considered. Sophistication of the present error models to evaluate the additional weighting factors is recommended to ensure compatible feasibility with accuracy/safety requirements. Generally though, component miniaturization and particularly extended measurement ranges are needed.

2. The effect of lunar local vertical anomalies upon the horizontal or planar dead reckoning error is negligible. For the vertical component of dead reckoning error, this error input is of secondary importance. Hence, relative navigation utilizing a dead reckoning process is little affected by the local vertical anomaly. However, position fix error

is a heavily weighted function of the anomalies, and absolute navigation to an extremely precise degree is significantly hindered regardless of the quality of the position fix navigational components unless compensation is provided to negate the anomaly effects.

3. For each navigation concept, a selenographic restriction exists. Concepts 1 and 3, the nongyro and RF systems, determine vehicle heading through earth azimuth measurement. These concepts are restricted to near-side operation. Also, vehicle operation must remain in a selenographic location where the locus of the earth subpoint does not approach the vehicle zenith, at which point the azimuth measurement becomes indeterminant. Due to error sensitivity coefficients, the vehicle selenographic locus should be constrained exterior to a 10° great circle arc of the earth subpoint.

   Polar navigation by the inertial concept is restricted, but this concept is operational at all longitudes, both far and near side. If 10^{-6} earth g accelerometers are used, the Coriolis and centripetal accelerations must be considered.

   Conventional pole shifting techniques will eliminate the polar singularity for the inertial concept. Similarly, for extremely precise dead reckoning navigation, pole shifting of the latitude-longitude grid to the earth subpoint minimizes error sensitivity coefficients of the earth tracking subsystems.

4. To relax both dead reckoning and position fix component accuracy requirements, homing range extension through the use of passive and active RF and optical beacons is needed. Therefore, the design and performance of experiments should be conducted to verify assumptions regarding optical beacon detection within line of sight and RF propagation beyond the line of sight on the lunar surface.

5. Distance sensor errors are the prime contributors to dead reckoning error. In most instances, one and two orders of magnitude accuracy improvement are required to satisfy concept requirements. Alternate techniques to solve the relative navigation problem requiring benchmark mapping might be hybrid distance-sensing techniques; e.g., short-term accelerometer data coupled with long-term odometer measurement. Also laser, RF, and optical ranging and angular measurement devices performing trilateration and triangulation might be feasible substitutes for mapping tasks. An error analysis of these techniques is recommended for research and development forecasting.

6. In many instances of the current study, particular component errors were obscured by the presence of a large error source in the concept. The doppler radar, an extremely inaccurate land vehicle navigation sensor, largely negated the performance of the remaining RF concept components. Hence, recommendations for component research are hindered since component requirements are a function of total concept functioning. However, analysis directed to the formation of a set of concepts from a matrix of navigation sensors would avert the problem and remove the concept constraint. Since the error models were constructed in generalized hybrid form, the extension of analysis to a matrix of sensors is simplified and this study is strongly recommended.

7. Due to center of radiation/earth centroid error, and large component errors, position fixing utilizing an RF or IR earth tracker measurement on the earth is not recommended.

8. Due to the adverse lunar environment, time independent navigation concepts should be stressed to prevent error growth during performance of auxiliary exploration functions.

9. To minimize position fix errors, and to substantially reduce position fix component requirements, adherence to the optimal celestial/vehicle geometry is recommended. Minimization of time required of the position fix operation should be

considered, and complete digital computation with automation is beneficial. In comparing celestial tracking and earth-based RF tracking, an error analysis of a nominal accuracy type position fix system shows that for comparable position fix accuracies, vertical anomalies as large as 0.1° can be traded off with one to two days of DSIF tracking time. Therefore, a primary mode of on-board position fixing is deemed a necessity.

A study to investigate the feasibility of using an on-board optical sight with intervening space suit masks should be performed since an emergency mode of navigation may require vehicle operation without internal pressurization. Additionally, television and its boresight axis reference may have to serve as backup either for a theodolite or a celestial tracker.

10. Due to the importance of minimum position fix error and the inherent ramifications upon all other sub-concept requirements and component development, vertical independent techniques such as navigational satellites using range and range rate measurements must be analyzed.

11. In summary, the more important recommendations resulting from the analysis of three navigation system concepts are as follows:

    a. Develop and analyze sets of navigation concepts derived from a matrix of navigation sensors. This would provide a greater selection range for system optimization.

    b. Expand the error models to include other important weighting factors such as reliability, weight, volume, power, and cost.

    c. Develop odometers or odometric systems that will provide 3σ errors that are less than 0.1% of distance traveled.

d. Develop accelerometers with a null threshold of 10^{-8} (earth g's).

e. Review present estimates of lunar local vertical deflections. If these estimates (large position errors) are confirmed, applications of navigational satellites and landmark recognition (triangulation) techniques should be analyzed to determine more accurate means for measuring static surface positions.

APPENDIX A

DEAD-RECKONING ERROR MODEL

Dead-reckoning basically involves measurement of the pitch and azimuth motions of the vehicle with respect to fixed references, and some measure of vehicle distance of travel, velocity, or acceleration. The measures of vehicle travel distance (or its derivatives) are resolved into the coordinates of the references by appropriate use of the pitch and azimuth measurements. These differential changes in the coordinates are summed to provide the change in vehicle position as a function of time. This process can be modeled analytically by reference to Figure A-1. Figure A-1 defines the relationship of the vehicle velocity vector to the reference xyz coordinate system.

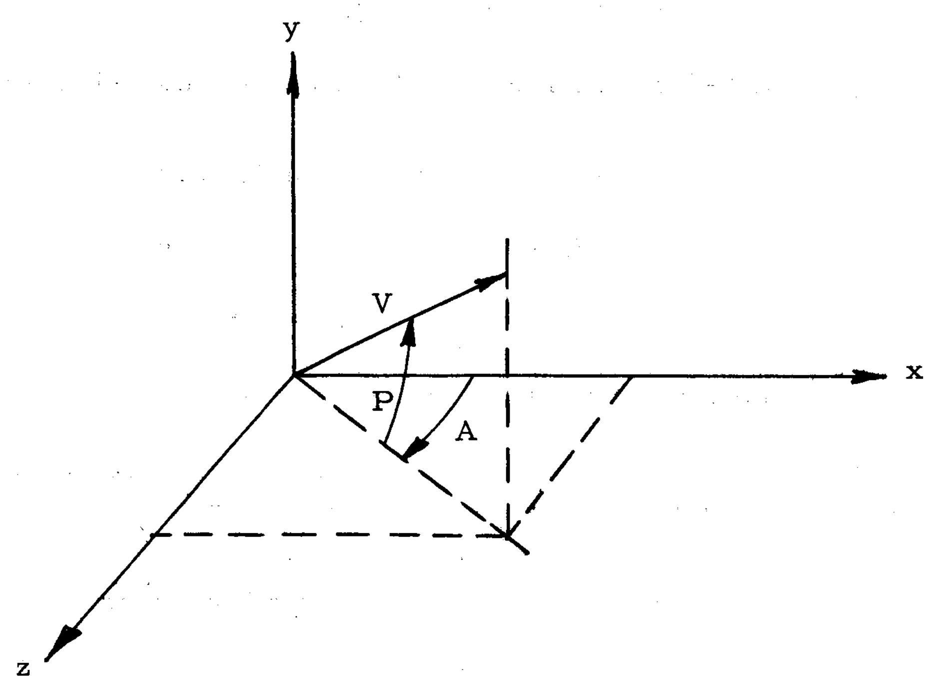

Figure A-1 Dead-Reckoning Reference Axes

From the figure,

$$V_y = V\sin P, \; V_x = V\cos P\cos A, \; V_z = V\cos P\sin A \qquad \text{(A-1)}$$

where

V = vehicle velocity

P = vehicle pitch motion with respect to the local horizontal

A = vehicle azimuth motion in the horizontal plane.

Equation A-1 can be written in terms of an altitude (h), latitude (Γ), longitude (Λ) system (with x axis nominally referenced to lunar north):

$$R\dot{\Gamma} = V\cos P\cos A, \; R\dot{\Lambda} = V\cos P\sin A, \; \dot{h} = V\sin P \qquad \text{(A-2)}$$

where R is the lunar radius (1738 km).

Equation A-2 can be integrated to find the new vehicle positions as:

$$\begin{aligned} R(\Gamma - \Gamma_o) &= \int V\cos P\cos A dt \\ R(\Lambda - \Lambda_o) &= \int V\cos P\sin A dt \\ h - h_o &= \int V\sin P dt \end{aligned} \qquad \text{(A-3)}$$

where the subscript o refers to initial values.

The effects of errors in pitch, azimuth, and velocity can be determined by taking the partial derivatives of Equation A-2.

$$\begin{aligned} \Delta\dot{\Gamma} &= \Delta V \frac{\partial \dot{\Gamma}}{\partial V} + \Delta P \frac{\partial \dot{\Gamma}}{\partial P} + \Delta A \frac{\partial \dot{\Gamma}}{\partial A} \\ \Delta\dot{\Lambda} &= \Delta V \frac{\partial \dot{\Lambda}}{\partial V} + \Delta P \frac{\partial \dot{\Lambda}}{\partial P} + \Delta A \frac{\partial \dot{\Lambda}}{\partial A} \\ \Delta\dot{h} &= \Delta V \frac{\partial \dot{h}}{\partial V} + \Delta P \frac{\partial \dot{h}}{\partial P} \end{aligned} \qquad \text{(A-4)}$$

where

$$\frac{\partial \dot{\Gamma}}{\partial V} = \left(\frac{1}{R}\right) \cos P \cos A, \quad \frac{\partial \dot{\Lambda}}{\partial V} = \left(\frac{1}{R}\right) \cos P \sin A, \quad \frac{\partial \dot{h}}{\partial V} = \sin P$$

$$\frac{\partial \dot{\Gamma}}{\partial P} = -\left(\frac{V}{R}\right) \sin P \cos A, \quad \frac{\partial \dot{\Lambda}}{\partial P} = -\left(\frac{V}{R}\right) \sin P \sin A, \quad \frac{\partial \dot{h}}{\partial P} = V \cos P$$

$$\frac{\partial \dot{\Gamma}}{\partial A} = -\left(\frac{V}{R}\right) \sin A \cos P, \quad \frac{\partial \dot{\Lambda}}{\partial A} = \left(\frac{V}{R}\right) \cos P \cos A.$$

Integration of Equation A-4 yields the following integral equations defining the effects of errors:

$$\Delta\Gamma = \int \frac{\Delta V}{R} \cos P \cos A\,dt - \int \frac{V}{R} (\Delta P) \sin P \cos A\,dt - \int \left(\frac{V}{R}\right) (\Delta A) \sin A \cos P\,dt$$

$$\Delta\Lambda = \int \frac{\Delta V}{R} \cos P \sin A\,dt - \int \frac{V}{R} (\Delta P) \sin P \sin A\,dt + \int \left(\frac{V}{R}\right) (\Delta A) \cos P \cos A\,dt \quad \text{(A-5)}$$

$$\Delta h = \int \Delta V \sin P\,dt + \int (\Delta P) V \cos P\,dt.$$

Treating the error quantities (V, ΔP, ΔA, ΔV, and R) as constant and noting that the vehicle azimuth can always be approximated by a constant over short distances, Equations A-5 can be rewritten as:

$$\Delta\Gamma = \frac{\Delta V}{V} (\Gamma - \Gamma_o) - \Delta A (\Lambda - \Lambda_o) - \frac{\Delta P (h - h_o) \cos A}{R}$$

$$\Delta\Lambda = \frac{\Delta V}{V} (\Lambda - \Lambda_o) + \Delta A (\Gamma - \Gamma_o) - \frac{\Delta P (h - h_o) \sin A}{R} \quad \text{(A-6)}$$

$$\Delta h = \frac{\Delta V}{V} (h - h_o) + (\Delta P) R (\Gamma - \Gamma_o) \cos A.$$

Note that Equations A-6 can be simplified by use of the relationship

$$\tan A = \frac{(\Lambda - \Lambda_o)}{(\Gamma - \Gamma_o)}.$$

This will reduce the variables by eliminating either A, $(\Lambda - \Lambda_o)$, or $(\Gamma - \Gamma_o)$.

Equations A-6 should be studied parametrically as a function of $(h-h_o)$, $(\Gamma - \Gamma_o)$, $(\Lambda - \Lambda_o)$, A, V, and the errors.

As an example, choose:

$$A = 45^o, \ (h-h_o) = 0.1 \text{ km}$$

$$R^2 (\Gamma - \Gamma_o)^2 + R^2 (\Lambda - \Lambda_o)^2 = 100 \text{ km})^2$$

Then:

$$R \, \Delta \Gamma = 70.7 \left(\frac{\Delta V}{V}\right) - 70.7 (\Delta A) - 0.0707 (\Delta P)$$

$$R \, \Delta \Lambda = 70.7 \left(\frac{\Delta V}{V}\right) + 70.7 (\Delta A) - 0.0707 (\Delta P)$$

$$\Delta h = 0.1 \left(\frac{\Delta V}{V}\right) + 50 (\Delta P).$$

If one is only interested in positional errors (not in altitude) then:

$$\text{Positional Error (P. E.)} = \left[R^2 (\Delta \Gamma)^2 + R^2 (\Delta \Lambda)^2 \right]^{1/2}.$$

Assuming independence:

$$\text{P.E.} = \sqrt{2} \left[\left(70.7 \, \frac{\Delta V}{V}\right)^2 + (70.7 \, \Delta A)^2 + (0.0707 \, \Delta P)^2 \right]^{1/2}.$$

APPENDIX B

ANALYSIS OF SYSTEM ERRORS

An initial evaluation of the effects of component errors on navigation performance is covered in Section 3 of this report. That phase of the effort was extended to obtain a more detailed analysis of errors using updated component and parameter data. This was desirable to isolate major error contributions before the computer error models had been completed so that component and parameter investigations could be redirected.

B. 1 POSITION FIX ERROR ANALYSIS

A definition of vectors follows:

$\bar{S}_1$ = unit vector in direction of star 1

$\bar{S}_2$ = unit vector in direction of star 2

P = unit vector directed from center of the moon to vehicle position.

These vectors have the following expressions in terms of selenographic latitude (Γ), longitude (Λ), and unit vectors $\underline{i}$, $\underline{j}$, $\underline{k}$ defining the selenocentric axes.

$$\bar{S}_1 = \underline{i} \cos \Gamma_1 \cos \Lambda_1 + \underline{j} \cos \Gamma_1 \sin \Lambda_1 + \underline{k} \sin \Gamma_1$$

$$\bar{S}_2 = \underline{i} \cos \Gamma_2 \cos \Lambda_2 + \underline{j} \cos \Gamma_2 \sin \Lambda_2 + \underline{k} \sin \Gamma_2$$

$$\bar{P} = \underline{i} \cos \Gamma \cos \Lambda + \underline{j} \cos \Gamma \sin \Lambda + \underline{k} \sin \Gamma$$

A position fix is obtained by measuring the angles between local vertical (assumed collinear with $\bar{P}$) and the directions $\bar{S}_1$ and $\bar{S}_2$ and then solving Equations B-1 for Γ and Λ.

$$\begin{aligned}
\bar{P} \cdot \bar{S}_1 &= \cos \rho_1 \\
\bar{P} \cdot \bar{S}_2 &= \cos \rho_2 \qquad \text{(B-1)} \\
\bar{P} \cdot \bar{P} &= 1
\end{aligned}$$

There are six independent variables: Γ_1, Λ_1, Γ_2, Λ_2, ρ_1, ρ_2. Letting τ denote one of these variables, one has

$$\begin{aligned}
\frac{\partial \bar{P}}{\partial \tau} \cdot \bar{S}_1 &= - \bar{P} \cdot \frac{\partial \bar{S}_1}{\partial \tau} - \sin \rho_1 \frac{\partial \rho_1}{\partial \tau} = a \\
\frac{\partial P}{\partial \tau} \cdot \bar{S}_2 &= - \bar{P} \cdot \frac{\partial \bar{S}_2}{\partial \tau} - \sin \rho_2 \frac{\partial \rho_2}{\partial \tau} = b \qquad \text{(B-2)} \\
\frac{\partial \bar{P}}{\partial \tau} \cdot \bar{P} &= 0
\end{aligned}$$

It can be verified (by taking dot products of Equation B-3 with $\bar{S}_1$, $\bar{S}_2$, and $\bar{P}$) that these equations have the solution

$$\frac{\partial \bar{P}}{\partial \tau} = \frac{a(\bar{S}_2 \times \bar{P}) - b(\bar{S}_1 \times \bar{P})}{\bar{S}_1 \times \bar{S}_2 \cdot \bar{P}} \qquad \text{(B-3)}$$

To investigate the effects of erroneous ephemeris data, it is assumed that the star trackers and vertical sensor are correctly aligned, but the ephemeris gives erroneous values for Γ_1 and/or Λ_1. In this case, the differential $d\bar{P}$ is given by

$$d\bar{P} = \frac{\partial \bar{P}}{\partial \Gamma_1} d\,\Gamma_1 + \frac{\partial \bar{P}}{\partial \Lambda_1} d\,\Lambda_1 . \qquad \text{(B-4)}$$

Using Equations B-3 and B-2, this becomes

$$d\bar{P} = \frac{-\bar{P} \cdot \left[\frac{\partial \bar{S}_1}{\partial \Gamma_1} d\Gamma_1 + \frac{\partial \bar{S}_1}{\partial \Lambda_1} d\Lambda_1\right] \left[\bar{S}_2 \times \bar{P}\right]}{\bar{S}_1 \times \bar{S}_2 \cdot \bar{P}}$$

$$= \frac{-\bar{P} \cdot d\bar{S}_1 [\bar{S}_2 \times \bar{P}]}{\bar{S}_1 \times \bar{S}_2 \cdot \bar{P}} . \qquad \text{(B-5)}$$

The square of the magnitude is

$$\left|d\bar{P}\right|^2 = d\bar{P} \cdot d\bar{P} = \frac{(\bar{P} \cdot d\bar{S}_1)^2 [\bar{S}_2 \times \bar{P}] \cdot [\bar{S}_2 \times \bar{P}]}{(\bar{S}_1 \times \bar{S}_2 \cdot \bar{P})^2}. \qquad \text{(B-6)}$$

Now $d\bar{S}_1$ can be shown to lie in a plane perpendicular to $\bar{S}_1$. Let $\underline{e}_1$ be a unit vector in the direction of the intersection of this plane with the plane of $\bar{P}$ and $\bar{S}_1$. Let $\underline{e}_2$ be a unit vector perpendicular to the plane of $\bar{P}$ and $\bar{S}_1$. Then $d\bar{S}_1$ may be represented as

$$d\bar{S}_1 = \underline{e}_1\, dS_{11} + \underline{e}_2\, dS_{12} \qquad \text{(B-7)}$$

It follows that

$$(\bar{P} \cdot d\bar{S}_1)^2 = (\bar{P} \cdot \underline{e}_1\, dS_{11} + \bar{P} \cdot \underline{e}_2\, dS_{12})^2$$

$$= (\bar{P} \cdot \underline{e}_1\, dS_{11})^2 \qquad \text{(B-8)}$$

$$= \sin^2 \rho_1 (dS_{11})^2$$

Noting that $\sin^2 \rho_2 = (\bar{S}_2 \times \bar{P}) \cdot (\bar{S}_2 \times \bar{P})$, Equation B-6 becomes

$$\left|d\bar{P}\right|^2 = \frac{dS^2_{11} \sin^2 \rho_1 \sin^2 \rho_2}{(\bar{S}_1 \times \bar{S}_2 \cdot \bar{P})^2} \qquad \text{(B-9)}$$

Denoting the mathematical expectation of X by E(X), it is observed that

$$\begin{aligned} E(d\bar{S} \cdot d\bar{S}) &= E\left[dS^2_{11} + dS^2_{12}\right] \\ &= E\,(dS^2_{11}) + E\,(dS^2_{12}). \end{aligned} \tag{B-10}$$

If the probability distribution of the magnitude of $d\bar{S}$ is independent of the direction of $d\bar{S}$, one has

$$E(dS^2_{11}) = E(dS^2_{12}) = E(d\bar{S} \cdot d\bar{S})/2. \tag{B-11}$$

To further reduce the expressions, one needs a vector identity

$$(\bar{S}_1 X\bar{P})\, X(\bar{S}_2\, X\bar{P}) \equiv \left[(\bar{S}_1\, X\bar{S}_2) \cdot \bar{P}\right] \bar{P}\,. \tag{B-12}$$

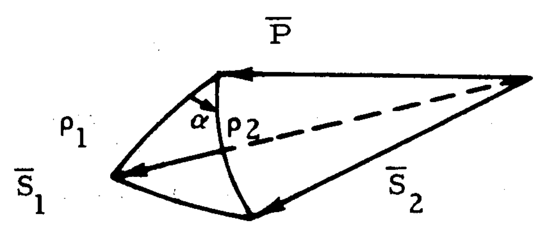

Figure B-1 Star Vector Position Vector Relationship

Referring to the Figure B-1, $\dfrac{\bar{S}_1\, X\bar{P}}{\sin\,\rho_1}$ is a unit vector perpendicular to the plane of $\bar{P}$ and $\bar{S}_1$ while $\dfrac{\bar{S}_2\, X\bar{P}}{\sin\,\rho_2}$ is a unit vector perpendicular to the plane of $\bar{P}$ and $\bar{S}_2$. Calling the angle between these planes α, one has

$$\sin^2 \alpha = \frac{\left[(\bar{S}_1 \ X\bar{P}) \ X(\bar{S}_2 X\bar{P})\right] \cdot \left[(\bar{S}_1 \ X\bar{P}) \ X(\bar{S}_2 X\bar{P})\right]}{\sin^2 \rho_2 \sin^2 \rho} \tag{B-13}$$

Using Equations B-9, B-11, B-12, and B-13, the final form of the error expression is

$$E(\left|dP\right|^2) = \frac{\csc^2 \alpha}{2} E(d\bar{S}_1 \cdot d\bar{S}_1). \tag{B-14}$$

It is readily seen that the same coefficient is obtained for $E(d\bar{S}_2 \cdot d\bar{S}_2)$.

Star tracker errors produce errors in the measured values of ρ_1 and ρ_2. Fixing all the independent variables except ρ_1, one has from Equations B-2 and B-3:

$$\frac{\partial \bar{P}}{\partial \rho_1} = \frac{-\sin \rho_1 (\bar{S}_2 \ X\bar{P})}{(\bar{S}_1 \ X\bar{S}_2) \cdot \bar{P}} \tag{B-15}$$

$$d\bar{P} \cdot d\bar{P} = \left(\frac{\partial \bar{P}}{\partial \rho_1} \cdot \frac{\partial \bar{P}}{\partial \rho_1}\right) d \rho_1^2$$

$$= \frac{\sin^2 \rho_1 (\bar{S}_2 \ X\bar{P}) \cdot (\bar{S}_2 \ X\bar{P})}{(\bar{S}_1 \ X\bar{S}_2 \cdot \bar{P})^2} d\rho_1^2 \tag{B-16}$$

$$= \csc^2 \alpha \ d\rho_1^2$$

The same coefficient is obtained for $d\rho_2^2$. It must be noted that $d\rho_1$ is a component (in the plane of $\bar{P}$ and $\bar{S}_1$) of the star tracker error. Hence, the variance of $d\rho_1$ is half the variance of the star tracker error.

Errors in sensing the local vertical or misalignment of the local vertical have the same effect on position determination, and this effect can be directly assessed. If all other errors are zero, ρ_1 and ρ_2 will be measured from the erroneous vertical, and the position vector obtained from Equation B-1 will be parallel to the erroneous vertical.

A timer error results in a position error equal to the distance the true position moves (moon's rotation) during the time error interval. The speed of a surface point is just the cosine of its latitude multiplied by the moon's angular velocity under the assumption that the polar axis and axis of rotation coincide.

Using 1738 km for the radius of the moon and 27 1/3 days for its sidereal period of revolution, the following expression for the variance of the position fix error is obtained:

$$\sigma_P^2 = \left(8.426 \times 10^{-3} \frac{\text{km}}{\text{sec}}\right)^2 \left[\sigma_1^2 + \sigma_5^2 + \csc^2\alpha \, (\sigma_2^2 + \sigma_4^2)\right]$$

$$+ \left(4.624 \times 10^{-3} \cos \Gamma \frac{\text{km}}{\text{sec}}\right)^2 \sigma_3^2$$

This expression is valid for the error sources considered, provided the errors are independent. The σ_i symbol refers to

$$\begin{aligned}
\sigma_1^2 &= \text{variance of L. V. sensor error (sec}^2) \\
\sigma_2^2 &= \text{variance of star tracker error (sec}^2) \\
\sigma_3^2 &= \text{variance of timer error (sec}^2) \\
\sigma_4^2 &= \text{variance of ephemeris errors (sec}^2) \\
\sigma_5^2 &= \text{variance of gravitational errors (sec}^2).
\end{aligned} \qquad \text{(B-18)}$$

The other parameters are defined as follows:

σ_P^2 = variance of position error (km^2)

α = angle between planes containing local vertical and the two stars

Γ = vehicle selenographic latitude.

The sensitivity coefficients are seen to depend only on the azimuth separation of the two stars (α) and vehicle latitude. The numerical quantities in Equation B-1 are computed from the radius of the moon and its spin velocity. Using Equation B-1 together with the vehicle and star positions used previously yields the following corrected values for the sensitivity coefficients:

$$C_1 = 8.43 \times 10^{-3} \text{ km/sec}$$

$$C_2 = 8.51 \times 10^{-3} \text{ km/sec}$$

$$C_3 = 4.61 \times 10^{-3} \text{ km/sec}$$

$$C_4 = 8.51 \times 10^{-3} \text{ km/sec}$$

Using the state-of-the-art numbers (3-sigma values) as shown in Section 3, the following position fix accuracies may be computed:

$$3\sigma_P = 1.83 \text{ km} \quad \text{(all errors included)}$$

$$3\sigma'_P = 1.59 \text{ km} \quad \text{(ephemeris errors neglected)}$$

$$3\sigma''_P = 1.52 \text{ km} \quad \text{(gravitational errors only).}$$

There is reason to believe that the state-of-the-art number previously used for ephemeris errors is grossly overestimated and that this error may be held to negligible size. The second of the above numbers would then be a better accuracy estimate than the first. The third number is presented to show the overwhelming dependence on uncertainties in the orientation of the gravity vector.

B.2 AZIMUTH REFERENCE ERROR ANALYSIS

The vectors $\bar{S}_1$ and $\bar{P}$ as previously defined are:

$$\bar{S}_1 = \underline{i}\cos\Gamma_1 \cos\Lambda_1 + \underline{j}\cos\Gamma_1 \sin\Lambda_1 + \underline{k}\sin\Gamma_1$$

$$\bar{P} = \underline{i}\cos\Gamma\cos\Lambda + \underline{j}\cos\Gamma\sin\Lambda + \underline{k}\sin\Gamma.$$

True azimuth is measured in the local tangent plant (which is perpendicular to $\bar{P}$) and referenced to the intersection of this plane with the plane containing $\bar{P}$ and $\bar{S}_1$. In the actual system, these planes are determined by the L. V. sensor and a star or earth tracker.

A unit azimuth reference $\bar{A}$ is defined by the expression

$$\bar{A} = \frac{[\bar{S}_1 - (\bar{P} \cdot \bar{S}_1)\,\bar{P}] \cos\alpha + \bar{P} \times \bar{S}_1 \sin\alpha}{[1 - (\bar{P} \cdot \bar{S}_1)^2]^{1/2}}. \tag{B-19}$$

The vector $\bar{A}$ lies in the plane normal to $\bar{P}$ and at an angle α measured counterclockwise from the plane of $\bar{P}$ and $\bar{S}_1$.

The differential contribution of an error in Λ_1 is

$$\frac{\partial \bar{A}}{\partial \Lambda_1} d\Lambda_1 = \left\{ \frac{\left[\frac{\partial \bar{S}_1}{\partial \Lambda_1} - \bar{P} \cdot \left(\frac{\partial \bar{S}_1}{\partial \Lambda_1}\right) \bar{P}\right] \cos\alpha + \bar{P} \times \frac{\partial \bar{S}_1}{\partial \Lambda_1} \sin\alpha}{[1 - (\bar{P} \cdot \bar{S}_1)^2]^{1/2}} + \frac{(\bar{P} \cdot \bar{S}_1)\left(\bar{P} \cdot \frac{\partial \bar{S}_1}{\partial \Lambda_1}\right) \bar{A}}{[1 - (\bar{P} \cdot \bar{S}_1)^2]} \right\} d\Lambda_1 \tag{B-20}$$

A similar expression holds for Γ_1. The differential change $d\bar{A}$ in $\bar{A}$ due to a differential change $d\bar{S}_1$ in $\bar{S}_1$ is the sum of the two expressions.

$$d\bar{A} = \frac{[d\bar{S}_1 - (\bar{P} \cdot d\bar{S}_1)\,\bar{P}] \cos\alpha + \bar{P} \times d\bar{S}_1 \sin\alpha}{[1 - (\bar{P} \cdot \bar{S}_1)^2]^{1/2}} + \frac{(\bar{P} \cdot \bar{S}_1)(\bar{P} \cdot d\bar{S}_1)\, A}{[1 - (\bar{P} \cdot \bar{S}_1)^2]} \tag{B-21}$$

Here, $d\bar{S}_1 = \frac{\partial \bar{S}_1}{\partial \Gamma_1} d\,\Gamma_1 + \frac{\partial \bar{S}_1}{\partial \Lambda_1} d\,\Lambda_1$ has been used. It can be verified that $\bar{A} \cdot d\bar{A} = \bar{P} \cdot d\bar{A} = 0$. Therefore, $d\bar{A}$ must be a scalar multiple of $\bar{P}x\bar{A}$. To evaluate this scalar, one forms

$$(\bar{P} x \bar{A}) \cdot d\bar{A} = \frac{\bar{P} \, x \, \bar{A} \cdot d\bar{S}_1 \cos \alpha + (\bar{P} \, x \, \bar{A}) \cdot \bar{P} \, x \, d\bar{S}_1 \sin \alpha}{[1 - (\bar{P} \cdot \bar{S}_1)^2]^{1/2}} . \tag{B-22}$$

But $(\bar{P} \, x \, \bar{A}) \cdot (\bar{P} \, x \, d\bar{S}_1 = [(\bar{P} \, x \, \bar{A}) \, x \, \bar{P}] \cdot d\bar{S}_1 = \bar{A} \cdot d\bar{S}_1$. Recalling the definition of α, it is readily verified that

$$\bar{P} x \bar{A} \cdot d\bar{A} = \frac{\bar{P} x \bar{S}_1 \cdot d\bar{S}_1}{[1 - (\bar{P} \cdot \bar{S}_1)^2]} . \tag{B-23}$$

Therefore,

$$d\bar{A} = \frac{\bar{P} x \bar{S}_1 \cdot d\bar{S}_1}{1 - (\bar{P} \cdot \bar{S}_1)^2} (\bar{P} x \bar{A}) \tag{B-24}$$

$$d\bar{A} \cdot d\bar{A} = \frac{(\bar{P} x \bar{S}_1 \cdot d\bar{S}_1)^2}{[1 - (\bar{P} \cdot \bar{S}_1)^2]^2} . \tag{B-25}$$

If one sets ρ_1 = angle between $\bar{P}$ and $\bar{S}_1$ and notes that $d\bar{S}_1$ lies in a plane parallel to the unit vector $\bar{P} x \bar{S}_1 \, [1 - (\bar{P} \cdot \bar{S}_1)^2]^{-1/2}$, the expected value of $d\bar{A} \cdot d\bar{A}$ is given by

$$\begin{aligned} E(d\bar{A} \cdot d\bar{A}) &= \frac{1}{[1 - (\bar{P} \cdot \bar{S}_1)^2]} E\left\{ \left[\frac{\bar{P} \, x \, \bar{S}_1}{[1 - (\bar{P} \cdot \bar{S}_1)^2]^{1/2}} \cdot d\bar{S}_1 \right]^2 \right\} \\ &= \frac{E \, (d\bar{S}_1 \cdot d\bar{S}_1)}{2 \sin^2 \rho_1} . \end{aligned} \tag{B-26}$$

In writing this last expression, it has been assumed that the magnitude of $d\bar{S}_1$ is independent of its orientation.

In the same manner that Equation B-21 was derived, the differential change $d\bar{A}$ of $\bar{A}$ due to a differential change $d\bar{P}$ of $\bar{P}$ may be obtained:

$$d\bar{A} = - \frac{\left[(\bar{S}_1 \cdot d\bar{P})\,\bar{P} + (\bar{P} \cdot \bar{S}_1)\,d\bar{P}\right] \cos\alpha + d\,\bar{P} \times \bar{S}_1 \sin\alpha}{\left[1 - (\bar{P} \cdot \bar{S}_1)^2\right]^{1/2}} + \frac{(\bar{P} \cdot \bar{S}_1)(\bar{S}_1 \cdot d\bar{P})\,\bar{A}}{\left[1 - (\bar{P} \cdot \bar{S}_1)^2\right]} . \tag{B-27}$$

It can be verified that $\bar{A} \cdot d\bar{A} = 0$. The projection of $d\bar{A}$ in the local horizontal plane is thus a scalar multiple of $\bar{P} \times \bar{A}$. To evaluate this scalar, one forms

$$\bar{P} \times \bar{A} \cdot d\bar{A} = - \frac{(\bar{P} \cdot \bar{S}_1)\,\bar{P} \times \bar{A} \cos\alpha + (\bar{P} \times \bar{A}) \times \bar{S}_1 \sin\alpha}{\left[1 - (\bar{P} \cdot \bar{S}_1)^2\right]^{1/2}} \cdot d\bar{P}. \tag{B-28}$$

Now $\bar{S}_1$ may be expressed

$$\bar{S}_1 = \left[1 - (\bar{P} \cdot \bar{S}_1)^2\right]^{1/2} \left[\bar{A} \cos\alpha - \bar{P} \times \bar{A} \sin\alpha\right] + (\bar{P} \cdot \bar{S}_1)\,\bar{P}. \tag{B-29}$$

Substituting for $\bar{S}_1$ in the cross product in Equation B-28 and simplifying yields

$$\bar{P} \times \bar{A} \cdot d\bar{A} = - \frac{(\bar{P} \cdot \bar{S}_1)}{\left[1 - (\bar{P} \cdot \bar{S}_1)^2\right]^{1/2}} \left[\bar{A} \sin\alpha + \bar{P} \times \bar{A} \cos\alpha\right] \cdot d\bar{P}. \tag{B-30}$$

Since we are interested in azimuth errors only, this is the only component which need be evaluated. The expected value of the square is

$$E\left\{[d\bar{A} - (\bar{P}\cdot d\bar{A})\bar{P}]\cdot[d\bar{A} - (\bar{P}\cdot d\bar{A})\bar{P}]\right\} = E[(\bar{P}x\bar{A}\cdot d\bar{A})^2$$
$$= \frac{\cot^2\rho_1}{2} E(d\bar{P}\cdot d\bar{P}) . \tag{B-31}$$

In writing the final expression, we have used the fact that $\bar{A}\sin\alpha + \bar{P}x\bar{A}\cos\alpha$ is a unit vector in a plane parallel to $d\bar{P}$. It is assumed that the magnitude of $d\bar{P}$ is independent of its orientation.

The effects of star (or earth) tracker errors may be identified with Equation B-8. Ephemeris errors enter indirectly in that α is measured properly but α itself will be incorrect. Nevertheless, ephemeris errors have the effect given in B-24. Errors in sensing the local vertical or in alignment of the gravitational vector may be identified with B-31.

The effect of a vehicle position error is an erroneous value for the bearing of the objective relative to the reference direction. This requires a separate analysis. Let $\bar{S}_1$, $\bar{P}$, and ρ_1 be defined as before. Let $\bar{S}_2$ be the position vector of the objective and let ρ_1 be the angle between $\bar{P}$ and $\bar{S}_1$. The angle between the plane of $\bar{P}$ and $\bar{S}_1$ and the plane of $\bar{P}$ and $\bar{S}_2$ is given by

$$\cos\alpha = \frac{(\bar{P}x\bar{S}_1)\cdot(\bar{P}x\bar{S}_2)}{[(\bar{P}x\bar{S}_1)\cdot(\bar{P}x\bar{S}_1)]^{1/2}[(\bar{P}x\bar{S}_2)\cdot(\bar{P}x\bar{S}_2)]^{1/2}} \tag{B-32}$$

The differential change in α due to a change $d\bar{P}$ in $\bar{P}$ is given by

$$d\alpha = \frac{d\bar{P}}{\sin\alpha}\cdot\left\{\frac{\cos\alpha}{\sin^2\rho_1}[\bar{S}_1 x(\bar{P}x\bar{S}_1)] + \frac{\cos\alpha}{\sin^2\rho_2}[\bar{S}_2 x(\bar{P}x\bar{S}_2)] - \frac{\bar{S}_1 x(\bar{P}x\bar{S}_2) + \bar{S}_2 x(\bar{P}x\bar{S}_1)}{\sin\rho_1 \sin\rho_2}\right\} \tag{B-33}$$

To evaluate this expression, a pair of vectors $\bar{e}_1$ and $\bar{e}_2$ is defined:

$$\bar{e}_1 \cdot \bar{e}_1 = \bar{e}_2 \cdot \bar{e}_2 = 1$$

$$\bar{e}_1 \cdot \bar{P} = \bar{e}_2 \cdot \bar{P} = 0$$

$$\bar{S}_1 = \bar{P} \cos \rho_1 + \bar{e}_1 \sin \rho_1$$

$$\bar{S}_2 = P \cos \rho_2 + \bar{e}_2 \sin \rho_2$$

$$\bar{e}_1 \cdot \bar{e}_2 = \cos \alpha .$$

Substituting for $\bar{S}_1$ and $\bar{S}_2$ in Equation B-33 and using the fact that $d\bar{P} \cdot \bar{P} = 0$, simplification of the result yields

$$d\alpha = d\bar{P} \cdot \left[\frac{\bar{e}_1 (\cot \rho_2 - \cot \rho_1 \cos \alpha) + \bar{e}_2 (\cot \rho_1 - \cot \rho_2 \cos \alpha)}{\sin \alpha} \right] . \quad \text{(B-35)}$$

The vector in brackets lies in a plane parallel to $d\bar{P}$. Hence, the expected value of $(d\alpha)^2$ is

$$E\left[(d\alpha)^2\right] = \frac{E(d\bar{P} \cdot d\bar{P})}{2} \left[\cot^2 \rho_1 + \cot^2 \rho_2 - 2 \cot \rho_1 \cot \rho_2 \cos \alpha \right] . \quad \text{(B-36)}$$

Here the coefficient of $E(d\bar{P} \cdot d\bar{P})/2$ is the square of the magnitude of the vector in Equation B-35 and it is assumed that the magnitude of $d\bar{P}$ is independent of its orientation.

Using 1738 km for the radius of the moon, the variance of the azimuth error becomes

$$\sigma_A^2 = \frac{\csc^2 \rho_1}{2} \left[\sigma_2^2 + \sigma_4^2 \right] + \frac{\cot^2 \rho_1}{2} \left[\sigma_1^2 + \sigma_5^2 \right]$$

$$+ (1.978 \text{ min/km})^2 \frac{\cot^2 \rho_1 + \cot^2 \rho_2 - 2 \cot \rho_1 \cot \rho_2 \cos \alpha}{2} \sigma_P^2 . \quad \text{(B-37)}$$

The σ_i symbol refers to

$$\sigma_1^2 = \text{variance of L. V. sensor error (min}^2)$$

$$\sigma_2^2 = \text{variance of star (or earth) tracker error (min}^2)$$

$$\sigma_4^2 = \text{variance of ephemeris errors (min}^2) \tag{B-38}$$

$$\sigma_5^2 = \text{variance of gravitational errors (min}^2)$$

$$\sigma_P^2 = \text{variance of present position error (km}^2).$$

The other quantities are defined as follows:

σ_1 = great circle angle from vehicle to star (or earth) subpoint

σ_2 = great circle angle from vehicle to objective

α = desired azimuth angle (angle between great circle to the reference subpoint and the great circle to the objective)

σ_A^2 = variance of azimuth error (min^2).

It is clear from Equation B-37 that the reference point should be chosen near the horizon and in the direction of the objective in order to minimize errors.

Assuming a vehicle position of 5° latitude and 30° longitude (as in Ref. 1), an earth tracker with earth subpoint at 0° latitude and 0° longitude, and an objective 100-km distant in a direction 45° from north, one has:

$\sigma_1 = 30^\circ\ 22.5'$

$\sigma_2 = 3^\circ\ 17.8'$

$\alpha = 143^\circ\ 34.8'$

and

$$(\csc^2 \rho_1)/2 = 1.9555$$

$$(\cot^2 \rho_1)/2 = 1.4554$$

$$\left[1.978 \frac{\text{min}}{\text{km}}\right]^2 \left[\cot^2 \rho_1 + \cot^2 \rho_1 - 2 \cot \rho_1 \cot \rho_2 \cos \alpha\right]/2 = 688.57\ \text{min}^2/\text{km}^2.$$

The following state-of-the-art numbers are used in computing the expected azimuth error:

$3\,\sigma_1$ = 0.5 min (L. V. sensor)

$3\,\sigma_2$ = 6.0 min (earth tracker)

$3\,\sigma_4$ = 1.8 min (ephemeris errors)

$3\,\sigma_5$ = 3.0 min (gravitational errors)

$3\,\sigma_{PP}$ = 1.6 km (present position error).

The present position error dominates

$3\,\sigma_A$ = 43.0 min (all errors included)

$3\,\sigma'_A$ = 43.0 min (present position error only).

The quantity computed here is 3 times the standard deviation of the error in selecting the direction to the objective. If one asks for 3 times the standard deviation of the error made in selecting a particular azimuth, ρ_2 becomes 85° (great circle distance to the north pole) and α is 98° 34.8'. Three σ_A becomes

$3\,\sigma_A$ = 10.2 min (all errors included)

$3\,\sigma'_A$ = 8.4 min (earth tracker only).

Timer errors have not been included in this analysis. However, they may be considered to affect the final accuracy by contributing to ephemeris uncertainty. In any event, it is to be expected that they may be held to a negligible level.

APPENDIX C

SELECTION OF A CELESTIAL OBSERVABLE

This appendix presents the equations necessary to transform a star position given in earth-based celestial coordinates to star subpoint position in lunar latitude and longitude. The star azimuth and elevation measured from an LRV at a point on the lunar surface can then be calculated. Thus, given the observable right ascension and declination, the lunar-based celestial tracker pointing angles may be calculated. A nominal lunar position in the earth orbit is required.

These equations represent an integral portion of the total lunar navigation problem, since it is doubtful that an LRV will perform a lunar mission without a celestial-based capability for position fixing. Hence, with these equations the following problem areas may be studied:

1. Of the 57 selected navigational stars used in earth navigation, which are suitable for lunar surface navigation?

2. Of the 57 selected observables, which fall into the region defined by minimal error sensitivity coefficients?

3. Are the available observables properly distributed spatially?

4. Which observables are affected by earth or solar occultation?

5. What observables, such as Canopus, are available as a lunar reference for which there have been extensive tracker hardware designs?

The above questions may be answered as a function of lunar mission or vehicle position with application of these equations. Also the reality of the error models is enhanced since specific observable positions may be analyzed.

The following nomenclature is used:

η_s	=	star right ascension
δ_s	=	star declination
η_m	=	moon right ascension
δ_m	=	moon declination

$\left.\begin{array}{l}\eta_s, \delta_s, \eta_m, \delta_m\end{array}\right\}$ earth-based celestial sphere

u	=	star latitude subpoint on moon
w	=	star longitude subpoint on moon
R_{E_m}	=	earth-to-moon distance
R_{E_s}	=	earth-to-star distance
R_{m_s}	=	moon-to-star distance
u_E	=	earth latitude subpoint on moon
w_E	=	earth longitude subpoint on moon
x	=	vehicle lunar latitude
y	=	vehicle lunar longitude
ϵ^*	=	star true elevation angle
$(\alpha^* + A_{n, n+1})$	=	star true azimuth angle

In Figure C-1, the celestial coordinate systems are defined. $(\vec{1}_X, \vec{1}_Y, \vec{1}_Z)$ defines an orthogonal triad with origin fixed at the earth center with

$\vec{1}_Z$ = pointing along the Celestial North Pole

$\vec{1}_X$ = pointing towards the Vernal Equinox

$\vec{1}_Y = \vec{1}_Z \times \vec{1}_X$.

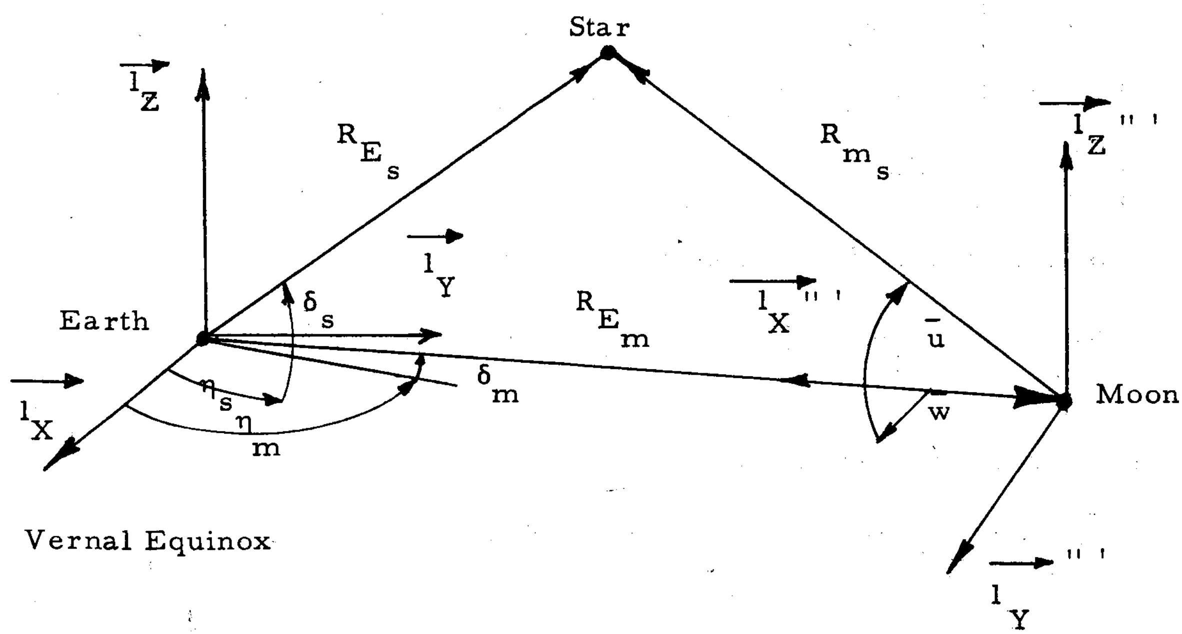

Figure C-1 Definition of Celestial Coordinate Systems

The transformation from earth space to moon space is made by:

1. Rotating $(\vec{1}_X, \vec{1}_Y, \vec{1}_Z)$ about $\vec{1}_Z$ through η_m to get $(\vec{1}_X', \vec{1}_Y', \vec{1}_Z')$
2. Then rotating $(\vec{1}_X', \vec{1}_Y', \vec{1}_Z')$ about $\vec{1}_Y'$ through δ_m to get $(\vec{1}_X'', \vec{1}_Y'', \vec{1}_Z'')$
3. Then rotating $(\vec{1}_X'', \vec{1}_Y'', \vec{1}_Z'')$ about $\vec{1}_Z''$ through 180° to yield $(\vec{1}_X''', \vec{1}_Y''', \vec{1}_Z''')$.

$(\vec{1}_X{}''', \vec{1}_Y{}''', \vec{1}_Z{}''')$ is the moon space with $\vec{1}_X{}'''$ pointing towards the earth along the earth/moon line of centers.

In matrix notation:

$$\begin{bmatrix} \vec{1}_X \\ \vec{1}_Y \\ \vec{1}_Z \end{bmatrix} = \begin{bmatrix} T \end{bmatrix} \begin{bmatrix} \vec{1}_X{}''' \\ \vec{1}_Y{}''' \\ \vec{1}_Z{}''' \end{bmatrix} \tag{C-1}$$

$$\begin{bmatrix} T \end{bmatrix} = \begin{bmatrix} -\cos\delta_m \cos\eta_m & \sin\eta_m & -\sin\delta_m \cos\eta_m \\ -\cos\delta_m \sin\eta_m & -\cos\eta_m & -\sin\delta_m \sin\eta_m \\ -\sin\delta_m & 0 & \cos\delta_m \end{bmatrix} \tag{C-2}$$

The position vector of the moon is given as:

$$\vec{R}_{E_m} = R_{E_m} \left[\cos\delta_m \cos\eta_m \vec{1}_X + \cos\delta_m \sin\eta_m \vec{1}_Y + \sin\delta_m \vec{1}_Z \right] \tag{C-3}$$

and the position vector of a star

$$\vec{R}_{E_s} = R_{E_s} \left[\cos\delta_s \cos\eta_s \vec{1}_X + \cos\delta_s \sin\eta_s \vec{1}_Y + \sin\delta_s \vec{1}_Z \right] . \tag{C-4}$$

The position vector of the star relative to the moon is

$$\vec{R}_{m_s} = \vec{R}_{E_s} - \vec{R}_{E_m} \tag{C-5}$$

$$\vec{R}_{m_s} = \begin{bmatrix} R_1 R_2 R_3 \end{bmatrix} \begin{bmatrix} \vec{1}_X \\ \vec{1}_Y \\ \vec{1}_Z \end{bmatrix} \tag{C-6}$$

which becomes in moon space

$$\vec{R}_{m_s} = \begin{bmatrix} R_1 R_2 R_3 \end{bmatrix} \begin{bmatrix} \\ T \\ \\ \end{bmatrix} \begin{bmatrix} \vec{1}_X''' \\ \vec{1}_Y''' \\ \vec{1}_Z''' \end{bmatrix} \tag{C-7}$$

$$R_1 = R_{E_s} \cos \eta_s \cos \delta_s - R_{E_m} \cos \eta_m \cos \delta_m \tag{C-8}$$

$$R_2 = R_{E_s} \sin \eta_s \cos \delta_s - R_{E_m} \sin \eta_m \cos \delta_m \tag{C-9}$$

$$R_3 = R_{E_s} \sin \delta_s - R_{E_m} \sin \delta_m \tag{C-10}$$

or

$$\vec{R}_{m_s} = \begin{bmatrix} R_4 R_5 R_6 \end{bmatrix} \begin{bmatrix} \vec{1}_X''' \\ \vec{1}_Y''' \\ \vec{1}_Z''' \end{bmatrix} \tag{C-11}$$

Upon manipulation, the unit pointing vector of the star relative to the lunar-based coordinates may be derived. In the derivation note that

$$R_{E_m} << R_{E_s} \text{ and } R_{m_s} \cong R_{E_s} .$$

The direction cosines defining the unit pointing vector are:

$$\frac{R_4}{\left|\vec{R}_{m_s}\right|} = D_X''' = -\cos \eta_s \cos \delta_s \cos \delta_m \cos \eta_m - \sin \eta_s \cos \delta_s \cos \delta_m \sin \eta_m - \sin \delta_s \sin \delta_m \tag{C-12}$$

$$\frac{R_5}{\left|\vec{R}_{m_s}\right|} = D_Y''' = \cos\eta_s \cos\delta_s \sin\eta_m - \sin\eta_s \cos\delta_s \cos\eta_m \tag{C-13}$$

$$\frac{R_6}{\left|\vec{R}_{m_s}\right|} = D_Z''' = -\cos\eta_s \cos\delta_s \sin\delta_m \cos\eta_m - \sin\eta_s \cos\delta_s \sin\delta_m \sin\eta_m + \sin\delta_s \cos\eta_m \tag{C-14}$$

Thus, the star subpoint, defined by the geometry of Figure C-1, may be expressed as general latitude and longitude angles $\bar{u}$ and $\bar{w}$.

$$\sin\bar{u} = D_Z''' \tag{C-15}$$

$$\cos\bar{w} = \frac{D_X'''}{\cos\bar{u}} \tag{C-16}$$

$$\sin\bar{w} = \frac{D_Y'''}{\cos\bar{u}} \quad . \tag{C-17}$$

However, since lunar optical and physical librations occur, the earth/moon line of centers does not pass through the lunar (0, 0) point. Hence

$$u = \bar{u} + u_E \tag{C-18}$$

$$w = \bar{w} + w_E \quad . \tag{C-19}$$

Thus, the star azimuth and elevation can be defined:

$$\epsilon^* = \sin^{-1}\left[\sin u \sin x + \cos u \cos x \cos(w-y)\right] \tag{C-20}$$

$$(\alpha^* + A_{n,n+1}) = \sin^{-1}\left[\frac{\sin(w-y)\cos u}{\cos\epsilon^*}\right] \tag{C-21}$$

A nominal lunar orbit is given in Table C-1.

TABLE C-1

NOMINAL LUNAR ORBIT

t Increasing	α_m (deg)	δ_m (deg)
t_o	17.000	0.0
t_1	30.198	7.833
t_2	35.682	10.140
t_3	48.912	15.146
t_4	65.689	20.100
t_5	102.000	24.000
t_6	139.544	20.145
t_7	169.629	10.180
t_8	193.000	0.0
t_9	208.362	- 7.058
t_{10}	245.722	-20.112
t_{11}	282.000	-24.000
t_{12}	349.702	-10.160
t_{13}	1.506	- 5.092
t_{14}	17.000	0.0

$t_{14} - t_o = 655.721$ hours

APPENDIX D

RF HOMING

Maximum RF homing ranges of the order of 80 to 200 km resulted from this study. These values are based on a number of assumptions including lunar soil constants, and local noise figure. Any marked differences between actual and hypothesized values may result in sizable changes in ranges which can be achieved.

D.1 SYSTEM LOSSES

L. E. Vogler (Ref. 100) has derived expressions for the power required to establish point-to-point communications on the surface of the moon, based on some simplifying assumptions which include the existence of a smooth spherical lunar surface and a homogeneous soil. The transmitted power required to achieve a specified signal-to-noise (S/N) ratio at the receiver terminals beyond line of sight is given by the expression:

$$P_T = 20 \log (4\pi d_o/\lambda) + A_t - (G_T + G_R) + R + F + B + 10 \log (k_B t_o) \qquad \text{(D-1)}$$

where

P_t = transmitter power expressed in db referred to 1 watt

d_o = range between transmitting and receiving antennas in meters (m)

λ = wavelength in meters

A_t = attenuation of the surface wave relative to free space due to effects of intervening terrain expressed in db (this factor is a complex function of range, height of antennas, wavelength, and of dielectric constant and conductivity of the terrain).

$G_{t,r}$ = gain of transmitting and receiving antennas, respectively, expressed in db referred to an isotrope

= $(D_t - L_{\eta t})$, $(D_r - L_{\eta r})$ where D_t, D_r = directivity of the respective transmitting and receiving antennas and $L_{\eta t}$, $L_{\eta r}$ = losses due to inefficiency of transmitting and receiving antennas (ohmic losses, matching network losses, etc).

R = minimum S/N ratio in db

F = effective noise figure due to external noise sources expressed in db

B = effective noise bandwidth expressed in db

k_B = Boltzmann's constant = 1.38×10^{-23} joule/deg

t_o = temperature in ^oK.

To derive quantitative results, the following assumptions have been made concerning a number of these parameters.

D. 1. 1 Surface Wave Attenuation (A_t)

The surface wave attenuation is a function of the electrical properties of the lunar soil, which are not presently known and probably will not be known accurately until samples have been tested. Considerable difference of opinion exists as to the nature of the lunar terrain. For the purpose of this study, values of dielectric constant of $\epsilon_R = 1.1$ and of $\sigma = 3.4 \times 10^{-4}$ mhos/m, which were derived by Senior and Siegel (Ref. 104), have been used. These constants imply a layer of dust extending to a considerable depth.

Values of A_t have been derived from parametric curves in Ref. 100, using these constants. Additional values can be derived based on values which might be representative of dry rock formations.

D. 1. 2 Antenna Gain (G_t, G_R)

For reasons which are apparent in the following section, a trans-horizon D/F system on the moon has to operate at frequencies below about 10 Mc, if any advantage is to be derived from the lower surface-wave attenuation. At these frequencies, the choice of antennas is somewhat limited by practical considerations of size, weight, and erectability.

It has been assumed that an omnidirectional beacon antenna is desirable; hence the use of a vertical mast or whip antenna (or a variant) operated over an artificial ground-plane appears to be a logical choice. The directivity of such an antenna ranges from 4.5 db if less than 0.1 wavelength high to 4.7 db if it is one-quarter wavelength. Estimates of the antenna efficiency are discussed in Section D.3.

The loop antenna has been selected as the prototype to be used for direction finding on the roving vehicle. At the frequencies in question, such an antenna would perforce be electrically small. The directivity of such an antenna is 1.5 db; estimates of the efficiency of practical configurations are also treated in Section D.3.

D.1.3 Minimum S/N Ratio (R)

A minimum S/N ratio of R = 10 db has been selected for estimating the required power. However, considerably lower S/N ratios may provide satisfactory service if correlation techniques are used to detect signals. Since an appreciable reduction in transmitter power levels might result, a more detailed study will be required to evaluate the trade-offs between system complexity, weight, response time, power, and range which would result from the use of such techniques.

D.1.4 Noise Figure (F)

This factor will not be known accurately until measurements have been made on the lunar surface. This factor has been roughly estimated in Vogler's article, on the basis of radio maps, as

$$F = 10 \log (1.585 \times 10^5 f_{Mc}^{-2.3}) \qquad \text{(D-2)}$$

at frequencies below 200 Mc, where f_{Mc} is the frequency in megacycles.

D.1.5 Bandwidth (B)

A modulating frequency of 40 cps (B = 16 db) has been arbitrarily selected for the present survey. Wider bandwidths are less demanding in terms of frequency stability, but also result in a substantial increase in transmitter power levels or a reduction in effective range. Conversely, a reduction in bandwidth to a modulating frequency such as 4 cps would result in an increase in range. A study which is beyond the scope of this investigation should be conducted on D/F requirements to determine the narrowest feasible operational bandwidth.

D. 1.6 Temperature (t_o)

A reference temperature of $t_o = 288.39^oK$, on which the factor F is based, has been used in this study.

D. 2 MAXIMUM RANGE OF HYPOTHETICAL OPTIMUM ANTENNAS

Before considering the effect of the losses of practical antennas on power and range, it is instructive to consider what these values might be in the case of hypothetical 100% efficient transmitting and receiving antennas. Inserting the appropriate values of those parameters which have been fixed so far, Equation D-1 can now be rewritten as:

$$P_T = 20 \log d_o - 20 \log (\lambda) + A_t + F + 246 \text{ db} \qquad \text{(D-3)}$$

since $L_{\eta t} = L_{\eta r} = 0$ for 100% efficient antennas.

This expression has been reduced to graphical form in Figure D-1 where P_T is plotted in db referred to 1 watt as a function of frequency for several values of range expressed in kilometers. As would logically be expected, these curves show a general decrease of required transmitter power for a given range as frequency decreases. Though it appears advantageous to select a very low operational frequency, the physically realizable antennas are very small in terms of wavelength and, in practice, such antennas are very inefficient. This efficiency is estimated in the following section.

D. 3 ANTENNA EFFICIENCY

Physical antennas such as monopoles and loops, whose principal dimension (length, in case of the stub, diameter in the case of loop) is of the order of a quarter of a wavelength, are generally close to 100% efficient if low resistivity conductors such as copper and low loss dielectrics are used in their construction. However, when these dimensions decrease below about one-tenth of a wavelength, their radiation resistance decreases to very small values. As a result, ohmic losses may become an appreciable

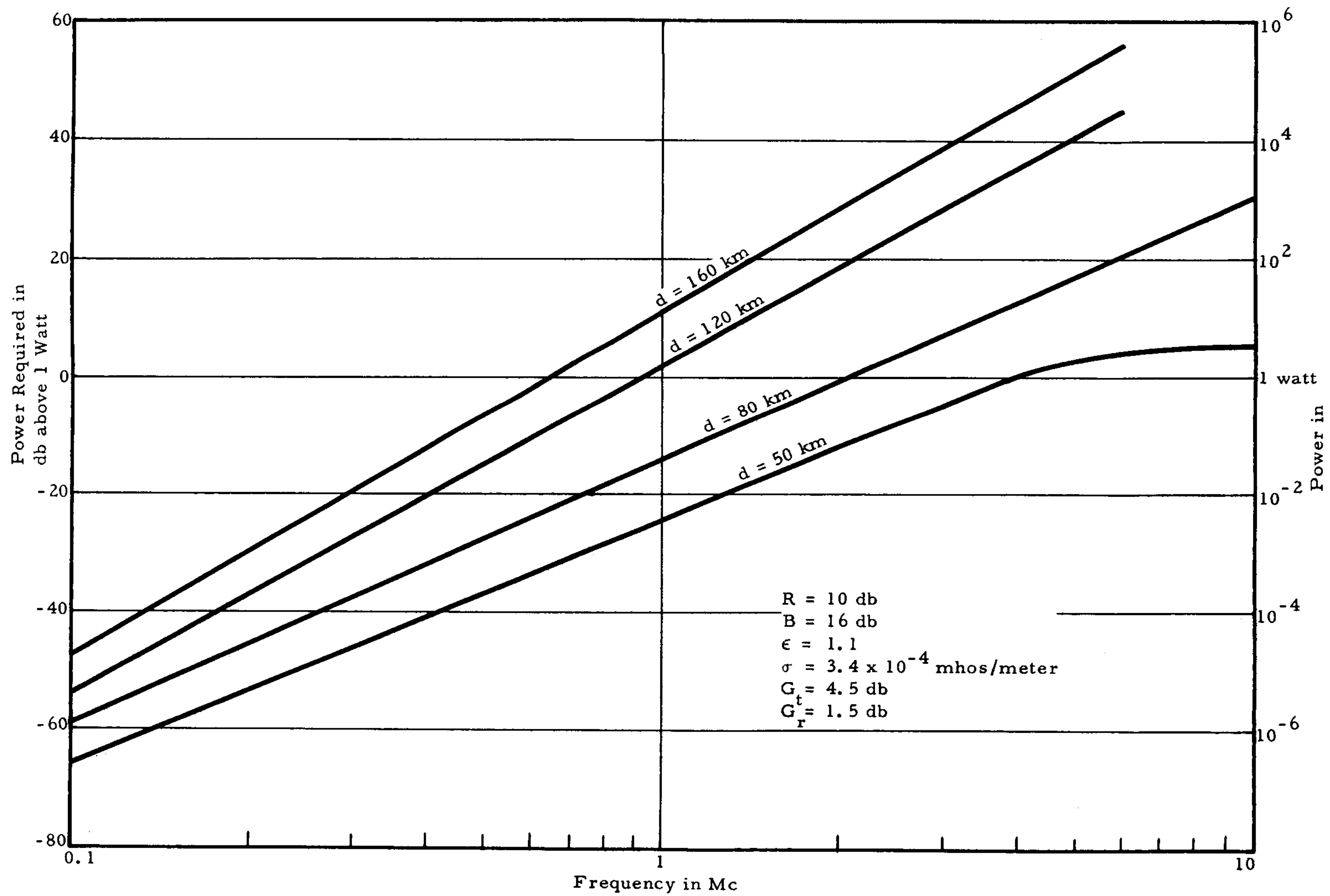

Figure D-1 Power Required for D/F Circuit on Moon, at Various Ranges, Assuming Hypothetical 100% Efficient Antennas proportion of the total input resistance. Furthermore, the low resistance coupled with a high reactance requires the use of a matching network to achieve an efficient transfer of power from the transmitter to space, or from space to the receiver. In the case of the short mast or whip, the reactance is capacitive, and a matching inductive reactance is required to cancel it. Practical inductors have finite losses which in the case of very high reactance antennas become appreciable. Even if such losses could be reduced to arbitrarily small values, it would be undesirable to do so, since it would be difficult to maintain the resultant very high Q circuit in tune.

The estimated losses of the antennas are dependent on the particular parameters such as height, diameter, construction, etc, which have been selected. Antenna parameters considered to be within a range currently achievable both in terms of transportation and erection on the lunar surface have been selected. In the case of the transmitter, a 0.0254-m diameter, 10-m tall mast has been selected. To demonstrate the improvement in performance which results from the use of a substantially taller structure, the efficiency of a 0.60-m effective diameter, 100-m high tower has been calculated for comparison purposes. (The 0.6-m effective diameter is considerably smaller than the actual physical size of the open strut tower and is used solely to estimate efficiency.)

For the receiving antenna, a 100-turn, 1 x 1 meter square loop of #20 copper wire (8.1×10^{-4} meter diameter) has been selected; this amounts to about 1.85 kg (nominally 4 lb) of copper wire with no estimate of the weight of the required support structure. This particular choice does not necessarily represent the optimum loop for a given weight of copper; optimization of the loop design is not treated in this report.

D.3.1 Transmitting Antenna

Figure D-2 shows the 0.25λ and 0.1λ heights of a mast as a function of frequency in the 0.1- to 10-Mc range, for general reference. Ideally, the mast should be $\lambda/4$ high (or very close to it). If the height is reduced substantially below 0.1 wavelength, the radiation resistance decreases porportionally to the square of its height and its reactance increases to a first approximation as the cotangent of its electrical height. Thus, the 0.1λ curve represents the height below which most losses become appreciable.

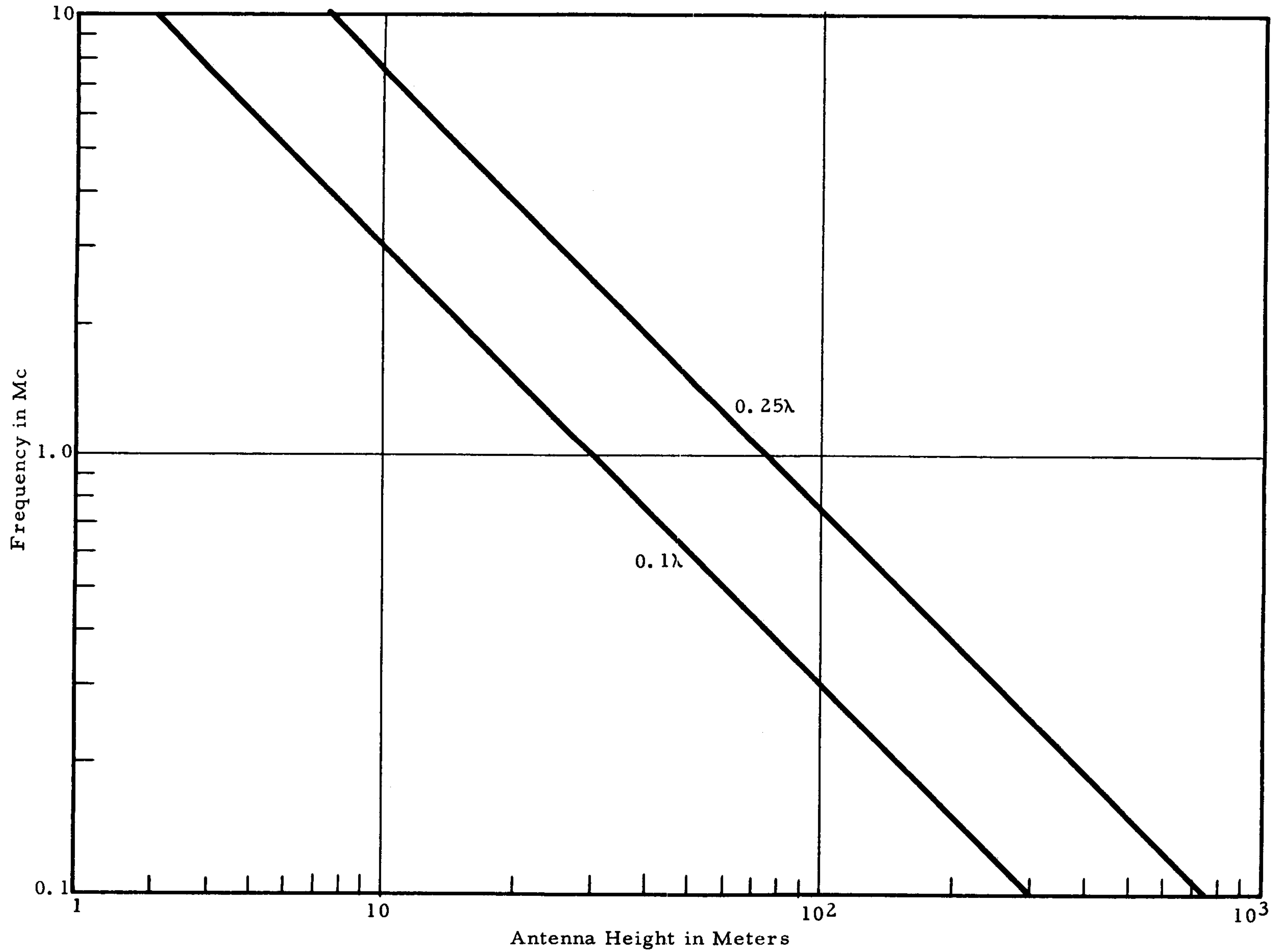

Figure D-2 Height of 0.25λ and 0.1λ Vertical Monopole Antennas as a Function of Frequency

It has been assumed that the Q of the associated matching network will be 300. The ohmic losses of the two postulated masts (10-m and 100-m) were calculated and found to be negligible, assuming the conductors to be copper clad. In addition of the ohmic and matching network losses, there are also losses in the ground system, particularly in the case of poor soil conductivity. These losses can be substantially reduced by laying out a system of ground wires around the base of the antenna to a radius equal to at least twice the height of the tower. Ground losses have not been estimated and have not been included in the calculations.

Figure D-3 shows the estimated efficiency losses of the 10-m mast and 100-m tower. In the case of the 10-m antenna these losses become appreciable (10 db) at 1 Mc; if the height is increased to 100 m, the losses become appreciable at one-tenth the frequency. At 0.1 Mc, increasing the height from 10 to 100 meters results in a 30-db decrease in antenna losses; the amounts are proportionately less at higher frequencies.

D.3.2 Receiving Antenna

The radiation resistance of a loop whose cross section is less than 0.1λ is proportional to the square of its area and to the square of number of turns, and inversely proportional to the fourth power of the wavelength. Thus, the radiation resistance of an electrically small loop is very low; considerable improvement in performance can be derived by making its cross section as large as practicable.

A 1 x 1 meter cross section was selected as a practical cross section; on a purely arbitrary basis, a nominal maximum weight of copper wire of 1.85 kg (4 lb) was selected. A comparison of the efficiency of several different combinations of wire size and number of turns showed that best performance is achieved with 100 turns of #20 wire. Though this is not necessarily the optimum for a given weight of copper, it appears to provide typical results. The estimated losses of this antenna, which are based on the ratio of radiation resistance to the sum of radiation resistance and ohmic losses, are presented in Figure D-4. The losses increase from about 2 db at 10 Mc to about 62 db at 0.1 Mc. The losses of the capacitive reactance network have been assumed to be negligible.

Since the losses in the loop are large, it is well to consider what steps could be taken to reduce them. The following conclusions are based

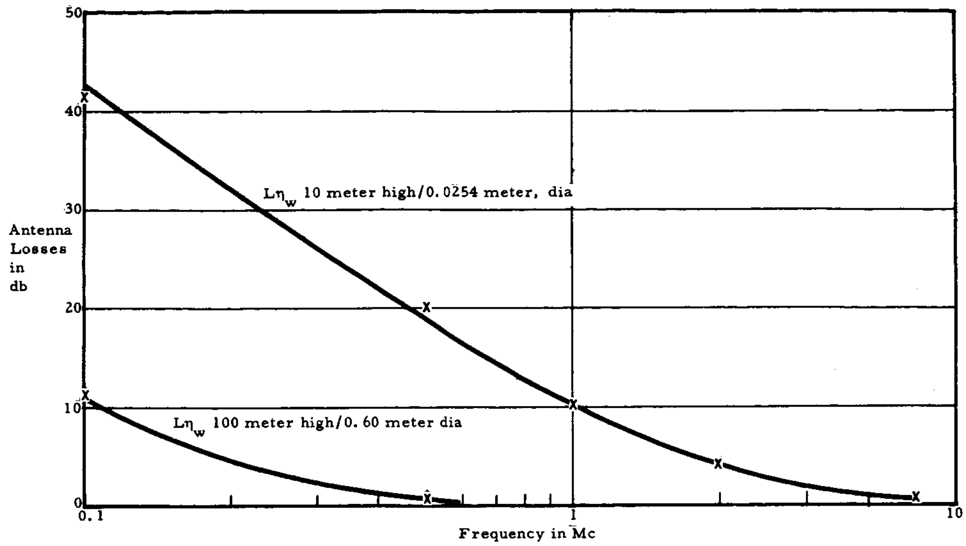

Figure D-3 Estimated Efficiency of 10-Meter Mast and 100-Meter Tower as a Function of Frequency

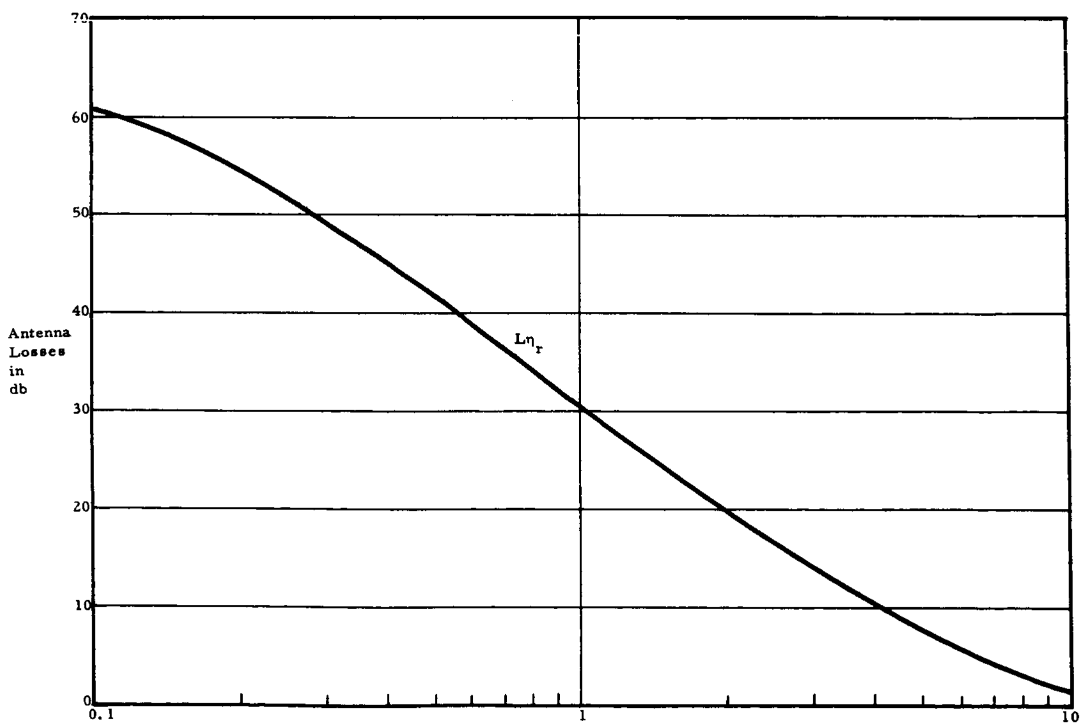

Figure D-4 Estimated Efficiency of 1 x 1 Meter Loop, 100 Turns, #20 Wire on the assumption that a solid conductor is used. Increasing the size of the square loop by a factor m will result in an increase in weight of copper by the factor m and a decrease in losses by a factor m^3 (30 log m db). Increasing the number of turns by n increases the weight by the factor n and decreases the losses by the factor n (10 log n db). An increase of the conductor cross section by a factor p results in an increase in weight of p^2 and a decrease in losses by the factor p (10 log p db).

D.4 POWER-RANGE RELATIONSHIPS FOR "PRACTICAL" ANTENNA SYSTEMS

Figure D-5 shows the power requirements as a function of frequency at several ranges for a 10-m mast transmitting antenna and a 100-turn, 1 x 1 meter loop receiver; at frequencies above 7.5 Mc, the use of a quarter wavelength mast (see Figure D-2) was assumed. Figure D-6 shows the power requirements for a 100-m tower transmitting antenna and the same receiving antenna; likewise at frequencies above 0.75 Mc, the use of a quarter wavelength structure, whose height can be determined from Figure D-2,was assumed. These curves should be compared with those in Figure D-1 which are based on hypothetical 100% efficient antennas. Several differences are immediately apparent. The power requirements no longer decrease indefinitely with decreasing frequency; an optimum frequency band appears in which power requirements for a given range are minimal. Thus, in the case of the 10-m mast at a range of 80 km, a minimum of 100 watts is required in the 2- to 5- Mc band. It is interesting to note that the location of this optimum frequency band shifts to lower frequencies with increasing range. Thus, at 120 km the minimum power requirement occurs around 1 Mc.

A comparison of Figures D-5 and D-6 shows that a substantial decrease in power requirements can be accomplished by increasing the antenna height and thus improving its efficiency. For 100-watt transmitter power, it is possible to D/F over a maximum range of about 80 km in the 2- to 5-Mc band with a 10-m mast. Increasing the height of the transmitting antenna to 100 m extends the range to an estimated 130 km, if the operational frequency is lowered to 0.2 Mc.

Further improvements in performance can be accomplished by increasing the efficiency of the loop. The most effective means of improving the loop performance results from an increase in its size. Doubling the

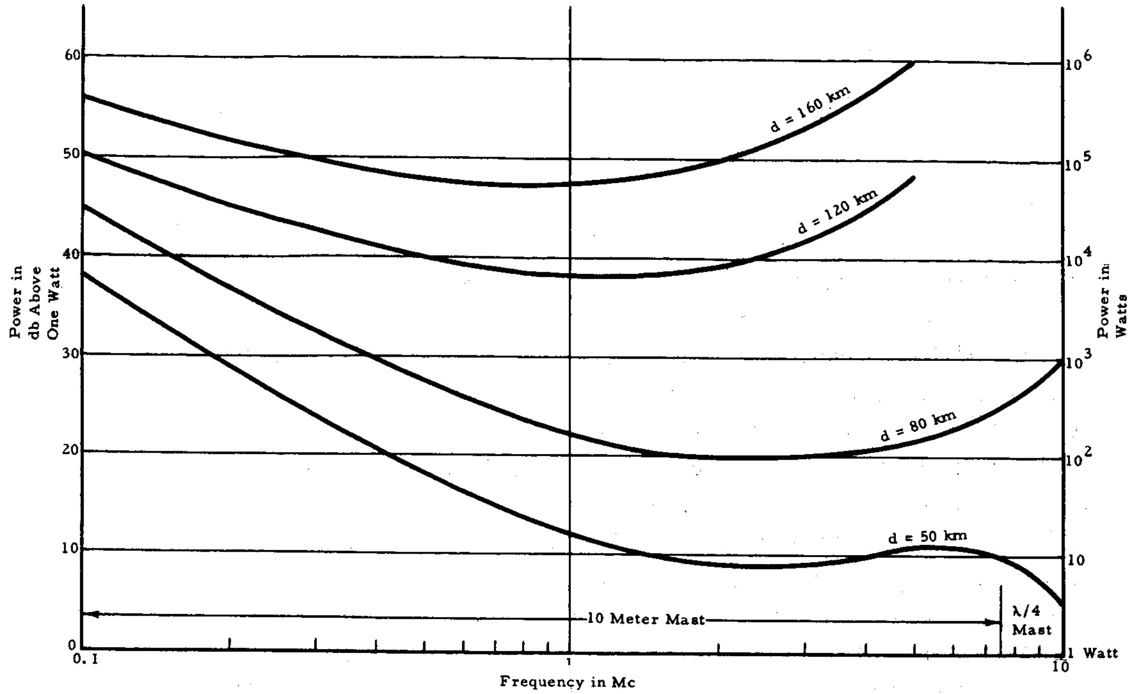

Figure D-5 Power Required for D/F Circuit on Moon, for 10-Meter Mast Beacon Antenna and 100-Turn, 1 x 1 Meter Loop

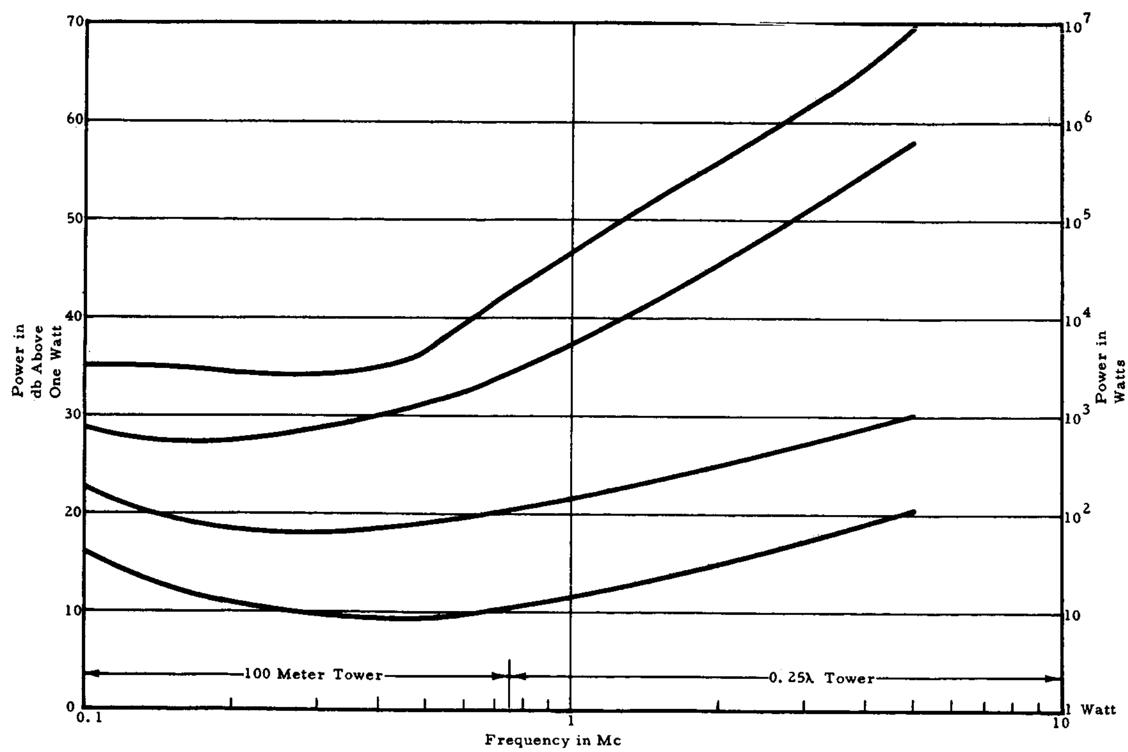

Figure D-6 Power Required for D/F Circuit on Moon, for 100-Meter Tower Beacon Antenna, and 100-Turn, #20 Wire, 1 x 1 Meter Loop

loop to a 2 x 2 meter size results in a 9-db improvement in performance. In addition to this and other changes which would increase the weight, it may be feasible to improve the efficiency by resorting to other than conventional techniques. In the example selected for this study, the conventional use of solid copper wire was postulated. Since the induced RF currents are substantially contained within one skin depth (2×10^{-4} m at 0.1 Mc) around the conductor periphery, it is desirable to increase the cross section of the conductor while leaving the center void. Thus a thin, film inflated plastic tube (such as Mylar) coated with a two-skin-depth thick layer of copper could form a very low weight/low resistance conductor. However, a gas inflated structure is not desirable in a high vacuum environment and is subject to puncture by micrometeorites or dust particles. Such a tube could be foamed in place with a low density 80 kg/m^3 (5 lb/ft^3) foam such as polyurethane. Since the expanded conductor would require considerable volume, assembly and erection of such a loop might have to be accomplished after lunar landing.

APPENDIX E

MEAN THEOREM APPLICATION TO GENERAL DEAD-RECKONING ERROR MODEL

This appendix presents the proof that the effect of

$$R \cos x\,(t) \cong R \cos\left(\frac{x_D + x_o}{2}\right)$$

is a satisfactory approximation for the dead-reckoning error model. It is to be shown that

$$\int_o^t \frac{V \cos P \sin A \;\; dt}{R \cos x} \cong \frac{1}{R \cos\left(\frac{x_D + x_o}{2}\right)} \int_o^t V \cos P \sin A \;\; dt \quad \text{(E-1)}$$

The term R cos x is the expression for the radius of equal latitude circles as a function of latitude. This term may be expressed by a Taylor series about an initial latitude x_o:

$$R\,(x) \cong R\,(x_o) - \sin\,(x_o)\,(S) \quad \text{(E-2)}$$

where higher order terms may be neglected for:

$$R\,(x) \triangleq R \cos x$$

and where S is the distance traveled in a northerly direction along a meridian of longitude measured from the parallel of latitude x_o.

Using the notation,

$$R\,(x) = c$$

$$-\sin\,(x_o) = b$$

Equation E-1 may now be written as:

$$\int_0^t \frac{V\cos P\sin A dt}{R\cos x} \cong \int_0^t \frac{V\cos P\sin A dt}{C' + bS} \qquad \text{(E-3)}$$

Assume over a short traverse that velocity V, pitch P, and azimuth A are constant (or average quantities). Since the variation of the denominator is greatest for a northerly traverse, and since we are interested in the magnitude of the variation about some mean value, assume A = 0.

Then,

$$\int_0^t \frac{V\cos P\sin A dt}{C+bS} = \int_0^t \frac{K\,dt}{C+bS} = \int_0^{Vt} \frac{K_1 dS}{C+bS} \triangleq I \qquad \text{(E-4)}$$

$$I = \frac{K_1}{b} \log \left| 1 + \frac{bVt}{C} \right| \qquad \text{(E-5)}$$

Expanding Equation E-5:

$$I = \frac{K_1}{b} \left[\frac{bVt}{C} - \frac{1}{2}\left(\frac{bVt}{C}\right)^2 + \frac{1}{3}\left(\frac{bVt}{C}\right)^3 + \ldots\ldots \right] \qquad \text{(E-6)}$$

For $\frac{bVt}{C} \ll 1$,

$$I \cong K_1 \left[\frac{Vt}{C} - \frac{b}{2}\left(\frac{Vt}{C}\right)^2 \right] \qquad \text{(E-7)}$$

Now from Equation E-1 and the assumptions following Equation E-3

$$I' \triangleq \int_0^t \frac{Kdt}{R\cos\left(\frac{x_D + x_o}{2}\right)} \qquad \text{(E-8)}$$

but

$$R\cos\frac{x_D + x_o}{2} \cong R\cos x_o - \sin x_o \left(\frac{S_D - S_o}{2}\right)$$

$$I' \cong \int_o^t \frac{Kdt}{C + b\left(\frac{Vt}{2}\right)} = \int_o^{Vt} \frac{K_1\, dS}{C + b\left(\frac{Vt}{2}\right)} \tag{E-9}$$

$$I' \cong \frac{K_1 Vt}{C + \frac{bVt}{2}} = \frac{K_1 Vt}{C} \left(\frac{1}{1 + \frac{bVt}{2C}}\right) \tag{E-10}$$

Since $\frac{bVt}{2C} << 1$ and taking the Maclaurin series,

$$I' \cong \frac{K_1 Vt}{C} \left[1 - \frac{bVt}{2C} + \left(\frac{bVt}{2C}\right)^2 \;\ldots\ldots\right] \tag{E-11}$$

$$I' \cong K_1 \left[\frac{Vt}{C} - \frac{b}{2}\left(\frac{Vt}{C}\right)^2\right] \tag{E-12}$$

hence

$I' \cong I$ from Equations E-7 and E-12. This expression is sufficient for S_{max} = 1 km and $x < 70^o$. At $x = 70^o$, the error is $1/(1.4 \times 10^6)$.

APPENDIX F

REFERENCES

1. "Lunar Radio Beacon Location by Doppler Measurements", Gabbard & Baker, AIAA Journal, April 63.

2. "Vis. Det. of Lite-Sources on or Near the Moon", Dole; AD 133032 Rand, 27 May 57.

3. Lunar Logistics System, Volume VI, "Tracking & Mission Control," Aeroballistics Div. NASA MSFC, MTP-M-63-1, 15 March 63.

4. "Apollo Logistics Support Systems MOLAB studies", Doyle Thomas Working Papers, Northrup, NSL E30-8, June 64.

5. "Radio Tracking Tech. and Perf. of USDSIF", Rezetti Fearey, Hall, Ostermier, AD 264261.

6. "Apollo Logistic Support Systems MOLAB Studies", Task rep. Sec 9 Thomas, Northrup, NASA TMX-53032.9, March 64.

7. "Methods for Estimating Instrumentation System Accuracies", IRIG of Range Comm. Conf., Document No. 104-62, Nov 62.

8. "On the Transformation of Prob. Ellipses into Circles for Impact Problems", Baur; Land Air Inc., Report No. 34, Contract N-123 (61756)19425 A/PMR.

9. "Logic of Approach to Analysis of Complex Systems", AD275534.

10. "Probability Applications to Weapon System Analysis", AD282648.

11. "Lunar Vehicle Guidance Study", AD273301.

12. "Selenographic Coordinates", Kalensher, JPL Report No. 32-41, Feb 61.

13. "Navigation Instruments", AD411758.

14. "Star Tracker Aerospace Reference Study", AD294927.

15. "A Dead-Reckoning Land Vehicle Navigation System," Wall, Aviation Electric Ltd., Montreal, Quebec, presented at 20th Annual Mtg. of the Institute of Navigation, 15-17 June 64, New York, N.Y.

16. "Extended Lunar Exploration", Evans, Advanced Manned Mission Prog.

17. "Preliminary MOLAB Navigation Study", TR7311-64-19R, The Bendix Corporation, Eclipse-Pioneer Division, Nov 64.

18. "Celestial Navigation Sensitivity Study", Breseke, Bendix Systems Division, IOM #64-261-837, Jan 64.

19. "Post-Apollo Lunar Program Phases & Possible Exploratory Mission Sequence", David Paul, MSFC, June 64.

20. "Preliminary ALSS Navigation", Breseke, Bendix Systems Division, IOM #64-261-806, Jan 64.

21. "Terrestial Navigation Using Satellites", N64-1110, NASA, October 62.

22. "Engineering Problems on Lunar Environment", N64-12678.

23. "Eqns. for Nav. by CW Doppler from Earth Satellites", N64-18389.

24. "Physical Constant Uncertainties on Lunar Orbit Determination", N64-18086.

25. "Lunar Orbit Stability", N64-17680.

26. "Strapped-Down Systems", N64-15258.

27. "A Study of Factors Affecting the Accuracy of Pos. Fix for Lunar Traj.", NASA Tn D-2178, Nov 63.

29. "An Analytical Study of the Magnetic Field Encountered by Artificial E. Sat. in Cir. Orb.", NASA TN D-2091.

30. "Guidance and Control State of the Art", AD 337-580.

31. "Normal Bivariate Density Function", AD412332.

32. "Monte Carlo", AD410290.

33. "A Critical Survey of in Orbit Guidance and Control Prob., A Functional Analysis of a Master Control Center", TD Rep. #ESD-TDR-63-482, Dec 63.

34. "Astrodynamic Constants", AD430017.

35. "Error Analysis the Covariance Method", AD296892.

36. "History of Inertial Guidance", AD419538.

37. "Orbit Determination Error Analysis", AD419467.

38. "Survey of Trajectory Guidance & Propulsion for Rendezvous", AD414106.

39. "Servo Analysis of an Inertial Platform", AD416538.

40. "Navigation & Guidance", AD405953.

41. "Estimating the Accuracy of Navigation Systems", AD427269.

42. "Error Analysis of Vehicular Navigation System", AD219999.

43. "Error Analysis of Vehicular Navigation System", AD219998.

44. "Bibliography on Extraterrestrial Research", AD410518.

45. "Soil Trafficability", AD410212.

46. "Terrain Sensing", AD407584.

47. "Lunar Landing & Takeoff", AD404744.

48. "Power Lines/Harmonic Induction Lines", AD419607.

49. "Bibliography of Lunar & Planetary Research", AD428471.

50. "Lunar Alignment Systems Investigation", AD419048.

51. "Optimal Thrust Programming for a Soft Lunar Landing", AD429017.

52. "Automatic Contour Display", AD417193.

53. "Timing & Space Navigation with Existing Ground Stations", AD246270.

54. "Lunar Photometry for Navigation", AD273310.

55. "Guidance & Navigation Systems for Lunar Missions", ARS Reprint 2294-61, October 61.

56. "Physical Phenomena for Space Navigation ", AD243695.

57. "Bibliography of Reports on Data Acquisition Instrumentation", AD275277.

58. "Fundamental Limitations on Inertial Measurements", ARS Reprint 1925-61, August 61.

59. "Submarine Doppler Navigation with Space Satellites", AD239793.

60. "Space Reference Systems", AD275853.

61. "Photometric Environment on the Lunar Surface", Bendix Systems Division, BSR 946, May 64.

62. "LRV Optical Studies Phase II Progress Report", Bendix Systems Division, BSR 913, March 64.

63. "Orbit Determination for a Lunar Satellite", JPL TR 32-483, March 64.

64. "Control System Lags and Man-Machine System Performance", NASA CR-83, July 64.

65. "Vehicle Navigation Study, Phase I, Error Analysis", AD219997.

66. "Radar Siting by Trilateration", AD601567.

67. "Navigation Systems for Land Vehicles", AD234604.

68. "Effects of Television Bandwidth on Target Identification", AD435746.

69. "JPL Celestial Sensor Activities, 1 June 60 through 1 Jan 63", FI 132, N64-13288, Jan 63.

70. "Inertial Guidance Engineering", Macomber & Fernandez, Prentice Hall Space Technology Series, 1962.

71. "Study to Estimate the Guidance and Navigation Subsystem for the Lunar Roving Vehicle", Honeywell Aero Rept., R-ED 25223, Nov 62.

72. "Effect of a Lunar Ionosphere on Lunar Surface Radio Communications", U of M Radio Astr. Observatory, Newbern Smith, Report No. 64-7, June 64.

73. "Development of Techniques for Prediction of System Effectiveness", RADC-TDC-63-407, Feb 64.

74. "Advanced Land Navigation, A Prototype Course", US Army, Ft. Benning, Ga., July 63.

75. "Experimental Investigations of the Land Navigation Process", US Army, Ft. Benning, Ga., Jan 64.

76. "Plotting Radiolocation Predictions and their Errors", Univ. of Illinois, RRL Report No. RRL-230, March 64.

77. "Calibration of Altazimuth Instruments by Means of Star Photography", Tech Note No. I. R. 37, Royal Aircraft Est., Feb 64.

78. "Factors Contributing to Errors in Inertial Navigation Systems", AD215886, 1959.

79. "The Theory of Visual Range of Aids to Navigation", AD242082.

80. "Indication of the Vertical From Moving Bases", AD158729.

81. "Antarctic Task Force 43", AD261144, 1961.

82. "Position and Velocity Determination within the Solar System From Measurement of Angles between Celestial Bodies", AD261168, 1961.

83. "Interplanetary Navigation Study: Stellar and Planetary Positions", AD261169.

84. "Traverse Navigation in Polar Regions" AD285221, 1962.

85. "Third Quarterly Report - Study of Multi-Function Sensors for Guidance Subsystems", AD405474.

86. "Relative Star Angle Comparator", AD430013.

87. "Spacecraft Bus for Lunar Logistics Systems", (STL), 8689-6007-TU-000, Vol. I., Dec 62.

88. "No-Gimbal Feasibility Flight Test Program", ASD-TDR-62-913, Nov 62.

89. "Methods for Estimating Accuracy of Position, Velocity and Acceleration Data", DR&CWG of IRIG, Document 103-64.

90. "X-20A Guidance Philosophy and Mechanization", SEG TDR 64-5, May 64.

91. "Non-Random Range, Azimuth, and Elevation Residuals Induced at the Observation Site", Aerospace Corp Report No. TOR-269 (4110-01)-46, June 64.

92. "A Computer Program for Automatic Star Identification", Ballistic Research Lab. Report No. 1535, Dec 63.

93. "Distance Estimation of Frequency-Coded and Uniformly Flashing Lights", FAA Tech Raport No. 12, Contract FAA/BRD-127, June 62.

94. "Assessment of AN/AVN-1 Astro-Navigational Set", AD405734.

95. "Orientation Determining Device", Patent Disclosure; Potter et al., US Patent 3,120,578.

96. "Space Position Fixing Techniques", AD224659.

97. "Constants and Related Data for Use in Trajectory Calculations", JPL Technical Report #32-604, March 64.

98. "Apollo Logistics Support Systems Molab Studies Task Order N-36 Report on Conceptual Navigation System", Doyle Thomas, NASA CR-61013, Oct 64.

99. "Report on NASA/CRPL - NBS Meeting, 15 October 1964", Bendix Systems Division, IOM #AP/319.

100. "Point to Point Communications on the Moon", L. E. Vogeler, Journal of Research, NBS, Vol. 67D, No. 1, Jan - Feb 63, pp 5-21.

101. "Optical Doppler Measurement Limitation," AD 252683.

102. "Service Test of Direction and Position Determining Indicating Instruments in Combat Vehicles", AD 277 259L.

103. "Report on Precision Celestial Navigation Experiments", H. Shuffeldt, on Contract #NONR-2449(00), Nov 57.

104. Senior and Siegal, "A Theory of Radar Back Scattering by the Moon", Journal of Research, NBS, Vol 67D, No. 3, p. 217, May-June 60.

105. "Measured Profiles on the Moon's Surface, and the Estimates of Magnitudes of the Errors in Relative Altitude," Gilbert Fielder, Dept. of Astronomy, University of Manchester, AD 243 276, Nov 59.

106. "Horizontal and Vertical Control for Lunar Mapping," Part One: Methods - Army Map Service, Technical Report, No. 29, AD 262 899, Aug 60.

107. "ALSS Scientific Mission Support Study," Bendix Systems Division, Final Report BSR 1112, March 65.

108. "The Earth and Its Gravity Field," Heiskanen and Vening Meinesz, McGraw-Hill, 1958.

109. Personal communication dated 17 December 1964 from Mr. W. M. Kaula to Mr. F. E. Digesu, MSFC.

110. ALSS SMSS Statement of Work, Enclosure 2, MSFC.

111. Pitman, Inertial Guidance, University of California Engineering and Physical Sciences Extension Series, John Wiley and Sons, Inc., 1962.

112. Ehricke, Space Flight-Dynamics, Principles of Guided Missile Design, D. Van Nostrand, Inc., 1962.

113. Parvin, Inertial Navigation, Principles of Guided Missile Design, D. Van Nostrand, Inc., 1962.

114. Dinsmore, "Introduction to the Moon", Derived from "Lunar Maps", prepared by NAA Space & Information Systems Div.

115. "Studies of Lunar Logistics System Payload Performance," Grumman Project 344, Section 6.4.10.2.

116. Bowditch, American Practical Navigator, H. O. Publication No. 9, 1962.

117. Dutton, Navigation and Piloting, United States Naval Institute, 1958.

118. IEEE Transactions on Aerospace and Navigational Electronics, Volume ANE-10, Sept 63.

119. "Lunar Maps" (MSC, ACIC & AFCRL Estimates of Lunar Map Accuracy). Also LUNAV #28 Information obtained informally from MSFC.

120. Macomber and Fernandex, Inertial Guidance Engineering, Prentice Hall Space Technology Series, 1962.

121. "Effect of Physical Constant Uncertainties Upon Lunar Orbit Determination," Dr. T. L. Gunckel, delivered at Berlin Air and Space Navigation, Congress, April 63, N64-18086.

122. "System Capabilities and Development Schedule of the Deep Space Instrumentation Facility 1963-1967," JPL Tech. Memo No. 33-83, 2 March 62.

123. "Lunar Logistic System, Volume VI, Tracking and Mission Control," MSFC, 15 March 63.

124. "Studies of LLS Payload Performance," Grumman Project 344 Summary Report, p. 8-8.

125. "Scope of Work, Preliminary Design Study of Logistics Support System (ALSS) Payloads": RFP, DCN 1-4-21-01015-01: MSFC, March 64.

126. Personal communication to S. W. Fordyce (NASA-Washington) from T. W. Hamilton (JPL), 8 December 1964 (re earth-based tracking).

127. Personal communication to The Bendix Corporation from R. L. Duncombe, Director of Nautical Almanac Office, June 64.

128. J. Opt. Soc. Am., 52, 949, 1962.

129. J. Opt. Soc. Am., 52, 253, 1962.

130. J. Opt. Soc. Am., 51, 1310, 1961.

131. J. Opt. Soc. Am., 51, 1251, 1961.

132. J. Opt. Soc. Am., 51, 719, 1961.

133. J. Opt. Soc. Am., 52, 1321, 1962.

134. J. Opt. Soc. Am., 52, 1310, 1962.

135. J. Opt. Soc. Am., 52, 1089, 1962.

136. J. Opt. Soc. Am., 53, 1096, 1963.

137. J. Opt. Soc. Am., 53, 1401, 1963.

138. J. Opt. Soc. Am., 48, 868, 1958.

139. J. Opt. Soc. Am., 49, 1135, 1959.

140. J. Opt. Soc. Am., 50, 214, 1960.

141. J. Opt. Soc. Am., 30, 464, 1940.

142. J. Opt. Soc. Am., 50, 203, 1960.

143. Jenkens and White, "Fundamentals of Optics", McGraw-Hill, 1959.

144. App. Opt., p. 1411, Dec 64.

145. App. Opt., p. 778, Jan 62.

146. Handbook of Chemistry and Physics, Chemical Rubber Publishing Company, 1963.

147. International Critical Tables, Vol. V, McGraw-Hill, 1929.

148. Satellite ANNA, Optical Program, Edgerton, Germeshausen and Grier, Dec 62.

149. SLRV - Phase I, Final Report, Bendix Systems Division, BSR 903, Vol. II, p. 5-2.

150. ALSS 439, Bendix Systems Division, Contact Report, H. Faram to E. Dungan, C. Hamilton, MSFC, 14 July 64.

151. Bendix Systems Division Contact Report 64-210-941, W. Green to J. Harden, MSFC, 26 June 64.

152. Personal communication from Mr. J. A. Downey to Contracting Officer's Rep. R-ASTR-AN, dated 15 Dec 64.

153. Personal communication from Mr. S. W. Fordyce, NASA Hg, to Mr. J. W. Harden, Jr., NASA MSFC, dated 28 Dec 64.

154. Jet Propulsion Laboratory, Interoffice Memo 312.7-93, 3 March 1965, by T. H. Elconin.

155. W. Kaula, "Statistical and Harmonic Analysis of Gravity," Journal of Geophysical Research, Vol. 54, No. 12, Dec 59

156. G. Bomford, Geodesy, Oxford at the Clarendon Press, 1952.